A STUDY OF THE WIND FORCES ON LOW RISE BUILDING ARRAYS AND THEIR APPLICATION TO NATURAL VENTILATION DESIGN METHODS

MAHMOOD HUSSAIN
B. Arch.

Thesis submitted to fulful the requirements
for the degree of

Doctor of Philosophy

at the

Department of Building Science,
University of Sheffield

November 1978

CONTAINS PULLOUTS

TEXT CUT OFF IN THE ORIGINAL

PAGE NUMBERS ARE CUT OFF IN THE ORIGINAL

To my parents
and
my wife Shahida
with love.

SUMMARY

A STUDY OF THE WIND FORCES ON LOW RISE BUILDING ARRAYS AND THEIR APPLICATION TO NATURAL VENTILATION DESIGN METHODS

MAHMOOD HUSSAIN

Due to the complicated flow phenomenon in urban areas, the assessment of wind pressure forces as well as the rates of natural ventilation for groups of low rise buildings is complex. As a result, the current design methods for the prediction of these forces are over-simplified and lead to inaccurate estimates of wind forces and ventilation rates in buildings.

A survey of previous studies regarding wind properties and their influence on pressure forces alongwith work related to natural ventilation, wind loading and air flow round buildings was carried out. The survey revealed that no general relationship exists which defines the interaction between the various aspects of flow. This thesis, therefore, attempts to enhance our knowledge about the flow around groups of buildings and suggests a means of quantifying the interaction between building shape, group geometry, flow properties and the resulting pressure forces.

The present study has been carried out in a simulated urban terrain atmospheric boundary layer flow. A series of model scale experiments were performed for different building shapes. The study starts with the investigation of the influence of upstream fetch on the central model drag before going on to the detailed measurements on various models covering a wide range of building shapes, group form and plan area density. The detailed measurements of mean pressure forces on model buildings situated within a variety of groups of similar form indicated three different trends in the behaviour of these forces, corresponding to the three flow regimes known to exist for flow over general

roughness elements. The existence of these flow regimes was confirmed by velocity profile measurements. A general correlation between group geometry, flow properties and the resulting pressure forces has been suggested.

In order to apply the foregoing results to full scale building arrays, a method has been proposed to yield the pressure difference across low rise buildings for the prediction of natural ventilation rates in an urban built form. This method takes into account the relevant built form and flow parameters which are ignored in the current IHVE design guide method (1970), (applicable to high rise buildings only). The suggested method includes the prediction of ventilation rates from the openings in the walls as well as in the roof. Suggestions have also been made to revise the British Standard Code of Practice for wind loading to incorporate the trends which have been found to be different to those currently recommended.

SUMMARY

LIST OF CONTENTS

LIST OF FIGURES

ACKNOWLEDGEMENTS

NOMENCLATURE

LIST OF FIGURES

ACKNOWLEDGEMENTS

I would like to thank my supervisor, Dr. B.E. Lee, for his invaluable guidance during the experimental stage of this work and his advice and constructive criticism during the writing of this thesis. I am also grateful to him for all the help he provided to make my stay in this country pleasant.

I also want to express my gratitude to all the staff and students of the Department of Building Science for their invaluable suggestions from time to time. Special thanks are due to Mr. C.G. Souster for his help regarding computing problems.

I also want to thank the members of the technical staff of the Department of Building Science, Mr. R. Webster, Mr. R. Skelton, Mr. P. Williams, Mr. A. Walker, Mr. M. Broady and Mr. T. Thomas, for their assistance in constructing the models used in this study.

I would particularly like to thank Mrs. L. Robertson for the care and diligence with which she typed this thesis.

The financial support provided by the Government of Pakistan is also acknowledged. My thanks are due also to the members of the University of Engineering and Technology, Lahore, Pakistan, particularly the Vice Chancellor and the staff of the Architecture Department.

Finally, I would like to thank my wife for her help and encouragement during the period of my research and her patience and understanding during all this time. Special thanks also to all the members of my family who have helped me in one way or the other.

NOMENCLATURE

A list of the nomenclature used in all the chapters of the thesis is given below.

List of Nomenclature

Symbol	
A	Area of the intervening smooth surface/roughness element, also site area/building.
A_1	Constant in equation 7.1.
A_f	Frontal aspect ratio (L/H).
A_p	Plan area associated with one roughness element.
A_s	Side aspect ratio (W/H).
a_i	Constant in equation 3.2.
a_f	Frontal area of one roughness element.
B	Constant in equation 5.2.
B_1	Constant in equation 4.2 and 4.5.
b	Breadth of two dimensional grooves in the flow direction.
b_i	Constant in equation 3.2.
C	Constant in equation 7.1
C_1	Constant in equation 2.4 - function of U_*, Z_o and f.
C_2	Constant in equation 4.15.
C_3	Constant in equation 4.16.
C_D	Drag coefficient.
C_{D_1}	Drag coefficient based on the free stream dynamic head.
C_{D_c}	Element's centre line drag coefficient based on the free stream dynamic head.
C_{D_H}	Drag coefficient based on the dynamic head at the building (or roughness element) height, H.

C_{D_m}	Drag coefficient based on the maximum pressure difference across the element.
C_f	Local skin friction coefficient.
C_{f_e}	Effective local skin friction coefficient, C_{D_1}/A.
C_i	Infiltration coefficient of the opening.
C_{L_1}	Roof lift coefficient based on free stream dynamic head.
C_{L_H}	Roof lift coefficient based on the dynamic head at the building (or roughness element) height, H.
C_p	Mean pressure coefficient.
C_{p_1}	Maximum mean pressure coefficient.
C_{p_b}	Leeward wall mean pressure coefficient.
$C_{p_{bc}}$	Leeward wall mean pressure coefficient at element centre line.
C_{p_l}	Roof mean pressure coefficient.
C_{p_o}	Minimum mean pressure coefficient.
C_t	Concentration of tracer gas at time t.
C_{p_w}	Windward wall mean pressure coefficient.
$C_{p_{wc}}$	Windward wall mean pressure coefficient at element centre line.
ΔC_L	Mean pressure difference across the roof of a building, (based on U_1).
ΔC_{L_H}	Mean pressure difference across the roof of a building, (based on U_H).
ΔC_p	Mean pressure difference coefficient across any opening in a vertical face of a building, (based on U_1).
ΔC_{p_H}	Mean pressure difference coefficient across any opening, (based on U_H).
ΔC_{p_o}	Mean pressure difference coefficient across two opposite faces of a building.
D	Drag force on a building or roughness element.

d	Zero plane displacement.
$\bar{d}$	Mean value of d.
E	Mean bridge voltage of the anemometer.
$\underline{E}$	Constant in equation 4.4.
E_d	The reattachment distance downstream the building or any roughness element.
E_f	Mean bridge voltage of the anemometer in the free stream.
E_o	Mean bridge voltage of the anemometer at zero velocity.
E_t	The sum of the separation and reattachment distances, E_u and E_d.
E_u	The separation distance upstream the building or any roughness element.
E_v	Dimension of the stable vortex in the flow direction.
ΔE	$\frac{E^2 - E_o^2}{E_f^2 - E_o^2}$ in equation 5.4.
F_1	Empirical function of the ratio δ^*/θ^* in equation 7.3.
F_3	Functional dependence of the windward pressure profile.
F_4	Functional dependence of the leeward pressure profile.
f	Coriolis parameter in equation 2.4.
f_o	Resistance coefficient in equations 4.15 and 4.16.
H	Building height, roughness element height.
$\bar{H}$	Average value of H.
H_1	Shape factor related to δ^*/θ^* in equation 7.3.
h	Central model height relative to the average height of the group.
K	Universal constant = 0.41.

k	Height of two dimensional roughness elements.
K_1	Constant in equation 3.3.
k_s	The equivalent sand grain roughness size.
L	Length of the building.
L_c	Crack length.
L_x	Distance of separation between buildings in the wind direction, also site length.
L_y	Site lateral dimension.
m	Roughness concentration indicator.
n	Exponent in equation 1.1.
p	Wind pressure on the building surface.
p_b	Leeward wall pressure.
p_o	The static pressure at the reference point.
Δp	Pressure difference acting across any opening.
Δp_o	Pressure difference between the two faces of a building.
q_1	The free stream dynamic head.
R	Group layout radius, also central model fetch.
R_1	Hydraulic radius of pipes in equation 4.15.
S	The roughness element spacing in the flow direction.
S_c	Roughness element clear spacing in the flow direction.
t	Time.
u	Mean velocity in the wind direction at any height.
U_1	Mean velocity in the free stream.
U_H	Mean velocity at roughness element height, H.
U_G	Gradient velocity.
U_{10}	Mean velocity at 10m above ground.

U_*	Friction velocity.
$\frac{\Delta U}{U_*}$	Roughness function.
V	Infiltration rate.
v	Vertical component of the mean velocity.
V_1	Volume of air entering the room.
V_o	Volume of the room.
W	Width of the building.
Y	Height above the ground.
Y_G	Gradient height.
Z_o	Roughness length.
$\overline{Z}_o$	Mean value of Z_o.
α	Exponent in the power law.
θ	Central model orientation angle with respect to wind direction.
θ^*	Boundary layer momentum thickness.
$\Delta\theta$	Temperature difference.
ϕ	The surrounding group angle of orientation with respect to wind direction.
λ	Density of the array.
λ_e	Spacing of two dimensional roughness elements.
λ_f	Frontal area density.
λ_p	Plan area density.
δ	Boundary layer thickness.
δ_i	Internal layer thickness.
δ^*	Displacement thickness.
ε	Error in origin for measuring y, ($H = \varepsilon + d$).
κ	Universal constant ($\simeq 0.4$).
ν	Kinematic viscosity of air.
ρ	Density of air.

τ_{oe}	Effective surface shear stress.
ψ_x	Ratio between building width, W and the site length, L_x.
ψ_y	Ratio between building length, L and the site lateral dimension, L_y.

CHAPTER 1

INTRODUCTION

1. INTRODUCTION

1.1 The fundamentals of natural ventilation

1.1.1 The knowledge of the amount of fresh air supplied to the building and the removal of excess heat, moisture and noxious products as close as possible to the point of generation is a fundamental rule of ventilation practice. This is important not only in the estimation of heating or cooling requirements of a building, but also in determining the quality of air within the buildings. The supply of air can be achieved in three different ways either by natural ventilation, by mechanical ventilation or by air conditioning. The choice of the method to deal with a particular situation effectively is the first important step in the planning of a ventilation system and is governed by either the architectural design principles or the cost and the required standards of the internal environment of the building. The type of ventilation technique used often dictates the shape of the building which in turn affects many other architectural design principles.

All methods of ventilation control have their advantages and disadvantages. Air conditioning and mechanical ventilation provide controllable internal conditions more suited to the needs of individuals or of a particular purpose, but involve additional capital investment and increased running cost. This may be acceptable in some buildings and essential in others and the cost may be wholly or partially recovered by possible compromises in certain other aspects of the design as well as in providing comfort to the occupants. Natural ventilation on the other hand is dependent on external climatic conditions which may be highly variable, as a result of which, the ventilation rates vary from time to time and desirable indoor conditions cannot be maintained.

1.1.2 Natural ventilation occurs in virtually all buildings from the designed provision of specified apertures in their fabric, such as openable windows, ventilators, shafts and so on and can usually be controlled to some extent by the occupant. The ventilation rates in a building depend not only on the external wind velocity but also to a great extent on the location, size, orientation and design of openings.

1.1.3 Infiltration on the other hand is the leakage of air through a building due to imperfections in the structures mainly as gaps and cracks around doors, windows and similar other joints and perforations between infill panels and cladding sheets. Whereas the flow of air through proper openings can be controlled, the infiltration cannot and is always at the mercy of natural forces and cannot be relied upon to provide a guaranteed rate of air change under all conditions. It is for this reason that efforts should be made to make all structures as airtight as possible when all doors and windows are closed to minimise unintentional flow of air.

1.1.4 The existence of a pressure difference across the building and the areas and resistance offered by the openings to air flow governs the rate of air flow through a building i.e. its natural ventilation. One of the motive forces responsible for natural ventilation is caused by the difference in the density of air due to the indoor and outdoor temperature difference. This is commonly known as the "stack effect" and in this case air will either move from low level inlets in a heated building to high level outlets or it may move in the opposite direction if the air in the building is cooler than the outside.

The other force causing the pressure difference is the wind force in which case air will enter through openings and cracks in the windward side and leave through openings in the leeward side or through the roof. Due to air flow

around a building different pressures are exerted on its external surfaces i.e. positive pressure normally develops on the windward face while negative pressure develops on the leeward face, side walls and the roof. Under some conditions, both the stack and the wind effect act together to produce natural ventilation. The pressure caused by the two effects are added to give the total pressure difference acting at any opening and hence, together with a knowledge of the open areas and their discharge coefficients, the ventilation rate can be determined.

1.1.5 There are certain other factors affecting the pressure difference across the openings in specific circumstances, such as the turbulence diffusion or the pressure fluctuations. The magnitude of air flowing through a building due to these two mechanisms is, however, very small compared to the wind force or the thermal force. In the absence of both the wind and the thermal forces, these could be of some weight.

1.1.6 Most design recommendations for calculating natural ventilation and infiltration rates are based on the results of digital analogue studies. Bilsborrow and Fricke (1975) studied these methods and found that due to the complex interaction of the factors affecting the ventilation potentials, almost all the natural ventilation rate calculation methods make a number of simplifying assumptions which have not been experimentally verified. Despite the fact that the experimental arrangement in which they carried out their study was not sufficiently rigorous to establish accurate values, their scale model studies in a wind tunnel showed the calculated ventilation rates to be up to 30% higher than the model ventilation rates.

1.2 Natural ventilation requirements and prediction techniques

1.2.1 A continuous supply of fresh air is essential in all buildings in order to maintain comfortable conditions

for human occupation. The supply of fresh air helps to provide adequate oxygen for breathing and to remove excess CO_2, excessive moisture, undesirable odours and any specific artificial contamination which may be produced in the environment by normal occupation. It also assists in controlling the thermal conditions in the space.

The provision of ventilation to satisfy the above requirements is directly related to the number of occupants in the building or the production of noxious products in specific cases such as kitchens, laundries or in certain laboratories. The two widely used methods of predicting natural ventilation or infiltration rates in buildings are the air change method and the crack method. Both methods are described in the IHVE Guide (1970) and the ASHRAE Guide (1972).

1.2.2 The air change method which is entirely empirical is based on the assumption that similar building types of typical construction and normal use in winter would have similar infiltration rates. The recommended values of design ventilation rates in the IHVE guide are, therefore, classified with respect to building types assuming normal exposure and an average of 25% openable windows and doors to the external walls. Allowance of 25 - 50% are then made for the degree of exposure and the higher ratios of openable areas and a reduction of up to 50% for unoccupied buildings. The guide also recommends a reduction of up to 33% for sheltered sites as compared to a 50% increase in the case of severely exposed sites. On the other hand, the air change method described in the ASHRAE guide gives the values applicable to residential buildings which are classified according to opening distributions in the external walls alongwith an allowance for weather stripping for which a reduction of up to 33% is recommended. This, however, does not allow for the shelter of the building and the amount of glazing.

1.2.3 The crack method of infiltration calculation, regarded as being more accurate,is used to calculate the ventilation rates from the estimated infiltration characteristics of the building fabric and design external pressure distribution. The method is based on the use of a single design wind speed which is corrected for building height and the type of terrain. A representative total leakage area is taken which depends upon the window distribution, and assuming a pressure coefficient of 0.55 across the crack area, a maximum infiltration rate is calculated. The following equation relates the ventilation rate, V, to the pressure difference, Δp, acting across any openings.

$$V = C_i \, L_c \, (\Delta p)^{1/n} \qquad 1.1$$

where C_i and L_c are the infiltration coefficient and the crack length and depend on the type and area of the opening respectively. Bilsborrow (1973) showed a relationship to exist between C_i and the exponent n, from his work on air flow through openings. In order, therefore, to determine the ventilation rate, V, in equation 1.1, Δp remains to be determined. The main source of information is to be found mainly in the work relating to air flow around buildings.

The IHVE guide assumes the velocity pressure of the wind at the roof top level to be approximately equal to the pressure difference between the windward and leeward faces of the building, Δp_o. This is then used to estimate the mean pressure difference across any opening, Δp. Therefore, for one design wind speed, three velocity pressure profiles, assumed to occur for three different types of terrain, are plotted in order to obtain Δp_o for buildings of any given height in the three site conditions. The estimates of Δp_o made in this manner do not account for the building form or for the influence of the group form and may result in considerable error. It is, therefore, important to consider

the factors affecting the pressure difference across the buildings in order to calculate the ventilation rates more reliably.

1.2.4 Neither the IHVE guide nor the ASHRAE guide make any mention about the rate of air flow through openings in the roof. Such openings may well be essential in certain types of buildings particularly in low rise buildings where the use of skylights cannot be avoided. In order to substantially improve the ventilation calculations through infiltration, it is essential to consider the factors affecting the pressure difference across any openings in the roof and include these in the guide.

1.3 The factors affecting the pressure difference across the windward and leeward faces as well as across the roof of buildings

1.3.1 The number of variables affecting the pressure difference across vertical faces of buildings as well as across the roof in the natural wind is large. The main source of information about the interaction between these variables is the work on scale model experiments. In particular, the work done on the drag (and hence Δp_o) of bluff bodies in turbulent boundary layers provide the basic information required. Such work has been reported by Morris (1955), Jensen and Franck (1965), Good and Joubert (1968), Joubert, Perry and Stevens (1971) and Wooding, Bradley and Marshall (1973). The work done on the roof suction of bluff bodies is, however, very rare. Although the flow in a turbulent boundary layer over rough surfaces is expected to be different to that of the wind flow over the earth's surface, the work done in turbulent boundary layers can be taken as a fundamental datum and the work done in atmospheric boundary layer flow can be compared to work done in rough wall turbulent boundary layers.

1.3.2 The drag exerted on any bluff body in boundary layer flow is the difference between the integral of windward and the leeward pressure distributions. On the other hand, the lift force exerted on the roof of a bluff body is the integral of the roof pressure distributions. These surface pressures are determined by the process of separation and reattachment of air flow round the body and depend on the form of the individual building as well as the group form in an urban area. Individual building form is the only form factor affecting the pressure forces and may be broken down to:

i. building shape
ii. building size, and
iii. building permeability.

1.3.3 The effect of varying the rectangular shape of isolated buildings on the drag coefficient has been studied by Joubert, Stevens and Perry (1962), where the drag coefficient was found to be sensitive to variations in frontal aspect ratio but was quite insensitive to variations in side aspect ratios over the normal range of interest in building construction. Furthermore, the British Standard Code of Practice CP3 (1972), gives values of the drag coefficient for varying shapes of buildings. On the other hand, the work of Good and Joubert (1968) and Jensen and Franck (1965) has demonstrated that for buildings with turbulent boundary layer, the size of building alone can influence the drag coefficient. This is probably due to the varying ratio between body height and the boundary layer height. The third property of individual form that affects the drag coefficient i.e. the building permeability, though outside the scope of present work has been found to reduce the pressure difference across one particular building by a factor of 30%, Newberry, Eaton and Mayne (1973).

1.3.4 In urban and suburban areas, however, the buildings in most cases are close enough to act in the form of a group. In such cases, the individual form of the building is overshadowed by the group form in influencing the surface pressure forces experienced by each building and hence the pressure difference across the vertical faces and suction on the roof. Some recent experimental work by Joubert, Perry and Stevens (1971) and Lee and Soliman (1977) has shown how the group geometry of roughness elements in a turbulent boundary layer flow affect the drag forces on each element.

1.3.5 The wind loads on buildings will also be affected by the factors mentioned above. The effect of varying the shape and form of the building on the resulting windloads is well documented in ESDU 71016 as well as in the British Standard Code of Practice for wind loads, CP3, Chapter 5, Part II, (1972). The method of determining the wind forces on buildings used in CP3 utilises a design wind speed and a drag coefficient C_{D_H}. The design wind speed is based on the maximum gust speed for the locality and takes into account the local topographic influences, the surface roughness of the environment and the design life of the building. For a particular case, the height of the building is taken into account since the reference dynamic head is that appropriate to the top of the building and the value of C_{D_H} takes into account the building geometry.

1.4 The problem and the pattern of investigation

1.4.1 The natural ventilation calculations are shown to depend on an accurate estimate of the pressure difference across the buildings and the roof suction acting on the buildings, which are found to be affected largely by the geometry of the building group and the properties of the natural wind. It is, therefore, necessary to obtain comprehensive information about the natural wind flow and the surface pressure forces acting on buildings in urban

areas. It is intended to carry out a detailed investigation on the interaction between group geometry, the resulting pressure forces and the properties of air flow with the object of establishing a relationship between the three parameters.

On the basis of work reported by Good and Joubert (1968) for a single case of a two dimensional isolated element in smooth surface flow, whereby a similar relationship was found to exist between the element form, the resulting pressure forces and the flow properties, it is suggested that a relationship of this type will also exist in the present investigation.

In the present study, an effort has been made to present the results in a systematic manner explaining in detail the different aspects of form and flow in urban areas so as to cover most building forms which are likely to be met in actual practice and their interaction in the natural wind. In order to make the investigation more comprehensive and to substantiate the experimental results, the theoretical aspects of turbulent boundary layer flow over rough surfaces have been included where possible. The following pattern of investigation was thus followed to meet the requirements.

1.4.2 In the first part of the thesis, Chapters 2-4, the properties of flow in the natural wind alongwith the relevant available information of previous work on the wind pressure and flow over two and three dimensional bodies are included. This work was carried out to obtain the theoretical basis and the available information to be used in the second section of the thesis. Since the properties of flow in the natural wind are important factors in determining the pressure forces on buildings, these are first considered in chapter 2. A review of the previous work on the wind pressure forces and flow over groups of buildings is made in chapter 3. Since buildings can be considered as roughness elements on the earth's surface over which the atmospheric boundary layer flows, the work done on flow over rough surfaces is discussed

in chapter 4.

1.4.3 The results of the work carried out in the first section of the thesis suggested that further investigation was needed to understand the interaction between flow properties and the resulting pressure forces for different building geometries and to close the gap between the idealised theoretical case and the practical case of buildings in the natural wind. Consequently in the second section of the thesis, chapters 5-10, the results of the experimental investigation carried out in the present study using a large number of building shapes tested in a simulated atmospheric boundary layer flow have been presented and discussed. The main variables considered in the investigation are as follows:

a) The building form: including the plan form variations and the height variations. The cube was taken as a simplified building form and the results for other building forms were related to the results obtained for the cube.

b) The group form: including a wide range of group density and layout pattern.

c) The upstream fetch: to investigate the optimum size of the model group for the stabilisation of pressure forces.

d) The resulting pressure forces on the windward and leeward faces as well as the roof of various building models: made from the pressure tapped models placed in the centre of the group in each case.

e) The velocity profiles: measured in front of two building models.

1.4.4 The experimental arrangements and the measurement techniques alongwith their accuracy levels are given in chapter 5. In chapter 6 the discussion of the experimental results for all the models in isolation is given. Following in chapter 7, a detailed investigation of the influence of upstream fetch on cube shaped buildings is included. The results of this investigation about the model group size required for the stabilisation of pressure forces were applied to all the subsequent investigations. The pressure and flow measurement results on a cube shaped element are given in chapter 8. On the basis of the effect of group geometry on the resulting pressure and velocity profile measurements, conclusions concerning the flow behaviour are drawn and different parameters correlated. In order to extend this study to other building forms, chapter 9 describes the pressure and flow measurement results for buildings of different plan forms. The results in this chapter were related to those found for cube shaped elements and the conclusions drawn in chapter 8 were substantiated and confirmed. In chapter 8 and 9 a clear picture of the existence of different flow regimes and their dependence on the shape of the buildings was formulated. Finally chapter 10 describes the effect of model height variations relative to the surrounding roughness alongwith a detailed discussion of the behaviour of forces acting on them.

1.4.5 In the last section of the thesis, a detailed discussion on the application of this study to the natural ventilation problems of buildings is presented and an alternative procedure for the prediction of the pressure difference across buildings is given in chapter 11. This alternative prediction procedure would result in a substantial improvement to the current IHVE guide method for the calculation of infiltration rates. In addition to this, a separate procedure is suggested to calculate the infiltration from the roofs of buildings to be added to the IHVE guide. Finally in chapter 12, the conclusions reached in this thesis are

summarised and the areas where uncertainty exists, over-simplifications made or the conservative values used, are outlined. Suggestions have also been made to reconsider some of the trends given in the British Standard Code of Practice for Wind Loads.

CHAPTER 2

THE PROPERTIES OF NATURAL WIND, THE SIMULATION TECHNIQUES IN THE WIND TUNNEL AND THEIR INFLUENCE ON PRESSURE FORCES ON BLUFF BODIES

2. THE PROPERTIES OF NATURAL WIND, THE SIMULATION TECHNIQUES IN THE WIND TUNNEL AND THEIR INFLUENCE ON PRESSURE FORCES ON BLUFF BODIES

2.1 Introduction

2.1.1 The atmospheric boundary layer is the lower region of the atmosphere from which momentum is extracted to compensate for the friction of the earth's surface. The structure of the atmospheric boundary layer is complicated and its properties highly variable. It is, therefore, essential to briefly describe the structure and behaviour of the natural wind before discussing the flow variables affecting the pressure forces on the buildings.

2.2 The structure and behaviour of the natural wind

2.2.1 Natural wind in the boundary layer developed over the surface of the earth varies widely in structure because of strong dependence upon topography, surface roughness features and the state of thermal stratification. Above the boundary layer the atmosphere is considered to be unaffected by surface friction and the air movement originally produced by large pressure gradients in the atmosphere is modified by the rotation of the earth to form the Geostrophic Wind. Thus the boundary layer may be regarded as a layer from which momentum is directly extracted and transferred downward to overcome the aerodynamic friction arising from the motion of the air relative to the earth's surface, Pasquill (1970).

2.2.2 The atmospheric boundary layer can be broken down to two regions of characteristically different properties. Close to the surface, the variation of shear stress with height is negligible. Wind direction in this region is also independent of height. This defines "the surface layer" or "the roughness layer" which extends from the ground up to about 30-100 metres depending upon the terrain, Cook (1971), Panofsky and Petersen (1972) and Counihan (1975).

Bounded at the bottom by the roughness layer and extending to the top of the atmospheric boundary layer is the "Ekman layer". In this layer, the shear stress decreases with height from its maximum value at the roughness layer to zero at the gradient height. This change in the shear stress is accompanied by a change in wind speed and direction. The change of wind direction known as the "Ekman spiral" is a clockwise rotation with increasing height in the northern hemisphere and the reverse in the southern hemisphere. The depth of the Ekman layer also varies from 300-600 metres depending upon the terrain. This would mean that the lowest height at which the wind velocity is equal to the gradient wind, i.e. the top of the atmospheric boundary layer, is of the order of 350-700 metres from the ground. Some research workers, however, do not agree with this and Harris (1977) has suggested the height of the boundary layer to be between 1000-3000 metres. Due to the highly complex nature of atmospheric boundary layer, a lot of information is still needed to establish its exact flow structure, flow pattern and its dimensions.

Within large surface roughness, such as in city centres, an "interfacial layer" may be present in which the downward flux of momentum is transferred to pressure forces acting on the surface roughness elements themselves, Pasquill (1970). This layer is characterised by wake flows and large variations of static pressure. Although the various sub-layers that form the whole atmospheric boundary layer blend into each other and the geostrophic conditions it is often convenient to assume sharp transition for practical purposes. Figure 2.1 details out the behaviour of the boundary layer as known under these conditions.

2.2.3 Over land, the earth's boundary layer is always adapting to changes of surface roughness such that an internal layer grows from every surface at a roughness change. This internal layer develops with the fetch to completely replace the old layer, Elliott (1958) and Munn (1966).

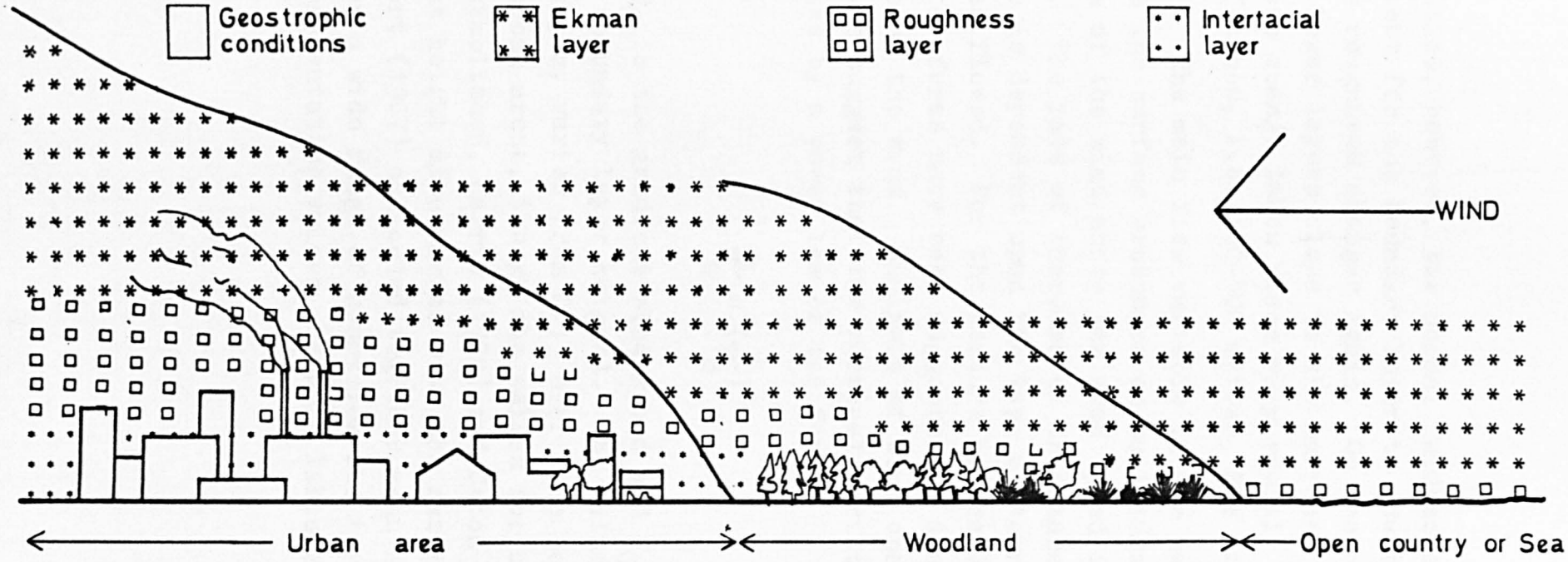

FIGURE 2.1 TYPICAL DEVELOPMENT OF THE ATMOSPHERIC BOUNDARY LAYER

In practice, however, the normal fetches of towns are not sufficient for the boundary layer to adapt fully before the surface roughness changes again. On the contrary, however, in the lower layers close to the surface, adaptation of roughness change takes place very rapidly at relatively short fetches, i.e. 100-500 metres, BRE digest 119 (1970).

2.2.4 The main flow variable in the natural wind that affects the surface pressures on buildings is the velocity profile of the wind where the wind speed increases with height. The rate of increase on the shape of the wind speed profile is dependent upon the type of terrain over which the wind has flowed. For the earth's boundary layer several empirical forms have been suggested to describe the velocity profile of the wind. Analysis of wind speed records over the years suggest that the vertical variation is well expressed by a power law of the form:

$$\frac{u}{U_G} = \left(\frac{Y}{Y_G}\right)^{\alpha} \qquad 2.1$$

where U_G is the gradient wind speed and Y_G is the gradient height (boundary layer height). The value of the power law exponent, α, varies from 0.13 over open country to 0.4 over rough urban areas, though the values for urban areas are less well established, Harris (1972) and Caton (1975). The gradient height also varies with the nature of the terrain. Davenport (1967) collected together mean wind speed profile data for a wide range of countries and terrains and suggested the representative values shown in Table 2.1 and Figure 2.2.

Table 2.1 Variation of the exponent α and the gradient height (After Davenport, 1967)

Type of terrain	Exponent α	Gradient height (m)
Flat open country	0.16	280
Woodlands and suburban areas	0.28	400
Heavily built up urban areas	0.40	430

2.2.5 Since the atmosphere in the surface layer is rarely adiabatic, the only satisfactory method of finding the power law index is by interpolation in measurements made over a range of thermal conditions. Jones et al (1971) have reported some measurements of the average wind speed and temperature at heights up to 1000 ft. at two urban sites to investigate the dependence of power law index, α, on temperature lapse rate, stability and wind speed. They found that both the power law index as well as the boundary layer thickness depend on thermal conditions in a certain range. This dependence was found to be negligible for temperature difference $\Delta\theta<0$ between the top and the bottom of the boundary layer and increases as the temperature difference increases. In their study covering a wide range of atmospheric thermal stability conditions they found the value of the power law index over Liverpool varying from 0.15 to 0.51 and suggested a value of 0.21 corresponding to the dry adiabatic lapse rate.

2.2.6 A survey of the available literature, however, shows that urban terrain power law exponents have been measured at various urban sites in the range from 0.21 to 0.40, Shellard (1963), Davenport (1963), Kamei (1955), Shiotani (1962), Jones et al (1971) and Caton (1975). The value of α = 0.23 was reported by Caton for central London which incorporates an allowance for the zero plane

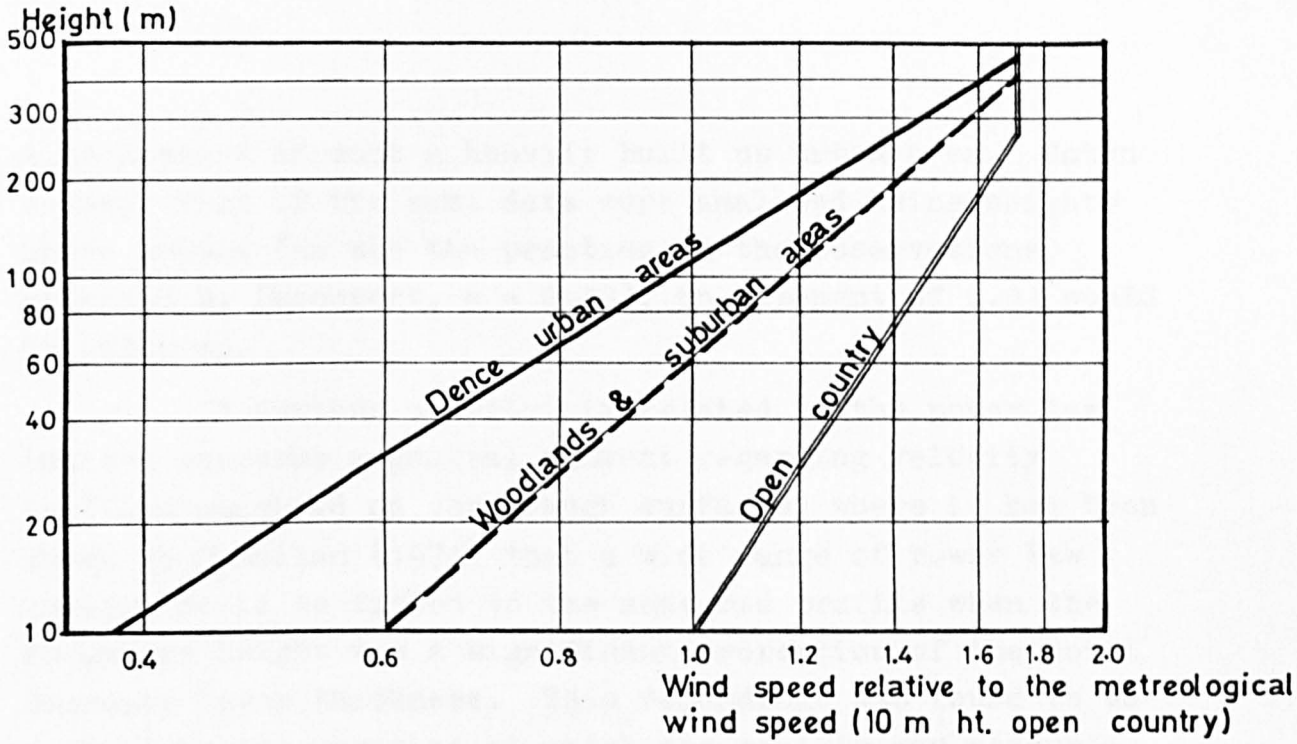

FIGURE 2.2 MEAN WIND VELOCITY PROFILES FOR SURFACES OF DIFFERENT ROUGHNESS (AFTER DAVENPORT)

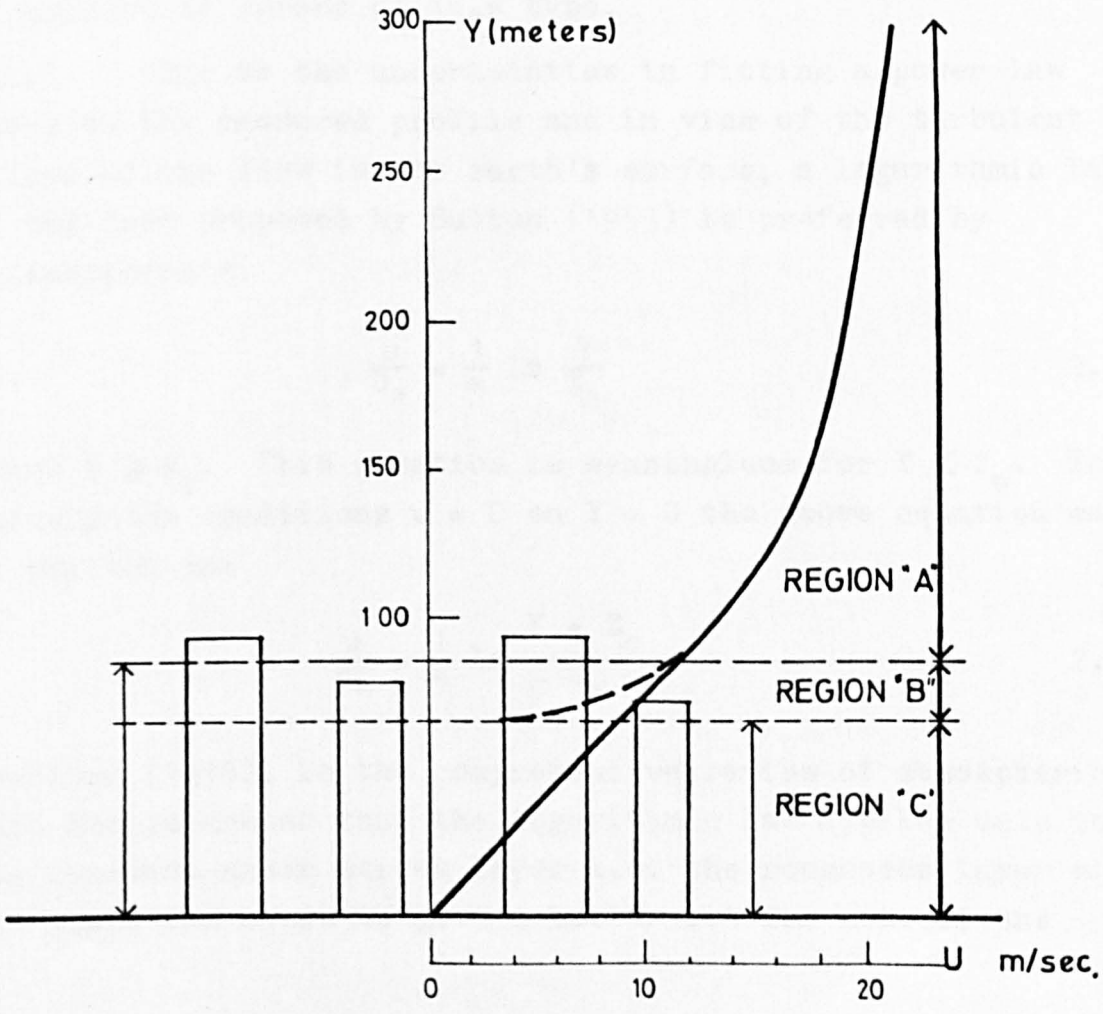

FIGURE 2.3 A MODEL FOR AIR FLOW IN URBAN AREAS (AFTER HARRIS 1972)

displacement of such a heavily built up urban area. Caton reports that if the same data were analysed using heights above ground (as was the practice in the observations reported by Davenport, $\alpha = 0.40$), an exponent of 0.33 would be obtained.

A further uncertainty related to the power law indices concerns a general comment regarding velocity profiles measured on very rough surfaces, where it has been shown by Counihan (1971) that a wide range of power law indices could be fitted to the measured profile when the roughness height was a significant proportion of the total boundary layer thickness. This dependence was found to be related to the position at which the profile was measured in relation to a particular roughness element and the height range over which the profile was fitted. Counihan suggests that some of the measurements reported by Kamei (1955) may be subject to errors of this type.

2.2.7 Due to the uncertainties in fitting a power law index to the measured profile and in view of the turbulent nature of the flow in the earth's surface, a logarithmic law of the form proposed by Sutton (1953) is preferred by meteorologists.

$$\frac{u}{U_*} = \frac{1}{\kappa} \ln \frac{Y}{Z_o} \qquad 2.2$$

where $Y > Z_o$. This equation is meaningless for $Y < Z_o$. To satisfy the conditions $u = 0$ on $Y = 0$ the above equation may be written as:

$$\frac{u}{U_*} = \frac{1}{\kappa} \ln \frac{Y + Z_o}{Z_o} \qquad 2.3$$

Counihan (1975), in the comprehensive review of atmospheric data has commented that the logarithmic law applies only to the constant shear stress layer i.e. the roughness layer while the power law seems to give a better fit for most of the

available data over a greater height range i.e. the Ekman layer, where the shear stress is no longer constant. In order to extend the validity of the logarithmic law to Ekman layer, a linear term should, therefore, be added in equation 2.3, Harris (1972).

$$\frac{u}{U_*} = \frac{1}{\kappa} \ln \frac{Y + Z_o}{Z_o} + C_1 fY \qquad 2.4$$

where f is the Coriolis parameter and C_1 is a function of U_*, Z_o, f and the gradient velocity and wind deviation between ground level and gradient height.

2.2.8 In the review given by Counihan (1975) he suggests that the rural area roughness length should fall in the range $0.01 \leqslant Z_o$ (m) $\leqslant 0.15$ and that for urban areas, the value of the roughness length will be of the order of 1 to 3m depending on the relative roughness element size. The ESDU Data Item (1972) covers a wide range of rural areas depending on the physical description of the terrain. Under the category of farmland, Z_o varies from 0.02m for uncut grass to 0.3m for terrain with many trees, hedges and few buildings. It also gives the value of Z_o in the range of 0.65m to 1.2 for centres of large towns and cities and values of 1.2 to 3.0m for centres of cities with very tall buildings.

2.2.9 In the case of flow over urban areas, the velocity profile undergoes a ground level displacement, d, therefore equation 2.2 should be modified to read:

$$\frac{u}{U_*} = \frac{1}{\kappa} \ln \frac{Y - d}{Z_o} \qquad 2.5$$

The model for flow in urban areas proposed by Harris (1972) shown in Figure 2.3 assumes three zones of flow, "A", "B" and "C". Zone "A" represents that part of the flow described by a logarithmic profile similar to the following modified form of equation 2.3:

$$\frac{u}{U_*} = \frac{1}{\kappa} \ln \frac{Y - d + Z_o}{Z_o} \qquad 2.6$$

In the region within the displacement height i.e. zone "C" no general law is applicable and the flow is determined by adjacent buildings while zone "B" is only a transition from region "A" to region "C".

2.2.10 The structure of atmospheric turbulence is usually described by the existence of eddies of different sizes and highly irregular shape in the atmospheric boundary layer. In general the eddy size increases with distance above the ground as there will be more room for larger eddies to grow. It is postulated that eddies comparable with the boundary layer height exist in the earth's boundary layer, Townsend (1951). As a result of this eddy cascade, the wind speed changes continuously with time, and the mean value of the wind speed is then dependent on the period taken for averaging. The energy contained in the eddies can be analysed for different frequencies to yield a spectrum similar to the one shown in Figure 2.4, Van der Hoven (1957).

2.2.11 In normal atmospheric conditions the wind speed and direction vary almost constantly throughout the year for various periods of time. The correct assessment of the prevailing wind conditions (speed and direction) at a particular site is essential in order to incorporate the wind effects likely to be experienced by a building or structure in its design life time. The statistical analysis of time and direction is known as a wind nose, Figure 2.5.

2.3 The simulation of the urban terrain atmospheric boundary layer flow

2.3.1 A comprehensive review of wind tunnel simulation mechanisms of the atmospheric boundary layer is given in a report on Euromech 50 (1975). Numerous applications of wind tunnel simulation techniques which are in use at various places have been described in the report and some conclusions about the validity, the limitation and future developments of wind tunnel simulation methods were reached

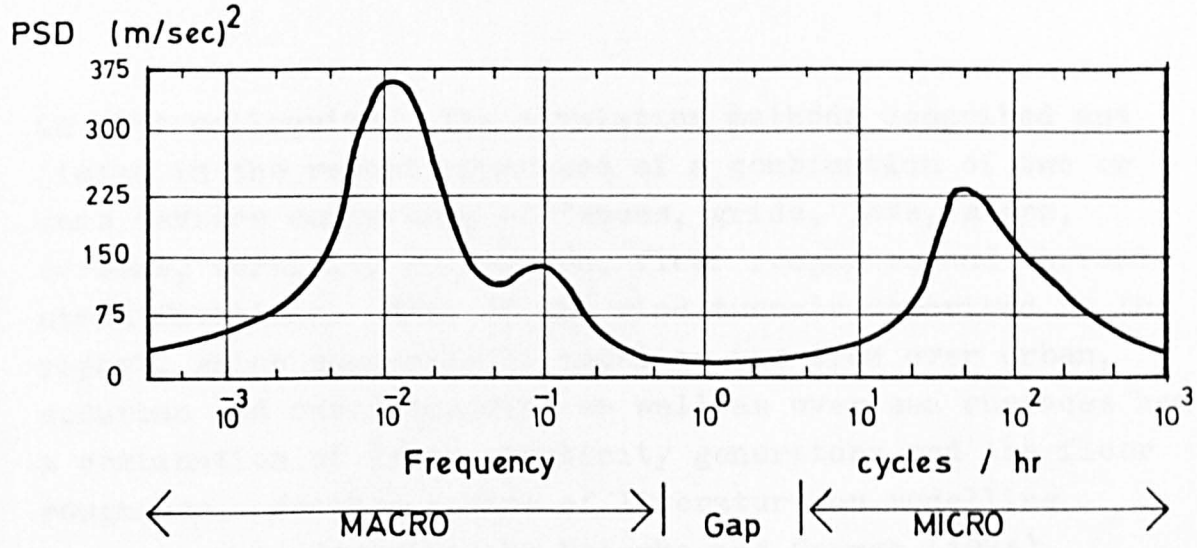

FIGURE 2.4 SPECTRUM OF THE HORIZONTAL WIND COMPONENT, (AFTER VAN DER HOVEN 1957)

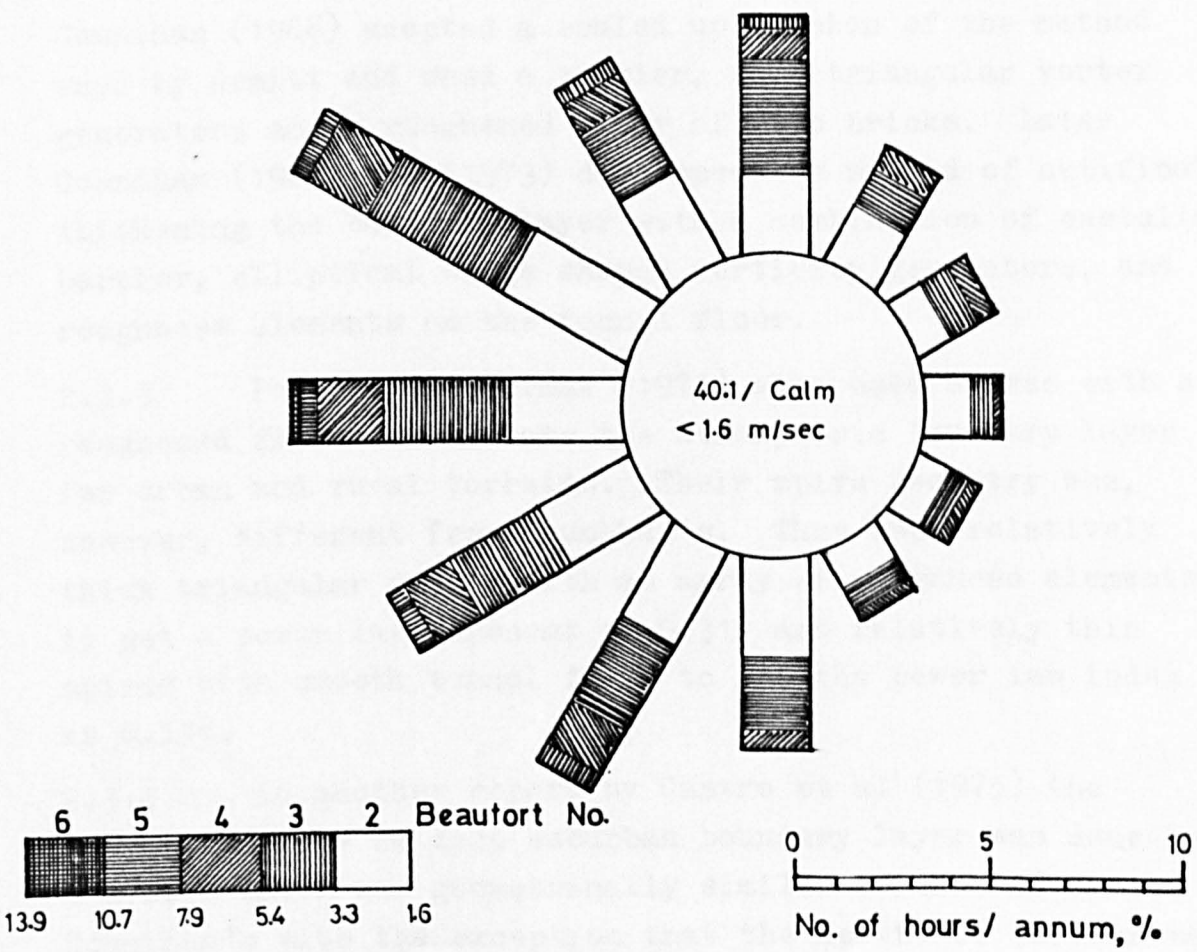

FIGURE 2.5 WIND ROSE DIAGRAM FOR SHEFFIELD (REPLOTTED FROM LEE 1975(b))

in that colloquium. The simulation methods described and listed in the report comprised of a combination of two or more devices comprising of fences, grids, jets, steps, screens, vorticity generators, floor roughness and thermal stratifications. Most of the wind tunnels described in the report, which successfully modelled the flow over urban, suburban and rural terrains as well as over sea surfaces had a combination of fence, vorticity generators and the floor roughness. Another review of literature on modelling techniques is described by Peterka and Cermak (1974).

2.3.2 An early use of fence and triangular vortex generators at the test entrance to simulate the natural wind was reported by Armitt (1966) and Armitt and Counihan (1968). Armitt used a combination of $\frac{1}{4}$" square bar, six 2" high vortex generators and floor roughened with corrugated cardboard in a 1' x 1' square working section of the Central Electricity Research Laboratory wind tunnel. Armitt and Counihan (1968) adopted a scaled up version of the method used by Armitt and used a barrier, four triangular vortex generators and a roughened floor of lego bricks. Later Counihan (1969) and (1973) developed the method of artifically thickening the boundary layer with a combination of castellated barrier, elliptical wedge shaped vorticity generators, and roughness elements on the tunnel floor.

2.3.3 Peterka and Cermak (1974) also used spires with a roughened floor to simulate the atmospheric boundary layer for urban and rural terrains. Their spire geometry was, however, different from Counihan's. They used relatively thick triangular spires with an array of roughness elements to get a power law exponent of 0.312 and relatively thin spires with smooth tunnel floor to get the power law index as 0.138.

2.3.4 In another report by Castro et al (1975) the simulation of a 2m deep suburban boundary layer was done by a system which was geometrically similar to that of Counihan's with the exception that the height of barrier was

adjustable and the distance between the barrier wall and vorticity generators was proportionally smaller.

2.3.5 On the basis of the above studies, it is suggested that the flow generated with the fence - spires - roughness method would represent an adequate simulation of the flow in the atmospheric surface layer. As a result of this it is expected that the wind pressures on the external surfaces of models tested in such a flow will provide sufficiently accurate estimates comparable to full scale results.

2.4 Effect of flow parameters on the mean pressure forces on the buildings

2.4.1 The effect of wind direction, turbulence and velocity profile parameters on the mean pressure difference across buildings experimentally studied in wind tunnels and the comparison of model results with full scale measurements provide the basic information. Some of the relevant work is reported below.

2.4.2 The effect of varying the wind direction on the pressure difference, Δp_o, is to produce completely different flow conditions due to variations of upstream roughness alongwith changing the pressure difference across the two opposite faces of a building. Tieleman and Reinhold (1976) in their wind tunnel model investigations for basic dwelling geometries have found that the mean as well as peak pressures vary a great deal with wind approach angle and pressure tap location. In another similar study Tieleman and Gold (1976), compared their results of wind tunnel investigation of a single family dwelling with its full scale results and found a reasonable agreement between the two. On the other hand Dick (1949) noted in his full scale studies on natural ventilation of houses that the wind direction is of negligible effect. This may be true for certain conditions but in the case of buildings of long plan shapes, buildings in groups and where the ventilation openings are only located on two

opposite faces of the building, the mean pressure difference across two opposite faces may range from a maximum at normal incidence to a minimum for the wind at right angle. Therefore, information about wind direction in nature is necessary if any estimates of Δ_{p_o} are required.

2.4.3 The effect of turbulence scale and intensity on the drag coefficient of two dimensional bodies has been investigated by Lee (1975(a)) and (1976) amongst others. Cook (1971) investigated the effects of turbulence scale or intensity on three dimensional rectangular forms. Jensen and Franck (1965) conducted wind tunnel experimental work in which the flow structure was varied using different surface roughness upstream of the model, on which the boundary layer naturally developed. Although no attempt was made to measure the associated turbulence characteristics or to reproduce the atmospheric turbulence structure, it was implied that modelling the correct ratio of H/Z_o in natural wind was closely related to modelling the turbulence properties. In general higher turbulence intensities reduce the pressure difference by increasing the negative leeward pressure. On the other hand, effects of turbulence scale would appear to be dependent on the ratio of eddy size to building dimensions. Dominant effects would occur at values of this ratio ranging between 0.5 - 10, Cook (1971) and Armitt (1974).

2.4.4 The main parameters of the boundary layer velocity profile known to affect the flow mechanism and hence the surface pressure forces on bluff bodies, are the boundary layer thickness, δ, the roughness length, Z_o and the zero plane displacement, d. The effect of increasing the ratio H/δ on the drag of a two dimensional plate normal to the flow on a smooth surface was investigated by Good and Joubert (1968) where it was shown that both C_{D_1} and C_{D_H} are dependent on H/δ, Figure 2.6.

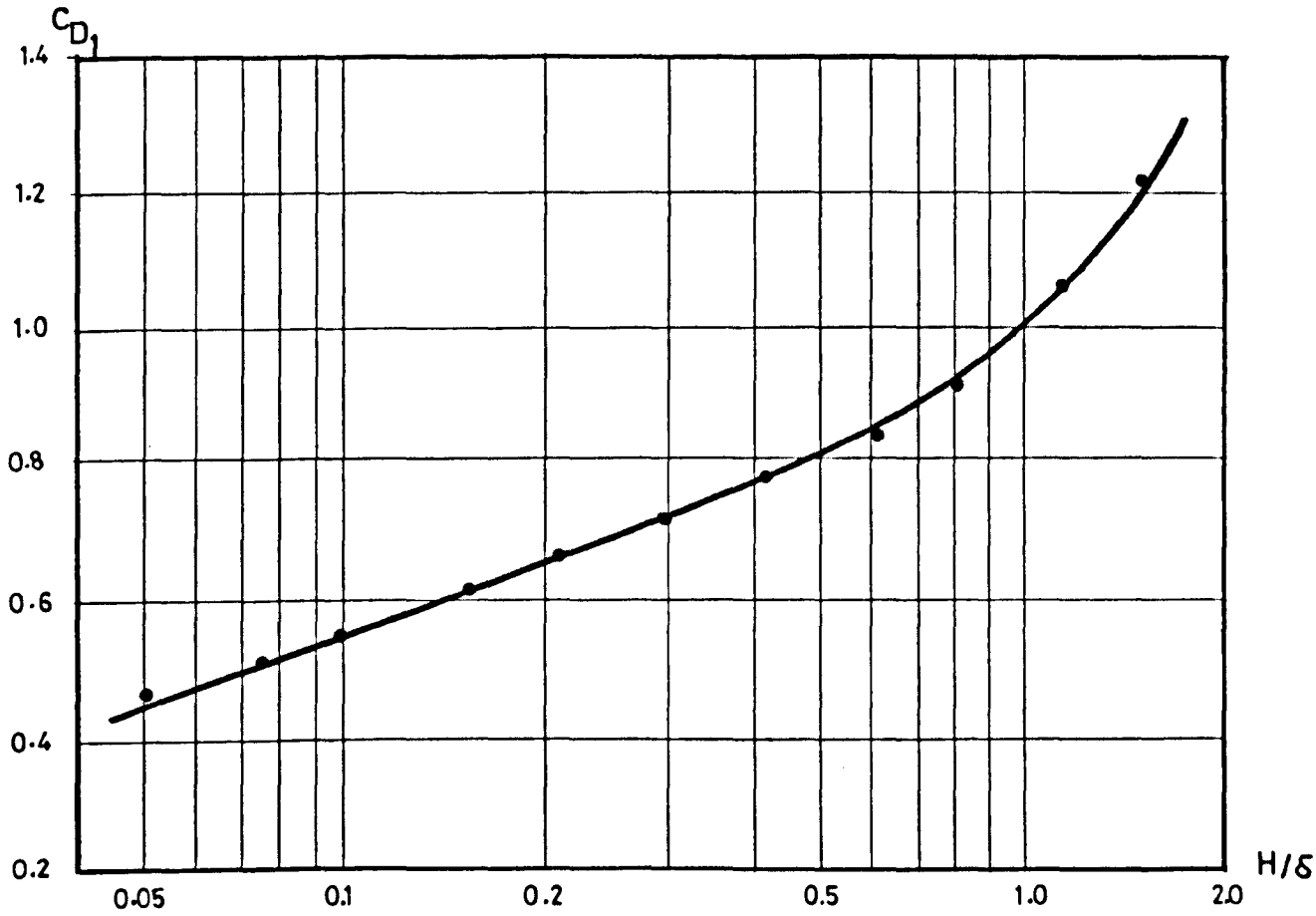

FIGURE 2.6 VARIATION OF C_{D_1} WITH H/δ (AFTER GOOD AND JOUBERT 1968)

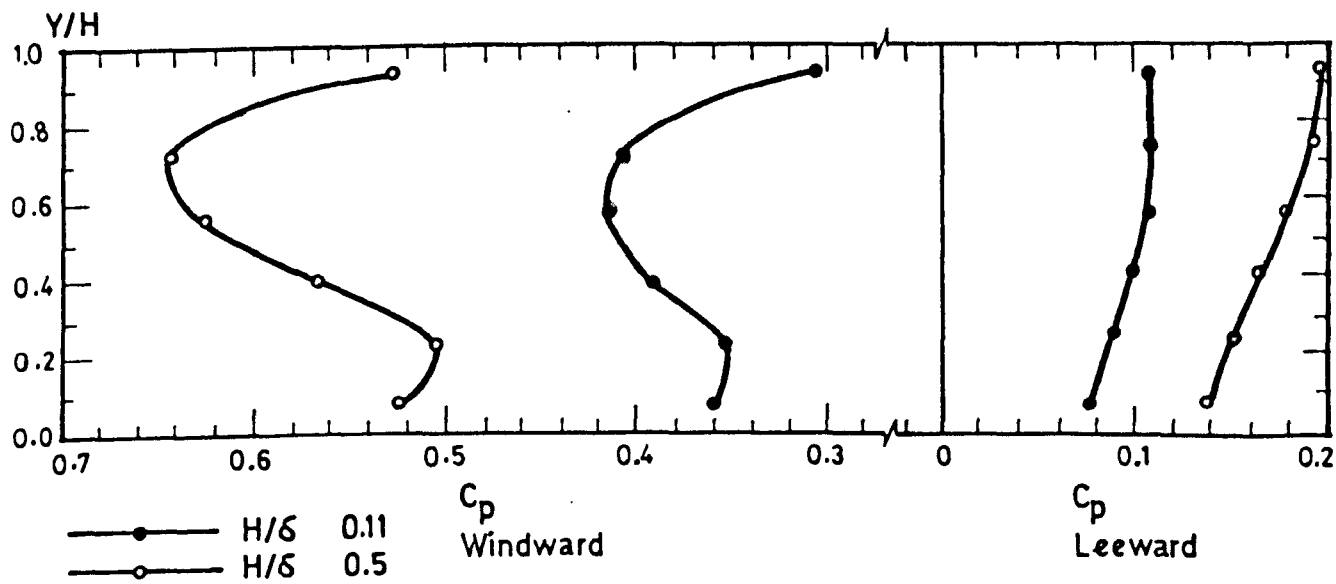

FIGURE 2.7 EFFECT OF H/δ ON SURFACE PRESSURE FORCES ON AN ISOLATED CUBE (AFTER SOLIMAN 1976)

2.4.5 Similar observations were also noted by Soliman (1976) from his work on wind pressure forces on groups of buildings in two different turbulent boundary layer flows with different values of the ratio H/δ. He showed a marked increase in the surface pressure forces with the increase of the ratio H/δ from 0.11 to 0.5, Figure 2.7.

2.4.6 The effect of the ratio H/Z_o for various rough surfaces on the pressure difference as well as on the pressure distributions has been shown by Jensen and Franck (1965). Although they did not make any allowance for the zero plane displacement, d, in determining the values of Z_o, the effect of the variation of Z_o as a parameter of value was clearly shown in their work, Figures 2.8 and 2.9. Due to the dependence of the roughness length on the zero plane displacement, d, in the cases where high roughness elements were used, large values of d are to be expected. Hence the corresponding values of roughness length are possibly an overestimate.

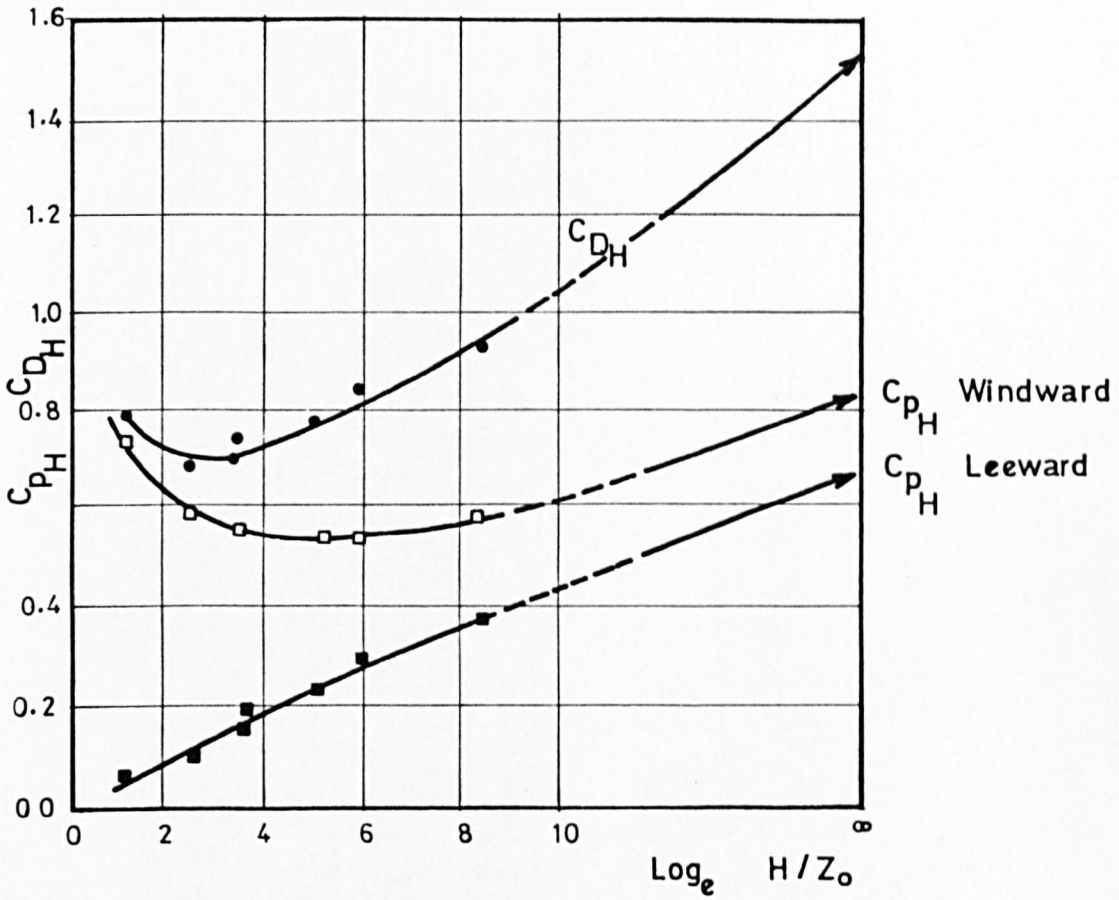

FIGURE 2.8 VARIATION OF C_{D_H} WITH H/Z_o AS DEDUCED FROM JENSEN AND FRANCK DATA, 1965

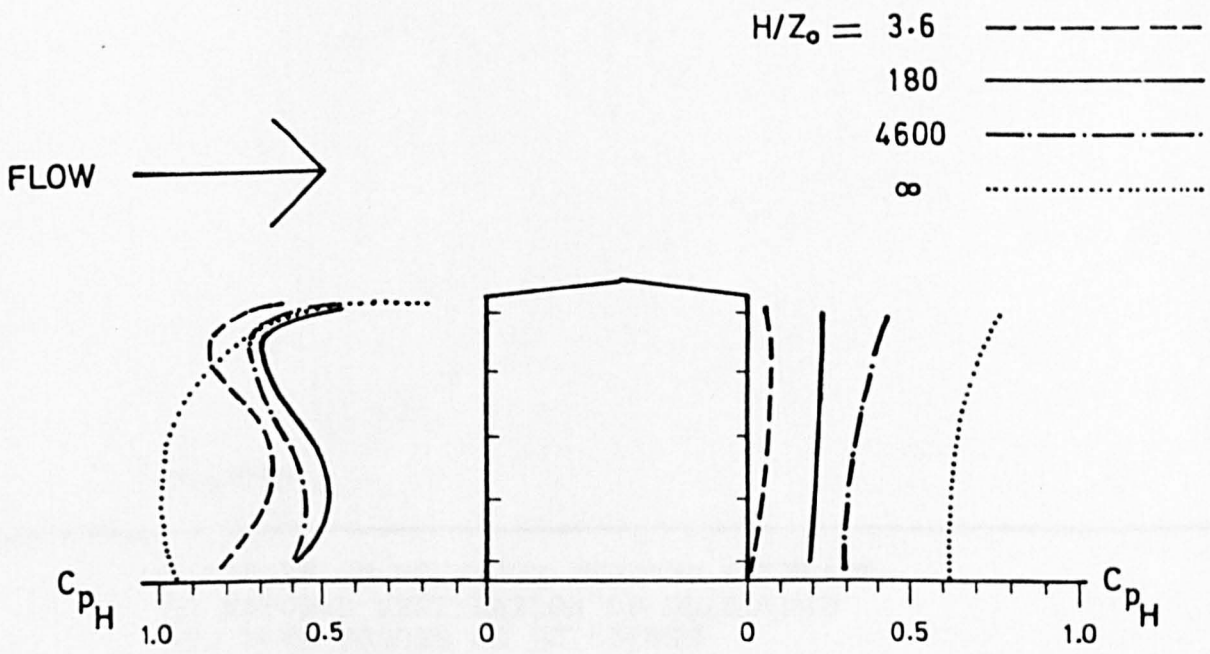

FIGURE 2.9 PRESSURE DISTRIBUTIONS ON A MODEL HOUSE FOR DIFFERENT VALUES OF H/Z_o (AFTER JENSEN AND FRANCK 1965)

CHAPTER 3

A REVIEW OF PREVIOUS STUDIES RELEVANT TO NATURAL VENTILATION OF BUILDINGS AND WIND FORCES ON BUILDINGS

3. A REVIEW OF PREVIOUS STUDIES RELEVANT TO NATURAL VENTILATION OF BUILDINGS AND WIND FORCES ON BUILDINGS

3.1 Introduction

3.1.1 The investigation of wind effects on buildings has been carried out in the past for the purposes of wind environment around structures, natural ventilation calculation of buildings and for wind loading purposes. Most of the work has, however, been concentrated on isolated buildings while the groups of buildings have received comparatively little attention. A few wind tunnel studies carried out for groups of buildings in rough wall turbulent boundary layer flows have ignored the simulation of upwind conditions which are likely to be met in practice. The findings of these investigations will no doubt serve a useful purpose because of the inter-relation between building form, wind flow and the resulting pressure forces. A review of previous works which follows will include the relevant work carried out on:

i) Air flow round isolated buildings.
ii) The effect of upstream fetch around the test model.
iii) Air flow round groups of buildings.
iv) Natural ventilation of building groups.
v) Wind loading on building groups.

3.2 Previous work on air flow round isolated buildings

3.2.1 Castro and Robins (1976) studied the flow round an isolated surface mounted cube in uniform and turbulent streams. In the thick incident boundary layer flow formed by vorticity generators and roughness elements, they placed their cube with a side dimension of 200mm, $3\frac{1}{2}$ boundary layer heights downstream of the vorticity generators. The roughness elements which were square blocks, 18mm high distributed at about 25% plan area density with taller blocks 38mm high, sparsely located in between surrounded the test model and the boundary layer height in which the tests were carried out was 10 times

the cube height. Their measurements in the wake of a surface mounted cube in both the uniform and turbulent upstream flows coupled with pressure measurements on the cube itself, have led to a fairly clear picture of the nature of the flow alongwith the upstream separation and downstream reattachment distances. For the flow normal to the front face, pulsed wire measurements in the reversed flow region directly behind the body have indicated that the addition of upstream turbulence and shear considerably reduce the size of this cavity zone.

3.2.2 Tieleman and Reinhold (1976) studied the wind loads on 32 basic dwelling geometries in a turbulent boundary layer which simulated the atmospheric surface layer in a low speed wind tunnel. The simulation devices in the wind tunnel consisted of spires and roughness elements. Pressure measurements were made on isolated models of varying geometry for wind approach angles between zero and 360 degrees. Models with gable roofs with slopes of 0, 10, 20 and 30 degrees with two different length to width ratios (L/W = 1.2 and 2.0) and with two different height to width ratios representing single and two storey dwellings were tested. Their results indicated that mean as well as peak pressures on the walls as well as on the roof vary a great deal with wind approach angle and roof pitch.

3.2.3 On the other hand a considerable amount of work has been reported on the wind forces on and wind environment around isolated tall buildings. Miyoshi, Ida and Maura (1971) investigated the wind pressure forces on exterior wall elements of an isolated tall building in a rough wall turbulent wind having a power law exponent of 0.25. Their results were, however, confined to the pressure distribution measurements with the aims of determining the pressure coefficients acting on cladding elements. Melbourne and Joubert (1971) studied the severe wind problems to pedestrians caused by tall buildings in suburban environments. Their tests were carried out in the natural wind generated by vorticity generators followed by roughness elements for a fetch length of five times the

boundary layer height with the value of $\alpha = 0.2$ and studied the causes of the problem. Davenport (1971) also studied the response of different plan shapes of tall buildings in the turbulent wind.

3.3 The effect of upstream fetch around the test model

3.3.1 Most of the work done on flow over two and three dimensional bluff bodies was performed for isolated buildings either in smooth flow where the boundary layer grew over the smooth floor of the tunnel or in rough flows where the boundary layer grew over a random roughness chosen arbitrarily. This is hardly the case in actual practice. Very few studies of the flow round groups of buildings were made in the past and the groupings were very specific as a result of which their conclusions could not be used to predicting the flow phenomenon in general terms.

Bailey and Vincent (1943) carried out a series of wind tunnel experiments to investigate proximity effects on the wind loading of buildings. The cases considered were mainly for two buildings, one downstream of the other alongwith one array of three identical buildings. All cases of building proximity investigated showed the effect of the obstruction by an upstream building.

Norton and Oldham (1975) also investigated the effects on surface pressures generated by regular arrays. This study was also confined to two or three identical buildings placed one behind the other in the direction of the flow. In one case, however, six buildings were placed in two rows. They found that a building model in a loose array (five width spacings) will undergo a reduction of up to 55% of the total lift, drag and overturning moment experienced by an isolated model.

3.3.2 In some cases, the simulation in the wind tunnel was the simulation of the actual site to produce the required conditions as in the full scale. In these cases, the simulation

sometimes extended up to the test model or some distance behind it. The complete modelling of the actual site in a wind tunnel is more expansive and time consuming and requires a very long wind tunnel and certain characteristics of the site such as large topographical features may not be possible to model.

Robertson and Chen (1969) modelled the whole of the area of Pittsburgh alongwith a complete model of US steel office building on the turntable to study the treatment of wind in the design of very tall buildings. Cockrell and Lee (1969) called for complete representation of terrain upstream of model situation which will need a long wind tunnel of large cross sectional area. In order to avoid a large wind tunnel, they suggested some compromises and studied the implications of such compromises.

3.3.3 Many people carried out the experiments in wind tunnels with the general roughness extending up to the edge of the turntable with the actual model of the site on the turntable but nobody has investigated the extent of actual modelling on or beyond the turntable to find out a boundary between the two.

Dalgliesh (1969) modelled all major structures to 1:400 scale within 1600 feet radius alongwith upwind land contours with the surface roughness beyond it for comparing full scale to model scale studies of a 34 storey office building in Montreal. Cermak et al (1969) modelled on the turntable, the two towers planned for the Atlantic Richfield Plaza in Los Angeles. The general roughness of modular bricks extended upwind with a smooth surface between the two to study the fluctuating moments on tall buildings produced by wind loading. Hillier (1973) modelled the Hartlepool power station switch house alongwith its surroundings (1140m dia) on the turntable beyond which the general roughness extended.

3.3.4 On the basis of work done at Bristol University by Beddingfield and Lapraik (1970) and Newberry and Obee (1971) with arrays of cubes and high aspect ratio elements used together, Cook (1972) and (1974) suggested that five rows of similarly sized elements are sufficient to mask the individual effect of an upstream row. This study was carried out for a very specific case and did not include the effect of varying the layout pattern or the group density of the elements. Therefore it cannot be adopted as a general rule.

3.3.5 Soliman (1976), however, considered the group density and layout pattern in his study of flow over three dimensional roughness elements in a rough flow, obtained from the boundary layer growing over a rough sheet placed upstream of the turntable on which the model group layout was placed. He suggested that the drag of the roughness elements stabilises at a fetch equal to 12 times the element height, $R/H = 12$, irrespective of the element density. His work remains inconclusive as he was unable to model larger fetches of roughness and did not see the effect of increased fetch lengths particularly at low densities where the use of $R/H = 12$ is questionable.

3.3.6 From the above review, the only broad outline available is to model on the turntable either up to 5 blocks or up to $R/H = 12$. The use of modelling 5 blocks around the test model is based on a very specific case and cannot be therefore generalised to be applicable to others. On the other hand, the suggestion of modelling a fetch equal to 12 times the element height is more reliable but cannot be applied to all cases due to its inconclusiveness. All other cases are very specific and do not give a definite extent of modelling round a test building.

3.4 Previous work on air flow around groups of buildings

3.4.1 Wise, Sexton and Lillywhite (1965) have reported some measurements of the flow round buildings in a wind tunnel simulating an artificially generated suburban velocity profile. The building types and their groupings under investigation consisted of (i) two low buildings, (ii) three low buildings and (iii) a slab building with a low building upstream. The dimensions of these models in terms of the low rise building height are given in Table 3.1.

Table 3.1 Dimension of the models used by Wise et al (1965)

Model	Height H	Length	Thickness
Low building	1	4	1
Slab building	3	4	1

where the length is the dimension normal to the flow and the thickness is the in-wind dimension. The buildings were relatively large in size compared with the boundary layer thickness, δ, i.e. $H/\delta = 0.22$, 0.67 for the low and slab buildings respectively. In all the tests the distance of separation was kept constant at double the low building height. The results showed that a vortex existed between the buildings in all cases. However, the wind speed at any point between the buildings compared with that at the same height far upstream is shown to be reduced in between the buildings in the first two groupings while in the third case, it increased by about 30% in the region close to the ground. It was also noted that relative speed observed in the first two cases was similar. Thus the effect of adding the third building in case (i) was negligible.

The particular geometric parameters considered in the above work coupled with the relaxation of simulating size parameters, i.e. H/δ or H/Z_o will tend to limit the general

applicability of results. Furthermore, the flow speed measurements at discrete points make it difficult to obtain any relation between the flow parameters and the group form parameters.

3.4.2 In order to relate the flow speed at one point to the geometrical parameters describing a group of two buildings Wise (1970) carried out a detailed investigation of the combination of a slab with an upstream low rise building i.e case (iii) described in 3.4.1. The geometrical parameters varied were the distance of separation, L_x, the slab building thickness and height, W and H. The main conclusion reached was that the velocity at one point between the two buildings and close to the ground is a complex function of the wind speed at the top of the slab building, the height of the point above the ground, the slab building length, L, height, H and thickness, W, as well as the low building height.

3.4.3 Olgyay (1963) presented a series of flow visualisation results in order to suggest improvements in the natural ventilation rates of low rise housing in different layout patterns. Six models were arranged in three rows at different spacings in each layout pattern. From the study, he concluded that the grid iron pattern causes more shelter to subsequent rows of buildings while the staggered pattern gives better ventilation. It was recommended that a spacing of seven times the building height should secure satisfactory ventilation for each unit. Similar comments are also given by Koenigsberger, Ingersoll, Mayhew and Szokolay (1973) where a distance of six times the building height is given as the satisfactory limit for adequate natural ventilation. In both these studies, however, the measure of satisfactory ventilation was not defined, nor was the form of the individual buildings considered, which is an important parameter.

3.5 Previous work on natural ventilation of building groups

3.5.1 Weston (1956) in his investigation of the effect of obstructing a simple industrial building by other different building forms placed at different upstream distances, measured the average internal air speed in a 1/16 scale model for different obstruction cases. He presented the results in the form of the percentage of the mean internal air speed obtained for the same buildings when unobstructed. Table 3.2 gives the dimensions of the experimental building together with average and extreme values of the different obstructing buildings normalised by the windward wall height, H, of the experimental building (4.57m in full scale).

Table 3.2 Dimensions of the buildings used by Weston (1956)

	Experimental building	Obstructing building		
		Min.	Avg.	Max.
Building length (across wind)	4H	3.07H	4.04H	6.67H
Building depth (along wind)	12H	1.0 H	2.71H	4.0 H
Building height	1H	0.67H	1.82H	2.73H

From the information given by Weston, the results obtained from the different obstructing buildings were averaged and the standard deviation was calculated. The form of presentation is shown in Figure 3.1 which shows the effect of the distance of separation on the internal air velocity. From his work Weston drew the following conclusions:

i) As a general rule, increasing the distance of separation between the building and its obstruction improves the natural ventilation.

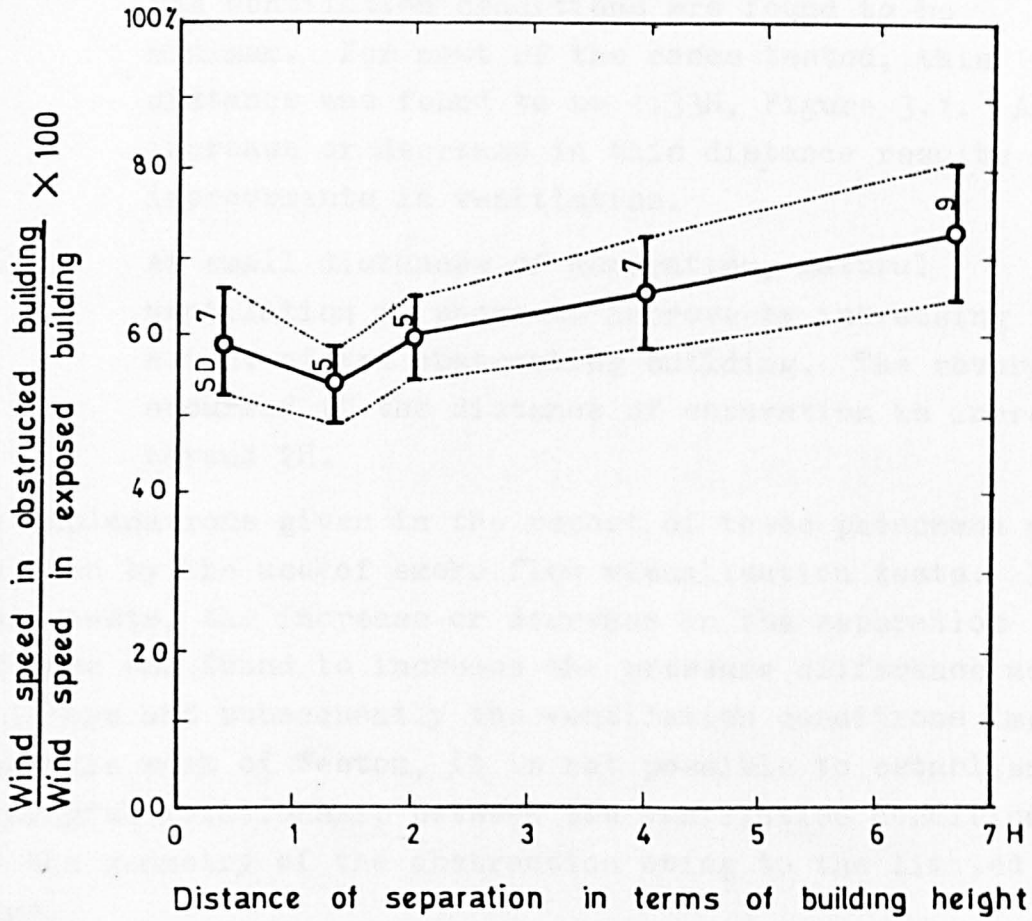

FIGURE 3.1 EFFECT OF DISTANCE OF SEPARATION ON THE RESULTING VENTILATION USING WESTON'S DATA (1965)

ii) There is a certain distance of separation at which a change of flow conditions appears to occur and the ventilation conditions are found to be minimum. For most of the cases tested, this distance was found to be 1.33H, Figure 3.1. Any increase or decrease in this distance results in improvements in ventilation.

iii) At small distances of separation, natural ventilation is shown to improve by increasing the height of the obstructing building. The reverse occurred if the distance of separation is increased beyond 2H.

The explanations given in the report of these phenomena were assisted by the use of smoke flow visualisation tests. In these tests, the increase or decrease in the separation distance was found to increase the pressure difference across buildings and subsequently the ventilation conditions improved. From this work of Weston, it is not possible to establish any meaningful relationship between the ventilation conditions and the geometry of the obstruction owing to the limited test range.

3.5.2 In a series of wind tunnel experiments reported by Givoni (1968) the effect of building group geometry on natural ventilation and air flow around building blocks was investigated. As no mention was made of the mean velocity gradient in the incident flow, it is reasonable to assume that the flow was uniform. In this study measurements of average air speed were made both inside and outside the models and expressed as a percentage of the wind speed at the same height upstream of the group arranged in two or three rows normal to the wind. The blocks were 600 x 200mm in plan and 400mm high. In the first case where only two blocks were used, one block in each row, the longitudinal distance of separation was varied from 0.75 to 3.25H at 0.25H intervals, where H is the block height. In the second case three rows

were considered and the longitudinal distance of separation took the values of 0.75H, 1H and 1.25H, while the lateral distance of separation between blocks in the same row varied from 0 to 1.25H at intervals of 0.25H. The main conclusions obtained were:

i) The effect of increasing the longitudinal distance of separation between blocks in two rows was to increase the air speed between the blocks whilst the internal air speed in the leeward block reflected an initial decrease followed by an increase.

ii) The effect of increasing the lateral distance of separation between blocks in the same row was to initially increase both internal and external air speeds then to reach a maximum followed by gradual decrease to a value approximately equal to the initial value where the lateral distance was zero.

Since the values of internal air speeds given is dependent largely on the block proportions and the wall opening details as well as the flow properties; the results obtained by Givoni cannot be applied to other situations.

3.5.3 In addition to model scale studies, Dick (1949) and (1951) carried out a series of investigations on full scale buildings on a number of specially constructed two storey, semi-detached experimental houses built in two rows. The standards and type of construction were designed to be typical of other new houses being built at that time and two sets of observations were made, one of these was taken at a time when the houses were under normal occupation. From these studies a series of empirical equations were deduced which could be applicable to buildings of this type.

The measurements of ventilation rates were made by introducing hydrogen tracer gas into the house and studying the rate of decay of the gas. The air change rate for the volume being considered was then deduced using an equation of

the form:

$$V_o \, \Delta C_t / \Delta \theta = V_1 \, C_t \qquad 3.1$$

where V_o is the volume of the room, V_1 is the volume of air entering the room in time t, C_t is the concentration of tracer gas at time t, and $\Delta\theta$ is the temperature difference. From these studies a series of empirical equations were presented showing the relationship between air filtration rate and wind speed and direction. It was also shown that the effect of wind direction was normally of secondary importance to wind speed and that a simpler and adequate relationship of the form:

$$V = a_i + b_i \, u \qquad 3.2$$

was acceptable for representing the whole house ventilation rate. In equation 3.2, V represents the infiltration rate, a_i and b_i are constants and u represents the wind speed. The houses when observed under normal occupation, where the users opened windows as they wished, the ventilation rates were generally found to be higher with higher wind speeds.

The full scale studies are of value because they establish empirical relationship between various factors affecting infiltration and ventilation, and give estimates of the wide range of infiltration rates likely to be present in these types of buildings but their value in terms of establishing predictive rules is limited by two significant factors. Firstly, the range of buildings studied is entirely limited and secondly, there is a lack of correlatable data from such studies and the empirical equations derived are only applicable to the particular buildings studied.

3.6 Previous work on wind loading on buildings

3.6.1 Bailey and Vincent (1943) carried out a series of wind tunnel experiments to investigate proximity effects on the wind loading of buildings. The cases considered were mainly for two buildings, one downstream of the other alongwith an array of three identical buildings. All of the cases of building proximity investigated showed the effect of the obstruction by an upstream building apart from one case where the effect of a downstream high building on a low building upstream was investigated. The geometrical variables considered in this study were the building shape, the group form and the distance of separation between buildings. The variations in the size and shape of buildings is given in Table 3.3.

Table 3.3 Description of the models used by Bailey and Vincent (1943)

Model	Height to eaves (mm)	Overall height (mm)	Length normal to wind (mm)	Thickness along the wind (mm)	Type of roof
A	30.5	42.7	127	53.8	Sloped at 23.5°
B	30.5	58.7	127	53.8	Sloped at 45°
C	63.5	91.7	127	53.8	Sloped at 45°
D	30.5	46.7	127	53.8	Sloped at 30°
E	30.5	31.2	127	53.8	Flat
F	63.5	64.2	127	53.8	Flat
G	-	132.1	203.2	50.8	Stepped

The distance of separation was varied in units of the building thickness from a minimum of zero to a maximum which varied from 3 to 20 for different models. Despite the early date of this report, consideration was given to the simulation of the natural wind profile at least in terms of velocity gradient. The profile simulated was that appropriate to flow in open country with a boundary layer thickness, δ, of 203mm. The profile shape was a close approximation to the following equation, suggested by the Meteorological Office at the time.

$$\frac{U_y}{U_{10}} = K_1(1.00 + 2.81 \log(y + 4.75)) \qquad 3.3$$

In the course of the investigation, the pressure measurements were obtained from a centre line row of tappings on the windward wall and the roof. The leeward wall pressures were, however, obtained from only one tapping near the top of the wall. The pressures were given in the form of coefficients non dimensionalised with respect to the dynamic load at a height of 50.8mm from the tunnel wall. From the results obtained, those concerning the wall pressures, considered most relevant are shown in Figure 3.2, (a) to (h) and the corresponding roof pressure variations are shown in Figure 3.3, (a) to (h). The main conclusions drawn by this study were:

i) The effect of a small building on the pressure difference across a high building downstream, Figure 3.2 (a), is small. The maximum reduction at any distance was about 20% of the isolated case.

ii) The effect of the number of models upstream, Figure 3.2 (b) and (c), was found to be small, therefore, the results would be expected to be representative of built up areas.

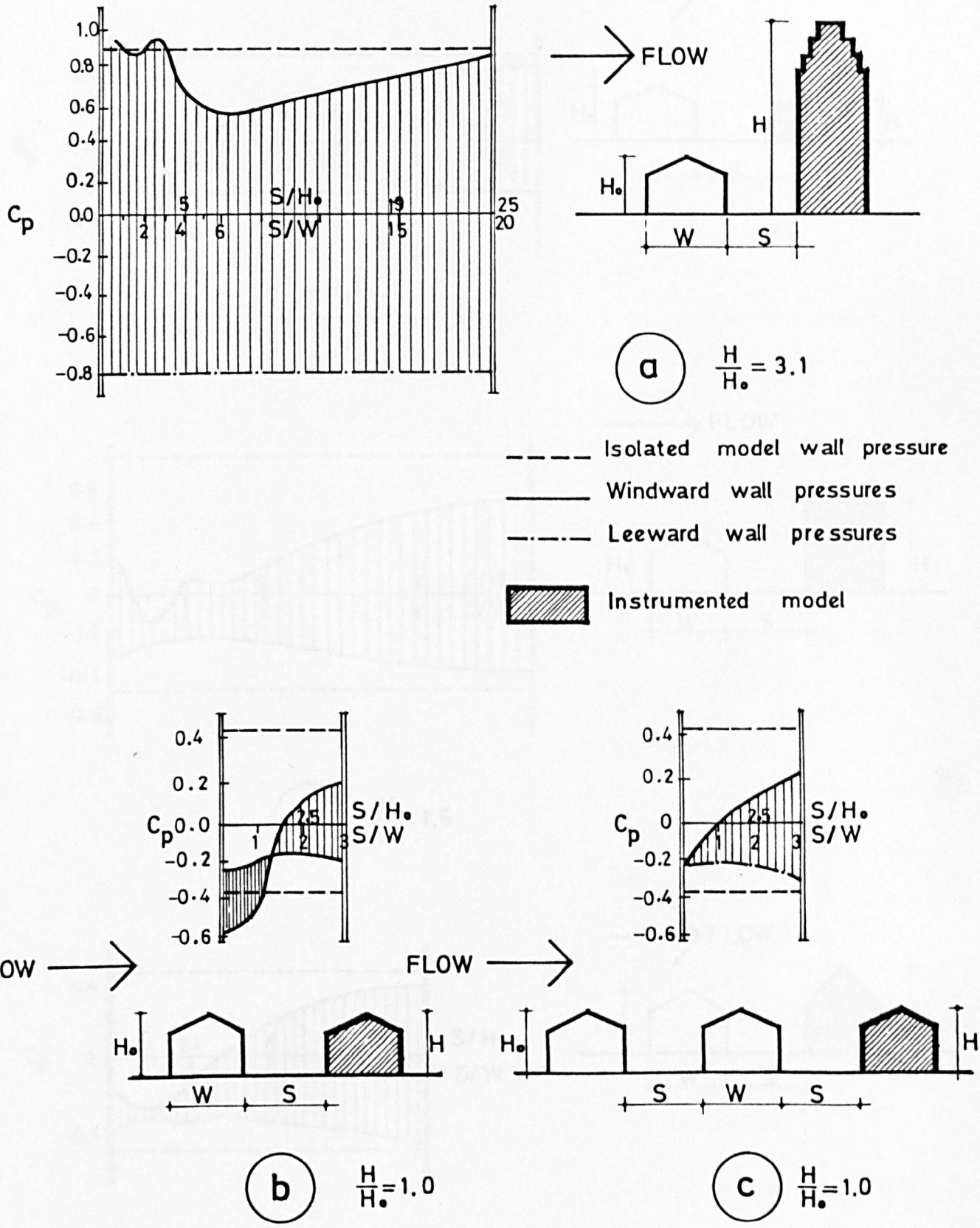

FIGURE 3.2 BAILEY AND VINCENT (1943) RESULTS FOR WALL PRESSURES.

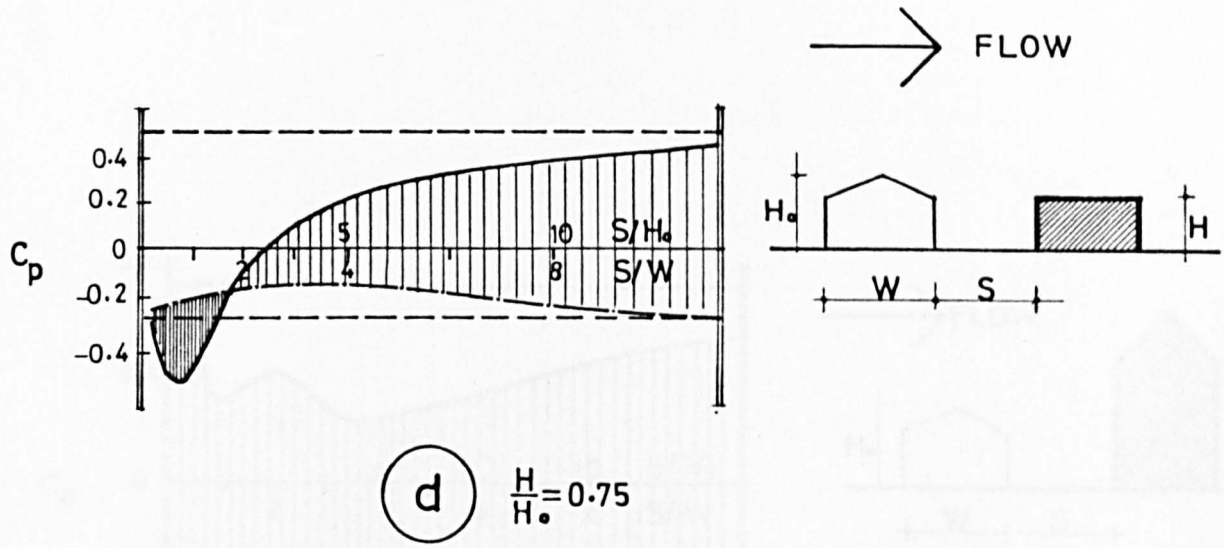

(d) $\frac{H}{H_0} = 0.75$

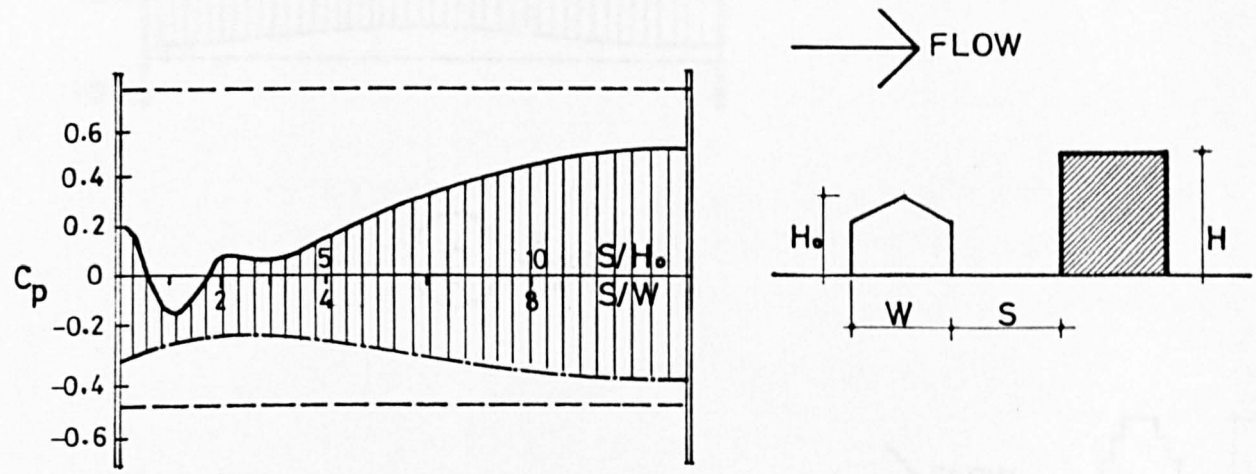

(e) $\frac{H}{H_0} = 1.5$

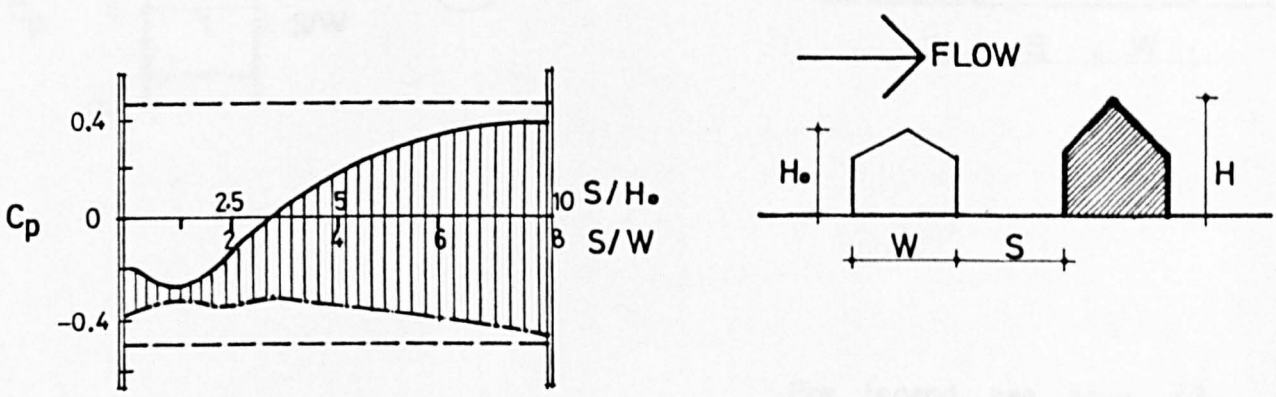

(f) $\frac{H}{H_0} = 1.4$

For legend see page

FIGURE 3.2 BAILEY AND VINCENT (1943) RESULTS FOR WALL PRESSURES.

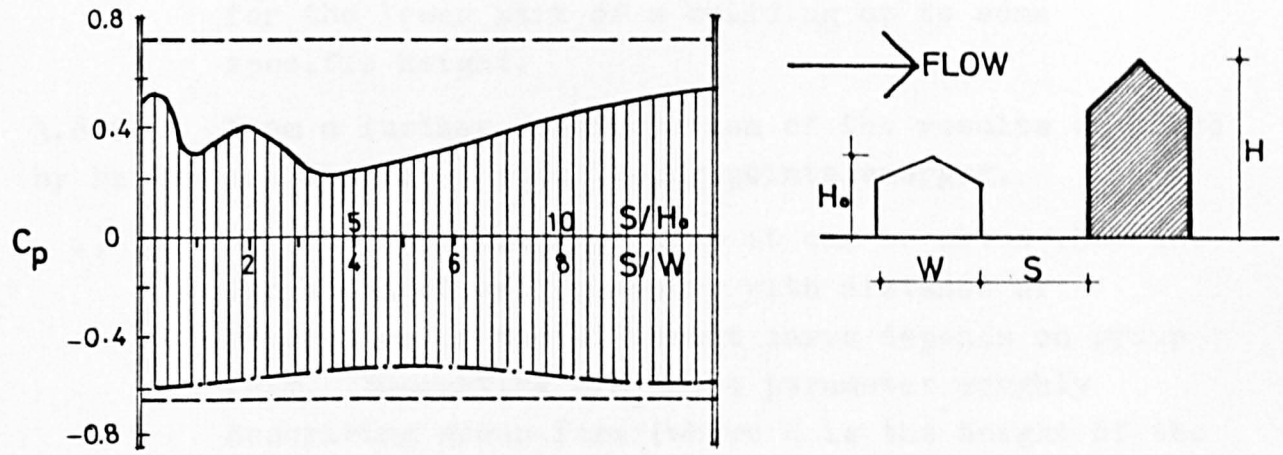

(g) $\frac{H}{H_0} = 2.2$

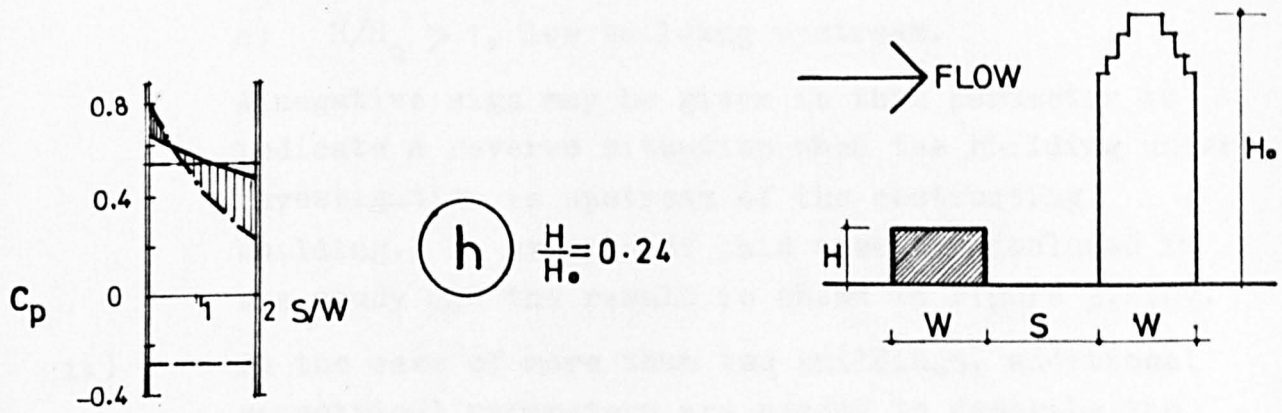

(h) $\frac{H}{H_0} = 0.24$

For legend see page 43

FIGURE 3.2 BAILEY AND VINCENT (1943) RESULTS FOR WALL PRESSURES.

iii) Due to the downwind shelter effect present in most cases even at large separation distances, allowance should be made to reduce the fully exposed values for the lower part of a building up to some specific height.

3.6.2 From a further consideration of the results obtained by Bailey and Vincent the following points emerged.

i) For the two building cases it can be shown that the variation of wall pressure with distance of separation in the different cases depends on group form. Suggesting H/H_o as a parameter roughly describing group form (where H is the height of the test building and H_o is the height of the obstructing building) different group forms regardless of roof shape may be written as:

a) $H/H_o < 1$, high building upstream

b) $H/H_o = 1$, two equal buildings

c) $H/H_o > 1$, low building upstream.

A negative sign may be given to this parameter to indicate a reverse situation when the building under investigation is upstream of the obstructing building. An example of this case was included in the study and the result is shown in Figure 3.2(h).

ii) In the case of more than two buildings, additional geometrical parameters are needed to describe the group form, where variation in individual building dimensions will add complexity to these parameters. Here only one simple case has been considered, Figure 3.2(c) where the three buildings tested were identical.

iii) A zone of negative pressure difference at certain distances of separation can be seen as a common feature in Figure 3.2(b) and (d). The significance of this observation is that these are the cases

where $H/H_o \leq 1$.

iv) In the cases where $H/H_o > 1$, i.e. Figure 3.2 (a), (e), (f) and (g), the pressure difference between the windward and leeward faces was positive at all distances and the shelter effect decreased as H/H_o increased.

v) A relevant point may be made concerning the case of more than two buildings shown in Figure 3.2(c). Here, contrary to the conclusions given in the paper which implies a negligible effect for the number of models, it can be seen by comparing Figures 3.2(b) and (c) that two major differences occur. Firstly the zone of negative pressure which was dominant in the two building case disappeared in the three building case, and secondly the point at which the pressure difference is zero occurs approximately at zero distance of separation.

vi) The roof pressures were found to be negative in all cases except on the windward face of the pitched roof where the slope was 45^{o}.

3.6.3 Two important conclusions may be drawn from this work. Firstly the parameters governing the flow and pressures in groups of two buildings are not the same as those for an array of more than two. Secondly, for pairs of buildings subject to the same incident flow conditions, the pressure difference between the windward and leeward faces as well as across the roof was affected both by the building form and the distance of separation.

3.7 Conclusions

3.7.1 From the above review the following conclusions may be drawn:

i) The flow and the pressure forces on buildings in isolation or in groups are dependent on both the individual building form, i.e. size and shape of

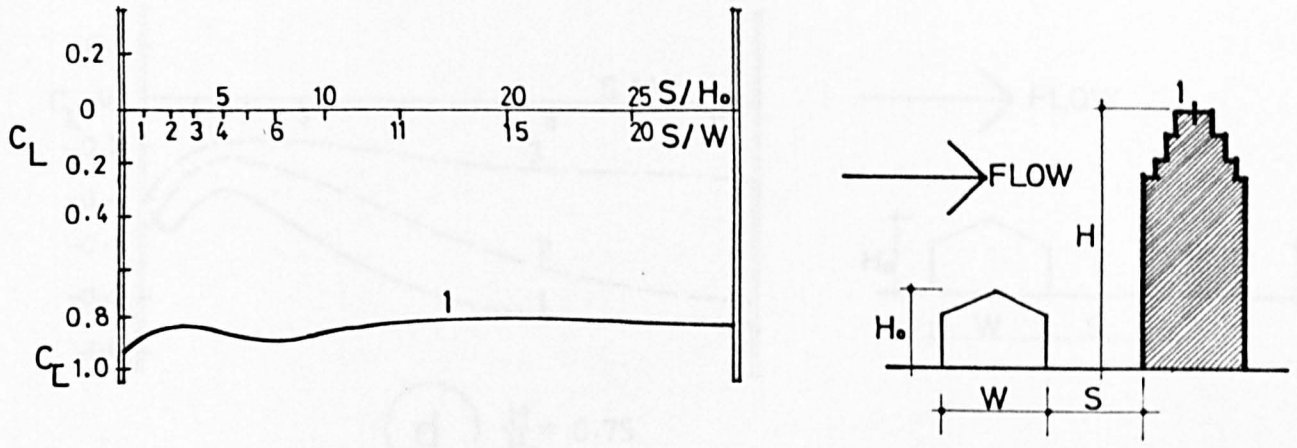

(a) $\frac{H}{H_o} = 3.1$

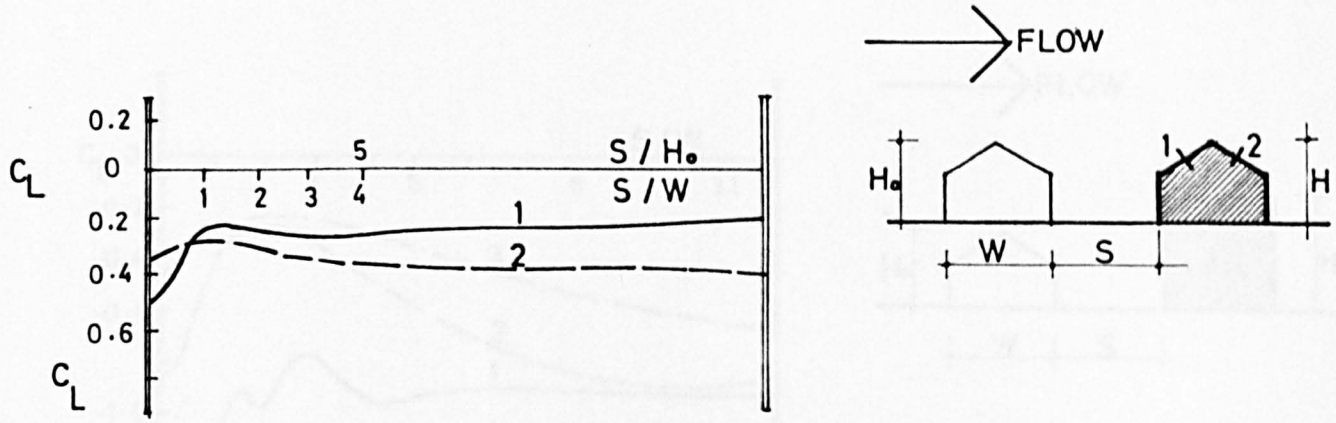

(b) $\frac{H}{H_o} = 1{\cdot}0$ Roof slope $23\frac{1}{2}°$

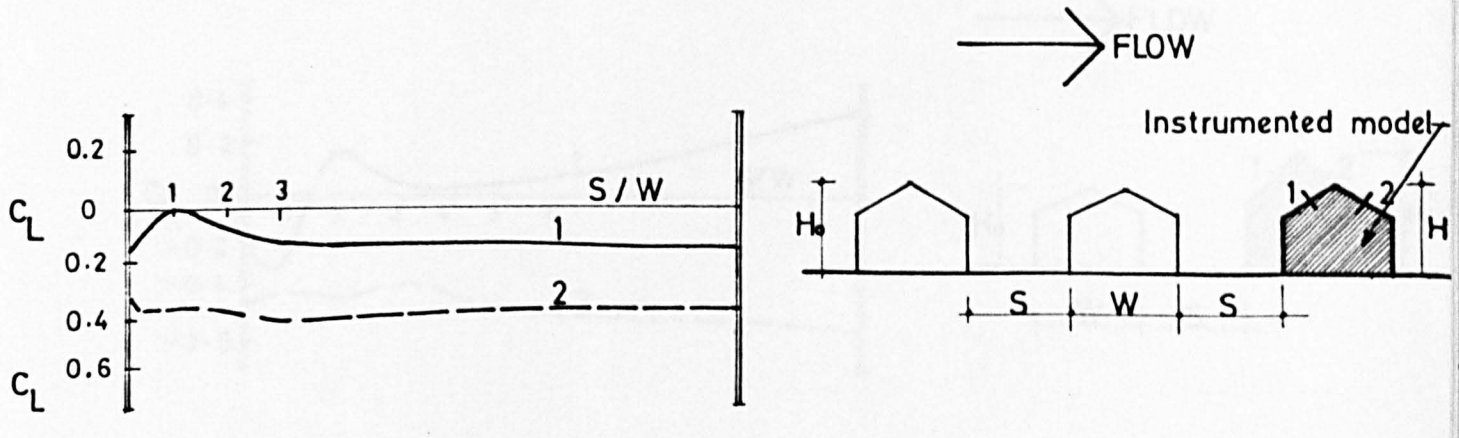

(c) $\frac{H}{H_o} = 1{\cdot}0$ Roof slope $23\frac{1}{2}°$

FIGURE 3.3 BAILEY AND VINCENT (1943) RESULTS FOR ROOF PRESSURES.

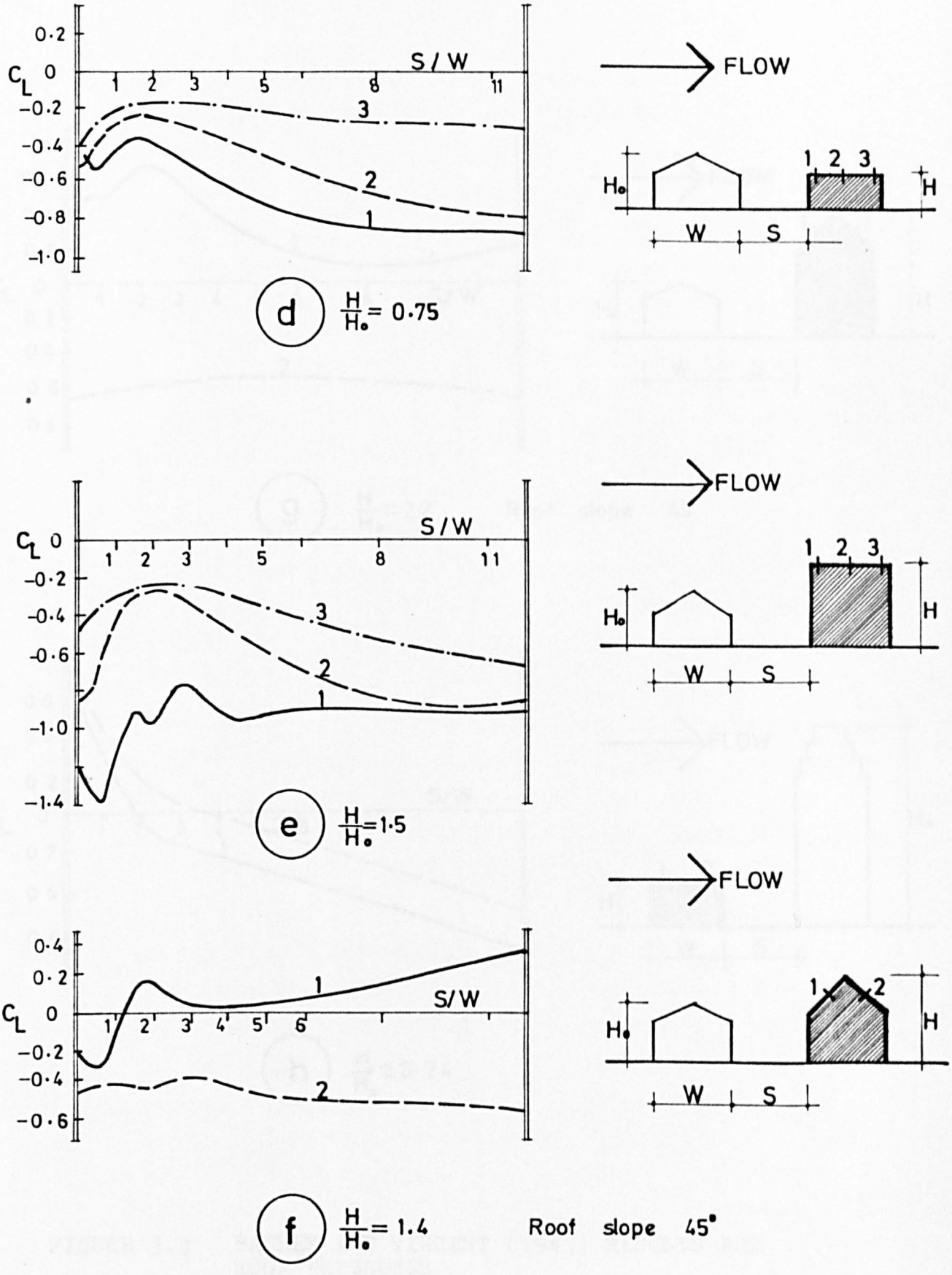

FIGURE 3.3 BAILEY AND VINCENT (1943) RESULTS FOR ROOF PRESSURES

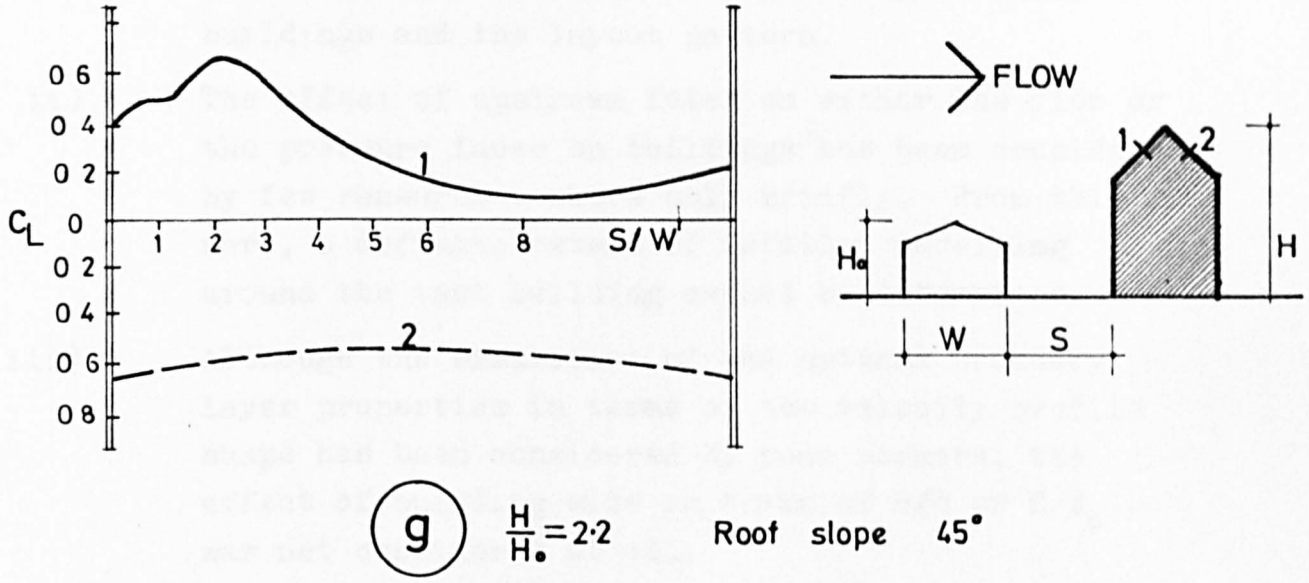

(g) $\frac{H}{H_o} = 2{\cdot}2$ Roof slope 45°

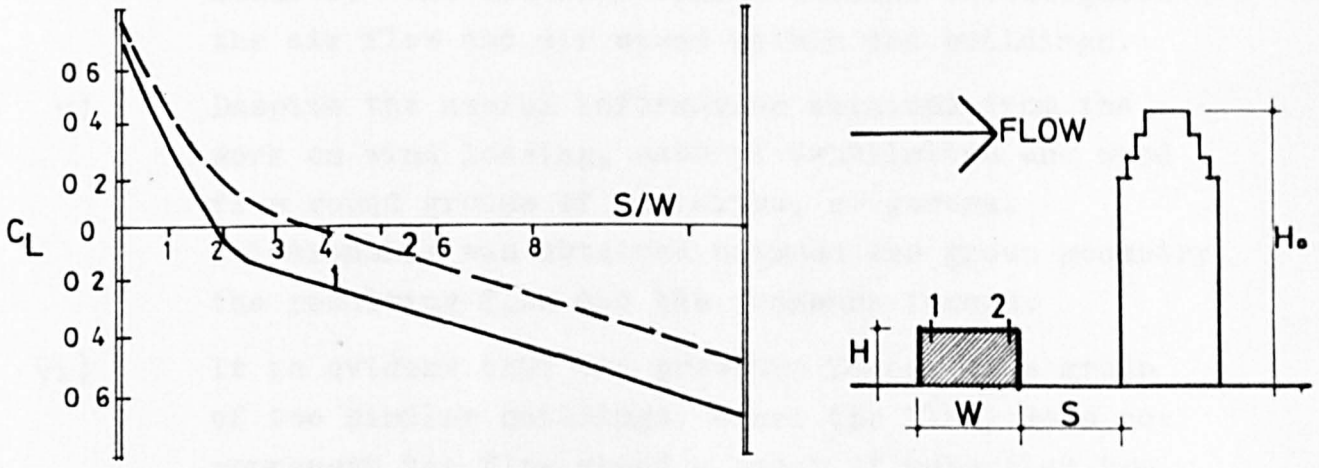

(h) $\frac{H}{H_o} = 0{\cdot}24$

FIGURE 3.3 BAILEY AND VINCENT (1943) RESULTS FOR ROOF PRESSURES

the building as well as the building group form which includes the relative size of individual buildings and the layout pattern.

ii) The effect of upstream fetch on either the flow or the pressure faces on buildings has been considered by few research workers only briefly. From this work, a definite extent of detailed modelling around the test building cannot be determined.

iii) Although the simulation of the natural boundary layer properties in terms of the velocity profile shape has been considered by some workers, the effect of building size in terms of H/δ or H/Z_o was not considered at all.

iv) Natural ventilation studies are mostly confined to either full scale studies or digital analogue studies. The few wind tunnel studies investigated the air flow and air speed within the buildings.

v) Despite the useful information obtained from the work on wind loading, natural ventilation and wind flow round groups of buildings, no general relationship was obtained between the group geometry, the resulting flow and the pressure forces.

vi) It is evident that the pressure forces on a group of two similar buildings, hence the flow, does not represent the flow round a group of more than two buildings, the case of urban areas.

3.7.2 The complexity of the problem indicated by the above conclusions suggests that in order to obtain any relationship between individual building form, building group form and size, as well as the resulting pressure forces, great limitations ought to be put to the variables involved. A more appropriate approach may then include the effect of building size, (in terms of H/δ) the building shape, (considering the height variations alongwith the frontal and the side aspect ratio variations) as well as the size and form of the building group

(in terms of upstream fetch) required to give representative results of the corresponding conditions in urban areas.

CHAPTER 4

FLOW OVER ROUGH SURFACES

4. FLOW OVER ROUGH SURFACES

4.1 Introduction

4.1.1 The problems of the forces and flow round isolated buildings as well as round arrays of similar buildings caused by the wind have been outlined in the previous chapters. As the buildings can be considered to be the roughness elements on the earth's surface, the forces on them are comparable to the forces on the roughness elements of a surface over which a turbulent boundary layer flow occurs. The application of the boundary layer theory to the flow over the earth's surface has been shown to be valid in the study of micro-meteorology and to be helpful in providing a flow model for wind tunnel simulation of the natural wind. In this chapter, therefore, consideration is given to the way in which the idealised problem of flow over rough surfaces has been studied in the past, which will help in solving the present problem.

4.1.2 The flow over roughness elements and consequently the effect of roughness geometry on the properties of flow will be reviewed in this chapter. The investigation will extend to consider possible relationships between the roughness geometry, flow properties and the resulting pressure forces. Theoretically, these idealised cases normally deal with an infinitely extending uniformly roughened surface which is not the case in actual practice, particularly for large roughness elements where the surface roughness changes take place very rapidly at relatively short fetches. Therefore, the effect of a step change in surface roughness will also be reviewed.

4.2 Principles of flow over rough surfaces

4.2.1 Although various methods exist for the calculation of the drag of aerodynamically smooth surface, it is beyond engineering or economic practicability to produce such surfaces. Some account, therefore, must be taken of the

expected departure from smoothness. Although many methods also exist to predict the development of turbulent boundary layers over smooth surfaces, unfortunately corresponding published data for rough surfaces are few.

Nikuradse (1933) made an exhaustive study of the effect of Reynolds number and relative roughness for dense sand grain roughness in pipe flows. The results of his study have since been used by many researchers to standardise their roughness effect in terms of the "equivalent sand grain roughness". From this fundamental work on the effect of sand grain roughness on pipe flow three flow conditions were established. These are as follows:

i) The completely smooth flow where the roughness size is small and contained within the laminar sub-layer

ii) The completely rough flow where the roughness extends completely outside the laminar sub-layer

iii) The intermediate roughness or transitional flow where the roughness extends partially outside the laminar sub-layer.

Nikuradse used sand grains as his roughness elements to the surface in the maximum possible concentration. His results for the three flow conditions may be expressed in terms of a Reynolds number based on the sand grain roughness height, k_s, as follows:

$$\frac{k_s U_*}{\nu} < 5 \qquad \text{Completely smooth flow}$$

$$5 < \frac{k_s U_*}{\nu} < 70 \qquad \text{Transitional flow}$$

$$\frac{k_s U_*}{\nu} > 70 \qquad \text{Completely rough flow}$$

4.2.2 The general structure of the turbulent boundary layer flow can be divided into two main layers, an inner layer usually called the wall layer and an outer layer alongwith a zone of overlap between the two, Figure 4.1. In the inner layer, the flow is entirely dependent on the turbulent friction due to the roughness elements while the flow in the outer layer is insensitive to the conditions at the surface and is mainly affected by pressure gradients and the velocity defect law applies. A zone of overlap also exists in which a logarithmic velocity distribution is obtained, Chauser (1956). Since the inner layer is the more relevant part of the turbulent boundary layer in the present study, it will be examined more closely.

4.2.3 In the inner layer three regions of flow may be identified. Very close to the wall, a very thin laminar sub-layer exists in which the velocity is linearly related to the distance from the wall, i.e.

$$\frac{u}{U_*} = \frac{y\ U_*}{\nu} \qquad 4.1$$

At the top end of the inner layer fully turbulent flow prevails in which the well known logarithmic velocity distributions may be written as:

$$\frac{u}{U_*} = \frac{1}{K} \ln \frac{y\ U_*}{\nu} + B_1 \qquad 4.2$$

In between the laminar sub-layer and the log layer, a transition zone is present. Figure 4.2 shows the graphical presentation of equation 4.2. The extension of the logarithmic line down to the surface gives a finite height known as the roughness length, Z_o, at which the velocity is theoretically zero, Figure 4.2.

4.2.4 Since the addition of roughness always increases turbulent skin friction, and hence U_*, the logarithmic line of the inner layer represented by equation 4.2 must then undergo a downward shift. Hence for rough wall flows,

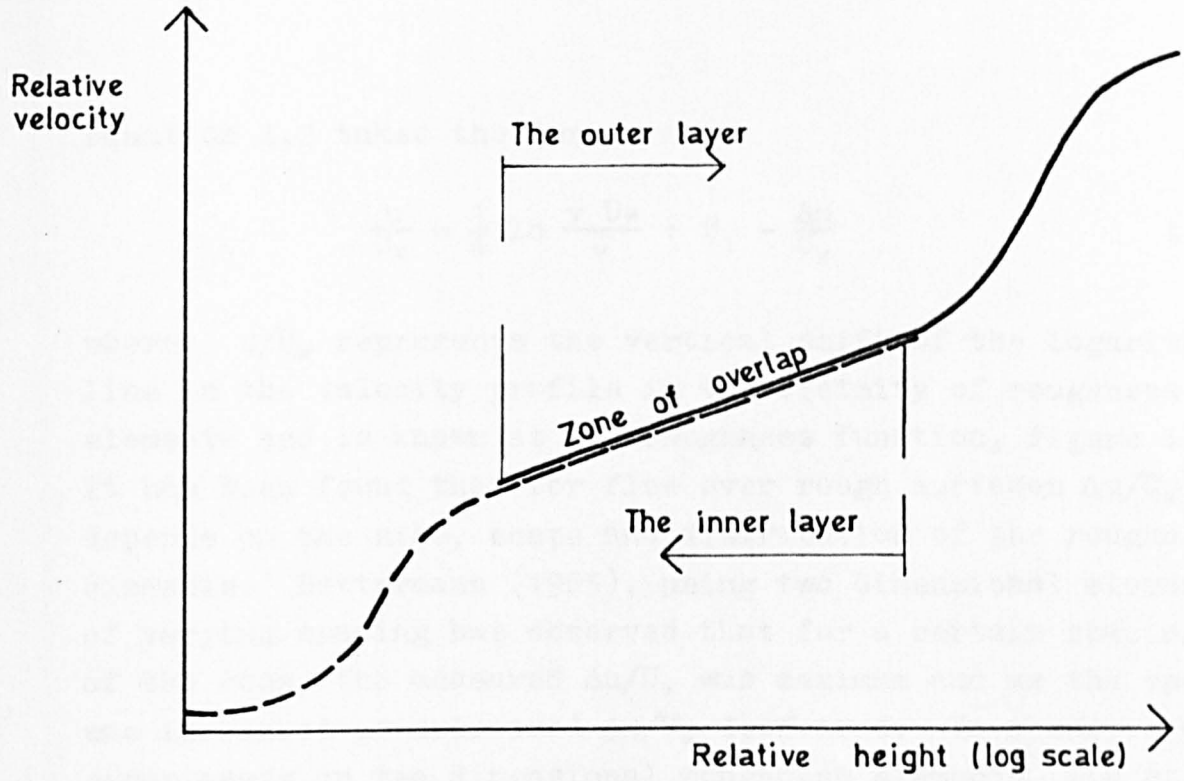

FIGURE 4.1 THE GENERAL STRUCTURE OF TURBULENT BOUNDARY LAYER FLOWS

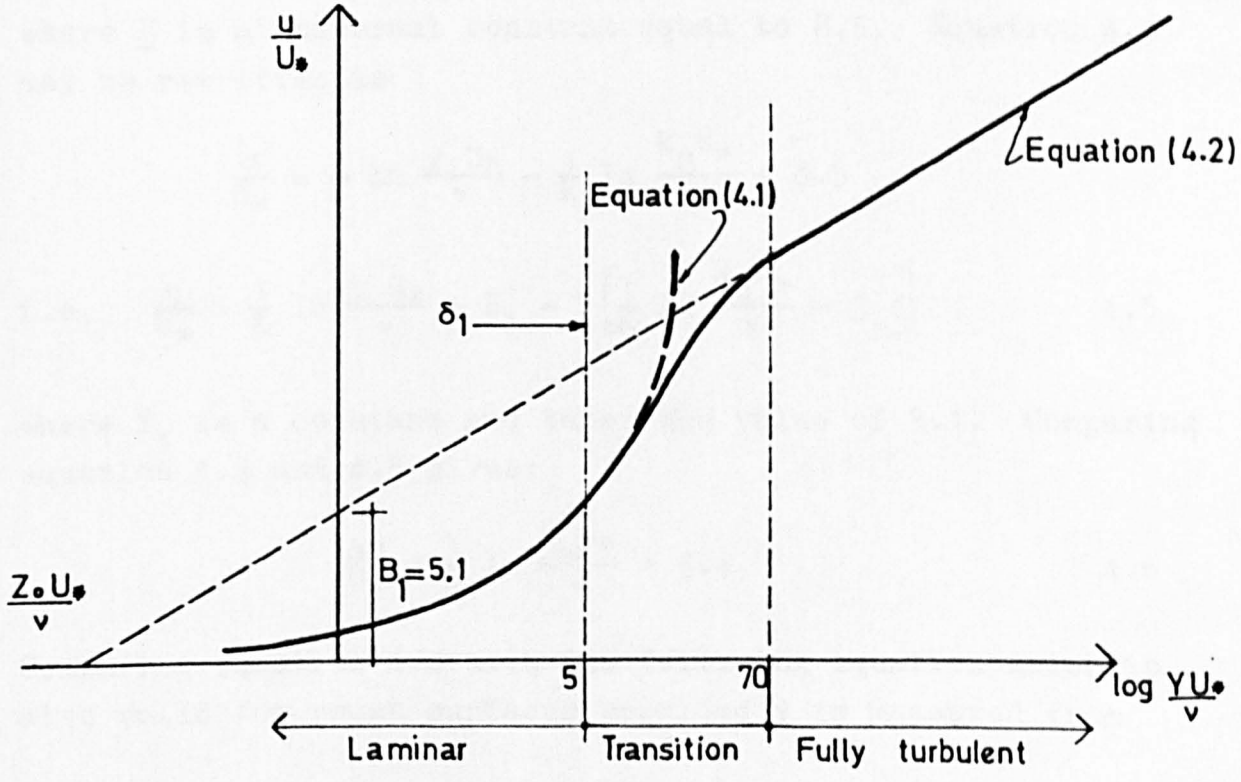

FIGURE 4.2 THE THREE REGIONS OF FLOW IN THE INNER LAYER OF THE BOUNDARY LAYER FLOW AND THE DEFINITION OF THE ROUGHNESS LENGTH, Z_o.

equation 4.2 takes the form:

$$\frac{u}{U_*} = \frac{1}{K} \ln \frac{y\,U_*}{\nu} + B_1 - \frac{\Delta u}{U_*} \qquad 4.3$$

where u/U_* represents the vertical shift of the logarithmic line in the velocity profile in the vicinity of roughness elements and is known as the roughness function, Figure 4.3. It has been found that for flow over rough surfaces $\Delta u/U_*$ depends on the size, shape and distribution of the roughness elements. Bettermann (1965), using two dimensional elements of varying spacing has observed that for a certain spacing of the rods, the measured $\Delta u/U_*$ was maximum and as the spacing was increased or decreased $\Delta u/U_*$ decreased. In a series of experiments on two dimensional roughness elements, Liu et al (1966) have also made the same observation.

4.2.5 In the fully rough flows, Schlichting (1968) shows that:

$$\frac{u}{U_*} = \frac{1}{K} \ln \frac{y}{k_s} + \underline{E} \qquad 4.4$$

where $\underline{E}$ is a universal constant equal to 8.5. Equation 4.4 may be rewritten as

$$\frac{u}{U_*} = \frac{1}{K} \ln \frac{y\,U_*}{\nu} - \frac{1}{K} \ln \frac{k_s U_*}{\nu} + 8.5$$

$$\text{i.e.} \quad \frac{u}{U_*} = \frac{1}{K} \ln \frac{y\,U_*}{\nu} + B_1 - \left[\frac{1}{K} \ln \frac{k_s U_*}{\nu} - 3.4\right] \qquad 4.5$$

where B_1 is a constant and takes the value of 5.1. Comparing equation 4.3 and 4.5 gives:

$$\frac{\Delta u}{U_*} = \frac{1}{K} \ln \frac{k_s U_*}{\nu} - 3.4 \qquad 4.6$$

Comparing equation 4.4 with the following equation which is also valid for rough surfaces provided y is measured from

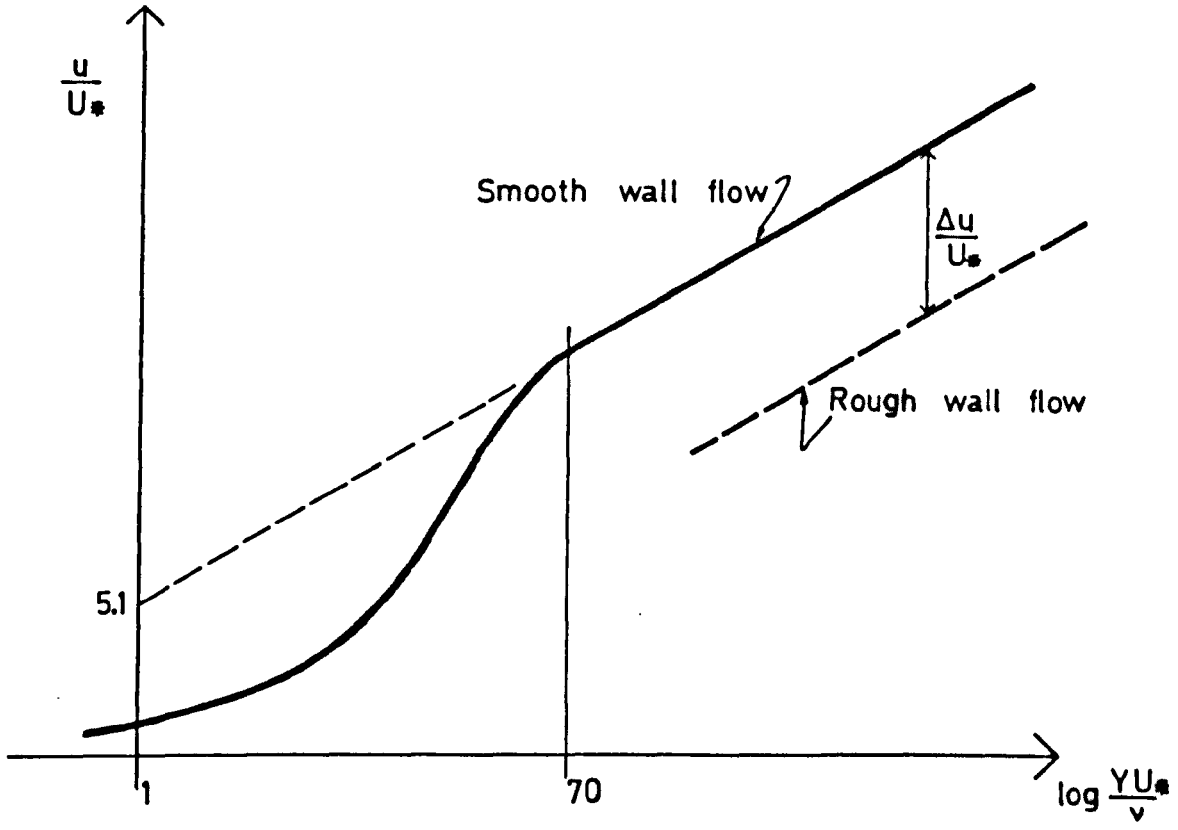

FIGURE 4.3 DEFINITION OF THE ROUGHNESS FUNCTION

the correct origin

$$\frac{u}{U_*} = \frac{1}{K} \ln \frac{y}{Z_o} \qquad 4.7$$

the following relationship is obtained for fully rough flows:

$$\frac{k_s}{Z_o} = 30 \qquad 4.8$$

4.2.6 Due to the irregularity of rough surfaces, the question will arise as to which origin should be taken for the measurement of y, whether it is more appropriate to choose the crest of roughness or the lowest point on the surface. However, if y is shifted by a constant amount, curvature will appear in the straight line logarithmic part of the velocity profile. Therefore, the experimental points measured from the wall may be shifted upward assuming a zero plane displacement, d, until a straight line is obtained, Chauser (1956). On the other hand, if y was taken from the crest of the roughness elements, a downward shift will be necessary to bring the origin of y at a distance ε below the crest such that, Perry and Joubert (1963):

$$H = \varepsilon + d \qquad 4.9$$

4.3 Effect of roughness geometry on the mean pressures and their distribution

4.3.1 A considerable amount of work has been done on the investigation of fully rough flows over rough surfaces consisting of regular arrays of geometrical roughness elements in different distribution concentrations. Due to the complexity of the problem and the great number of parameters which can be considered to fully specify the element shape and distribution on the surface, the majority of the work has been done on the simple case of two dimensional roughness elements. An excellent review on this case is given by Liu, Kline and Johnston (1966). In regular

arrays of three dimensional elements, the parameters required to fully describe the roughness geometry, i.e. element shape and distribution, may also be simplified to depend on either the plan area density, λ_p or the frontal area density, λ_f. This simplification can be made if both the frontal and the side aspect ratio, A_f and A_s respectively as well as the spacing ratio ψ_x/ψ_y, which defines the pattern of distribution are kept constant. This may explain why in most of the investigations, the correlations are made with the roughness density neglecting the other variables. However, in the analytical review made by Wooding, Bradley and Marshall (1973), the inclusion of an aspect ratio factor was suggested.

4.3.2 On the basis of work done on the investigation of the effect of roughness geometry and their distribution on two and three dimensional elements, different flow regimes were suggested which are as follows. Morris (1955) was the first to introduce the classification of the flow over roughness elements into three flow regimes. These flow regimes which are applicable to pipe flows, open channel flows and flat plate boundary layer are denoted as isolated roughness flow, wake interference flow and the skimming flow. Perry and Joubert (1963) and Perry, Schofield and Joubert (1969) reported the work on two dimensional square sectioned roughness elements and suggested two types of roughness geometry, "k" type and "d" type roughness corresponding to the wake interference and the skimming flow regimes respectively.

In the isolated roughness flow, the roughness elements are sufficiently far apart such that each element acts in isolation and behind which the wake and the separation bubble develop completely and the reattachment occurs before the next element is reached. In the wake interference flow the roughness elements are close enough to each other so that the separation bubble associated with each element does not have room to develop fully. In the skimming flow, the roughness elements are closer still so that the stable vortices are created in the space between the elements

and the flow appears to skim on the crest of the elements. It can, therefore, be concluded that the main effect of roughness geometry, characterised by its density, is to change the flow from one regime to the other. Attention is given here to the resulting drag forces on the roughness elements as well as to their pressure distributions in each of the three flow regimes.

4.3.3 In the case of a rough surface with the roughness density so low that the total drag on the surface is approximately equal to the frictional drag on the smooth intervening boundary, the total drag will be a function of the Reynold's number based on the freestream velocity and the fetch. In the present investigation, this hardly is the case as for fully rough flows (usually taken as $H\ U_*/\nu \geqslant 70$) the viscosity is of negligible importance and the drag occurring on the roughness elements is essentially by pressure rather than shear forces, Gartshore (1977). As the density increases, the flow changes from isolated roughness flow to the wake interference flow and subsequently to skimming flow where the total drag is only due to the form drag on the elements. For identical roughness elements with flat top surfaces, the flow may once again experience a transition from a fully rough to a smooth surface flow on top of the elements as the density, λ_p, reaches 100%.

4.3.4 The element's drag coefficient may be written as:

$$C_{D_1} = D/q_1\ a_f \qquad 4.10$$

and the effective shear on the surface, τ_{oe}, may be written as:

$$\tau_{oe} = D/A \qquad 4.11$$

Hence the effective local skin friction may be represented as:

$$C_{f_e} = \tau_{oe}/q_1 \qquad 4.12$$

Substituting from equation 4.10 and 4.11 gives:

$$C_{f_e} = \frac{C_{D_1} a_f}{A} = C_{D_1} \lambda_f \qquad 4.13$$

4.3.5 Due to the scarcity of data on the drag of regular arrays of roughness elements in the isolated roughness flow regime, we will have to rely on the analogy between this flow and the smooth wall flow round a single element being reasonably correct. However, some differences may occur due to the different properties of incident flow in each case. For example, the value of d, which will be zero for the smooth flow incident on a single roughness element, is only approaching zero at very low densities. From the work of Good and Joubert (1968) on two dimensional bluff flat plate (fence) in smooth wall flow, the main conclusions may be summarised as follows:

i) The drag coefficient C_{D_1} is dependent on the ratio of body height to boundary layer height, H/δ, see Figure 2.6.

ii) A linear relationship was found to exist between the windward and the leeward pressure coefficients provided that the element height is within the inner layer of the incident velocity profile. The same result was also noted by Plate (1964).

iii) A drag coefficient, C_{D_m}, based on the maximum pressure difference over the bluff plate was approximately constant, i.e.

$$C_{D_m} = \frac{D}{(P_{max} - P_b)H} \simeq 0.945$$

This agrees well with the corresponding value of 0.95 obtained by Plate.

iv) Normalised pressure distributions with respect to the maximum pressure were obtained as a function of the relative height on the plate face, y/H. The pressure distribution was of an "S" form with the peak pressure occurring at $y/H \simeq 0.6$, Figure 4.4. Such a pressure distribution form is usually obtained for isolated buildings.

Since the above work was carried out in smooth wall flow, some difference would be expected for fully rough surfaces. The difference would be mainly due to the introduction of the zero plane displacement, d, and the variation of Z_o with roughness density.

4.3.6 Soliman (1976) carried out some pressure measurements on groups of three dimensional bluff bodies in a rough turbulent boundary layer flow growing over a random layout of wooden blocks. His measurements showed the following:

i) The drag coefficient C_{D_1} is dependent on the ratio of body height to the boundary layer height H/δ.

ii) The method of normalising the windward pressures using the maximum pressure suggested by Good and Joubert (1968) proved successful only in the isolated roughness flow regime. The pressure distribution was an "S" form with the peak pressure occurring at $y/H \simeq 0.75$, Figure 4.5.

iii) In groups of bodies, the isolated roughness flow regime was obtained when the spacing S/H was large enough so that the separation and the downward reattachment zones of flow round the cube did not interfere with the next element.

iv) A linear relationship was also found to exist between both the windward and leeward pressure coefficients with the spacing in the isolated roughness flow.

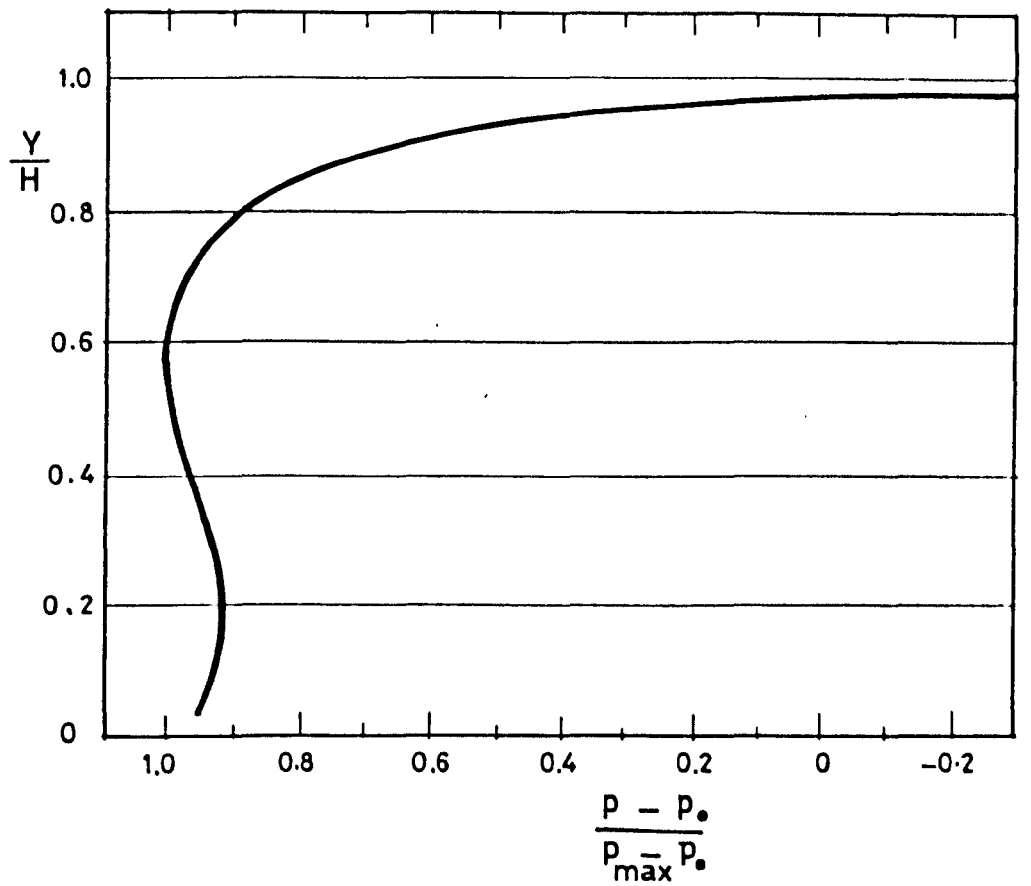

FIGURE 4.4 THE PRESSURE DISTRIBUTION ON AN ISOLATED BODY, (GOOD AND JOUBERT, 1968).

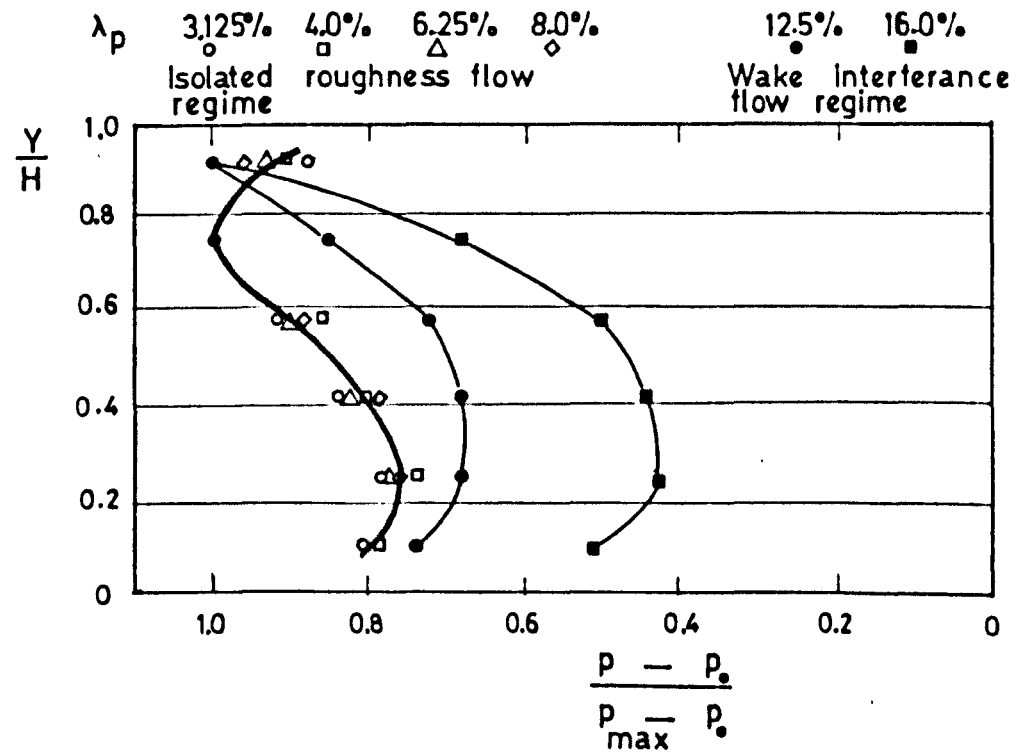

FIGURE 4.5 NORMALISED WINDWARD PRESSURE PROFILES WITH RESPECT TO THE MAXIMUM PRESSURE IN THE ISOLATED ROUGHNESS FLOW REGINE, (SOLIMAN 1976)

4.3.7 In the wake interference flow regime, owing to the increase of the zero plane displacement, the drag coefficient C_{D_1} is expected to decrease as the density increases. The pressure distributions on the face of the elements is different from that of the isolated roughness flow regime in that the "S" form is slightly distorted and would be better represented by a reversed "C" over 95% of the element height, Schofield, Perry and Joubert (1974), Figure 4.6. Similar results though less accurate at the lower and the upper parts on the element were obtained from the work of Antonia and Luxton (1971). On the leeward face, the pressure distribution is approximately uniform. These distributions are obtained from two dimensional square roughness elements in zero pressure gradients.

Similar observations on three dimensional roughness elements were reported by Soliman. In spite of the fact that the shape of pressure distributions on the windward face of models reported by Soliman was a reversed "C" form over the whole of the element height, it is suggested that a transition range between the two must exist where the "S" form of pressure distribution slowly changes to the reversed "C" form.

4.3.8 In the skimming flow regime, the rate of change of the zero plane displacement with density is less than the corresponding rate in the other two regimes, (see Counihan (1971)). This would imply that the drag coefficient C_{D_1} is less sensitive to variations in density. However, significant effects on C_{D_1} were observed due to the vertical misalignment of the element crests, Perry, Schofield and Joubert (1969). Joubert, Perry and Stevens (1971) also showed the variation in drag coefficient C_{D_1} of the order of approximately 70% with only 1% change in height for two dimensional elements with stable vortices between them. From these observations it seems that in the skimming flow regime, where ε is very small, a small fraction of the element height could be very large relative to the value of ε.

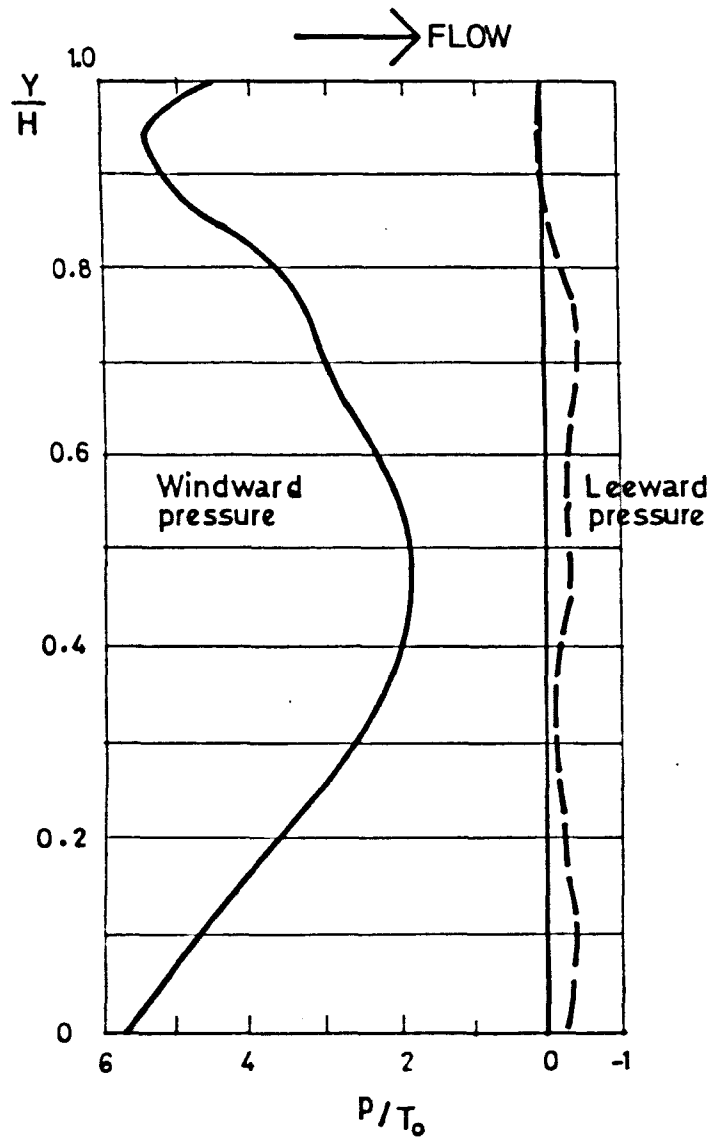

FIGURE 4.6 THE PRESSURE DISTRIBUTIONS ON AN ELEMENT IN THE WAKE INTERFERENCE FLOW REGIME, (SCHOFIELD ET AL, 1974)

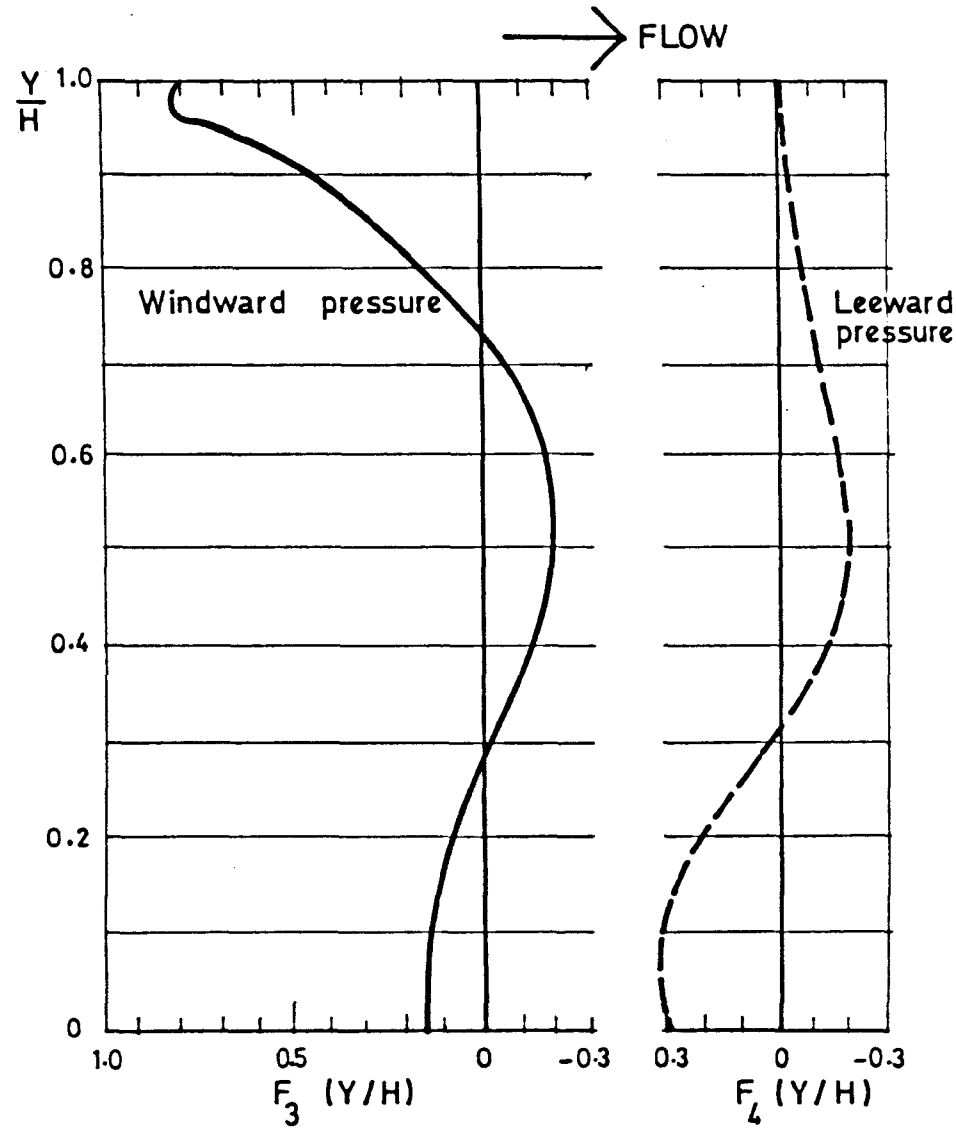

FIGURE 4.7 THE PRESSURE DISTRIBUTIONS ON AN ELEMENT IN THE SKIMMING FLOW REGIME (SCHOFIELD ET AL 1974)

The pressure distributions on the front face of a two dimensional square element are rather similar in the skimming flow regime to those corresponding to the wake interference regime, where the reversed "C" form of the pressure profile now covers up to 98% of the element height, Figure 4.7. The pressures on the upper part have higher values than those on the lower part of the face. On the leeward face, the pressure profile becomes non uniform and similar to the windward face pressure in the lower half of the face with minimum pressure occurring at mid height, Schofield, Perry and Joubert (1974). Such variation on the leeward face is characteristic of the stable vortex created in the space between elements, Roshko (1955).

Soliman reported similar observations for flow over three dimensional bluff bodies in a turbulent boundary layer flow. The shape of the pressure profiles in the skimming flow regime on both the windward and the leeward faces of the element was similar to those on two dimensional elements. He, however, observed a sudden decrease in the leeward pressure coefficient at the start of the skimming flow regime before starting to increase again as the density increased. This change was also reflected in the drag coefficient in the form of a sudden jump in the value of C_{D_1}.

4.4 Effect of roughness geometry on the velocity profile parameters

4.4.1 The classification of the flow over roughness elements into three flow regimes as introduced by Morris (1955) and their effect on pressure distributions has already been discussed in the last section. The work done on the investigation of the effect of roughness geometry and distribution on the resulting flow is reviewed below.

4.4.2 The variation of $\bar{d}/H$ with roughness density, λ_p, was investigated by Counihan (1971) and Cook (1976). For approximately cubical roughness elements, (the elements were square in plan with 15.9mm side length and 9.5mm high) Counihan found that $\bar{d}/H$ increased linearly with λ_p and suggested that beyond a value of λ_p approximately 50%, $\bar{d}/H$ will follow an asymptotic line to reach a maximum value of 1.0 at λ_p = 100%. Cook (1976) also studied the variation of d/H for flow over three dimensional blocks (100 x 50mm in plan, 50mm high) in a staggered layout pattern and found similar results.

Soliman (1976) compared the results of his investigation of the variation of d/H with roughness density for an array of cubes with corresponding results of Counihan and found a similar trend. Soliman's values of d/H were, however, larger than the values obtained by Counihan. This is suggested to be due to differing ratios of H/δ in both the investigations.

4.4.3 The variation of Z_o/H with λ_p was also studied by Counihan (1971) and was found to be different to the corresponding variation of $\bar{d}/H$ in that it increased linearly with λ_p to reach a maximum value and then decreased with increasing λ_p. Here it may be noted that this variation is expected to be similar to that of k_s/H with density reported by Koloseus and Davidian (1966) due to the proportionality between k_s and Z_o in the fully rough flow, (see equation 4.8). The maximum in Z_o/H was at λ_p = 25% for Counihan's results compared with λ_f = 15% for the cubical roughness elements reported by Koloseus et al. This discrepancy is thought to be attributed to the difference in the definition of density used in each case. Transforming λ_p used by Counihan to λ_f using the following relation:

$$\lambda_f = \lambda_p / A_s \qquad 4.14$$

and knowing that A_s for Counihan's roughness elements was 1.67, gives a correction factor of 0.597 to be multiplied by his values of λ_p. Therefore, λ_p at 25% will be corresponding to λ_f at 14.9% which is only 0.1% different from that noted by Koloseus et al of 15%.

Cook (1976) and Soliman (1976) also investigated the variation of Z_o/H with λ_p for the roughness element described in section 4.4.2 and found similar trends. Small differences in the magnitude of Z_o/H with λ_p in the three experiments described above are considered to be either due to the different shapes of roughness elements or due to differing nature of flows.

4.4.4 The effect of changing roughness density on the velocity profile parameters has been investigated by Koloseus and Davidian (1966). They studied the influence of roughness geometry on the value of k_s/H. Wooding, Bradley and Marshall (1973) explained the results and analysis of Koloseus et al on the grounds of three flow regimes of Morris. The results showed how the parameter k_s/H increases linearly with the density, λ_f, in the isolated roughness flow regime reaching a maximum value in the transition to the wake interference regime and subsequently decreases in the skimming flow regime. It may be noted however that the distinction between the wake interference and the skimming flow regime is not clear. From the comparison between roughness elements of different geometrical forms it is evident that the behaviour of each of them is characterised by a particular line on a plot of k_s/H against λ_f. Although all the lines showed the same trend, they all showed variation in the location of the maxima, Figure 4.8.

Koloseus et al found that the data for various roughness elements are well represented by a linear relation between log k_s/H and log λ over a large range in roughness concentration. The slope of these lines varies in an unsystematic fashion about a value of 1. As a result, they modified the equation of the law of resistance for flow over

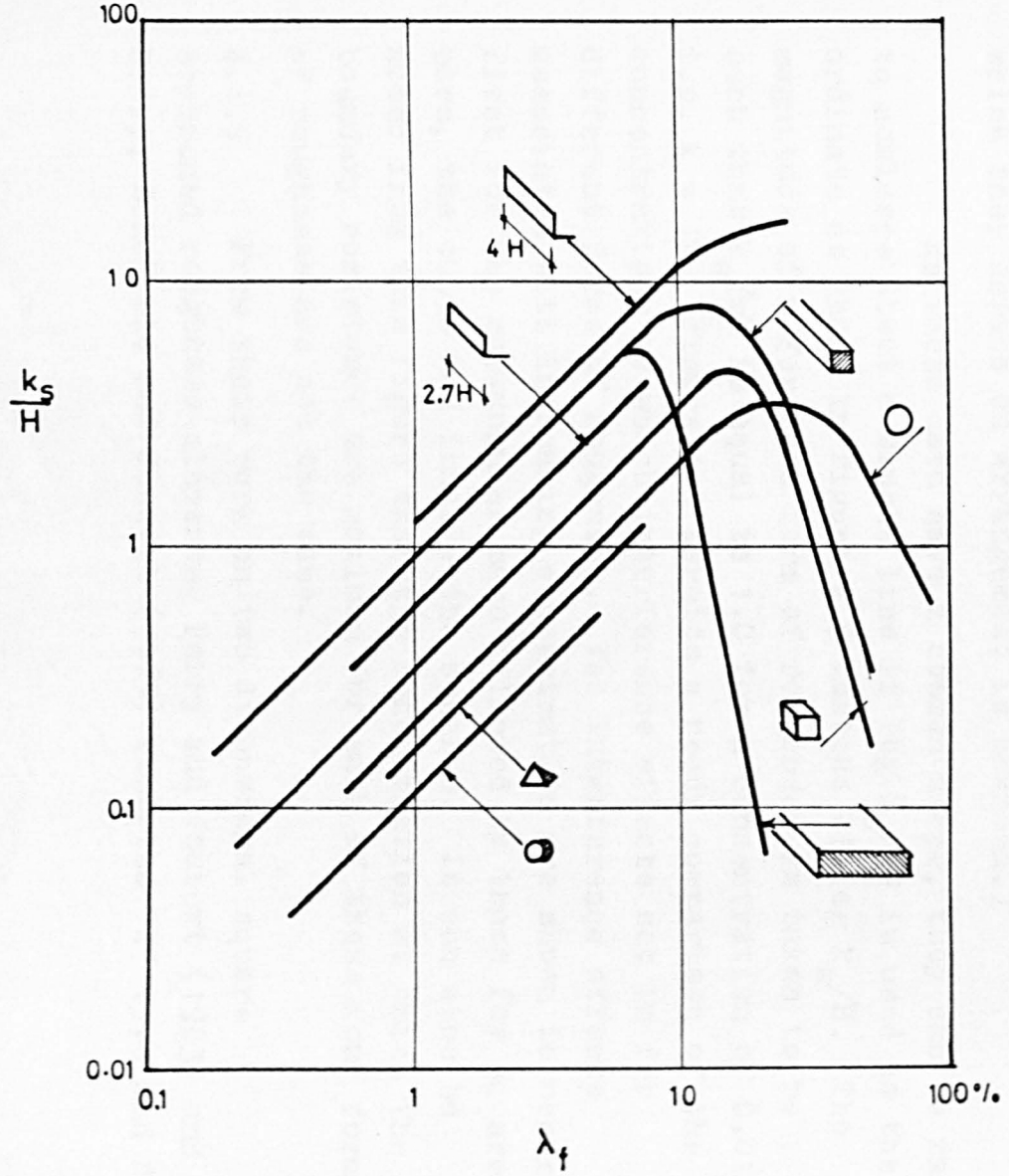

FIGURE 4.8 VARIATION OF K_s/H WITH λ_f FOR DIFFERENT ELEMENT FORMS

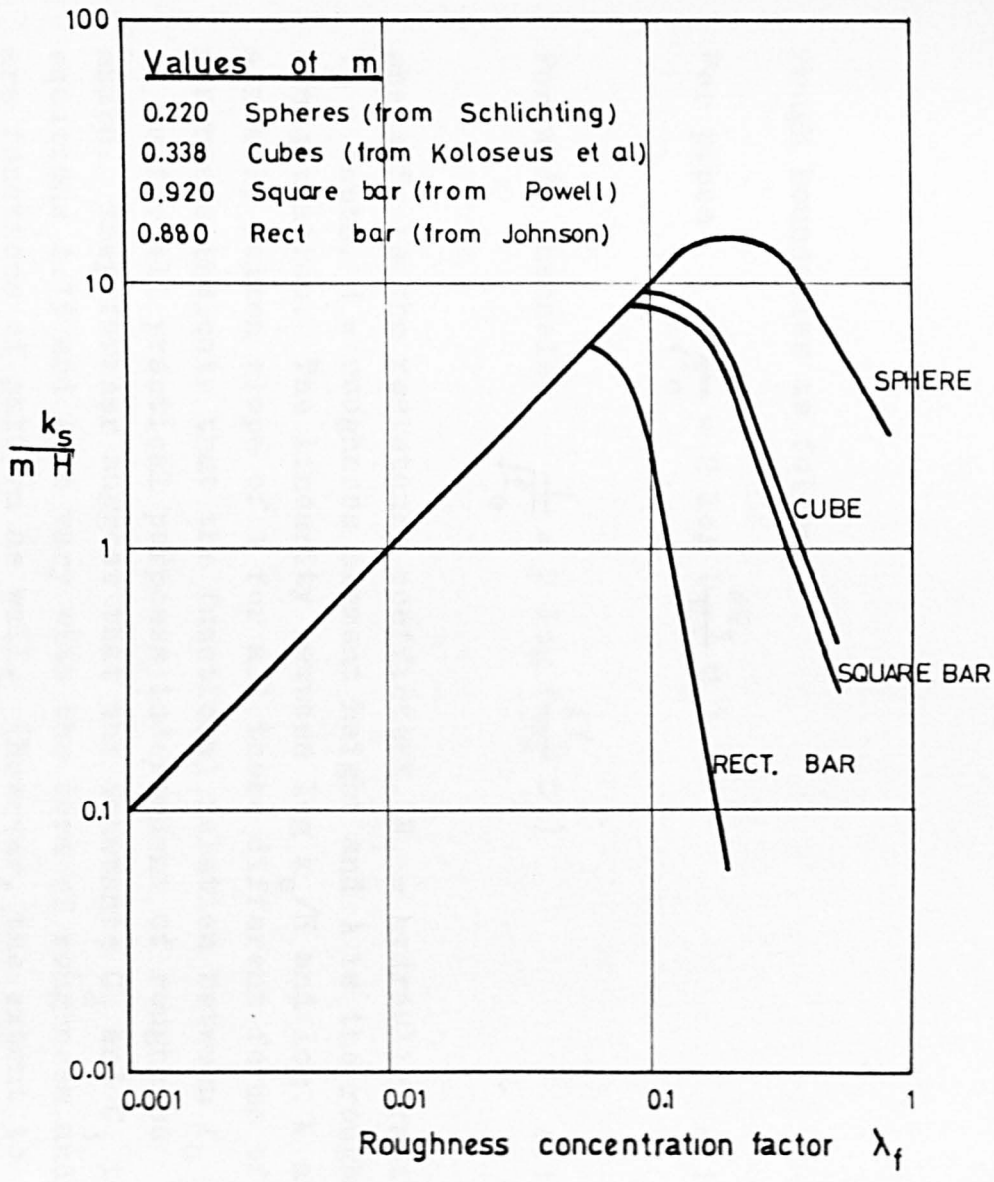

FIGURE 4.9 INTERFERENCE EFFECTS OF ROUGHNESS ELEMENT CONCENTRATION

rough boundaries as follows:

For pipes $$\frac{1}{\sqrt{f_o}} = 2 \log \left(\frac{4R_1}{H\lambda} C_2\right) \qquad 4.15$$

For wide channels $$\frac{1}{\sqrt{f_o}} = 2 \log \left(\frac{4Y_o}{H\lambda} C_3\right) \qquad 4.16$$

where f_o is the resistance coefficient, R_1 = hydraulic radius, Y_o = depth, H = roughness element height and λ is the roughness concentration. The linearity between log k_s/H and log λ at a nearly common slope of 1 for all these different forms of roughness indicate that the functional relation between f_o and λ is for all practical purposes independent of roughness shape. They further suggest that the constants C_2 and C_3 in equations 4.15 and 4.16 vary with the form of roughness and are functions of pattern as well. (However, the extent to which they depend on arrangement is unknown.)

As these data have a common slope, they can be made to coalesce about a single line if log k_s/mH is used as the ordinate as shown in Figure 4.9 instead of log k_s/H. The magnitude of m for each form of roughness is taken to be such that k_s/mH is equal to 1.0 for a concentration of 0.01 i.e. λ = 1%. Figure 4.9 permits a ready comparison of the concentrations at which interference effects set in for different forms of roughness. The interference effects associated with increasing concentration are shown to occur, first for the rectangular bars followed by those for square bars, the cubes and finally the spheres. It can also be noted from this figure that the concentration at which the boundary resistance are maximum for each of these four forms of roughness are not the same.

4.4.5 From their work on two dimensional square sectioned roughness elements, Perry and Joubert (1963) and Perry, Schofield and Joubert (1969) reported "k" type and "d"

type roughness geometry corresponding to the wake interference and skimming flow regimes respectively. The error in origin ε in the wake interference flow was shown to be proportional to the roughness height, H, while in the skimming flow regime, ε was shown to be proportional to the boundary layer thickness, δ. From their work on the flow structure for both the flow regimes, Perry et al (1969) were able to offer the following explanation of the flow mechanism.

i) In the wake interference flow, eddies with a length scale proportional to the roughness height H are assumed to be shed into the flow, forming a sub-layer structure having a thickness of some factor times H. Further away from the crests, this sub-layer structure blends smoothly with the flow described by the logarithmic law, Figure 4.10(a).

ii) In the skimming flow regime, the stability of the vortices between the elements results in negligible eddy shedding from the elements into the flow. The outer flow rides over the elements relatively undisturbed and the sub-layer structure forming on top of the elements approaches zero, Figure 4.10(b).

4.5 Effect of a step change in surface roughness

4.5.1 The discussion so far has been limited to surfaces of uniform roughness elements extending for long fetches, so that the flow stability is assumed to have been achieved. This is hardly the case in nature. In situations, therefore, where a step change in surface roughness occurs, an internal layer is known to grow on the new rough surface and develops in the flow direction to replace the older layer as the fetch increases. This problem is of great interest to the studies of air flow in the atmosphere as such surface changes are frequently met on the earth's surface, see for example Elliott (1958), Bradley (1968), Panofsky and Townsend (1964) and Blom and Warner (1969). The main conclusions from the

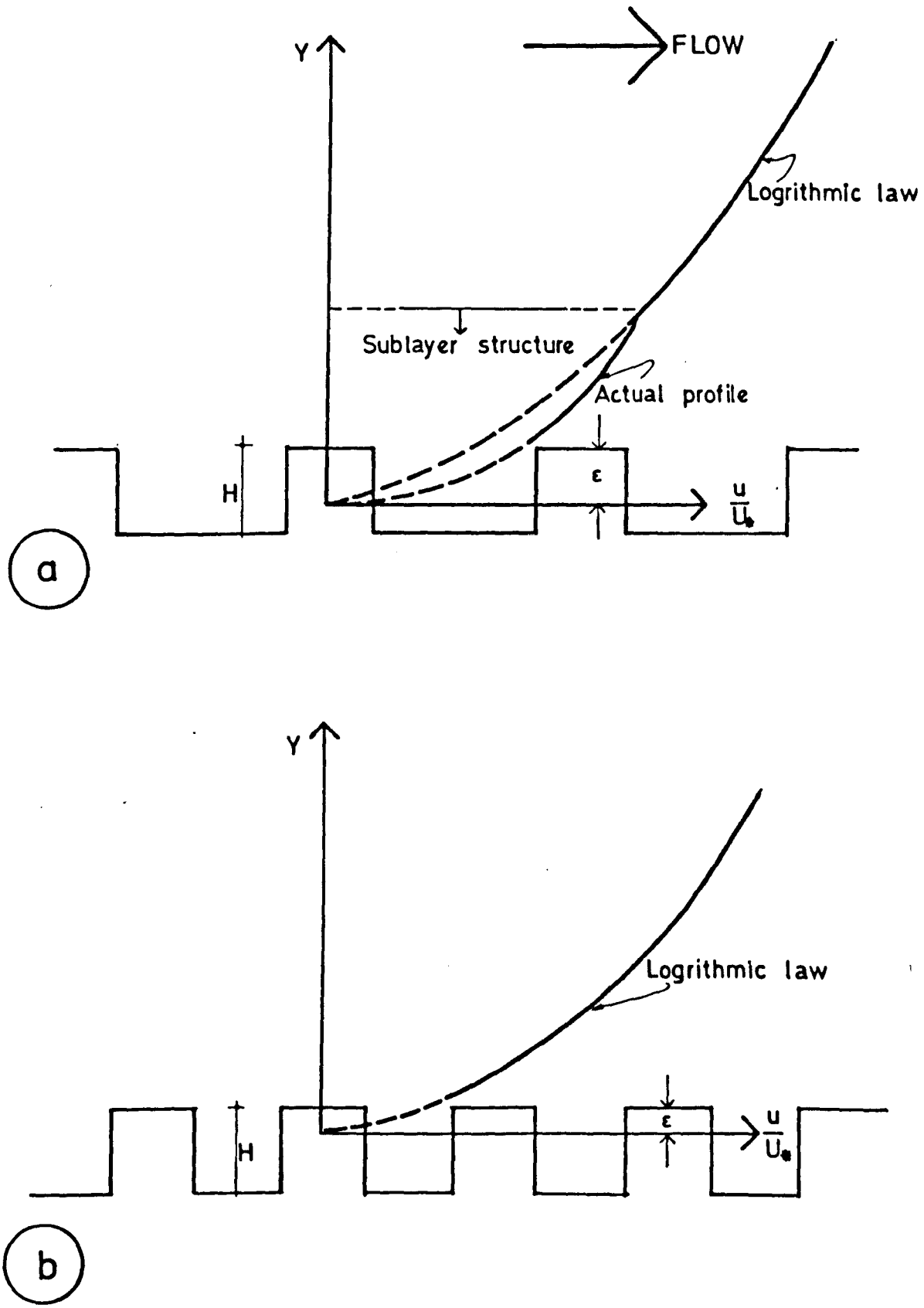

FIGURE 4.10 THE FLOW STRUCTURE FOR
a) WAKE INTERFERENCE FLOW REGIME
b) SKIMMING FLOW REGIME (PERRY ET AL 1969)

results of these investigations is that the adaptation of the surface shear stress to the new boundary condition takes place fairly rapidly, therefore, reliable values of the drag forces on an element may be obtained at a relatively short fetch compared with that required for the whole boundary layer to adapt.

4.6 Conclusion

4.6.1 In this chapter, it has been shown that the main effect of changing the roughness geometry and pattern of distribution is to produce different flow regimes. It is also shown that the velocity profile parameters, i.e. Z_o and d as well as the resulting drag forces are dependent on the flow regime and hence the roughness geometry. Since air flow in urban areas in strong winds is completely rough, it is considered that the results obtained for the different regimes may well extend to include arrays of similar buildings in full scale conditions. However, as most of the work reported has been for two dimensional roughness elements, further work on three dimensional roughness elements covering a wide range of densities and patterns is required. This will provide relevant information on the behaviour of the element drag, hence the natural ventilation potential in different flow regimes.

CHAPTER 5

EXPERIMENTAL ARRANGEMENT AND TECHNIQUES

5. EXPERIMENTAL ARRANGEMENT AND TECHNIQUES

5.1 Introduction

5.1.1 In order to attempt a comprehensive investigation of the effect of building shapes and their geometry on the resulting wind pressure forces, an extensive series of wind tunnel model studies were made. A large number of building shapes were studied systematically to find a relationship between surface pressure forces and the geometry of buildings. Since the cube is the only three dimensional body form that is characterised by a single dimension, the study started with a detailed investigation of flow around cube shaped elements before going to other building forms.

5.2 Details of wind tunnel and model mounting technique

5.2.1 A low speed wind tunnel of the Department of Building Science, University of Sheffield was used for all the experiments. The wind tunnel has a large working section with an inlet flare upstream and a small working section downstream joined to the large working section by a smooth transition piece, Figure 5.1. The present investigations were carried out in the large section of the wind tunnel which measures 1.2 x 1.2m and has an overall length of 7.2m, incorporating a 1.1m diameter turntable whose centre lies 5.4m downstream of the entry point. A honeycomb, 150mm thick with 15mm cell size, is positioned in the inlet flare to act as a flow straightener.

In order to simulate the dominant characteristics of the urban terrain boundary layer, the general approach suggested by Counihan (1973) is followed in the wind tunnel and the simulation arrangement consists of a castellated fence, a row of spires and a regular array of roughness elements on the wind tunnel floor. The castellated fence, which spans the width of the working section, has heights of

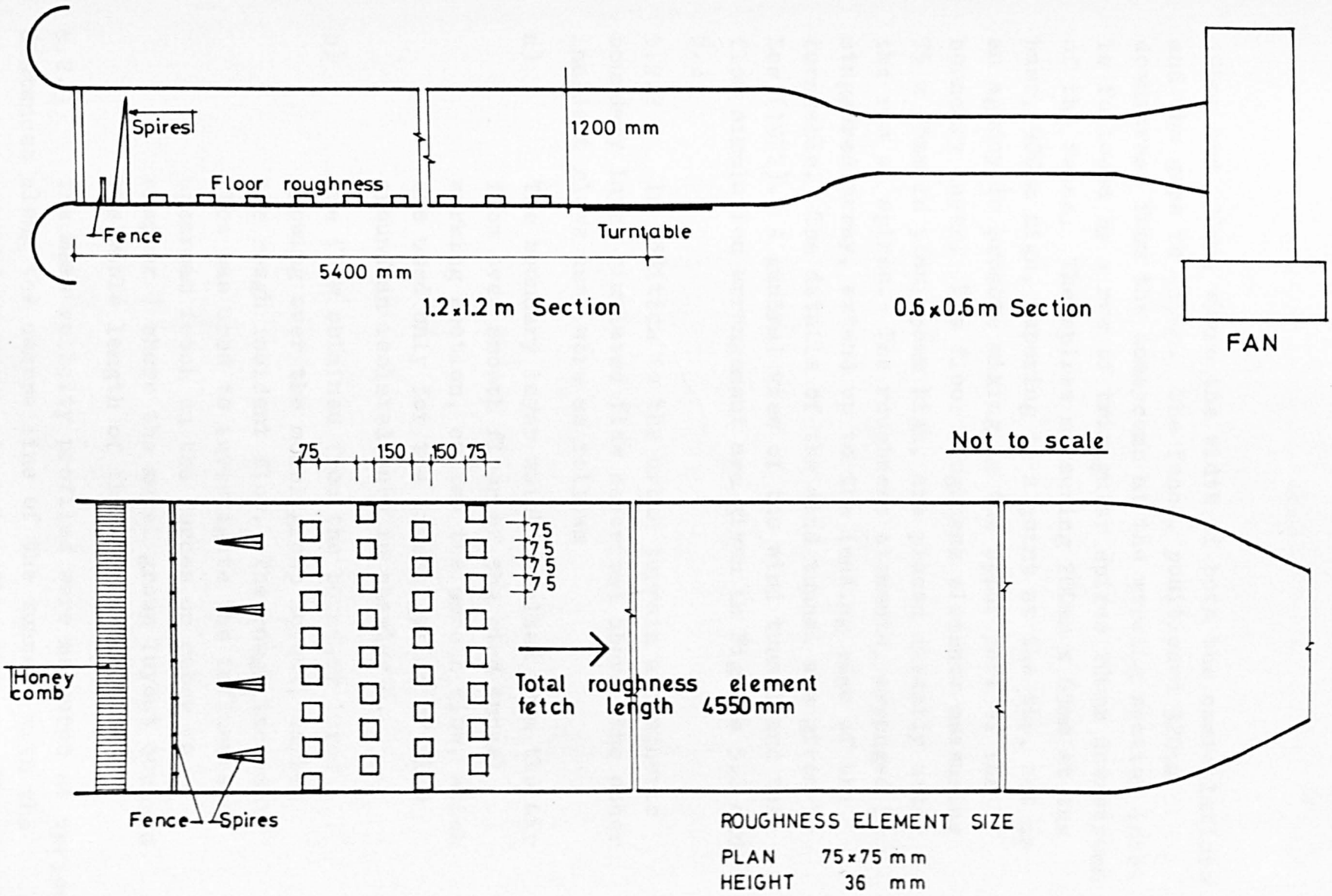

FIGURE 5.1 DETAILS OF THE WIND TUNNEL AND THE URBAN TERRAIN BOUNDARY LAYER SIMULATION ARRANGEMENT

195mm and 230mm, where the width of both the castellations and the gaps is 150mm. The fence, positioned 320mm downstream from the honeycomb at the working section inlet is followed by a row of triangular spires 200mm downstream of the fence. The spires measuring 200mm x 65mm at the base, 900mm high, tapering to a point at the top, act as an agency to promote mixing in the upper part of the boundary layer. The floor roughness elements measuring 75 x 75mm in plan, 36mm high, are placed directly after the row of spires. The roughness elements, arranged in a staggered array, extend up to the leading edge of the turntable. The details of the wind tunnel are given by Lee (1977). A general view of the wind tunnel and the flow simulation arrangement are given in Figures 5.2 and 5.3.

5.2.2 In addition to the urban terrain atmospheric boundary layer simulated flow described above, the other incident glows used were as follows

a) The boundary layer which resulted from the air flow over smooth floor of the wind tunnel working section, called the smooth flow, which was used only for the investigation of flow around an isolated cube in chapter 6.

b) The flow obtained from the boundary layer growing over the model group layout, called the rough incident flow. The rough incident flow was used to investigate the influence of upstream fetch on the forces on cubes in chapter 7 where the model group layout covered the whole length of the working section.

5.2.3 The mean velocity profiles were measured at various distances along the centre line of the tunnel, with the atmospheric boundary layer simulated flow upwind. The velocity profile was measured at the turntable centre in the first instance. Further profiles were measured at

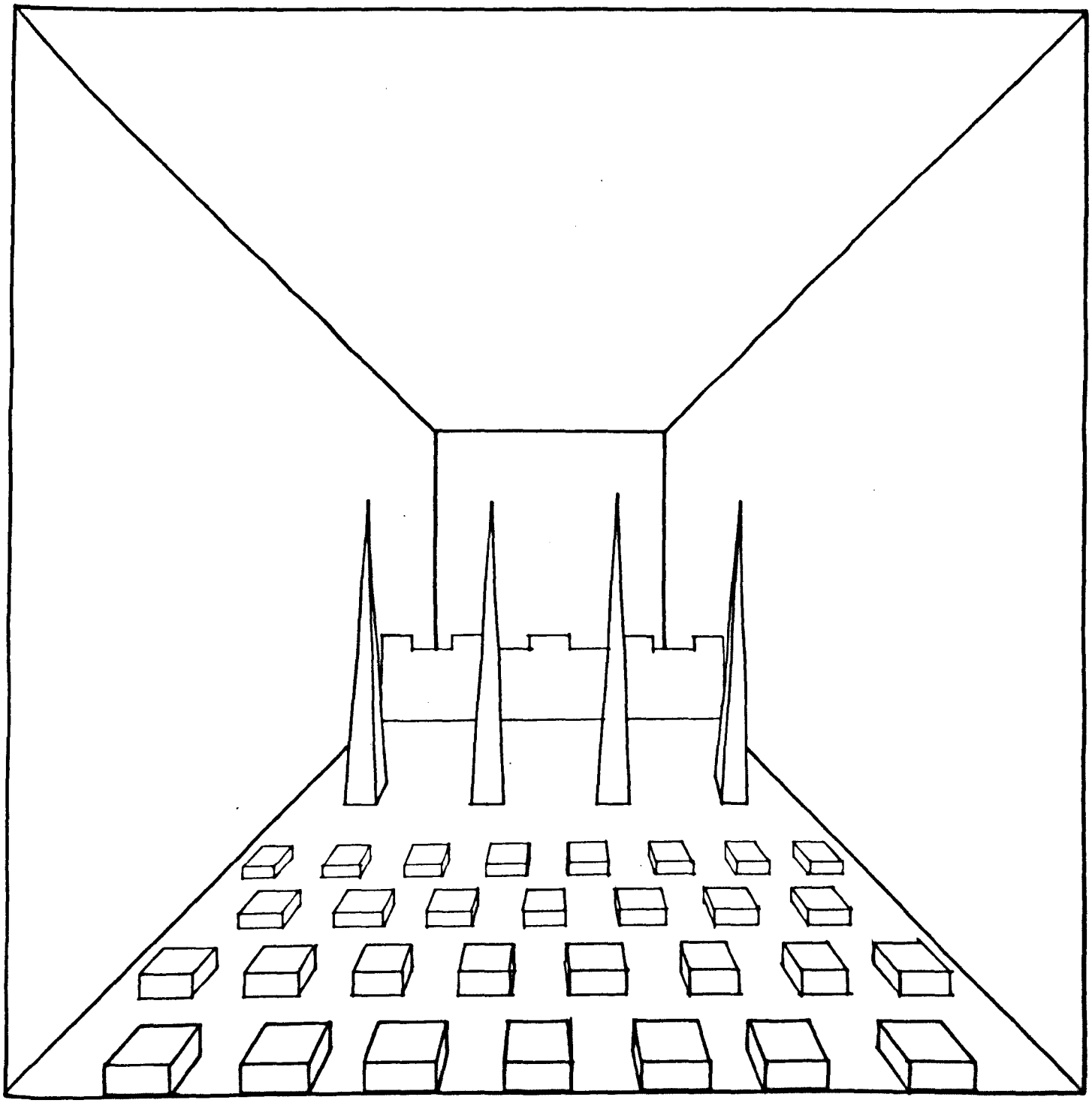

FIGURE 5.2 WIND TUNNEL TEST ENTRANCE SHOWING THE FENCE, SPIRES AND ROUGHNESS ELEMENTS.

FIGURE 5.3 A PHOTOGRAPH OF THE INTERIOR OF THE TUNNEL

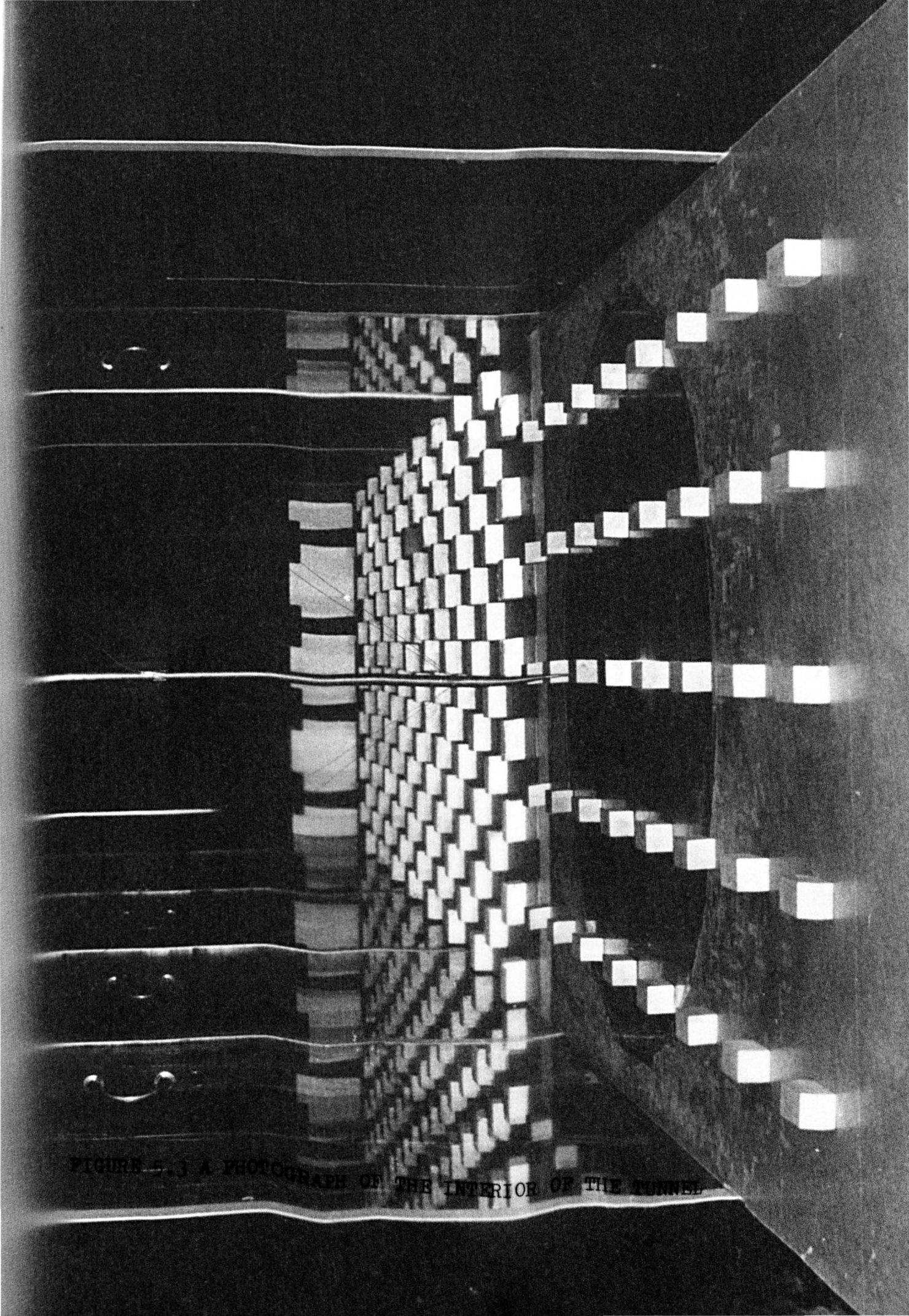

FIGURE 5.3 A PHOTOGRAPH OF THE INTERIOR OF THE TUNNEL

distances of 180, 720 and 1080mm upwind from the centre of the turntable in the streamwise direction. These results are shown plotted in Figure 5.4. The profiles show that a maximum velocity of 9.65 m/s is attained at a height of 800mm, the physical thickness of the boundary layer. Above this boundary layer, a region of constant velocity exists which extends to the roof boundary layer. Figure 5.5 shows the present profiles plotted alongwith similar results of Counihan (1973) and Peterka and Cermak (1974).

The power law velocity profile measured at the turntable centre and defined by the equation:

$$\frac{u}{U_1} = \left(\frac{y}{\delta}\right)^{\alpha} \qquad (5.1)$$

is shown in Figure 5.6. An inflection in the velocity profile is found at about y = 150mm in Figure 5.6. Consequently two values of the exponent, α, were found, i.e. $\alpha = 0.16$ corresponding to the lower part of the profile growing over the smooth surface of the turntable and $\alpha = 0.28$ which corresponds to the upper part of the profile and represents the boundary layer flow. The value of $\alpha = 0.28$ representing the urban terrain boundary layer flow is in good agreement with similar figures assessed from full scale measurements by various research workers for various urban areas, i.e. Jones et al (1971), Kamei (1955), Shiotani (1962), Shellard (1963), Davenport (1963) and Caton (1975), where the value of urban power law exponent is found to vary from 0.21 to 0.40. The value of $\alpha = 0.28$ can, therefore, be taken to represent an adequate description of the urban boundary layer power law profile.

5.2.4 The details of the turbulence intensity, Reynold stresses, the turbulence spectra and the simulated urban boundary layer scale factors for this simulation are found to be an adequate representation of the full scale boundary layers, Lee (1977). No correction for wind tunnel

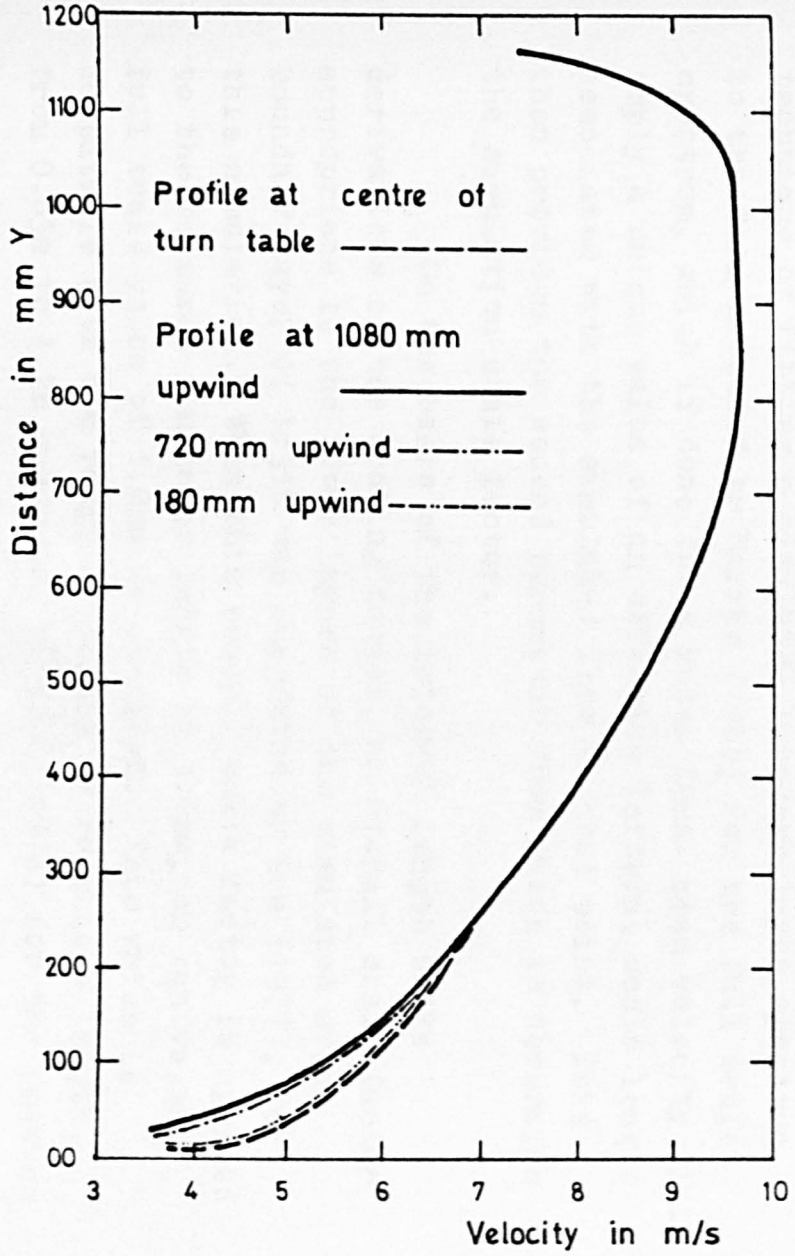

FIGURE 5.4 INCIDENT FLOW PROFILES

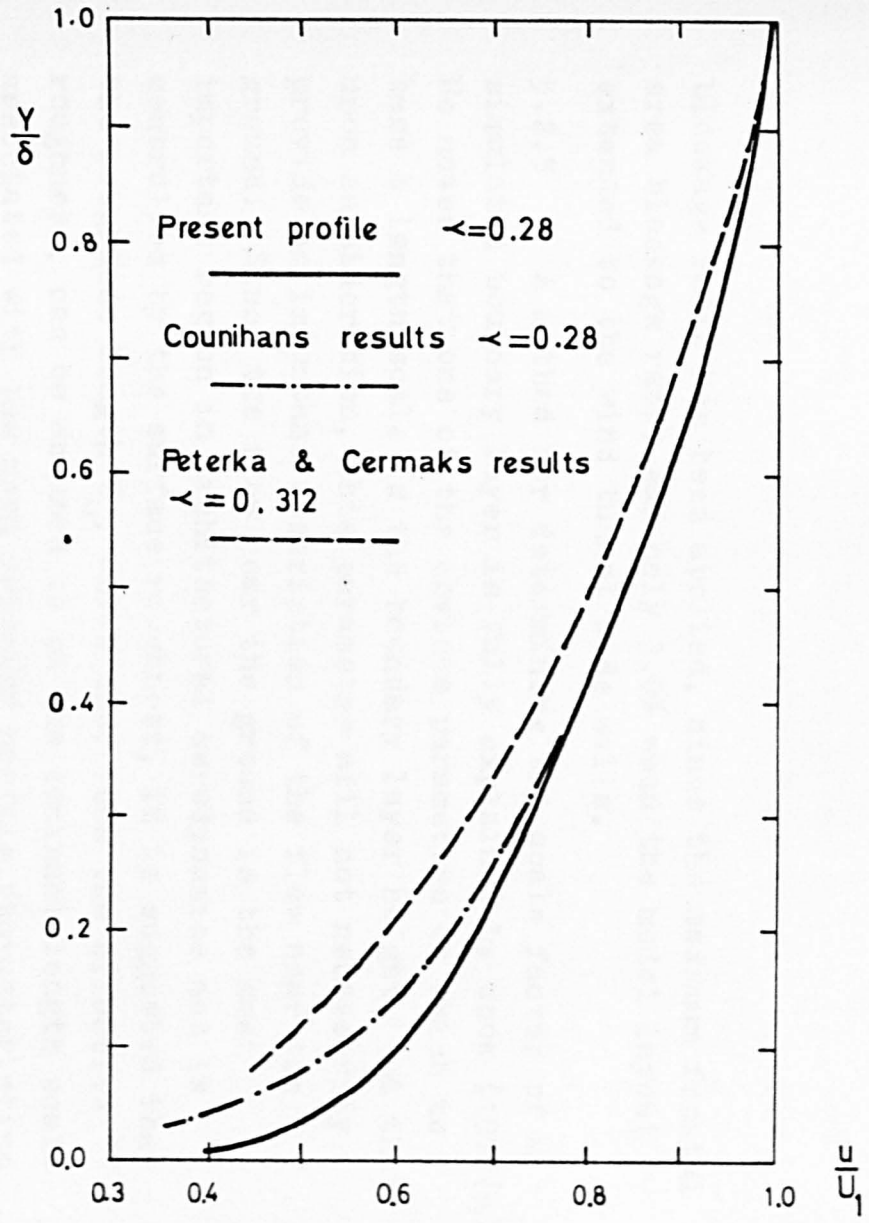

FIGURE 5.5 INCIDENT FLOW PROFILES, (A COMPARISON)

blockage ratio has been applied, since the maximum frontal area blockage ratio was only 3.0% when the model layout extended to the wind tunnel side walls.

5.2.5 A method for determining the scale factor of a simulated boundary layer is fully explained by Cook (1976(a)). He notes that one of the obvious parameters on which to base a length scale is the boundary layer height, but that upon consideration, this parameter will not necessarily provide an important description of the flow near the ground. Since the flow near the ground is the most important region in architectural aerodynamics and is controlled by the surface roughness, it is suggested that the roughness length Z_o, which describes the effective roughness, can be assumed to be the dominant length scale associated with the mean velocity profile characteristics.

Since this length parameter describes the mean velocity characteristics of the simulated flow a further length parameter is required which describes the turbulence characteristics. Cook then proceeds to explain the technique of fitting a simulated boundary layer spectrum to the form proposed by Harris (1968) for the full scale spectrum, which if done for a known local mean velocity will imply a unique value of an effective integral scale length associated with the simulated flow at that point. This then provides the second parameter from which to determine the simulation scale factor.

On the basis of the integral length scale derivations of the scaling factor, an overall scale factor appropriate to the lower layers of the simulated urban boundary layer of 1:350 was suggested by Lee (1977), for this simulation. When this overall scale factor is applied to the measured roughness length of 3.0mm, an equivalent full scale value of 1.05m is obtained. This value is compatable with the range of values of roughness length from 0.65m to 1.2m suggested by ESDU (1972) for the centres

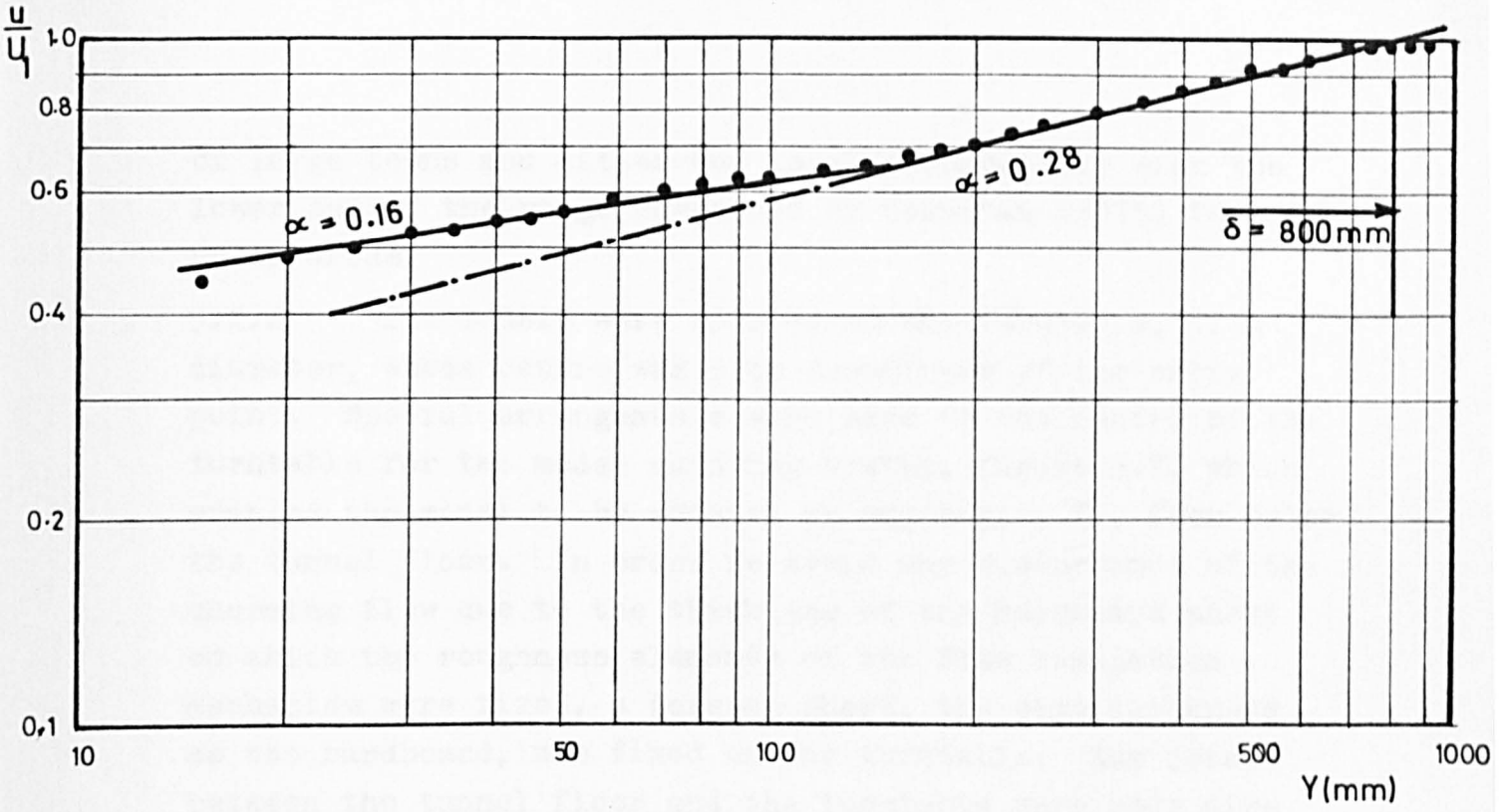

FIGURE 5.6 INCIDENT FLOW PROFILE AT THE TURNTABLE CENTRE, POWER LAW FORM.

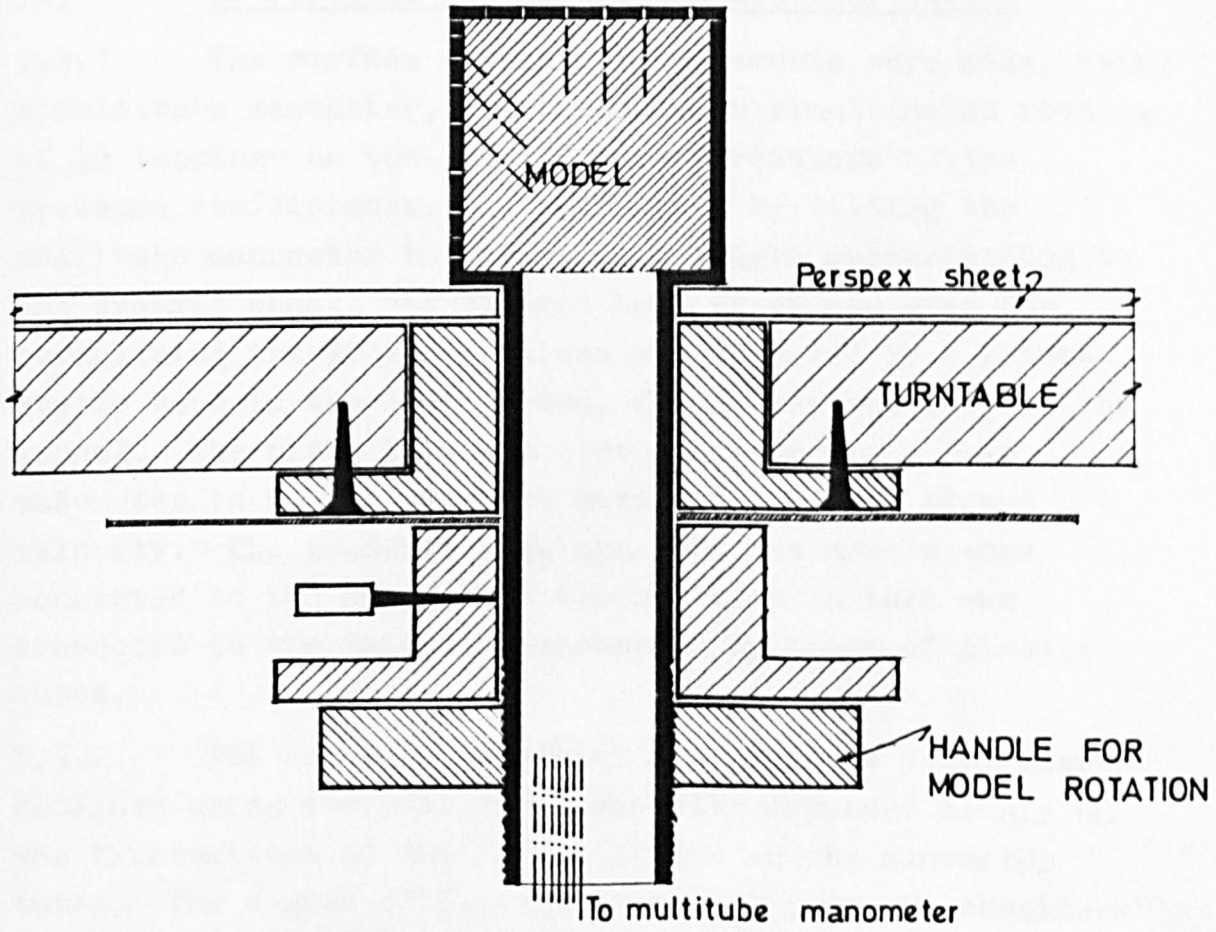

FIGURE 5.7 MODEL MOUNTING SYSTEM

of large towns and cities and is also compatible with the lower end of the range suggested by Counihan (1975) for urban areas.

5.2.6 The models were mounted on the turntable, 1.1m diameter, whose centre was 5.4m downstream of the entry point. Special arrangements were made at the centre of the turntable for the model mounting system, Figure 5.7, which enabled the model to be rotated to any angle, θ , from below the tunnel floor. In order to avoid any disturbance of the oncoming flow due to the thickness of the hardboard sheet on which the roughness elements of the flow simulation mechanism were fixed, a perspex sheet, the same thickness as the hardboard, was fixed on the turntable. Any joints between the tunnel floor and the turntable were made air-tight with sellotape.

5.3 Measurement techniques and accuracy levels

5.3.1 The surface pressure measurements were made, using a multitube manometer, which enabled a simultaneous reading of 33 tappings on the model. Direct readings of the pressure coefficients, C_p, were taken by tilting the multitube manometer to give a unit length corresponding to the dynamic head. The dynamic head which was used for normalising the pressure values was measured by a pitot-static tube in the free stream, fixed from the roof of the tunnel. The pitot tube was also connected to a Betz manometer to keep a constant watch on the free stream velocity. The pressure tappings from the models were connected to the hypodermic tubing which in turn was connected to the multitube manometer by means of plastic tubes.

5.3.2 The accuracy levels of the pressure measurements obtained using the multitube manometer depended mainly on the fluctuations of the liquid levels in the manometer tubes. The degree of fluctuations was, however, considerably reduced by using long hypodermic tubes as well as by

inserting the dampers in the plastic tubes. The fluctuations of the liquid levels in the manometer tubes were found to be different on either faces of the model and depended largely on the group density. As a result of this, the accuracy level would also be expected to be different. Therefore higher accuracy levels $\pm$ 2% would be expected at higher densities and an accuracy level of $\pm$ 5% would be anticipated at lower density groups.

5.3.3 In the initial stages of the investigation, the mean velocity profile measurements were made by a Betz manometer using a pitot tube. The vertical traversing of the pitot tube was done manually. Due to the shape of the pitot tube as well as the uncertainty of flow direction and high turbulence levels within the roughness elements, the velocities in the portion below the element crest could not be measured.

In the later stages, where higher accuracy levels were required and the portion of the velocity profile below the element crest was to be measured, a DISA constant temperature hot wire anemometer, type 55M01, fitted with a straight miniature probe model 55P11 was used. For the purposes of traversing the hot wire probe vertically over the turntable, an automatically controlled traversing mechanism was used which enabled the operator to control the vertical steps of the traverse in the range of 2 to 30mm as well as the time delay between steps in the range of 10 - ∞ seconds. This traversing mechanism was already available in the department. The signals from the hot wire, at the end of each vertical step of the traverse mechanism, were fed into the anemometer which was in turn connected to a digital voltmeter. At each point in the velocity profile, 5 readings of the hot wire output were taken at 2 second intervals, the average value was then used for the calculation of the mean velocity at that point. Figure 5.8 show the experimental set up used for the pressure measurements as well as the mean velocities. Figure 5.9

FIGURE 5.3 A PHOTOGRAPH OF THE EXPERIMENTAL SET UP

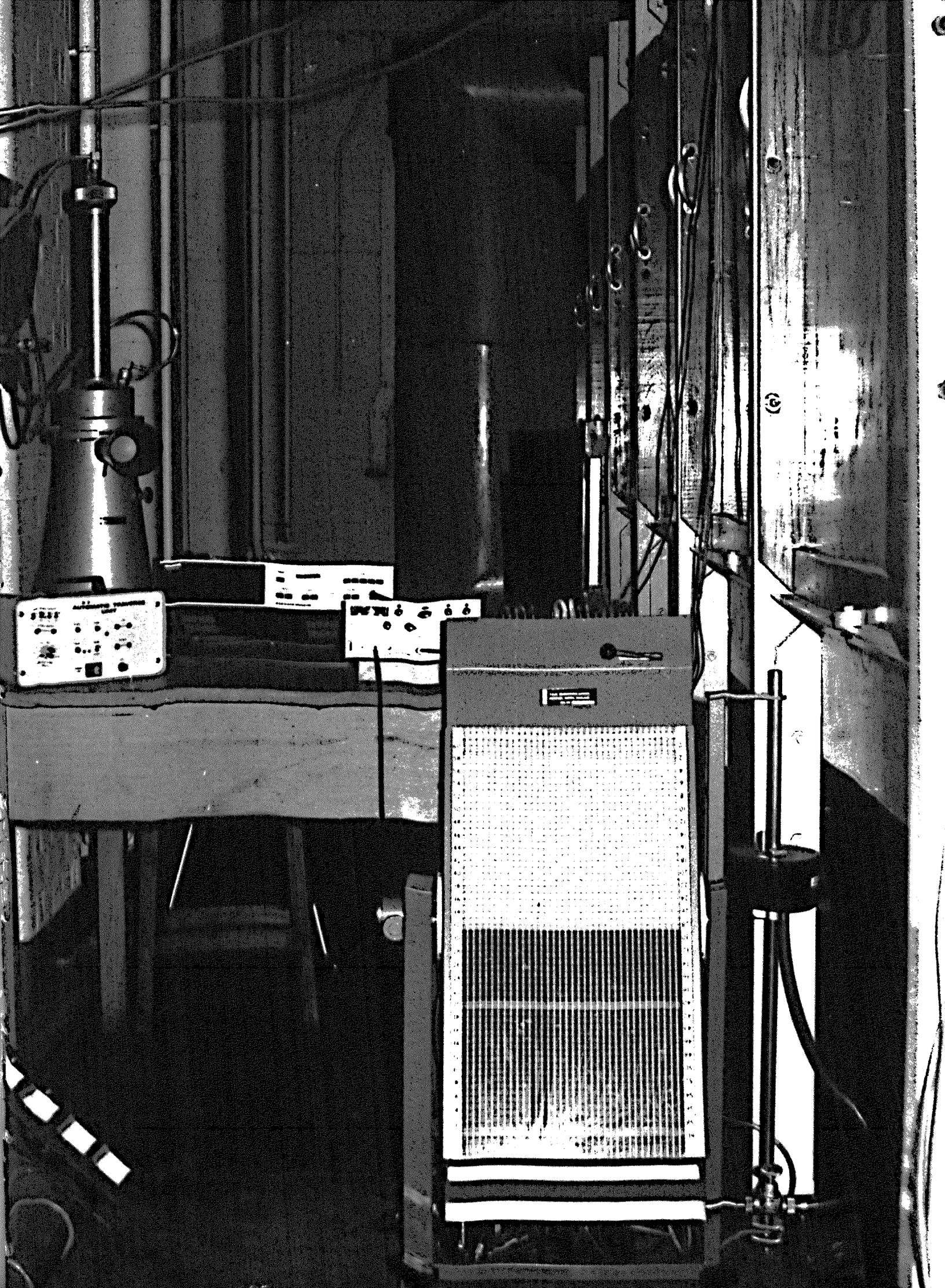

FIGURE 5.3 A PHOTOGRAPH OF THE EXPERIMENTAL SET UP

FIGURE 5.9 A PHOTOGRAPH OF TRAVERSE MECHANISM ON ROOF OF THE WIND TUNNEL

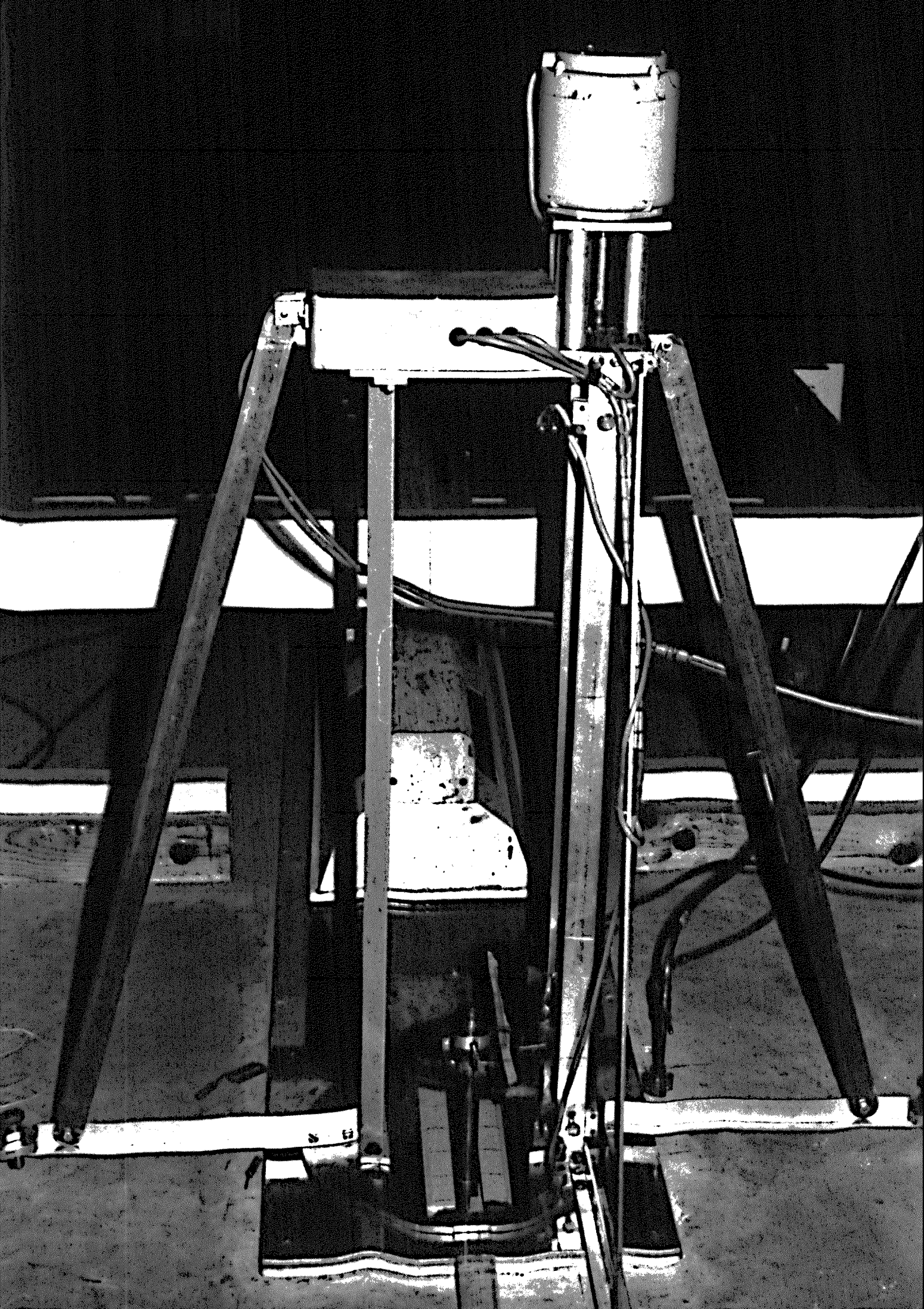

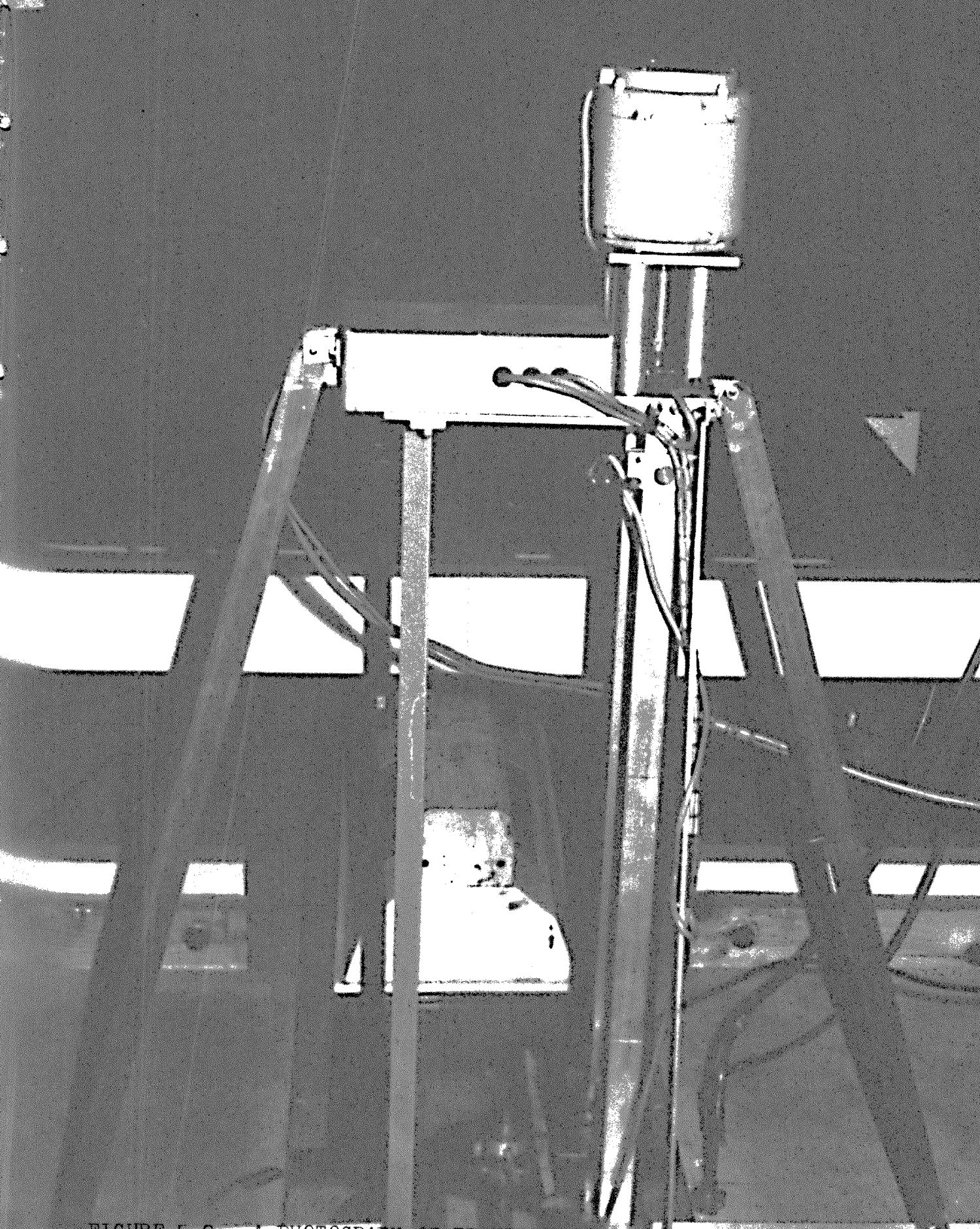

FIGURE 5.9 A PHOTOGRAPH OF TRAVERSE MECHANISM ON ROOF OF THE WIND TUNNEL

shows the traversing mechanism on the roof top of the wind tunnel.

5.3.4 Neglecting the fluctuating components of the flow due to turbulence, hence its corresponding fluctuating voltage output, the response of a hot wire placed normal to the flow may be described by the King's law as follows:

$$E^2 = E_o^2 + B\sqrt{u} \qquad (5.2)$$

where E is the mean bridge voltage of the anemometer at any point and u is the mean velocity at that point. E_o is the mean bridge voltage of the anemometer at zero velocity and is thus constant and B is also a constant independent of the flow velocity. Similarly at the free stream velocity:

$$E_f^2 = E_o^2 + B\sqrt{U_1} \qquad (5.3)$$

where E_f and U_1 are the mean bridge voltage of the anemometer and the mean velocity in the free stream. dividing equation 5.2 by 5.3:

$$\left[\frac{E^2 - E_o^2}{E_f^2 - E_o^2}\right]^2 = \frac{u}{U_1} \qquad (5.4)$$

Let $\Delta E = \dfrac{E^2 - E_o^2}{E_f^2 - E_o^2}$

$$u = U_1 \times \Delta E^2 \qquad (5.5)$$

The value of the freestream velocity, U_1, was found by means of a pitot tube placed in the free stream, connected to a Betz manometer, while the mean bridge voltages of the anemometer at various points were found by the output of the hot wire. Thus the mean velocity at each vertical step of the traverse mechanism was calculated from equation 5.5.

5.3.5 In an earlier investigation, Soliman (1976) used an x-configuration hot wire probe type 55P63 for the measurements of velocity profiles in arrays of 20mm cubes at various densities. From these measurements he found the velocity component in the vertical direction, v, alongwith the mean velocity in the wind direction, u, using Dean's (1974) method. Table 5.1 gives the measurements of both the components of the velocity made by Soliman in his investigation of flow over cubes for an 8% density in the normal layout pattern. In almost all cases, he found the vertical component of the velocity too small to be of any significance in the results. On the basis of his results, a straight wire miniature probe was used and only the mean velocity in the horizontal direction was measured in the present investigation.

Table 5.1 Velocity profile measurements for 8% density in normal pattern, Soliman (1976)

Height mm.	u m/s	v m/s	v/u
4	4.0764	0.0623	0.0153
8	5.0670	-0.5738	-0.1132
12	5.0386	0.3387	0.0672
16	6.4623	0.1427	0.0221
20	7.4968	-0.4215	-0.0562
24	10.4690	-0.5444	-0.0520
28	13.0571	-0.1441	-0.0110
32	13.8671	0.0879	0.0063
36	14.3211	0.1625	0.0113
40	16.2322	0.4501	0.0277
44	15.9077	0.1822	0.0115
48	16.0844	-0.3521	-0.0219
54	17.5063	0.3766	0.0215

5.3.6 Due to the manual traversing of the pitot tube for the measurements of velocity profiles in the early stages of the experiments in chapter 7, the magnitude of error in the positioning of the tube could be estimated to be $\pm$ 10%. In the later phases of the experimental investigations when the flow velocity measurements were made using the hot wire anemometer, the overall accuracy limits for the velocity profiles are estimated to be $\pm$ 5%. In the lower part of the velocity profiles, however, the measurements made between the roughness elements are thought to be less accurate owing to the high levels of turbulence. The accuracy limits here are estimated to be $\pm$ 10%.

5.4 Ranges of parameter considered and the details of models

5.4.1 The pressure tapped model used in the first two phases of the investigation was the cube having a side dimension of 36mm, made from brass and was machined to give sharp edges. The other models used in the subsequent phases were made from aluminium. The windward pressure coefficient measurements were made from tappings on one face of the models which could be rotated through an angle of $\pm$ 180^{o} to get the measurements on the leeward face. The tappings on the roof of models were used to get the surface pressure measurements on the roof. All models had a different number of pressure tappings distributed on the vertical face and the roof of models. The maximum number of tappings on any model was 33. The pressure tappings were connected to hypodermic tubing gauge 19, 0.648mm inside diameter which were made flush with the faces of models. The hypodermic tubes were in turn connected to the multitube manometer by plastic tubes.

5.4.2 The instrumented models were accurately machined to give the exact size and sharp edges and corners. The

surrounding building models used for the array, made from wood, were nominally identical to the instrumented models in every phase of the investigations. Accurately sized hardwood models were used immediately around the model, while less accurate blocks were used for the remainder of the roughness element layout. As the surrounding blocks could not be made as exact in size as the instrumented models, this may well have resulted in an error of $\pm$ 5%. Other sources of error might possibly have arisen from the accuracy with which the roughness elements could be positioned in the model group. This positioning error of $\pm$ 5% would tend to cancel out in a large element array. Double coated, adhesive tape was used to hold the surrounding blocks in position.

5.4.3 The instrumented models were kept at the centre of the turntable which also formed the centre of the group in this parametric study. The following variations of parameters were considered in various phases of this investigation, see Figure 5.10.

a) The building group density, defined by plan area, was varied from $2.5\% < \lambda_p < 60.0\%$ for various models.

b) The building group pattern i.e. the normal and the staggered layout patterns.

c) The building group layout size, R/H, was varied from 3 to 145.

d) The incident flow direction was kept constant at $\theta = \phi = 0$ for the whole of the investigation.

5.4.4 In order to cover most of the building forms which occur in practical life, the following variations of model shapes were studied, Figure 5.10.

a) Since the cube is the only three dimensional rectangular body form that is characterised by a single dimension, it was chosen for a very extensive parametric study. This study is then

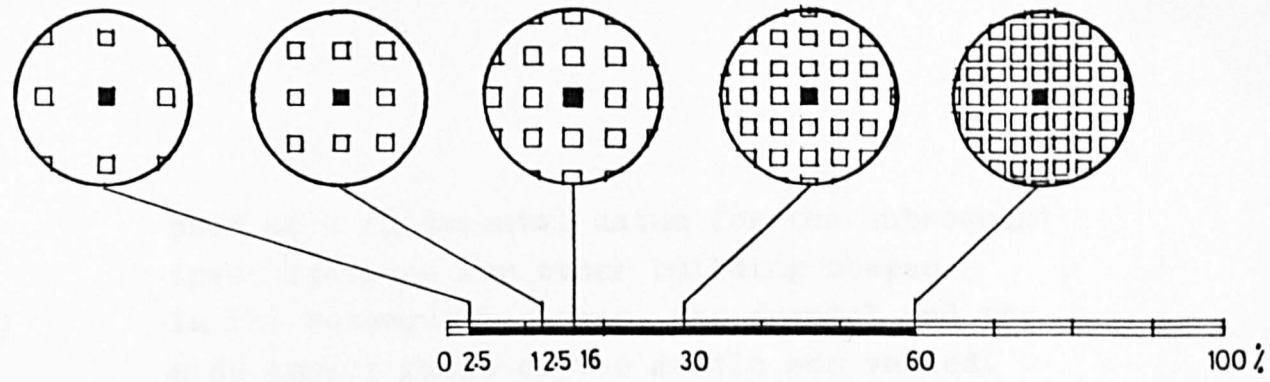

○ GROUP DENSITY

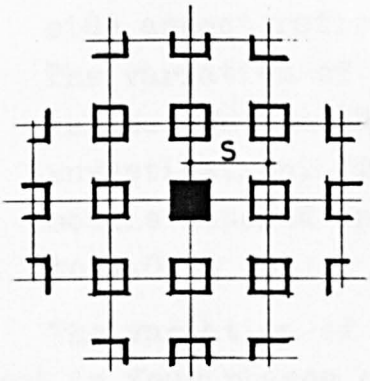

Normal pattern

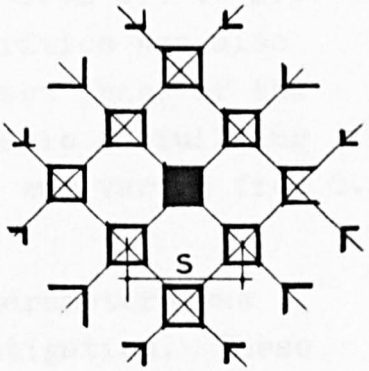

Staggered pattern

○ LAYOUT PATTERN

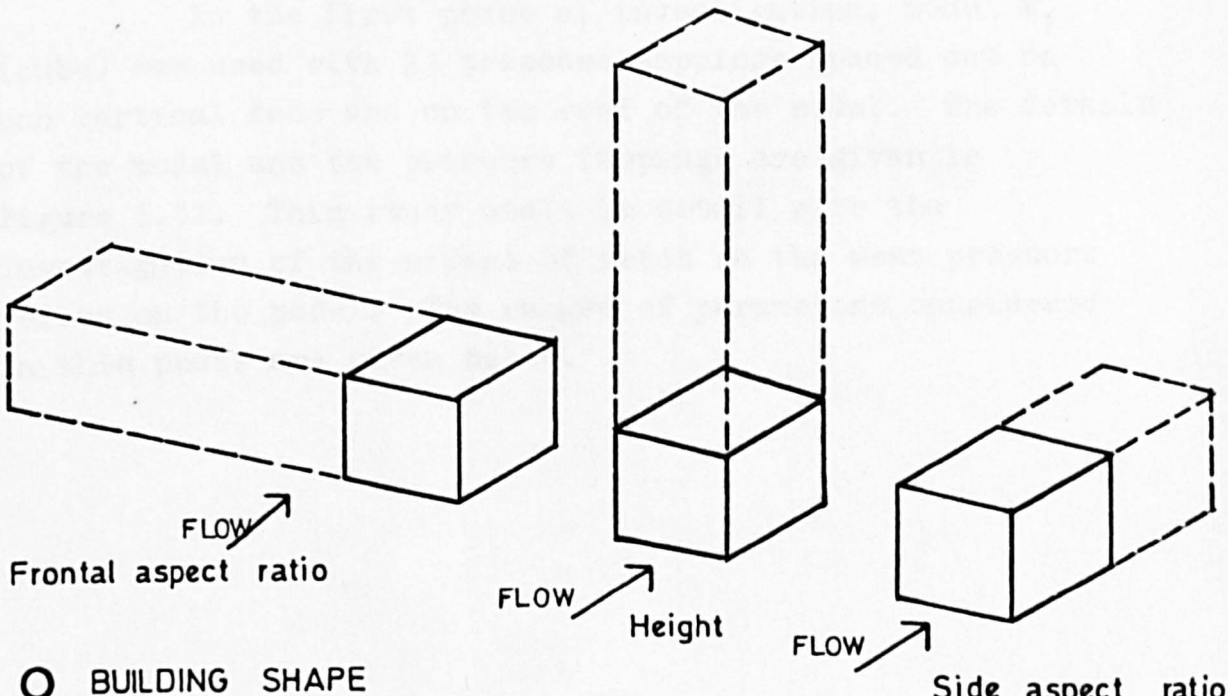

○ BUILDING SHAPE VARIATION

FIGURE 5.10 THE PARAMETERS CONSIDERED IN THE PRESENT STUDY

used as a fundamental datum for the subsequent investigations for other building shapes.

b) In the subsequent phases, the frontal and the side aspect ratio of the models was varied. The cube was taken to be having both the frontal as well as the side aspect ratio of 1 and other building models were related to it. The frontal aspect ratio was varied from 0.5 to 4.0 and the side aspect ratio was varied from 0.5 to 2.0.

c) The variation of the height ratios was also related to the cube in the last phase of the investigation. The height ratio of building models studied in this phase was varied from 0.5 to 4.0.

5.4.5 The variation of the above parameters was considered in four phases of the investigation. These phases alongwith the details of models and their pressure tappings are given below in the sequence in which the results are presented in the subsequent chapters.

In the first phase of investigation, model M_1 (cube) was used with 33 pressure tappings spaced out on one vertical face and on the roof of the model. The details of the model and the pressure tappings are given in Figure 5.11. This study dealt in detail with the investigation of the effect of fetch on the mean pressure forces on the model. The ranges of parameters considered in this phase are given below.

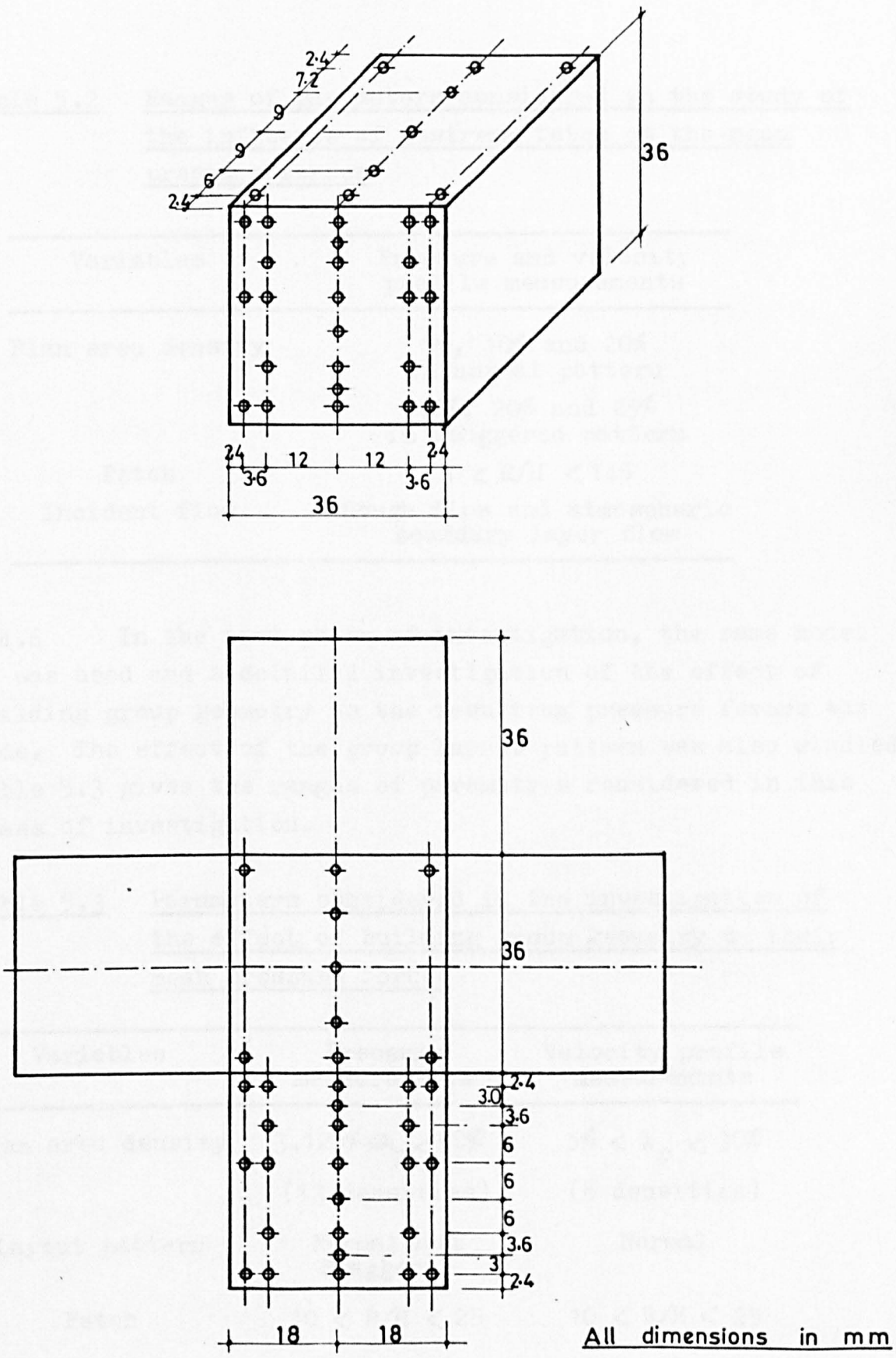

FIGURE 5.11 DETAILS OF PRESSURE TAPPINGS ON MODEL M_1 (THE CUBE)

Table 5.2 Ranges of parameters considered in the study of the influence of upstream fetch on the mean pressure forces

Variables	Pressure and velocity profile measurements
Plan area density	5%, 10% and 20% in normal pattern 10%, 20% and 25% in staggered pattern
Fetch	$3 < R/H < 145$
Incident flow	Rough flow and atmospheric boundary layer flow

5.4.6 In the next phase of investigation, the same model M_1 was used and a detailed investigation of the effect of building group geometry on the resulting pressure forces was made. The effect of the group layout pattern was also studied. Table 5.3 gives the ranges of parameters considered in this phase of investigation.

Table 5.3 Parameters considered in the investigation of the effect of building group geometry on their mean pressure forces

Variables	Pressure measurements	Velocity profile measurements
Plan area density	$3.125\% < \lambda_p < 50\%$ (13 densities)	$5\% < \lambda_p < 30\%$ (8 densities)
Layout pattern	Normal and Staggered	Normal
Fetch	$10 < R/H < 25$	$10 < R/H < 25$
Incident flow	Atmospheric Boundary Layer Flow	Atmospheric Boundary Layer Flow

5.4.7 In the third phase of investigation, various models of plan form variations were used to investigate the effect of varying the frontal and the side aspect ratios of models on their resulting pressure forces. Four different models M_{101} - M_{104} of varying frontal aspect ratios were used. These were of frontal aspect ratios of 0.5, 1.5, 2.0 and 4.0 respectively. The details of the models alongwith the distributions of the pressure tappings are given in Figure 5.12. Three models, M_{201} - M_{203} of different side aspect ratios of 0.5, 1.5 and 2.0 were also used. The details are given in Figure 5.13. Table 5.4 gives the variables considered.

Table 5.4 Parameters considered in the investigation of the effect of plan form variations of models on their resulting pressure forces

Variables	Pressure measurements	Velocity profile measurements
Frontal aspect ratio	0.5 to 4.0	2.0
Side aspect ratio	0.5 to 2.0	-
Plan area density	$2.5 < \lambda_p < 60.0$ (At least 15 densities in each case)	$5\% < \lambda_p < 40\%$ (7 densities)
Layout pattern	Normal	Normal
Fetch	$10 < R/H < 25$	10 R/H 25
Incident flow	Atmospheric boundary layer flow	Atmospheric boundary layer flow

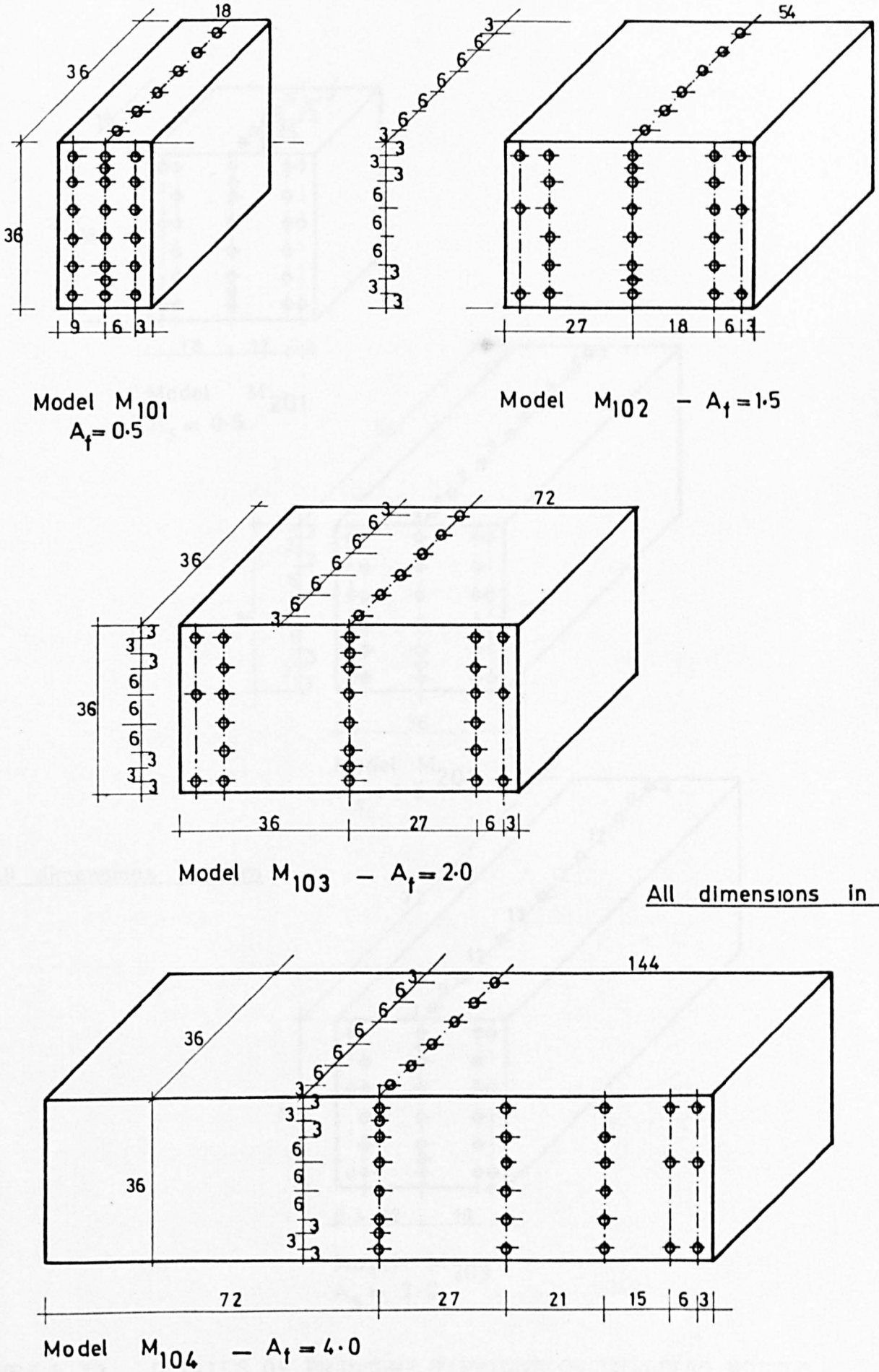

Model M_{101} $A_f = 0.5$

Model M_{102} — $A_f = 1.5$

Model M_{103} — $A_f = 2.0$

All dimensions in mm

Model M_{104} — $A_f = 4.0$

FIGURE 5.12 DETAILS OF PRESSURE TAPPINGS ON BUILDING MODELS WITH VARYING FRONTAL ASPECT RATIO

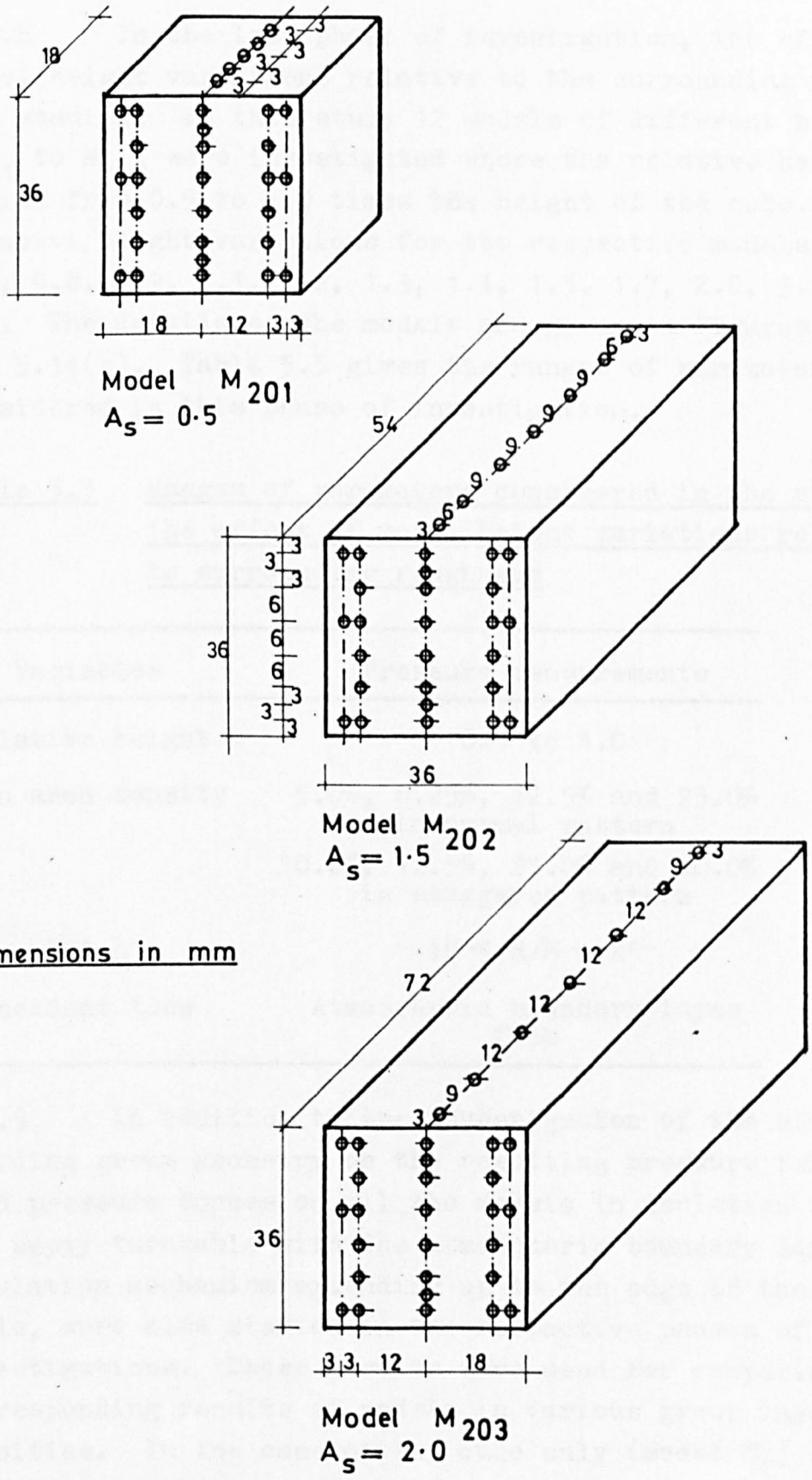

FIGURE 5.13 DETAILS OF PRESSURE TAPPINGS ON BUILDING MODELS WITH VARYING SIDE ASPECT RATIOS

5.4.8 In the last phase of investigation, the effect of model height variations relative to the surrounding roughness was studied. In this study 12 models of different heights, M_{301} to M_{312} were investigated where the relative height varied from 0.5 to 4.0 times the height of the cube. The relative height variations for the respective models were 0.5, 0.8, 0.9, 1.1, 1.2, 1.3, 1.4, 1.5, 1.7, 2.0, 3.0 and 4.0. The details of the models are given in Figures 5.14(a) and 5.14(b). Table 5.5 gives the ranges of parameters considered in this phase of investigation.

Table 5.5 Ranges of parameters considered in the study of the effect of model height variations relative to surrounding roughness

Variables	Pressure measurements
Relative height	0.5 to 4.0
Plan area density	5.0%, 6.25%, 12.5% and 25.0% in normal pattern
	10.0%, 12.5%, 25.0% and 40.0% in staggered pattern
Fetch	$10 < R/H < 25$
Incident flow	Atmospheric boundary layer flow

5.4.9 In addition to the investigation of the effects of building group geometry on the resulting pressure forces, the wind pressure forces on all the models in isolation placed on the empty turntable with the atmospheric boundary layer simulation mechanism extending up to the edge of the turntable, were also studied in the respective phases of investigations. These results were used for comparing the corresponding results of models in various group layout densities. In the case of the cube only (model M_1) detailed pressure measurements were also made in a smooth wall boundary layer which resulted from the air flow in an empty wind tunnel.

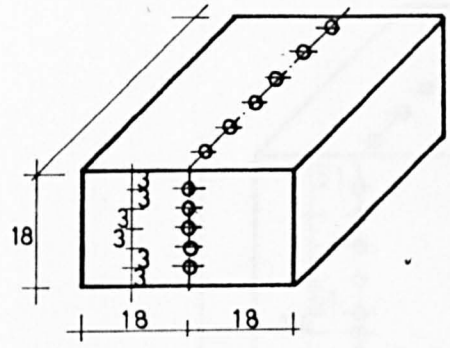

Model M_{301}
h = 0·5

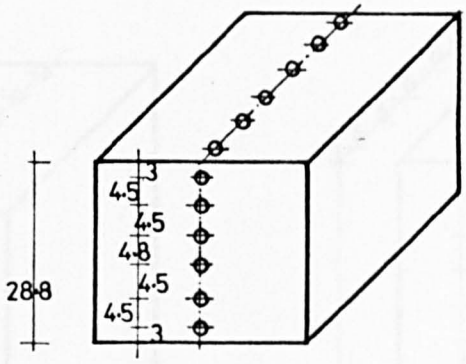

Model M_{302}
h = 0·8

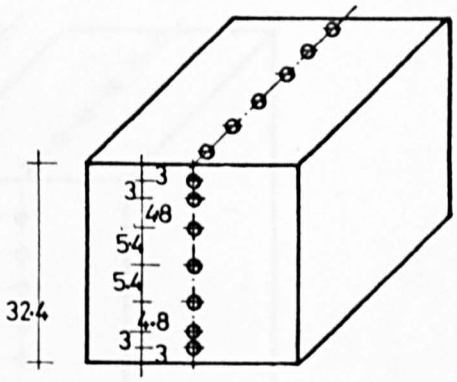

Model M_{303}
h = 0·9

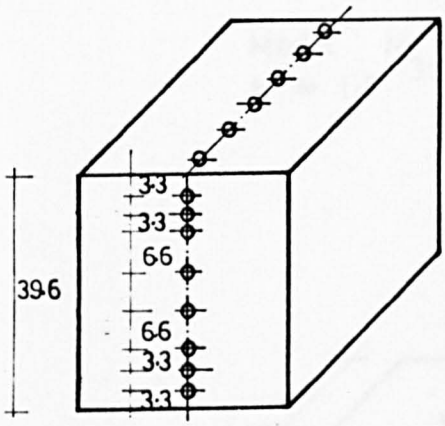

Model M_{304}
h = 1·1

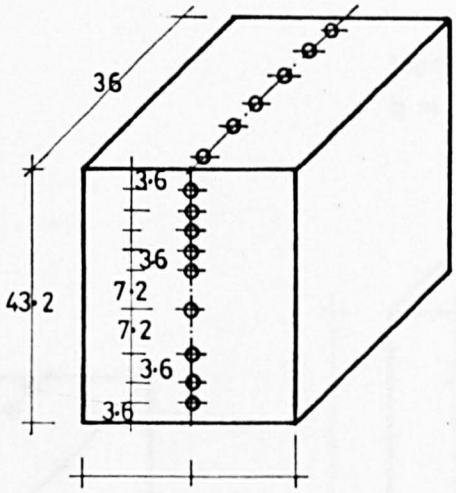

Model M_{305}
h = 1·2

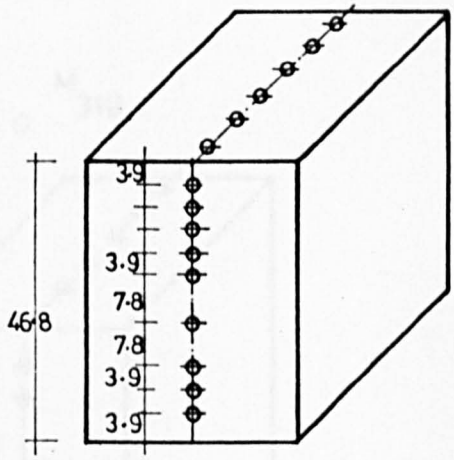

Model M_{306}
h = 1·3

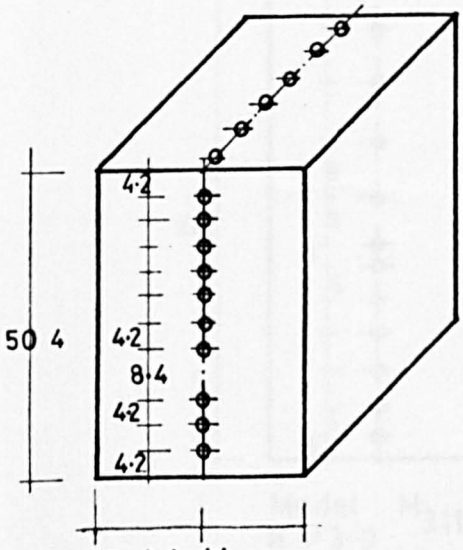

Model M_{307}
h = 1·4

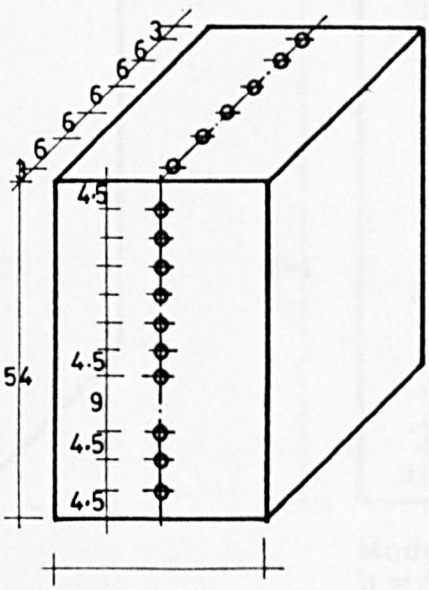

Model M_{307}
h = 1·5

All dimensions in mm

FIGURE 5.14 DETAILS OF PRESSURE TAPPINGS ON MODELS OF VARYING HEIGHT RATIOS

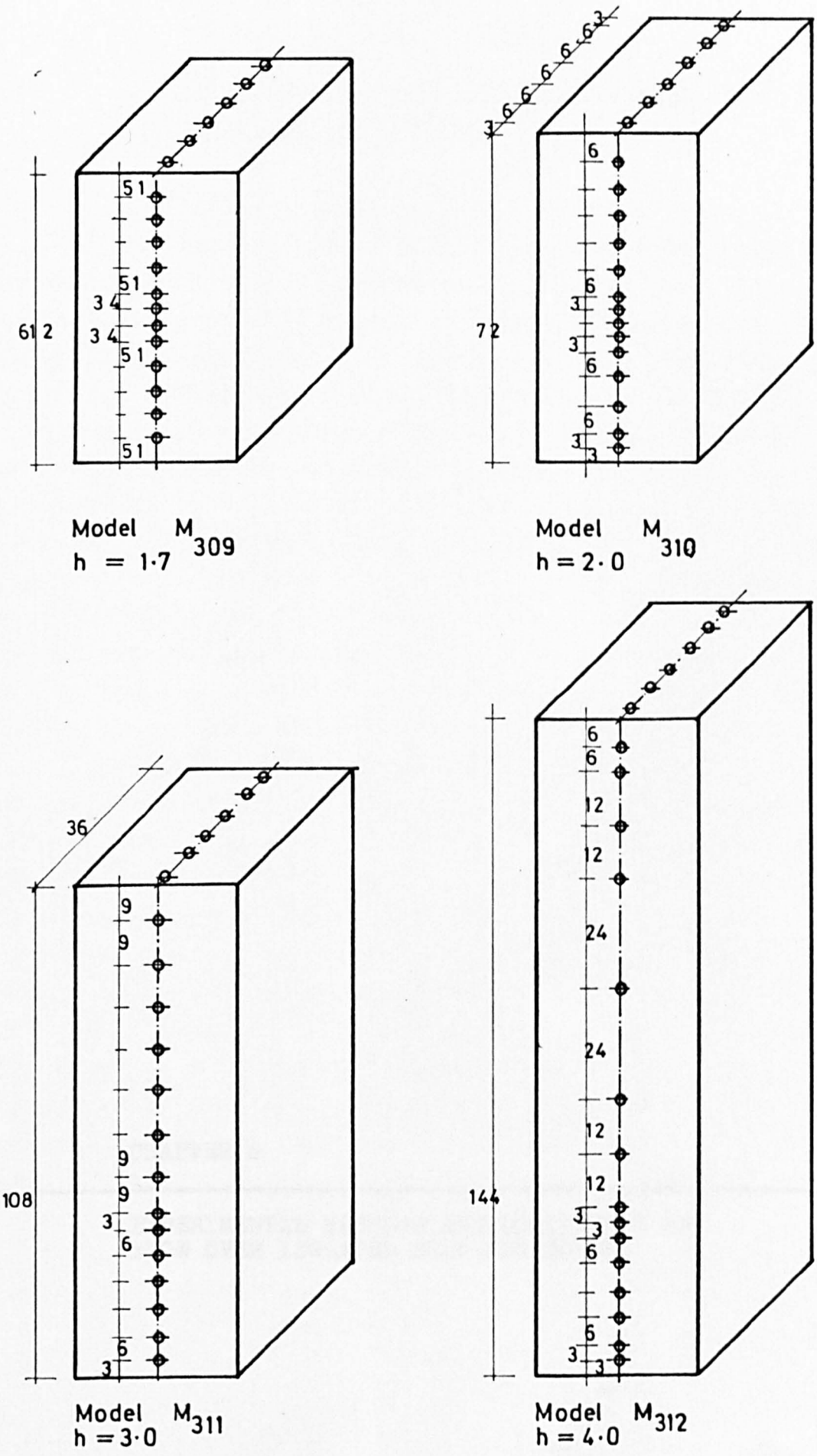

FIGURE 5.14 DETAILS OF PRESSURE TAPPINGS ON MODELS OF VARYING HEIGHT RATIOS

CHAPTER 6

EXPERIMENTAL RESULTS AND DISCUSSION OF FLOW OVER ISOLATED BUILDING MODELS

6. EXPERIMENTAL RESULTS AND DISCUSSION OF FLOW OVER ISOLATED BUILDING MODELS

6.1 Introduction

6.1.1 There has been a significant increase in the study of bluff body aerodynamics in recent years, though the attention of most research workers has been directed to the flow around two dimensional bodies. Such studies are often regarded as a datum for assessing the effects of incident flow variations on the body. On the contrary, however, the flow around three dimensional bodies, has received relatively little attention. Most of the work done on flow over three dimensional bluff bodies has been restricted to isolated cube shaped elements either in smooth or in rough flows without any consideration to the upwind effects appropriate to full scale conditions. Castro and Robins (1977) and Yu (1975) studied the flow around an isolated surface mounted cube in uniform and turbulent streams. Arrays of different building shapes, on the other hand, have been considered in only a few cases. Bailey and Vincent (1943) and Norton and Oldham (1975) investigated the wind pressure forces on buildings of various shapes both in isolation and in groups of two or three bodies. Although the grouping of structures should be considered for practical design purposes, the case of an isolated roughness element is, nevertheless, important as a fundamental datum on such cases. In this chapter, the wind pressure forces and the flow around isolated models of various shapes are investigated. The study starts with the investigation on the cube before going to other model forms. The results of the investigation made on the cube are taken as a reference in the subsequent studies.

6.2 The flow around an isolated cube

6.2.1 Detailed pressure measurements, on an isolated cube, were made in a smooth as well as a simulated atmospheric boundary layer flow. This was the only case in which the model was tested in a smooth wall boundary layer, which resulted from the air flow in an empty wind tunnel. An example of the pressure coefficient distributions on the centre line of both the windward and leeward faces of the cube are shown in Figure 6.1 for an orientation angle $\theta = 0$. The mean windward and leeward pressure coefficients, C_{pw} and C_{pb}, were calculated from these pressure distributions, the algebraic difference of these, then yields the drag coefficient, C_{D_1}. The mean lift coefficient, C_{L_1}, was calculated by the integration of pressure coefficient distributions on the roof, also shown in Figure 6.1.

6.2.2 It is clear from Figure 6.1 that the pressure forces on an isolated cube are reduced drastically in the atmospheric shear flow compared with the smooth wall boundary layer flow. This is thought to be due to the change in the ratio of boundary layer thickness, δ, to that of the element height, H, which is increased from 4 in the smooth flow to 22 in the atmospheric shear flow. Similar observations were also reported by Soliman (1976). In order, therefore, for such results to be applicable to low rise housing, a large discrepancy in the value of $\frac{\delta}{H}$ would result in an inaccurate estimate of the wind forces.

6.2.3 For the purposes of wind load calculations, the pressure coefficients are generally normalised with respect to the velocity at building height, U_H. The pressure coefficient results of the present study were, therefore, normalised with reference to the velocity at cube height, U_H, by multiplying the relevant pressure coefficients by $(U_1/U_H)^2$. These are shown replotted in Figure 6.2 alongwith comparable results for cubes

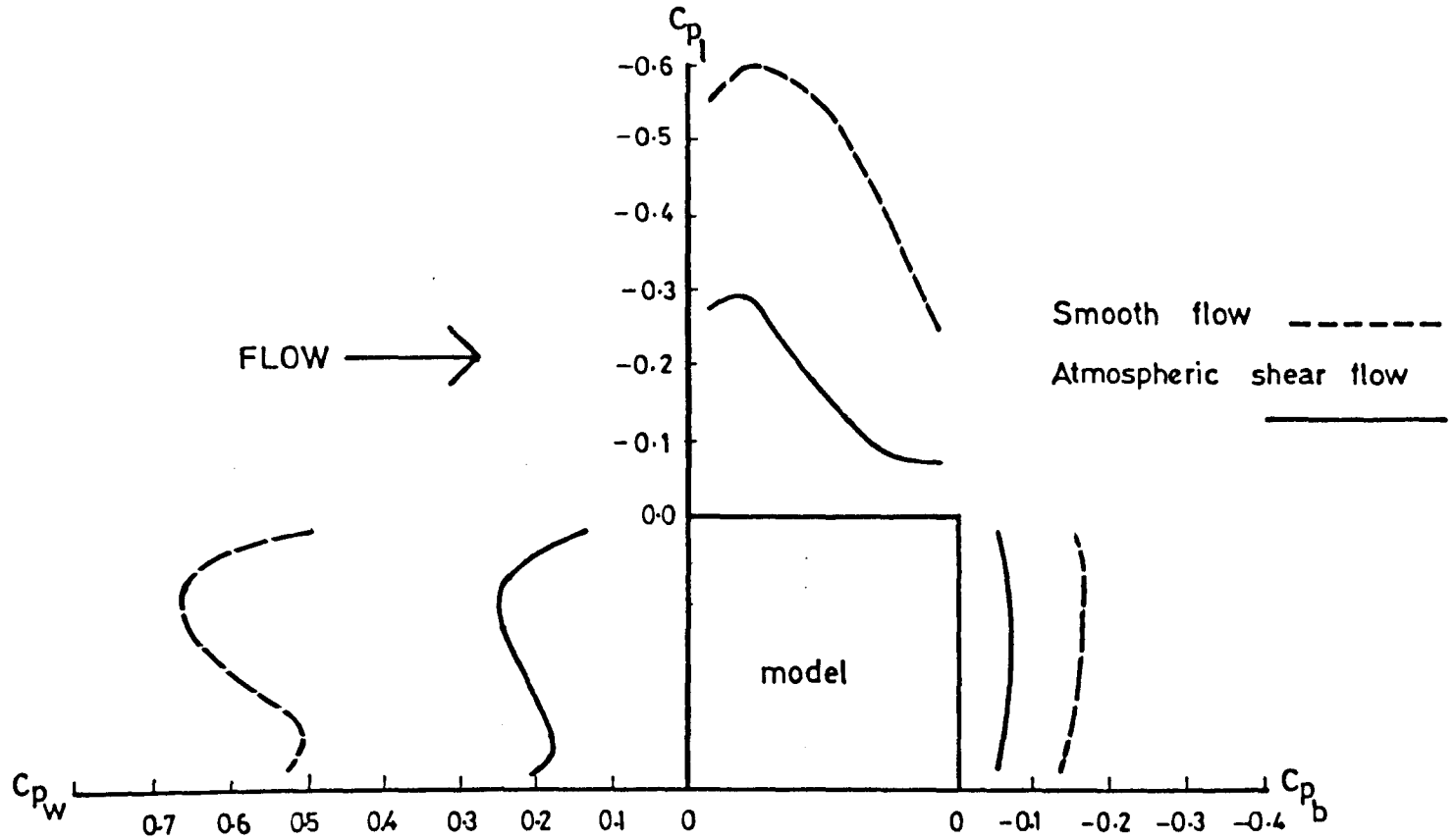

FIGURE 6.1 PRESSURE COEFFICIENT DISTRIBUTIONS ON AN ISOLATED CUBE (BASED ON U_1)

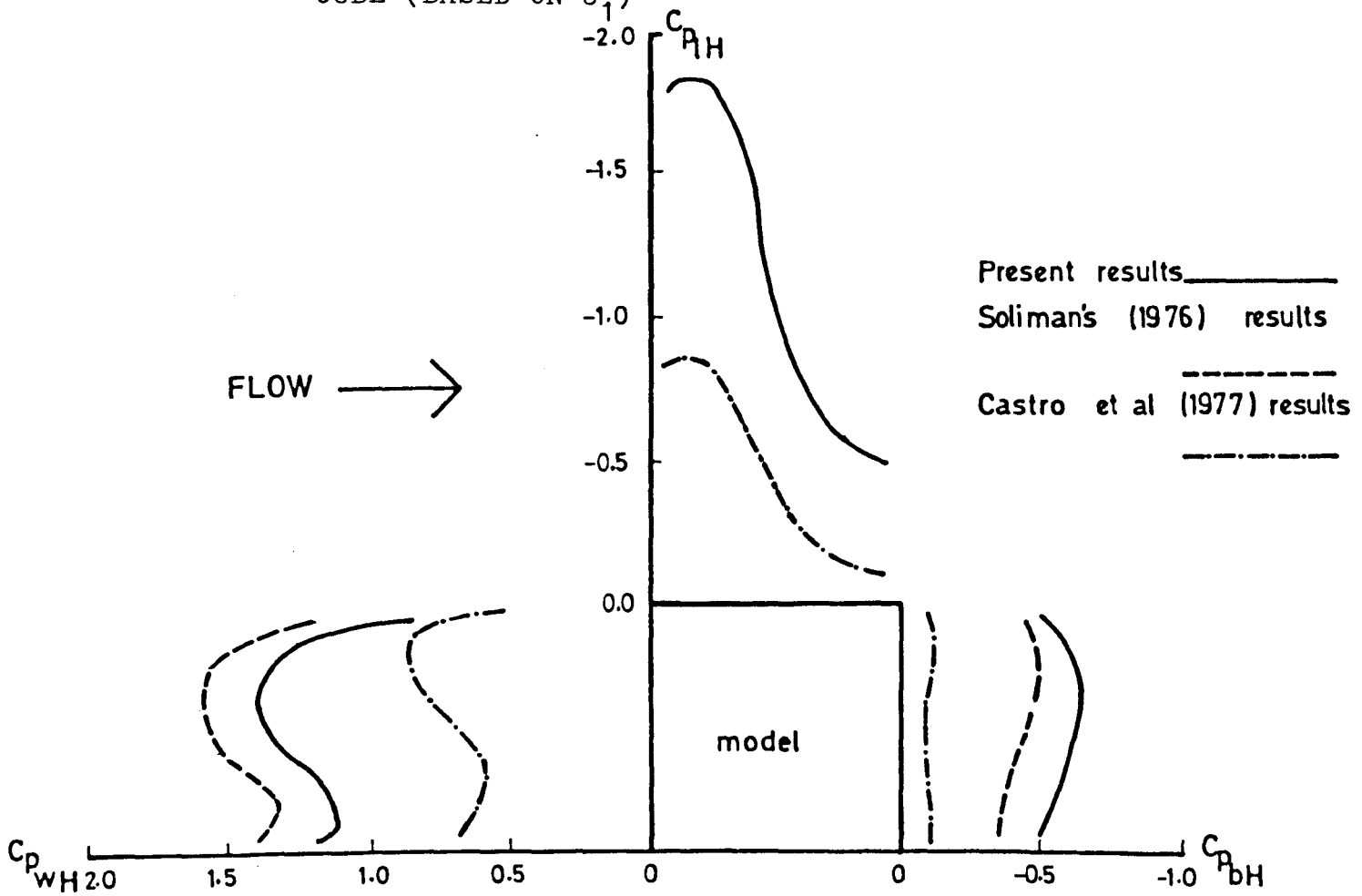

FIGURE 6.2 PRESSURE COEFFICIENT DISTRIBUTIONS ON AN ISOLATED CUBE AND THEIR COMPARISON (BASED ON U_H)

obtained by Soliman (1976) and Castro et al (1977). Soliman performed his experiments in a rough flow obtained from the boundary layer growth on a rough sheet placed upstream of the turntable, the rough sheet consisted of a random layout of wooden blocks. The differing nature of the flows, probably accounts for the difference in magnitude between Soliman's results and the present results. Castro et al on the other hand, in their study of measurements on a surface mounted cube in a thick incident boundary layer flow, formed by vorticity generators and roughness elements, placed their cube, with a side length of 200 mm, $3\frac{1}{2}$ boundary layer heights downstream of the vorticity generators. The roughness elements, which were square blocks 18 mm high, distributed at 25% plan area density with taller blocks 38 mm high, sparsely located in between, surrounded the test model. In such an arrangement, the cube under investigation is not truly isolated and so comparatively, the values, in the present investigation, Figure 6.2, are expected to be higher than those of Castro et al. The most significant aspect of the roof pressure coefficient variation is that the maximum negative pressure occurs very close to the leading edge of the cube and is followed by a region of steep pressure recovery.

The computed values of the drag C_{D_H}, for the present study is 1.57 as compared to 1.76 and 1.1 suggested by Soliman and Castro et al respectively. The corresponding values of C_{D_H} suggested by both the Engineering Science data item, ESDU 71016 and the British Standard Code of Practice is 1.2 which indicates that the use of the code of practice may lead to inaccurate wind loads on low rise buildings.

6.2.4 The three dimensional flow pattern around the isolated cube, as suggested by Yu (1975) seems to substantiate the results of pressure distributions in the present study. This flow pattern around an isolated cube,

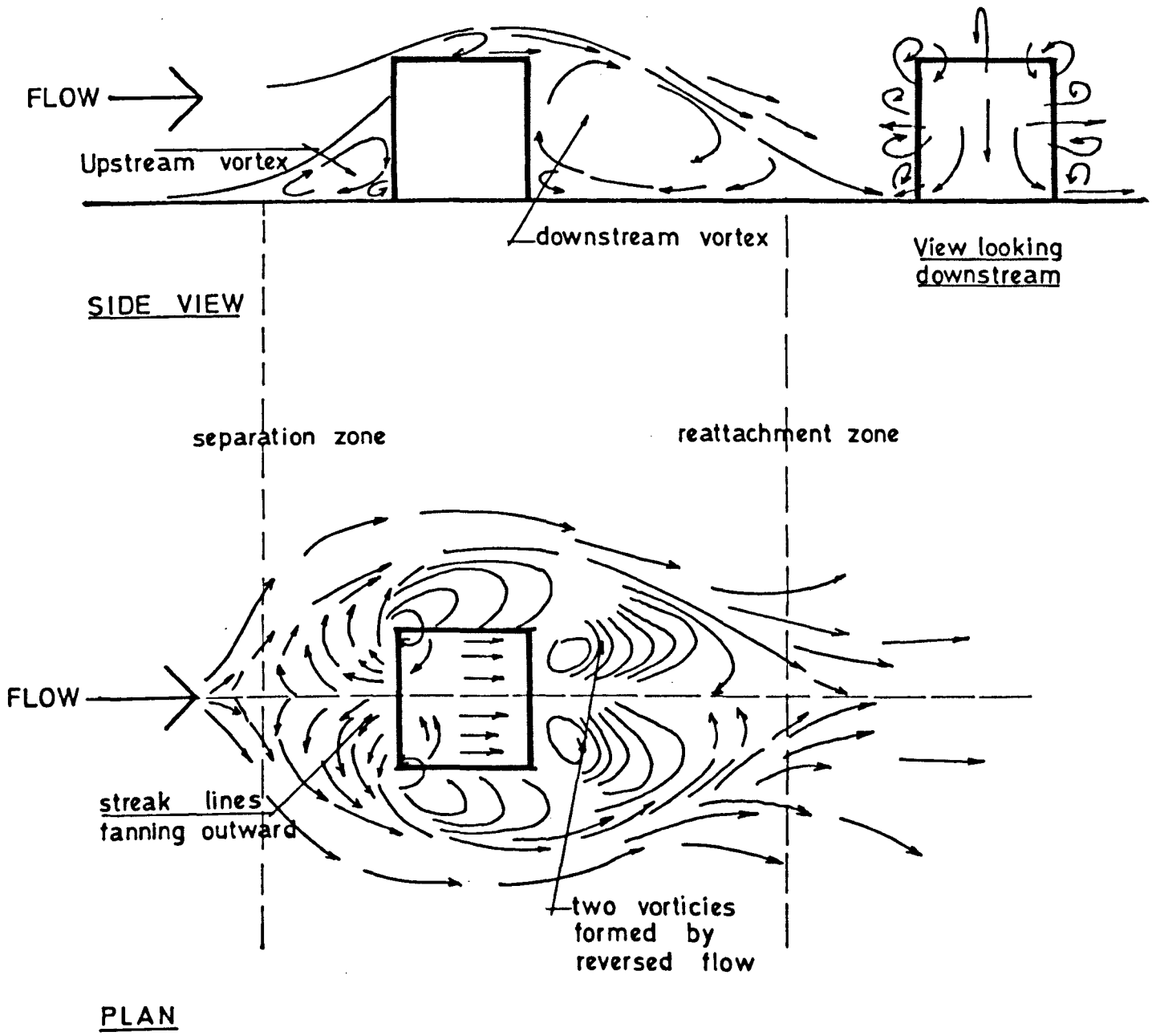

FIGURE 6.3 THE FLOW PATTERN AROUND AN ISOLATED CUBE

given in Figure 6.3, shows an upstream separation region and downstream re-attachment region. The horse shoe vortex which curves round and wraps itself around the model divides the downstream eddy bubble into two vortices forming at the leeward cube wall. The negative pressure near the leading edge of the roof of the model suggests that separation must occur at this edge. The negative pressure, however, starts rising towards the leeward edge almost immediately after the high suction.

6.3 The flow around isolated models of varying heights

6.3.1 The investigations of three dimensional bluff body flows have been restricted to a few ad hoc studies of either low rise or high rise building models. No systematic study on the effect of varying the height from low rise to high rise, is known to the author. This lack of information has led to the adoption of similar values of wind forces on both low rise and high rise buildings, which may be misleading. In this section a detailed study of the flow around isolated models, of square base, equal to the cube, with relative height varying from 0.5 to 4, has been reported. The height ratio of the cube in this study is taken as 1 and all other body heights are related to it. This study intends to indicate a distinction between the low rise and high rise buildings.

6.3.2 The vertical distribution of pressure coefficients measured on the centre line of the windward and leeward faces of various models for an orientation angle $\theta = 0$ are shown in Figure 6.4. These pressure distributions were integrated to give the mean windward and leeward pressure coefficients, $C_{p_{wc}}$ and $C_{p_{bc}}$ and the algebraic difference of these in each case yields the drag coefficient C_{D_c}. The pressure coefficient distributions on the centre line of the roof of the model, Figure 6.5, were integrated to get the lift coefficient, C_{L_1}, in each case.

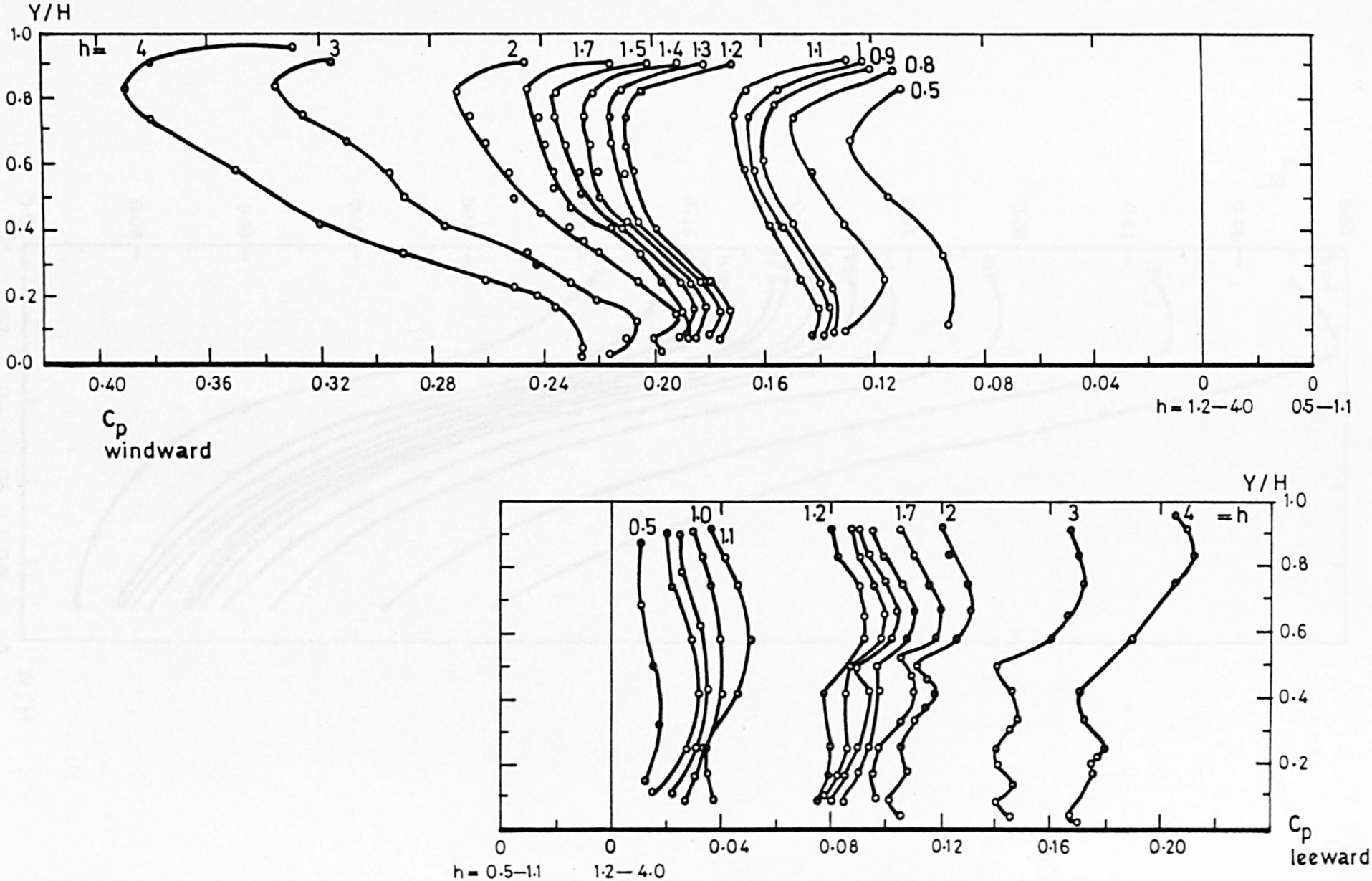

FIGURE 6.4 WINDWARD AND LEEWARD PRESSURE COEFFICIENT DISTRIBUTIONS ON THE CENTRE LINE OF ISOLATED MODELS OF VARYING HEIGHTS

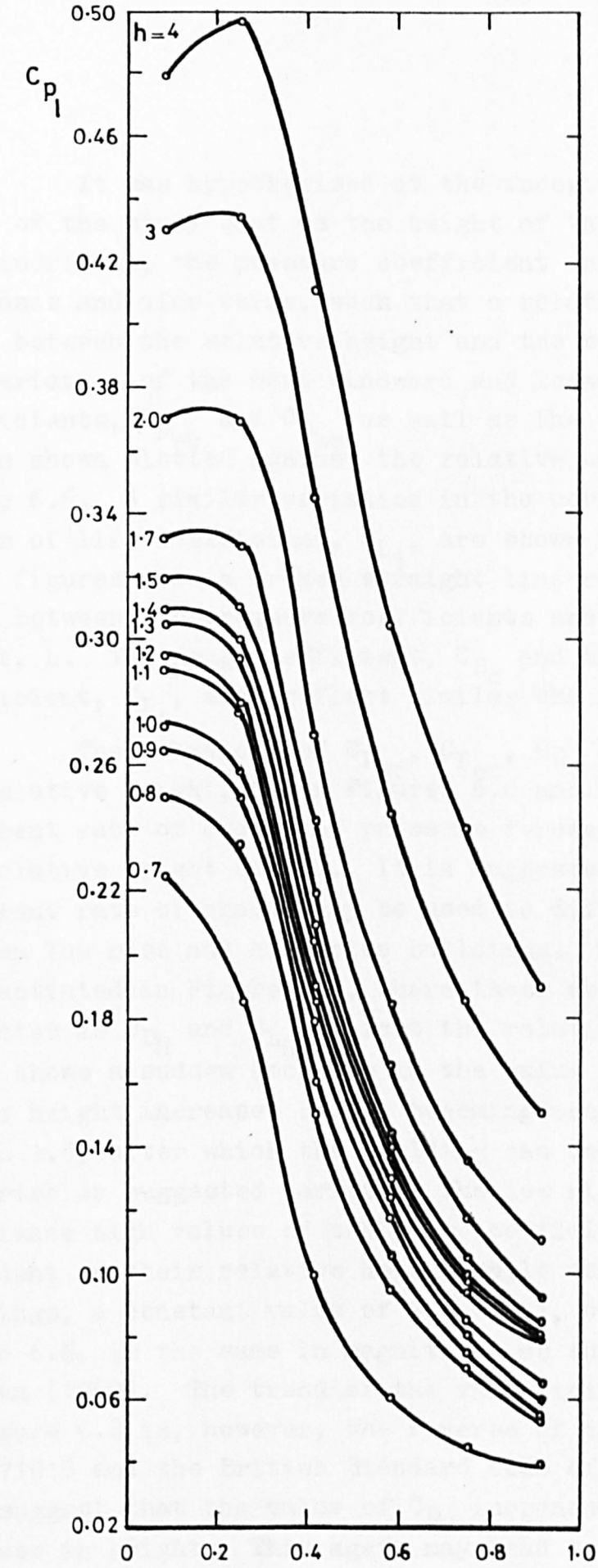

FIGURE 6.5 ROOF PRESSURE COEFFICIENT DISTRIBUTIONS ON ISOLATED MODELS OF VARYING HEIGHTS

6.3.3 It was hypothesised at the inception of this phase of the study that as the height of the individual body increases, the pressure coefficient on the body also increases and vice versa, such that a relationship must exist between the relative height and the pressure forces. The variation of the mean windward and leeward pressure coefficients, $C_{p_{wc}}$ and $C_{p_{bc}}$ as well as the drag coefficient C_{D_c} is shown plotted against the relative height in Figure 6.6. A similar variation in the corresponding values of lift coefficient, C_{L_1}, are shown in Figure 6.7. These figures show a broken straight line relationship to exist between the pressure coefficients and the relative height, h. The drag coefficient, C_{D_c} and the lift coefficient, C_{L_1}, also reflect similar changes.

6.3.4 The behaviour of $C_{p_{wc}}$, $C_{p_{bc}}$, C_{D_c} and C_{L_1} with the relative height, h, in Figures 6.6 and 6.7 show a different rate of change of pressure forces below and above the relative height of 1.6. It is suggested that this different rate of change may be used to differentiate between low rise and high rise buildings. The concept is substantiated in Figure 6.8, where these results have been replotted as C_{D_H} and C_{L_H} against the relative height. The graph shows a sudden decrease in the value of C_{D_H} and C_{L_H} as the height increases before becoming constant at a value of h = 1.6, after which the building can be taken to the high rise as suggested earlier. The low rise buildings experience high values of the drag coefficient, C_{D_H}, dependent on their relative height while for the high rise buildings, a constant value of C_{D_H} = 1.1, obtained from Figure 6.8, is the same in magnitude, as suggested by Jackman (1969). The trend of the variation of C_{D_H} given in Figure 6.8 is, however, the reverse of that given in ESDU 71016 and the British Standard Code of Practice, which noth suggest that the value of C_{D_H} increases with the increase in height. This again may lead to the under-estimation of wind loads on low rise buildings.

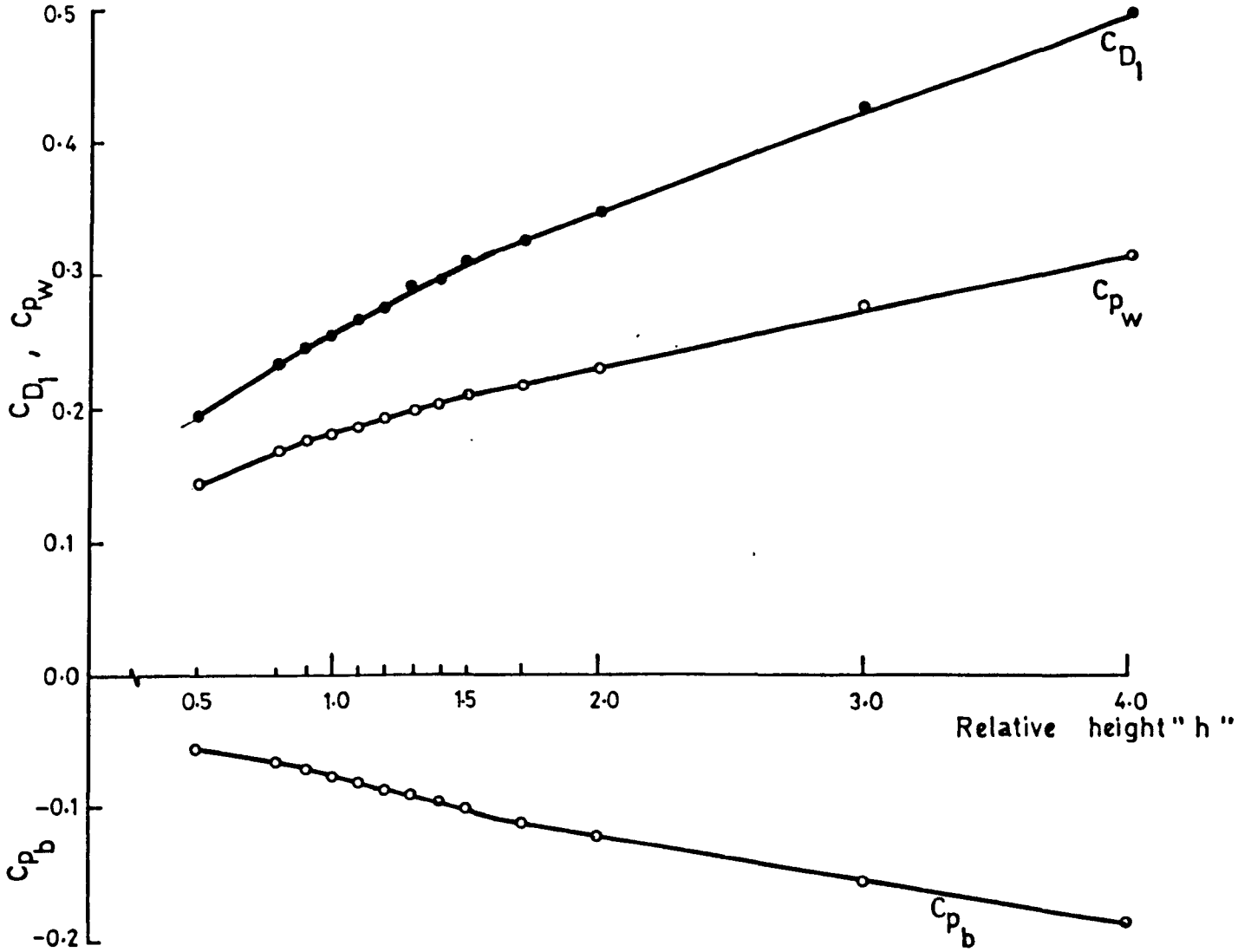

FIGURE 6.6 VARIATION OF THE WALL PRESSURE COEFFICIENTS AND THE DRAG COEFFICIENT WITH RELATIVE HEIGHT OF ISOLATED MODELS

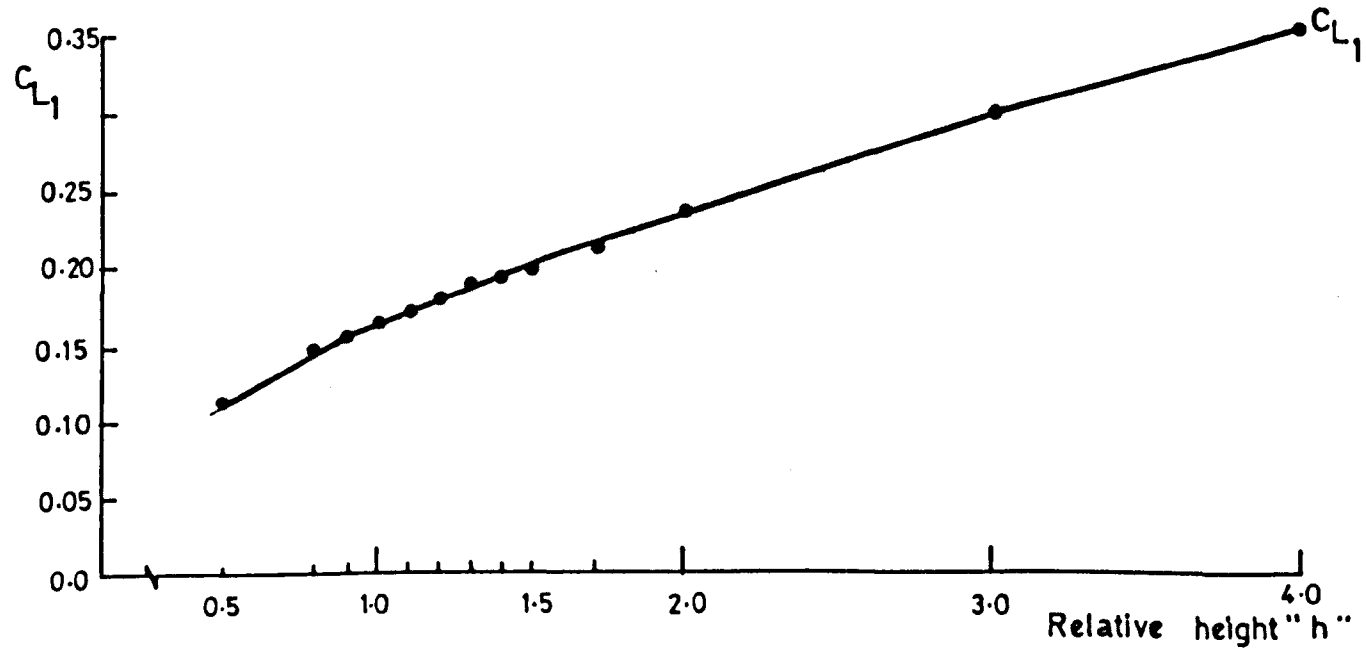

FIGURE 6.7 VARIATION OF C_{L_1} WITH RELATIVE HEIGHT OF ISOLATED MODELS

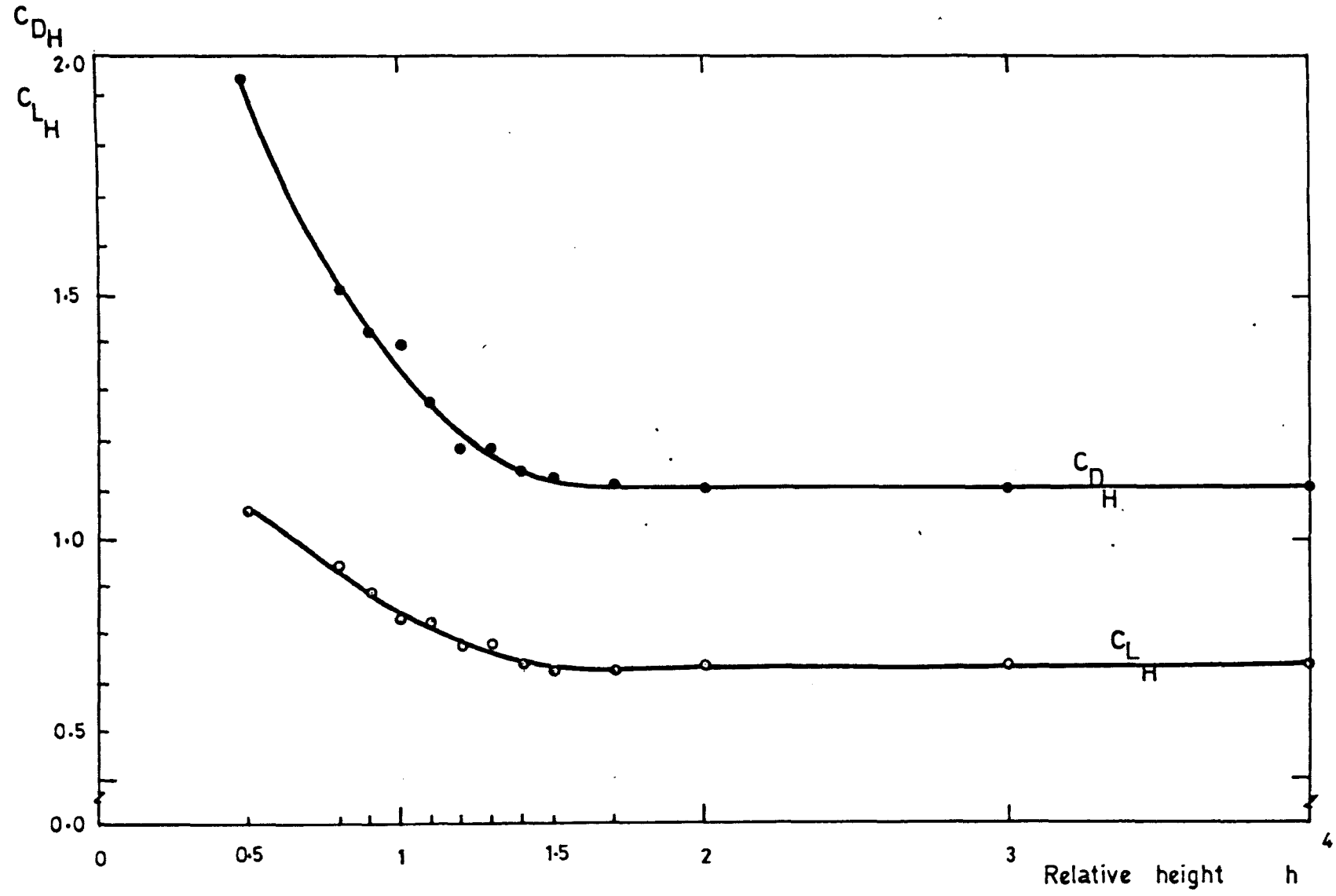

FIGURE 6.8 VARIATION OF C_{D_H} AND C_{L_H} WITH RELATIVE HEIGHT – ISOLATED MODELS

6.4 Flow around isolated models of varying frontal and side aspect ratios

6.4.1 There is very little data available in the literature on bluff body flows to enable a systematic assessment to be made of the effect of varying the side or frontal aspect ratios of low rise buildings on the resultant wind forces. Only Joubert et al (1962) investigated the effect of aspect ratios on wind forces on building models but this study was too restricted as they did not vary the aspect ratio over a wide range. This section, therefore, sets out to provide some data on isolated models of varying plan shapes. The cube was taken as having both side and frontal aspect ratio of 1.0. The frontal aspect ratio was varied from 0.5 to 4.0 and the side aspect ratio varied from 0.5 to 2.0. In this way, most of the common building shapes which occur in practice were covered in the tests.

6.4.2 The vertical distribution of pressure coefficients measured on the centre line of the windward and the leeward faces of the models of varying aspect ratios are shown in Figure 6.9. In all these distributions, the orientation angle θ was kept at 0. Other pressure coefficient distributions on the faces of the models, on either side of the centre line alongwith these centre line distributions were integrated to give the mean windward and leeward pressure coefficients, the difference of which yields the drag coefficient C_{D_1} in each case. Similar pressure coefficient distributions on the roof centre line of each model are shown plotted in Figure 6.10, the integration of which gives the lift coefficient, C_{L_1}, in each case.

6.4.3 In spite of the fact that Joubert et al (1962) in their study of the effect of aspect ratio on wind forces on building models, did not vary the aspect ratio over a wide range, they concluded that the significant parameter determining the drag coefficient of building

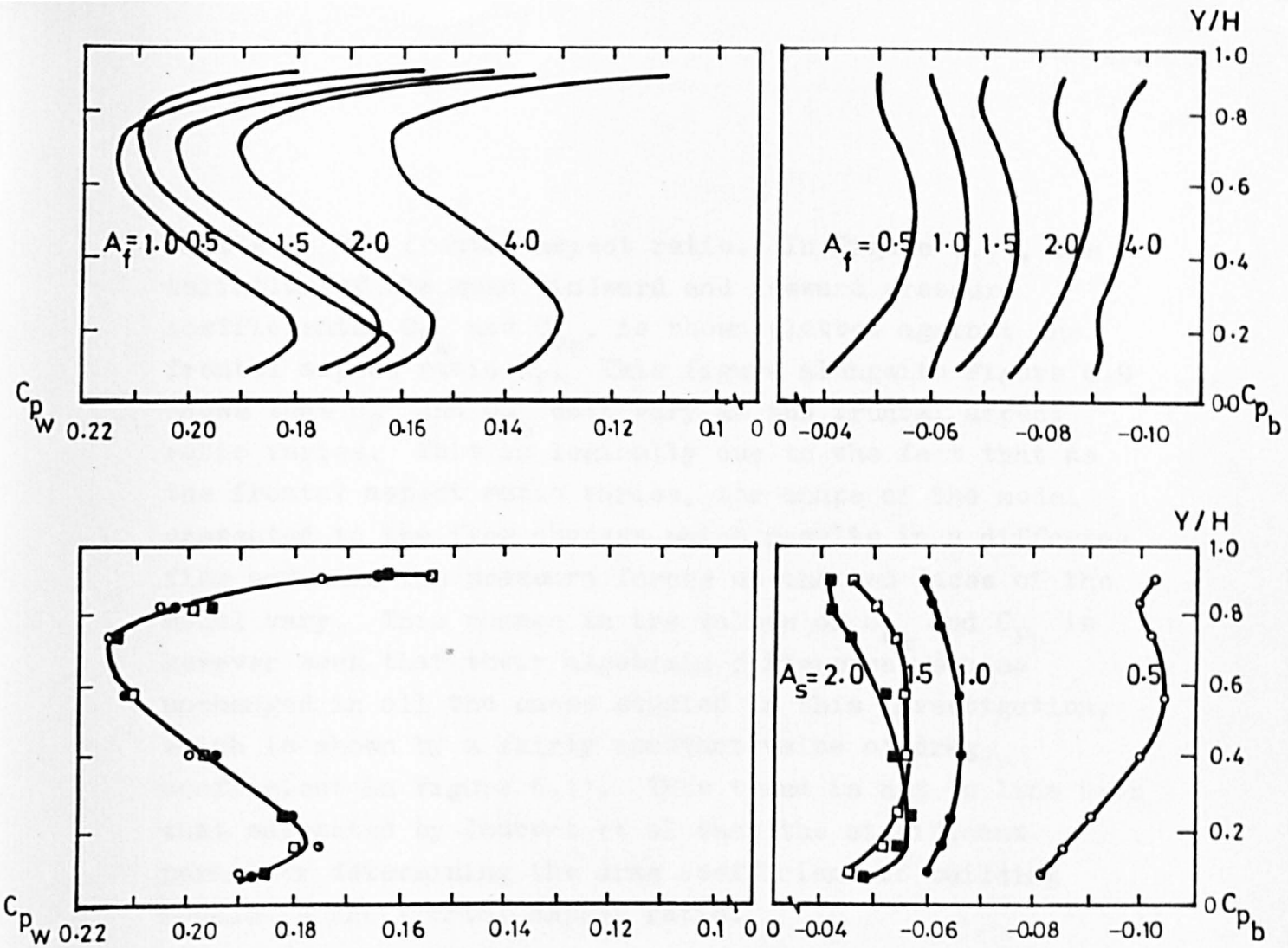

FIGURE 6.9 VERTICAL PRESSURE COEFFICIENT DISTRIBUTIONS ON ELEMENT CENTRE LINE FOR VARIOUS ASPECT RATIO MODELS

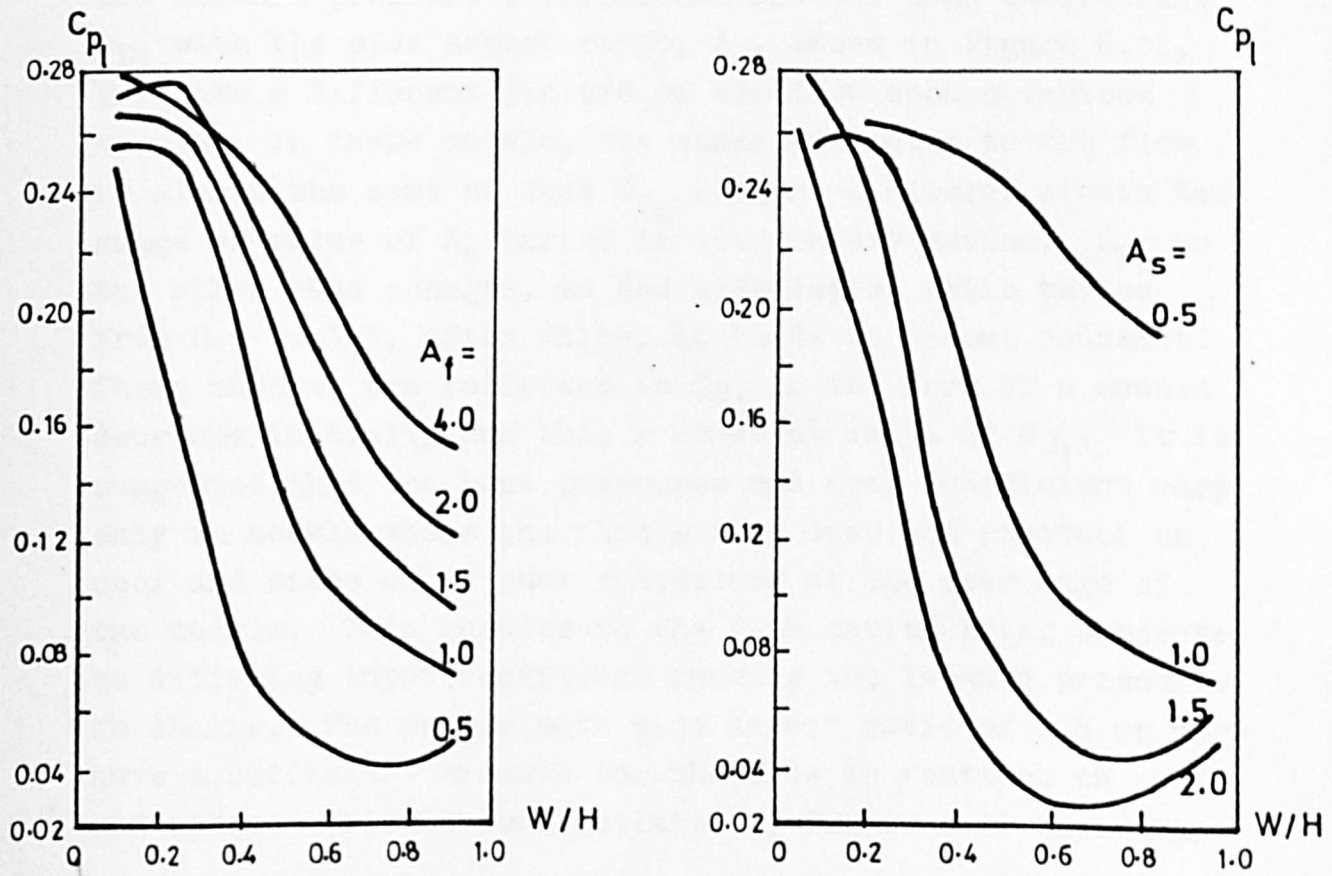

FIGURE 6.10 PRESSURE COEFFICIENT DISTRIBUTIONS ON ROOFS OF ISOLATED MODELS

models is the frontal aspect ratio. In Figure 6.11, the variation of the mean windward and leeward pressure coefficients, C_{p_w} and C_{p_b}, is shown plotted against the frontal aspect ratio A_f. This figure alongwith Figure 6.9 shows that C_{p_w} and C_{p_b} both vary as the frontal aspect ratio varies. This is logically due to the fact that as the frontal aspect ratio varies, the shape of the model presented to the flow changes which results in a differing flow and thus the pressure forces on the two faces of the model vary. This change in the values of C_{p_w} and C_{p_b} is however such that their algebraic difference remains unchanged in all the cases studied in this investigation, which is shown by a fairly constant value of drag coefficient in Figure 6.11. This trend is not in line with that suggested by Joubert et al that the significant parameter determining the drag coefficient of building models is the frontal aspect ratio.

6.4.4 The corresponding variations of the mean windward and leeward pressure coefficients and the drag coefficient C_{D_1} with the side aspect ratio, A_s, shown in Figure 6.12, presents a different picture of the flow around various models. In these models, the shape presented to the flow is always the same so that C_{p_w} remains unaltered within the range of value of A_s varied in this investigation. C_{p_b} on the other hand changes, as the side aspect ratio varies from 0.5 to 1.5, after which, it tends to become constant. These changes are reflected in C_{D_1} in the form of a sudden decrease initially and then a constant value of C_{D_1}. It is suggested that the base pressures and drag coefficient vary only in models where the flow either does not reattach on roof and sides or it just reattaches at the rear edge of the models. This results in the base cavity being subjected to differing input conditions causing the leeward pressures to change. The models with side aspect ratio of 1.5 or more have a sufficient breadth for the flow to reattach on roof and sides. This is substantiated by Figure 6.10 where the

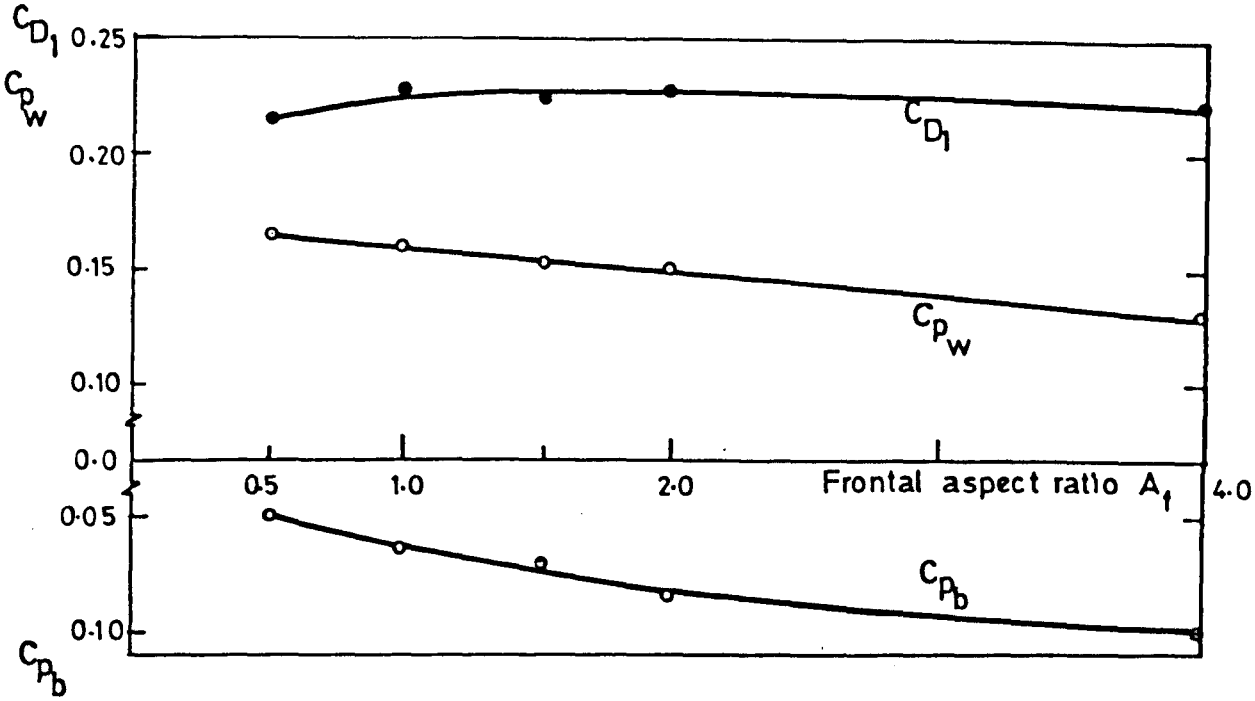

FIGURE 6.11 VARIATION OF THE WALL PRESSURES AND THE DRAG FORCE WITH FRONTAL ASPECT RATIO - ISOLATED MODELS

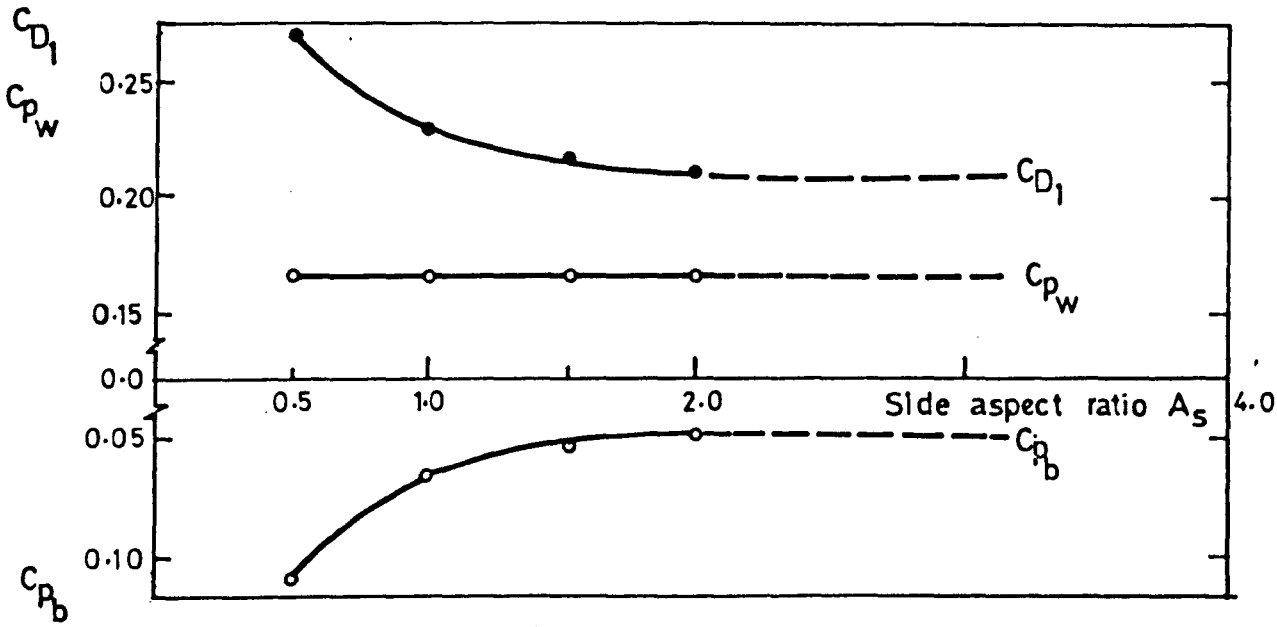

FIGURE 6.12 VARIATION OF THE WALL PRESSURES AND THE DRAG FORCES WITH SIDE ASPECT RATIO - ISOLATED MODELS

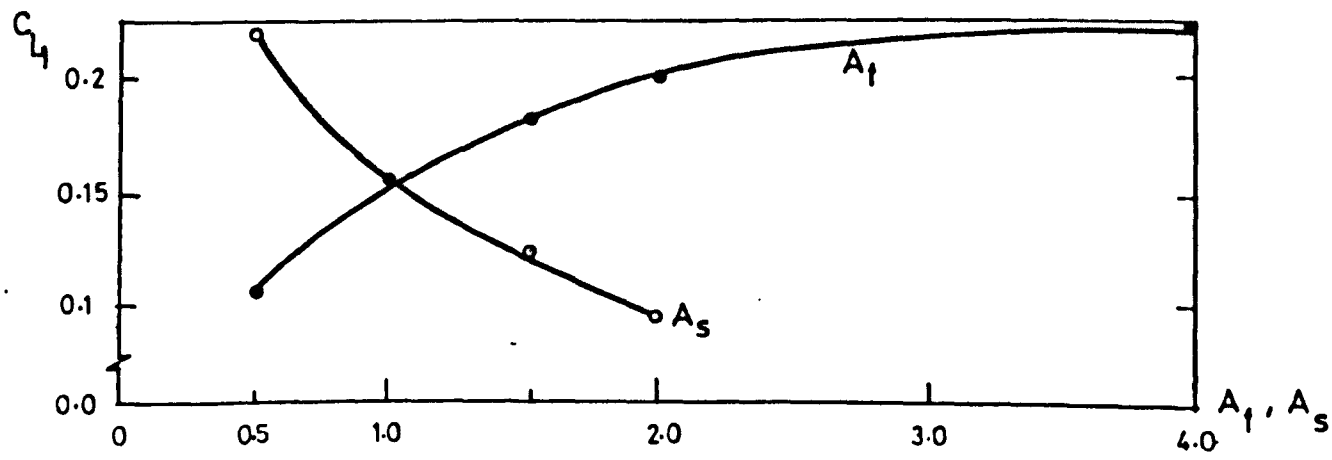

FIGURE 6.13 VARIATION OF THE ROOF LIFT COEFFICIENT WITH ASPECT RATIO OF ISOLATED MODELS.

roof pressure distribution for models of A_s = 1.5 and 2.0 show a pressure minimum towards the leeward edge of the models. This point where the pressure minimum occurs is suggested to be the region of reattachment of the flow, in contrary to Hillier's (1978) suggestion that the flow reattaches at the point where the pressure recovery has the greatest slope. This finding of Hillier may well only be appropriate to the determination of the reattachment position on bodies with a sufficient streamwise dimension to ensure reattachment.

6.4.5 The present results of roof pressure distributions shown in Figure 6.10, for various aspect ratios, shows the maximum negative pressure near the windward edge of the models, which agrees with the findings of Castro and Robin (1977) and Jensen and Franck (1965). Figure 6.13 shows the variation of mean lift coefficient with the aspect ratio. The lift coefficient, C_{L_1}, is shown to increase with the increase of frontal aspect ratio, A_f, before becoming constant at a value of $A_f \simeq 4$. On the other hand, as the side aspect ratio, A_s, increases, C_{L_1} decreases, because the maximum suction near the windward edge of the models have to be averaged over a large area.

6.5 Conclusions

6.5.1 The effect of changing the incident flow type, and thus the parameter $\frac{\delta}{H}$ from 4 in the smooth incident flow to 22 in the simulated atmospheric boundary layer flow, resulted in a large reduction in pressure forces on an isolated cube. In order to be applicable to low rise housing, a large discrepancy in the value of $\frac{\delta}{H}$ would result in an inaccurate estimate of the wind forces (Figure 6.1).

6.5.2 The computed value of drag coefficient normalised with respect to the velocity at cube height, C_{D_H}, for the isolated cube was found to be larger than the comparable value suggested by British Standard Code of Practice.

6.5.3 The roof pressure coefficients for the isolated models were always negative with the maximum suction occurring near the windward edge and decreasing towards the rear edge (Figure 6.1, 6.5 and 6.10).

6.5.4 From the graph showing the variation of mean windward and leeward pressure coefficient, drag and lift coefficient with relative height h, it is shown that the rate of change of pressure with building height is different below and above a value of h = 1.6. It is suggested that the lower region may be thought of as encompassing low rise buildings whilst the upper region includes high rise buildings (Figure 6.6 and 6.7).

6.5.5 The drag coefficient normalised with respect to the velocity at model height, C_{D_H}, decreases as the height increases for low rise buildings. On the other hand, the value of C_{D_H} remains constant for high rise buildings (Figure 6.8).

6.5.6 The low rise buildings experience high values of the drag coefficient dependent of their relative height. The drag decreases as the height increases. This trend is the reverse of that given by ESDU 71016 and the British Standard Code of Practice.

6.5.7 As the frontal aspect ratio increases, the shape presented to the flow varies. This affects the windward and leeward pressure coefficients but the overall drag coefficient remains unaffected (Figure 6.11).

6.5.8 The drag coefficient is also affected by the side aspect ratio until such time that the flow reattaches on the roof and sides of the model, after which the side aspect ratio does not affect the drag (Figure 6.12).

6.5.9 The lift coefficient, C_{L_1}, increases as the frontal aspect ratio increases and decreases with the increase of side aspect ratio (Figure 6.13).

CHAPTER 7

EXPERIMENTAL RESULTS AND DISCUSSIONS: INFLUENCE OF UPSTREAM FETCH ON FORCES ON THREE DIMENSIONAL BLUFF BODIES

7. EXPERIMENTAL RESULTS AND DISCUSSIONS: INFLUENCE OF UPSTREAM FETCH ON FORCES ON THREE DIMENSIONAL BLUFF BODIES

7.1 Introduction

7.1.1 The wind loading studies of buildings, in an urban or rural environment, require the simulation in a wind tunnel of the appropriate atmospheric boundary layer in order to satisfy the scaling laws. However, the simulation appropriate to a particular site requires the production of a detailed site model of the area which is both expensive and time consuming. The extent of detailed modelling has, therefore, been determined by these two considerations and very few attempts were made to find the optimum extent of detailed modelling and the effect of the general simulation upstream. Thus, the tests are often carried out in wind tunnels where the upstream general roughness extends up to the working section, leaving only a small area for detailed modelling. Occasionally, the detailed modelling is omitted altogether and the tests are carried out on buildings in isolation, a case unlikely to be encountered in reality.

7.1.2 Pasquill (1972) estimated the extent of surface roughness that dominantly affects the flow conditions at various heights and derived a table of "roughness footprint" dimensions. If every part of the surface roughness that affected a point in the simulated flow should be accurately modelled then in the case of the wind tunnel used for these investigations, a simulation to the roughness height of 500mm at 1/250 scale would require the 4.0 metre fetch of general roughness to be replaced by a detailed model. Fortunately, this is not necessary. Where the "roughness footprint" contains a large number of similar roughness elements i.e. buildings, the individual effect of a single element is indistinguishable from the combined effect of others and here a form of general roughness can be used. The problem lies in assessing just where to place the boundary between detailed model and the general roughness.

Cook (1972), on the basis of work done at Bristol University with arrays of cubes and high aspect ratio elements used together, suggested that five rows of similarly sized elements are sufficient to mask the individual effect of an upstream row. This study was carried out for a very specific case and did not include the effects of varying the layout pattern or the group density of the elements. Therefore, it cannot be adopted as a general rule.

Soliman (1976), however, considered the group density and layout pattern in his study of flow over three dimensional roughness elements in a rough flow obtained from the boundary layer growing over a rough sheet placed upstream of the turntable on which the model group layout was placed. He suggested that the drag coefficient of the roughness elements stabilise at a fetch equal to 12 times the element height, R/H = 12, irrespective of the group density, Figure 7.1. As this figure shows, the use of R/H = 12 for all tests is questionable particularly at low densities. His work remains inconclusive in this respect since he was unable to model larger fetches of roughness.

The present study details out the way in which the surface pressures of a model low rise building as part of a large array of similar buildings are influenced by both the array size as well as the general atmospheric shear flow upstream of the array. An effort has been made to arrive at the optimum use of both the array size as well as the general incident flow which dominates the flow conditions.

7.1.3 In this investigation, the upstream fetch of the model array, R/H, comprising of similarly sized elements, was varied from 3 to 145 and the downstream fetch was varied from 3 to 25. The model group, therefore, took the form of free standing cubes on the smooth floor of the tunnel, hence the oncoming flow underwent a change of

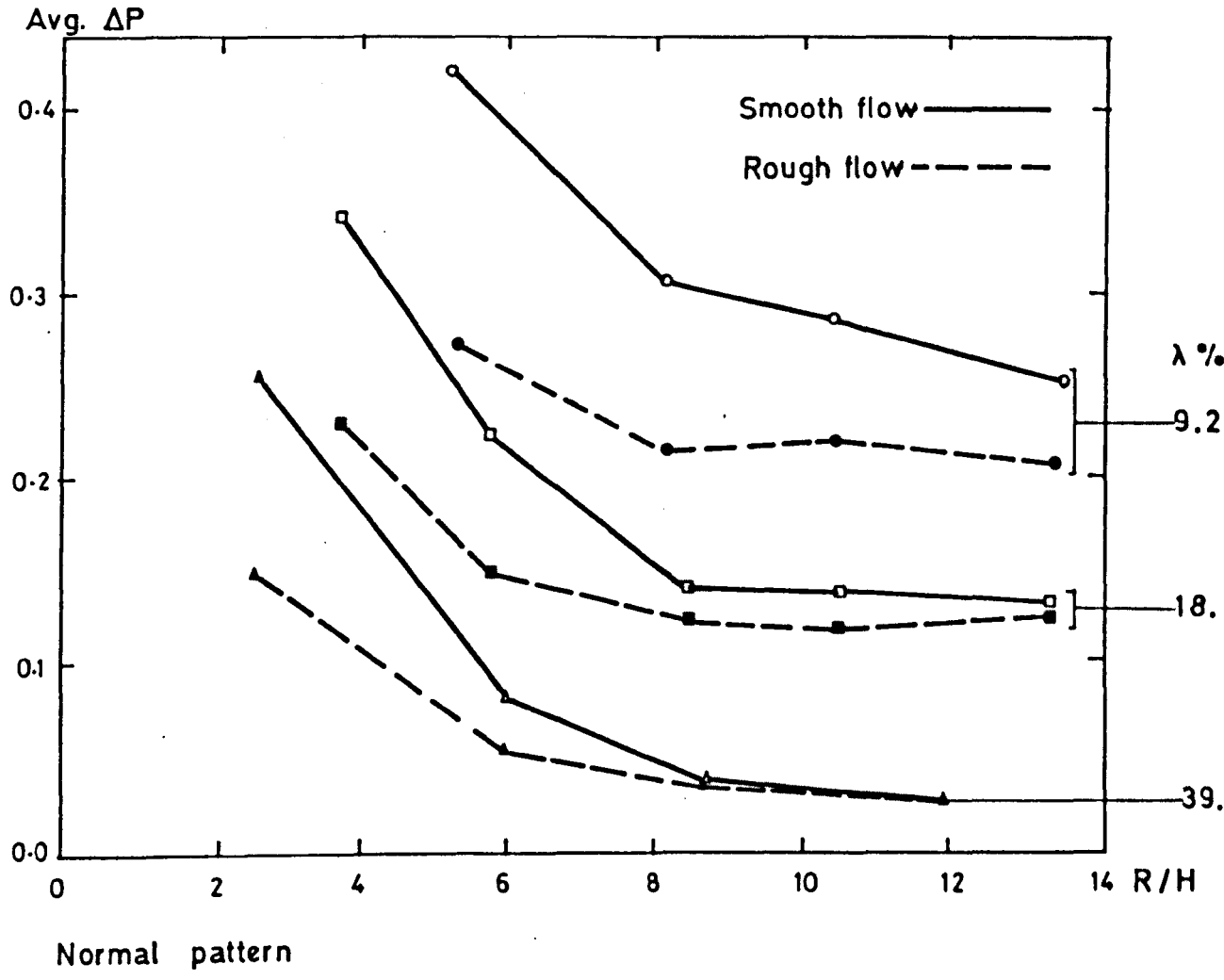

FIGURE 7.1 VARIATION OF PRESSURE DIFFERENCE COEFFICIENT WITH FETCH (SOLIMAN 1976)

surface roughness, when it reached the group layout. The effect of this disturbance on the incident smooth wall boundary layer flow has been investigated to determine the model group layout size required for the surface pressure forces to stabilise. At a value of R/H = 145, the whole length of the wind tunnel was occupied by the roughness elements. During this stage of investigation the surface pressures of the test model were found to stabilise at different values of fetch lengths in various layout densities.

When the surface pressures in a particular density stabilised and further increase in fetch resulted in only nominal changes, the atmospheric boundary layer simulation mechanism was introduced upwind in the tunnel. Various combinations of the model group fetch lengths and the general roughness in the simulation mechanism were then studied to find their effect on the stabilised pressure forces.

7.1.4 Detailed pressure measurements were made for the flows both in the case in which the roughness elements alone were present as well as those which included the atmospheric boundary layer simulation devices. A series of velocity profile measurements were also made for the various fetches of roughness elements. Three values of element plan area density were chosen in each of the layout patterns. Table 7.1 gives the variables considered in this phase of the investigation.

Table 7.1 Variables considered in this phase of the investigation

Variables	Pressure and velocity profile measurements
Plan area density	5%, 10% and 20% in the normal pattern 10%, 20% and 25% in the staggered pattern
Fetch	$3 < R/H < 145$
Orientation	$\theta = \phi = 0$

7.2 Pressure coefficient distributions and the array size

7.2.1 The vertical distributions of the pressure coefficients measured on the centre line of the windward and leeward faces of the cube, for various fetch lengths in both the normal and the staggered patterns, are shown in Figures 7.2 to 7.7. These centre line pressure distributions alongwith four other vertical pressure profiles on the faces of the model were integrated to give the mean windward and leeward pressure coefficients, C_{p_w} and C_{p_b}. The algebraic difference of these pressure coefficients in each case yields the drag coefficient, C_{D_1}.

7.2.2 The variation of the drag coefficient, C_{D_1}, with fetch, R/H, for various densities is shown in Figure 7.8, for both the normal and staggered layout patterns. The figure indicates that in almost all cases, the drag coefficient is found to decrease with the increase of fetch. The rate at which this reduction takes place is, however, different in various densities. For the lowest densities, 5% in the normal pattern and 10% with the staggered pattern, the reduction in the drag coefficient was found to be gradual, when the fetch was increased from 3H to

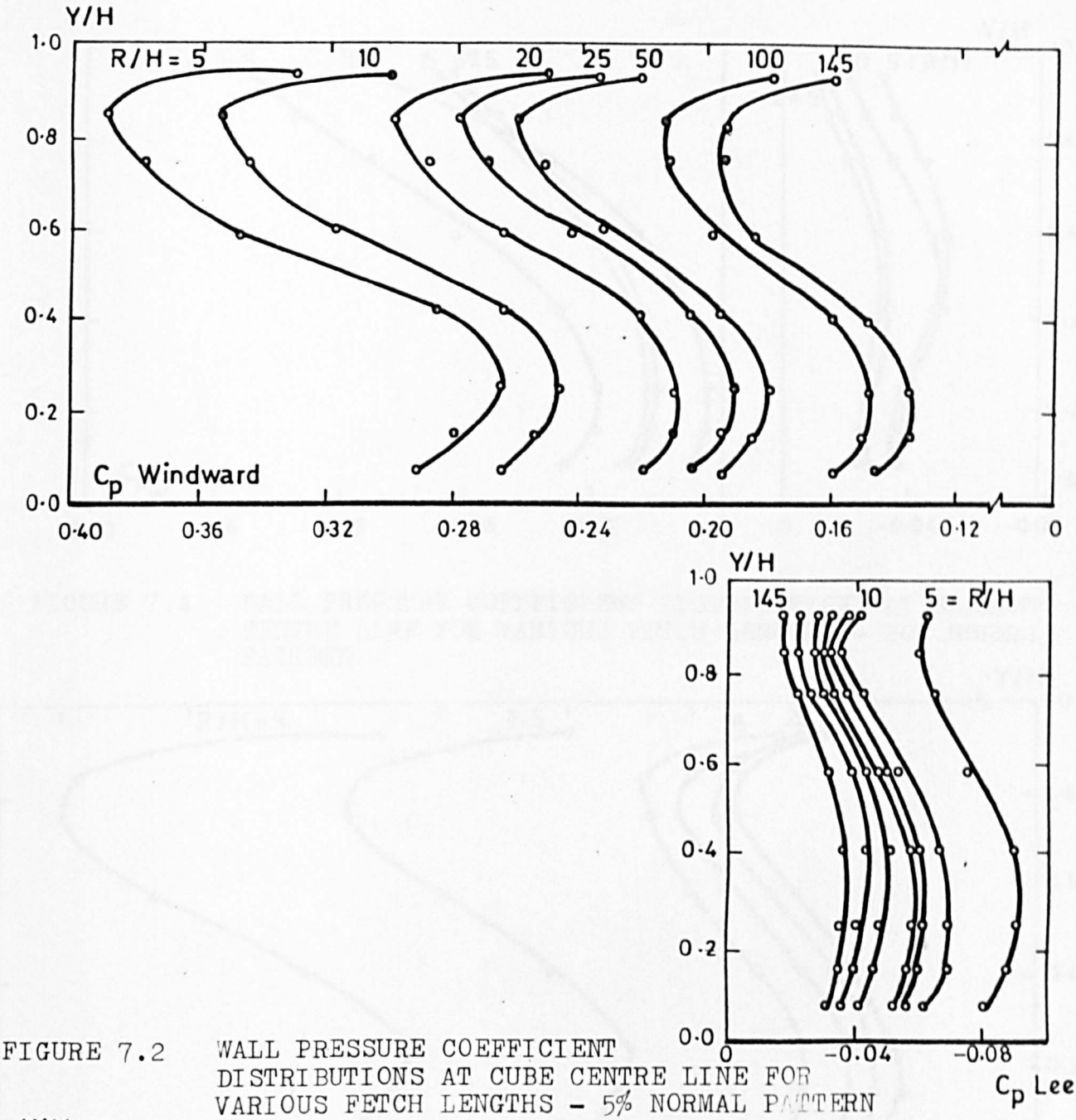

FIGURE 7.2 WALL PRESSURE COEFFICIENT DISTRIBUTIONS AT CUBE CENTRE LINE FOR VARIOUS FETCH LENGTHS - 5% NORMAL PATTERN

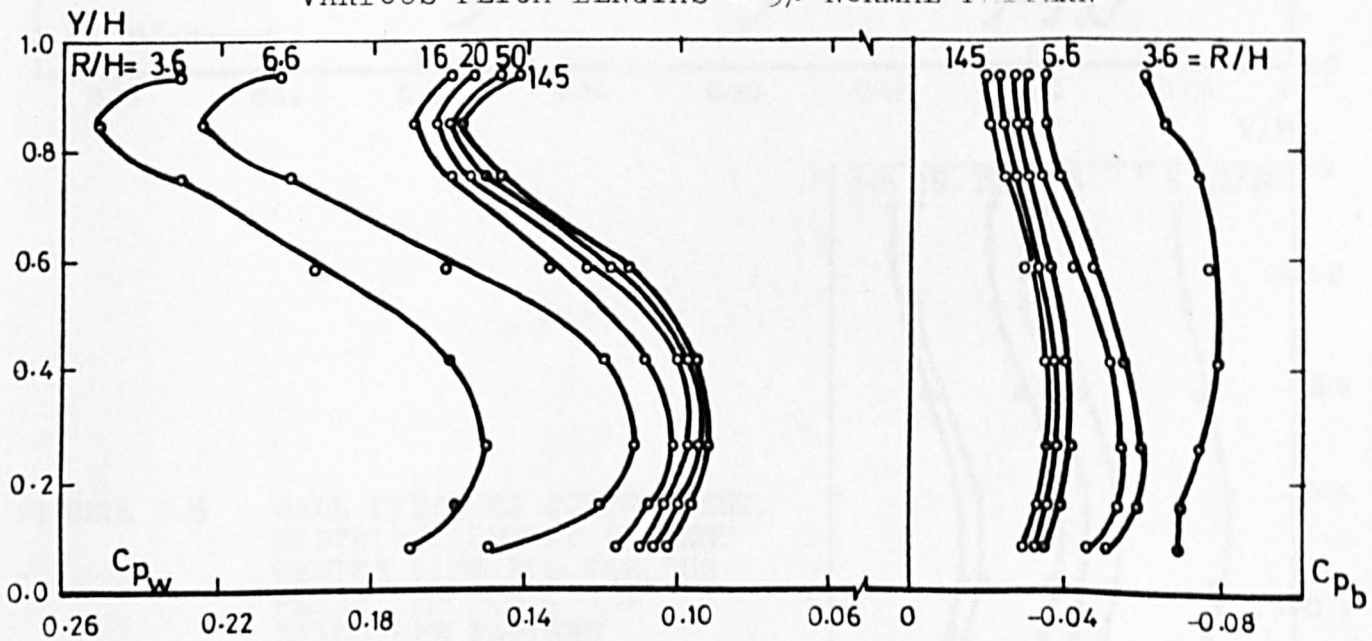

FIGURE 7.3 WALL PRESSURE COEFFICIENT DISTRIBUTIONS AT CUBE CENTRE LINE FOR VARIOUS FETCH LENGTHS - 10% NORMAL PATTERN

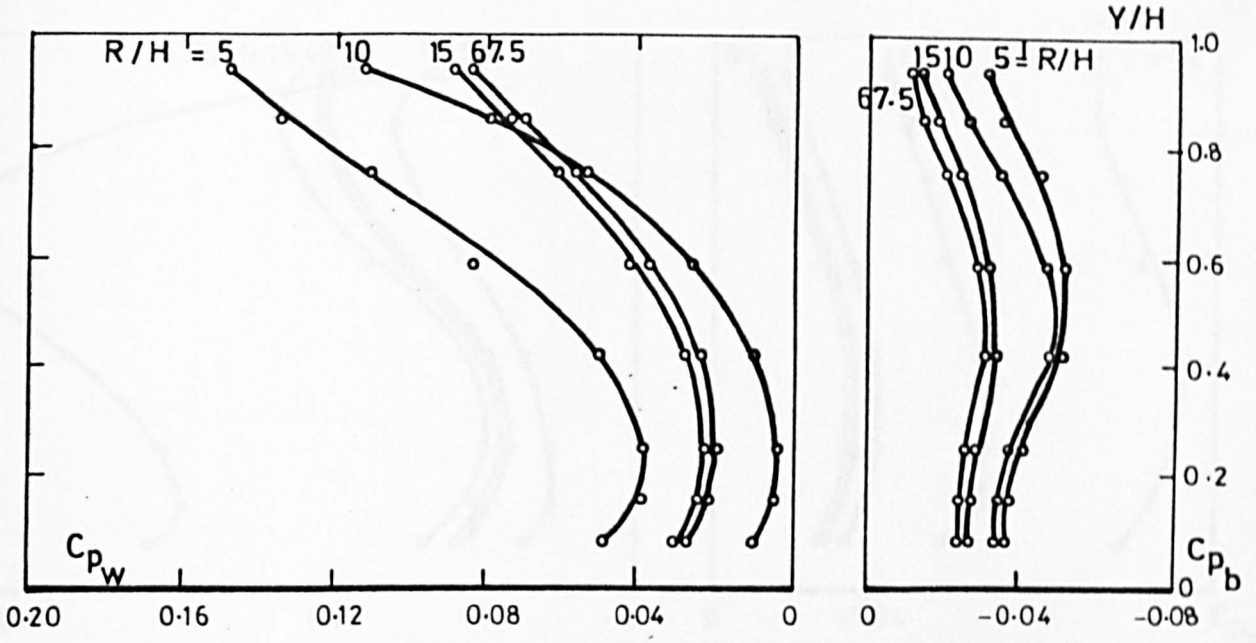

FIGURE 7.4 WALL PRESSURE COEFFICIENT DISTRIBUTIONS AT ELEMENT CENTRE LINE FOR VARIOUS FETCH LENGTHS - 20% NORMAL PATTERN

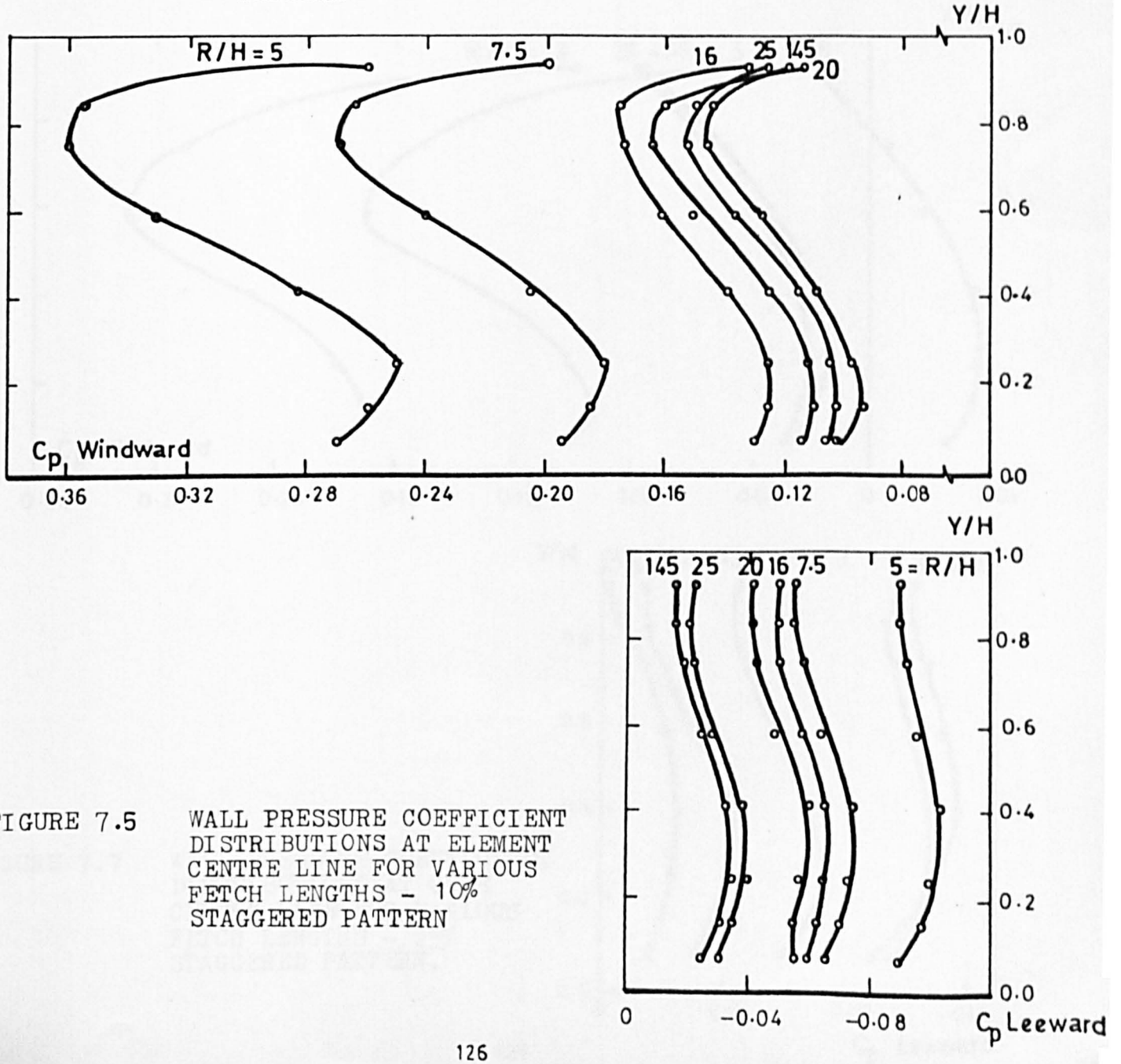

FIGURE 7.5 WALL PRESSURE COEFFICIENT DISTRIBUTIONS AT ELEMENT CENTRE LINE FOR VARIOUS FETCH LENGTHS - 10% STAGGERED PATTERN

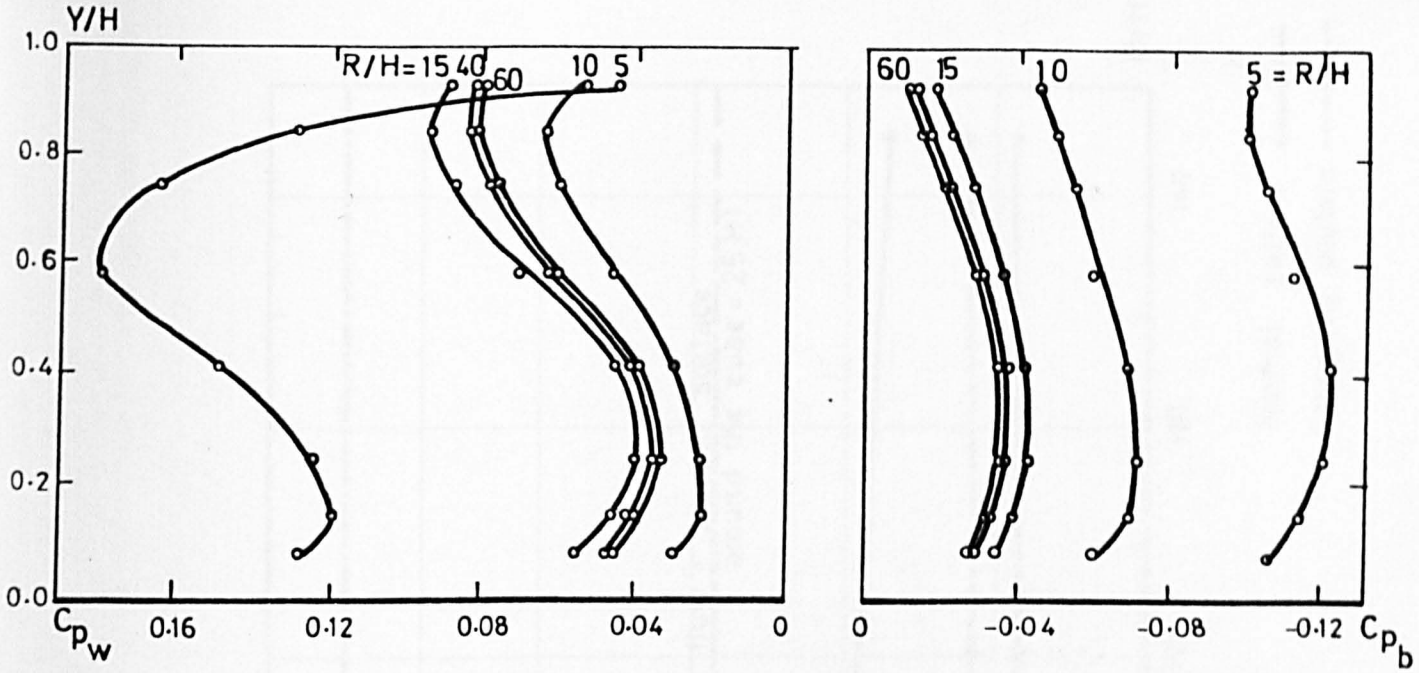

FIGURE 7.6 WALL PRESSURE COEFFICIENT DISTRIBUTIONS AT CUBE CENTRE LINE FOR VARIOUS FETCH LENGTHS - 20% STAGGERED PATTERN

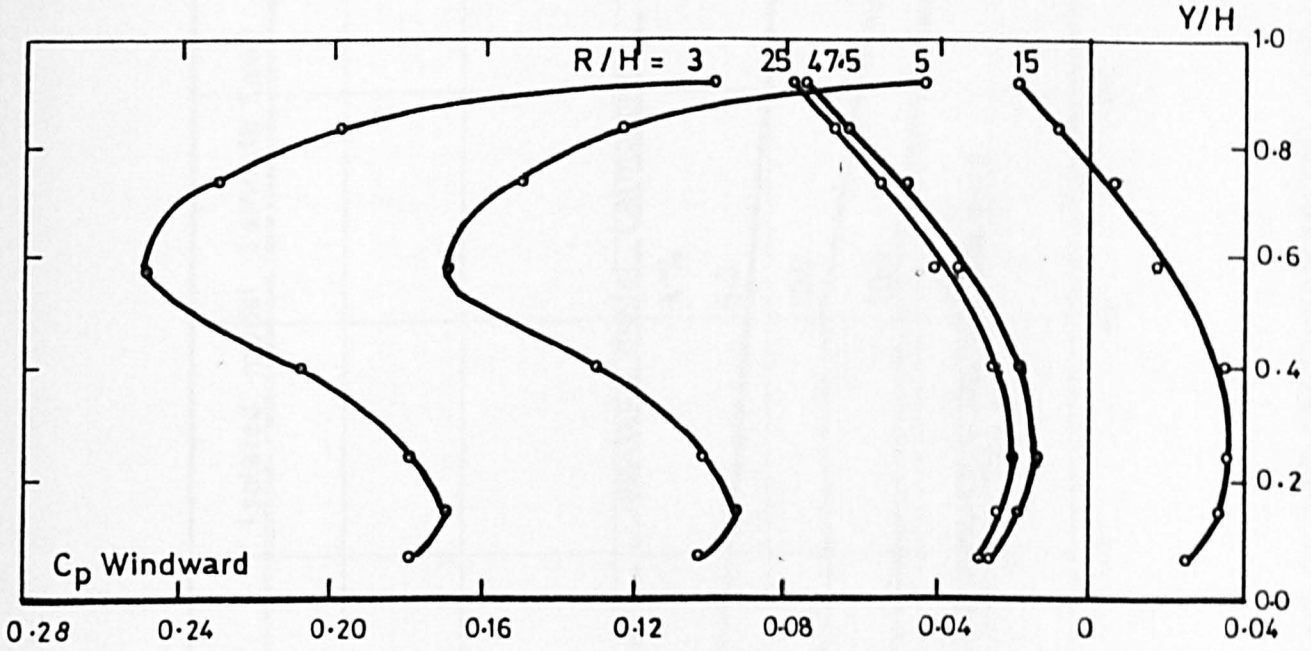

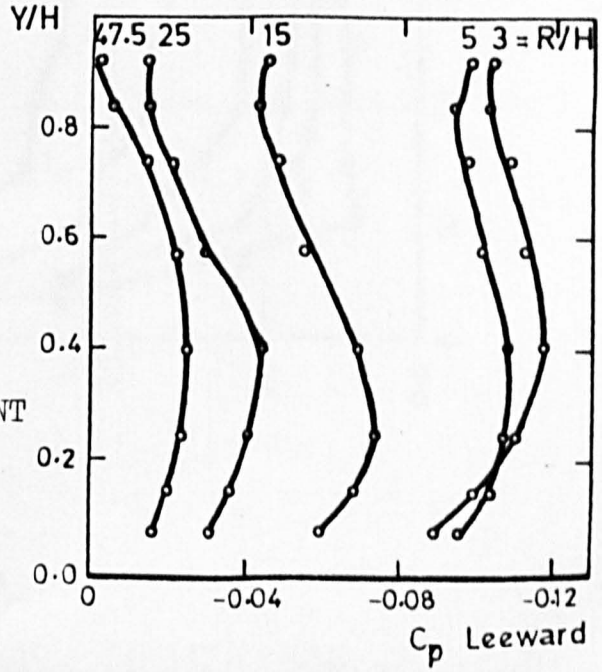

FIGURE 7.7 WALL PRESSURE COEFFICIENT DISTRIBUTIONS AT CUBE CENTRE LINE FOR VARIOUS FETCH LENGTHS - 25% STAGGERED PATTERN.

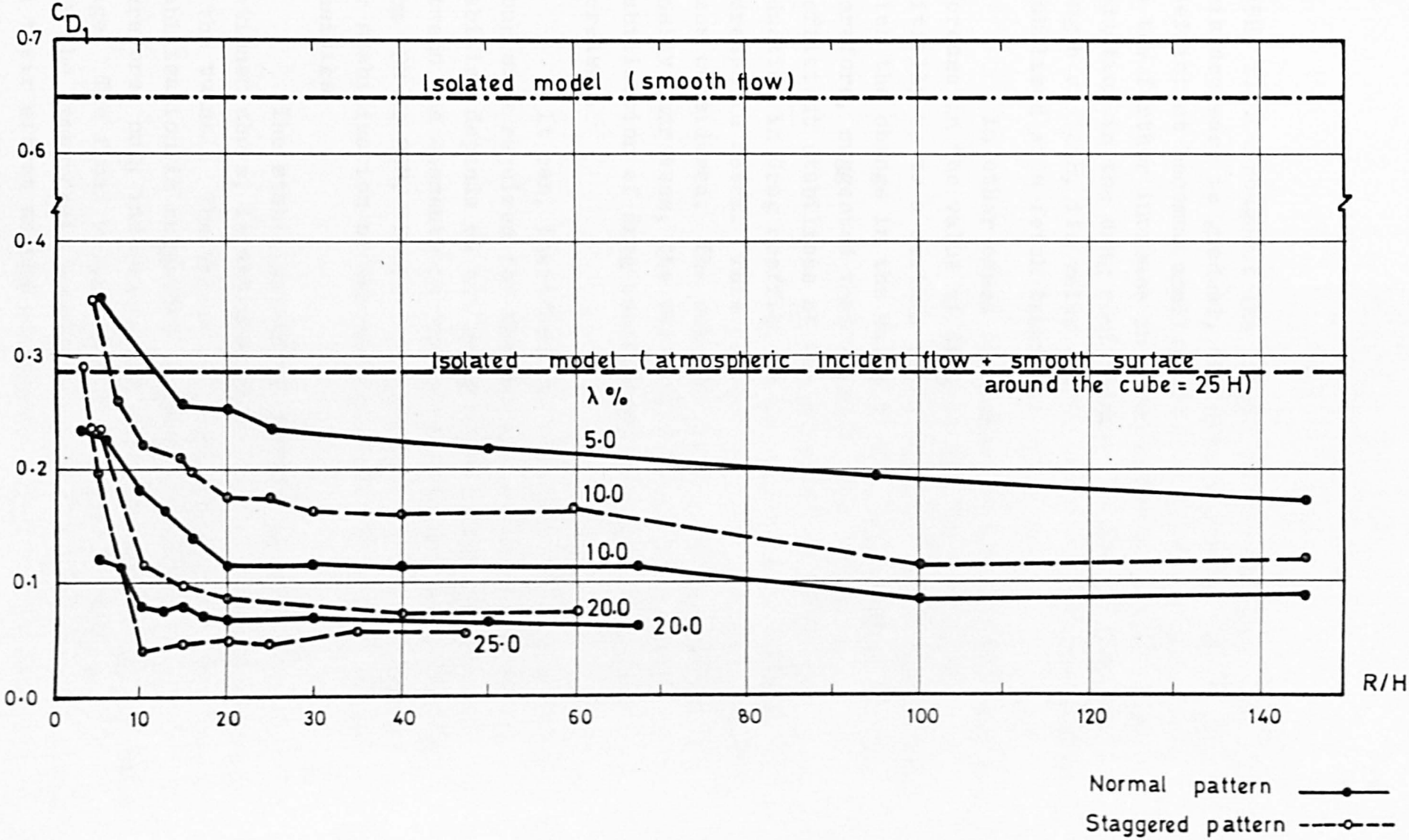

FIGURE 7.8 VARIATION OF THE DRAG COEFFICIENT WITH FETCH.

145H, i.e. throughout the length of the tunnel. Although this decrease is gradual, the rate of change of the drag coefficient becomes smaller after a fetch length of 25H. As the further increase in fetch results in only a small reduction in the drag coefficient i.e. 20% at a fetch length of 145H, its value can be taken to have approximately stabilised at a fetch length of R/H = 25.

In other cases of higher densities, however, the decrease in the value of drag coefficient is abrupt initially up to a certain value of the fetch length, after which the change in the value of C_{D_1} is nominal. It is, therefore, suggested that in such cases the drag coefficient stabilises at the point after which the reduction in drag coefficient is nominal with further increase in fetch. This is true for the remaining density cases considered. The only difference being that as the density increases, the value of R/H, at which the stabilisation of drag coefficient is found to occur, decreases.

It can, therefore, be concluded that the model group size required for the surface pressure forces to stabilise depends on the group density and the spacing between the elements in the group, and is found to vary from 10H to 25H. Shorter fetches are normally required for stabilisation of the mean pressure forces at higher densities.

The stabilisation of surface pressure forces, mentioned above, is achieved with regular roughness arrays in the tunnel. The values of fetch lengths at which the stabilisation is suggested to have taken place are, therefore, only indicators and not the final values at this stage. The final values of R/H with their combinations with the atmospheric boundary layer flow simulation devices and their effect on the stabilised drag coefficients will be shown in the next section.

7.2.3 Figures 7.2, 7.3 and 7.5 show that the windward pressure coefficients decrease with the increase of fetch length for smaller densities of 5% and 10% in the normal pattern and 10% in the staggered pattern. On the other hand, the windward pressure coefficients in higher density cases behave slightly differently. In these cases, the windward pressure coefficients were found to first increase as the fetch increased before decreasing at larger values of fetch. Figures 7.4, 7.6 and 7.7 show this phenomenon for 20% density in the normal pattern and 20% and 25% densities in the staggered layout pattern. Conversely, the leeward pressure coefficients keep on increasing with the increase of fetch length in all the densities considered.

The behaviour of windward pressure coefficients at higher densities is suggested to be due to the zero plane displacement which occurs for element groupings. In higher densities, as the fetch increases, the displacement gets greater and the effective height is decreased, resulting in the increased windward pressure coefficients initially. Once the zero plane displacement has achieved its maximum value the windward pressure coefficients begin to decrease with the increase in fetch.

The velocity profiles in this phase of the investigation were taken on top of the cubes and the portion below the element crest was not covered. During the analysis of the velocity profiles, it was found that there were either insufficient experimental points or none at all falling on the logarithmic straight line portion of the profiles. Due to this, the zero plane displacement could not be measured from the velocity profiles in this phase of the investigation. Therefore the above hypothesis could not be substantiated by the experimental results and remains only a suggestion.

7.2.4 As the fetch length required for the stabilisation of surface pressure forces on the model varies with the density of the model group, a constant value of R/H cannot be taken for all group densities normally used for low rise housing. Therefore the suggestion made by Cook (1972) that five rows of similarly sized elements are sufficient to mask the individual effect of an upstream row cannot be generalised.

On the other hand, the conclusions drawn by Soliman (1976) whereby he used a value of fetch, R/H = 12, for all his experiments seem to be applicable to higher density groupings only. At lower densities, however, this value of R/H = 12 would result in an over-estimation of the surface pressure forces.

7.3 Effect of array size and the incident atmospheric shear flow

7.3.1 The fetch length,at which the drag coefficient stabilises, was found to vary depending upon the density of model group and the element spacing in the model group. At such a point the atmospheric boundary layer flow mechanism was introduced upwind of the array size to see the effect on the stabilised drag of the test model. The boundary layer flow mechanism is explained fully in chapter 5. In order to find a boundary between the extent of modelling around the test building as part of a large array and the atmospheric incident flow, two or three combinations of both the array size and the roughness of the atmospheric flow simulation mechanism were studied. In some cases, an open space of the order of 10H was also left between the two to find its influence.

7.3.2 The vertical distributions of the pressure coefficients measured on the centre line of the windward and leeward faces of the model in these arrangements for various densities are shown in Figures 7.9 to 7.14. A further drop

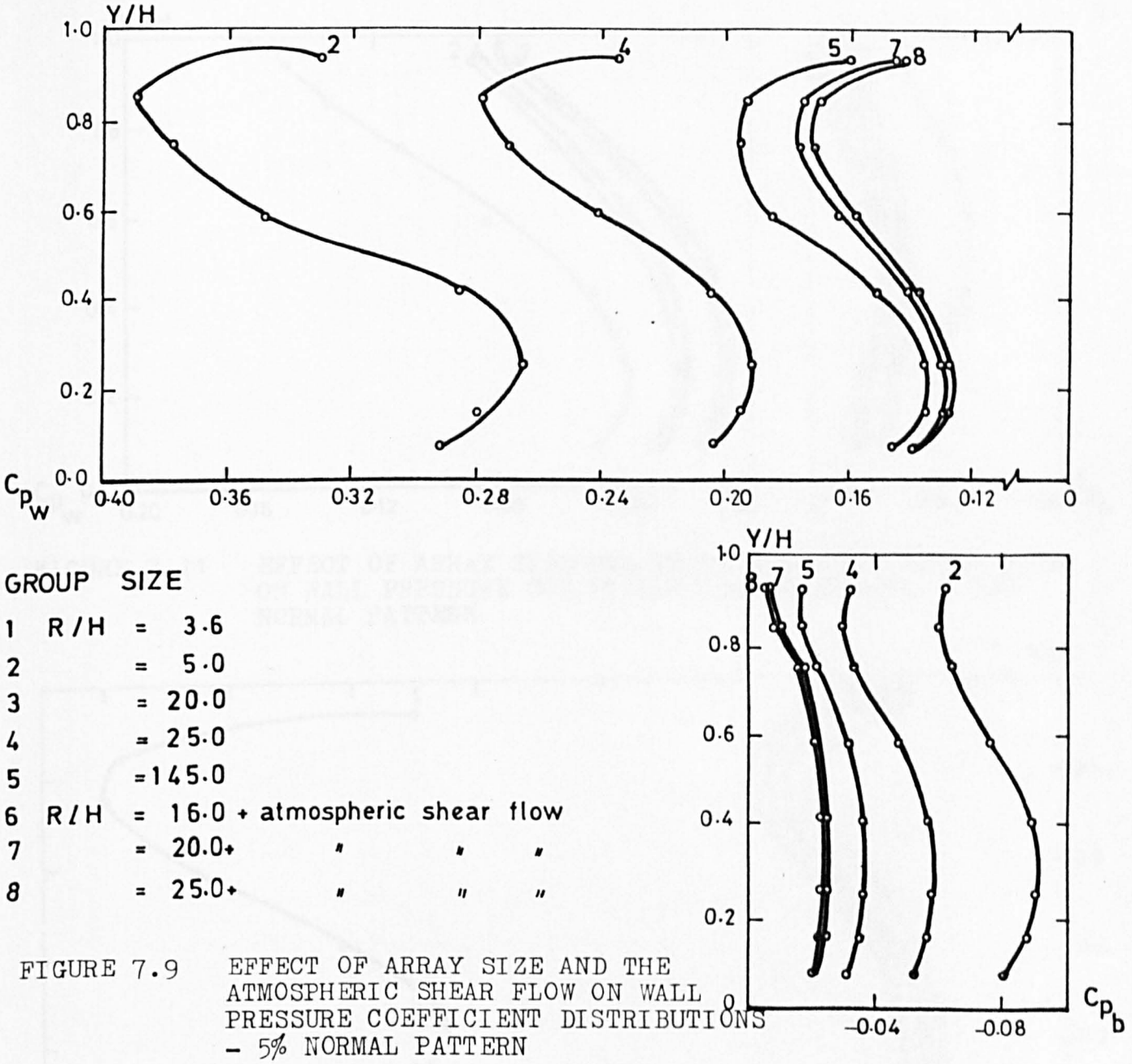

FIGURE 7.9 EFFECT OF ARRAY SIZE AND THE ATMOSPHERIC SHEAR FLOW ON WALL PRESSURE COEFFICIENT DISTRIBUTIONS – 5% NORMAL PATTERN

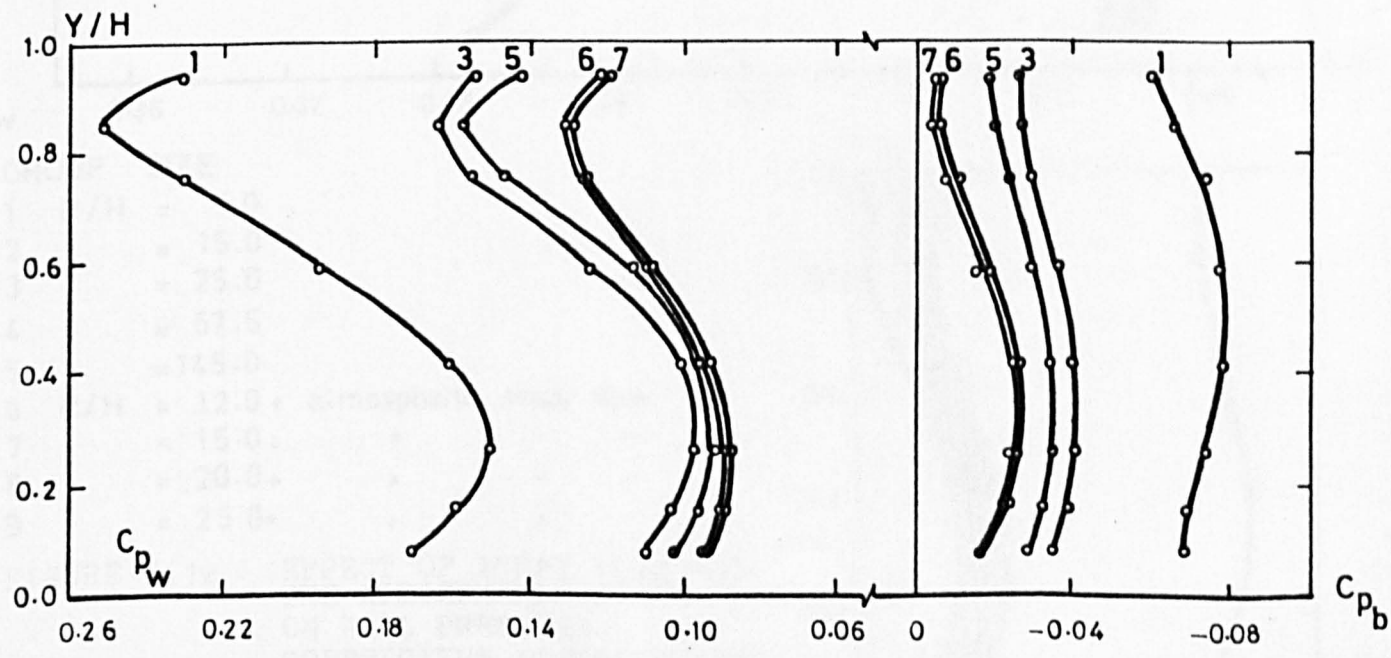

FIGURE 7.10 EFFECT OF ARRAY SIZE AND THE ATMOSPHERIC SHEAR FLOW ON WALL PRESSURE COEFFICIENT DISTRIBUTIONS – 10% NORMAL PATTERN

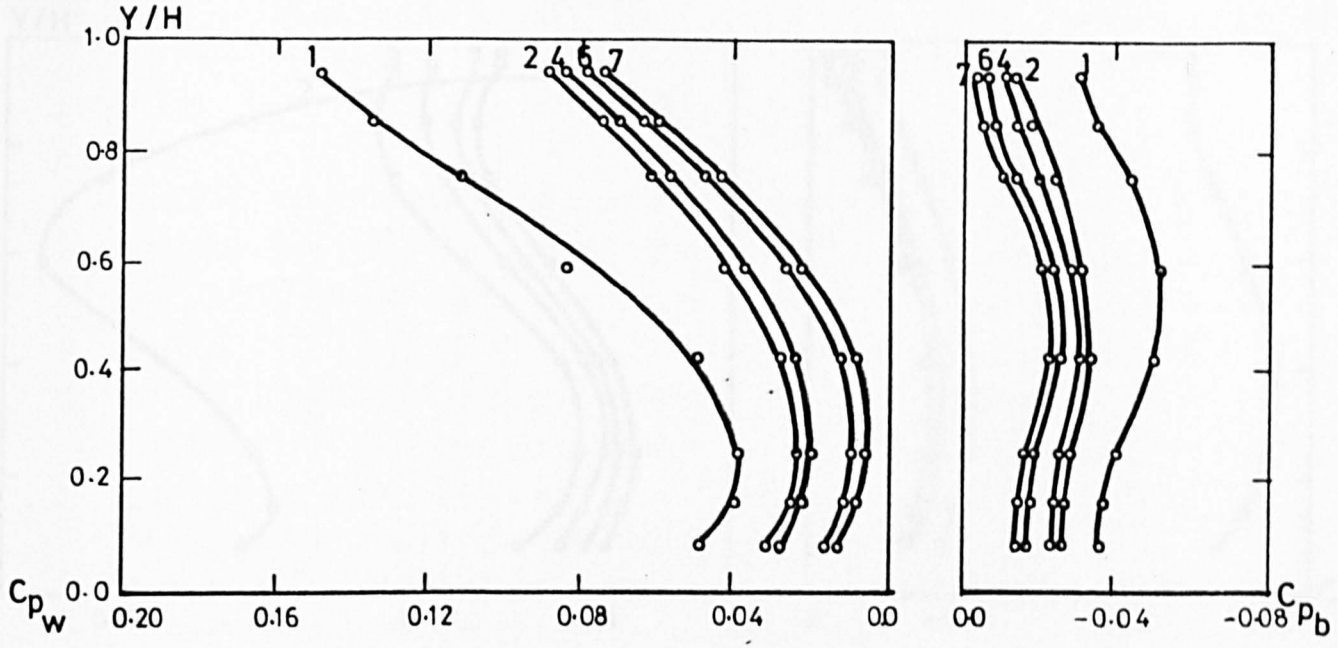

FIGURE 7.11 EFFECT OF ARRAY SIZE AND THE ATMOSPHERIC SHEAR FLOW ON WALL PRESSURE COEFFICIENT DISTRIBUTIONS – 20% NORMAL PATTERN

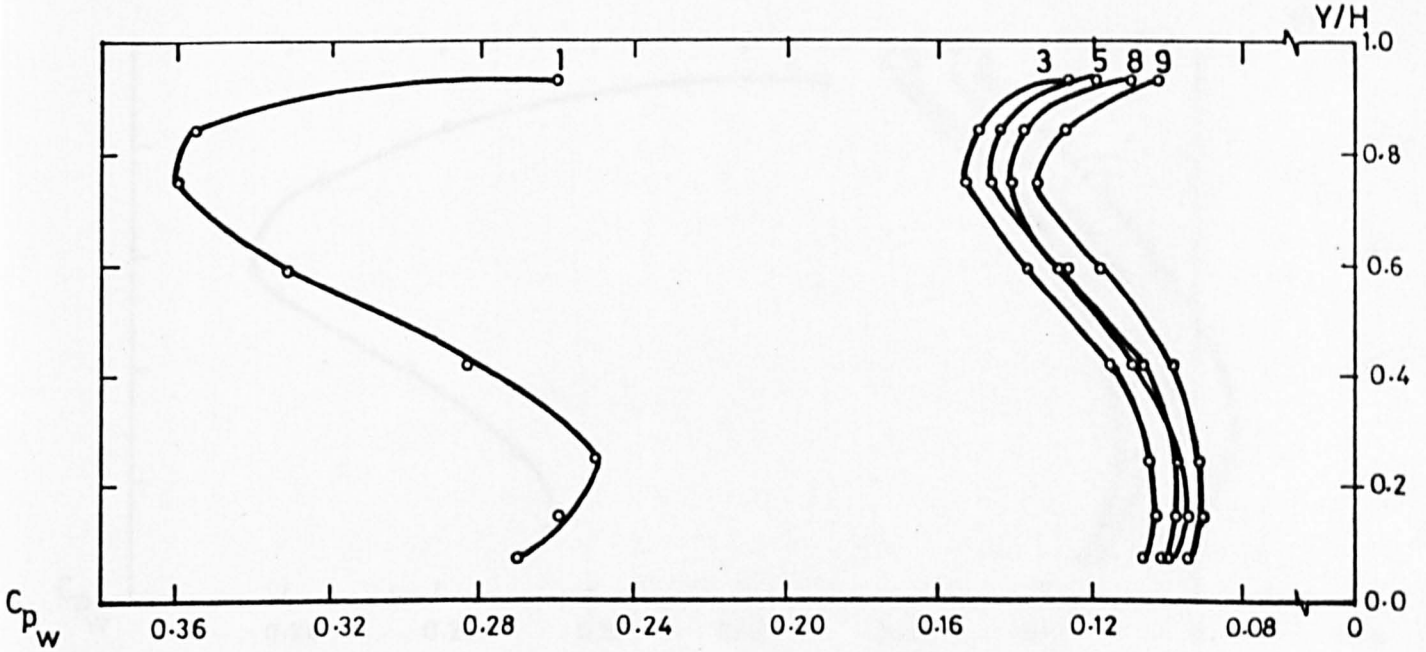

GROUP SIZE

1 R/H = 5.0
2 = 15.0
3 = 25.0
4 = 67.5
5 = 145.0
6 R/H = 12.0 + atmospheric shear flow
7 = 15.0 + " " "
8 = 20.0 + " " "
9 = 25.0 + " " "

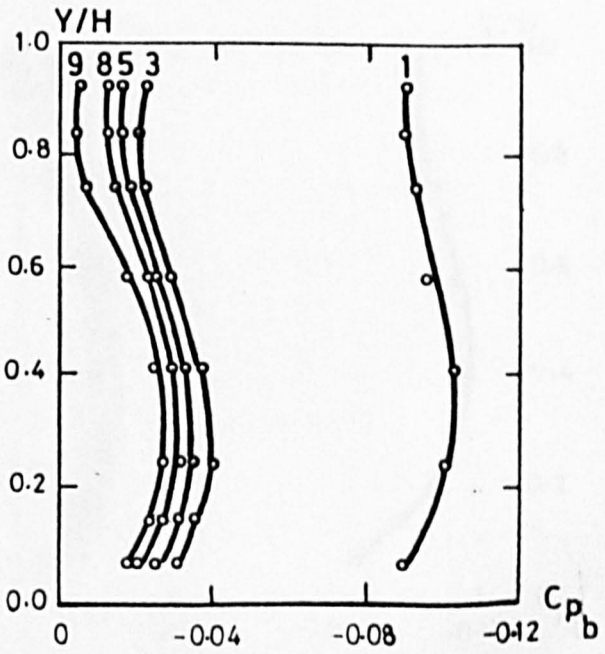

FIGURE 7.12 EFFECT OF ARRAY SIZE AND THE ATMOSPHERIC SHEAR FLOW ON WALL PRESSURE COEFFICIENT DISTRIBUTIONS – 10% STAGGERED PATTERN

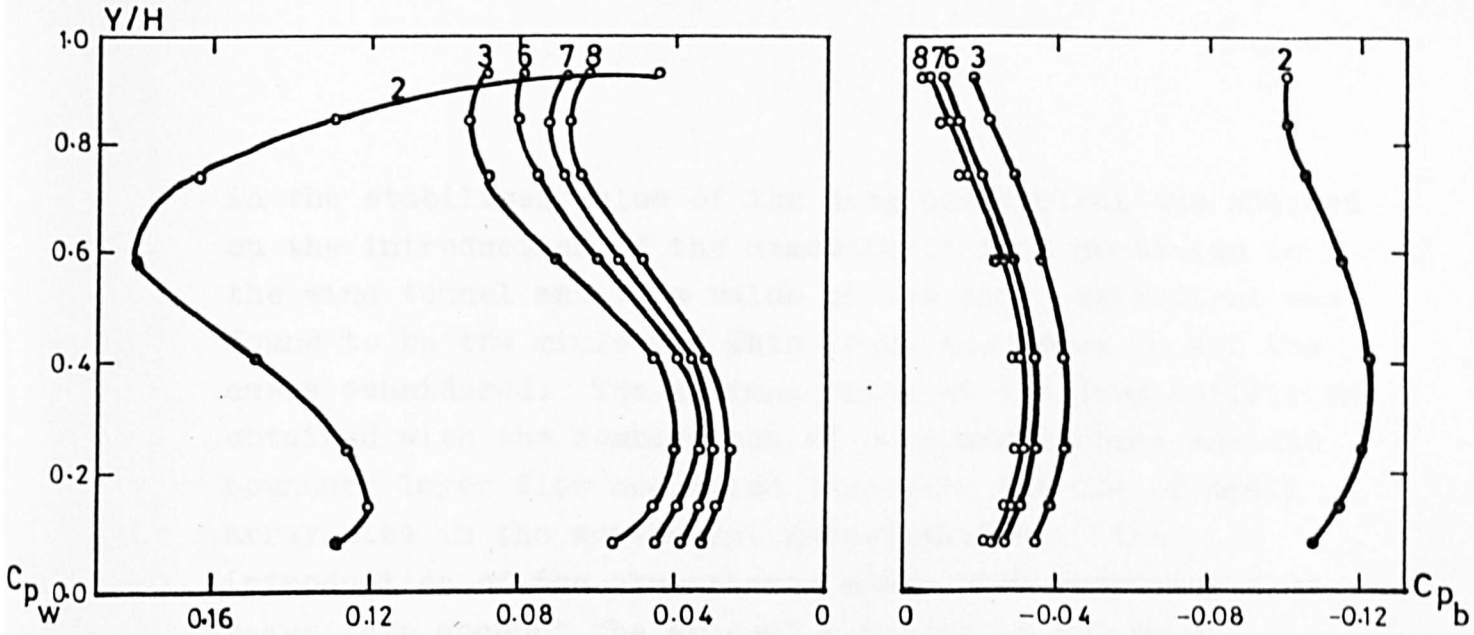

FIGURE 7.13 EFFECT OF ARRAY SIZE AND THE ATMOSPHERIC SHEAR FLOW ON WALL PRESSURE COEFFICIENT DISTRIBUTIONS – 20% STAGGERED PATTERN

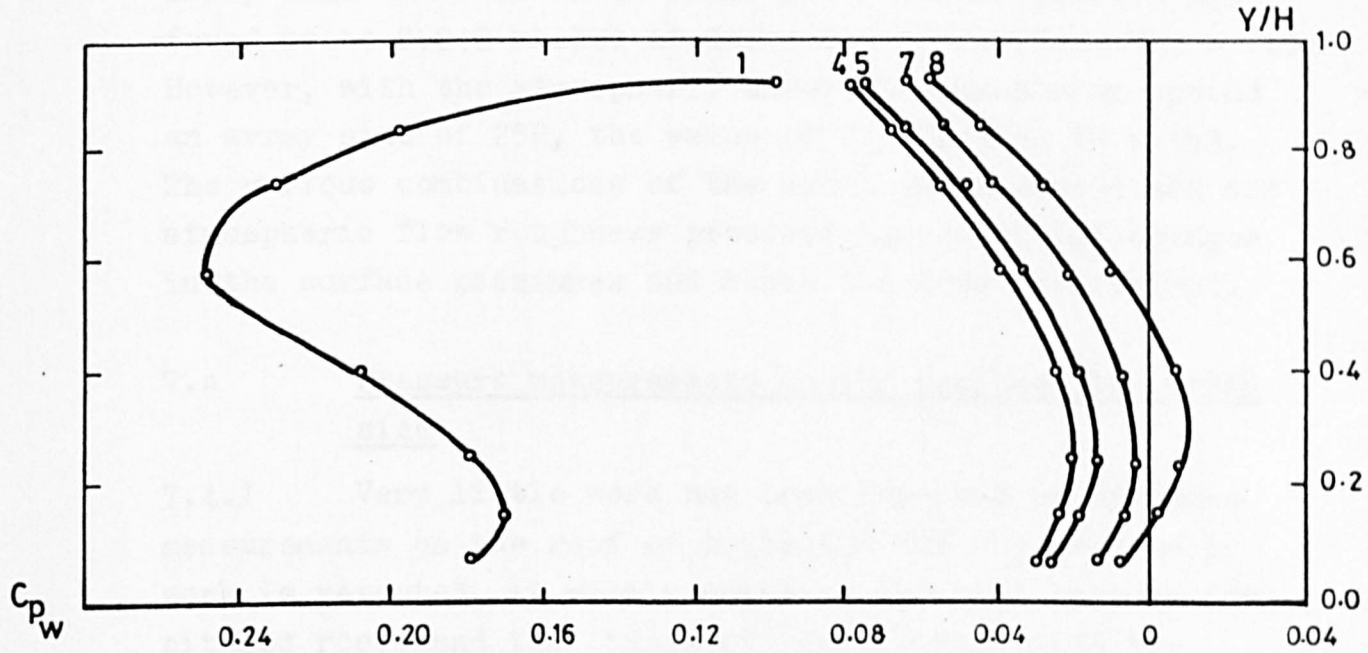

GROUP SIZE

1 R/H = 3.0
2 = 5.0
3 = 15.0
4 = 25.0
5 = 47.5
6 = 67.5
7 R/H = 12.0 + atmospheric shear flow
8 = 15.0 + " " "

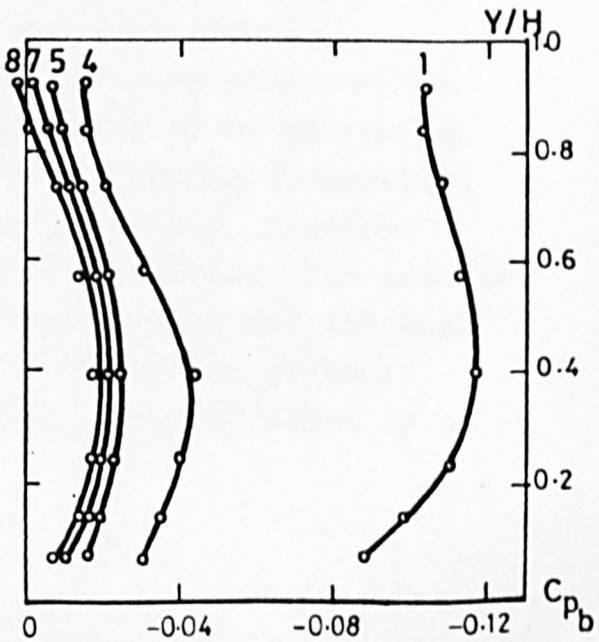

FIGURE 7.14 EFFECT OF ARRAY SIZE AND THE ATMOSPHERIC SHEAR FLOW ON WALL PRESSURE COEFFICIENT DISTRIBUTIONS – 25% STAGGERED PATTERN

in the stabilised value of the drag coefficient was noticed on the introduction of the atmospheric flow mechanism in the wind tunnel and this value of the drag coefficient was found to be the minimum. This trend was found in all the cases considered. The minimum value of the drag coefficient obtained with the combination of such array sizes and the boundary layer flow mechanism justifies the use of small array size in the subsequent investigations. The introduction of the atmospheric shear flow mechanism also takes into account the gradual decrease of the drag coefficient at large fetch lengths found in the lowest densities. The value of the drag coefficient for roughness array size R/H = 25 in 5% density for normal pattern was found to be 0.249 whilst it decreased to 0.172 at R/H = 145. However, with the atmospheric shear flow mechanism upwind an array size of 25H, the value of C_{D_1} dropped to 0.153. The various combinations of the model group layout and the atmospheric flow roughness produced insignificant changes in the surface pressures and hence the drag coefficient.

7.4 Pressure measurements on the roof and the array size

7.4.1 Very little work has been reported on pressure measurements on the roof of buildings and wherever such work is reported, it mainly concerns the roof suction for pitched roofs and the change of roof suction with the variation of pitch, Eaton, Mayne and Cook (1976). Kelnhofer (1971), however, carried out some experimental investigation to determine the influence of neighbouring building models on the flat roof wind loading of parallel building models, changing their height ratio, distance between the two models and the wind direction. His results show that depending on the model combination and the wind direction, the minimum flat roof wind suction pressure coefficient may be favourably or adversely affected by a neighbouring building.

7.4.2 In the present study detailed roof pressure measurements were made. The pressure coefficient distributions on the centre line of the model roof for various fetch lengths in different densities are shown in Figures 7.15 to 7.20. The roof lift coefficient, C_{L_1}, was calculated by integrating these pressure coefficient distributions and its variation with the upstream fetch is shown in Figure 7.21.

7.4.3 The roof pressure distributions in various densities for different fetch lengths shown in Figures 7.15 to 7.20 show the maximum negative pressure near the windward edge of the model which agrees with the trend established in chapter 6 for isolated models. The magnitude of these pressure coefficients keep on decreasing with the increase of fetch, though the variation is found to be small at larger fetch lengths.

7.4.4 The trend in the variation of the roof lift coefficient with fetch for both the layout patterns is broadly similar to the corresponding variation of the drag coefficient. The only slight difference in the behaviour of the two is, that the roof lift coefficient does not show a distinct point where its value can be taken to have stabilised as was shown by similar variation of drag coefficient at higher densities. The variation in the value of the roof lift coefficient, C_{L_1}, with upstream fetch is however small when the fetch length is increased beyond the value required for stabilisation of drag forces found in section 7.2. The values of C_{L_1} can, therefore, be taken to have stabilised at the same values of fetch.

7.4.5 The roof lift coefficient was also found to decrease to its lowest value when the atmospheric incident flow was introduced in the wind tunnel upwind the array size required for the stabilisation of pressures. Various combinations of both the array size and the roughness of the atmospheric flow simulation mechanism, identical to those described in section 7.3, did not produce any

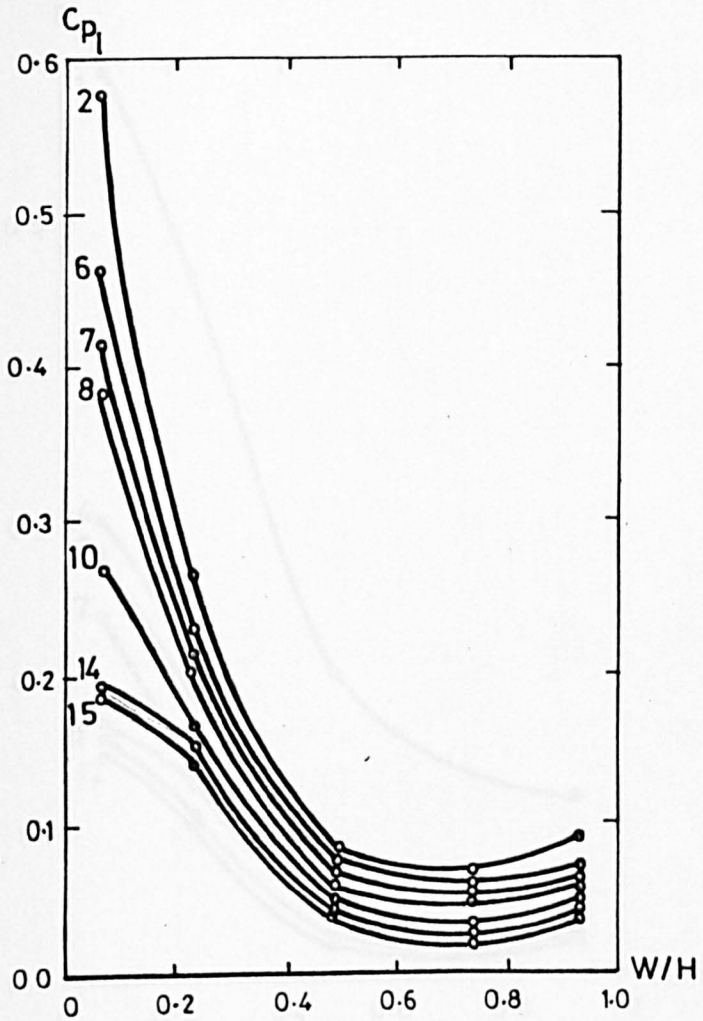

FIGURE 7.15 VARIATION OF ROOF PRESSURE COEFFICIENT DISTRIBUTIONS WITH FETCH LENGTH - 5% NORMAL PATTERN

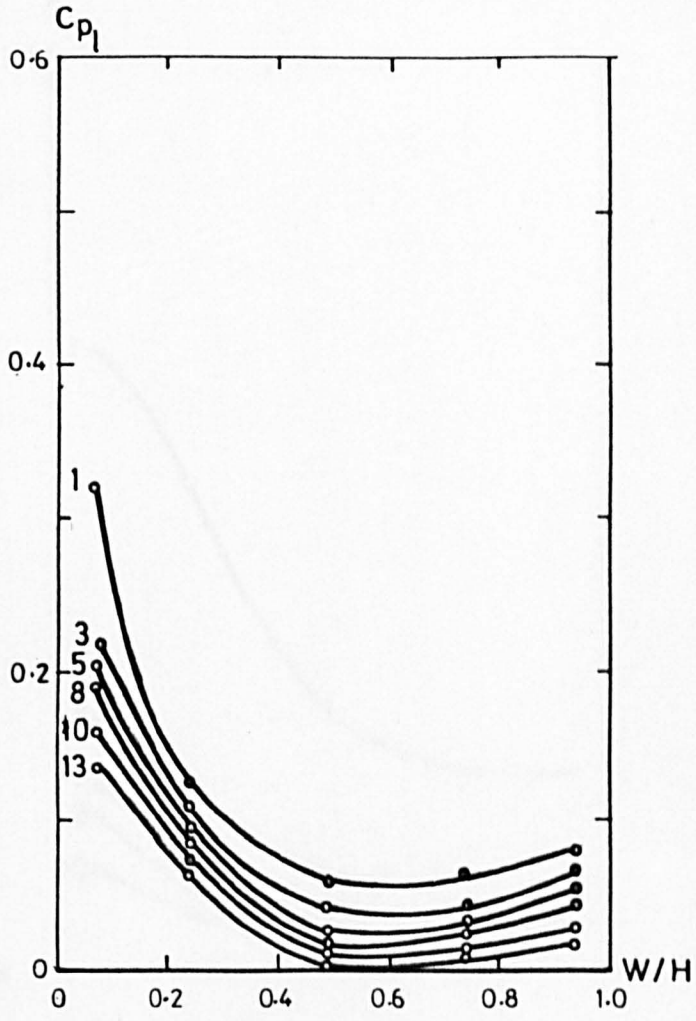

FIGURE 7.16 VARIATION OF ROOF PRESSURE COEFFICIENT DISTRIBUTIONS WITH FETCH LENGTH - 10% NORMAL PATTERN

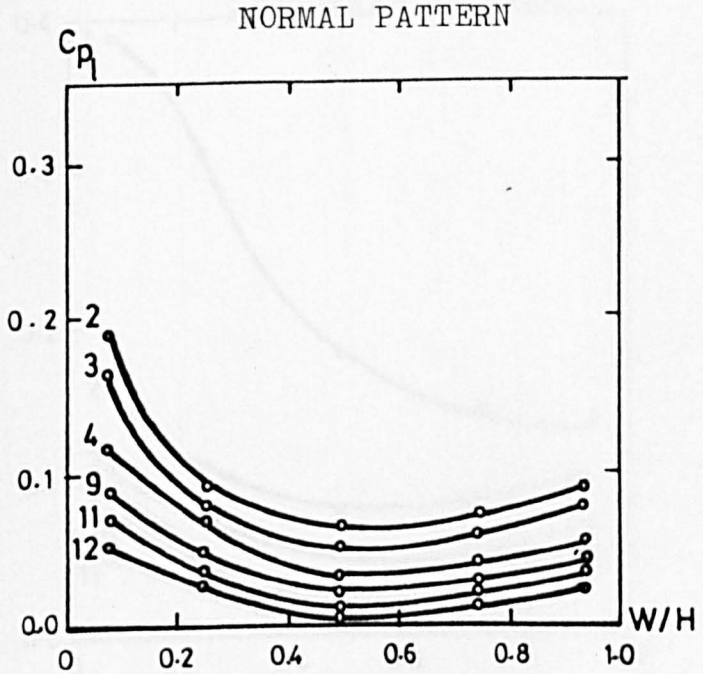

FIGURE 7.17 VARIATION OF ROOF PRESSURE COEFFICIENT DISTRIBUTIONS WITH FETCH LENGTH - 20% NORMAL PATTERN

GROUP	SIZE			
1	R/H = 3.6			
2	= 5.0			
3	=10.0			
4	=15.0			
5	=16.0			
6	=20.0			
7	=25.0			
8	=50.0			
9	=67·5			
10	=145.0			
11	R/H =12.5+	atmos.	shear	flow
12	=15.0+	"	"	"
13	=16.0+	"	"	"
14	=20.0+	"	"	"
15	=25.0+	"	"	"

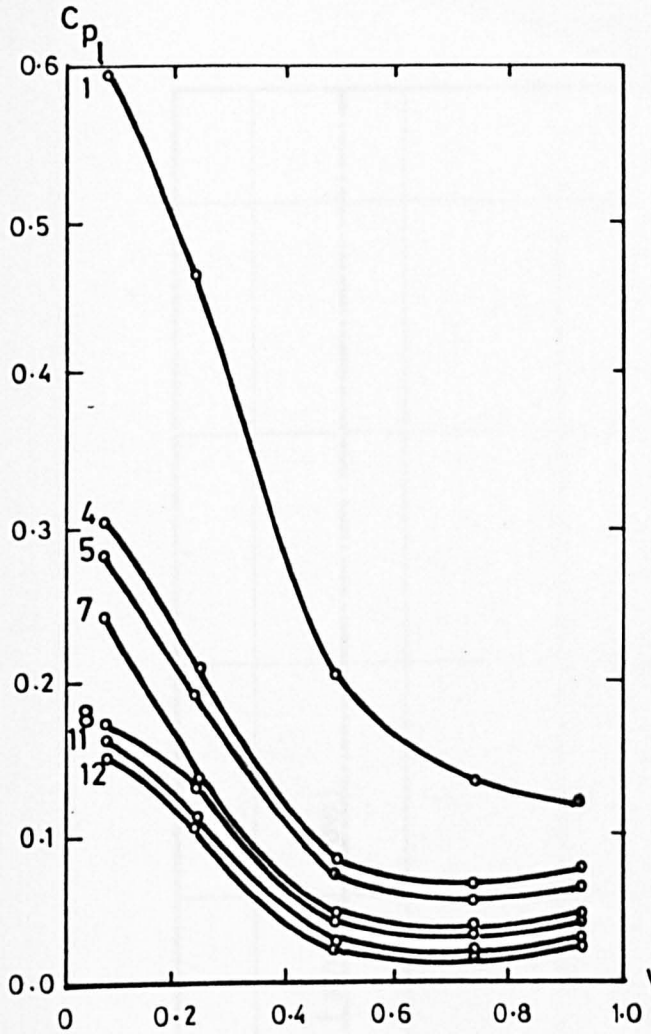

FIGURE 7.18 VARIATION OF ROOF PRESSURE COEFFICIENT DISTRIBUTIONS WITH FETCH LENGTH - 10% STAGGERED PATTERN

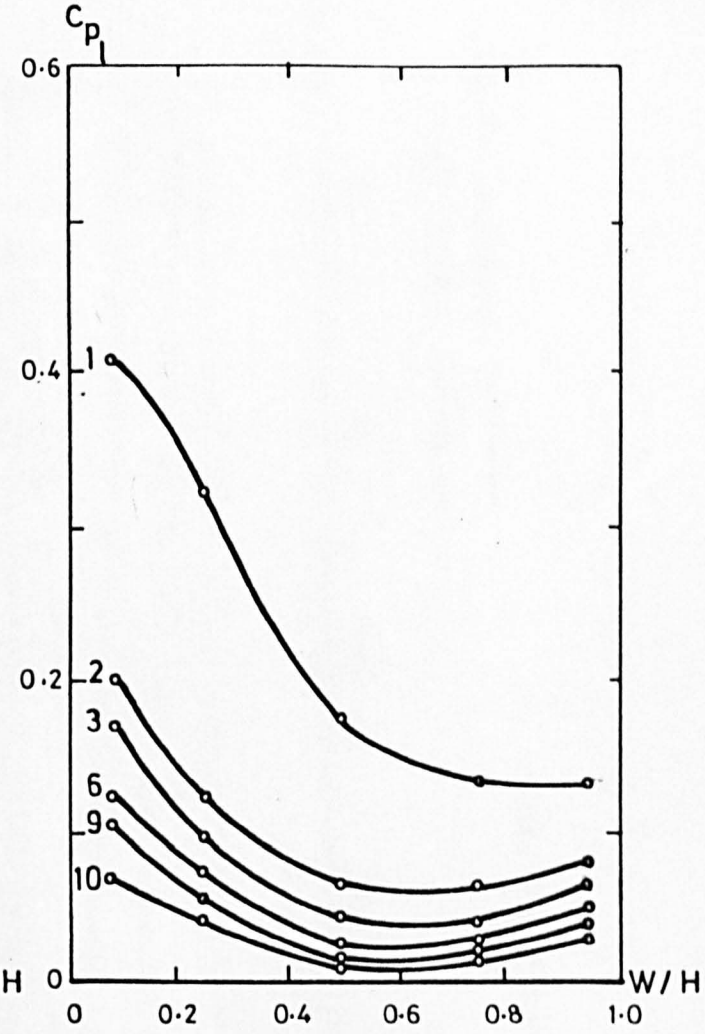

FIGURE 7.19 VARIATION OF ROOF PRESSURE COEFFICIENT DISTRIBUTIONS WITH FETCH LENGTH - 20% STAGGERED PATTERN

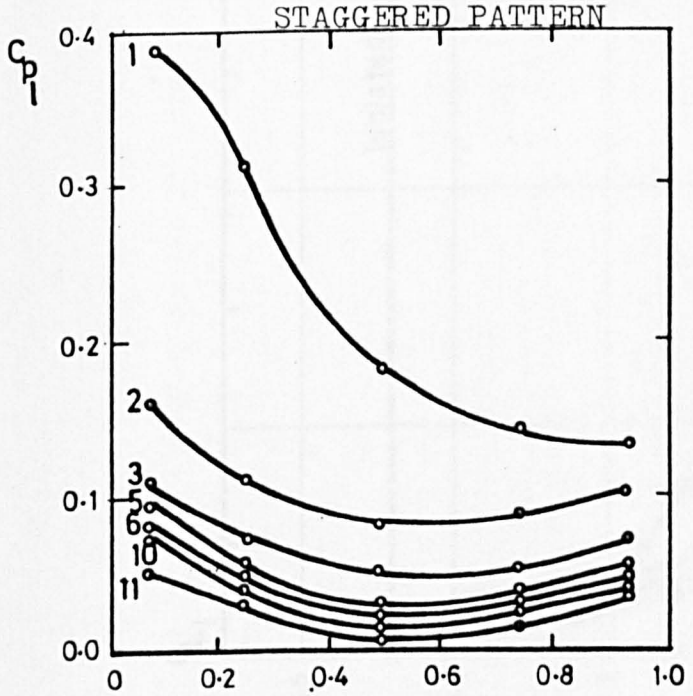

FIGURE 7.20 VARIATION OF ROOF PRESSURE COEFFICIENT DISTRIBUTIONS WITH FETCH LENGTH - 25% STAGGERED PATTERN

GROUP	SIZE
1	R/H = 5·0
2	=10·0
3	=15·0
4	=20·0
5	=25·0
6	=67·5
7	=100·0
8	=145·0
9	R/H =12·5 + atmospheric shear flow
10	=15·0 + " "
11	=20·0 + " "
12	=25·0 + " "

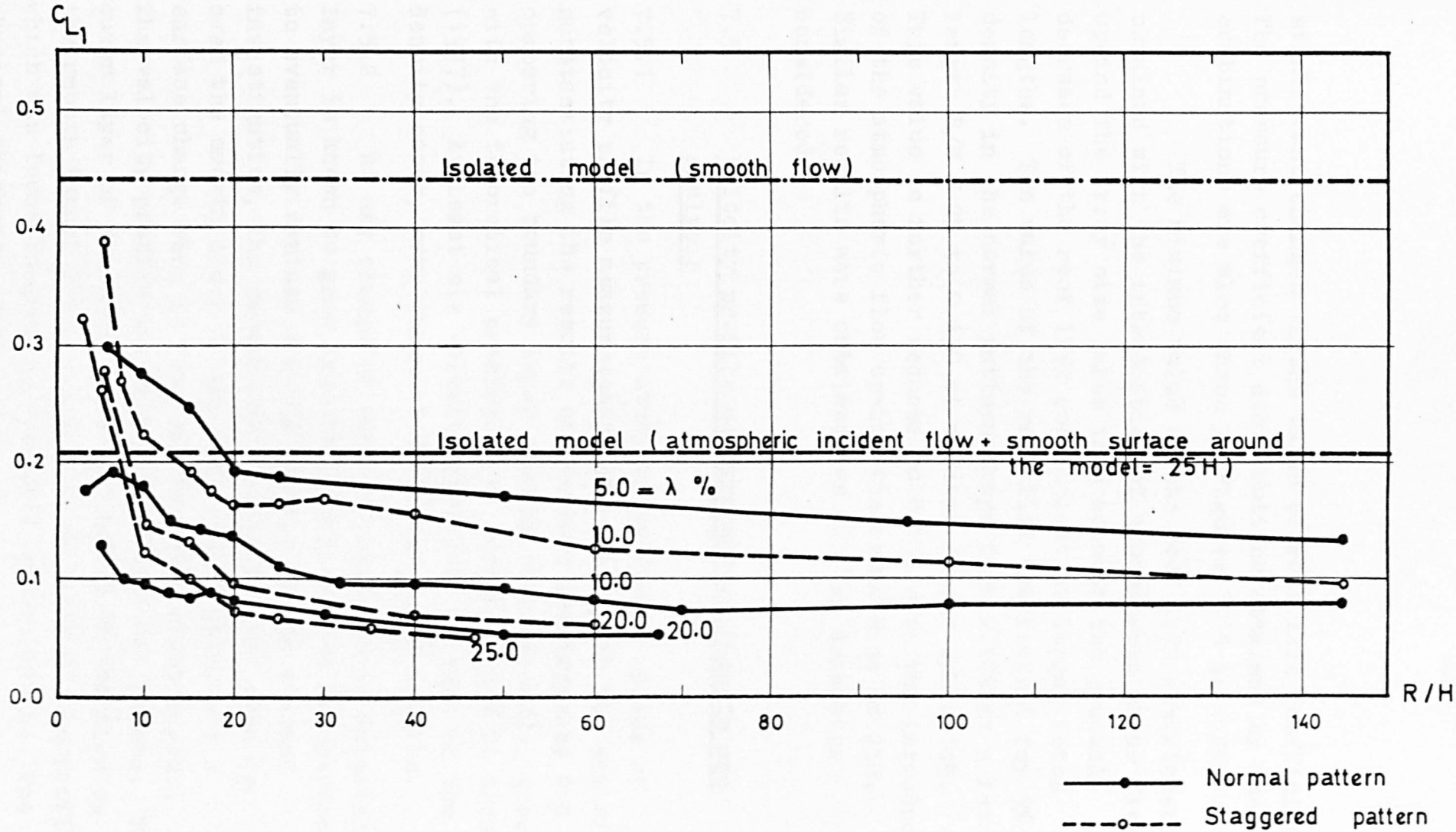

FIGURE 7.21 VARIATION OF ROOF LIFT COEFFICIENT WITH FETCH

significant changes in the value of roof lift coefficient. The pressure coefficient distributions obtained by these combinations are also shown in Figures 7.15 to 7.20.

The minimum value of the roof lift coefficient obtained with the introduction of atmospheric shear flow upwind the array size takes into account the gradual decrease of the roof lift coefficient at larger fetch lengths. The value of the roof lift coefficient for 5% density in the normal pattern drops from 0.185 at a fetch length R/H = 25 to 0.130 at a fetch length R/H = 145. This value is further reduced to 0.115 with the introduction of the atmospheric flow upwind the array size of 25H. Similar results were obtained for all the densities considered.

7.5 Velocity profile measurements: results and analysis

7.5.1 In the present study an extensive series of velocity profile measurements were taken with the aim of substantiating the results of pressure measurements and comparing the boundary layer growing over the model group with the theoretical prediction of Gartshore and De Croos (1977). At least six velocity profiles, in each of the density cases, were taken at different fetch lengths.

7.5.2 At any change of surface roughness an internal layer is known to grow from the origin of the new surface to eventually replace the old layer. In the present investigation, the smooth wall boundary layer growing over the smooth floor of the wind tunnel underwent a surface change when it reached the model group layout. The velocity profile was thus composed of two layers. The outer layer of the profile corresponding to the flow on the smooth tunnel floor and the inner layer of the profile which was found to grow on the model group layout. The physical thickness of the inner layer increased with the

fetch and completely replaced the outer smooth wall boundary layer profile in the case of smaller densities where the model group layout extended the whole length of the tunnel. Figure 7.22 shows the increase of inner layer profile with the fetch length. The vertical origin of the velocity profile measurements was on the cube centre line and on top of the cubes.

7.5.3 Previous empirical studies of rough wall boundary layers have related the wall shear stress to some integral boundary layer thickness parameters usually the displacement thickness δ^*, to calculate the shape of the boundary layer. Dvorak (1969) has given an extensive review of the results obtained using square two dimensional bar roughness elements. He related the bar height, k, and the bar spacing, λ_e, to the effective wall shear stress, $_o$ and the displacement thickness, δ^*, using the form proposed by Clauser (1954), as follows.

$$\frac{U_1}{U_\tau} = \frac{1}{K} \ln \frac{U_1 \delta^*}{U_\tau k} + A_1 - C \qquad 7.1$$

where $\frac{U_\tau}{U_1} = \left(\frac{\tau_o}{\rho U_1^2}\right)^{\frac{1}{2}}$

U is the shear velocity, is the density of air, A, C and K are constants. Gartshore et al (1977) calculated the shape of the boundary layer in equilibrium by relating it to the roughness beneath, using Dvorak's data correlation and a semi empirical calculation method. As few natural rough boundaries can be approximated by a pattern of square bars normal to the flow, it is necessary to generalise the above results to three dimensional roughness elements of various shapes. Gartshore et al have done this by defining an effective spacing between two dimensional bars which produce the surface drag per unit area equal to that of the more

general roughness pattern and related the effective streamwise spacing between two dimensional roughness bars to the spacing between three dimensional roughness elements with the following equation

$$\frac{\lambda_e}{k} = \frac{A_p}{a_f} \qquad 7.2$$

where A_p is the plan area associated with one roughness element and a_f is the frontal area of one roughness element.

Head's method of empirically relating the entrainment rate to the shape factor, described by Dvorak (1969), when applied to zero pressure gradient boundary layers becomes:

$$\frac{d}{d_x}(\theta^* H_1) = F_1(\frac{\delta^*}{\theta^*}) \qquad 7.3$$

where F_1 is a known empirical function of the ratio δ^*/θ^*, θ^* is the boundary layer momentum thickness and H_1 is a shape factor related empirically to δ^*/θ^*.

Based on this relationship Gartshore then went on to relate the velocity profile power law exponent, α, to the three dimensional roughness elements with the equation:

$$\alpha = fn[\frac{\delta}{H}, \frac{\lambda_e}{k}] \qquad 7.4$$

and produced a graph relating the power law exponent with δ/H for equal values of λ_e/k, valid for equilibrium situations.

7.5.4 Figure 7.23 shows the theoretical graph suggested by Gartshore et al (1977) alongwith the results of the present investigation for equivalent values of λ_e/k as well as the values measured by Gartshore for $\lambda_e/k = 32$.

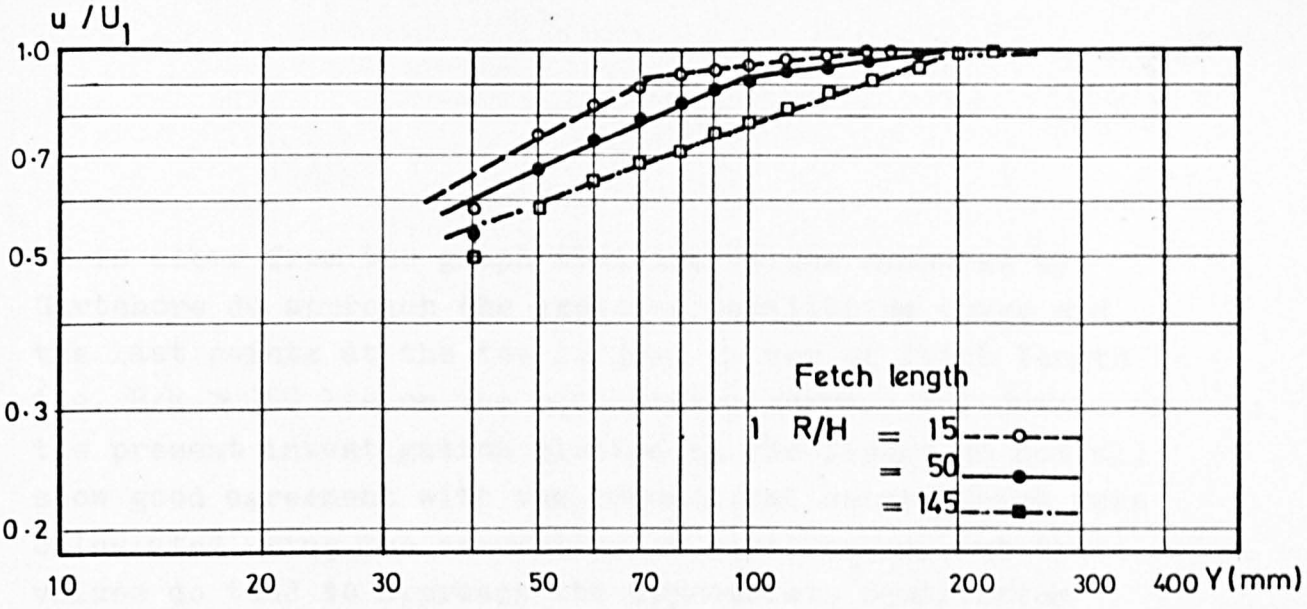

FIGURE 7.22 DEVELOPMENT OF INTERNAL LAYER WITH THE FETCH – 5% NORMAL PATTERN

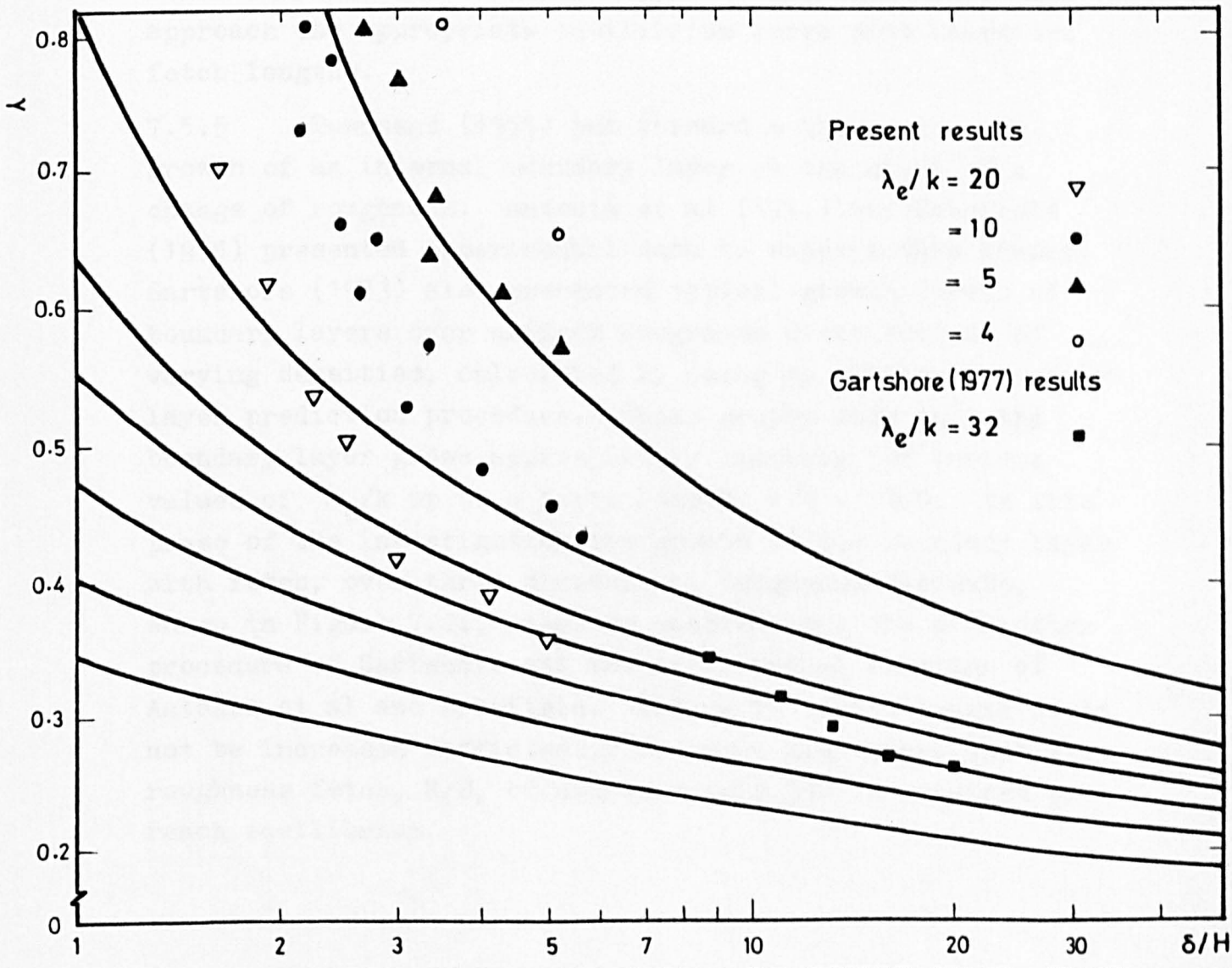

FIGURE 7.23 EFFECT OF ROUGHNESS GEOMETRY ON PROFILE SHAPE, EXACT EQUILIBRIUM CONDITIONS (AFTER GARTSHORE 1977) ALONGWITH THE PRESENT RESULTS

It is clear from the graph that the values measured by Gartshore do approach the expected equilibrium curve and the last points at the two largest values of fetch length i.e. $R/k > 350$ lie on the equilibrium curve. The data from the present investigation plotted in the figure do not all show good agreement with the theoretical curves which were calculated using the assumption of equilibrium, but these values do tend to approach the appropriate equilibrium curve. The agreement is, however, good for the last three values of $\lambda_e/k = 20$, where the model group extended to the whole length of the tunnel. From the trend in their variation of other values it appears that they would also approach the appropriate equilibrium curve with increased fetch lengths.

7.5.5 Townsend (1965) put forward a theory for the growth of an internal boundary layer at the start of a change of roughness. Antonia et al (1971) and Schofield (1975) presented experimental data to support this theory. Gartshore (1973) also presented typical growth curves of boundary layers over uniform roughness distributions of varying densities, calculated by using an integral boundary layer prediction procedure. These graphs show that the boundary layer grows approximately linearly for various values of λ_e/k up to a fetch length, $R/H = 1000$. In this phase of the investigation the growth of the boundary layer with fetch, over three dimensional roughness elements, shown in Figure 7.24, seems to substantiate the prediction procedure of Gartshore and the experimental findings of Antonia et al and Schofield. Though the fetch length could not be increased sufficiently to prove his theory that the roughness fetch, R/H, of approximately 350 is required to reach equilibrium.

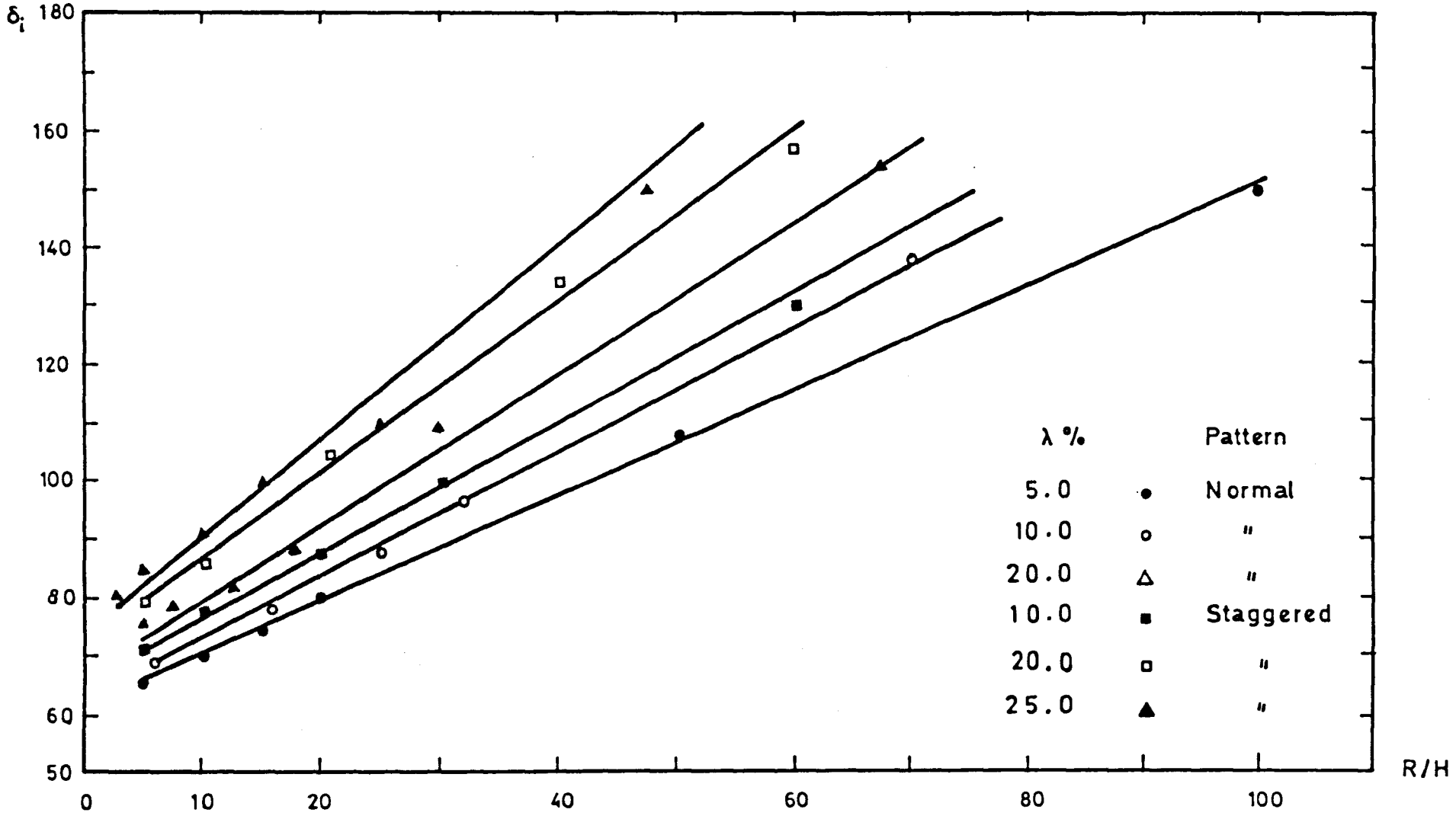

FIGURE 7.24 GROWTH OF INTERNAL LAYER WITH THE FETCH LENGTH

7.6 Conclusions

7.6.1 The drag coefficient was found to decrease with the increase of fetch in all cases considered. The variation was, however, found to be gradual in lower density cases with large element spacing. In these cases, though the reduction in the value of drag coefficient was gradual, the rate of decrease was, however, found to be smaller after a fetch length of 25H. On the other hand, in higher densities the variation of drag coefficient was abrupt initially after which the change was nominal. The extent of the array size after which the reduction in the value of drag coefficient is nominal depends on the group density and is found to decrease with the increase of density.

7.6.2 The model group size required for the surface pressure forces to stabilise depends on the group density and the spacing between the elements and is found to vary from 10H to 25H. Shorter fetches are normally required for stabilisation of the mean pressure forces at higher densities.

7.6.3 At higher densities the windward pressure coefficients were found to undergo a small increase with the increase of fetch initially before decreasing at larger fetch lengths. This is suggested to be due to the larger values of zero plane displacement in high density groupings resulting in decreased effective height. Once the zero plane displacement has achieved its maximum value, the windward pressure coefficients begin to decrease with the increase of fetch. This phenomenon was not observed in low density groups due to smaller zero plane displacement.

7.6.4 With the introduction of atmospheric boundary layer simulated flow upstream of the array size required for the stabilisation of surface pressures, the drag coefficient dropped to its lowest value. This lowest value of drag coefficient was found not to be affected by small variations in the combination of array size and the

atmospheric flow simulation mechanism.

7.6.5 The minimum value of drag coefficient obtained with the combination of array size and the atmospheric boundary layer flow mechanism takes into account any reduction in the value of drag coefficient which might occur at larger array sizes and therefore justifies the use of small array size in the subsequent investigations.

7.6.6 The roof pressure coefficients were always negative with the maximum suction occurring near the windward edge of the roof and decreasing towards the rear edge.

7.6.7 The variation of roof lift coefficient with the fetch was found to be similar to the corresponding variations in the drag coefficient and stabilised at similar values of fetch lengths. The effect of the introduction of the atmospheric boundary layer flow upwind of the array size required for stabilisation was also similar to the one found for the drag coefficient.

7.6.8 The growth of the boundary layer over three dimensional cubical arrays was found to be in reasonable agreement with the theoretical prediction of Gartshore correlating the shear stress with integral boundary layer properties and the three dimensional roughness geometry.

7.6.9 The surface pressure forces on the model were found to stabilise before the boundary layer reached equilibrium.

7.6.10 The linear growth of the boundary layer showed good agreement with the previous results and the theoretical prediction of Gartshore.

CHAPTER 8

EXPERIMENTAL RESULTS AND DISCUSSIONS: FLOW OVER GROUPS OF CUBE SHAPED ROUGHNESS ELEMENTS

8. EXPERIMENTAL RESULTS AND DISCUSSIONS: FLOW OVER GROUPS OF CUBE SHAPED ROUGHNESS ELEMENTS

8.1 Introduction

8.1.1 The purpose of the experiments to be explained in this chapter are to define the way in which group geometry governs the mean pressure forces on a group of identical roughness elements. This chapter alone follows the work of Soliman (1976), who looked at this problem earlier and whose work was restricted to the measurement of windward and leeward face pressures on a cube shaped roughness element. Soliman's work has been criticised, in that, his experimental arrangements were not sufficiently rigorous to establish accurate values during his investigation, though the trends he reported would be expected to be of great value, Lee and Soliman (1977) and Gartshore (1977). The present arrangement differs from that of Soliman in that the atmospheric boundary layer has been more rigorously established, resulting in better accuracy of the nature of flow and the model fetch lengths are greater thereby ensuring flow stabilisation. Also the ratio of physical thickness of boundary layer to the model height is large enough to be considered an acceptable compromise for wind tunnel testing. Thus the present results can be directly applied to low rise housing.

8.2 The effect of fetch on the central model drag

8.2.1 In the present investigation the model group took the form of free standing cubes on a smooth surface with the urban terrain atmospheric boundary layer simulation upwind. Thus the oncoming atmospheric flow underwent an abrupt change of surface roughness when it reached the group layout. The effect of this disturbance on the atmospheric boundary layer flow and its effect on the stabilisation of the surface pressure forces has been investigated in detail in Chapter 7.

The element drag was found to vary with the fetch length of the model layout before becoming stabilised when surrounded by an array of similarly sized elements. The extent of the array size, R/H, at which the drag stabilises varies from 10 to 25 depending upon the spacing between adjacent roughness elements or on the plan area density, λ_p. Normally shorter fetches were required for stabilisation of the mean pressure forces at higher densities.

8.2.2 The roof suction, C_{L_1}, was found to behave in a similar manner to the drag, C_{D_1}, in its variation with the group layout size. This variation was found to be appreciable up to a certain value of the array size which corresponded to the value of R/H where the value of drag was also found to stabilise. Further increases in the fetch were found to result in only nominal variations in the roof suction which could also be taken to be stabilised for practical purposes. The extent of the fetch required to produce only nominal changes in C_{L_1} depended on the group layout density and was found to vary from R/H = 10 to 25. Full details of these results are given in Chapter 7.

8.2.3 On the basis of conclusions drawn in Chapter 7, the model group layout size, R/H, in all subsequent investigations was varied from 10 to 25 depending upon the density. In the lowest density considered, the array size was kept at 25H and it was progressively reduced to 10H for the highest density.

8.3 The variables considered in this stage of investigation

8.3.1 An extensive series of mean pressure measurements and velocity profile measurements have been undertaken with a view to establishing a clear picture of the flow around a cube shaped roughness element positioned at the centre of a large group of similar elements. Table 8.1 gives the ranges of the parameters considered in this stage of the investigations.

Table 8.1 Variables considered in this stage of investigations

Variables	Pressure Measurements	Velocity Profile Measurements
Plan area density	$3.125\% < \lambda_p < 50\%$	$5\% < \lambda_p < 30\%$ (8 densities)
Pattern	Normal and staggered	Normal
Fetch	$10 < \frac{R}{H} < 25$	$10 < \frac{R}{H} < 25$
Orientation	$\theta = \phi = 0$	$\theta = \phi = 0$
Incident Flow	Simulated Atmospheric Boundary Layer Flow	Simulated Atmospheric Boundary Layer Flow

8.4 Pressure measurements on the windward and leeward faces

8.4.1 The vertical distribution of pressure coefficients measured on the centre line of the windward and leeward faces of the model in various layout densities for both the normal and staggered patterns are shown in Figures 8.1 and 8.2. In all these distributions, the orientation angles are $\theta = 0$ and $\phi = 0$. From these pressure coefficient distributions, the centre line windward and leeward pressure coefficients, $C_{p_{wc}}$ and $C_{p_{bc}}$, were calculated. In addition, these centre line pressure distributions were integrated, alongwith four other vertical pressure profiles on the faces of the model to give the mean windward and leeward pressure coefficients, C_{p_w} and C_{p_b}. The algebraic difference of these pressure coefficients in each case yields the drag coefficient, C_{D_1}.

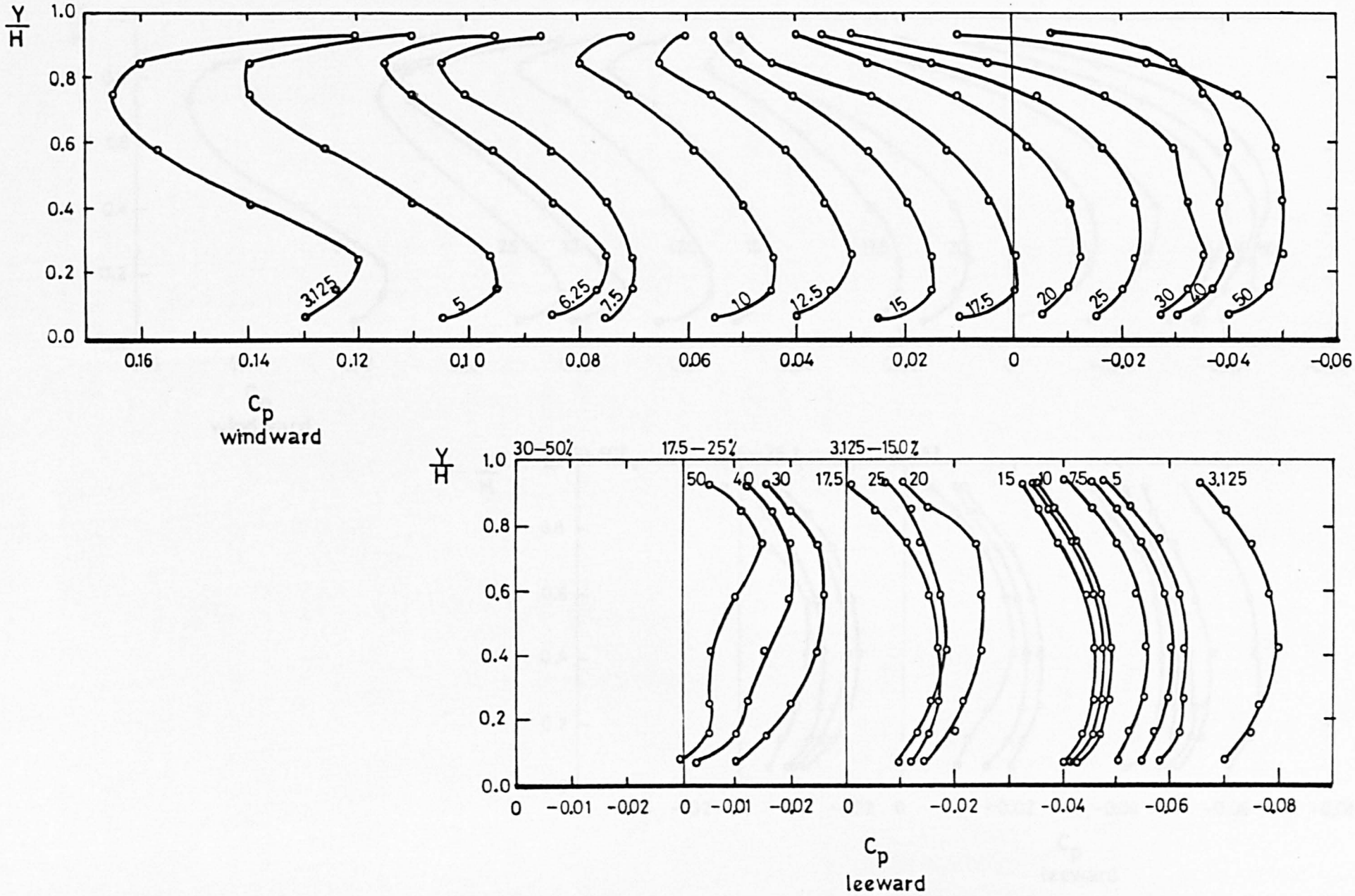

FIGURE 8.1 WALL PRESSURE COEFFICIENT DISTRIBUTIONS ON CUBE CENTRE LINE AT VARIOUS DENSITIES - NORMAL PATTERN.

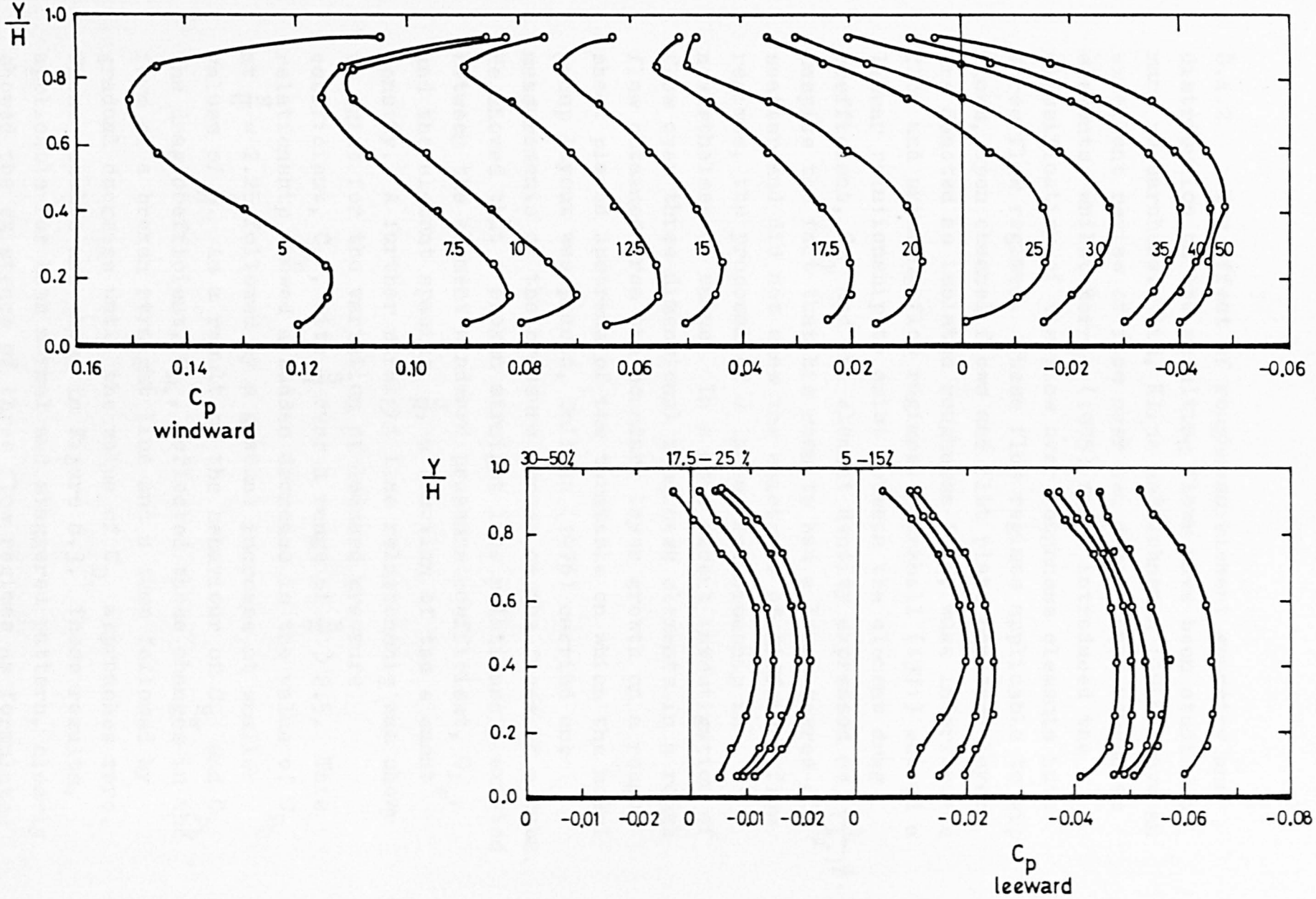

FIGURE 8.2 WALL PRESSURE COEFFICIENT DISTRIBUTIONS ON CUBE CENTRE LINE AT VARIOUS DENSITIES - STAGGERED PATTERN.

8.4.2 The effect of roughness element geometry and distribution on the resulting flows have been studied by many researchers. Liu, Kline and Johnston (1966) gave an excellent review of flow over two dimensional roughness elements, whilst Morris (1955) first introduced the classification of the flow over roughness elements into three flow regimes. These flow regimes applicable to pipe flows, open channel flows and flat plate boundary layers are denoted as isolated roughness flow, wake interference flow and skimming flow regimes. Marshall (1971) showed a linear relationship to exist between the element drag coefficient, C_{D_1} and the element density expressed as $\frac{1}{(\lambda_f)^{\frac{1}{2}}}$. Despite the fact that his results had a large degree of scatter and did not show the existence of different flow regimes, the proposal of a linear relationship is nevertheless of value. In a more recent investigation of flow over three dimensional roughness elements in a rough flow obtained from the boundary layer growth on a rough sheet placed upstream of the turntable on which the model group layout was placed, Soliman (1976) carried out measurements of the pressure forces on the faces of a cube. He showed that a broken straight line relationship existed between the element windward pressure coefficient, C_{p_w}, and the element spacing, $\frac{S}{H}$, a function of the element density. A further straight line relationship was shown to exist for the variation of leeward pressure coefficient, C_{p_b}, with $\frac{S}{H}$ over a range of $\frac{S}{H} > 2.5$. This relationship showed a sudden decrease in the value of C_{p_b} at $\frac{S}{H} = 2.25$ followed by a gradual increase at smaller values of $\frac{S}{H}$. As a result of the behaviour of C_{p_w} and C_{p_b} the drag coefficient, C_{D_1}, reflected these changes in the form of a broken straight line and a jump followed by gradual decrease until the value of C_{D_1} approaches zero. These results are shown in Figure 8.3.[1] These results, applicable for both normal and staggered pattern, clearly showed the existence of three flow regimes as formulated by Morris.

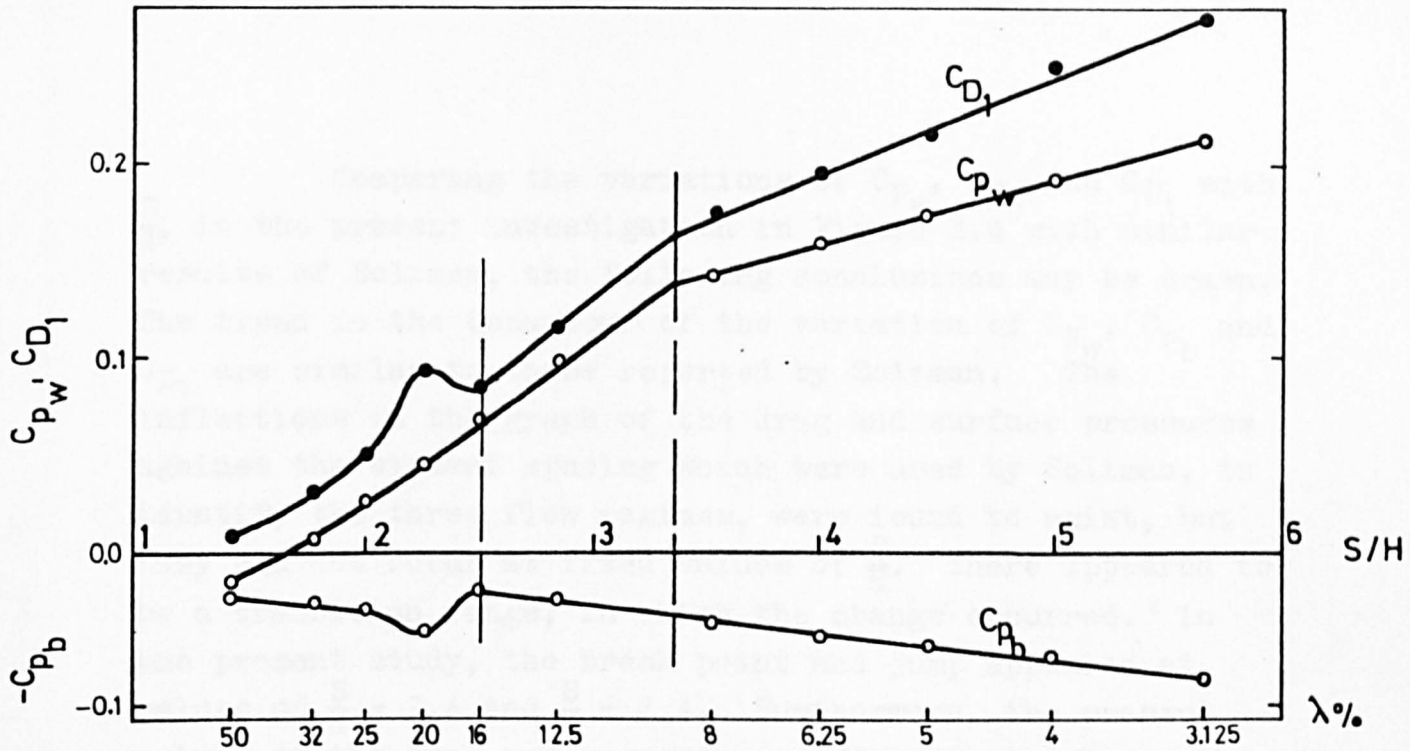

FIGURE 8.3 VARIATION OF THE WALL PRESSURES AND THE DRAG FORCE WITH THE CUBE SPACING - NORMAL PATTERN, ROUGH FLOW (AFTER SOLIMAN 1976)

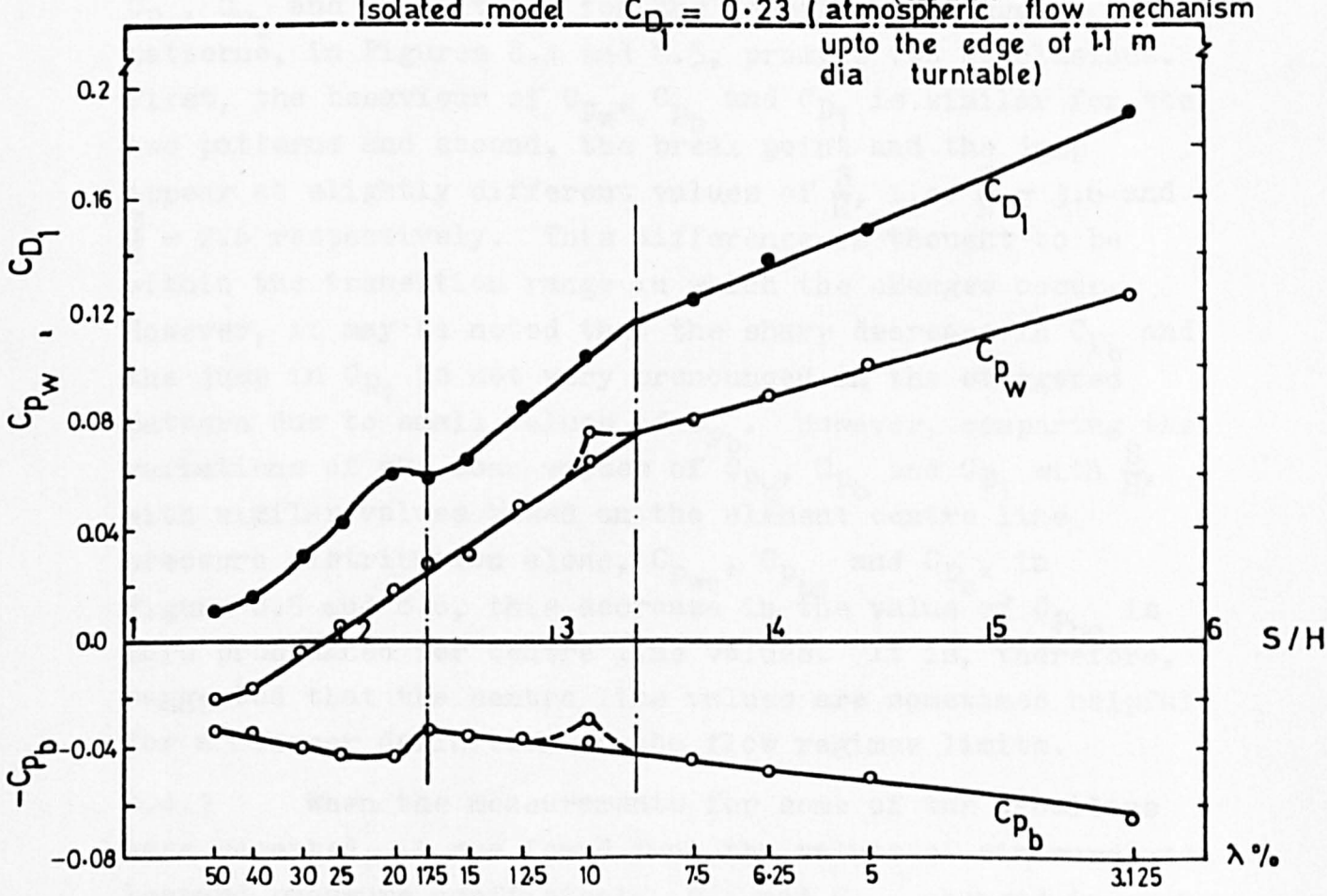

FIGURE 8.4 VARIATION OF THE WALL PRESSURES AND THE DRAG FORCE WITH THE CUBE SPACING - NORMAL PATTERN.

Comparing the variations of C_{p_w}, C_{p_b} and C_{D_1} with $\frac{S}{H}$, in the present investigation in Figure 8.4 with similar results of Soliman, the following conclusions may be drawn. The trend in the behaviour of the variation of C_{p_w}, C_{p_b} and C_{D_1} are similar to those reported by Soliman. The inflections in the graph of the drag and surface pressures against the element spacing which were used by Soliman, to identify the three flow regimes, were found to exist, but they did not occur at fixed values of $\frac{S}{H}$. There appeared to be a transition range, in which the change occurred. In the present study, the break point and jump appeared at values of $\frac{S}{H} \simeq 3.4$ and $\frac{S}{H} \simeq 2.4$. Furthermore, the present values of the drag and pressure coefficients are lower than those reported by Soliman. It is suggested that this difference arises from the differing nature of the incident flows in the two experiments. Comparing the variation of C_{p_w}, C_{p_b} and C_{D_1} with $\frac{S}{H}$, for the normal and staggered patterns, in Figures 8.4 and 8.5, prompts two conclusions. First, the behaviour of C_{p_w}, C_{p_b} and C_{D_1} is similar for the two patterns and second, the break point and the jump appear at slightly different values of $\frac{S}{H}$, i.e. $\frac{S}{H} \simeq 3.6$ and $\frac{S}{H} \simeq 2.6$ respectively. This difference is thought to be within the transition range in which the changes occur. However, it may be noted that the sharp decrease in C_{p_b} and the jump in C_{D_1} is not very pronounced in the staggered pattern due to small values of C_{p_b}. However, comparing the variations of the mean values of C_{p_w}, C_{p_b} and C_{D_1} with $\frac{S}{H}$, with similar values based on the element centre line pressure distribution alone, $C_{p_{wc}}$, $C_{p_{bc}}$ and C_{D_c}, in Figure 8.5 and 8.6, this decrease in the value of $C_{p_{bc}}$ is more pronounced for centre line values. It is, therefore, suggested that the centre line values are sometimes helpful for a clearer definition of the flow regimes limits.

8.4.3 When the measurements for some of the densities were repeated, it was found that the values of windward and leeward pressure coefficients, C_{p_w} and C_{p_b}, changed in such

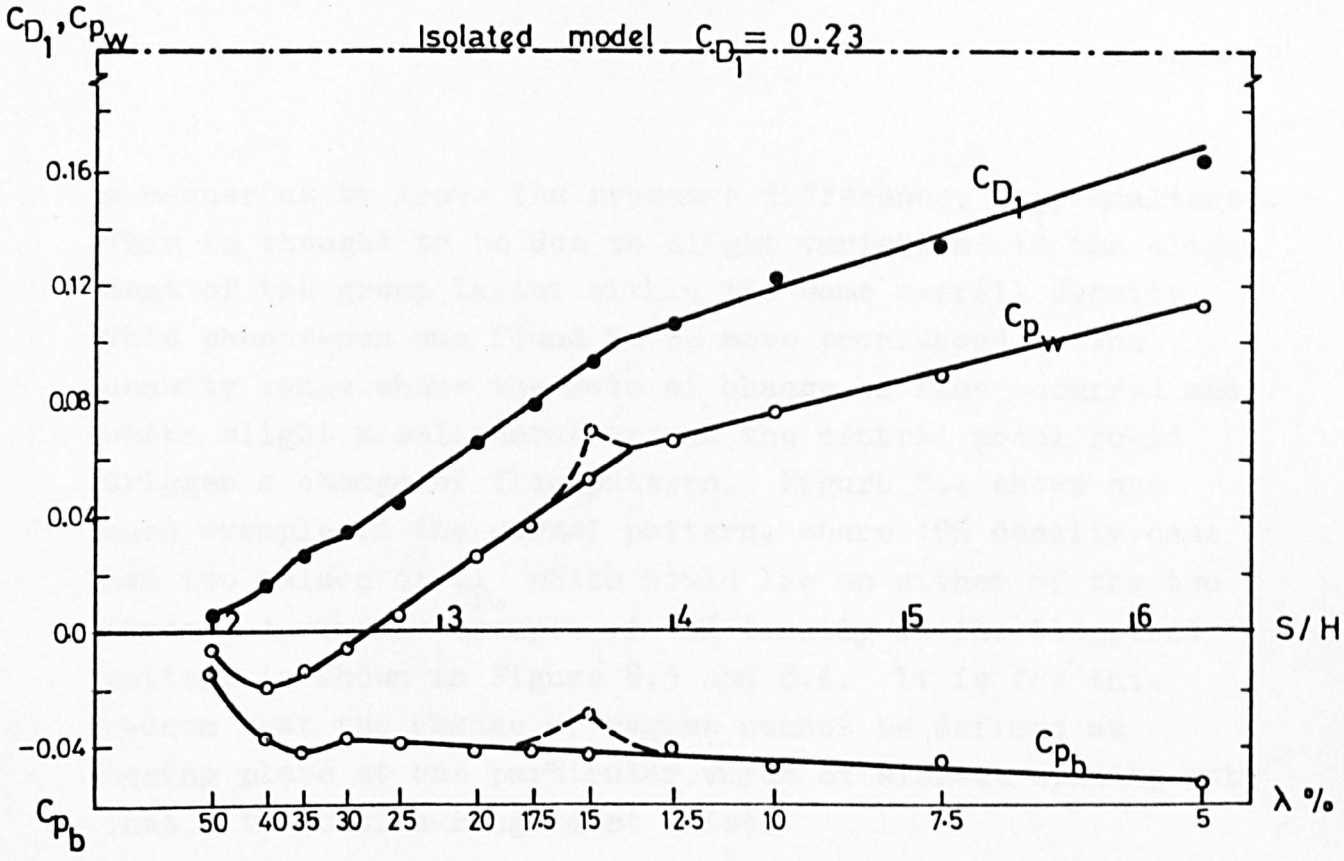

FIGURE 8.5 VARIATION OF THE WALL PRESSURES AND THE DRAG FORCE WITH THE CUBE SPACING - STAGGERED PATTERN

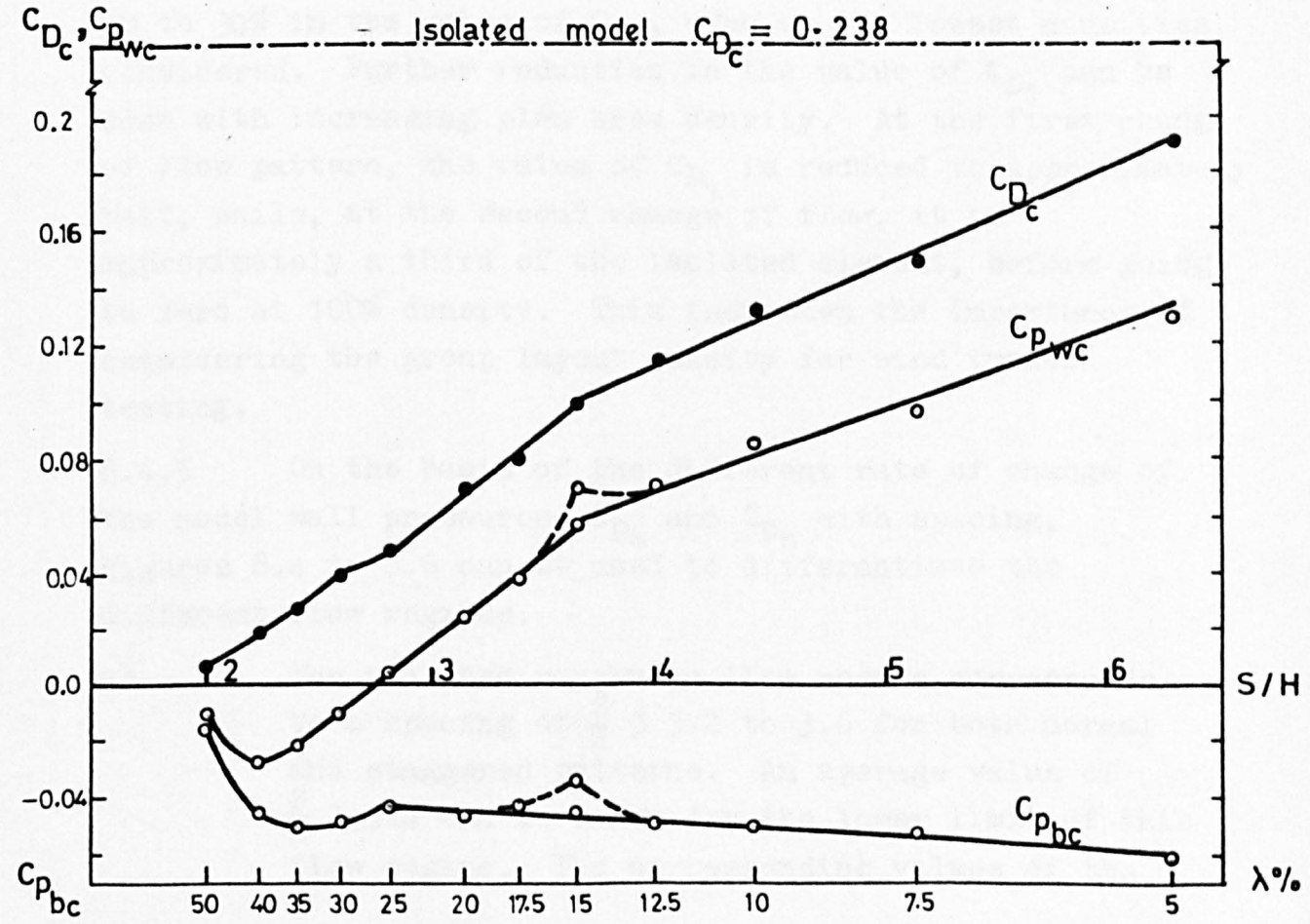

FIGURE 8.6 VARIATION OF THE WALL PRESSURES AND THE DRAG FORCE WITH THE CUBE SPACING (CENTRE LINE VALUES) - STAGGERED PATTERN

a manner as to leave the pressure difference, C_{D_1}, unaltered. This is thought to be due to slight variations in the alignment of the group layout within the same overall density. This phenomenon was found to be more pronounced in the density range where the rate of change of flow occurred and where slight misalignment around the central model could trigger a change of flow pattern. Figure 8.4 shows one such example in the normal pattern, where 10% density case has two values of C_{p_w} which could lie on either of the two lines. A similar example of 15% density in the staggered pattern is shown in Figure 8.5 and 8.6. It is for this reason that the change of regime cannot be defined as taking place at one particular value of element spacing but that a transition range must exist.

8.4.4 Figure 8.4 to 8.6 also show the drag coefficient, C_{D_1}, of an isolated element in the atmospheric flow. It is clear from these figures that there is an immediate drop of up to 30% in the value of C_{D_1}, even at the lowest densities considered. Further reduction in the value of C_{D_1} can be seen with increasing plan area density. At the first change of flow pattern, the value of C_{D_1} is reduced to approximately half, while, at the second change of flow, it is approximately a third of the isolated element, before going to zero at 100% density. This indicates the importance of considering the group layout density for wind tunnel testing.

8.4.5 On the basis of the different rate of change of the model wall pressures, C_{p_w} and C_{p_b} with spacing, Figures 8.4 to 8.6 can be used to differentiate the different flow regimes.

a) The isolated roughness flow regime corresponds to a spacing of $\frac{S}{H} > 3.2$ to 3.6 for both normal and staggered patterns. An average value of $\frac{S}{H} > 3.4$ can be taken for the lower limit of this flow regime. The corresponding values of the

plan area density are $\lambda_p < 8.5\%$ in the normal and $\lambda_p < 17\%$ in the staggered pattern.

b) The skimming flow regime corresponds to an element spacing of $\frac{S}{H} < 2.2$ to 2.6 which can be averaged to 2.4 giving the corresponding values of the plan area density, $\lambda_p > 17\%$ in the normal pattern and $\lambda_p > 34\%$ in the staggered pattern.

c) The wake interference flow regime corresponds to an element spacing of $2.4 < \frac{S}{H} < 3.4$ in both the patterns, i.e. $8.5\% < \lambda_p < 17\%$ in the normal pattern and $17\% < \lambda_p < 34\%$.

8.4.6 It has been suggested by Soliman (1976) that the change from isolated roughness flow regime to wake interference flow regime occurs when the total spacing between the elements is equal to the sum total of upstream separation distance and the downstream reattachment length of an isolated cube as shown in Figure 6.3. He found these distances as 0.83H and 1.53H and suggested a distance 3.36H between the elements, before interference occurs. Similarly Castro and Robins (1977) in their investigation of the wake structure of a surface mounted cube in a turbulent stream have shown that the reattachment occurs at 1.5H from the rear face of the cube. If their value of upstream separation region length of 0.9H for a uniform flow is added to the downstream separation, this will give a spacing of 3.4H before the flow interference occurs. These values are in good agreement with a spacing of $\frac{S}{H} = 3.4$ at which the change of regime from isolated roughness flow to the wake interference flow is suggested in 8.4.5 for the present study. The flow pattern in the wake interference flow regime, where each cube face interfered with the separation bubble of the upstream cube, as suggested by Soliman is shown in Figure 8.7.

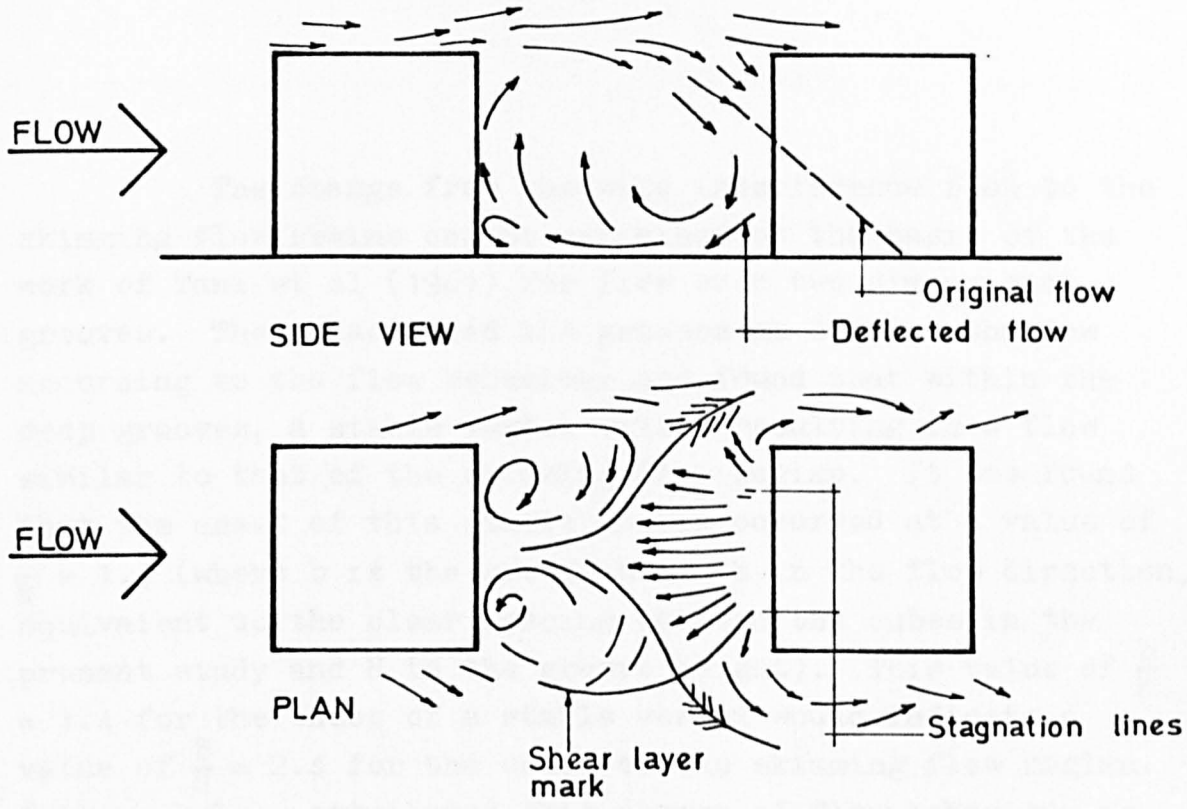

FIGURE 8.7 FLOW PATTERN IN THE WAKE INTERFERENCE FLOW REGIME

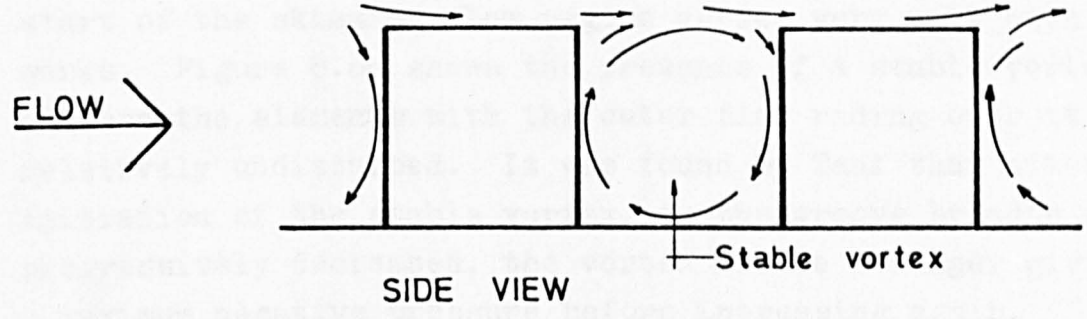

FIGURE 8.8(a) FLOW PATTERN IN THE SKIMMING FLOW REGIME

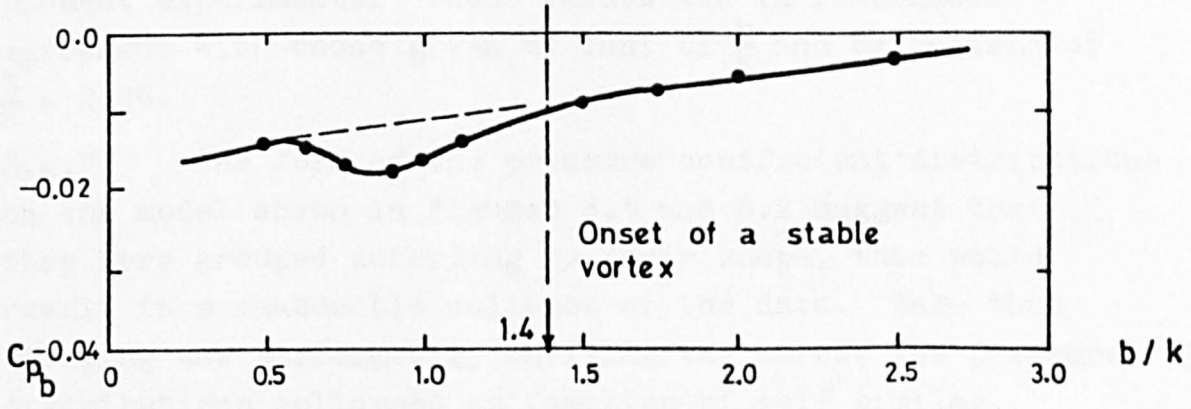

FIGURE 8.8(b) A REPLOT OF THE RESULTS OF TANI ET AL (1961) FOR THE LEEWARD GROOVE WALL PRESSURES

The change from the wake interference flow to the skimming flow regime can be explained on the basis of the work of Tani et al (1961) for flow over two dimensional grooves. They classified the grooves as deep or shallow according to the flow behaviour and found that within the deep grooves, a stable vortex exists resulting in a flow similar to that of the skimming flow regime. It was found that the onset of this stable vortex occurred at a value of $\frac{b}{k} = 1.4$ (where b is the groove breadth in the flow direction, equivalent to the clear spacing between the cubes in the present study and H is the groove height). This value of $\frac{b}{k} = 1.4$ for the onset of a stable vortex would indicate a value of $\frac{S}{H} = 2.4$ for the onset of the skimming flow regime. Soliman, also, attributed this change of flow behaviour to the initiation of a stable vortex and gave a value of $\frac{S}{H} = 2.5$. Thus the value of $\frac{S}{H} = 2.4$ given in 8.4.5 for the start of the skimming flow regime agrees very well with other works. Figure 8.8a shows the presence of a stable vortex between the elements with the outer flow riding over it relatively undisturbed. It was found by Tani that after the initiation of the stable vortex, as the groove breadth was progressively decreased, the vortex became stronger giving a maximum negative pressure before increasing again, Figure 8.8b. The maximum value of the negative pressure due to the vortex formation was found to occur at $\frac{S}{H} = 2$ in the normal pattern and 2.3 in the staggered pattern in the present experiments. These values are in reasonable agreement with those given by Tani of $\frac{b}{k}$ and by Soliman of $\frac{S}{H} = 2.25$.

8.4.7 The form of the pressure coefficient distributions on the model shown in Figures 8.1 and 8.2 suggest that if they were grouped according to their shape, this would result in a reasonable collapse of the data. When this grouping was performed, by shifting the zeros, the pressure distributions collapsed as families of self similar profiles. This is shown in Figures 8.9a and 8.9b, where

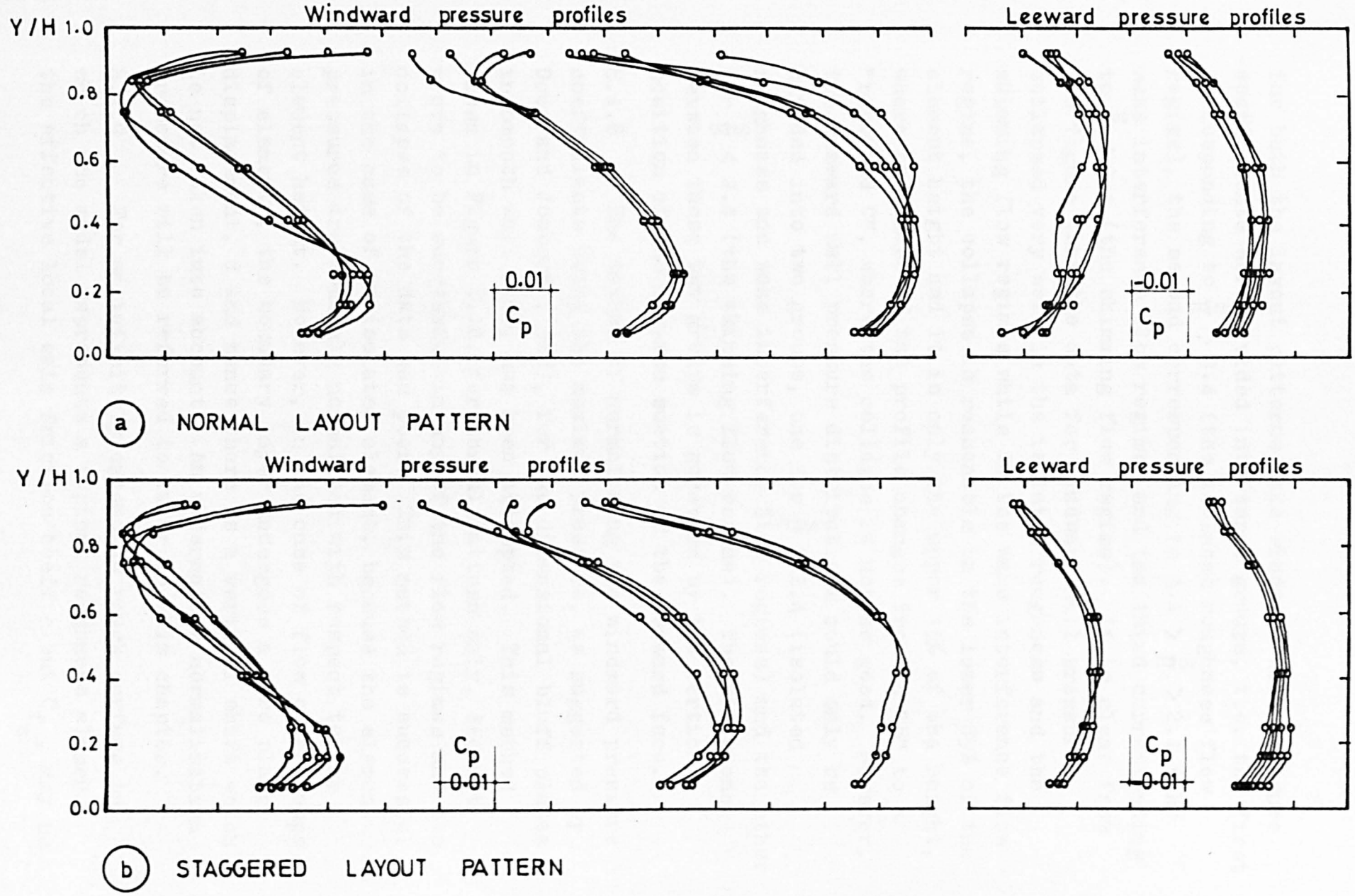

FIGURE 8.9 GROUPING OF WINDWARD AND LEEWARD PRESSURE DISTRIBUTIONS ACCORDING TO FLOW REGIMES

for both the layout patterns, the windward wall pressure coefficients were divided into three groups, i.e. the first corresponding to $\frac{S}{H} > 3.4$ (the isolated roughness flow regime), the second corresponding to $3.4 > \frac{S}{H} > 2.4$ (the wake interference flow regime) and the third corresponding to $\frac{S}{H} < 2.4$ (the skimming flow regime). It is clear from the figure that the data for windward wall pressures collapsed very well in the isolated roughness and the skimming flow regimes while in the wake interference flow regime, the collapse is reasonable in the lower 85% of the element height and it is only the upper 15% of the height, where the shape of the profile changes from an "S" to a "reversed C", where the collapse is not so good. However, the leeward wall pressure distributions could only be divided into two groups, one for $\frac{S}{H} > 2.4$ (isolated roughness and wake interference flow regimes) and the other for $\frac{S}{H} < 2.4$ (the skimming flow regime). The difference between these two groups is governed by the vertical position of the maximum suction of the leeward face.

8.4.8 The method of normalising the windward pressure coefficients using the maximum pressure, as suggested by Good and Joubert (1968), for two dimensional bluff plates in smooth wall flow, has been attempted. This method shown in Figure 8.10, for normal pattern only, did not prove to be successful in any of the flow regimes and the collapse of the data was poor. This method is successful in the case of an isolated element, because the element pressures are commonly normalised with respect to the element height. However, in the case of flow over groups of elements, the boundary layer undergoes a zero plane displacement, d and hence there is a vertical shift which is not taken into account. An alternative normalisation procedure will be referred to later in this chapter.

8.4.9 For an infinitely extending rough surface in which the model represents a typical roughness element, the effective local skin friction coefficient C_{f_e}, may be

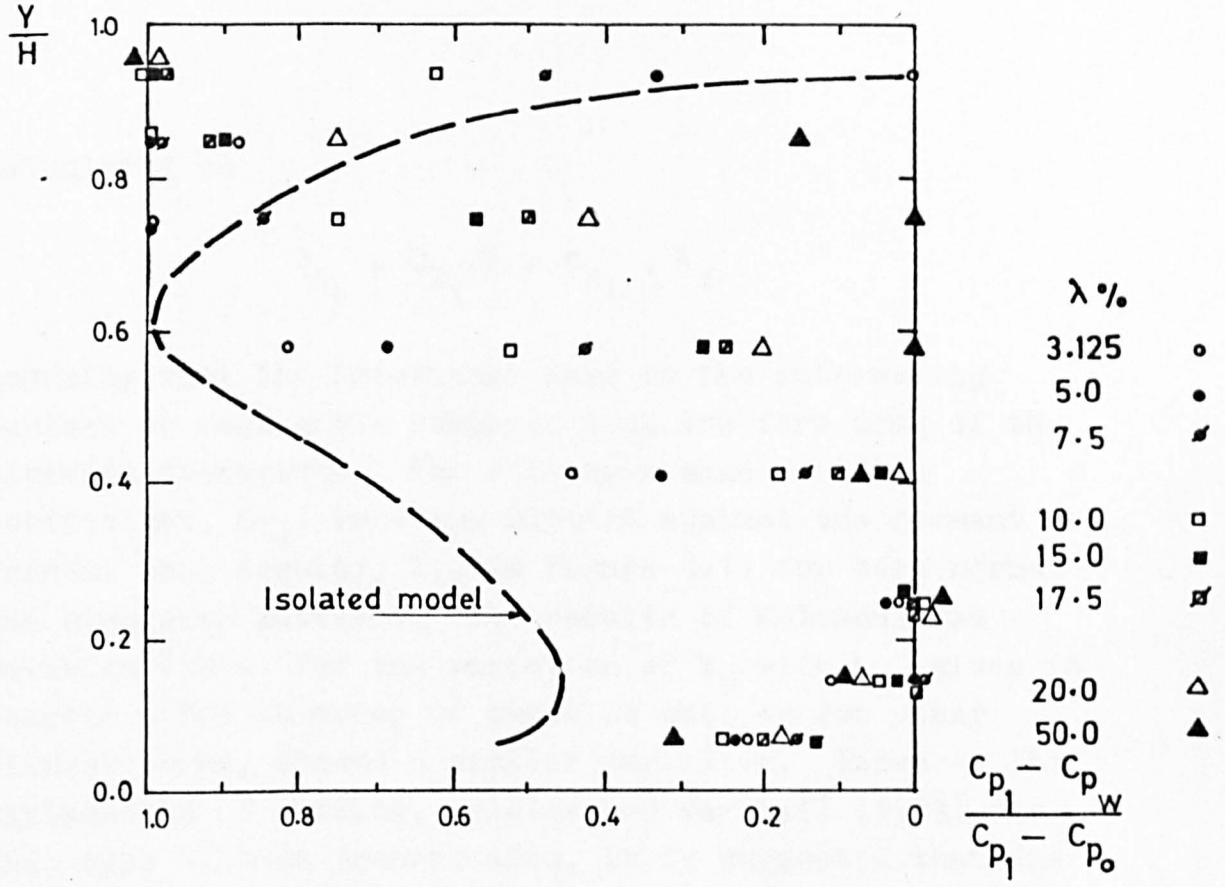

FIGURE 8.10 WINDWARD PRESSURE PROFILES NORMALISED WITH THE MAXIMUM PRESSURE

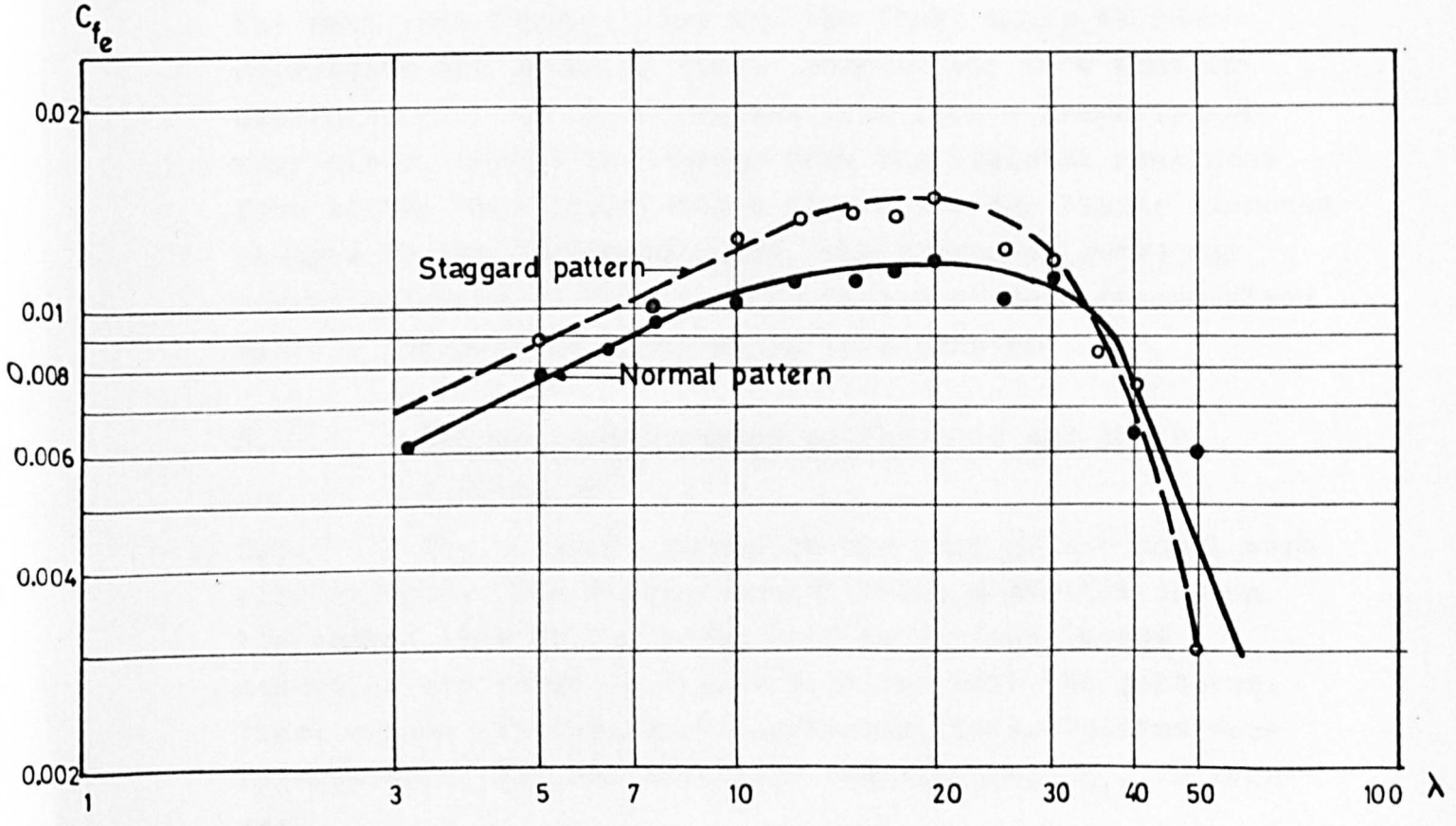

FIGURE 8.11 VARIATION OF C_{f_e} WITH λ

calculated as

$$C_{f_e} = C_{D_1}/A = C_{D_1} \cdot \lambda_f$$

assuming that the frictional drag on the intervening surface is negligible compared with the form drag of the elements themselves. The effective skin friction coefficient, C_{f_e}, is shown plotted against the element frontal area density, λ_f, in Figure 8.11 for both normal and staggered patterns. The results of Koloseus and Davidian (1966) for the variation of k_s with λ_f, given in chapter 4 for an array of cubes as well as for other element forms, showed a similar variation. Based on the explanation of Wooding, Bradley and Marshall (1973) for this type of data presentation, it is suggested that the initial linear increase of log C_{f_e} with log λ_f represents the isolated roughness flow, the subsequent levelling off and slow decrease of the curve represents the wake interference flow and the final sharp decrease represents the skimming flow. Despite the fact that the distinction of the flow regimes from such a graph is not very clear, except the change from the isolated roughness flow to the wake interference flow where the linear increase changes to the flattened curve, the suggested curve may nevertheless be of value. This method of data presentation will be referred to later on in this chapter.

8.5 Pressure measurement on the roof and their discussion

8.5.1 The pressure forces on the roof of the model were also studied. The pressure coefficient distributions on the centre line of the model roof in various layout densities are shown in Figure 8.12 for both the patterns. These centre line pressure coefficient distributions were integrated to get the mean lift coefficient, C_{L_1}, in each case.

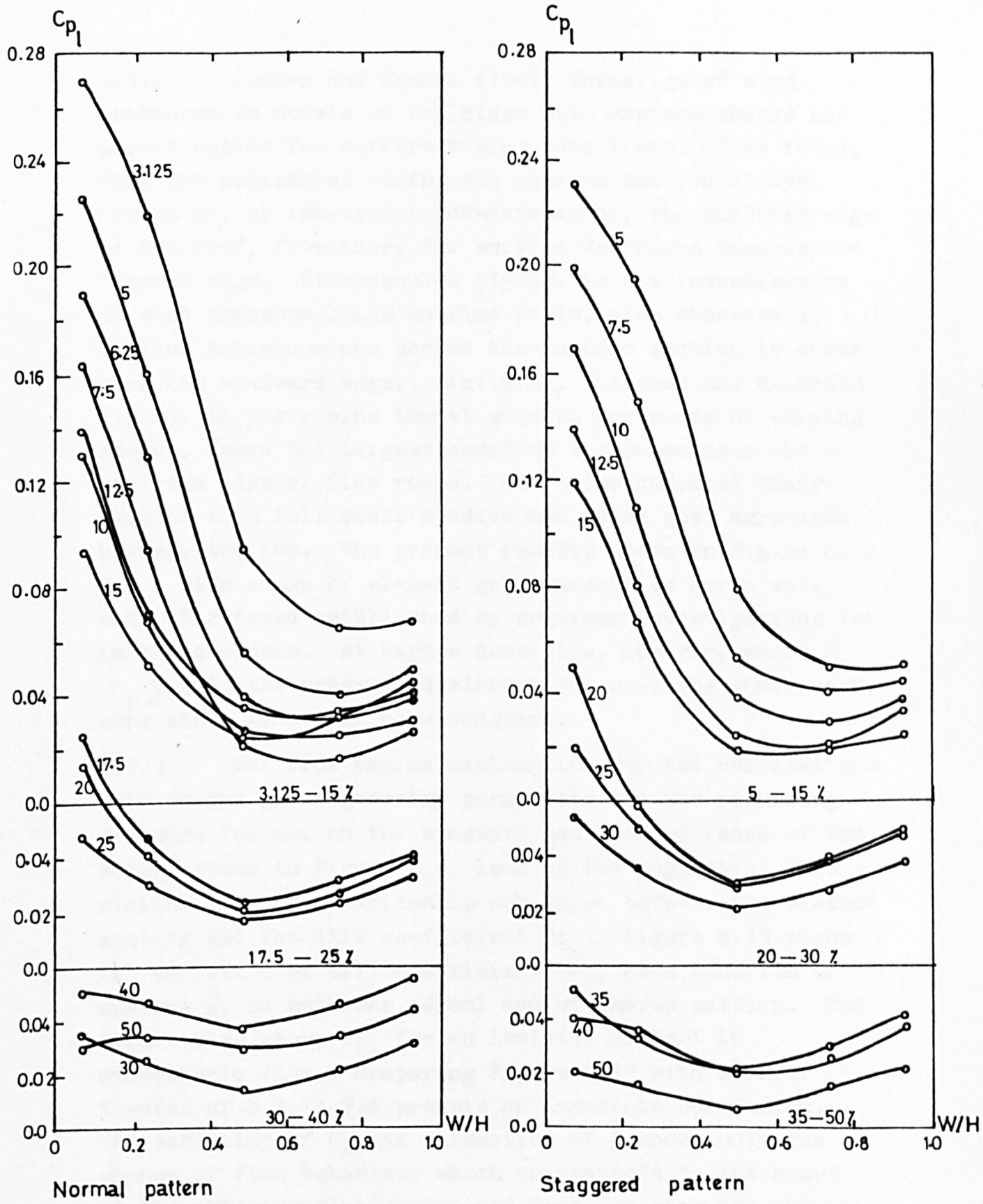

FIGURE 8.12 ROOF PRESSURE COEFFICIENT DISTRIBUTIONS AT VARIOUS DENSITIES

8.5.2 Jensen and Franck (1965) investigated wind pressures on models of buildings with various shapes and aspect ratios for different wind conditions. They found, that for horizontal roofs, the maximum suction always occurs at, or immediately downstream of, the windward edge of the roof, from there the suction decreases towards the leeward edge. Stathopoulos (1975), in his investigation of wind pressure loads on flat roofs, also observed a similar behaviour and showed the maximum suction to occur near the windward edge. Similarly, Tieleman and Reinhold (1976), in their wind tunnel studies for roofs of varying slopes, found the largest negative pressures near the upstream edge of flat roofs. They also compared their results with full scale studies and found good agreement between the two. The present results shown in Figure 8.12 for a wide range of element group densities agree well with this trend established by previous investigations for isolated models. At higher densities, however, where $\lambda_p \geqslant 40\%$, the pressure distributions over the whole roof, were shown to become more constant.

8.5.3 The flow regime explanation for the correlations between the group geometry parameters and the resulting pressure forces, on the windward and leeward faces of the model, shown in Figure 8.4, lead to the suggestion that a similar type of relationship may exist between the element spacing and the lift coefficient C_{L_1}. Figure 8.13 shows the variation of lift coefficient C_{L_1}, as a function of spacing $\frac{S}{H}$, in both the normal and staggered pattern. The figure also shows C_{L_1} for an isolated element in atmospheric flow. Comparing Figure 8.13 with earlier figures of 8.4 to 8.6 prompts an immediate conclusion. The variation of C_{L_1} as a function of $\frac{S}{H}$ shows only one change of flow behaviour which corresponds to the start of the skimming flow regime and does not show the change of behaviour between the isolated roughness flow and wake interference flow regimes. This change of behaviour at

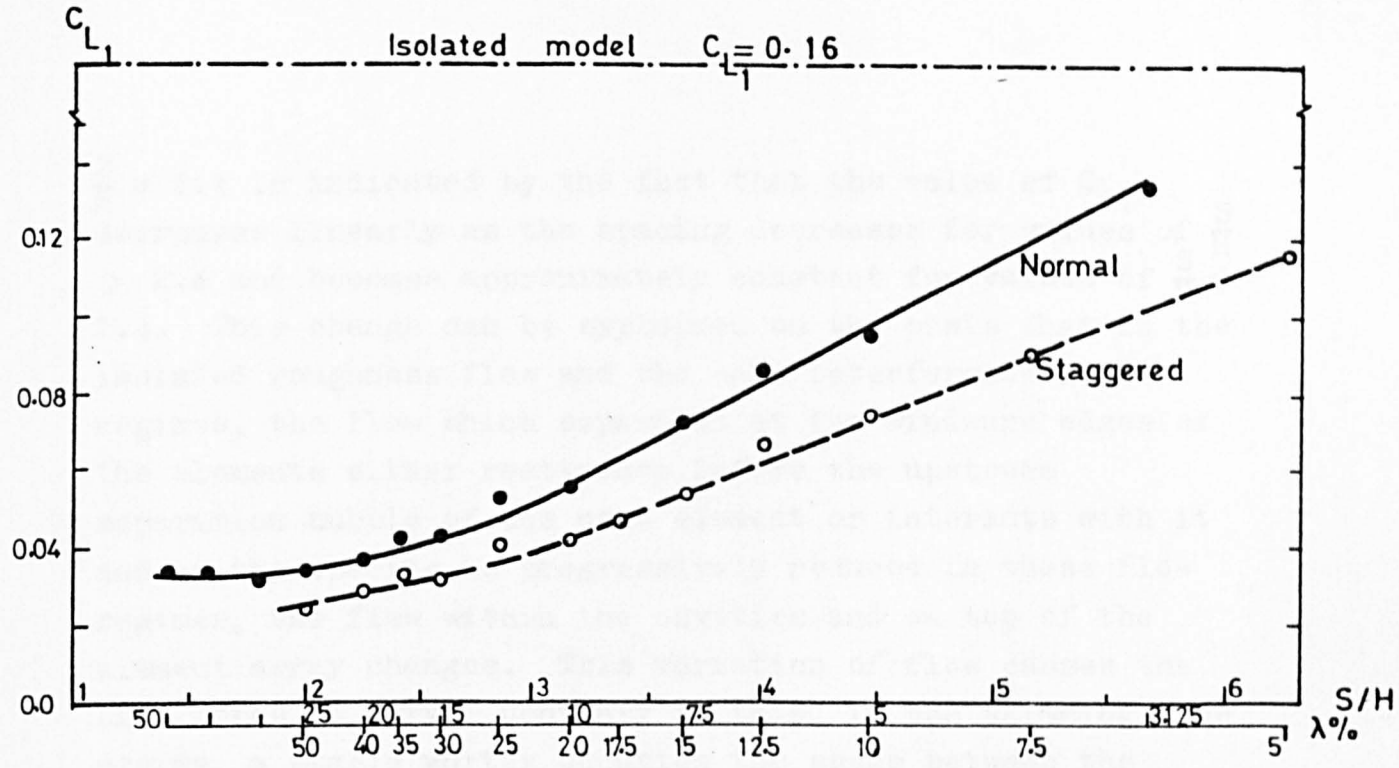

FIGURE 8.13 VARIATION OF THE ROOF LIFT COEFFICIENT WITH CUBE SPACING

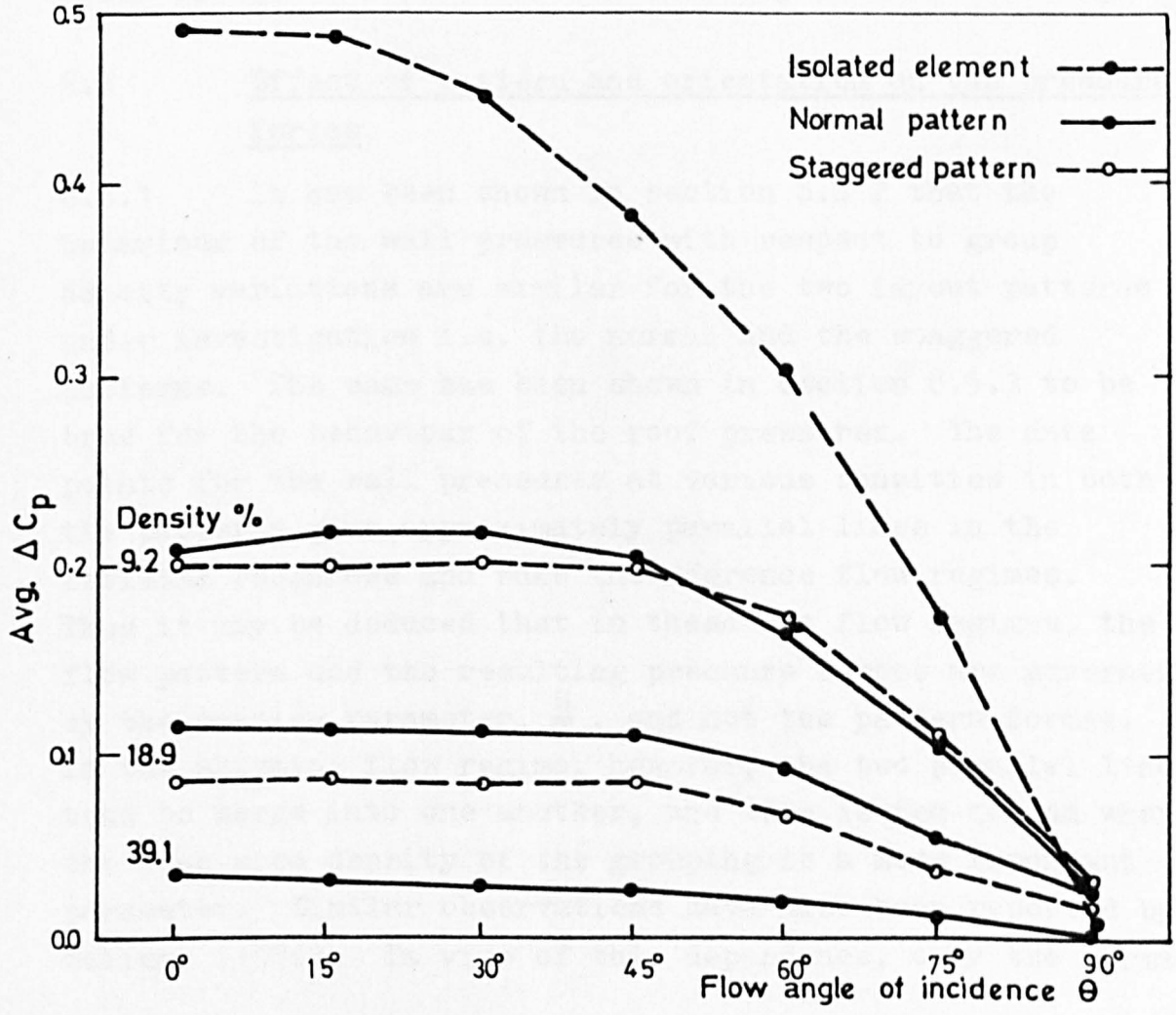

FIGURE 8.14 VARIATION OF ΔC_p WITH THE ORIENTATION ANGLE FOR VARIOUS DENSITIES (AFTER SOLIMAN 1976)

$\frac{S}{H} \simeq 2.4$ is indicated by the fact that the value of C_{L_1} decreases linearly as the spacing decreases for values of $\frac{S}{H} > 2.4$ and becomes approximately constant for values of $\frac{S}{H} < 2.4$. This change can be explained on the basis that in the isolated roughness flow and the wake interference flow regimes, the flow which separates at the windward edges of the elements either reattaches before the upstream separation bubble of the next element or interacts with it and as the spacing is progressively reduced in these flow regimes, the flow within the cavities and on top of the element array changes. This variation of flow causes the lift force to vary. Contrary to this, in the skimming flow regime, a stable vortex occupies the space between the cubes whilst the flow rides relatively undisturbed on top of the cube layout. Due to this undisturbed flow, the value of C_{L_1} does not vary with density in this flow regime.

8.6 Effect of pattern and orientation on the pressure forces

8.6.1 It has been shown in section 8.4.2 that the behaviour of the wall pressures with respect to group density variations are similar for the two layout patterns under investigation i.e. the normal and the staggered patterns. The same has been shown in section 8.5.3 to be true for the behaviour of the roof pressures. The data points for the wall pressures at various densities in both the patterns give approximately parallel lines in the isolated roughness and wake interference flow regimes. Thus it may be deduced that in these two flow regimes, the flow pattern and the resulting pressure forces are governed by the spacing parameter, $\frac{S}{H}$, and not the pattern format. In the skimming flow regime, however, the two parallel lines tend to merge into one another, and this is the region where the plan area density of the grouping is a more important parameter. Similar observations have also been reported by Soliman (1976). In view of this dependence, only the normal

pattern will be considered in the further investigations of models with varying plan forms and also in the velocity profile measurements.

8.6.2 The variation of the average pressure difference across the two faces of the model, ΔC_p, with model orientation, θ, for various densities has been investigated in detail by Soliman (1976), see Figure 8.14. He found that the effect of model orientation on the values of ΔC_p in the range $0 < \theta < 60$, is negligible for the three densities considered in the range of $9\% < \lambda_p < 40\%$. He did, however, suggest that smaller values of the layout densities i.e. larger values of $\frac{S}{H}$ representing the isolated roughness flow regime might increase the effect of orientation. He further suggested that the effect of group layout orientation angle, ϕ, becomes less important, as the fetch increases. On the basis of his observations, neither of the orientation angle θ nor ϕ were changed in the present investigation.

8.7 Velocity profile measurements: results and analysis

8.7.1 A series of velocity profile measurements were taken with the aim of substantiating the pressure measurement results. Eight values of the plan area density, λ_p, were chosen to cover the three flow regimes which emerged from the analysis of the pressure measurements. These were 5.0%, 6.25% and 7.5% in the isolated roughness flow regime, 10.0%, 12.5% and 15.0% in the wake interference flow regime and 25.0% and 30.0% in the skimming flow regime.

8.7.2 At any change of surface roughness, an internal layer is known to grow from the origin of the new surface to eventually replace the old layer. In the present investigation, the atmospheric incident flow underwent only one change when it reached the model group layout. Although the fetch of the group layout on the turntable was sufficient to allow the surface wall pressures to stabilise, it was too small to allow for complete profile adaptation.

8.7.3 In most of the previously reported works, the velocity profiles have been measured over two dimensional roughness element arrays and the flow regimes considered have been the wake interference and the skimming flow regimes. In such cases, the velocity profiles remain invariant in the transverse direction and differ very little in the streamwise direction. However, Soliman (1976) in his investigation of flow over cubes, in the normal pattern, measured two sets of velocity profiles, one at longitudinal cube axis and the other at the corresponding street axis. Each set of profiles consisted of measurements taken at distances of 0, 1H, 2H and 3H upstream of the centre of the model. He observed large variations in the two sets of profiles and an example showing these variations for profiles taken 1H upstream for λ_p = 4.0% and 12.5% is given in Figure 8.15. Conversely, he observed relatively less variations in the velocity profiles between those taken at different fetches in a particular density. An example of this is given in Figure 8.16 at 4.0% density on cube centre line. Later on when analysing his velocity profile measurements, he found that, since the value of C_{f_e} for the street centre line was not known, the slope of the logarithmic region of the internal layer profile and hence the value of the zero plane displacement, d, and roughness length, Z_o, could not be determined. Thus, the street centre line profiles could not be used in a profitable manner to substantiate the flow pattern hypothesis. Furthermore, a careful study of Figure 8.16 revealed that the logarithmic portion of the internal layer profile did not extend beyond the element height. Since the logarithmic region is the backbone of the velocity profile analysis, the profiles measured on top of the cubes could also not be used.

On the basis of these observations only one velocity profile was measured in each of the eight densities in the present investigation. The vertical origin of the velocity profile measurements was the smooth surface between

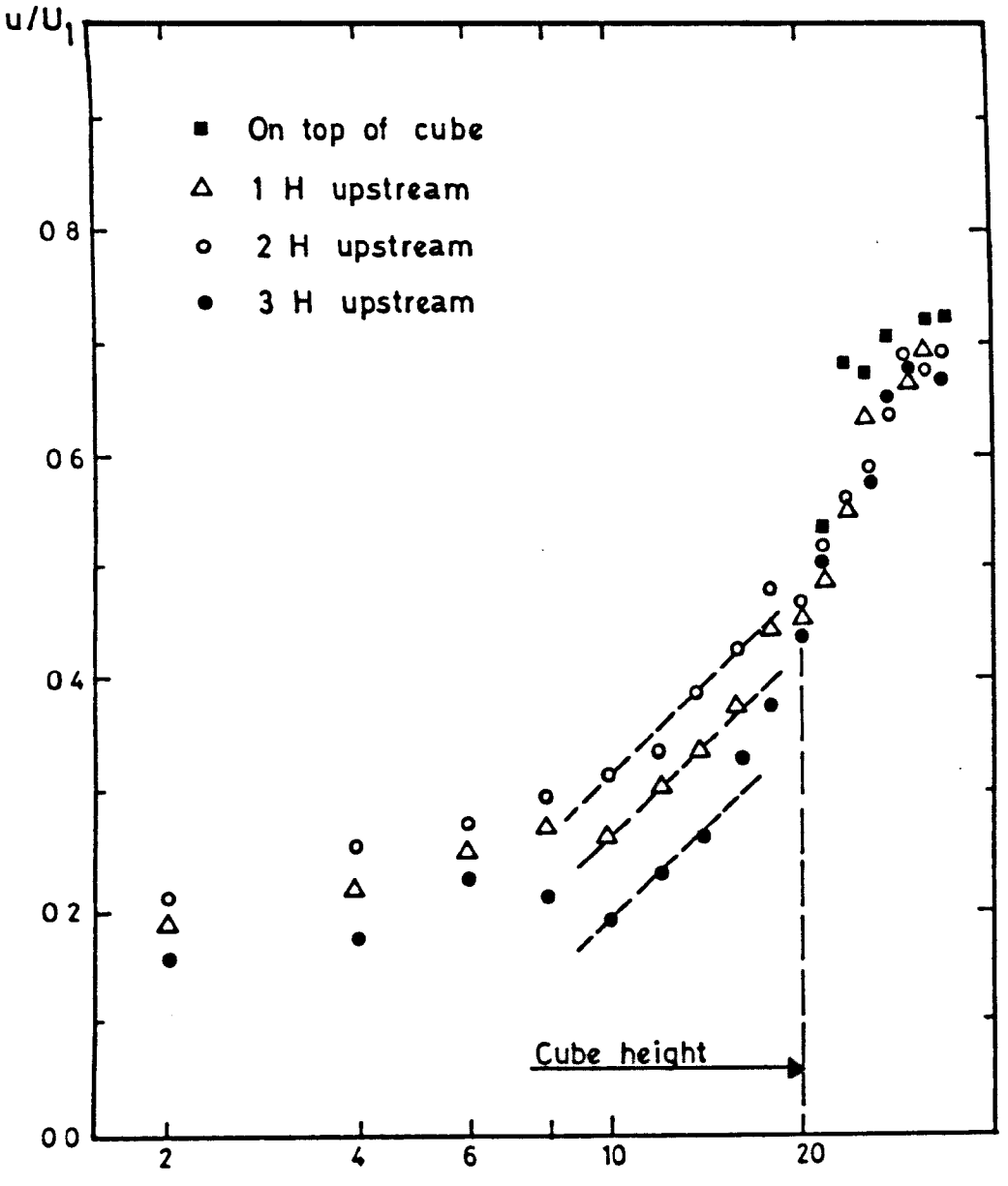

FIGURE 8.15 COMPARISON BETWEEN CUBE CENTRE LINE AND STREET CENTRE LINE VELOCITY PROFILES (AFTER SOLIMAN 1976)

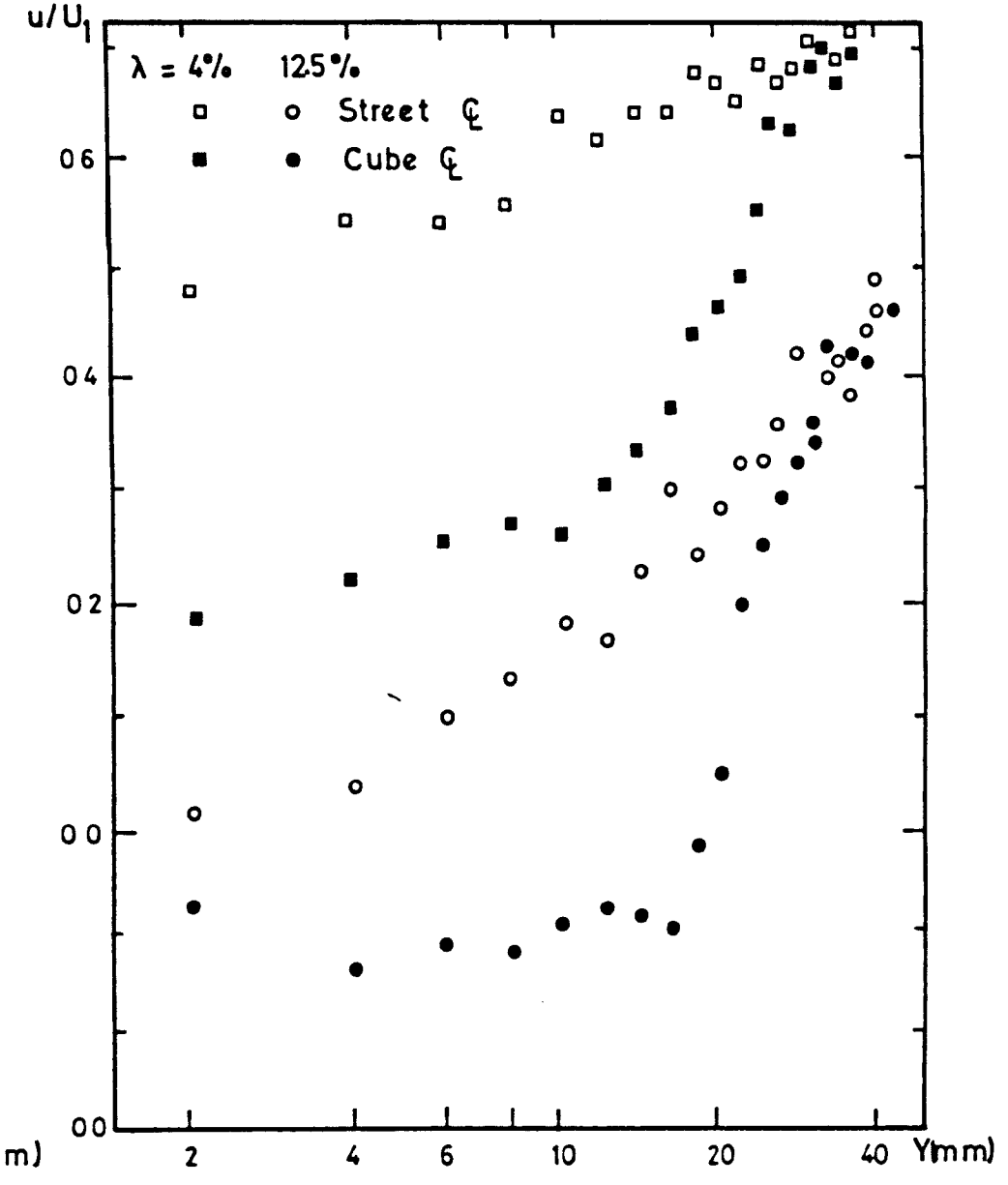

FIGURE 8.16 VARIATION OF VELOCITY PROFILES WITH FETCH AT CUBE CENTRE LINE, $\lambda = 4\%$ (AFTER SOLIMAN 1976)

the elements, on the cube centre line, at a distance of 1H upstream of the centre of the model. Figure 8.17 shows the locations of velocity profile measured at various densities.

8.7.4 A comparison between different profiles for various densities, including the profile of the empty turntable, is given in Figure 8.18. A careful study of these profiles shows that an internal layer, δ_i, either grows on the smooth turntable or on the new roughness composed of the group layout. The depth of this internal layer depends on the fetch and the roughness density. It can also be seen from this figure that in the outer layers, the data points for various densities collapse on one another. Therefore in the rest of the velocity profile analysis, consideration will be confined to the internal zone only, which is the most relevant to the model layout underneath.

8.7.5 In order to estimate the magnitude of the zero plane displacement, d, and the roughness length, Z_o, the graphical method of Perry and Joubert (1963) has been used. The application of this method requires a prior knowledge of the slope of the logarithmic region of the internal layer profile. In the present study, the values of C_{f_e} obtained originally from the pressure measurements were used to make the log-region slope compatable with the profiles measured 1H upstream of the model on the cube centre line. The slope of the log-region was calculated as $5.75\sqrt{C_{f_e}/2}$ (refer Soliman (1976). Table 8.2 gives the values of C_{D_1}, C_{f_e} and the slope of the log-region for each density. The application of this graphical method is shown in Figures 8.19 to 8.26.

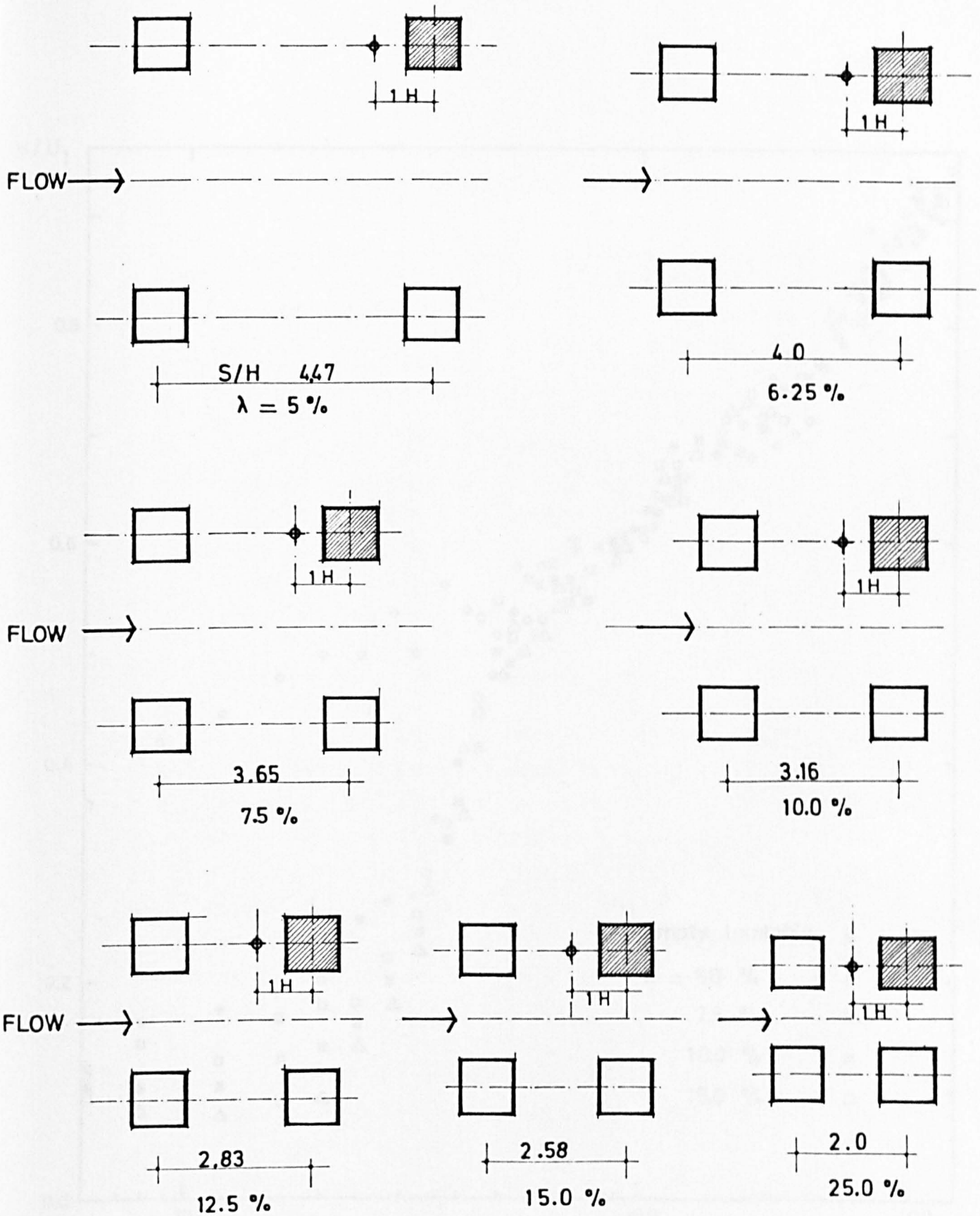

FIGURE 8.17 LOCATION OF VELOCITY PROFILES MEASURED AT VARIOUS DENSITIES

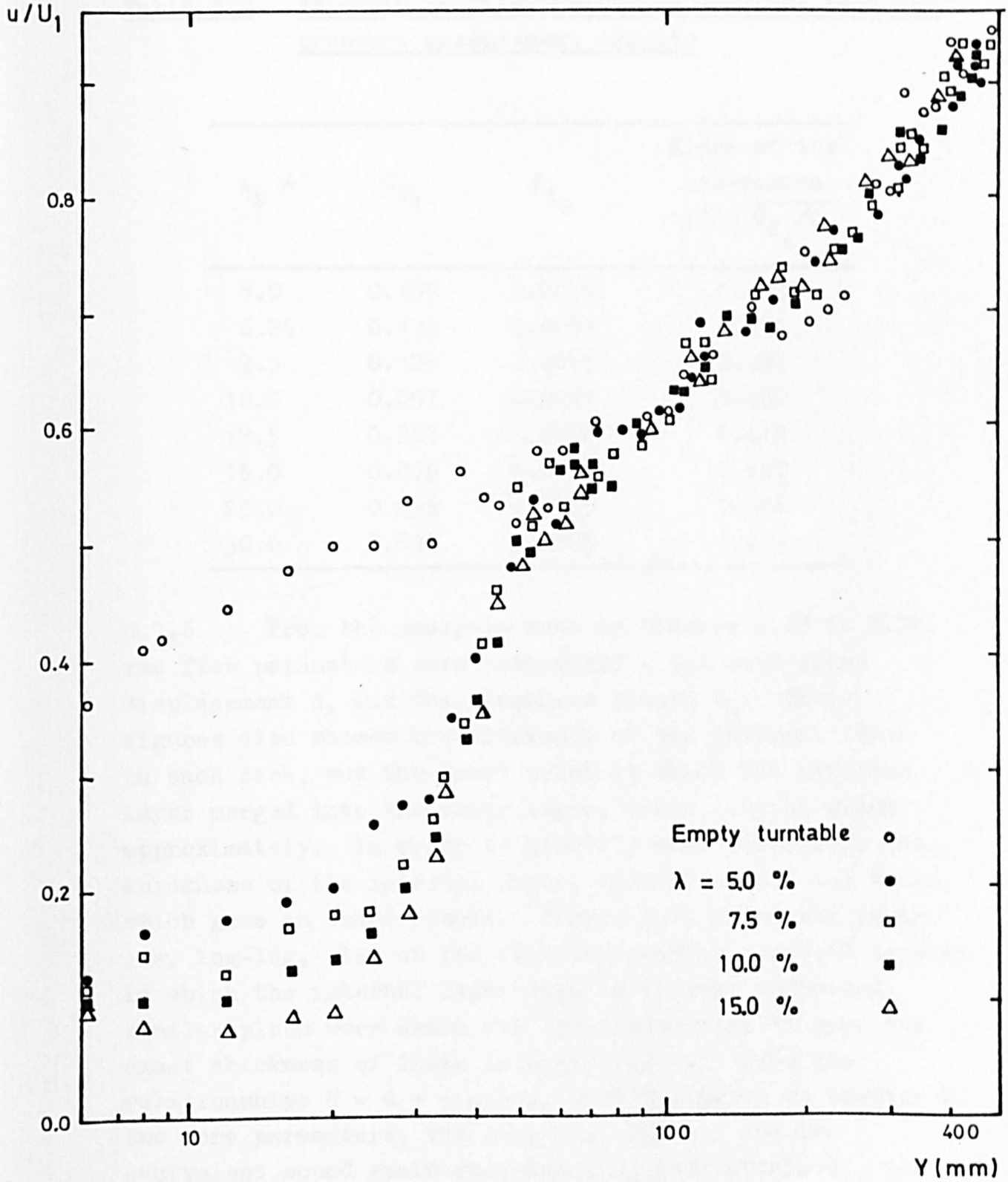

FIGURE 8.18 COMPARISON BETWEEN CUBE CENTRE LINE PROFILES AT VARIOUS DENSITIES SHOWING THE EFFECT OF CHANGE OF SURFACE ROUGHNESS

Table 8.2 Velocity profile parameters obtained from the pressure measurement results

λ_p %	C_{D_1}	C_{f_e}	Slope of the log-region $5.75\sqrt{C_{f_e}/2}$
5.0	0.159	0.0079	0.363
6.25	0.136	0.0085	0.375
7.5	0.126	0.0095	0.395
10.0	0.097	0.0097	0.400
12.5	0.085	0.0106	0.419
15.0	0.070	0.0105	0.417
25.0	0.038	0.0095	0.396
30.0	0.035	0.0105	0.416

8.7.6 From the analysis made in Figures 8.19 to 8.26, two flow parameters were determined - the zero plane displacement d, and the roughness length Z_o. These figures also showed the thickness of the internal layer in each case, but the exact point at which the internal layer merged into the outer layer, could only be given approximately. In order to identify more precisely, the thickness of the internal layer, another method was tried, which gave an exact result. Figure 8.27 shows the power law, log-log, plot of the velocity profile for 5.0% density in which the internal layer edge is clearly indicated. Similar plots were drawn for other densities to give the exact thickness of their internal layers. From the relationships $H = d + \varepsilon$ and $k_s = 30\ Z_o$, given in chapter 4, two more parameters, the error in origin ε and the equivalent sound grain roughness, k_s were obtained. All these parameters are given in Table 8.3.

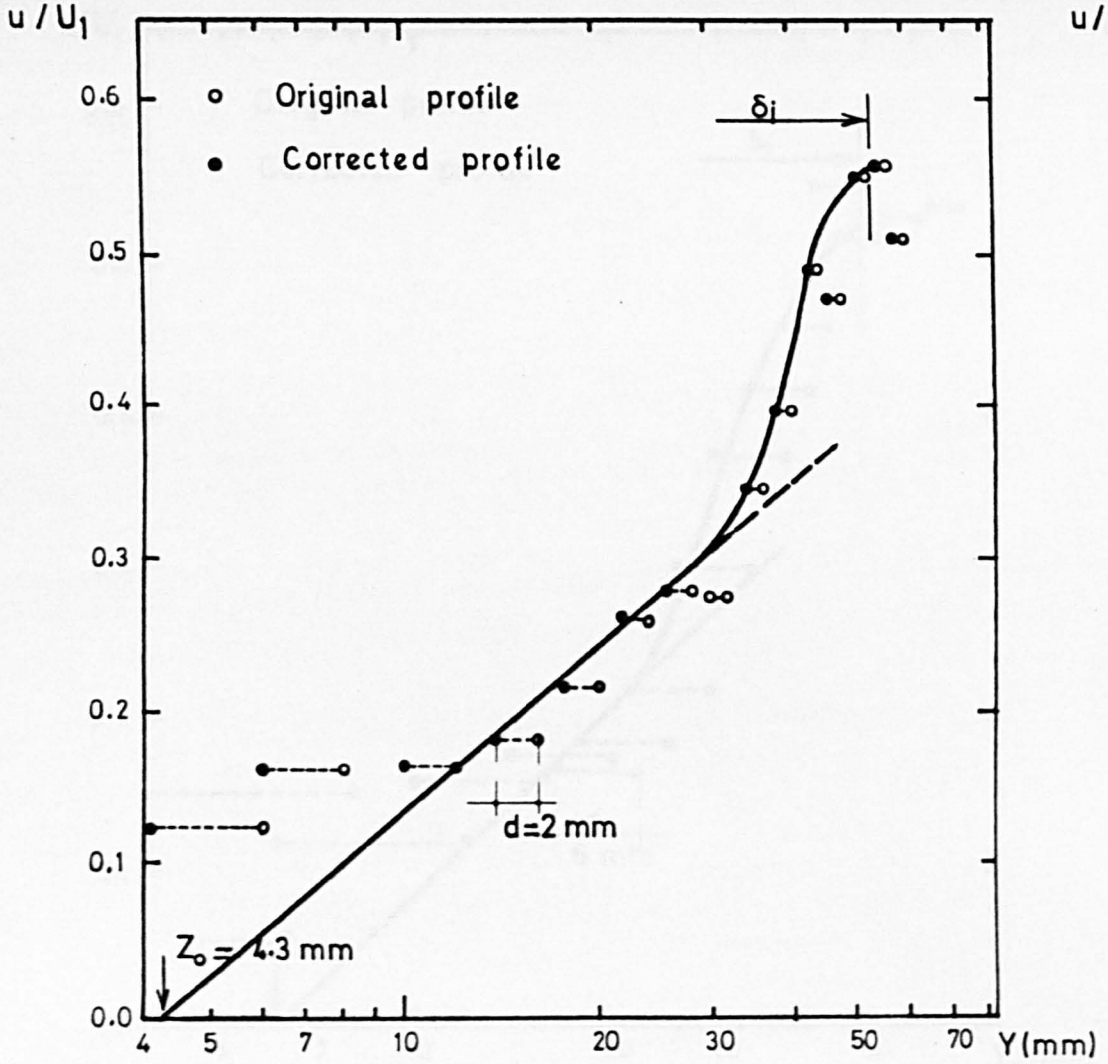

FIGURE 8.19 THE GRAPHICAL METHOD FOR DETERMINING THE ZERO PLANE DISPLACEMENT, d, (λ = 5%)

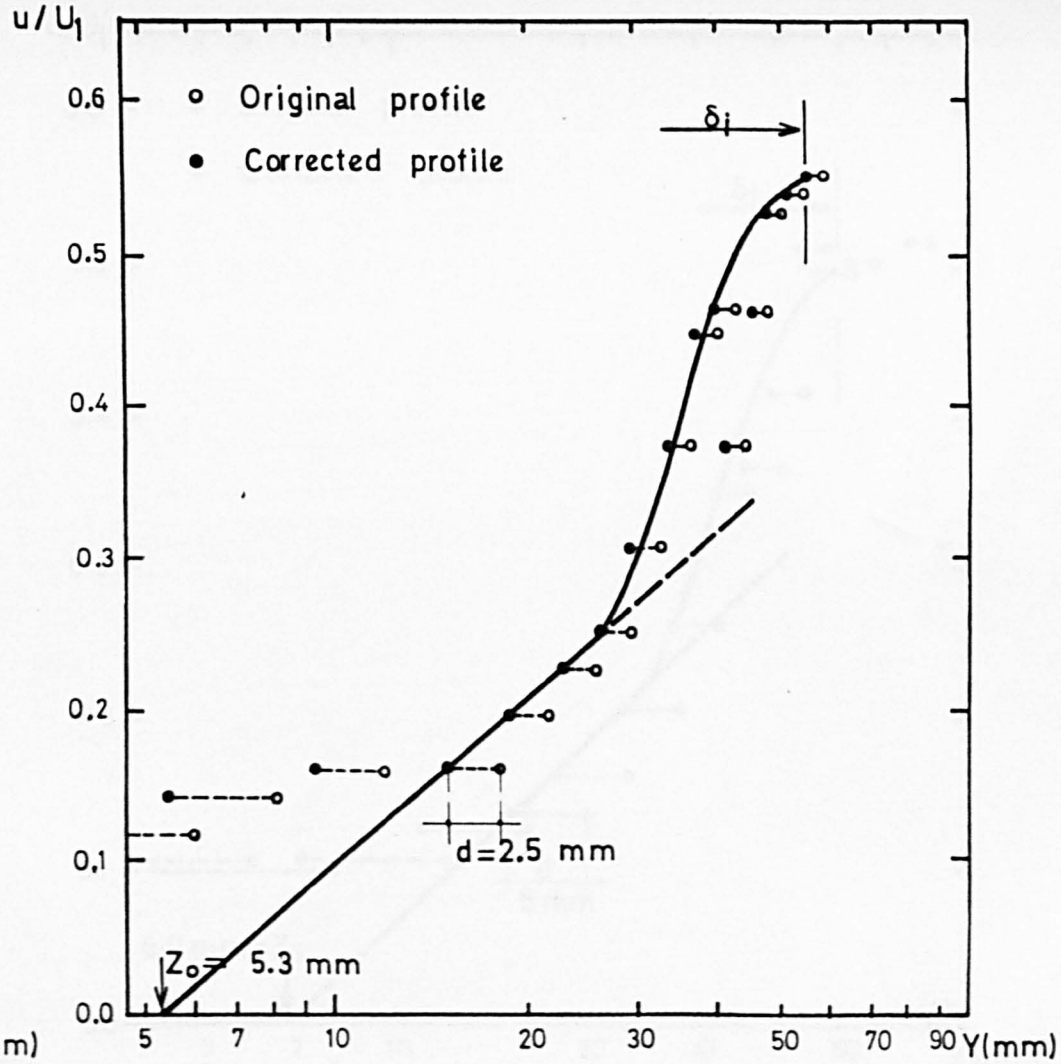

FIGURE 8.20 THE GRAPHICAL METHOD OF DETERMINING THE ZERO PLANE DISPLACEMENT, d, (λ = 6.25%)

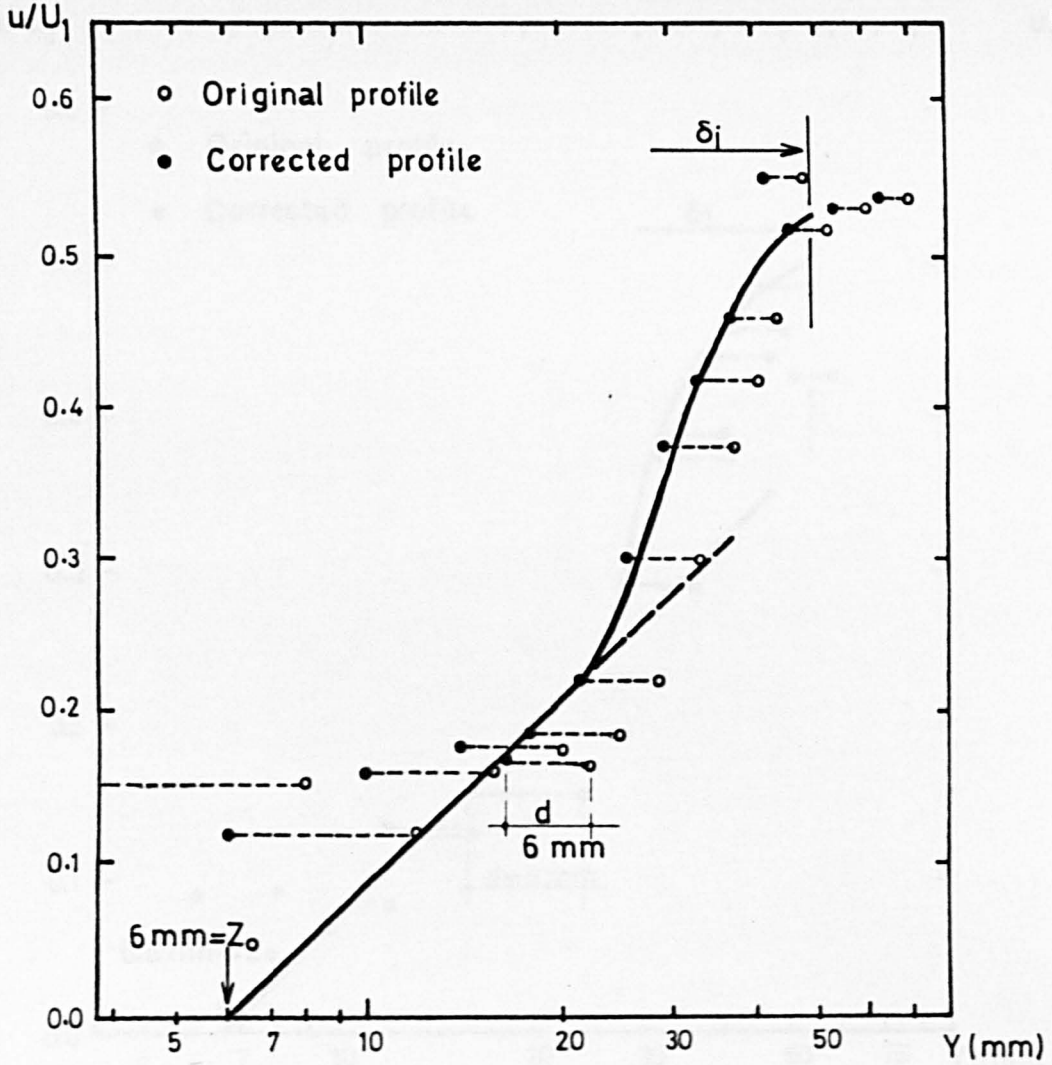

FIGURE 8.21 THE GRAPHICAL METHOD OF DETERMINING THE ZERO PLANE DISPLACEMENT, d, (λ = 7.5%)

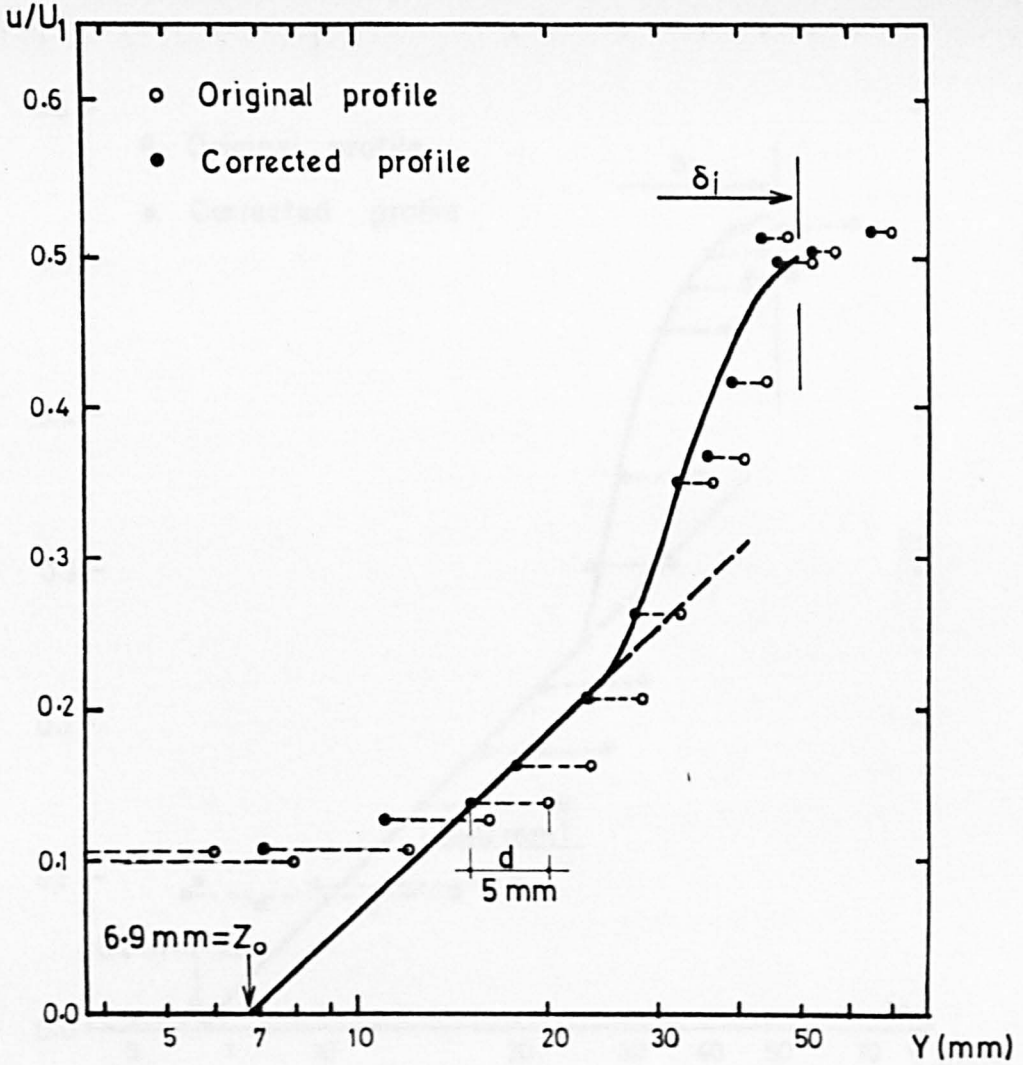

FIGURE 8.22 THE GRAPHICAL METHOD OF DETERMINING THE ZERO PLANE DISPLACEMENT, d, (λ = 10.0%)

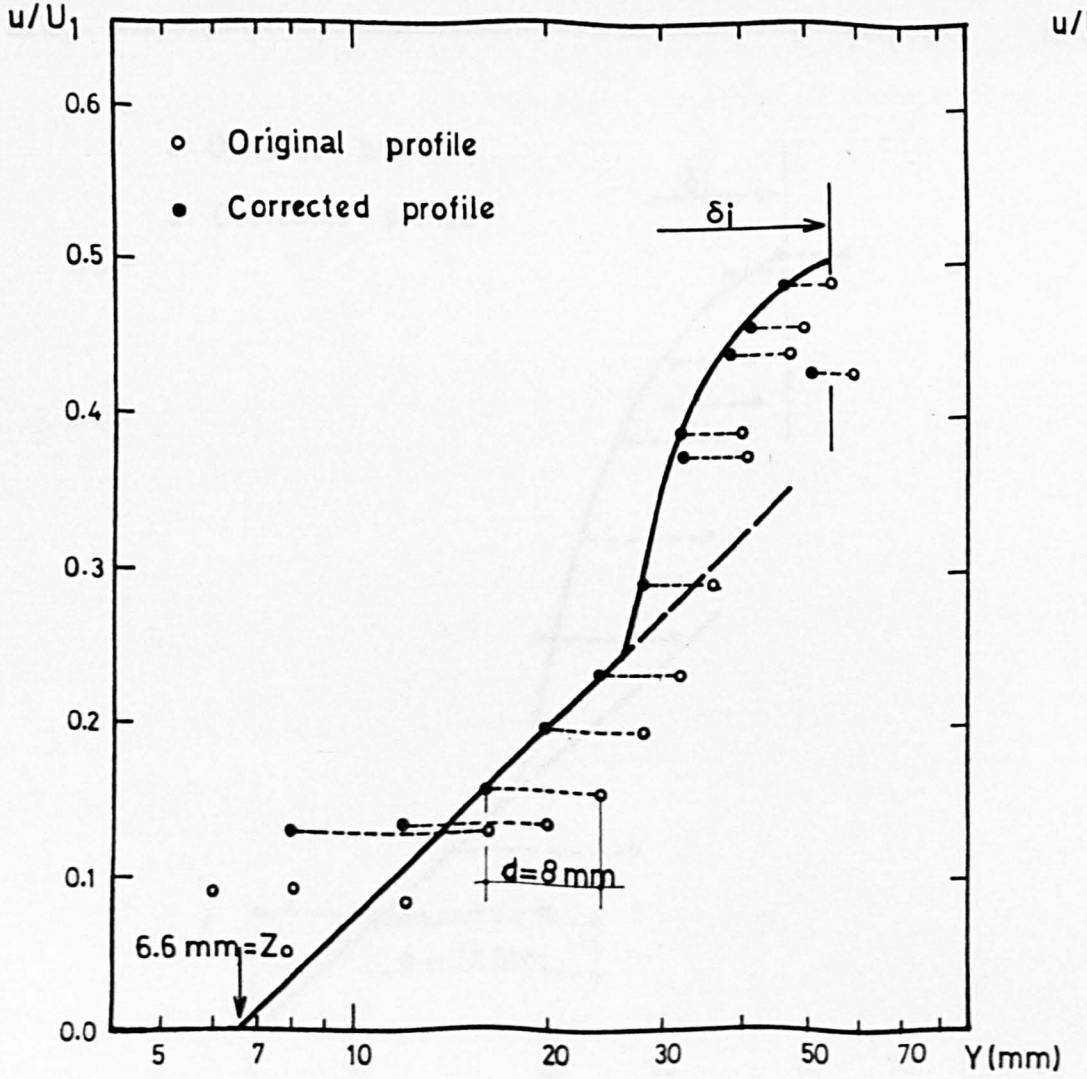

FIGURE 8.23 THE GRAPHICAL METHOD OF DETERMINING THE ZERO PLANE DISPLACEMENT, d, (λ = 12.5%)

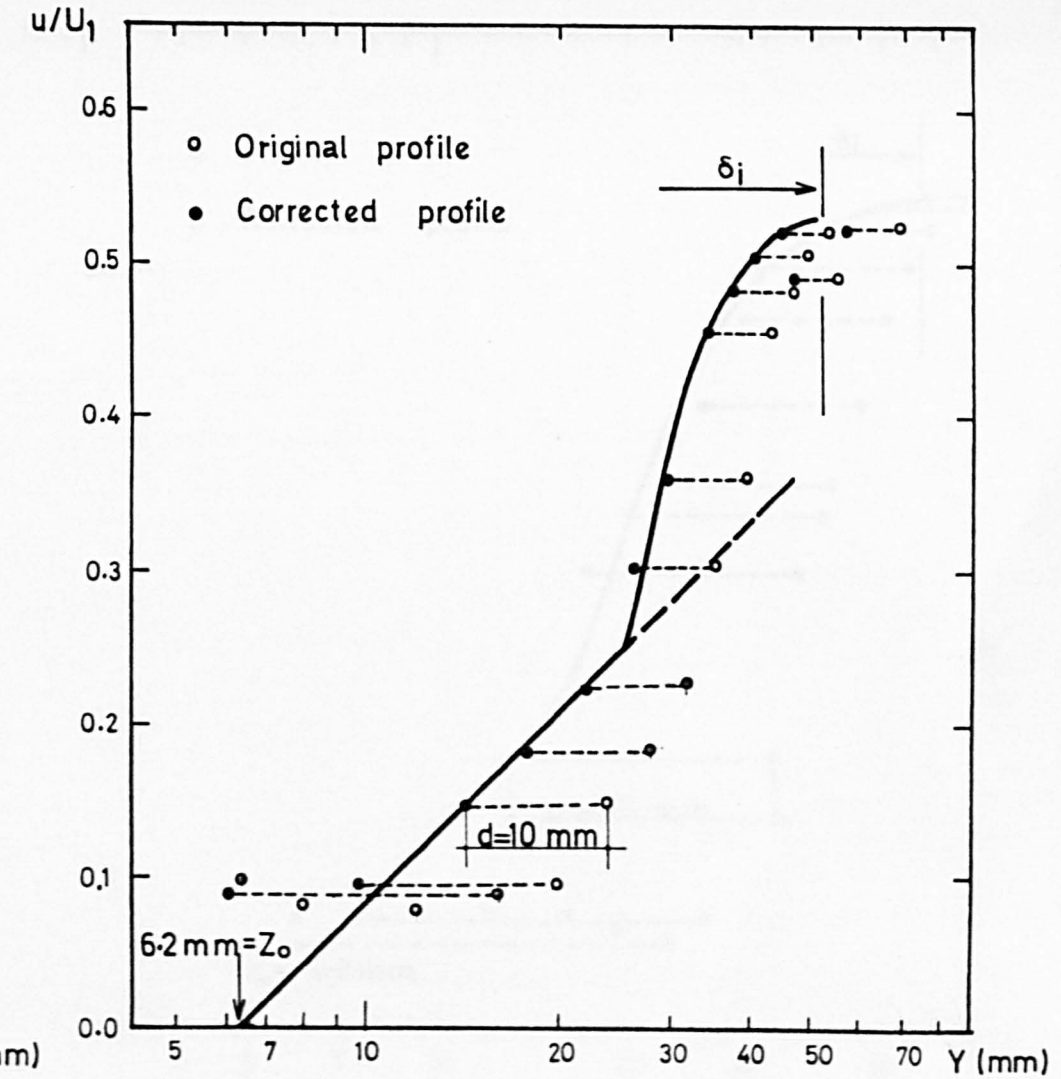

FIGURE 8.24 THE GRAPHICAL METHOD OF DETERMINING THE ZERO PLANE DISPLACEMENT, d, (λ = 15.0%)

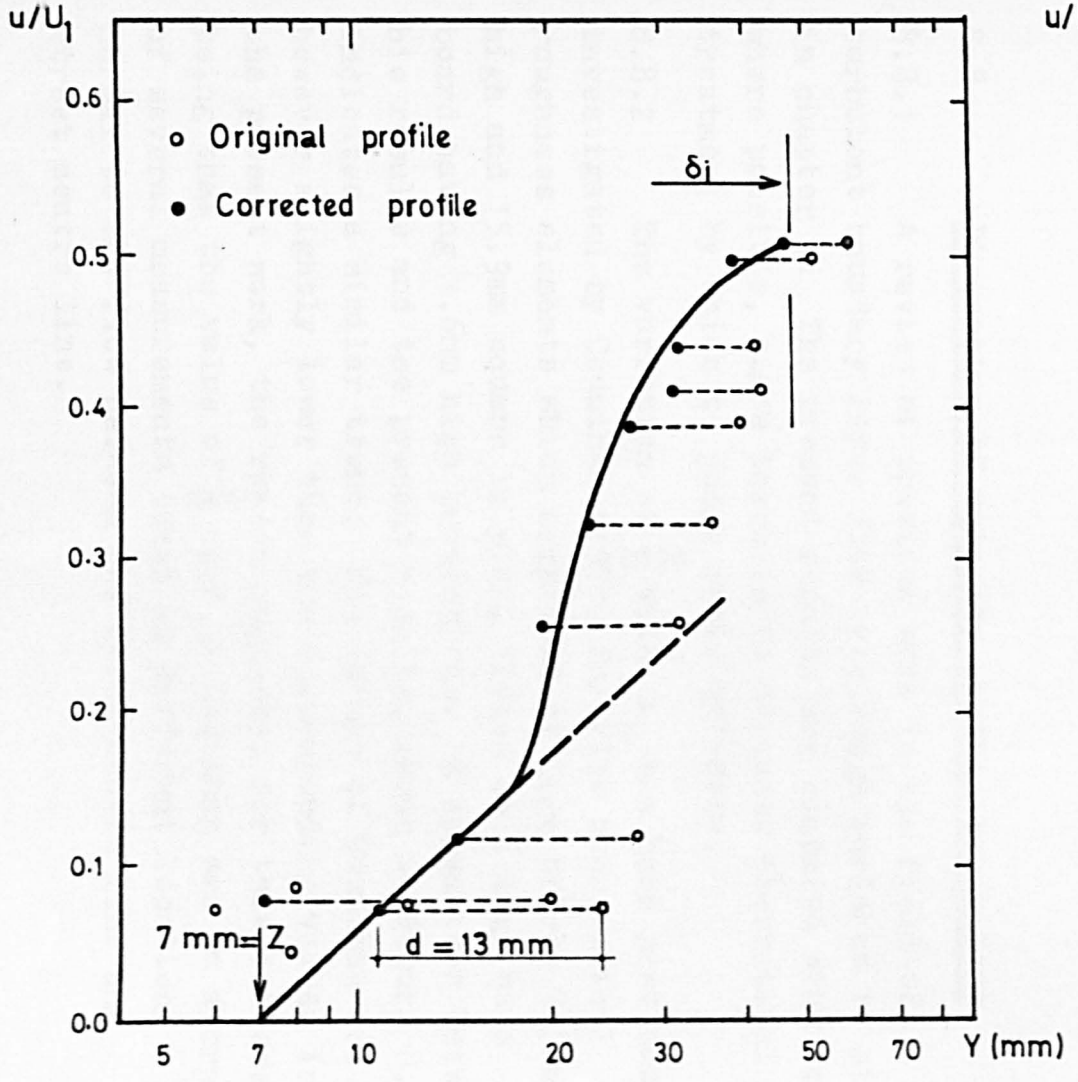

FIGURE 8.25 THE GRAPHICAL METHOD OF DETERMINING THE ZERO PLANE DISPLACEMENT, d, (λ = 25.0%)

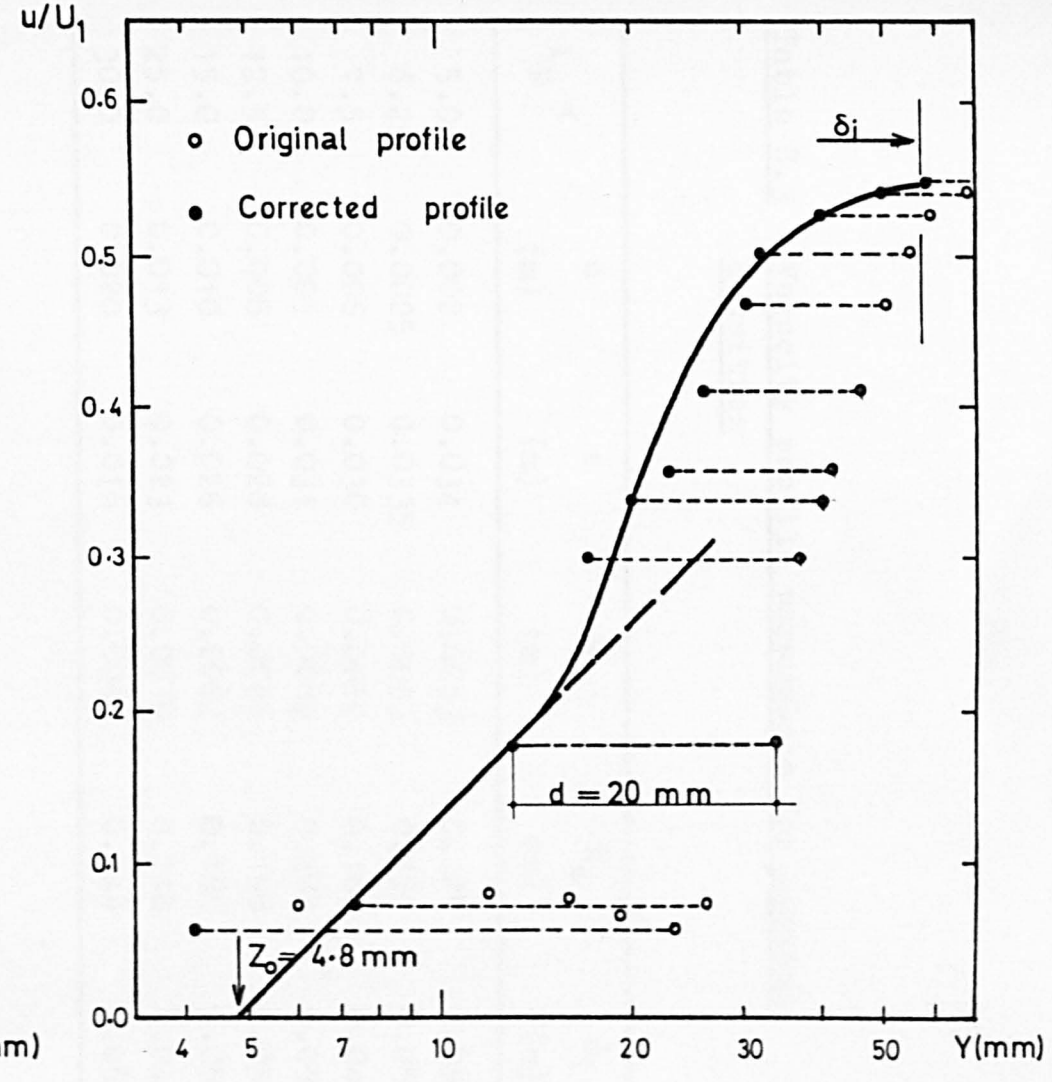

FIGURE 8.26 THE GRAPHICAL METHOD OF DETERMINING THE ZERO PLANE DISPLACEMENT, d, (λ = 30.0%)

Table 8.3 Velocity profile parameters for various densities

λ_p %	d (m)	ε (m)	Z_o (m)	k_s (m)	δ_i (m)
5.0	0.002	0.034	0.0043	0.129	0.055
6.25	0.0025	0.0335	0.0053	0.159	0.056
7.5	0.006	0.030	0.0060	0.180	0.048
10.0	0.005	0.031	0.0069	0.207	0.050
12.5	0.008	0.028	0.0066	0.198	0.054
15.0	0.010	0.026	0.0062	0.186	0.052
25.0	0.013	0.023	0.0070	0.210	0.048
30.0	0.020	0.016	0.0048	0.144	0.058

8.8 Discussion of velocity profile parameters

8.8.1 A review of previous work in the field of turbulent boundary layer flow over rough surfaces is given in chapter 4. The present results are compared with these, where possible, since there is no adequate theoretical treatment by which to judge their validity.

8.8.2 The variation of $\frac{\bar{d}}{H}$ with λ_p has been previously investigated by Counihan (1971) for flow over cubical roughness elements which comprised of lego bricks 9.5mm high and 15.9mm square in plan, fitted on a lego base board having 1.6mm high protrusions. A comparison between his results and the present results, shown in Figure 8.28, indicates a similar trend. The values of Counihan are however slightly lower than the corresponding values in the present work, the reason suggested for this difference being that the value of $\frac{\bar{d}}{H}$ used by Counihan was an average of several measurements taken at different locations normal to the flow between the block centre line and street centre line.

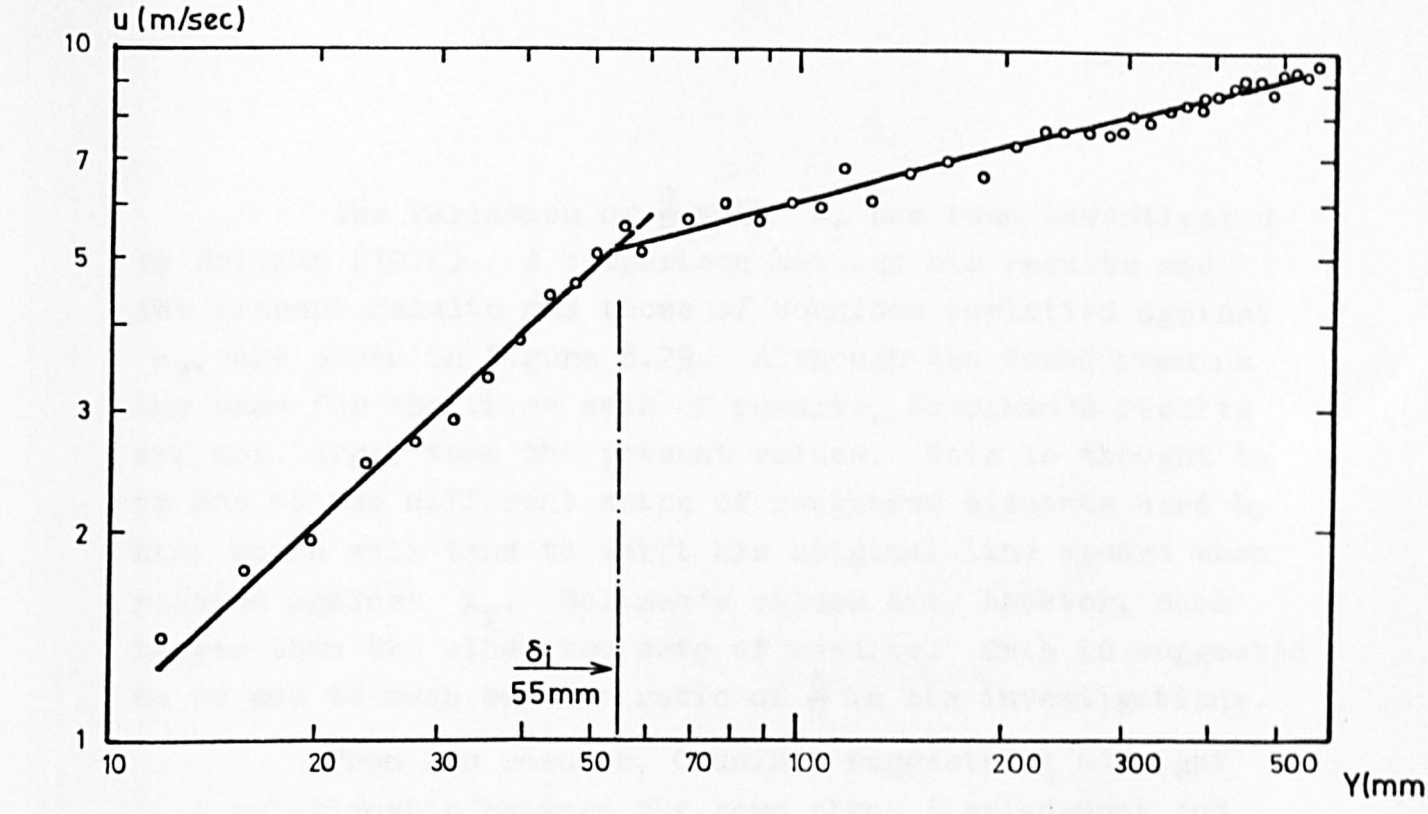

FIGURE 8.27 POWER LAW LOG-LOG PLOT TO DETERMINE THE INNER LAYER DEPTH

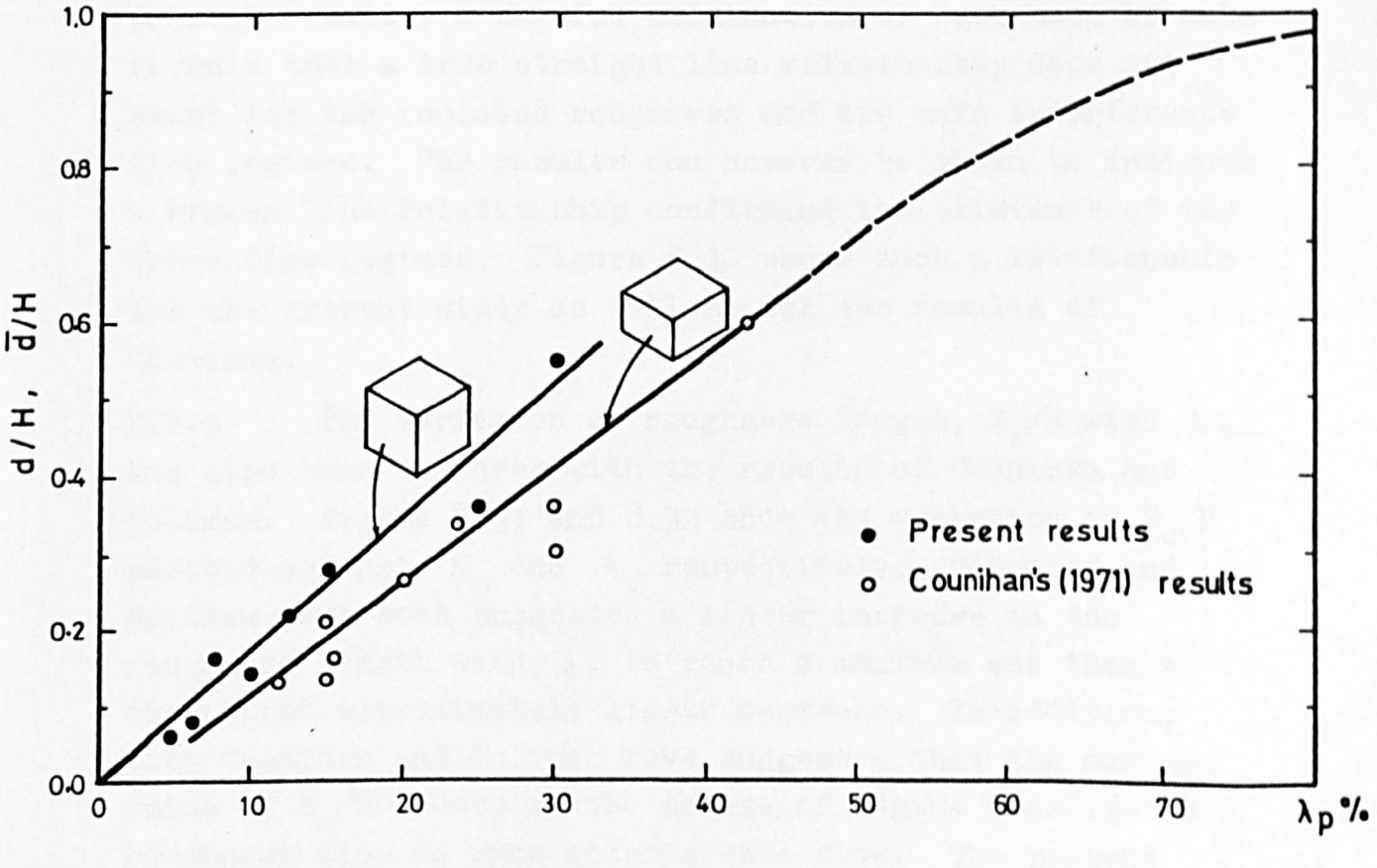

FIGURE 8.28 VARIATION OF d/H WITH PLAN AREA DENSITY

The variation of $\frac{d}{H}$ with λ_f has been investigated by Soliman (1976). A comparison between his results and the present results and those of Counihan replotted against λ_f, are shown in Figure 8.29. Although the trend remains the same for the three sets of results, Counihan's results are now larger than the present values. This is thought to be due to the different shape of roughness elements used by him, which will tend to shift his original line upward when plotted against λ_f. Soliman's values are, however, much larger than the other two sets of results. This is suggested to be due to much smaller ratio of $\frac{\delta}{H}$ in his investigations.

From his results, Counihan suggested a straight line relationship between the zero plane displacement and the density in the isolated roughness and the wake interference flow regimes and a separate relationship for the skimming flow regime shown by the dotted line in Figure 8.29. Although a similar trend is exhibited by the present results, a careful examination of both sets of data reveals that a true straight line relationship does not exist for the isolated roughness and the wake interference flow regimes. The results can however be shown to indicate a broken line relationship confirming the existence of the three flow regimes. Figure 8.30 shows such a relationship for the present study as well as for the results of Counihan.

8.8.3 The variation of roughness length, Z_o/H with λ, has also been compared with the results of Counihan and Soliman. Figure 8.31 and 8.32 show the variation of Z_o/H plotted against λ_p and λ_f respectively. Counihan and Soliman have both suggested a linear increase in the roughness length with λ, to reach a maximum and then a subsequent approximately linear decrease. In addition, both Counihan and Soliman have suggested that the maximum value of Z_o/H occurs at the change of regime from isolated roughness flow to wake interference flow. The present results show a broadly similar trend to those mentioned

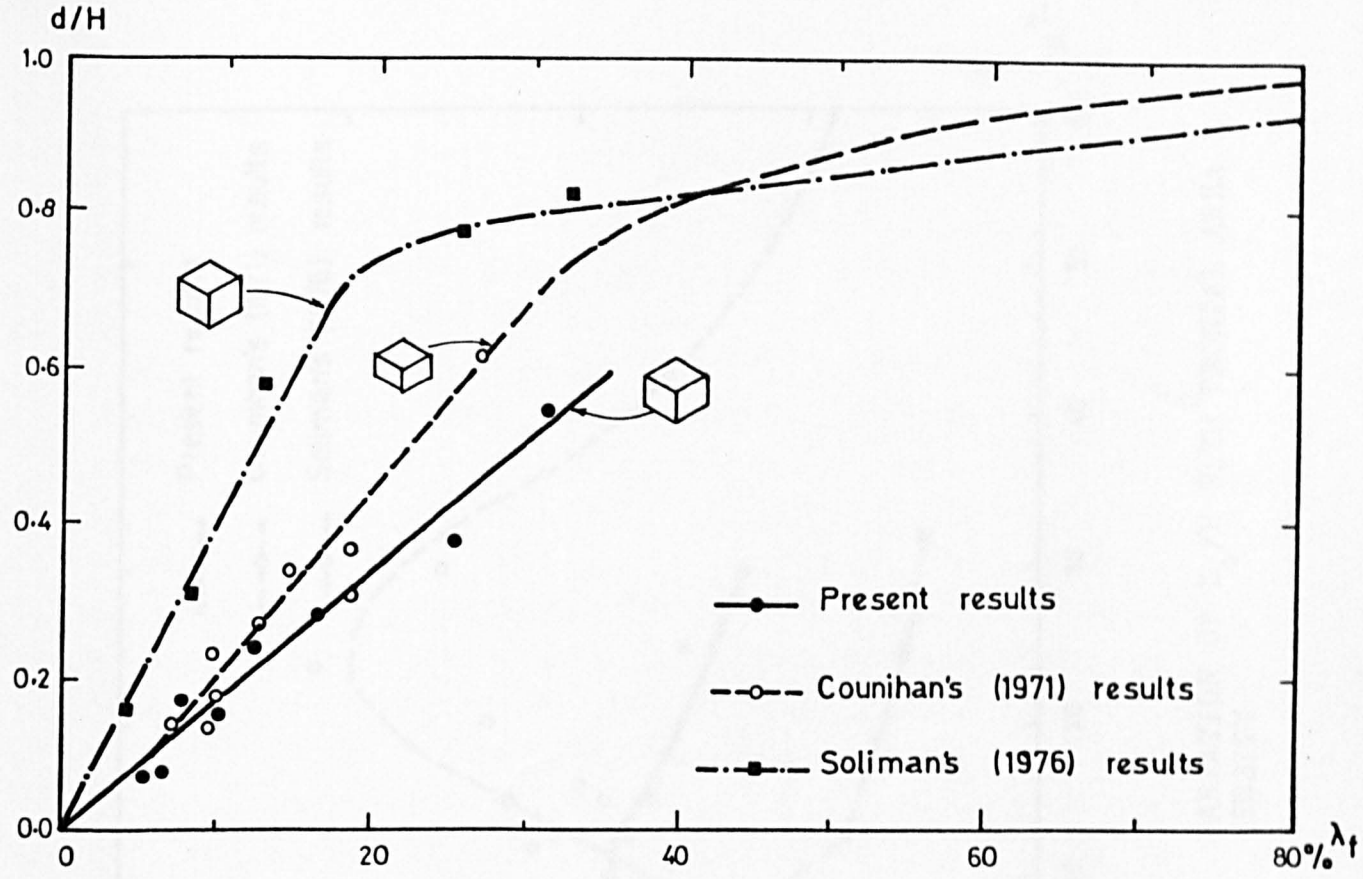

FIGURE 8.29 VARIATION OF d/H WITH FRONTAL AREA DENSITY

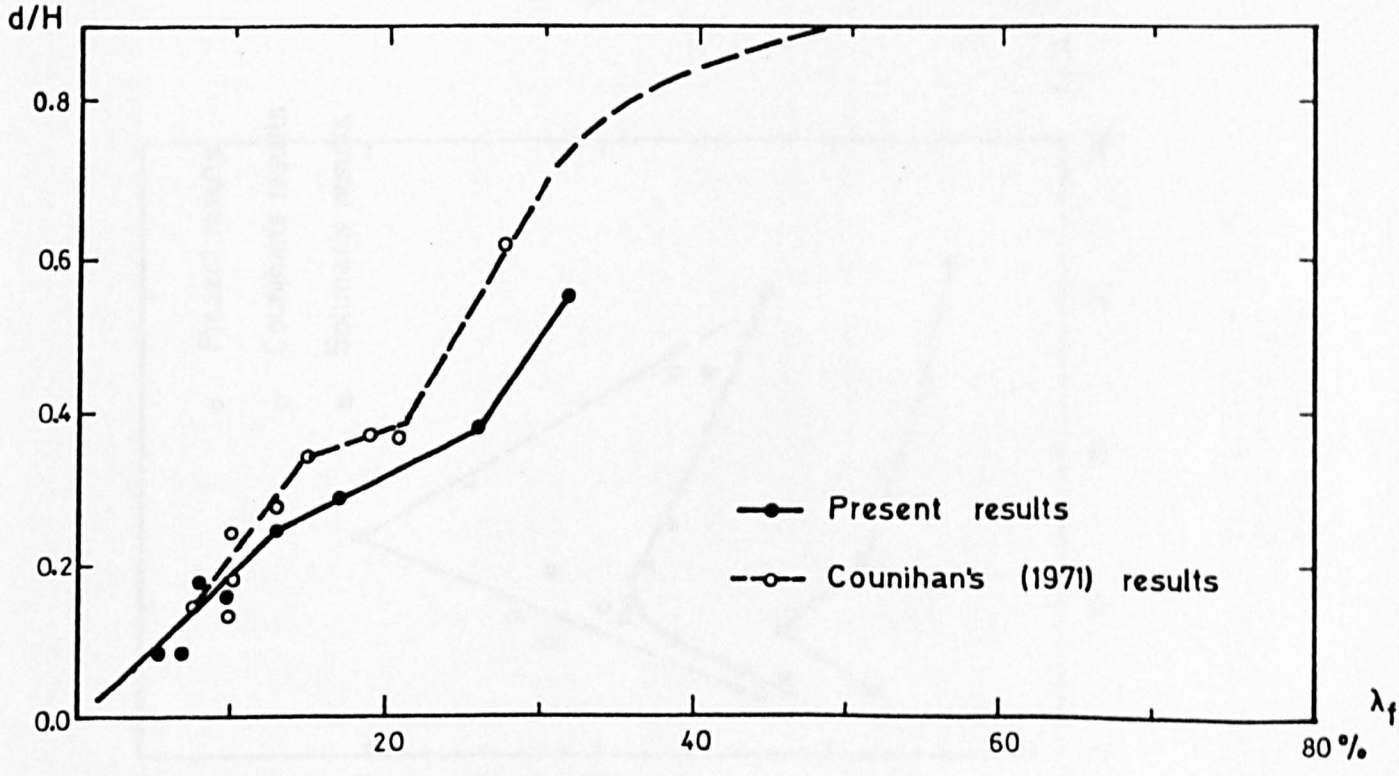

FIGURE 8.30 SUGGESTED VARIATION OF d/H WITH FRONTAL AREA DENSITY ACCORDING TO FLOW REGIMES

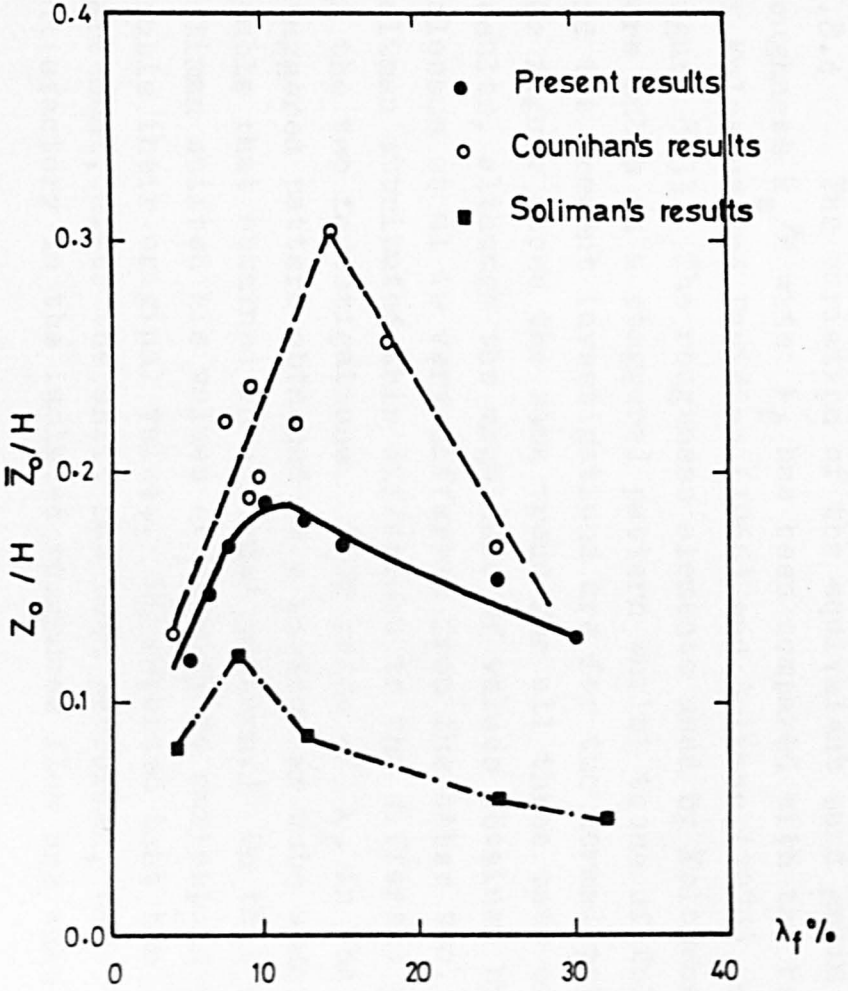

FIGURE 8.32 VARIATION OF Z_o/H WITH FRONTAL AREA DENSITY

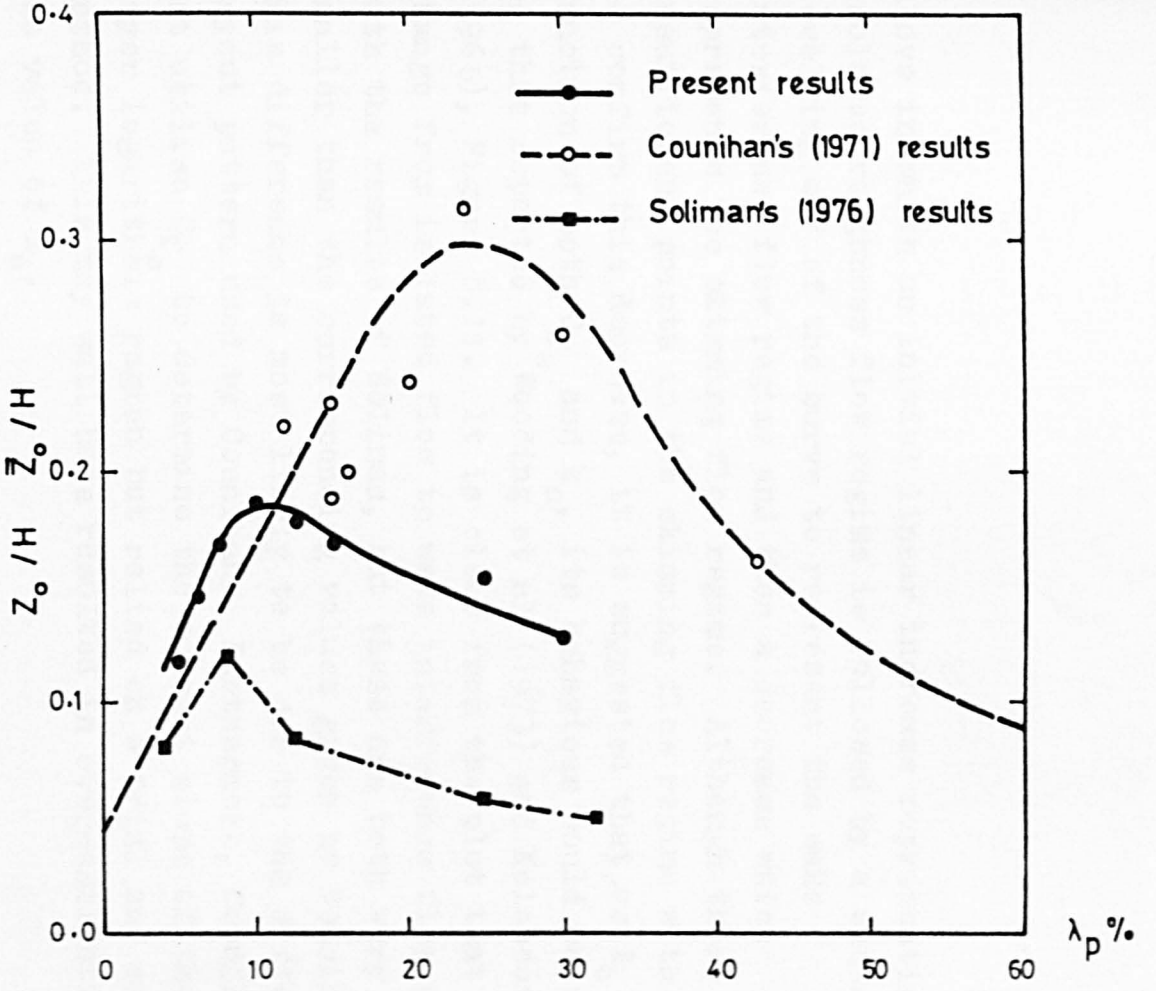

FIGURE 8.31 VARIATION OF Z_o/H WITH FRONTAL AREA DENSITY

above in which an initial linear increase representing the isolated roughness flow regime is followed by a subsequent levelling off of the curve to represent the wake interference flow regime and then a decrease which represents the skimming flow regime. Although there are insufficient points in the skimming flow regime with which to confirm this decrease, it is suggested that as Z_o is a function of both C_{f_e} and k_s, its behaviour would be similar to that reported by Wooding et al (1973) and Koloseus et al (1966), Figure 8.11. It is clear from the plot that the change from isolated flow to wake interference flow agrees with the results of Soliman, but these are both very much smaller than the corresponding values given by Counihan. This difference is most likely to be due to the different layout pattern used by Counihan. Furthermore, Counihan did not utilise C_{f_e} to determine the correct slope of the inner layer logarithmic region but relied on a trial and error method. This may well have resulted in over-estimation of the value of Z_o.

8.8.4 The variation of the equivalent sand grain roughness k_s/H with λ_f has been compared with the results of Koloseus and Davidian (1966) and Soliman (1976) in Figure 8.33. The roughness elements used by Koloseus et al were cubes in a staggered pattern whilst those of Soliman and the present investigations are for the normal pattern. The figure shows the same trend for all three sets of results, although the magnitude of values obtained by Koloseus et al is very different from the other two. Soliman attributed this difference to the different patterns in the two investigations. (The value of λ_f in the staggered pattern obtained at a particular cube spacing $\frac{S}{H}$ is double that obtained in a normal pattern.) On this basis Soliman shifted his values of density to correspond to double their original values. He reported that the agreement, after the shift had been performed, was satisfactory in the isolated roughness flow and wake

interference flow regimes, whilst in the skimming flow regimes, k_s/H depends primarily on the group density rather than the spacing parameter. Since the present results and those of Soliman's are similar in magnitude, the same conclusion is true for the results of the present investigation.

In addition to this, a more universal comparison was made for the present results. Koloseus et al collated a large amount of data from various investigations for different roughness element forms. They found that these data are well represented by a linear relation between log k_s/H and log λ over a large range in roughness concentration. The slope of these lines varies in an unsystematic fashion about a value of 1. Figure 8.33 shows that for the present investigation the first few data points in the isolated roughness flow regime are well represented by a linear relationship between log k_s/H vs log λ where the slope of this line is approximately 1. This line is then extrapolated to determine the value of m, the intercept on the log k_s/H axis for a value of λ_f = 1.0%. This value of m has been shown by Koloseus et al to be an indicator of the roughness concentration for the surface i.e. m varies directly with the surface roughness. The value of m given by Koloseus et al for their cubes in a staggered pattern is 0.338 and the corresponding values for cubes in the normal pattern in the present study is 0.72, which is logically approximately double the value found by Koloseus et al. A similar value of m, found by extrapolating Soliman's results in Figure 8.33, gives a value of 0.65 which is comparable to our value. If the vertical ordinate were then replotted to incorporate this roughness indicator, m, the resultant graph ought then to collapse all the data for the isolated roughness flow regime. Figure 8.34 shows this variation of k_s/mH with λ and its comparison with the other data.

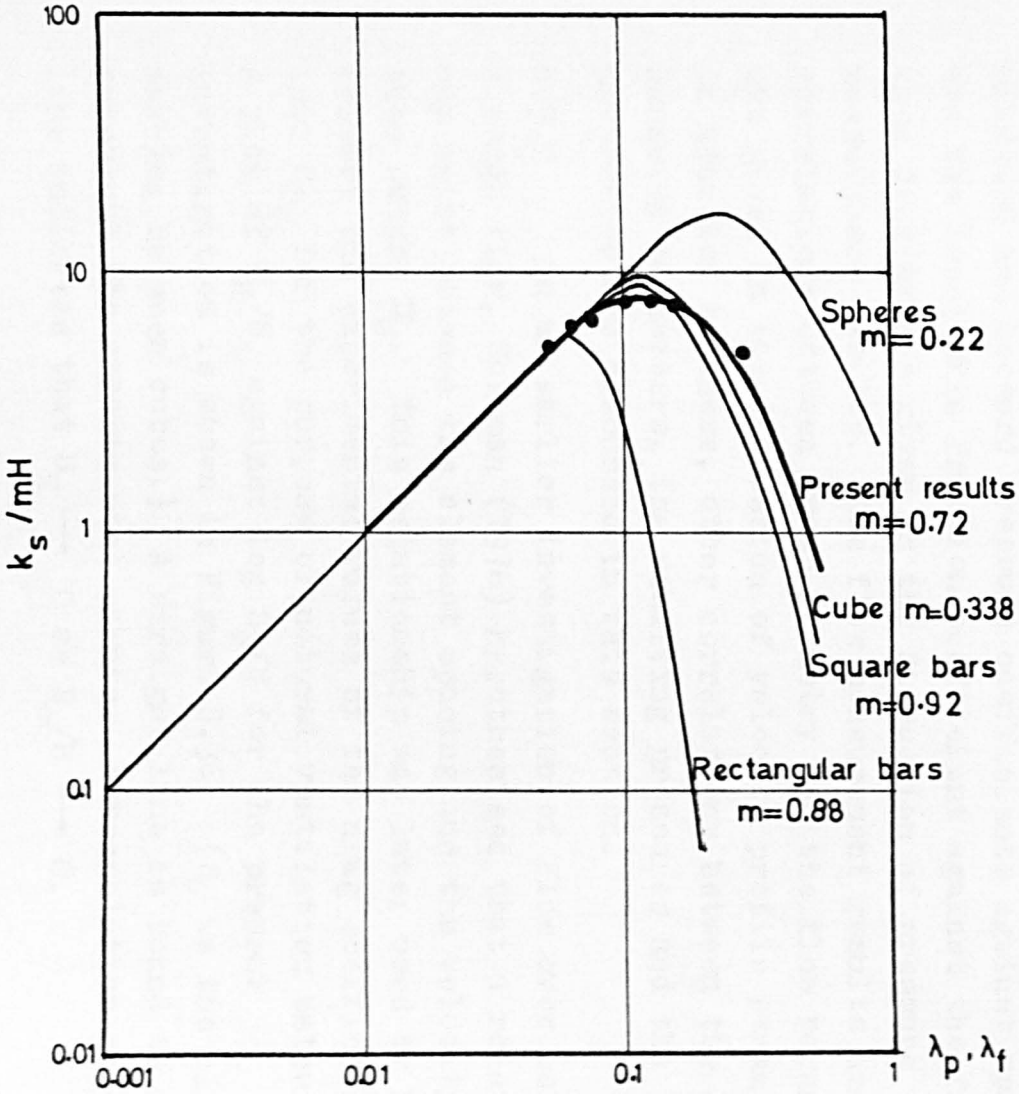

FIGURE 8.34 INTERFERENCE EFFECTS OF ROUGHNESS ELEMENTS WITH DENSITY (BASED ON KOLOSEUS AND DAVIDIAN 1966)

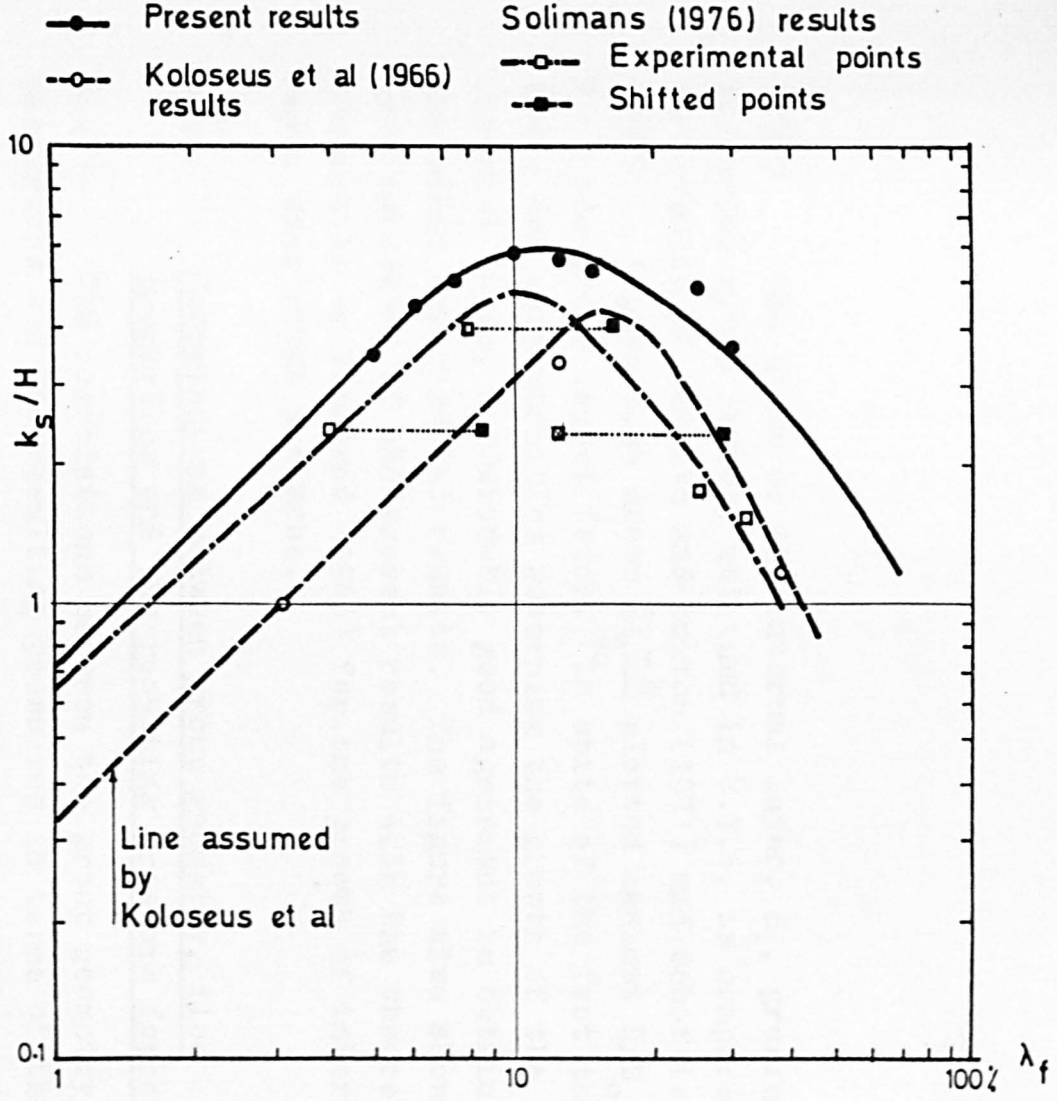

FIGURE 8.33 VARIATION OF k_s/H WITH FRONTAL AREA DENSITY

8.8.5 The depth of the internal layer, δ_i, growing over the model group layout, obtained in 8.7.6, is compared with the results of Antonia and Luxton (1971) and Schoffield (1975). Figure 8.35 shows $\frac{\delta_i - d}{Z_o}$ plotted against R/Z_o, where R is the group layout fetch. In spite of the fact that there are many variables governing the growth of the internal layer, a reasonably good agreement is obtained with the other experimental results. The figure also shows a good agreement of the present results with the theoretical prediction by Townsend (1965) for the growth of internal layer over rough surfaces.

8.9 Correlations between group geometry, flow properties and the resulting pressure forces

8.9.1 The correlations between the group geometry parameters and the resulting pressures in terms of the windward and leeward pressure coefficients against spacing and the local skin friction coefficient against the frontal area density are given in the discussion of pressure measurement results. The flow measurement results and the correlations between group geometry and the flow parameters are given in the discussion of velocity profile parameters. In addition to these, other correlations between the group geometry parameters, the resulting pressures and the flow properties are discussed in this section.

8.9.2 In an earlier investigation of flow over cubes in a rough flow, Soliman (1976) hypothesised that a relationship may exist between the element spacing and the velocity at cube height U_H. This relationship was later used by him to convert the experimental values of the drag coefficient, C_{D_1}, into C_{D_H} for the purpose of natural ventilation calculations. A plot of U_H/U_1 against log S_c/H for the present investigation is shown in Figure 8.36. (S_c is the clear spacing between cubes.) A straight line is found to represent the experimental points. Extrapolation of this line indicates that $U_H \longrightarrow 0$ as $S_c/H \longrightarrow 0$.

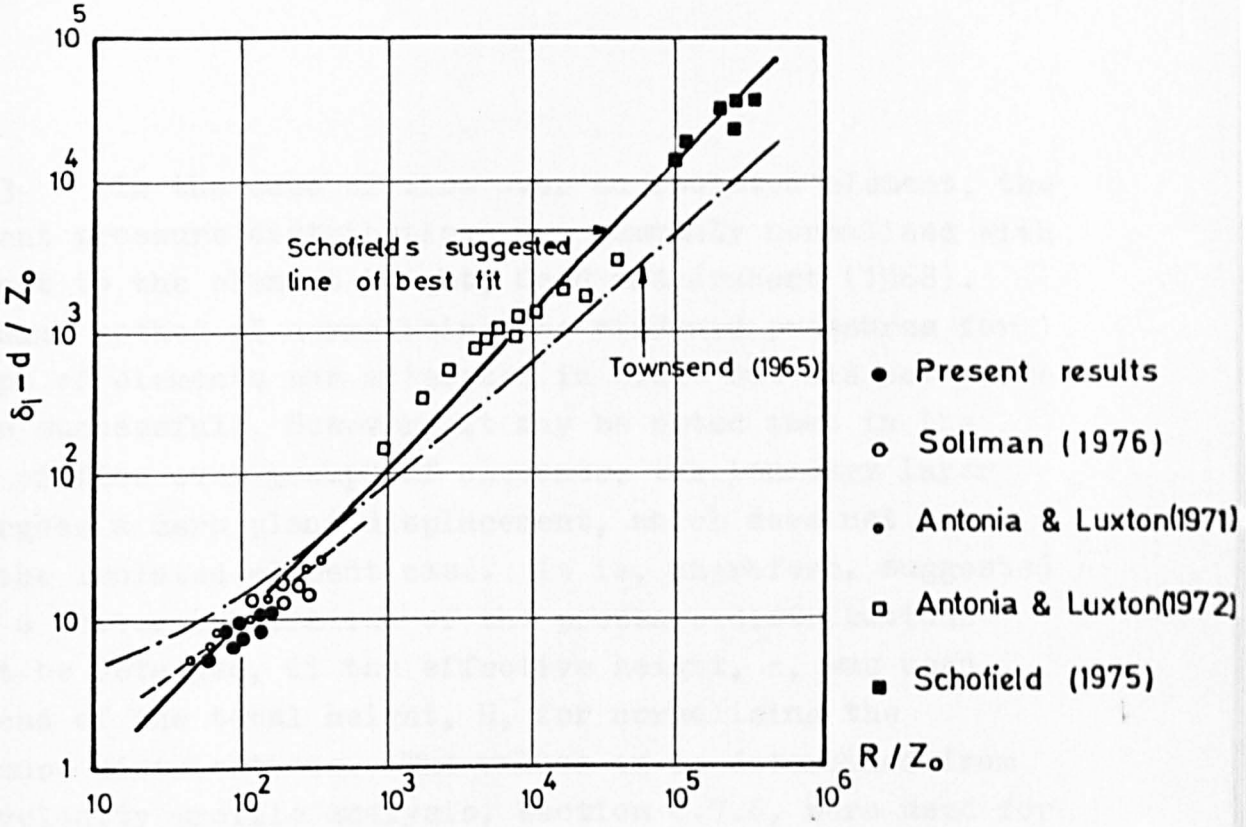

FIGURE 8.35 COMPARISON OF EXPERIMENTAL GROWTH OF INTERNAL LAYER WITH THEORY AND PRESENT RESULTS

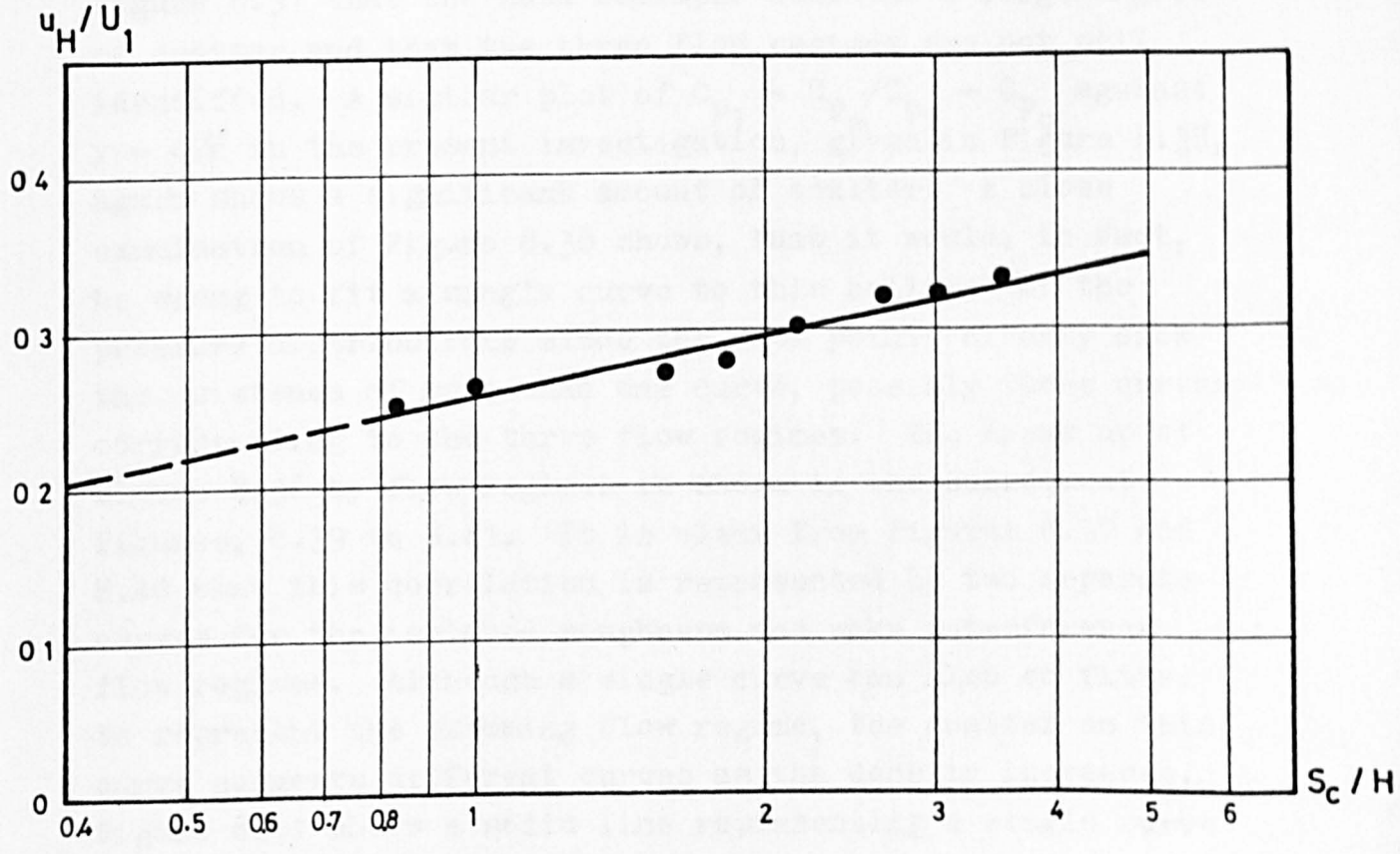

FIGURE 8.36 VARIATION OF U_H/U_1 WITH S_c/H

8.9.3 In the case of flow over an isolated element, the element pressure distributions are commonly normalised with respect to the element height, Good and Joubert (1968). The same method of normalising the windward pressures for groups of elements was attempted in 8.4.7 but did not prove to be successful. However, it may be noted that in the case of flow over groups of elements, the boundary layer undergoes a zero plane displacement, which does not occur for the isolated element case. It is, therefore, suggested that a better correlation of the pressure distributions might be obtained, if the effective height, ε, was used instead of the total height, H, for normalising the pressure distributions. The values of ε, determined from the velocity profile analysis, section 8.7.6, were used for this purpose. A similar plot by Soliman, given in Figure 8.37, showed the pressure distributions approximately grouped around a single curve. However, it is clear from Figure 8.37 that the data collapse contains a large degree of scatter and that the three flow regimes are not well identified. A similar plot of $C_{p_1} - C_{p_w}/C_{p_1} - C_{p_o}$ against $y - d/\varepsilon$ in the present investigation, given in Figure 8.38, again shows a significant amount of scatter. A close examination of Figure 8.38 shows, that it would, in fact, be wrong to fit a single curve to this collapse of the pressure distributions since the data points clearly show the existence of more than one curve, possibly three curves corresponding to the three flow regimes. The break up of Figure 8.38 by flow regimes is shown in the subsequent figures, 8.39 to 8.41. It is clear from Figures 8.39 and 8.40 that this correlation is represented by two separate curves for the isolated roughness and wake interference flow regimes. Although a single curve can also be fitted to represent the skimming flow regime, the scatter on this curve suggests different curves as the density increases. Figure 8.41 shows a solid line representing a single curve for the entire skimming flow regime and a number of broken

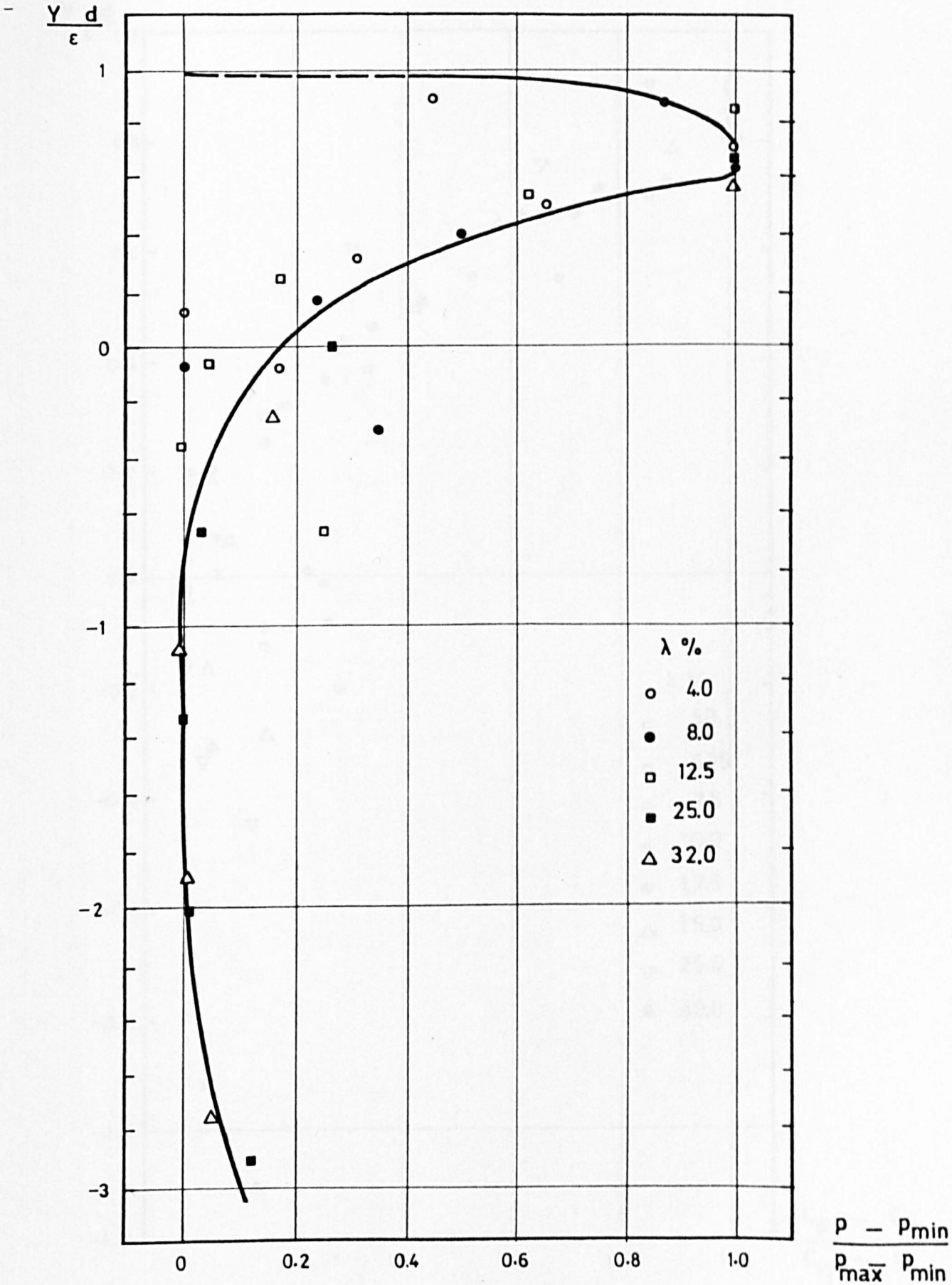

FIGURE 8.37 NORMALISED PRESSURE PROFILES FOR THREE FLOW REGIMES (SOLIMAN 1976)

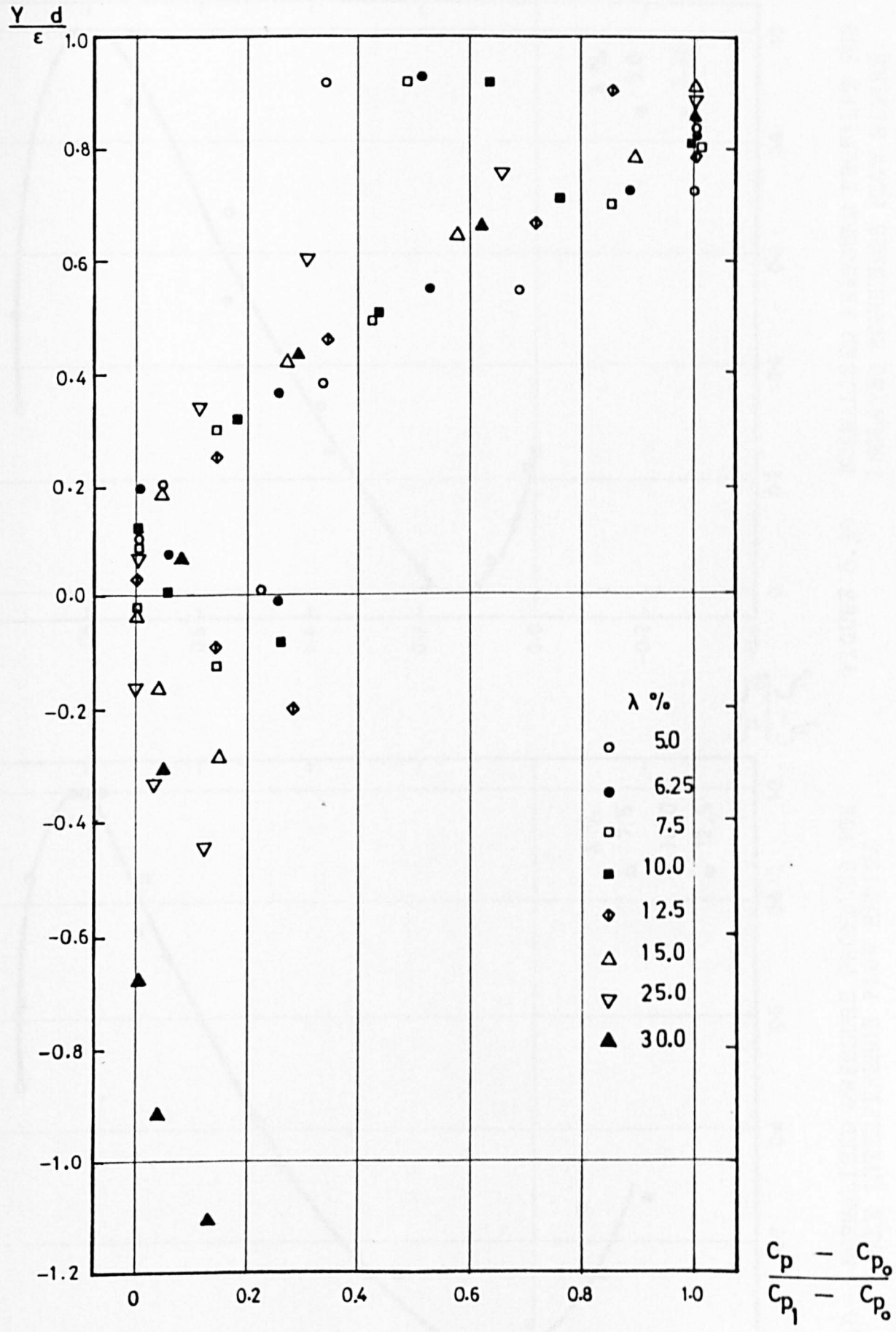

FIGURE 8.38 NORMALISED PRESSURE PROFILES FOR THE PRESENT RESULTS (THREE FLOW REGIMES)

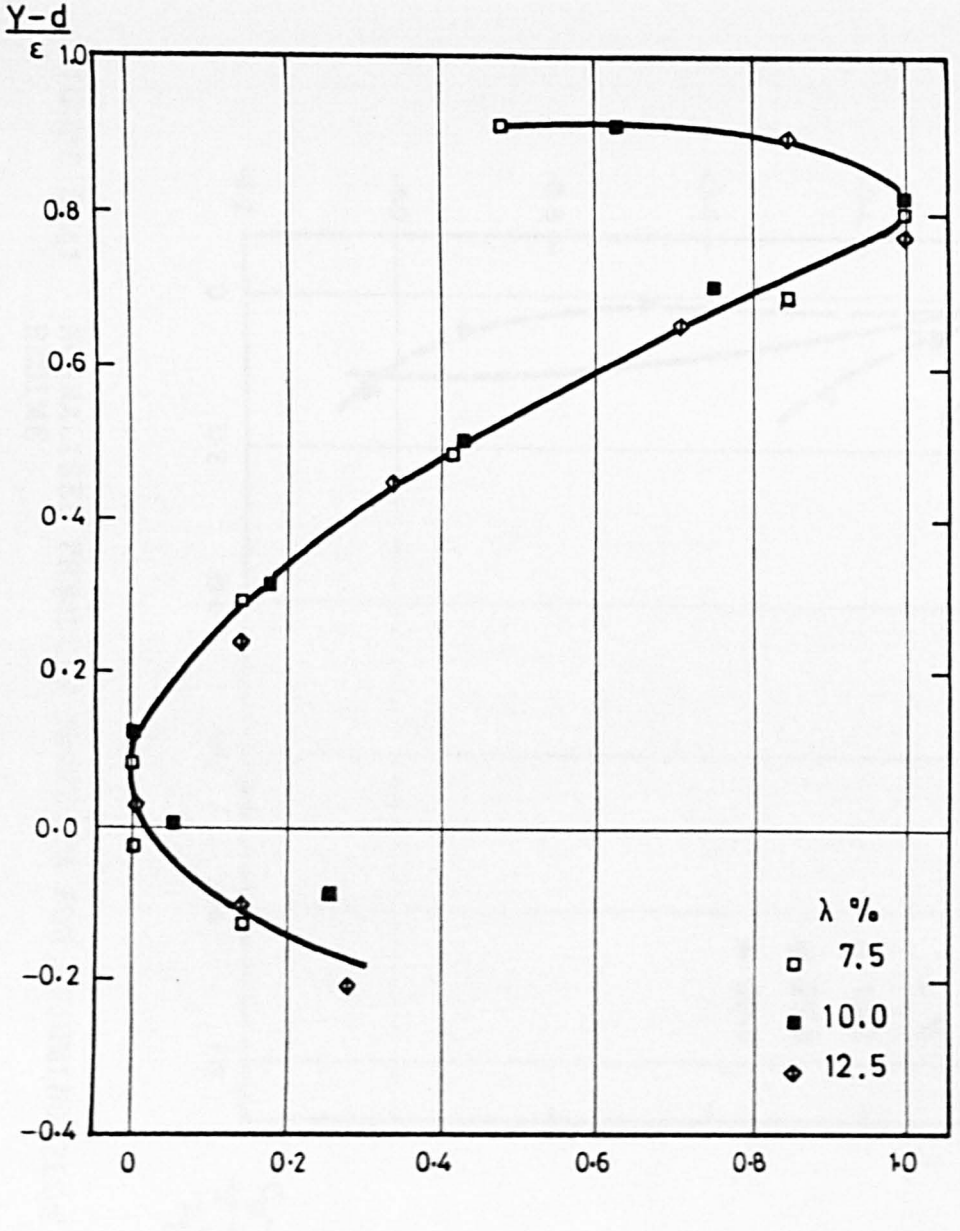

FIGURE 8.40 NORMALISED PRESSURE PROFILES FOR WAKE INTERFERENCE FLOW REGIME

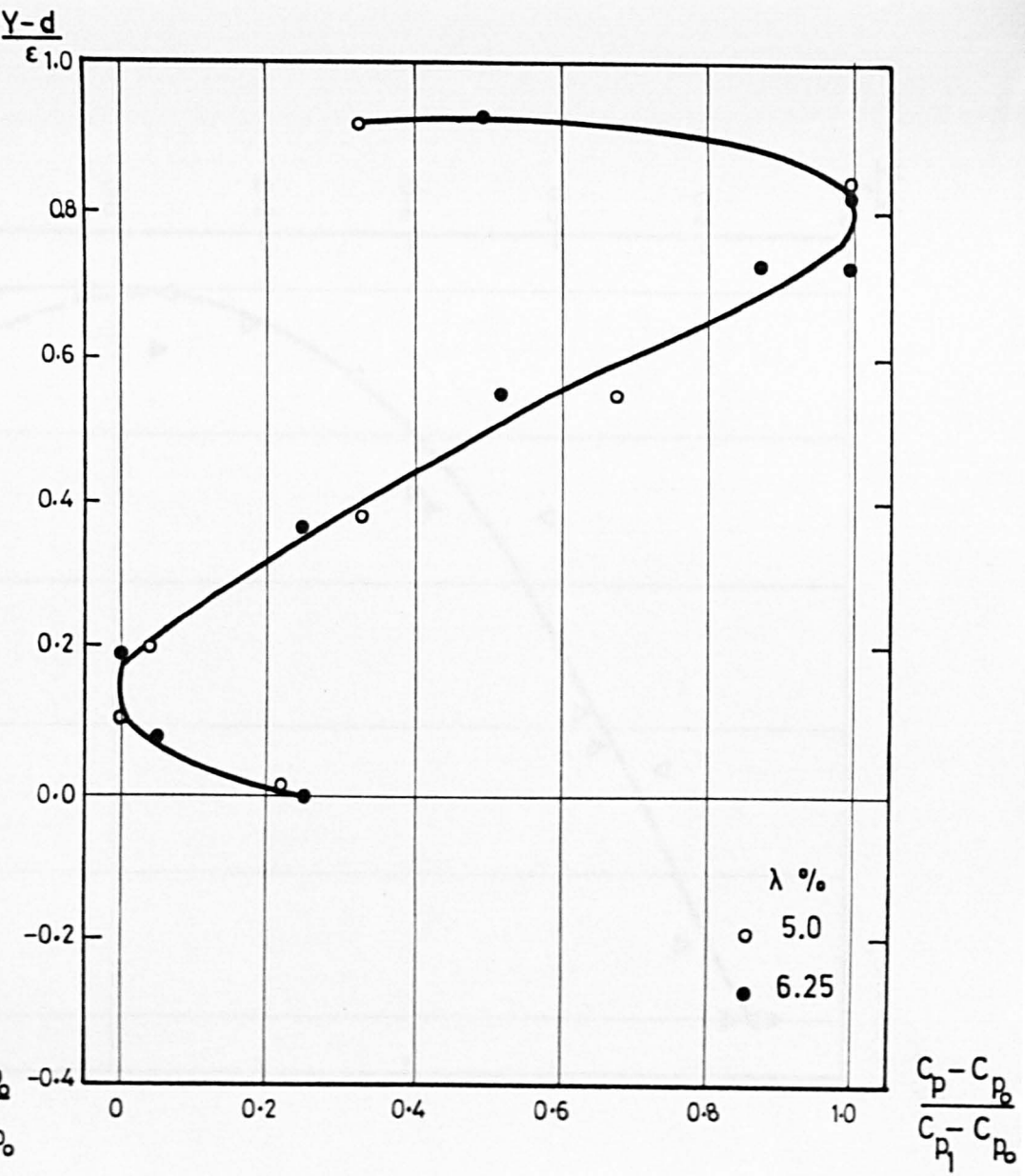

FIGURE 8.39 NORMALISED PRESSURE PROFILES FOR ISOLATED ROUGHNESS FLOW REGIME

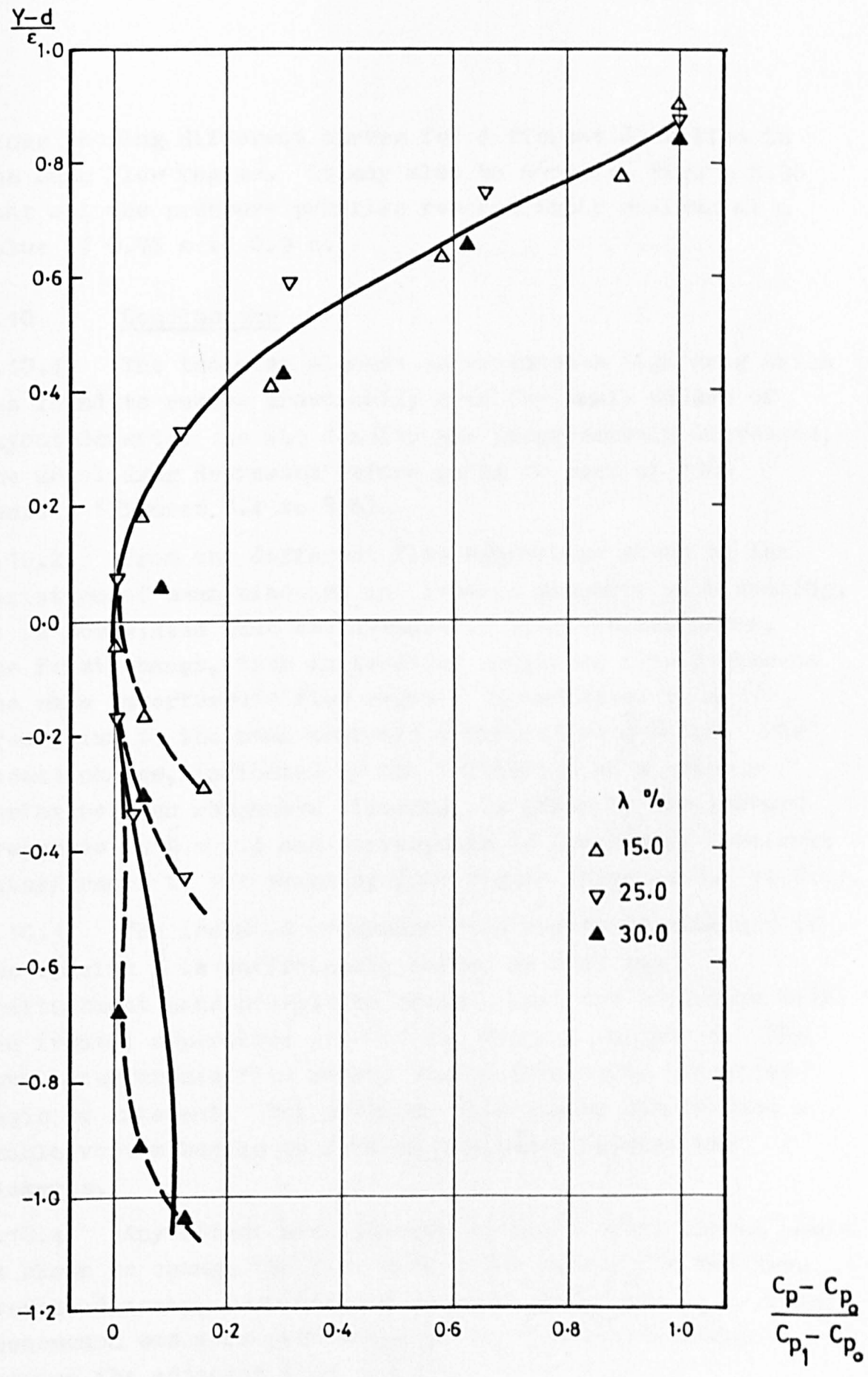

FIGURE 8.41 NORMALISED PRESSURE PROFILES FOR SKIMMING FLOW REGIME

lines showing different curves for different densities in the same flow regime. It may also be noted in Figure 8.38 that all the pressure profiles reached their maximum at a value of 0.75 ε to 0.9 ε.

8.10 Conclusions

8.10.1 The isolated element experienced a high drag which was found to reduce drastically even for small values of layout density. As the density was progressively increased, the model drag decreased before going to zero at 100% density (Figures 8.4 to 8.6).

8.10.2 From the different flow behaviours shown by the variation of mean windward and leeward pressure with spacing, it is postulated that two changes of flow regimes occur. The first change, from an isolated roughness flow regime to the wake interference flow regime, is indicated by a breakpoint in the mean windward pressures at $\frac{S}{H} \simeq 3.4$. The second change, indicated by the initiation of a stable vortex between roughness elements, is shown by the leeward pressures at $\frac{S}{H} \simeq 2.4$ and corresponds to the change from wake interference to the skimming flow regime (Figures 8.4 to 8.6).

8.10.3 The isolated roughness flow regime is obtained if the spacing $\frac{S}{H}$ is sufficiently large, so that the reattachment zone behind the element does not interfere with the frontal separation zone of the element behind it. The wake interference flow regime starts when these two zones begin to interact. The skimming flow regime starts when a stable vortex begins to form in the space between the elements.

8.10.4 Any slight misalignment in the element layout could be shown to change the flow within the cubes, for the same overall density, resulting in changes of C_{p_w} and C_{p_b}. This phenomenon was more pronounced in the transition range between the adjacent flow regimes.

8.10.5 A collapse of the windward pressure distribution profiles was obtained when the profiles were classified by flow regimes. These profiles, in the isolated flow regime took the form of an "S" and those in the skimming flow regime took the form of a reversed "C" while the profiles in the wake interference flow regimes, collapsed only in the lower 85% of their height. In the remaining 15% of the element height, the collapse was poor, owing to the transition from an "S" to a reversed "C" shape. A similar attempt was made to collapse the leeward pressure profiles. These profiles in the isolated roughness and wake interference flow regimes were of a more uniform distribution and collapsed as one family, whilst they were found to be no longer uniform in the skimming flow regime (Figure 8.9).

8.10.6 The normalisation scheme suggested by Good and Joubert (1968) for isolated body windward pressure profiles could not be successfully applied to groups of elements (Figure 8.10).

8.10.7 The variation of the effective skin friction coefficient with density reflected a behaviour similar to the behaviour of equivalent sand grain roughness with density. The variation of the layout pattern affected the values of C_{f_e} obtained in the isolated roughness and the wake interference flow regimes but not in the skimming flow regime (Figure 8.11).

8.10.8 The roof pressure coefficients were always negative with the maximum suction occurring near the windward edge of the roof and decreasing towards the rear edge. At higher densities, however, the pressure distributions were shown to become more constant over the roof (Figure 8.12).

8.10.9 From the single break point in the graph, showing the variation of the roof lift coefficient, C_{L_1} with spacing, at a value of $\frac{S}{H} = 2.4$, it is concluded that as the spacing is progressively reduced in the isolated roughness and the

wake interference flow regimes, the flow within the cavities and on top of element array changes. This variation of flow causes the lift force to vary. In the skimming flow regime, the value of C_{L_1} remains constant due to the undisturbed flow on top of roughness elements (Figure 8.13).

8.10.10 The flow and the resulting pressure forces are governed by the spacing parameter in the isolated roughness and the wake interference flow regimes while the group density is more important in the skimming flow regime. The behaviour of C_{p_w} and C_{p_b} is however similar for the two pattern, i.e. normal and staggered. The effect of model orientation θ is negligible in the range $0 < \theta < 60$ and the effect of group layout orientation ϕ becomes less important as the fetch increases (Figure 8.14).

8.10.11 The simulated atmospheric boundary layer flow underwent only one surface change, when it reached the model group layout. An internal layer was found to be growing over the group layout (Figure 8.18).

8.10.12 The logarithmic region of the internal layer of the cube centre line profiles did not extend above the cube height in any case (Figures 8.19 to 8.26).

8.10.13 A broken line relationship is shown to exist between the zero plane displacement and the group layout density. The break points correspond to the three flow regimes already suggested (Figure 8.30).

8.10.14 The variation of roughness length with increasing group layout density was shown to exhibit a trend similar to that of skin friction coefficient. The initial linear increase of roughness length represented the isolated roughness flow regime, with the subsequent levelling off of the curve corresponding to the wake interference flow regime and then a decrease to show the skimming flow regime (Figure 8.31 and 8.32).

8.10.15 The variation of equivalent sand grain roughness with increasing density, showed good agreement between the present results and the results of Koloseus and Davidian (Figures 8.33 and 8.34).

8.10.16 The depth of the internal layer obtained indicated good agreement with both previous results and the theoretical prediction by Townsend (Figure 8.35).

8.10.17 A relationship is suggested to exist between the velocity at the cube height and the clear spacing between cubes (Figure 8.36).

8.10.18 A normalisation scheme for the windward pressure distribution profiles, which takes into account the effect of the zero plane displacement and uses the effective height, has been suggested. In this scheme, all the pressure distribution profiles collapsed on three different curves representing the three flow regimes (Figures 8.38 to 8.41).

CHAPTER 9

EXPERIMENTAL RESULTS AND DISCUSSIONS: FLOW OVER GROUPS OF MODELS OF VARYING FRONTAL AND SIDE ASPECT RATIOS

9. EXPERIMENTAL RESULTS AND DISCUSSIONS: FLOW OVER GROUPS OF MODELS OF VARYING FRONTAL AND SIDE ASPECT RATIOS

9.1 Introduction

9.1.1 The shape of buildings and their grouping arrangements have been shown to be important parameters in determining the flow and, hence, the pressure forces on them. The few ad hoc studies of flows around different building shapes, made in the past were too restrictive to enable a systematic assessment to be made of the effects of varying the frontal or the side aspect ratios of low rise buildings on their resulting wind forces. A systematic study around isolated models of varying frontal and side aspect ratios was made in chapter 6, where it was found that the mean windward and leeward pressure coefficients as well as the roof lift coefficient vary as the aspect ratio varies. In an attempt to extend the investigation, this chapter describes in detail the manner in which the group geometry governs the mean pressure forces on groups of identical roughness elements of varying frontal and side aspect ratios. This study will also be used to identify the flow regimes for building groups of varying plan forms. Similar studies were made in the past, by Evan (1957) and Soliman (1976), but their work was restricted to the surface flow visualisation tests, as a result of which, a quantitative assessment was not possible. In this study, the cube has been taken as having both side and frontal aspect ratio of 1.0 and all other models are related to it. In order to cover most of the common building shapes which occur in practice, the frontal aspect ratio was varied from 0.5 to 4.0 and the side aspect ratio was varied from 0.5 to 2.0

9.1.2 In the present investigation the model group took the form of free standing roughness elements on the smooth surface of the turntable with the urban terrain atmospheric boundary layer simulation upwind. Thus the oncoming atmospheric flow underwent an abrupt change of surface roughness, when it reached the group layout. The effect of a similar disturbance on the simulated boundary layer flow and its effects on the stabilisation of the surface pressure forces in a group layout of cube shaped roughness elements has been investigated in chapter 7. On the basis of conclusions drawn in chapter 7 and their application of the investigation of cubes in chapter 8, it was thought that the drag forces and roof suction in this phase of the investigation would also behave in a similar manner. Thus the model group layout size, R/H, was kept between 10 to 25 depending on the plan area density. Shorter fetches were required for stabilisation of pressure forces at higher densities.

9.1.3 The effect of both normal and staggered layout patterns, on the resulting pressure forces has also been investigated in detail in chapter 8. Here, it was found that strong similarities existed between the results for the two layout patterns. On the basis of these results, only the normal pattern has been considered in this phase of the investigation.

9.1.4 On the basis of the investigation by Soliman (1976) concerned with the effect of model orientation angle, θ, and the group layout orientation angle, ϕ, on the resulting pressure forces on the cube shaped elements, both of the orientation angles θ and ϕ were kept at zero in the present investigation.

9.1.5 In a similar investigation of flow over cube shaped elements, the effect of roughness geometry has been studied in detail in chapter 8 where a broken straight line relationship was shown to exist between the elements

windward pressure coefficient, C_{p_w} and the element spacing, S/H, a function of the density. Another straight line relationship was found for the variation of leeward pressure coefficient, C_{p_b}, with S/H over a range of S/H > 2.4. This relationship showed a sudden decrease in the value of C_{p_b}, at a spacing of S/H $\simeq$ 2.4, followed by a gradual increase at smaller values of S/H. As a result of the behaviour of the windward and leeward pressure coefficients, the drag coefficient, C_{D_1}, reflected these changes in the form of a broken straight line and a jump followed by gradual decrease, until the value of C_{D_1} approached zero at 100% density. These inflections in the graph of the drag and surface pressures against the element spacing were used to identify three flow regimes. These results for the cube in the normal layout pattern, reproduced in Figure 9.1 show that the isolated roughness flow regime corresponds to a spacing of S/H > 3.4, the wake interference flow regime corresponds to an element spacing of 2.4 < S/H < 3.4 and the skimming flow regime to S/H < 2.4. A study of the pressure variations on the roof of the cube showed only one change of behaviour for the variation of the lift coefficient, C_{L_1}, as a function of element spacing, S/H, which corresponds to the start of the skimming flow regime at S/H = 2.4.

9.1.6 A series of mean pressure measurements have been undertaken for all the models while only one set of velocity profiles were taken for the model with a frontal aspect ratio of 2.0. Table 9.1 gives the ranges of the parameters considered in the two stages of this phase of the investigation.

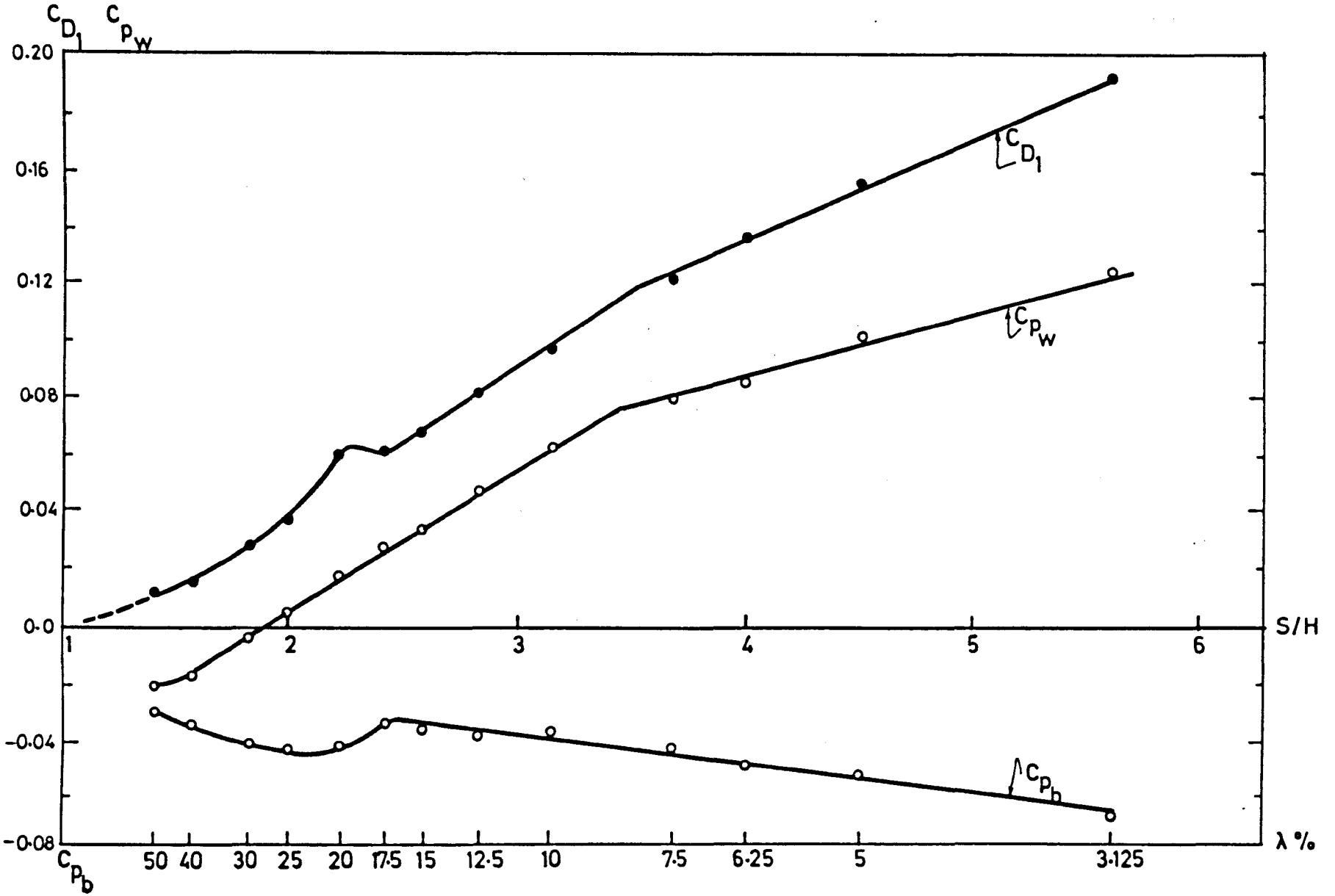

FIGURE 9.1 VARIATION OF THE WALL PRESSURES AND THE DRAG WITH THE CUBE SPACING - NORMAL PATTERN (FRONTAL AND SIDE ASPECT RATIO = 1.0)

Table 9.1 Variables considered in this investigation

Variables	Pressure measurements	Velocity profile measurements
Frontal aspect ratio	0.5 to 4.0	2.0
Side aspect ratio	0.5 to 2.0	-
Plan area density	$2.5\% < \lambda_p < 60.0\%$	$5.0\% < \lambda_p < 40.0\%$
Pattern	Normal	Normal
Fetch	$10 < R/H < 25$	$10 < R/H < 25$
Orientation	$\theta = \phi = 0$	$\theta = \phi = 0$
Incident flow	Simulated atmospheric boundary layer flow	Simulated atmospheric boundary layer flow

9.2 Pressure measurements on the windward and leeward faces of models having varying frontal aspect ratio

9.2.1 The vertical distribution of pressure coefficients measured on the centre line of the windward and leeward faces of all the models in various layout densities are shown in Figures 9.2 to 9.5. Other pressure coefficient distributions on the faces of the models, on either side of the centre line, (pressure tappings shown in chapter 5) alongwith these centre line distributions were integrated to give the mean windward and leeward pressure coefficients, C_{p_w} and C_{p_b}. The algebraic difference of these pressure coefficients, in each case, yields the drag coefficient, C_{D_1}.

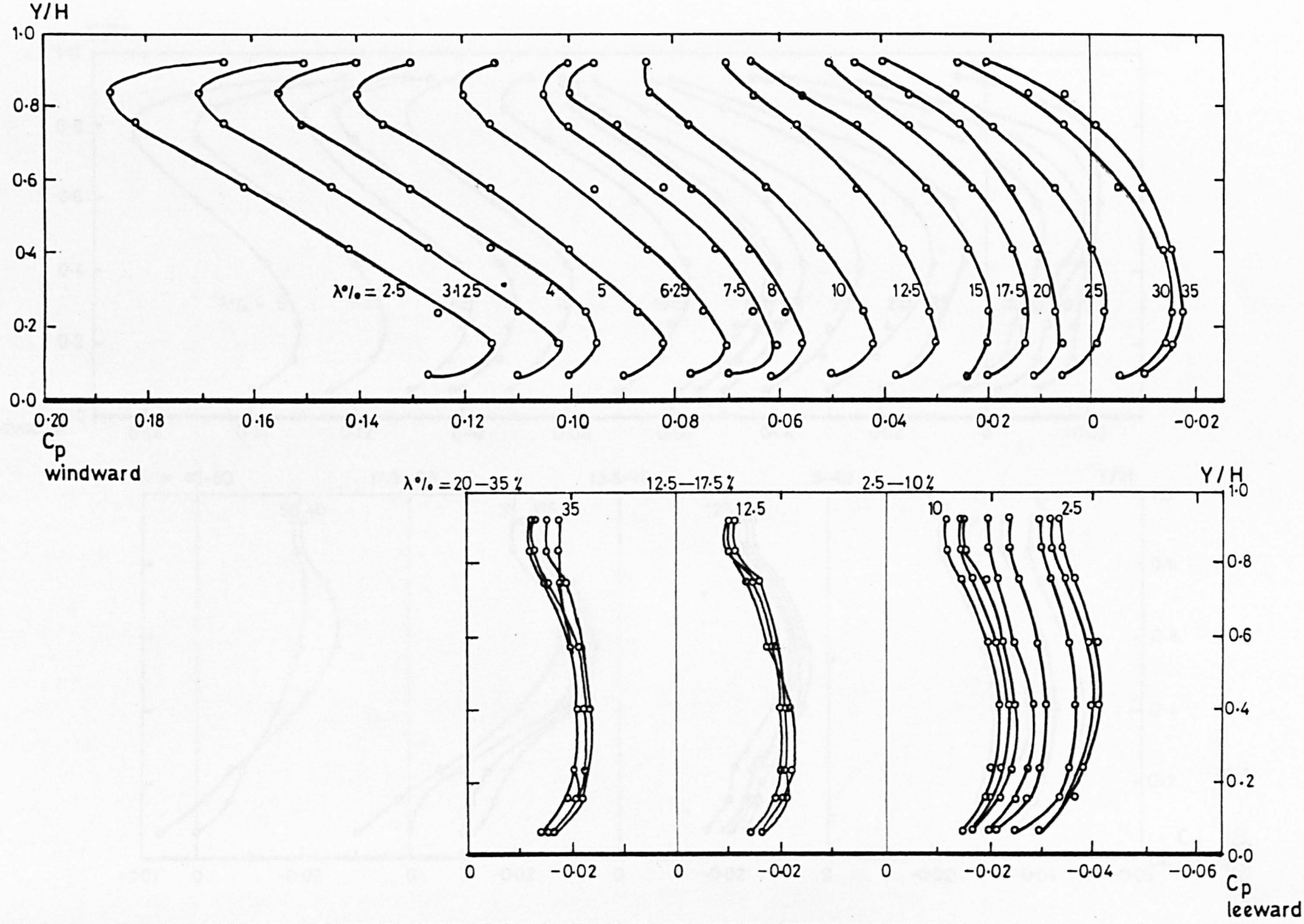

FIGURE 9.2 WALL PRESSURE COEFFICIENT DISTRIBUTIONS ON MODEL CENTRE LINE AT VARIOUS DENSITIES - A_f = 0.5

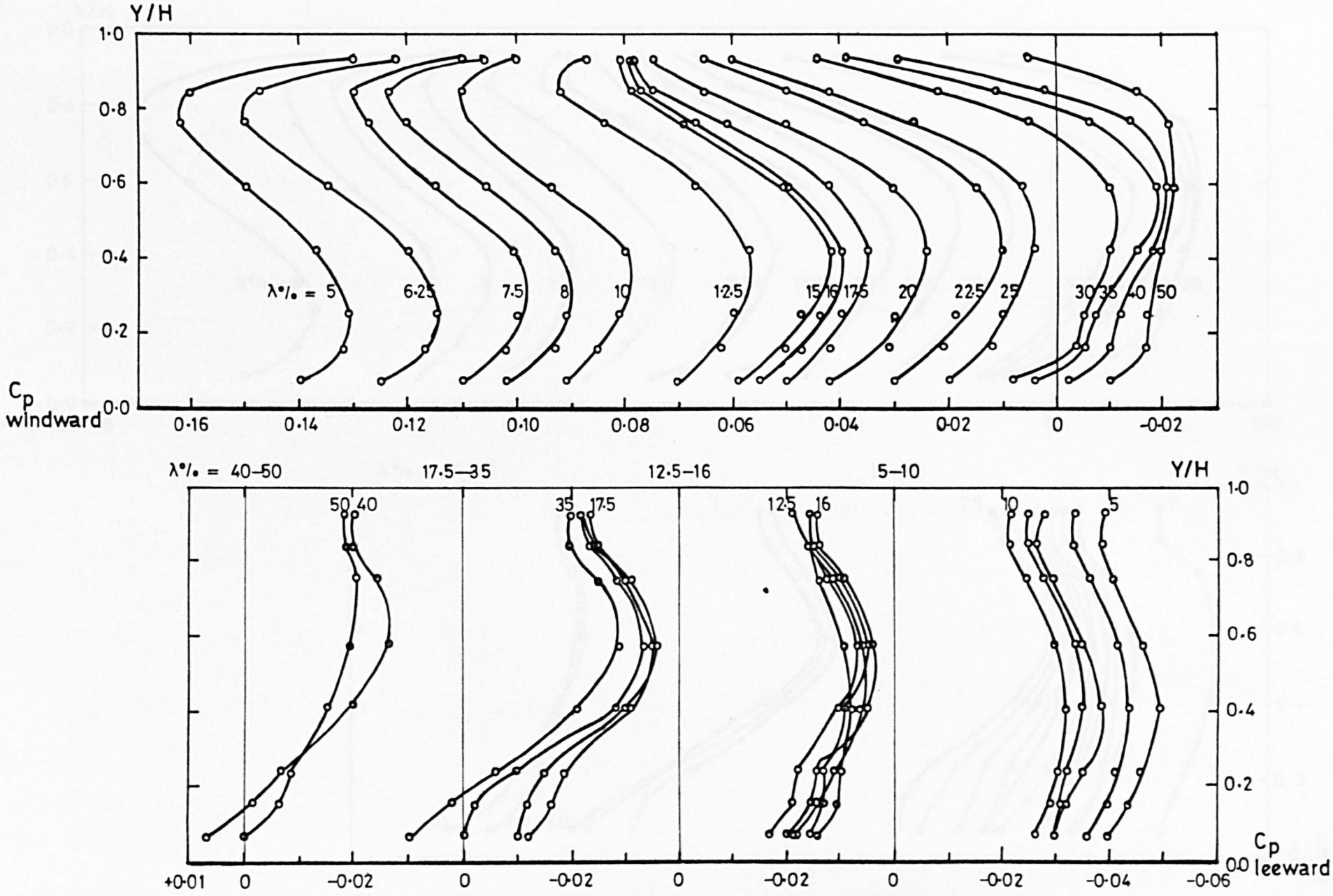

FIGURE 9.3 WALL PRESSURE COEFFICIENT DISTRIBUTIONS ON MODEL CENTRE LINE AT VARIOUS DENSITIES - A_f = 1.5.

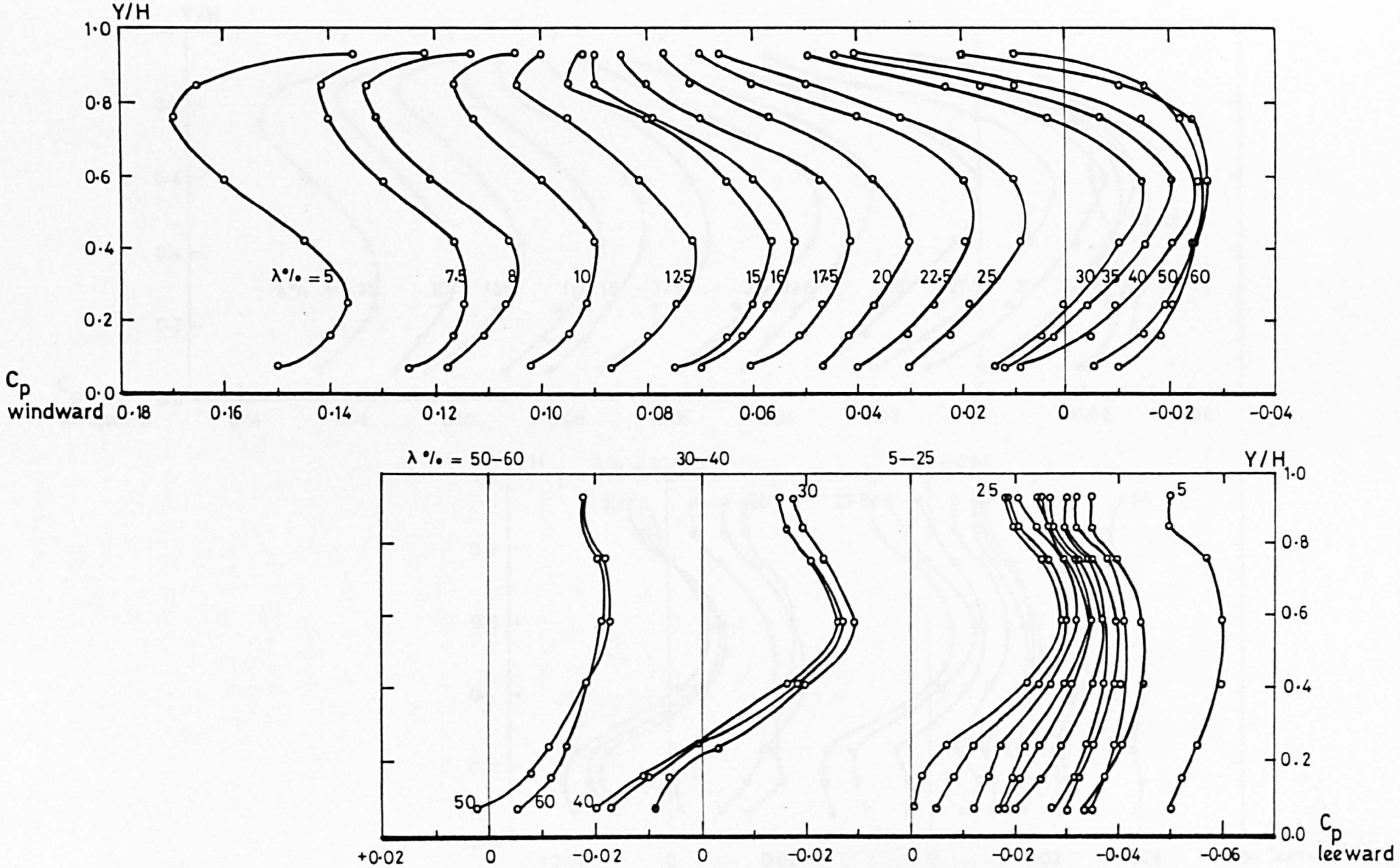

FIGURE 9.4 WALL PRESSURE COEFFICIENT DISTRIBUTIONS ON MODEL CENTRE LINE AT VARIOUS DENSITIES - $A_f = 2.0$

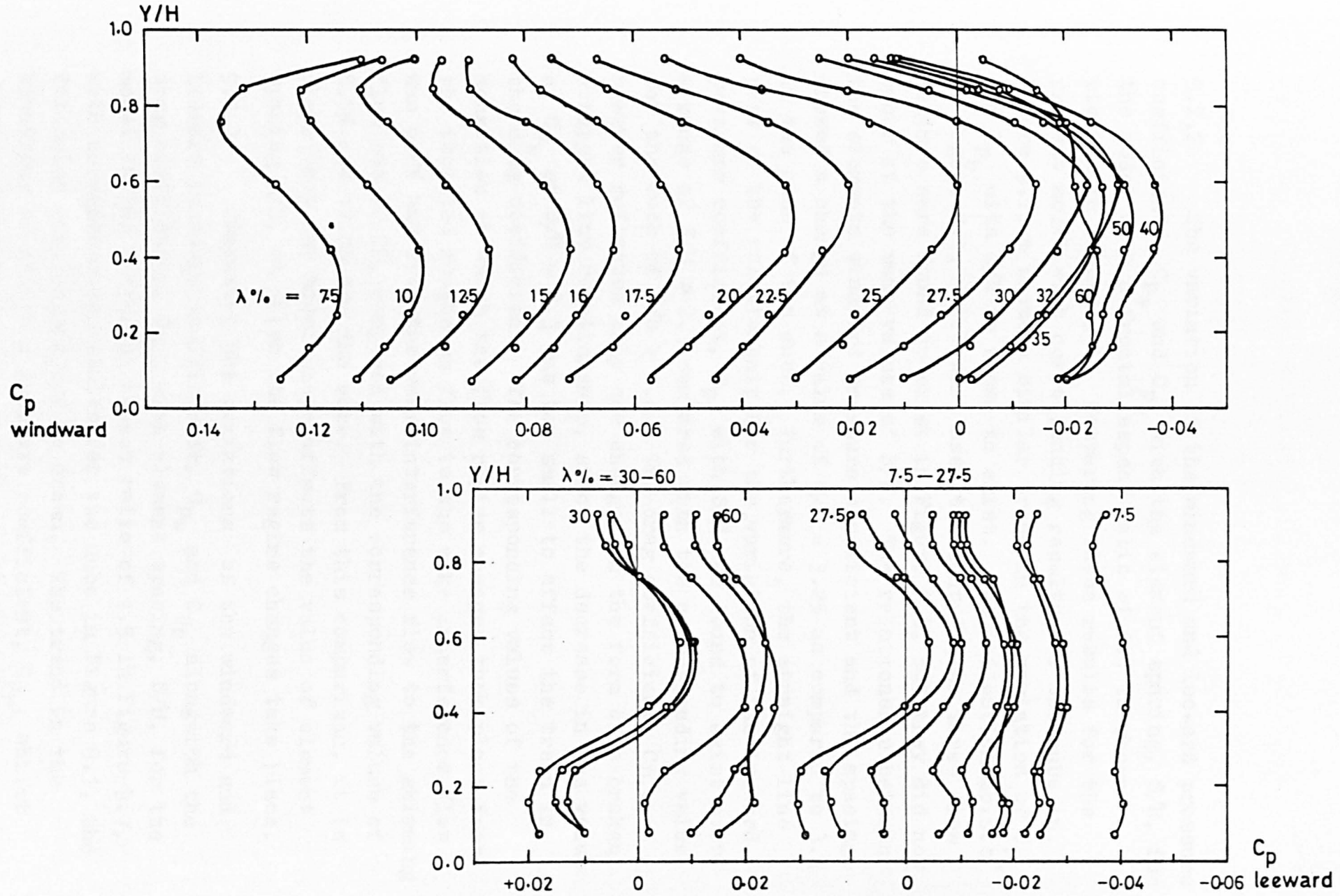

FIGURE 9.5 WALL PRESSURE COEFFICIENT DISTRIBUTIONS ON MODEL CENTRE LINE AT VARIOUS DENSITIES - A_f = 4.0

9.2.2 The variation of the windward and leeward pressure coefficients, C_{p_w} and C_{p_b} with the element spacing, S/H, for the model with a frontal aspect ratio of 0.5 is shown plotted in Figure 9.6. Comparing these results for the present model with corresponding results for the cube in Figure 9.1, a broadly similar trend in the variation of C_{p_w} and C_{p_b} with S/H is shown to exist. The inflection points in Figure 9.1, which were used to identify the three flow regimes were found to exist in Figure 9.6, but they did not occur at the same values of S/H. The relationship between the elements windward pressure coefficient and the spacing, showed a change at a value of S/H = 3.25 as compared to 3.4 in the case of the cube. Furthermore, the straight line part of the relationship for the variation of the leeward pressure coefficient, C_{p_b} with S/H was found to exist over a range of S/H $>$ 2.3 compared with the corresponding value for the cube of S/H $>$ 2.4. The drag coefficient, C_{D_1}, however reflected only one change, in the form of a broken straight line relationship, since the decrease in the value of C_{p_b} at S/H = 2.3 was too small to affect the trend in the drag coefficient. The corresponding values of the densities at which the flow regime changes took place from the isolated roughness flow to the wake interference flow was 6.0% and from the wake interference flow to the skimming flow was 12.0%, compared with the corresponding values of 8.5% and 17.0% for the cube. From this comparison, it is clear that the model shape affects the value of element spacing S/H, at which the flow regime changes take place.

9.2.3 Comparing the variations of the windward and leeward pressure coefficients, C_{p_w} and C_{p_b} alongwith the drag coefficient, C_{D_1}, with element spacing, S/H, for the model having a frontal aspect ratio of 1.5 in Figure 9.7, with corresponding results for the cube in Figure 9.1, the following conclusions may be drawn. The trend in the behaviour of windward pressure coefficient, C_{p_w}, whilst similar to that reported for the cube, shows a break point

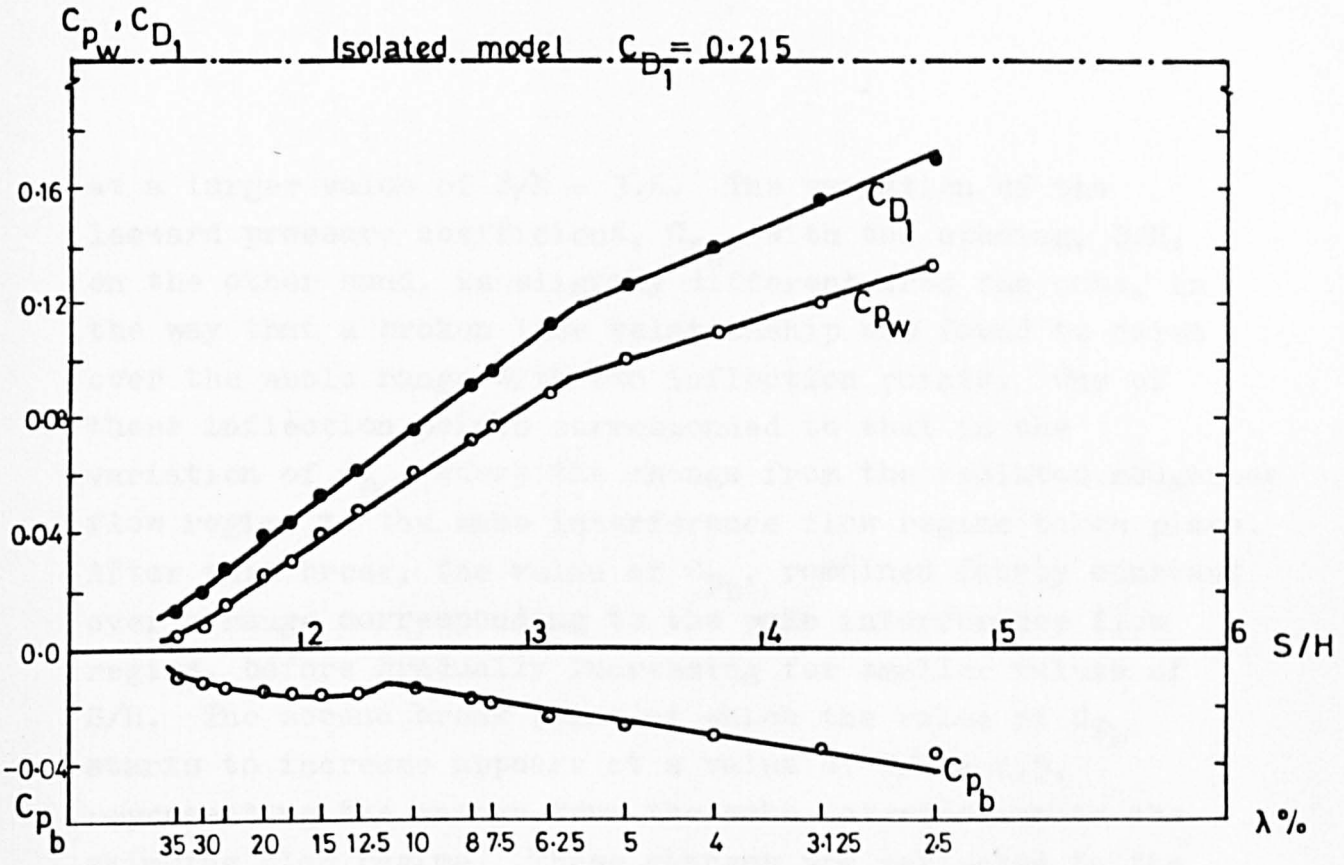

FIGURE 9.6 VARIATION OF THE WALL PRESSURES AND THE DRAG WITH SPACING - $A_f = 0.5$

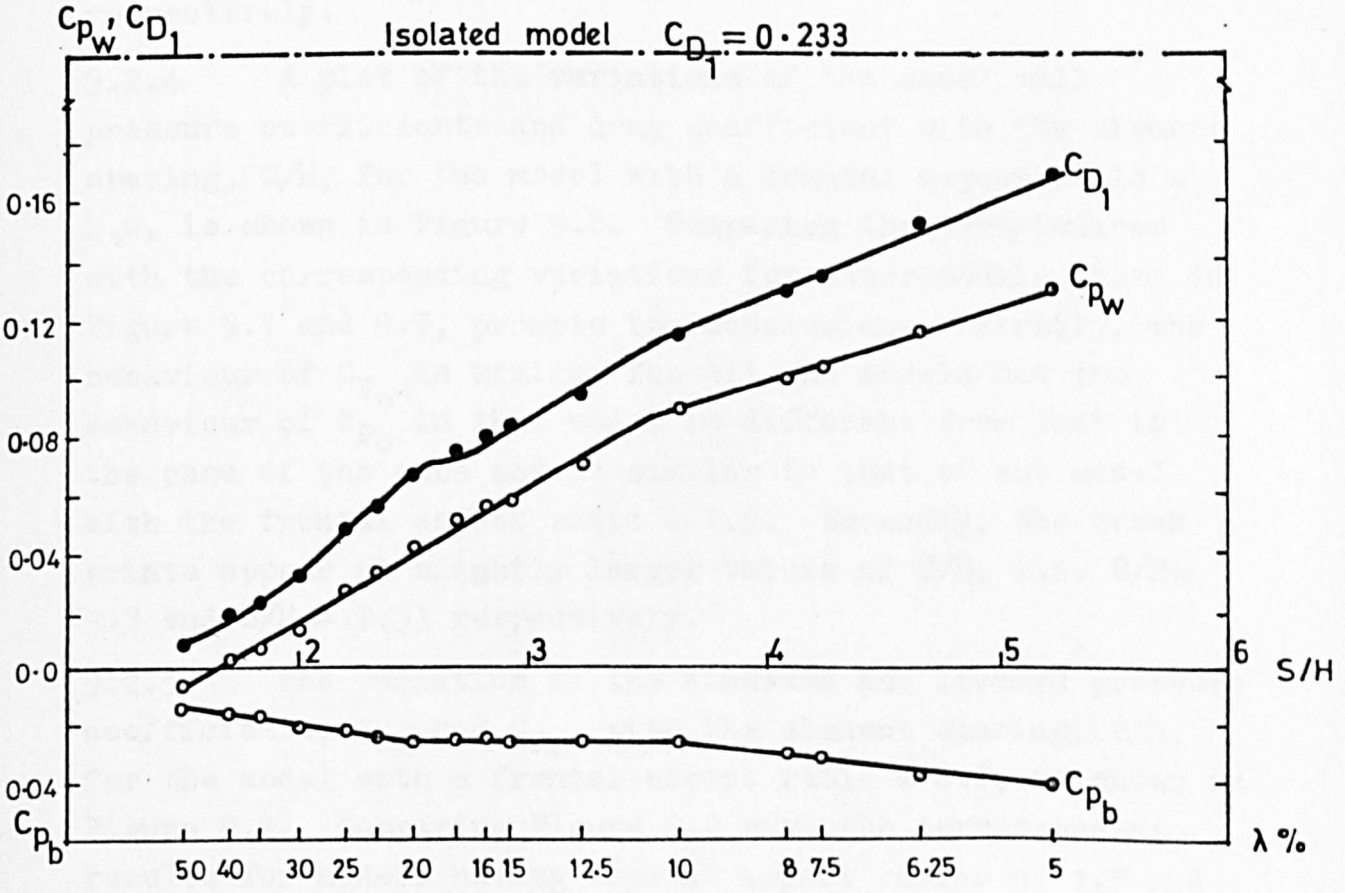

FIGURE 9.7 VARIATION OF THE WALL PRESSURES AND THE DRAG WITH SPACING - $A_f = 1.5$

at a larger value of S/H = 3.6. The variation of the leeward pressure coefficient, C_{p_b}, with the spacing, S/H, on the other hand, is slightly different from the cube, in the way that a broken line relationship was found to exist over the whole range with two inflection points. One of these inflection points corresponded to that in the variation of C_{p_w}, where the change from the isolated roughness flow regime to the wake interference flow regime takes place. After this break, the value of C_{p_b}, remained fairly constant over a range corresponding to the wake interference flow regime, before gradually increasing for smaller values of S/H. The second break point at which the value of C_{p_b} starts to increase appears at a value of S/H = 2.5, representing the change from the wake interference to the skimming flow regime. These changes are reflected in the variation of C_{D_1} in the form of a broken straight line relationship. The corresponding values of density at which these changes of flow require take place are 10.0% and 20.0% respectively.

9.2.4 A plot of the variations of the model wall pressure coefficients and drag coefficient with the element spacing, S/H, for the model with a frontal aspect ratio = 2.0, is shown in Figure 9.8. Comparing these variations with the corresponding variations for other models shown in Figure 9.1 and 9.7, prompts two conclusions. Firstly, the behaviour of C_{p_w} is similar for all the models but the behaviour of C_{p_b} in this model is different from that in the case of the cube and is similar to that of the model with the frontal aspect ratio = 1.5. Secondly, the break points appear at slightly larger values of S/H, i.e. S/H$\simeq$ 3.7 and S/H $\simeq$ 2.53 respectively.

9.2.5 The variation of the windward and leeward pressure coefficients, C_{p_w} and C_{p_b}, with the element spacing, S/H, for the model with a frontal aspect ratio = 4.0, is shown in Figure 9.9. Comparing Figure 9.9 with the corresponding results for models having frontal aspect ratios of 1.5 and

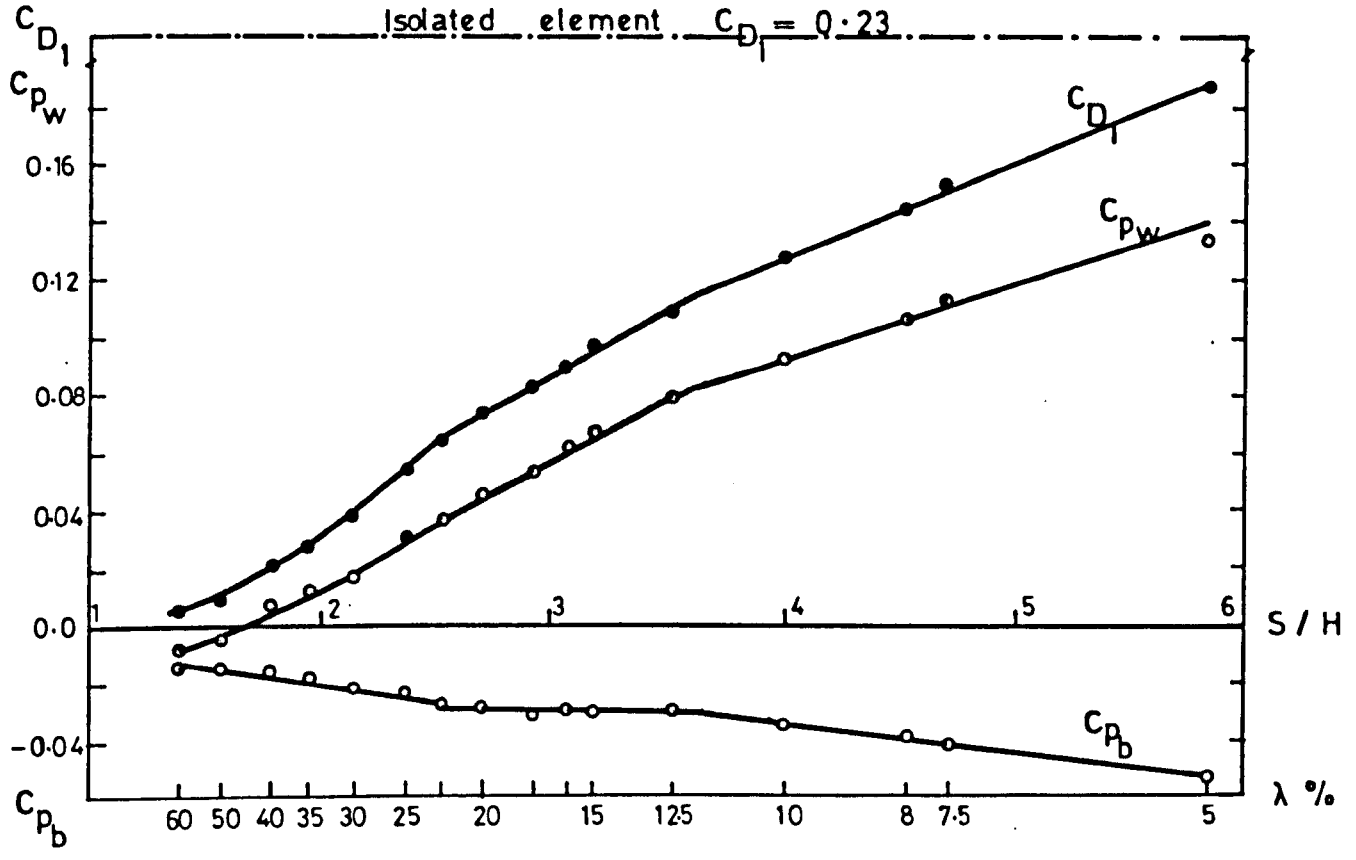

FIGURE 9.8 VARIATION OF THE WALL PRESSURES AND THE DRAG WITH SPACING - $A_f = 2.0$

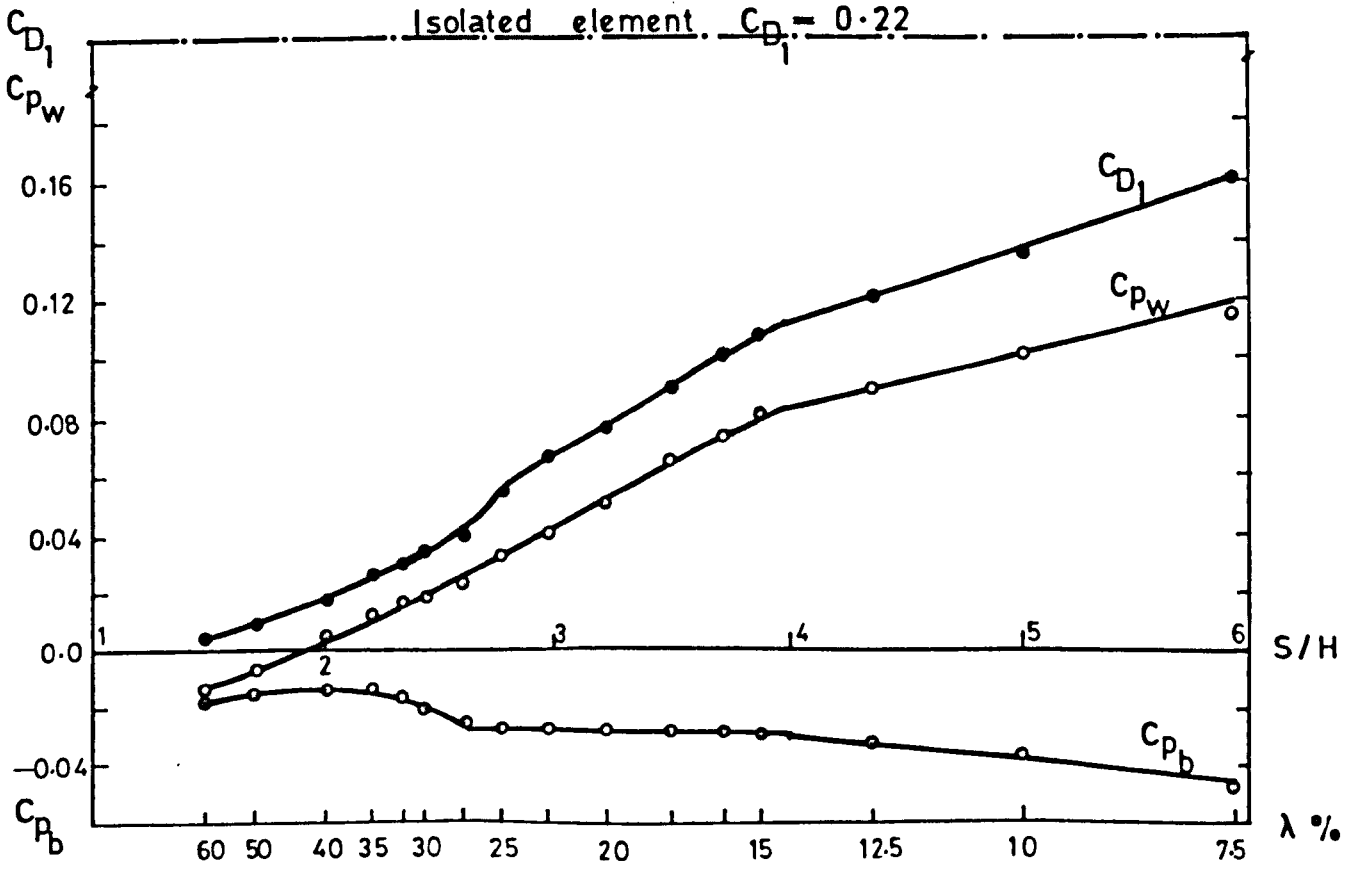

FIGURE 9.9 VARIATION OF THE WALL PRESSURES AND THE DRAG WITH SPACING - $A_f = 4.0$

2.0 in Figures 9.7 and 9.8, show a similar trend in the behaviour of the wall pressures for all the three models. The break points in Figure 9.9 appear at values of $S/H \simeq 4.0$ and 2.55 respectively which are slightly larger than comparable values for the previous model. The values of the leeward pressure coefficient, C_{p_b}, remained fairly constant in the range $4.0 > S/H > 2.55$ representing the wake interference flow regime. The variation of the drag coefficient, C_{D_1}, with S/H was also shown by a broken straight line relationship.

9.2.6 On the basis of the behaviour of the model wall pressures, C_{p_w} and C_{p_b}, with spacing, S/H, for models of varying frontal aspect ratios in Figures 9.6 to 9.9, the following observations can be made.

a) The isolated element drag shown in each Figure undergoes an immediate drop of up to 30% even at the lowest densities considered. The value of C_{D_1} is further reduced to approximately half at the first change of flow regime, while at the second change of flow regime, its value is approximately a third of the isolated model, before going to zero at 100% density.

b) The inflections in the graph of the drag and surface pressures against the element spacing, which were used to identify the flow regimes for the flow around cube shaped elements, were found to exist with small variations. These inflection points can similarly be used to identify the various flow regimes.

c) The values of element spacing, S/H, at which the change of flow regime occurs, varies with the frontal aspect ratio. The change from the isolated roughness flow regime to the wake interference flow regime was found to occur at an element spacing S/H = 3.25 in the case of the model with frontal

aspect ratio of 0.5 and it progressively increased to a value of S/H = 4.0 for the model with a frontal aspect ratio of 4.0. The corresponding values for the change from the wake interference flow to the skimming flow regime were found to vary from 2.3 to 2.55.

d) As the frontal aspect ratio increases for values greater than 1.0, the trend in the variation of base pressures changes from that found in the case of flow around cubes. In these models, the leeward pressure coefficient, C_{p_b}, increased linearly with decrease in spacing over a range representing the isolated roughness flow regime. The first inflection point in C_{p_b} appears at the start of the wake interference flow regime and the value of C_{p_b} remains fairly constant in this flow regime before it starts to gradually increase in the skimming flow regime.

9.2.7 The variation of the base pressures, C_{p_b}, with the element spacing, S/H, in the case of model of frontal aspect ratio A_f = 0.5, exhibited a trend similar to the one found to exist for corresponding variations for the cube, Figures 9.1 and 9.6. However, as the frontal aspect ratio increased, the behaviour of C_{p_b} in its variation with S/H was found to change, Figures 9.7 to 9.9. It is suggested that this change of behaviour can be explained by the position of the vortex which occupies a part of the cavity between adjacent roughness elements.

For models with large frontal aspect ratios, the flow which separates at the leading edge of the model does not reattach on the roof and the sides. Thus the base cavity vortex will be induced to form close behind the element. Due to the position of the vortex, as the spacing is progressively reduced, the position and the flow in the vortex remain effectively unchanged until such time that the

spacing is small enough for a stable vortex to occupy the whole cavity. This results in a constant value of the leeward pressure coefficient in this region, which is identified as the wake interference flow regime. Figure 9.10(a) shows the position of the vortex behind such models. The horizontal pressure distributions across the rear face of the models in such cases might be expected to show a local minimum at the centre caused by the close proximity of the base cavity vortex, Figure 9.10(b).

9.2.8 It has been shown in chapter 8 that the first change of regime from isolated roughness flow to the wake interference flow is related to the distances of upstream separation and downstream reattachment around an isolated cube. Evan (1957) carried out some surface flow visualisation tests on buildings of varying aspect ratios, and found that the downstream reattachment distance, E_d, increases as the frontal aspect ratio increases up to a value of $A_f = 10$, after which it tends to become constant. Similar flow visualisation results were reported by Soliman (1976) for various building shapes.

On the other hand the change from wake interference flow regime to the skimming flow regime was shown to coincide with the initiation of a stable vortex in the space between adjacent cubes at an element spacing $S/H = 1.4$ (chapter 8). From the previous works reported on the flow over two dimensional rectangular cut outs and grooves, Rushko (1955), Tani et al (1961) and Maul and East (1963), the vortex dimension, E_v, seems to be related to the groove height and not the groove length normal to the flow. It seems, therefore, that the change from wake interference flow to the skimming flow regime will not be significantly influenced by increasing the frontal aspect ratio.

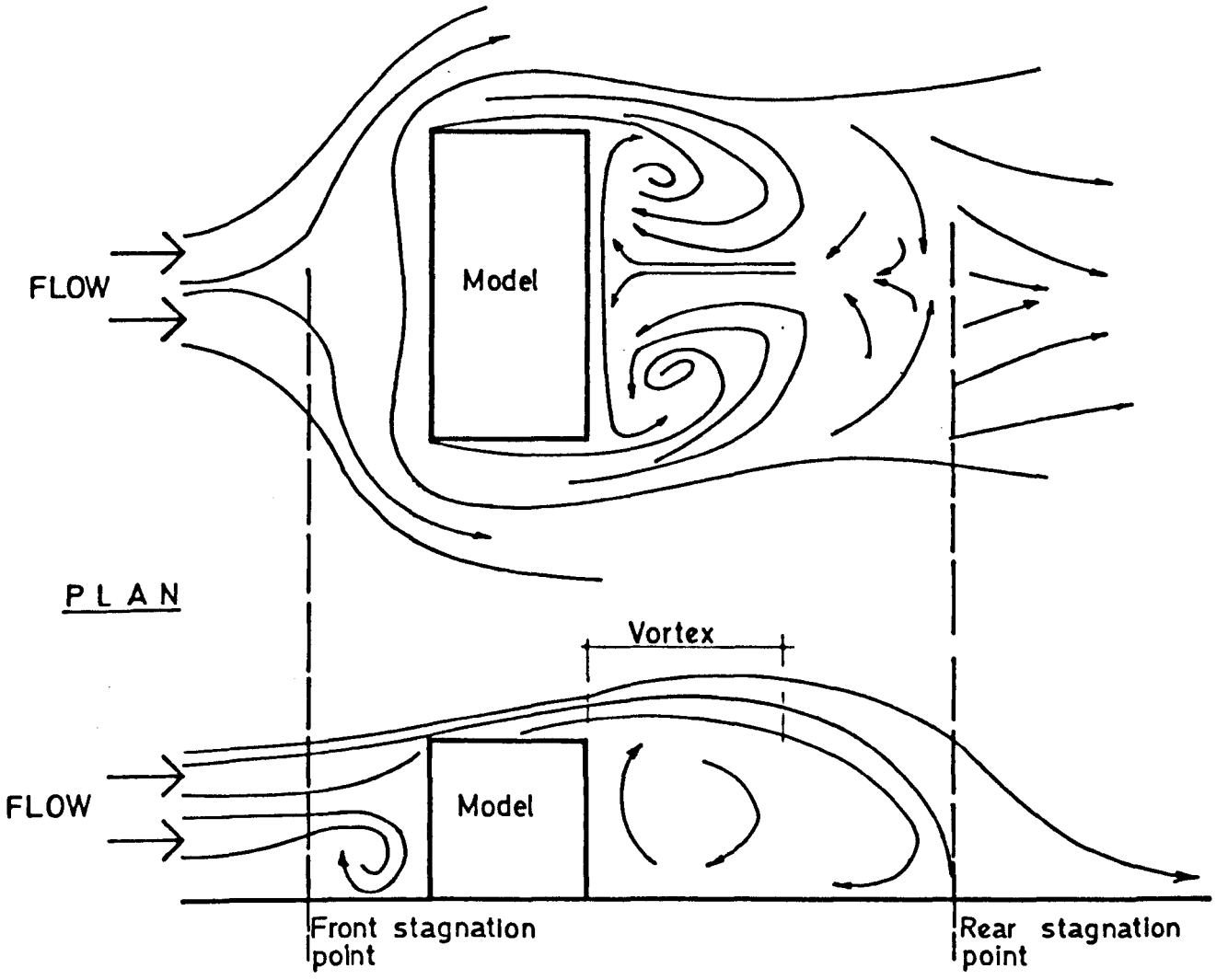

FIGURE 9.10(a) THE FLOW PATTERN AROUND A SHORT AFTERBODY MODEL

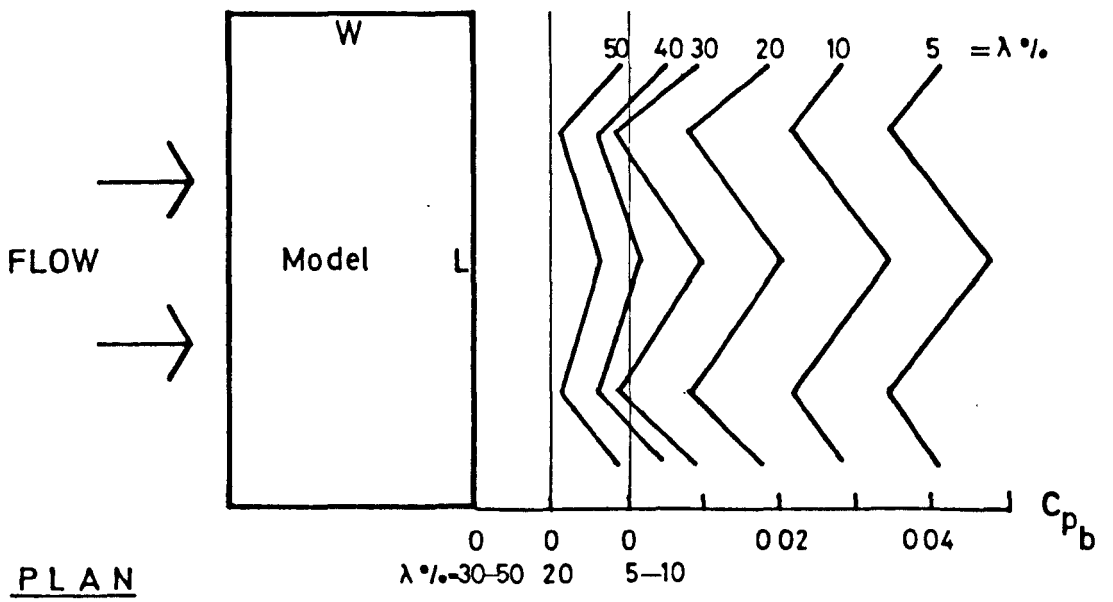

FIGURE 9.10(b) HORIZONTAL PRESSURE DISTRIBUTIONS ACROSS A SHORT AFTERBODY MODEL

9.2.9 Figure 9.11 shows the graph of frontal aspect ratio against C_{D_1} for equal spacing increments together with the spacing limits of the various flow regimes. This figure, alongwith Figures 9.6 to 9.9, shows that the element spacing, S/H, at which the isolated roughness flow regime changes to wake interference flow regime increases with the increase of frontal aspect ratio within the range of A_f considered in this investigation. As the change from isolated roughness to wake interference flow regime is directly related to the downstream reattachment distance these results seem to substantiate the findings of Evan and Soliman that the downstream reattachment distance depends on the frontal aspect ratio.

Figure 9.11 also shows that the change from wake interference flow regime to the skimming flow regime is relatively insensitive to the element spacing, compared with the first change. The small difference which exists in the value of S/H for this change is for models having a frontal aspect ratio $\leqslant 1.5$ where the flow is affected by the side flows. Conversely, the models, with the frontal aspect ratio > 1.5, behave in a manner similar to the two dimensional grooves and thus the element spacing at which this change takes place is not affected.

9.3 Pressure distributions on model roofs

9.3.1 The pressure coefficient distributions on the centre line of the roof of different models in various densities are shown in Figure 9.12 and 9.13. These pressure coefficient distributions were integrated to get the mean lift coefficient, C_{L_1}, in each case. The pressure coefficient distributions for all the models agreed well with the trend, established in chapter 8, for the cube. Over a wide range of element group densities covered for various models the maximum suction was found to occur near the windward edge. From there, the suction decreased towards the leeward edge. The magnitude of the maximum

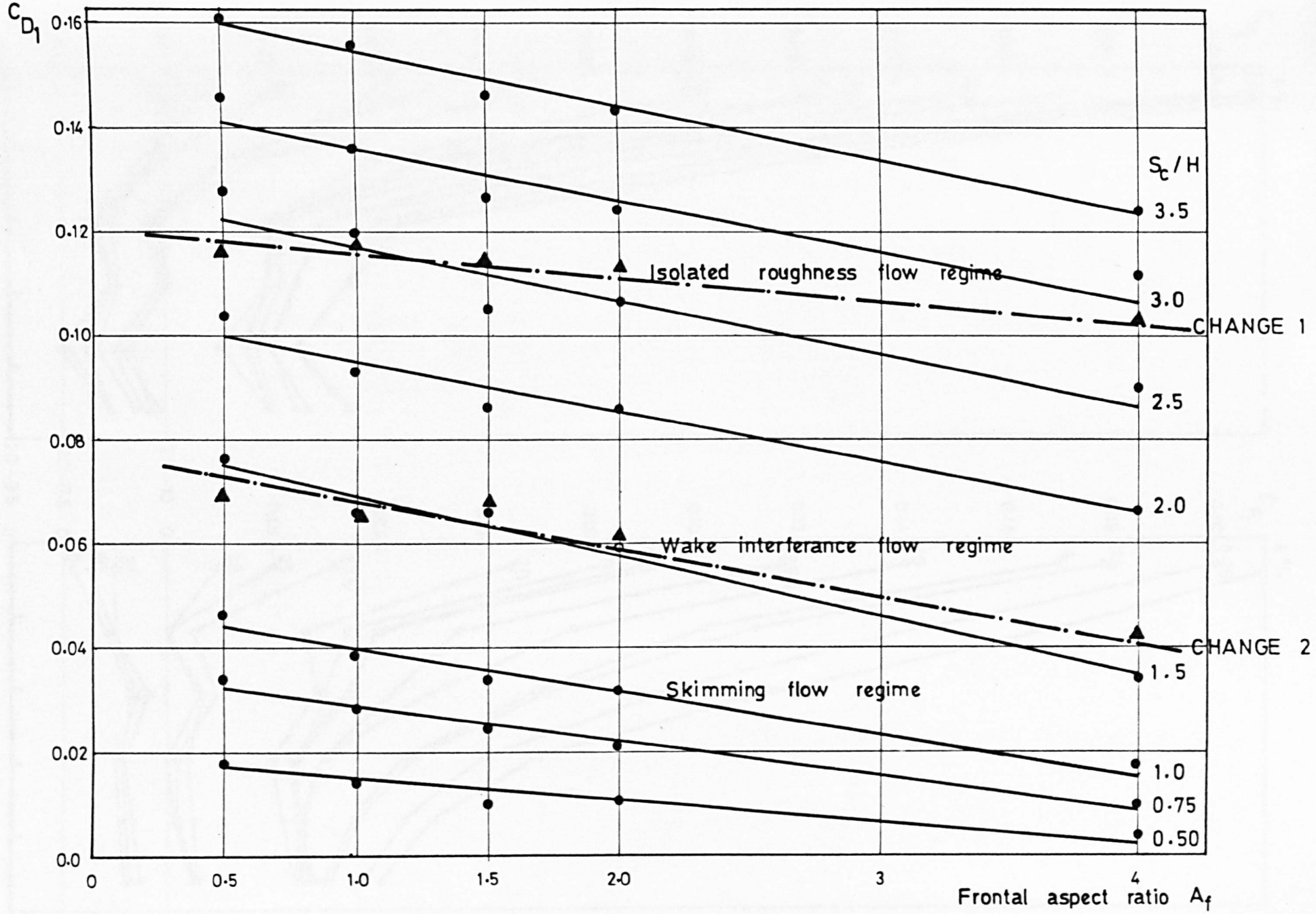

FIGURE 9.11 VARIATION OF C_{D_1} WITH FRONTAL ASPECT RATIO FOR EQUAL SPACING INCREMENTS

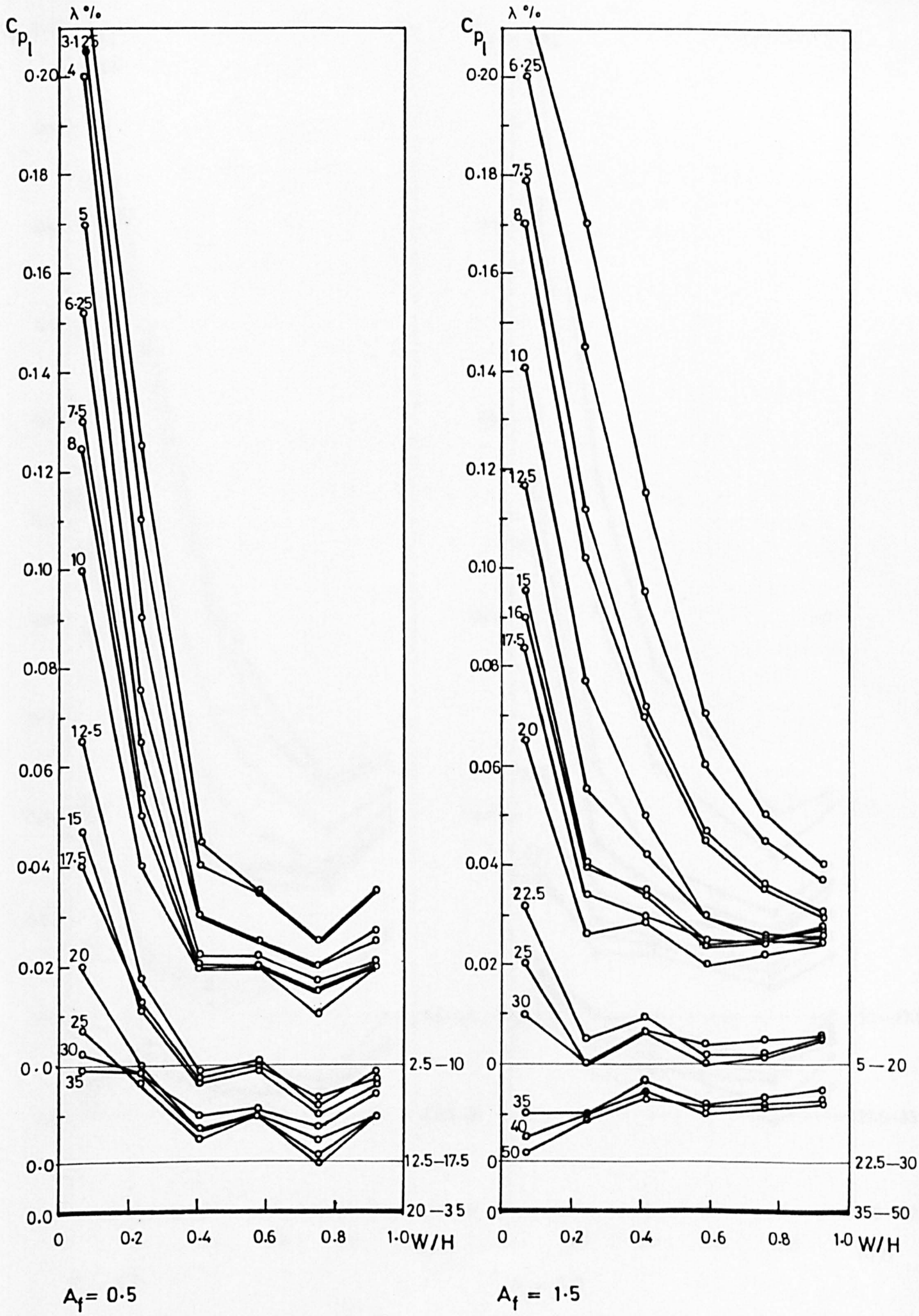

FIGURE 9.12 PRESSURE COEFFICIENT DISTRIBUTIONS ON ROOF CENTRELINE AT VARIOUS DENSITIES - A_f = 0.5 and 1.5

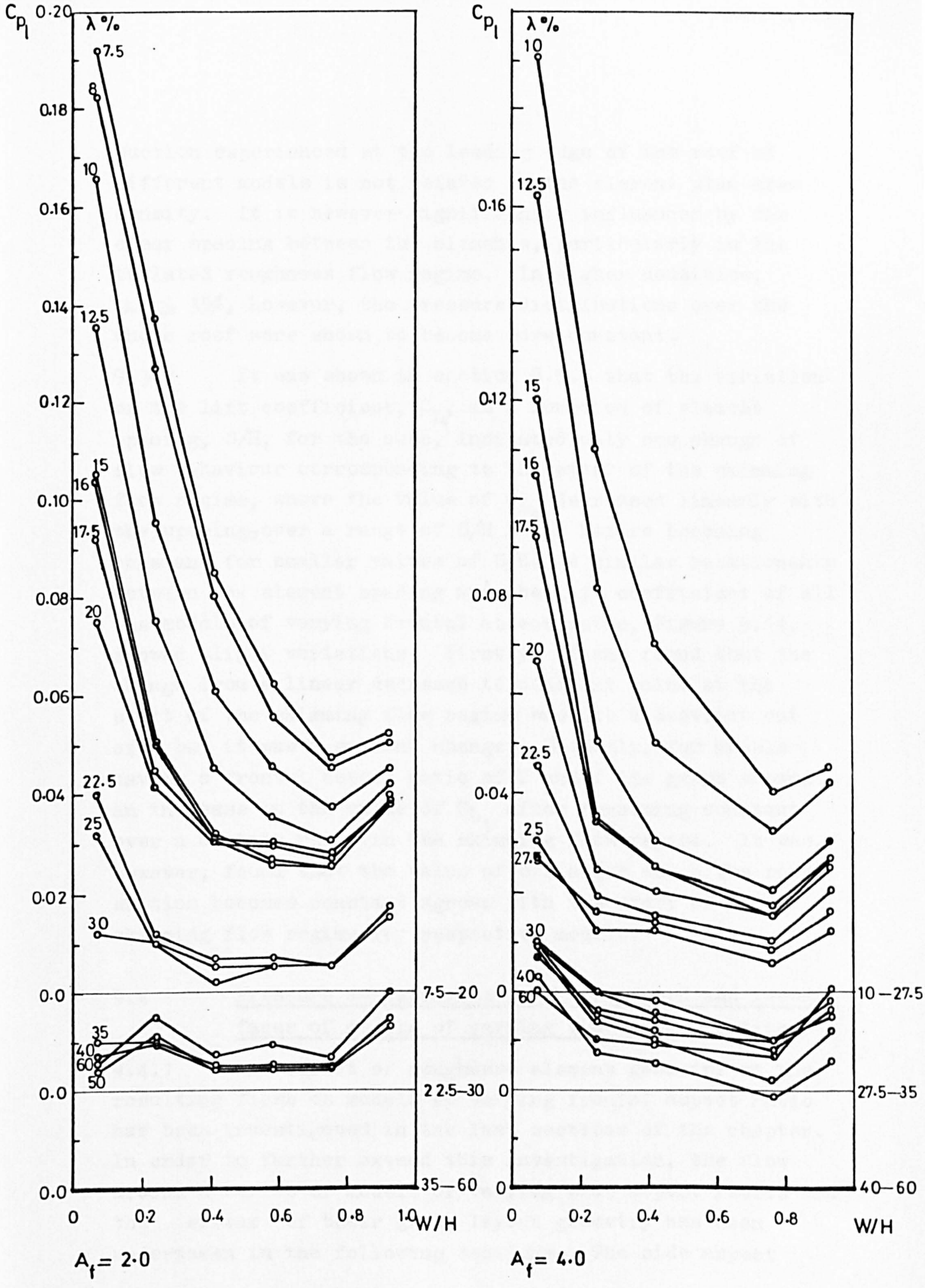

FIGURE 9.13 PRESSURE COEFFICIENT DISTRIBUTIONS ON ROOF CENTRELINE AT VARIOUS DENSITIES - A_f = 2.0 and 4.0

suction experienced at the leading edge of the roof of different models is not related to the element plan area density. It is however significantly influenced by the clear spacing between the elements, particularly in the isolated roughness flow regime. In higher densities, $\lambda_p \geq 35\%$, however, the pressure distributions over the whole roof were shown to become more constant.

9.3.2 It was shown in section 8.5.3 that the variation of the lift coefficient, C_{L_1}, as a function of element spacing, S/H, for the cube, indicated only one change of flow behaviour corresponding to the start of the skimming flow regime, where the value of C_{L_1} decreased linearly with the spacing over a range of $S/H > 2.4$ before becoming constant for smaller values of S/H. A similar relationship between the element spacing and the lift coefficient of all the models of varying frontal aspect ratio, Figure 9.14, showed slight variations. Firstly, it was found that the change from a linear decrease to constant value at the start of the skimming flow regime was not a distinct cut off, but it was a gradual change. Secondly, for models having a frontal aspect ratio of 2 and 4 the graph showed an increase in the value of C_{L_1} after remaining constant over a certain range in the skimming flow regime. It was, however, found that the value of S/H after which the roof suction becomes constant agrees with the start of the skimming flow regime for respective models.

9.4 Pressure measurements on the windward and leeward faces of models of varying side aspect ratios

9.4.1 The effect of roughness element geometry on the resulting flows on models of varying frontal aspect ratio has been investigated in the last sections of the chapter. In order to further extend this investigation, the flow around a series of models of varying side aspect ratios and the effect of their group layout geometry has been undertaken in the following sections. The side aspect

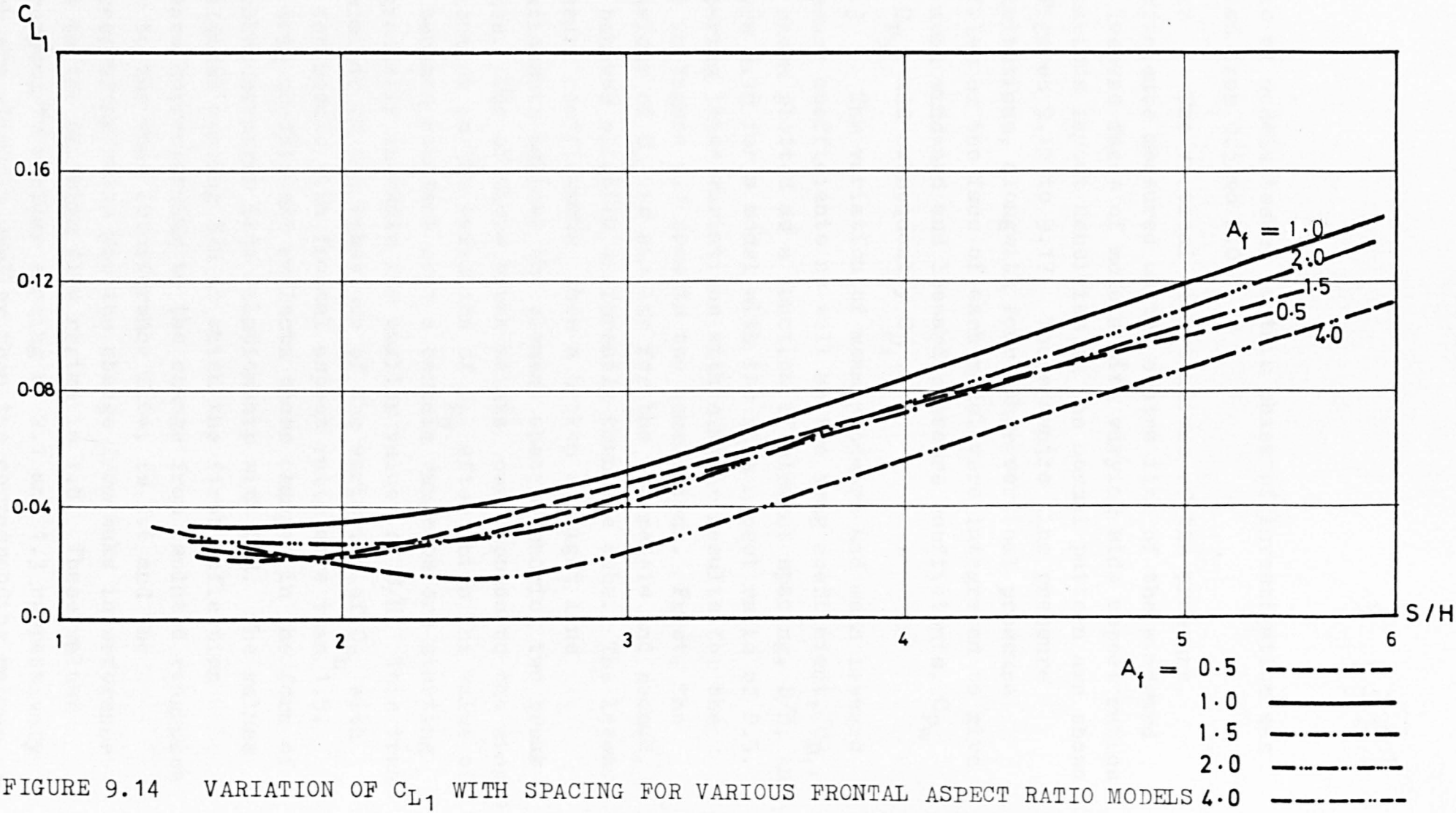

FIGURE 9.14 VARIATION OF C_{L_1} WITH SPACING FOR VARIOUS FRONTAL ASPECT RATIO MODELS

ratio of models tested in this phase of investigation was varied from 0.5 to 2.0.

9.4.2 The vertical distributions of the pressure coefficients measured on the centre line of the windward and leeward faces of models with varying side aspect ratios in various layout densities in the normal pattern are shown in Figures 9.15 to 9.17. These centre line pressure distributions, alongwith four other vertical pressure profiles on the face of each model,were integrated to give the mean windward and leeward pressure coefficients, C_{p_w} and C_{p_b}, and subsequently C_{D_1}.

9.4.3 The variation of mean windward and mean leeward pressure coefficients as well as the drag coefficient, C_{D_1}, are shown plotted as a function of element spacing, S/H, in Figure 9.18 for a model with the side aspect ratio of 0.5. Comparing these variations with similar results for the cube in Figure 9.1 prompts two conclusions. First, the behaviour of C_{p_w} is similar for the two models and second, C_{p_b} behaves slightly differently than the cube. The leeward pressure coefficients show a broken straight line relationship against the element spacing showing two break points. One of these break points corresponds to the single inflection in the variation of C_{p_w} after which the value of C_{p_b} becomes constant over a certain range before starting to gradually increase for smaller values of S/H. This trend is similar to the behaviour of the variation of C_{p_b} with S/H for models with frontal aspect ratio more than 1.5. The drag coefficient reflects these changes in the form of a broken straight line relationship with S/H. The values of element spacing S/H at which the first inflection appears corresponding to the change from isolated roughness flow to the wake interference flow, is 2.6 and the corresponding value for the change from wake interference flow to the skimming flow regime is 1.8. These values correspond to a clear spacing of 2.1 and 1.3 respectively which are slightly smaller than the corresponding values of

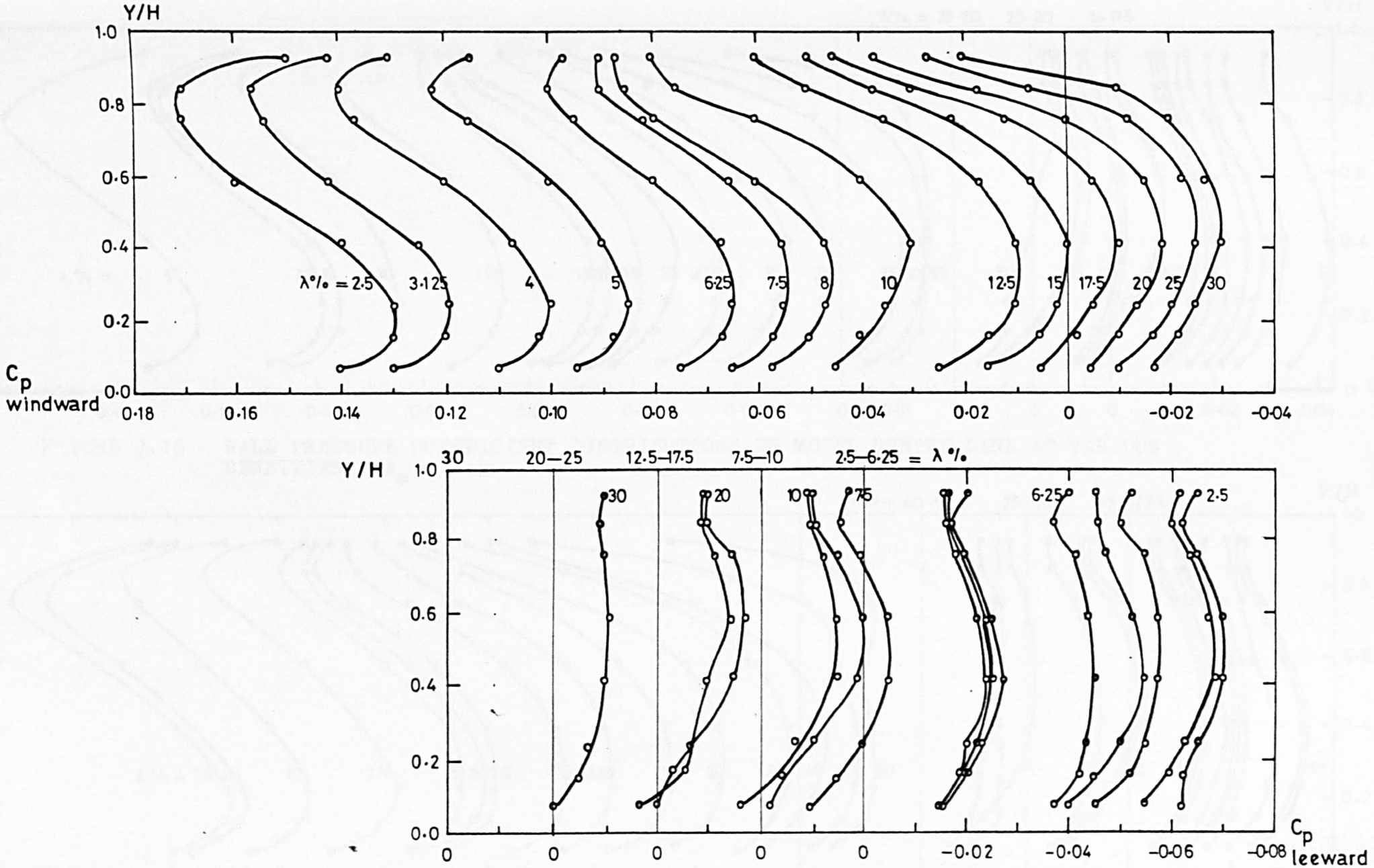

FIGURE 9.15 WALL PRESSURE COEFFICIENT DISTRIBUTIONS ON MODEL CENTRELINE AT VARIOUS DENSITIES - $A_s = 0.5$

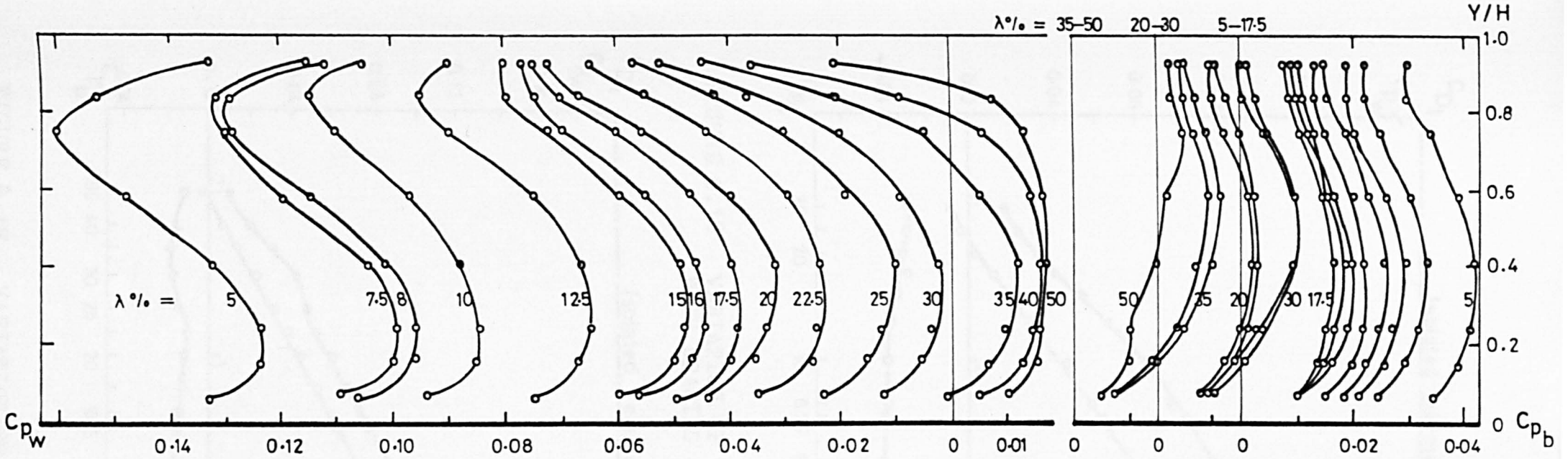

FIGURE 9.16 WALL PRESSURE COEFFICIENT DISTRIBUTIONS ON MODEL CENTRE LINE AT VARIOUS DENSITIES - A_s = 1.5

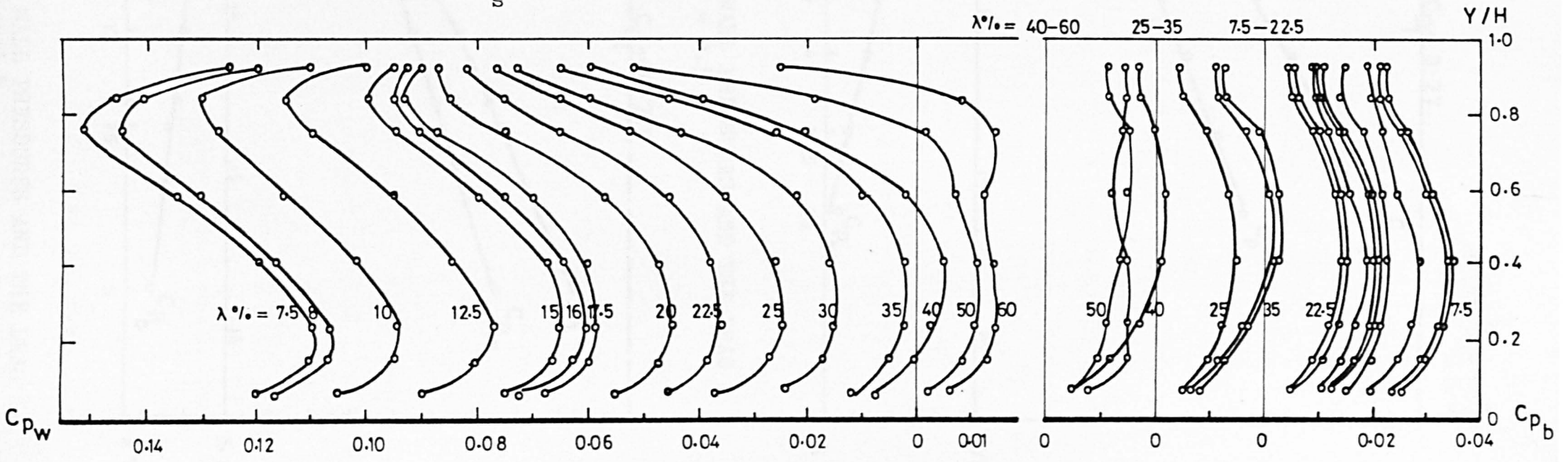

FIGURE 9.17 WALL PRESSURE COEFFICIENT DISTRIBUTIONS ON MODEL CENTRE LINE AT VARIOUS DENSITIES - A_s = 2.0

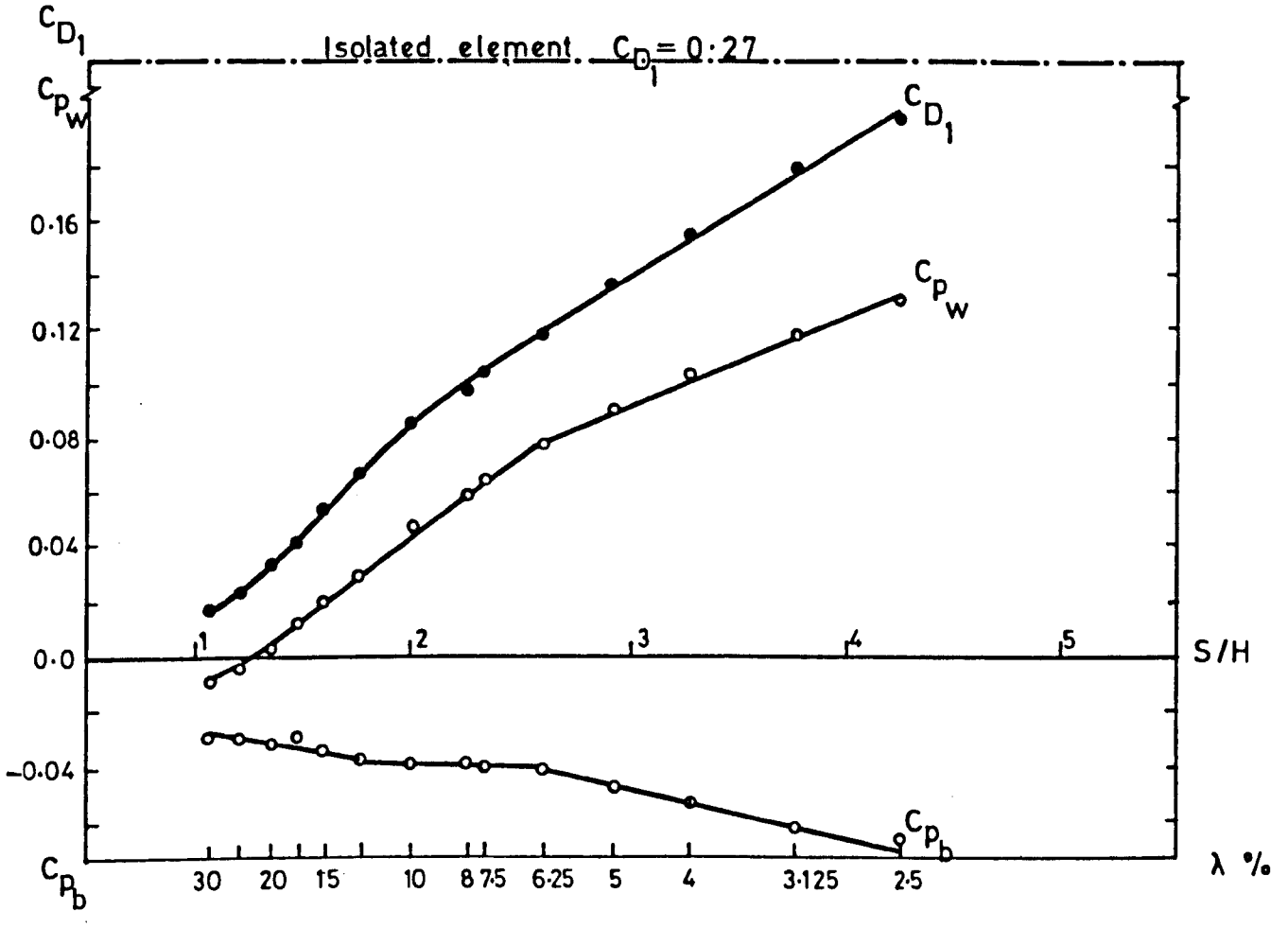

FIGURE 9.18 VARIATION OF THE WALL PRESSURES AND THE DRAG WITH SPACING - $A_s = 0.5$

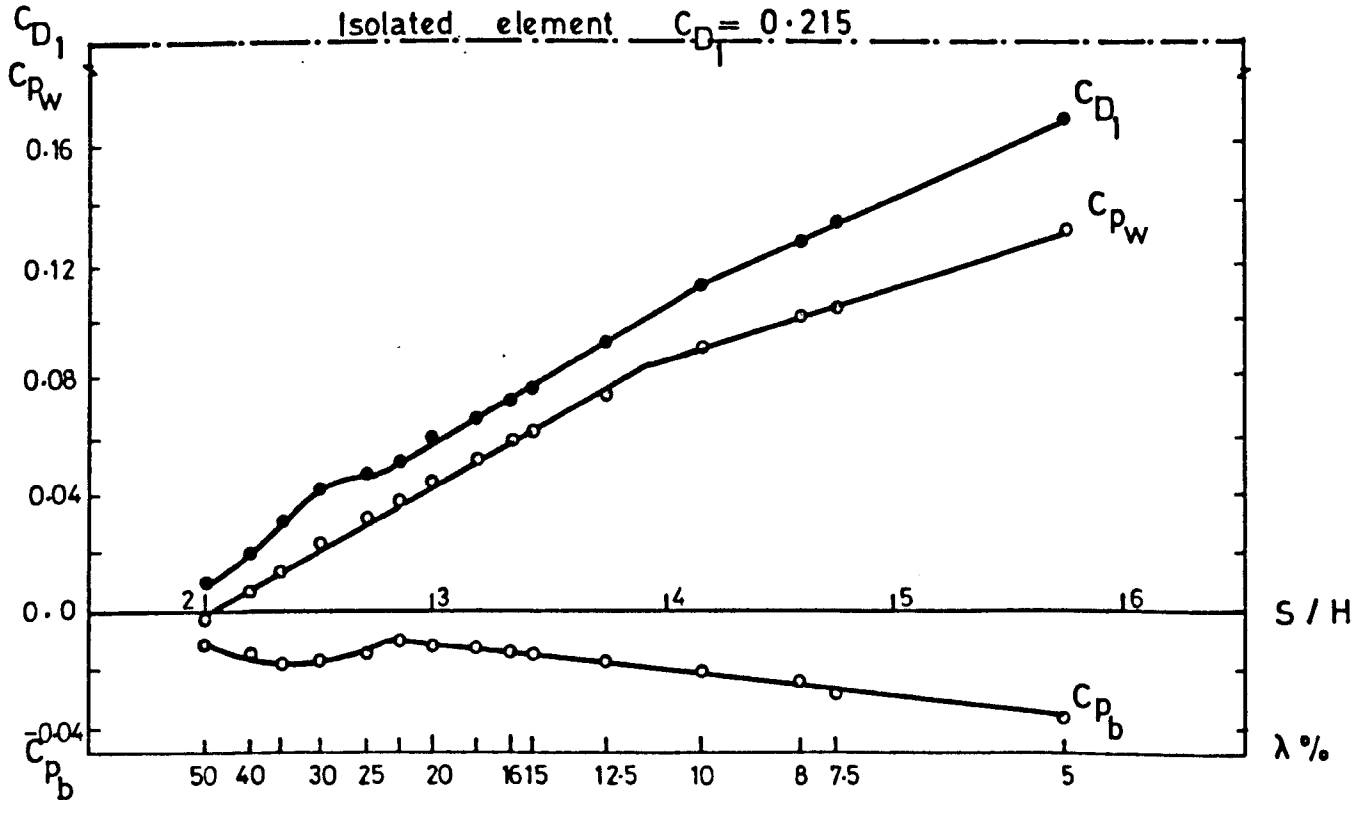

FIGURE 9.19 VARIATION OF THE WALL PRESSURES AND THE DRAG WITH SPACING - $A_s = 1.5$

2.4 and 1.4 in the case of the cube. The comparable values of densities, λ_p, at which these changes take place are 6.25% and 12.5%.

9.4.4 Comparing the variations of C_{p_w}, C_{p_b} and C_{D_1} with S/H, for the model having a side aspect ratio of 1.5 in Figure 9.19 with similar variations for the cube in Figure 9.1 indicates a similar pattern of behaviour to exist for both the models giving the break points at an element spacing of S/H = 4.0, i.e. the clear spacing of $S_c/H = 2.5$ which is only slightly different than 2.4 found in the case of the cube when the isolated roughness flow changed to wake interference flow regime. The decrease in the value of C_{p_b} before beginning to increase gradually corresponding to the break point between the wake interference flow regime and the skimming flow regime was however found to occur at the same clear spacing, S_c/H, of 1.4. The values of densities, λ_p, at which these changes occur are 11.0% and 22.5% respectively.

9.4.5 The variation of model wall pressures C_{p_w}, C_{p_b} as well as the drag coefficient C_{D_1} with the element spacing S/H for the model of side aspect ratio = 2, shown in Figure 9.20, again exhibits a broadly similar trend to those found in Figure 9.1 and 9.19 for cube and the model with the side aspect ratio = 1.5 respectively. Figure 9.20 indicates that the first inflection point appears at a slightly higher value of $S_c/H = 2.6$, compared to 2.4 in Figure 9.1 and 2.5 in Figure 9.19 while the second change from wake interference flow regime to the skimming flow regime occurs at the same value of $S_c/H = 1.4$.

9.4.6 On the basis of the behaviour of model wall pressures C_{p_w} and C_{p_b} and the drag coefficient C_{D_1} with the element spacing for models of varying side aspect ratio in Figures 9.18 to 9.20, the following observations can be made

a) The isolated element drag shown in each figure undergoes an immediate drop in its value, when surrounded by an array of similarly sized elements. This reduction is identical in magnitude to that found in the case of models of varying frontal aspect ratios in section 9.2.6.

b) The inflection points in the graphs of model wall pressures against the element spacing, which were used to identify the flow regimes for flow around cube shaped elements, were found to exist with slight differences.

c) The value of the element clear spacing S_c/H at which the isolated roughness flow regime changes to wake interference flow regime increases from 2.1 in the case of model with $A_s = 0.5$ to 2.6 in the case of model with $A_s = 2.0$. Conversely the value of S_c/H at which the second change of flow regime occurs remain approximately constant at 1.4.

d) The behaviour of the variation of C_{p_b} with S/H, for the model with the side aspect ratio of 0.5, is different from that found in the case of the cube. Its trend is broadly similar to the trend exhibited by models of large frontal aspect ratios.

9.4.7 The behaviour of C_{p_b} with S/H for the model with the side aspect ratio of 0.5 showed a behaviour similar to the one shown by models of larger frontal aspect ratio. This is thought to be due to similar proportions of the model dimensions, which would have the same flow phenomenon in the base cavity as discussed in section 9.2.7. On the other hand, the variation of C_{p_b} with S/H for models having side aspect ratios of 1.5 and 2.0 as well as the model with the frontal aspect ratio = 0.5 is similar to the behaviour of C_{p_b} in the case of the cube. This is explained as follows.

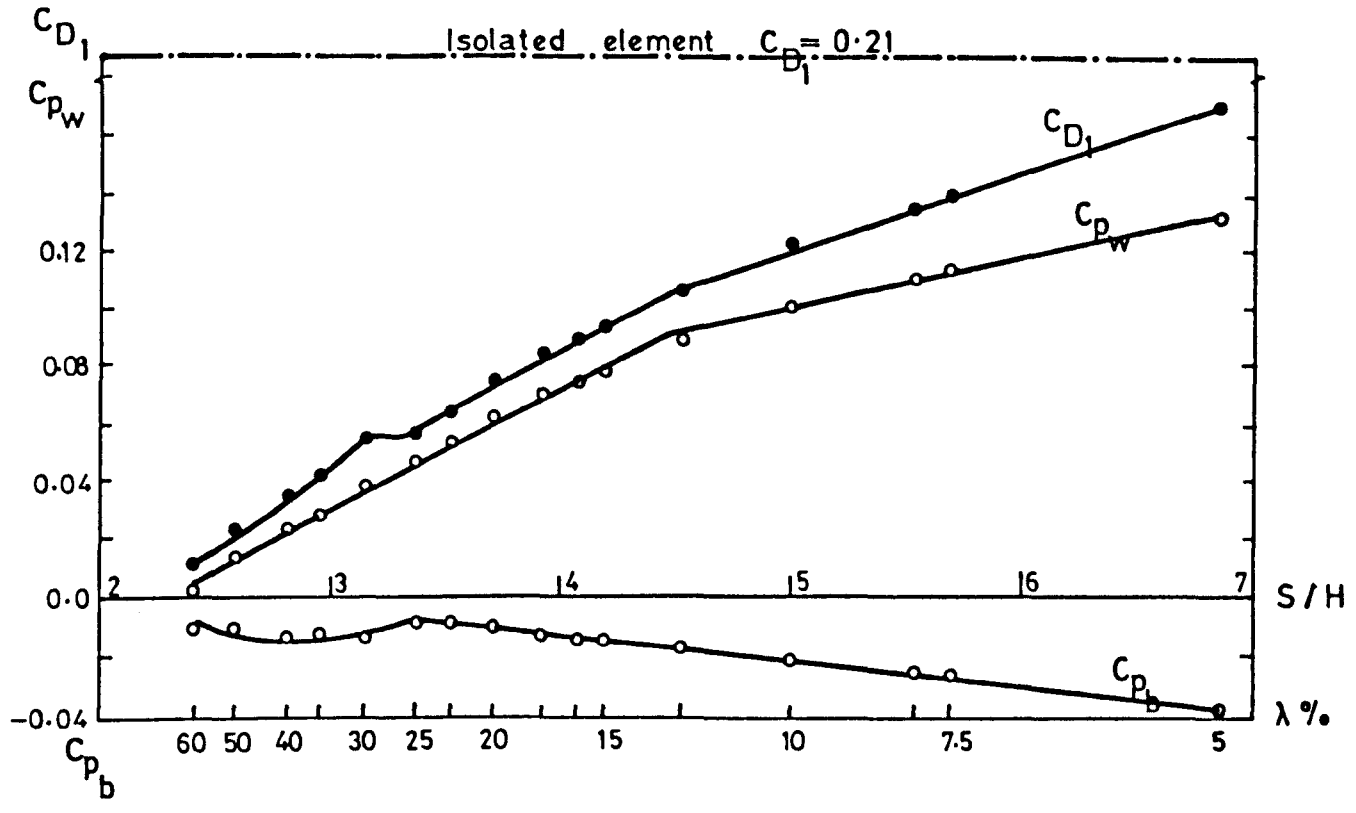

FIGURE 9.20 VARIATION OF THE WALL PRESSURES AND THE DRAG WITH SPACING - $A_s = 2.0$

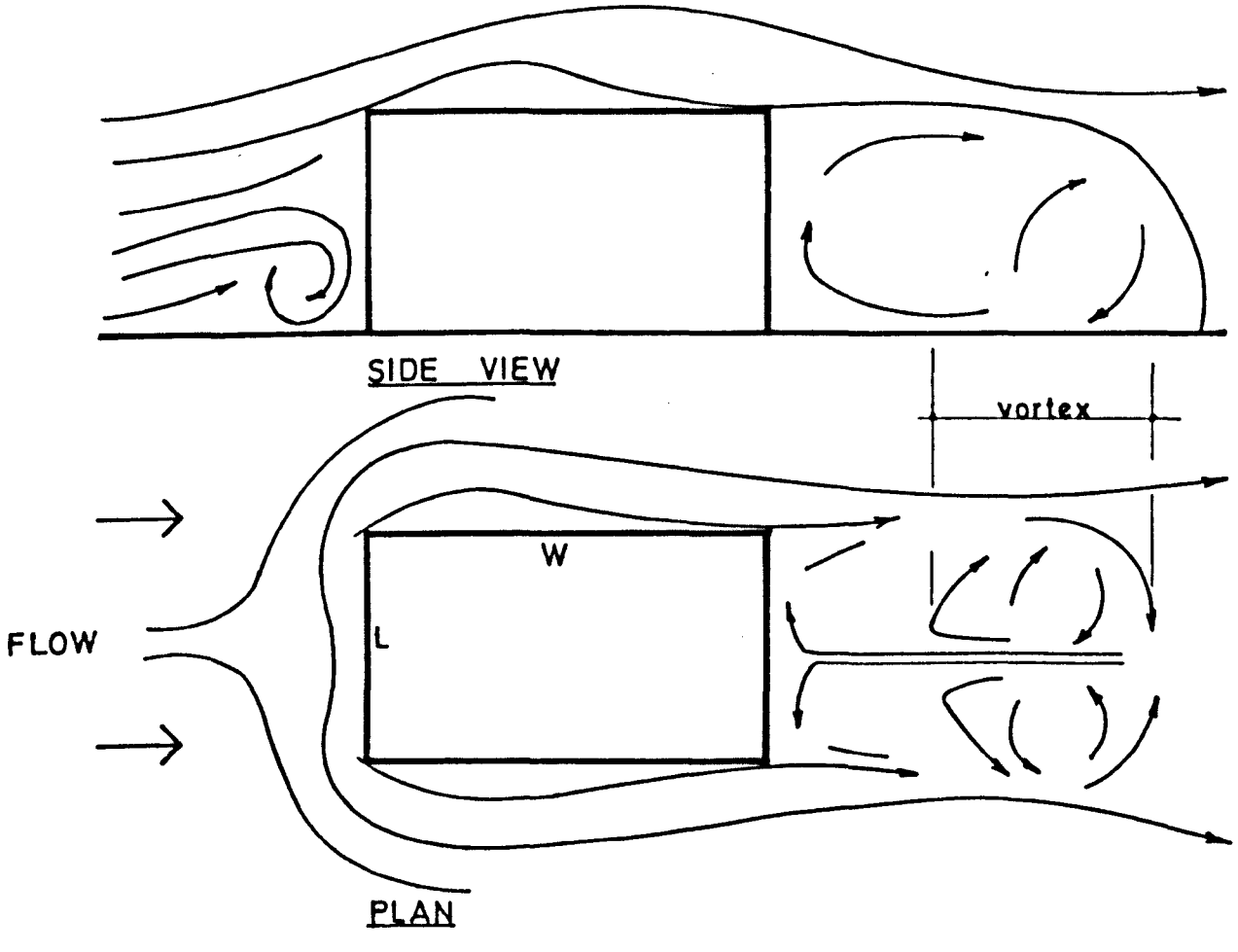

FIGURE 9.21(a) THE FLOW PATTERN AROUND A LONG AFTERBODY MODEL - $A_s = 1.5$

In these cases it is suggested that by virtue of their long afterbody shape, the flow reattaches on the roof and the sides of the models. Due to this flow reattachment the shear layers, which feed the base cavity vortex, are deflected outwards and thus the core of the vortex forms further downstream than if side flow reattachment had not occurred. The downstream limit of this vortex position will then be defined by the position of the next roughness element in the array. This is shown schematically in Figure 9.21(a). In such a situation, when the spacing between the elements is decreased progressively, the vortex is pushed nearer and nearer to the rear face of the model, causing the flow pattern and thus the base pressures to vary progressively. This hypothesis would then explain the experimental observation that for all such models the leeward pressures vary as the spacing varies, even in the wake interference flow regime. As the position of the base cavity vortex behind the model is far away from it, the horizontal pressure distributions across the rear face of the models should be invariant across their length. Figure 9.21(b) shows reasonably uniform horizontal profiles which tend to substantiate this explanation of the flow phenomenon for long afterbody model shapes. This figure may be compared with the corresponding horizontal pressure profiles shown in Figure 9.10(b) for the case of short afterbody model shapes.

9.4.8 Figure 9.22 shows the variation of drag coefficient with the side aspect ratio for equal spacing increments, alongwith the spacing limits of various flow regimes. The figure shows that the element spacing at which the flow regime changes from the isolated roughness flow to the wake interference flow is a function of the side aspect ratio more so for short afterbody models than for longer ones, in which case the side length is sufficient for the flow to have reattached on the roof and the side. Conversely, the change from the wake interference flow to the skimming flow regime,

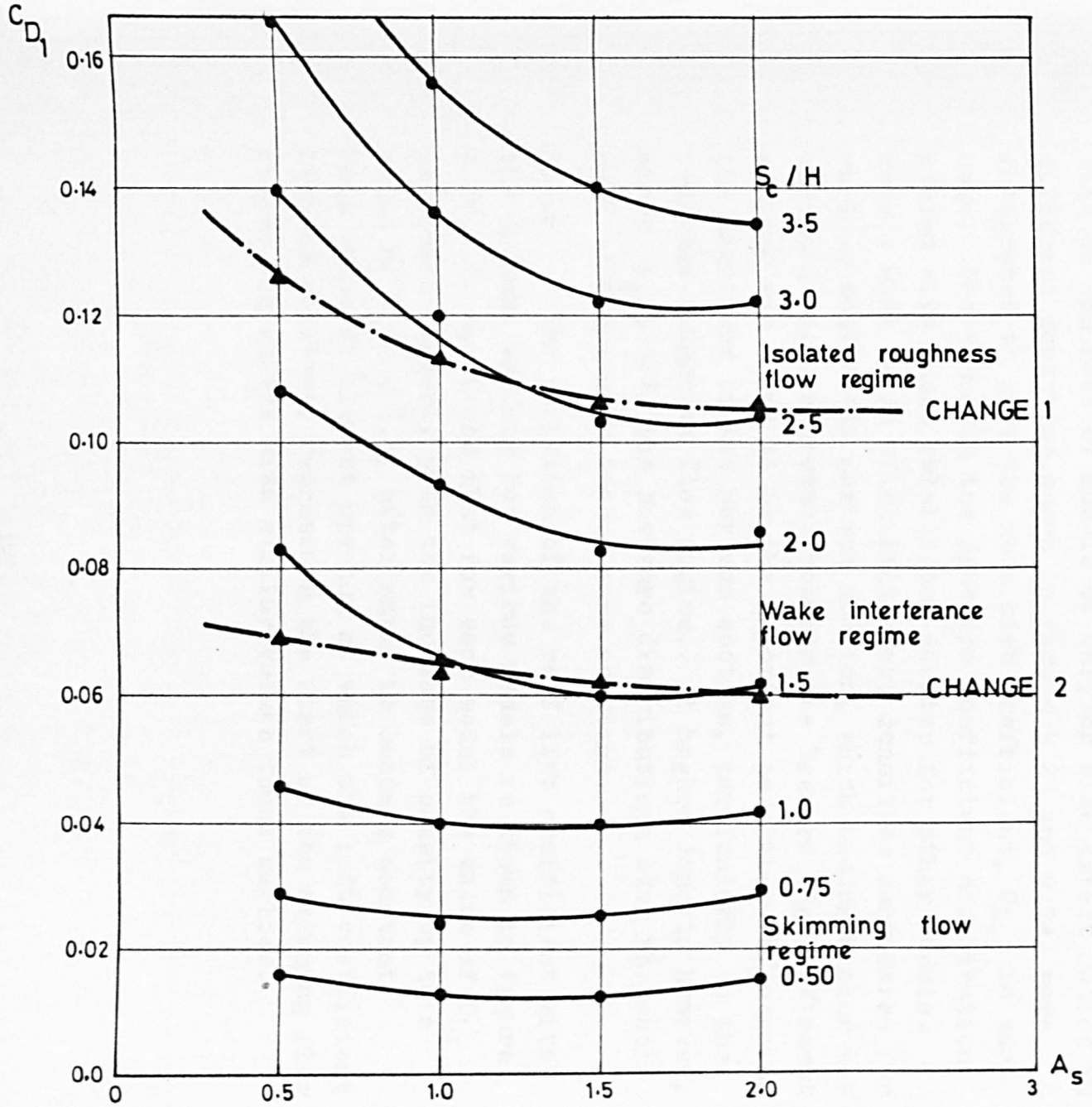

FIGURE 9.22 VARIATION OF C_{D_1} WITH SIDE ASPECT RATIO FOR EQUAL SPACING INCREMENTS

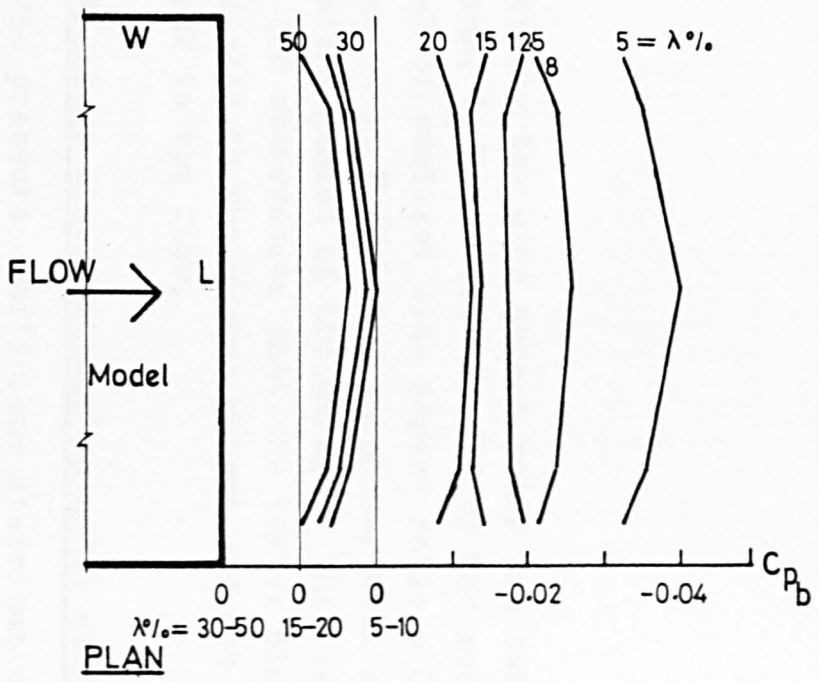

FIGURE 9.21(b) HORIZONTAL PRESSURE DISTRIBUTIONS ACROSS A LONG AFTERBODY MODEL - A_s = 1.5

is unaffected by the side aspect ratio and takes place at a clear spacing, S_c/H, of 1.4 in most of the models. However, in one model of smallest side aspect ratio = 0.5, this change occurred at $S_c/H = 1.3$ which may well have been due to slight misalignment of the arrays. This lends further support to the observation that the vortex dimension is directly related to the groove height and not the groove length normal to the flow.

9.5 Pressure distributions on model roofs

9.5.1 The pressure coefficient distributions on the centre line of the roof of models of varying side aspect ratios in different densities, shown in Figure 9.23 and 9.24, were integrated to give the mean lift coefficient, C_{L_1}, in each case. The trend in the pressure coefficient distributions agreed with those established earlier for other models. Over a wide range of element group densities considered for various models the maximum suction, which occurred near the windward edge, decreased towards the leeward edge. Element spacing was found to be the important parameter influencing the magnitude of the maximum suction, particularly in the isolated roughness flow regime. At higher density however, where $\lambda_p \geq 35\%$, the pressure distributions over the whole roof were shown to become more constant.

9.5.2 The variation of the roof lift coefficient with the element spacing for various models is shown in Figure 9.25. It was found that for each model the value of C_{L_1} decreases linearly with the increase of density up to a value of $S_c/H \simeq 1.4$, after which it becomes constant. This value of element spacing at which the lift coefficient becomes constant, represents the start of the skimming flow regime and agrees with similar values found earlier.

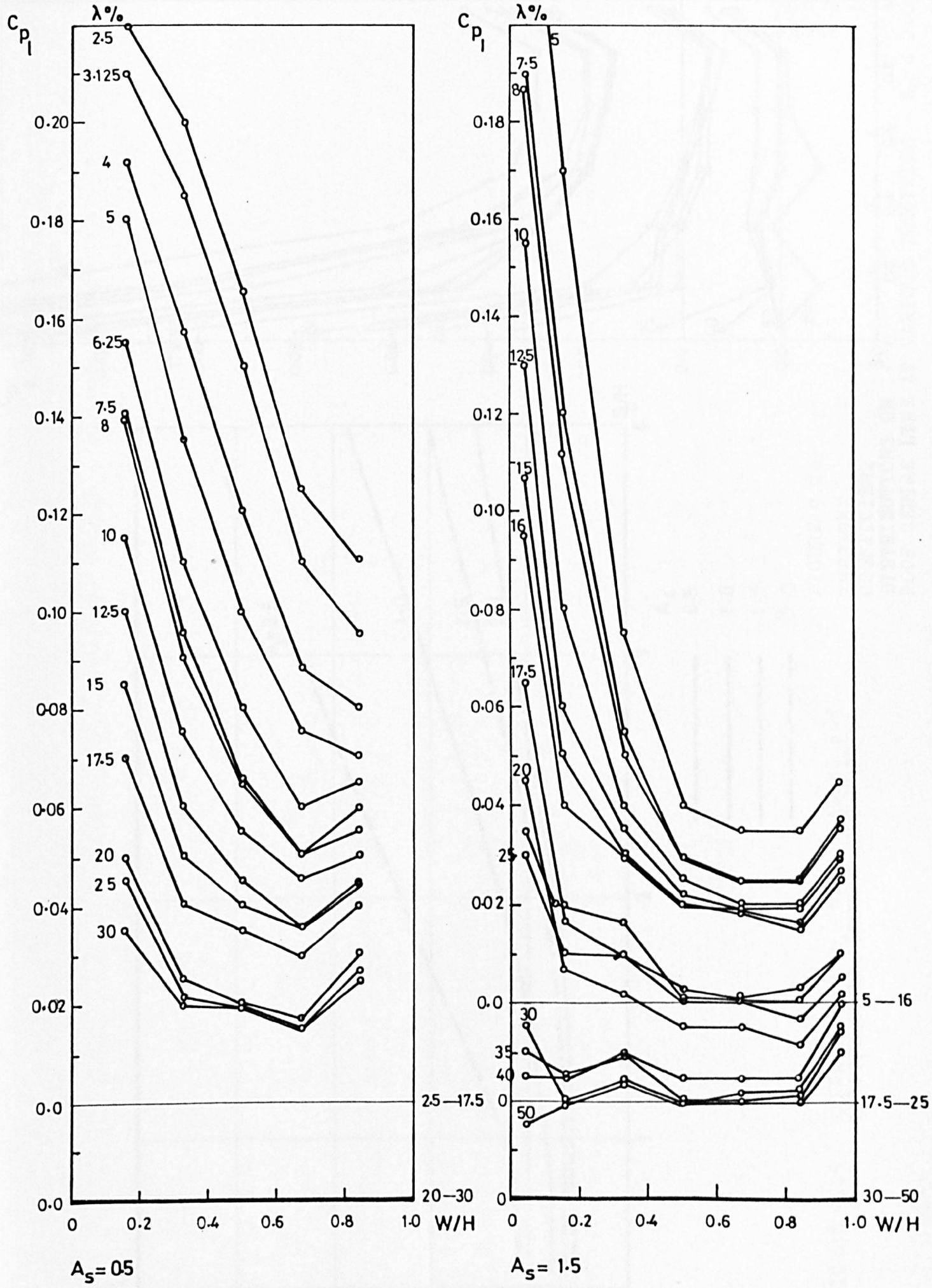

FIGURE 9.23 PRESSURE COEFFICIENT DISTRIBUTIONS ON ROOF CENTRE LINE AT VARIOUS DENSITIES - A_s = 0.5 and 1.5.

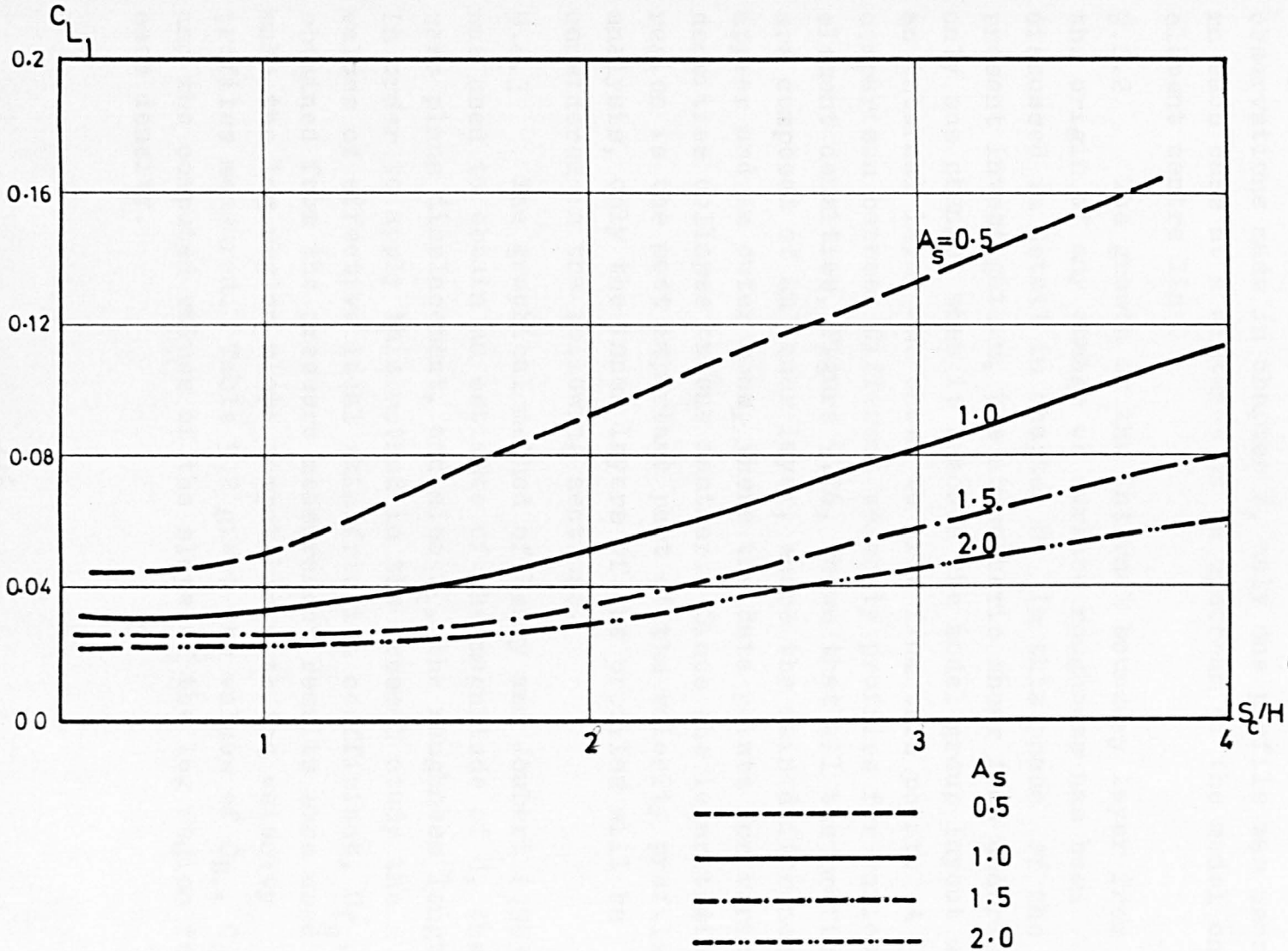

FIGURE 9.25 VARIATION OF C_{L_1} WITH SPACING FOR VARIOUS SIDE ASPECT RATIO MODELS

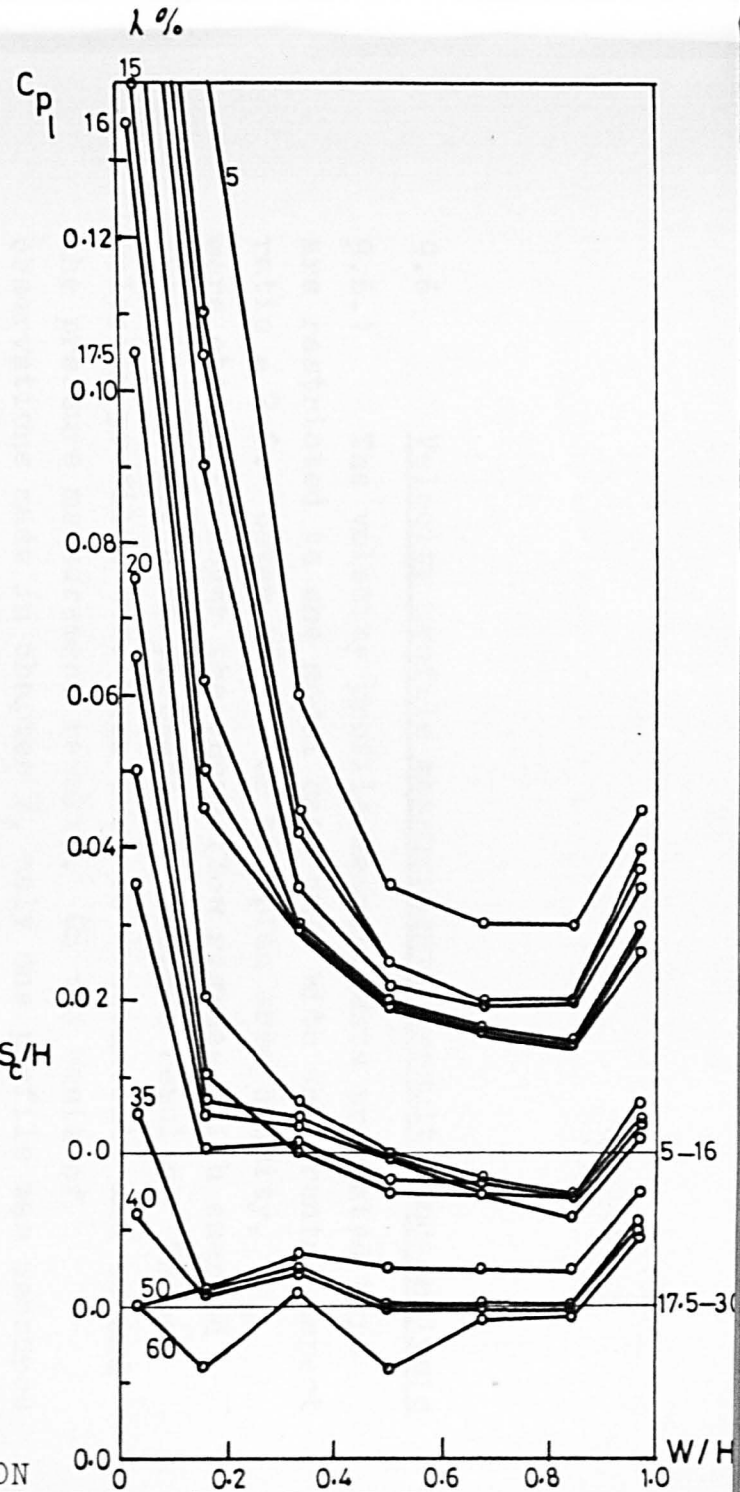

FIGURE 9.24 PRESSURE COEFFICIENT DISTRIBUTIONS ON ROOF CENTRE LINE AT VARIOUS DENSITIES – A_S = 2.0

9.6 Velocity profile measurements: results and analysis

9.6.1 The velocity profile measurements presented here are restricted to one model case only with the frontal aspect ratio = 2.0. Seven values of the plan area density, λ_p, were chosen to cover the three flow regimes which emerged from the analysis of pressure measurement results. These velocity profiles were then used to substantiate and extend the pressure measurement results. On the basis of observations made in chapter 8, only one profile was measured in each case at a distance of 1H upstream of the model on element centre line.

9.6.2 The growth of the internal boundary layer from the origin of any change of surface roughness has been discussed in detail in chapter 8. In this phase of the present investigation, the atmospheric shear flow underwent only one change, when it reached the model group layout and an internal layer was shown to grow from this point. A comparison between different velocity profiles for various element densities, Figure 9.26, shows that all the profiles are composed of an inner layer, where the main differences appear and an outer zone, where the data points for various densities collapse on one another. Since the logarithmic region is the most important part of the velocity profile analysis, only the inner layers of the profiles will be considered in the following sections.

9.6.3 The graphical method of Perry and Joubert (1963) was used to obtain an estimate of the magnitude of d, the zero plane displacement, and also Z_o, the roughness length. In order to apply this method in the present study the values of effective local skin friction coefficient, C_{f_e}, obtained from the pressure measurement results were used to make the log region slope compatable with the velocity profiles measured. Table 9.2 gives the values of C_{D_1}, C_{f_e} and the computed values of the slope of the log region for each density.

Table 9.2 Velocity profile parameters obtained from the pressure measurement results

λ_p %	C_{D_1}	C_{f_e}	Slope of the log region $5.75\sqrt{C_{f_e}/2}$
5.0	0.189	0.0095	0.395
10.0	0.125	0.0125	0.455
12.5	0.110	0.0138	0.477
16.0	0.090	0.0144	0.488
22.5	0.059	0.0133	0.468
30.0	0.037	0.0111	0.428
40.0	0.023	0.0092	0.390

9.6.4 The graphical method of analysis of the velocity profiles, measured over the range of element densities, is shown in Figures 9.27 to 9.33. The figures also show the thickness of the internal layer, δ_i, in each case. The point, at which the inner layer merges with the outer layer, was identified more precisely by the power law, log-log plot of the velocity profiles in each density, in a manner similar to that described in chapter 8. Two more flow parameters, the error in origin, ε, and the equivalent sand grain roughness, k_s, were obtained from the relationships $H = d + \varepsilon$ and $k_s = 30\ Z_o$, discussed in chapter 4. These parameters are given in Table 9.3

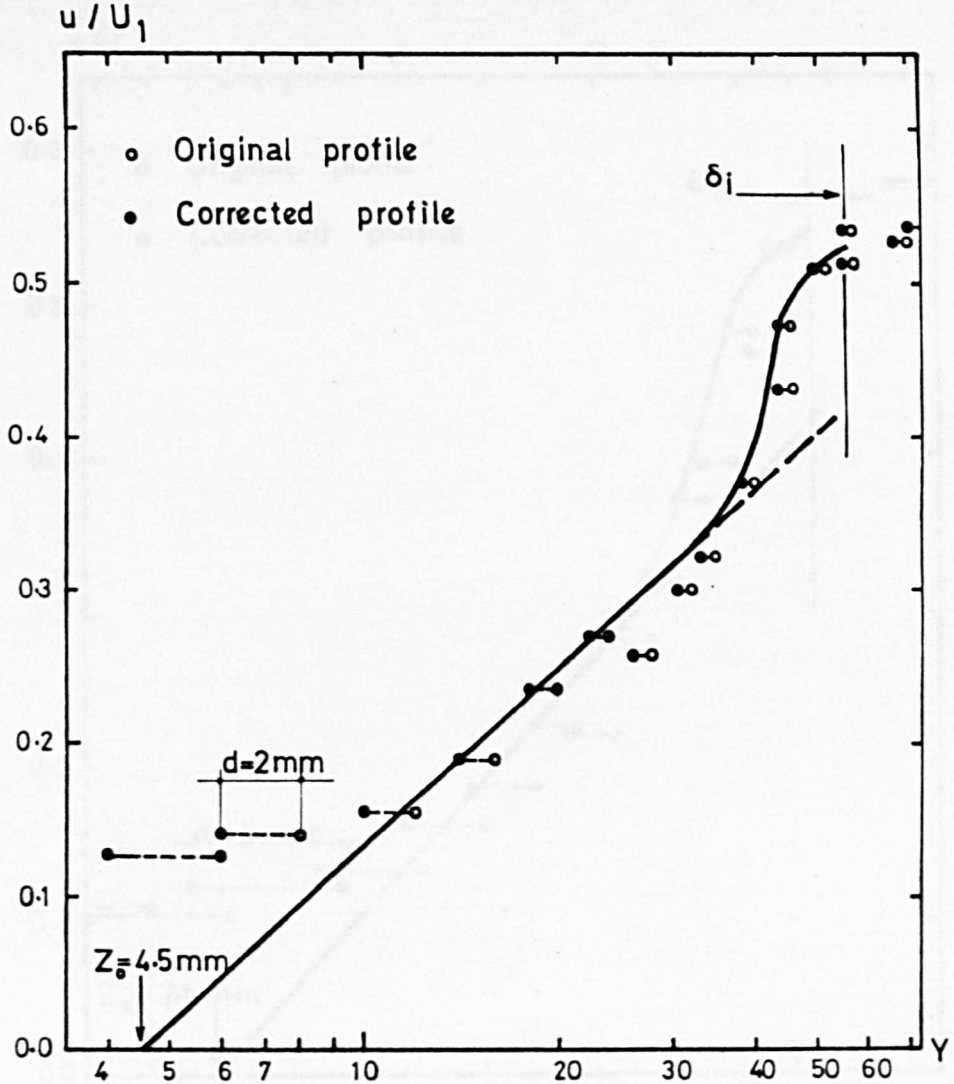

FIGURE 9.27 THE GRAPHICAL METHOD OF DETERMINING THE ZERO PLANE DISPLACEMENT (λ = 5%)

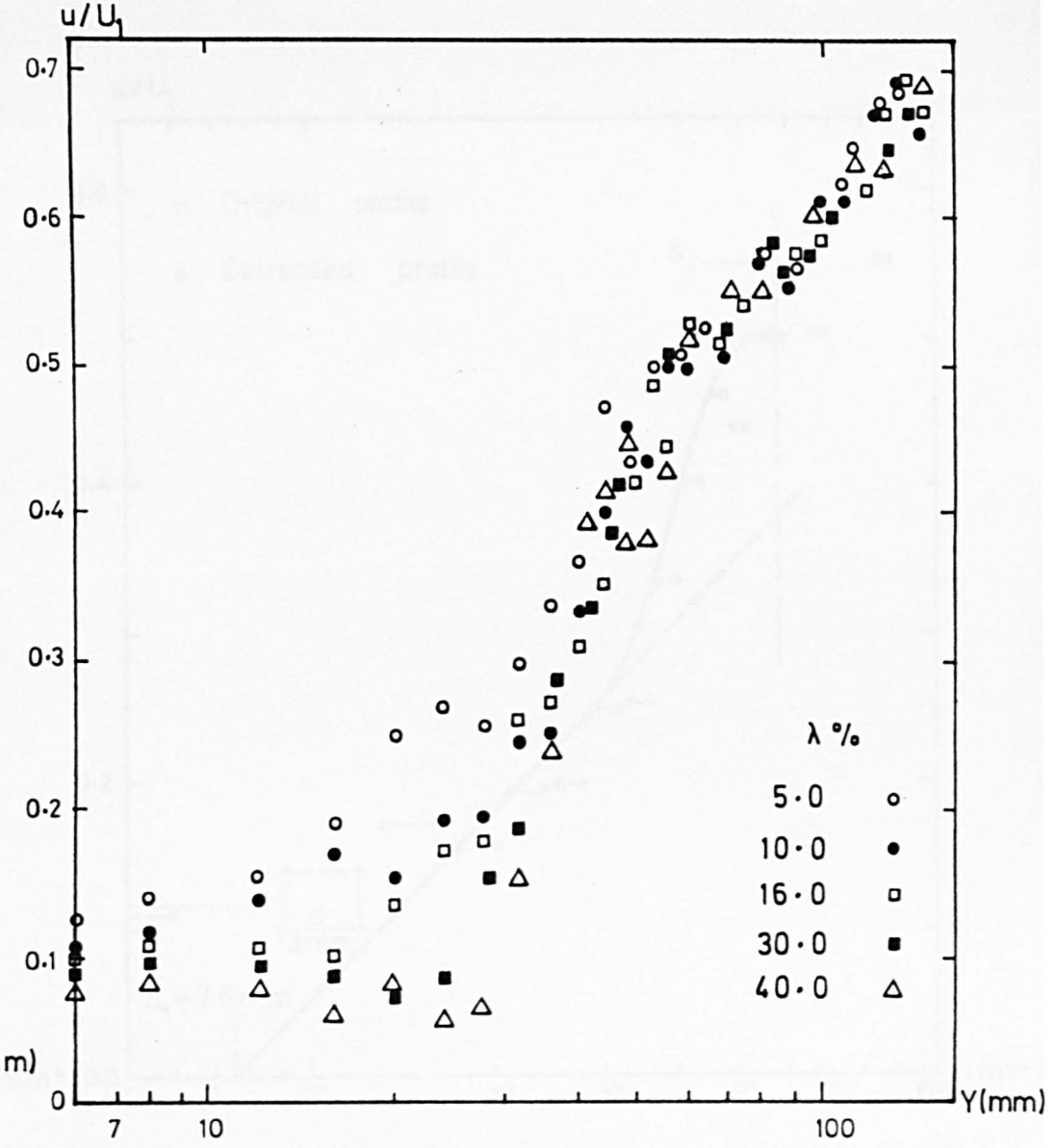

FIGURE 9.26 COMPARISON BETWEEN DIFFERENT PROFILES SHOWING THE EFFECT OF CHANGE OF SURFACE ROUGHNESS

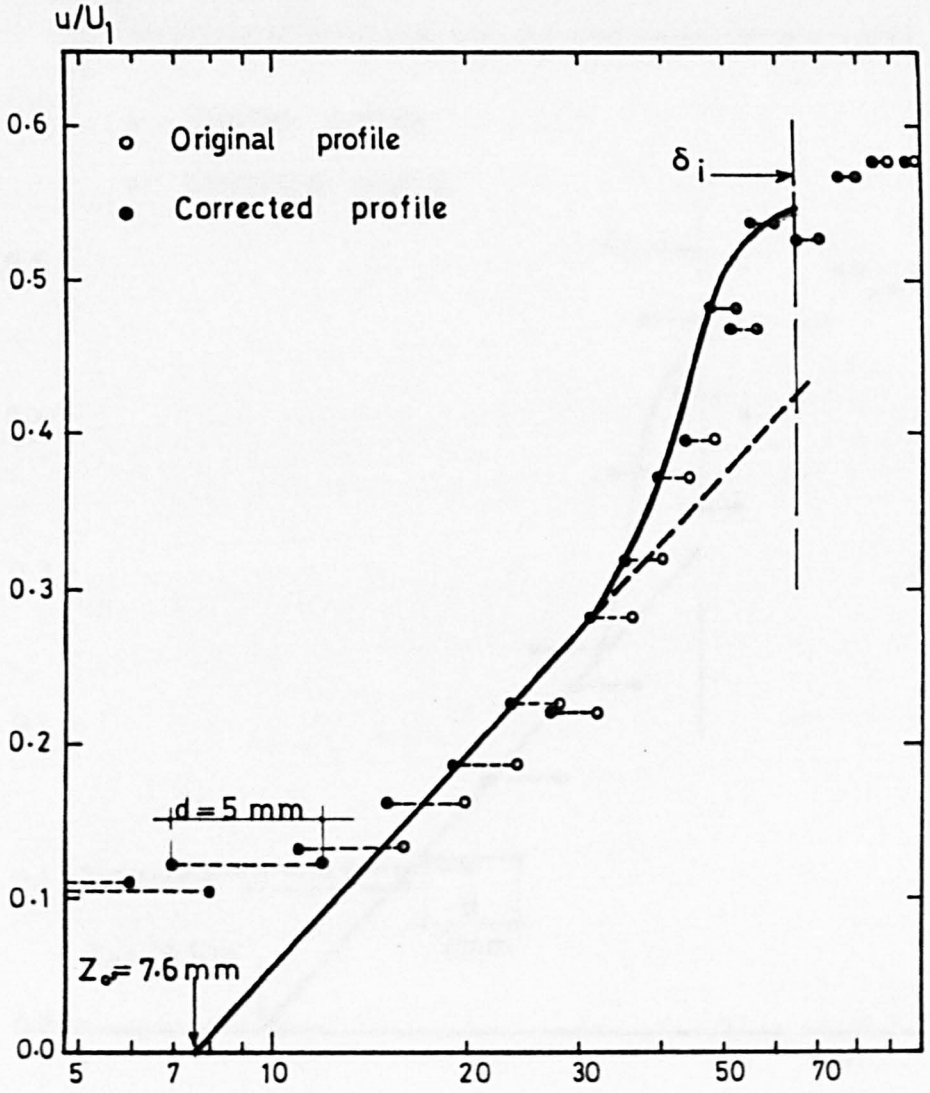

FIGURE 9.29 THE GRAPHICAL METHOD OF DETERMINING THE ZERO PLANE DISPLACEMENT, (λ = 12.5%)

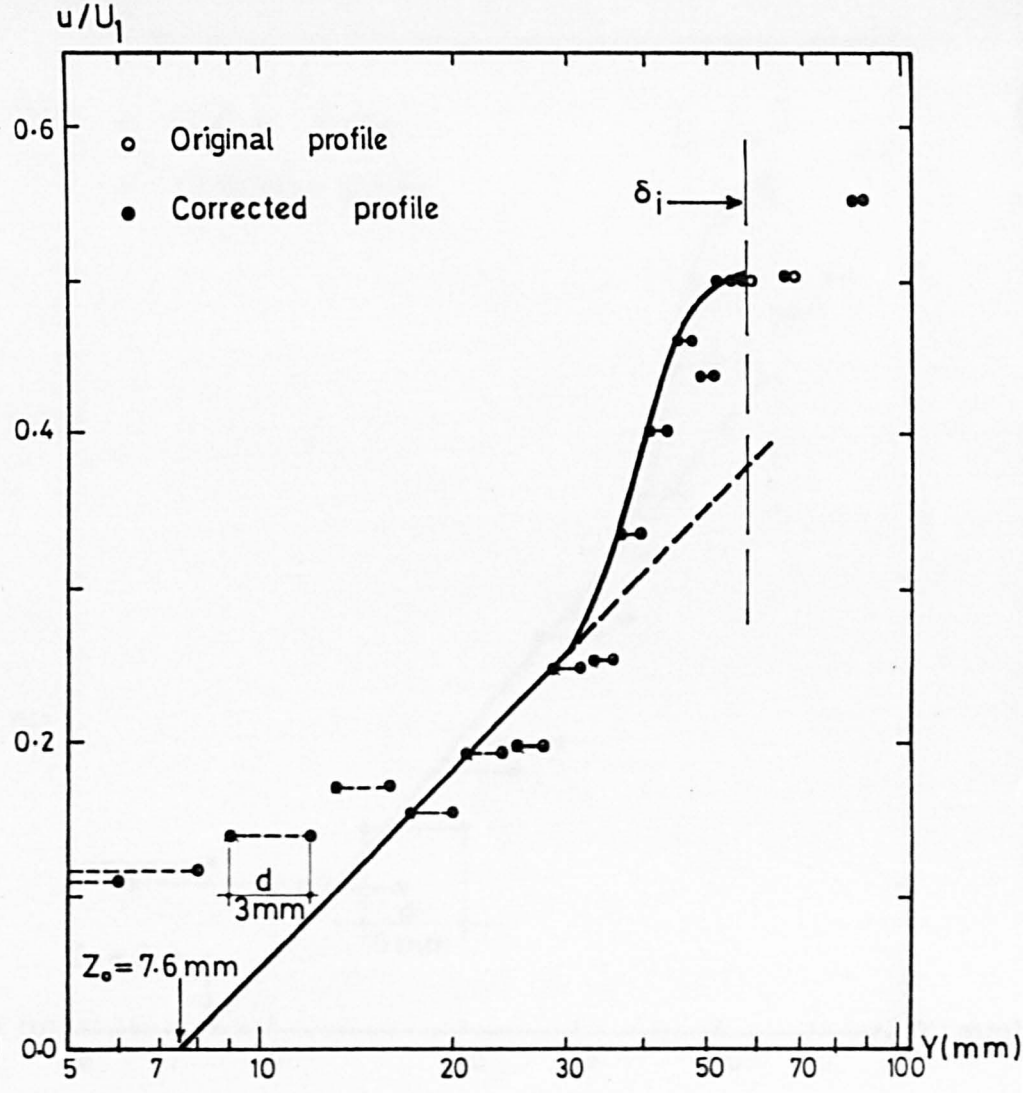

FIGURE 9.28 THE GRAPHICAL METHOD OF DETERMINING THE ZERO PLANE DISPLACEMENT, (λ = 10%)

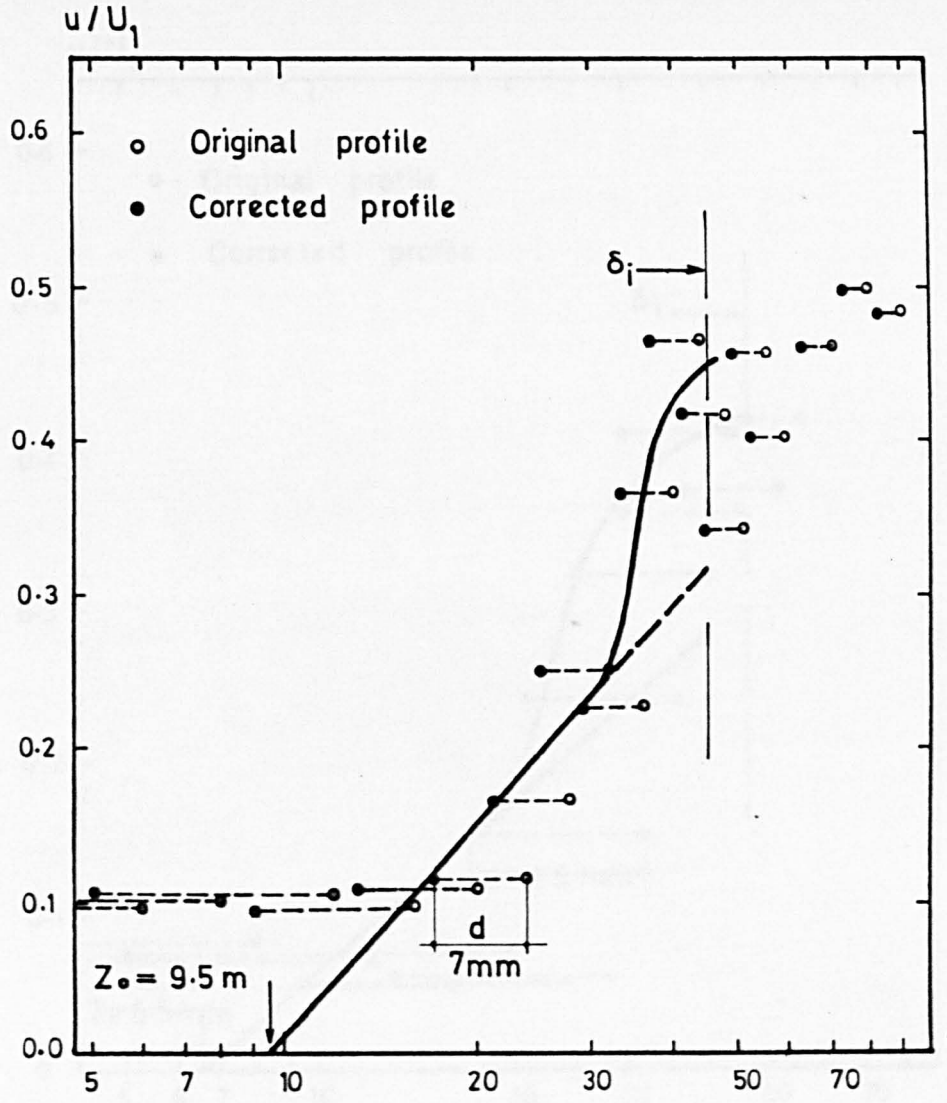

FIGURE 9.31 THE GRAPHICAL METHOD OF DETERMINING THE ZERO PLANE DISPLACEMENT (λ = 22.5%)

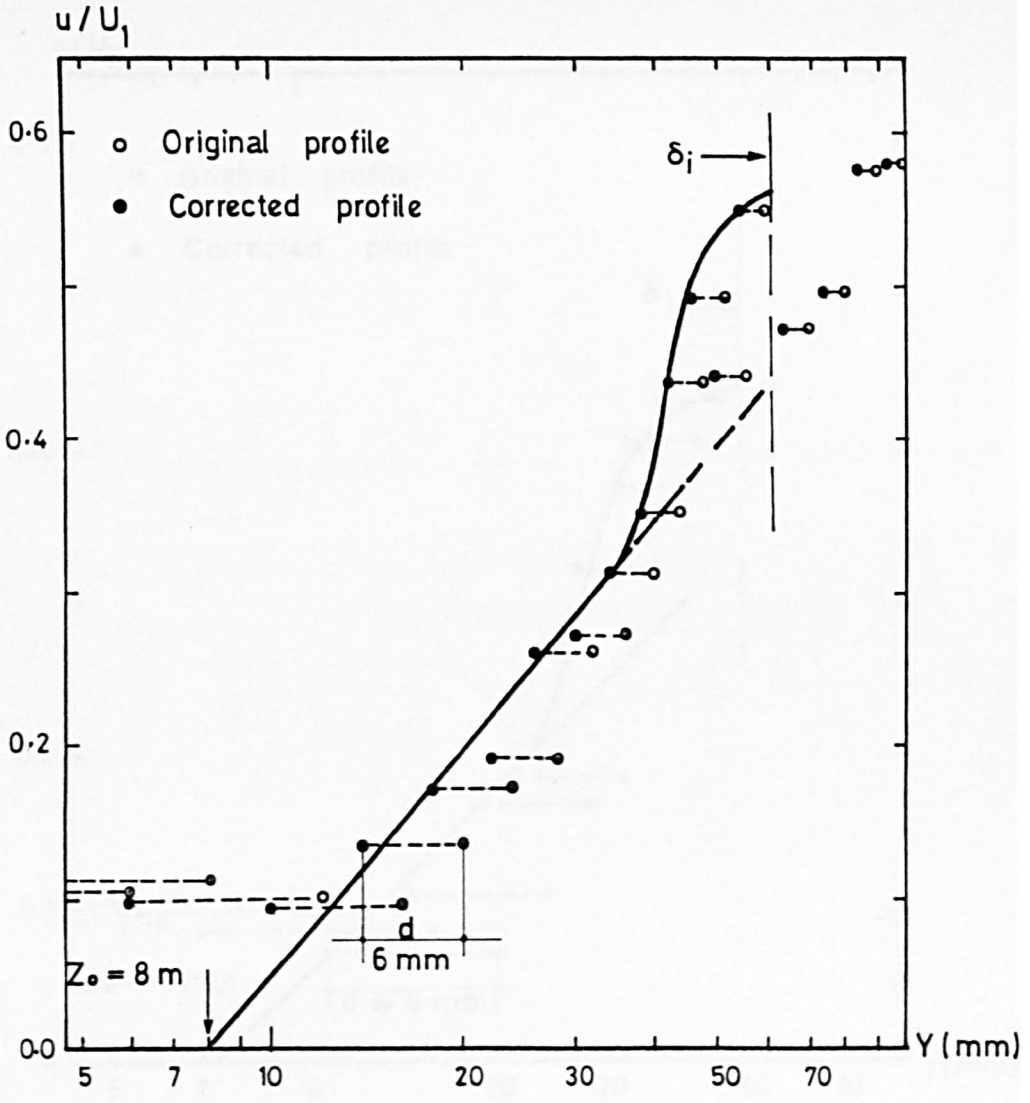

FIGURE 9.30 THE GRAPHICAL METHOD OF DETERMINING THE ZERO PLANE DISPLACEMENT (λ = 16.0%)

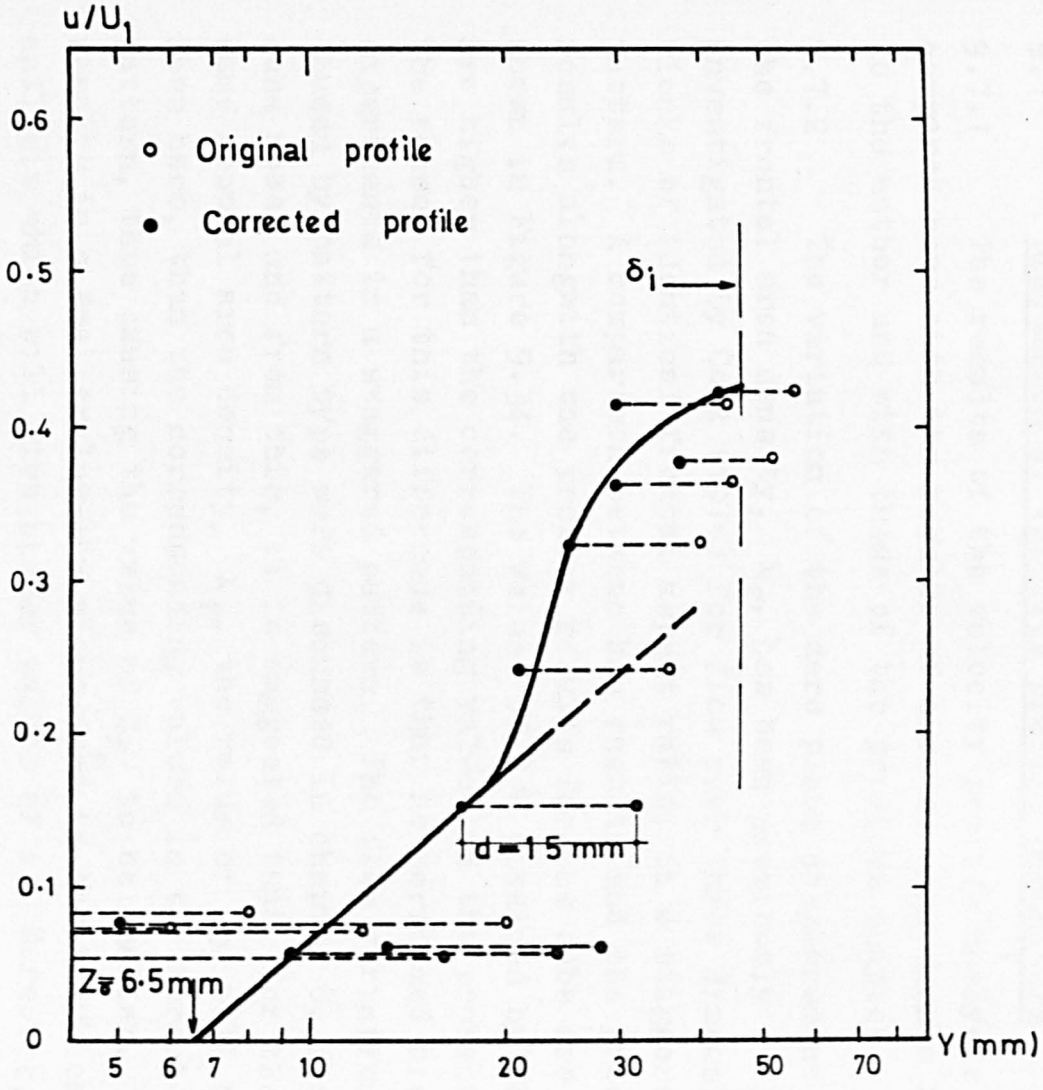

FIGURE 9.33 THE GRAPHICAL METHOD OF DETERMINING THE ZERO PLANE DISPLACEMENT, (λ = 40%)

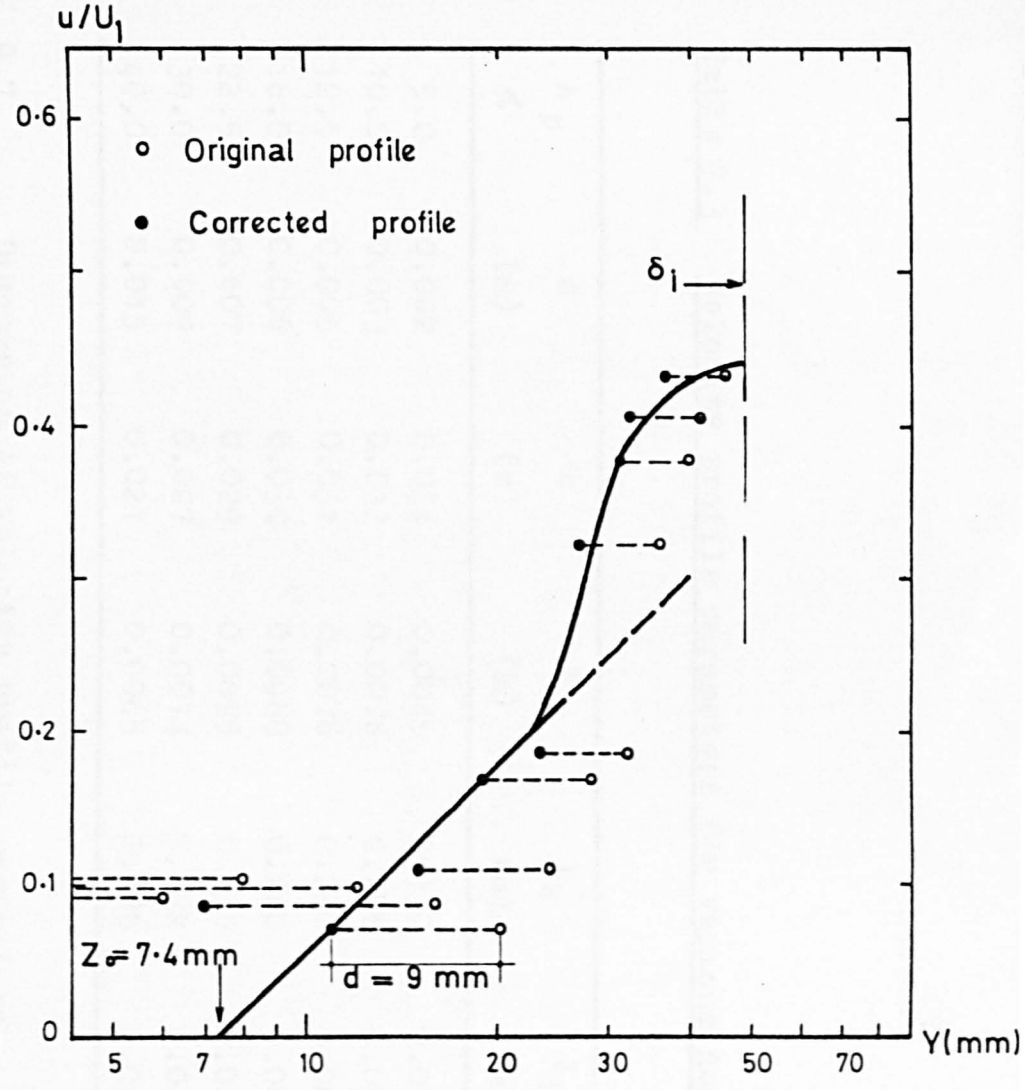

FIGURE 9.32 THE GRAPHICAL METHOD OF DETERMINING THE ZERO PLANE DISPLACEMENT, (λ = 30%)

Table 9.3 Velocity profile parameters for various densities

λ_p %	d (m)	ε (m)	Z_o (m)	k_s (m)	δ_i (m)
5.0	0.002	0.034	0.0045	0.135	0.054
10.0	0.003	0.033	0.0076	0.228	0.058
12.5	0.005	0.031	0.0076	0.228	0.064
16.0	0.006	0.030	0.0080	0.240	0.060
22.5	0.007	0.029	0.0095	0.285	0.045
30.0	0.009	0.027	0.0074	0.222	0.049
40.0	0.015	0.021	0.0065	0.195	0.047

9.7 Discussion of velocity profile parameters

9.7.1 The results of the velocity profile analysis are compared here with the results of similar experiments known to the author and with those of the previous chapter.

9.7.2 The variation of the zero plane displacement with the frontal area density, λ_f, has been previously investigated by Cook (1976) for flow over three dimensional blocks of identical frontal aspect ratio, in a staggered pattern. A comparison between his results and the present results alongwith the present results for the cube are shown in Figure 9.34. The values of d/H obtained by Cook are higher than the corresponding values in the present work. The reason for this difference is that he performed his experiments in a staggered pattern. The flow variations caused by pattern type were discussed in chapter 8, for the cube model and from this, it is suggested that, for the same frontal area density, λ_f, the value of C_{D_1} will be less here, than the corresponding values in the normal pattern, thus causing the value of C_{f_e} to be smaller. This results in a smaller log-law slope used in the graphical analysis which will give higher values of d. Moreover, he

has only shown rough values without fitting the measured C_{f_e} to the slope which might have resulted in an overestimation of the zero plane displacement.

In comparing the present results with those for the cube shaped model in chapter 8 for like values of λ_f, the value of drag coefficient has been shown to be smaller for the cubes, also resulting in higher values of d.

From his data points, Cook has suggested a straight line relationship to exist between the zero plane displacement and the density. This is similar to that suggested by Counihan (1971) and Soliman (1976). Although a similar trend is exhibited by the present results, Figure 9.34, a careful examination of the data reveals that a true straight line relationship does not exist. The data can, however, be shown to indicate a broken line relationship confirming the existence of three flow regimes. Figure 9.35 shows this relationship which is similar to the relationship suggested in the case of results for the cube in the last chapter.

9.7.3 The variation of Z_o/H, the roughness length, with λ_f has also been compared with the results obtained by Cook (1976) alongwith the results obtained for the cube in chapter 8, and is shown in Figure 9.36. The three sets of data show a broadly similar trend, in which an initial linear increase representing the isolated roughness flow regime is followed by a subsequent levelling off of the curve to represent the wake interference flow regime and then a decrease showing the skimming flow regime. Although there are insufficient points in the skimming flow regime with which to confirm this decrease, it is suggested that, as Z_o is a function of both C_{f_e} and k_s, its behaviour would also be similar to that reported by Wooding et al (1973) and Koloseus et al (1966), see chapter 8. The difference in magnitude of the present results and those of Cook is thought to be due to the reason that the log-law slope in

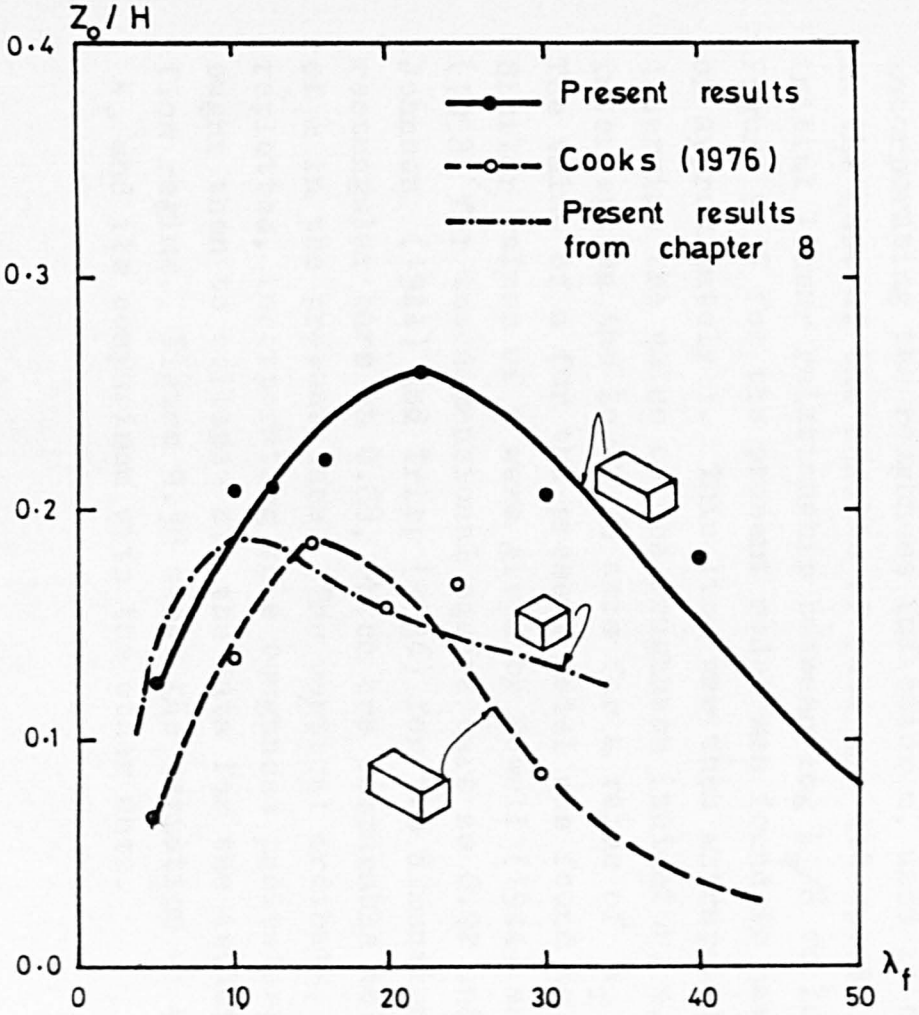

FIGURE 9.36 VARIATION OF Z_o/H WITH FRONTAL AREA DENSITY

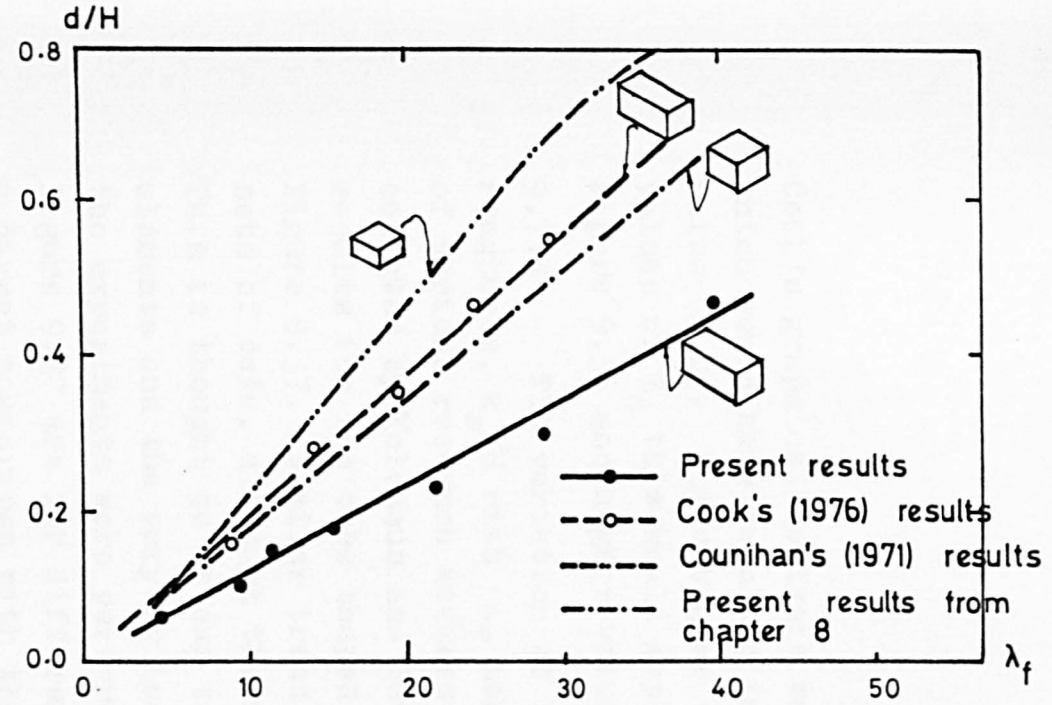

FIGURE 9.34 VARIATION OF d/H WITH FRONTAL AREA DENSITY

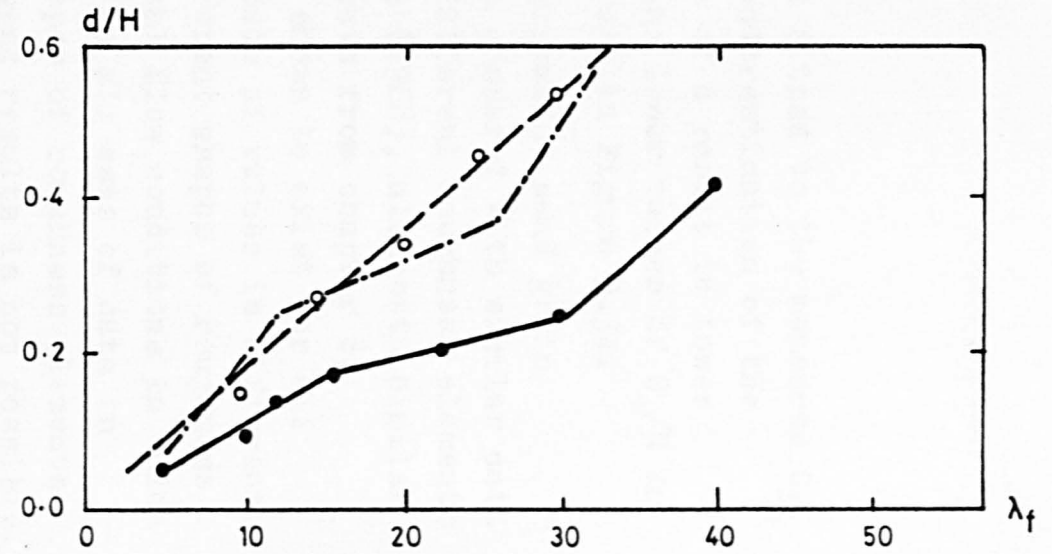

FIGURE 9.35 SUGGESTED VARIATION OF d/H WITH λ_f ACCORDING TO FLOW REGIMES

Cook's graphical analysis was not fitted to the measured C_{f_e} which would have resulted in an underestimation of the value of Z_o. Since higher values of d result in lower values of Z_o this would explain the lower values of Z_o/H in Figure 9.36 and higher values of d/H in Figure 9.34.

9.7.4 The variation of the equivalent sand grain roughness, k_s/H with λ_f has been compared with similar data of various research workers for different roughness elements collated by Koloseus and Davidian (1968), alongwith similar results for the cube shaped elements from chapter 8, Figure 9.37. Similar trends are shown to exist for all sets of data, although the magnitude of values is different. This is thought to be due to different shapes of roughness elements and the varying incidental flow conditions in which the experiments were performed. As all sets of data in Figure 9.37 are for different shapes of roughness elements a direct comparison with the present results is not possible.

Additionally, a more universal comparison incorporating the roughness indicator m, used in chapter 8 in the case of the results of cube was attempted. The initial linear relationship between log k_s/H vs log λ_f in Figure 9.37 for the present model was found to have a slope of approximately 1. This line was then extrapolated to determine the value of the roughness indicator, m, the intercept on the log k_s/H axis for a value of $\lambda_f = 1.0\%$. The value of m for the present model was found to be 0.8. Similar values of m were given by Powell (1944) and Rand (1952) for two dimensional square bars as 0.92 and by Johnson (1944) and Tripp (1936) for two dimensional rectangular bars as 0.88, which are comparable to the value of m in the present case. The vertical ordinate, if now replotted, incorporating this roughness indicator, m, ought then to collapse all the data for the isolated roughness flow regime. Figure 9.38 shows the variation of k_s/mH with λ_f and its comparison with the other data.

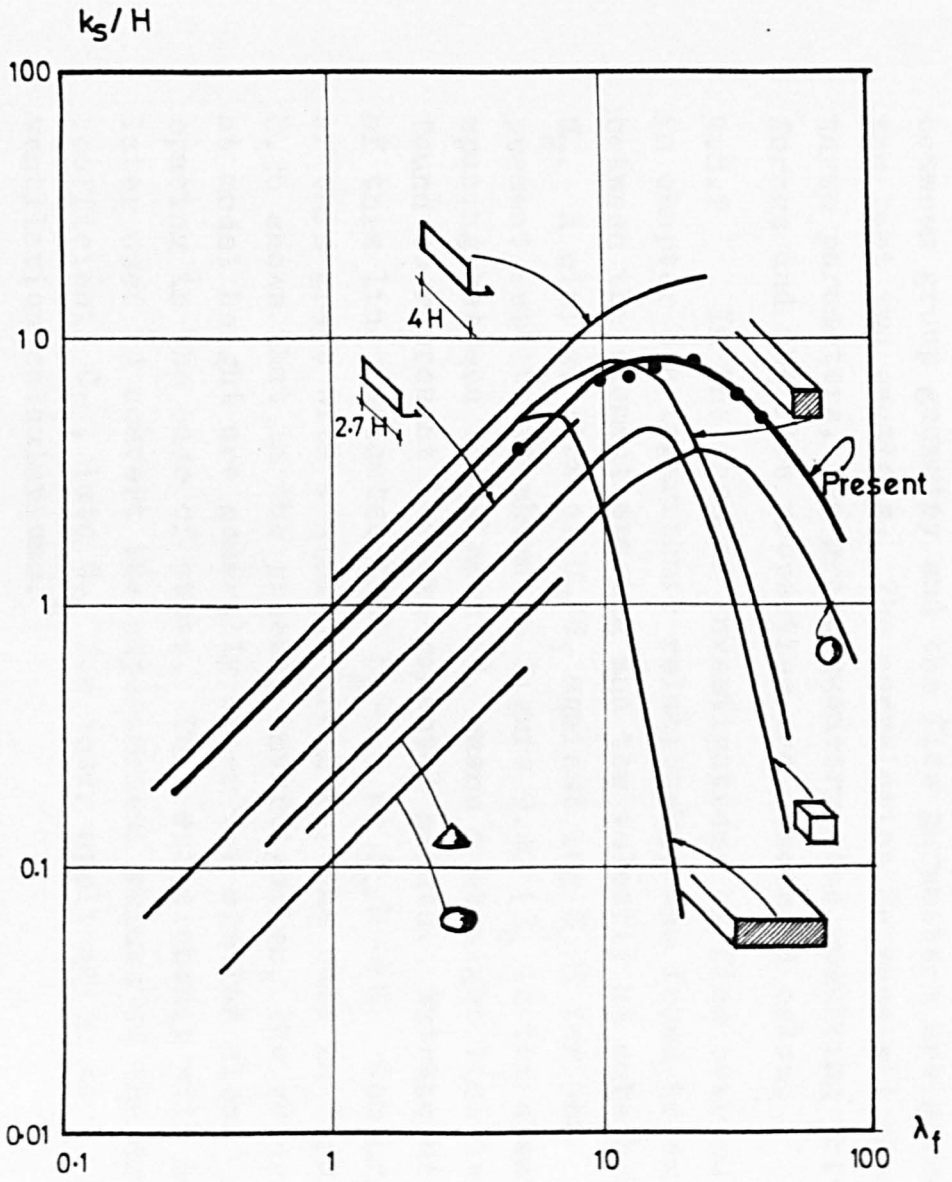

FIGURE 9.37 VARIATION OF k_s/H WITH λ_f AND THE COMPARISON WITH OTHER ELEMENT FORMS

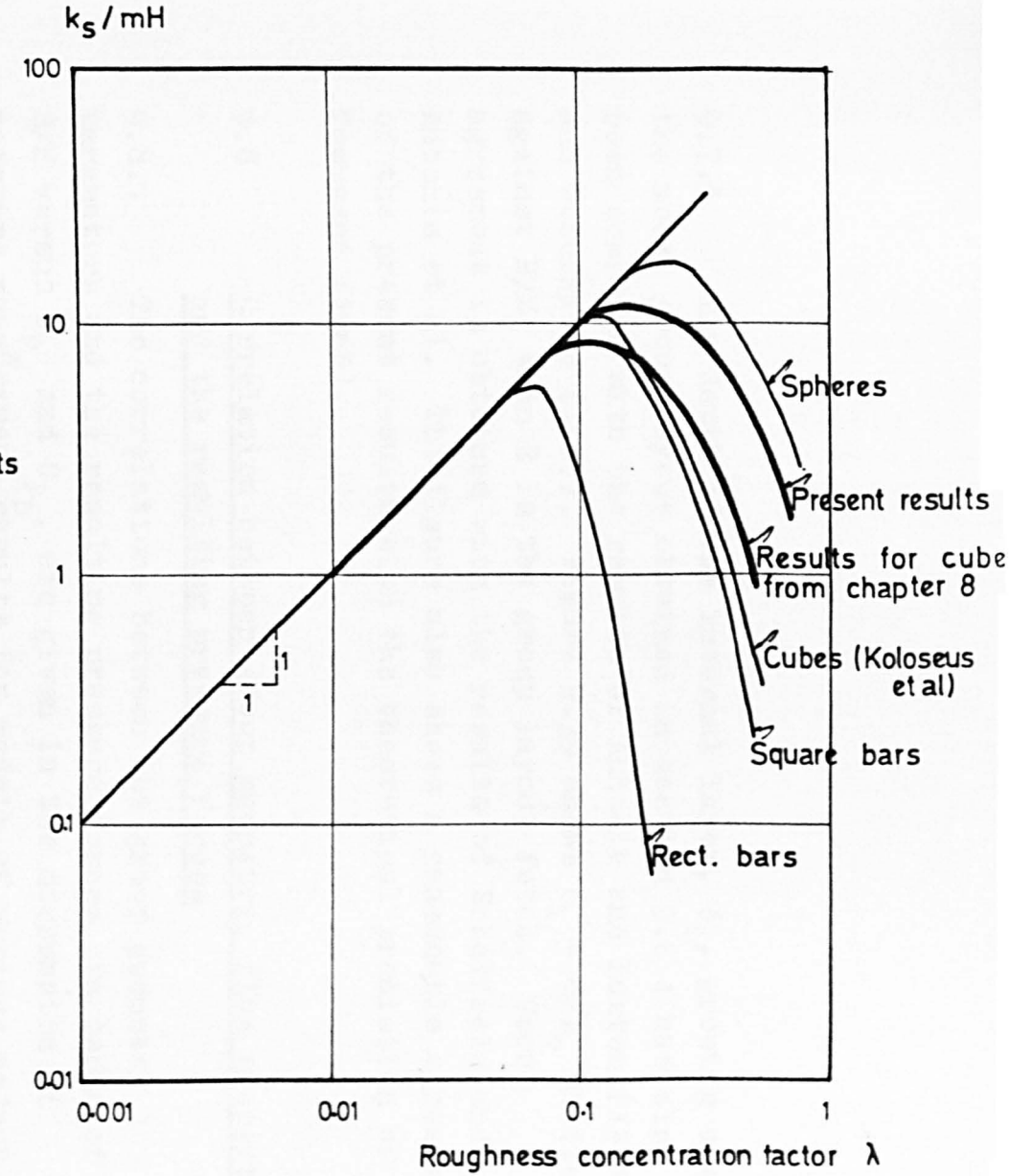

FIGURE 9.38 INTERFERENCE EFFECTS OF ROUGHNESS ELEMENTS WITH DENSITY (BASED ON KOLOSEUS AND DAVIDIAN 1966)

9.7.5 The depth of the internal layer, δ_i, growing over the model group layout obtained in section 9.6.4 has also been compared with the results of Antonia and Luxton (1971) and Schoffield (1975). Figure 9.39 shows $\delta_i - d/Z_o$ plotted against R/Z_o when R is the group layout fetch. Good agreement is obtained with the results of Schoffield and Antonia et al. The figure also shows a reasonable agreement of the present results with the theoretical prediction of Townsend (1965).

9.8 Correlation between group geometry, flow properties and the resulting pressure forces

9.8.1 The correlations between the group geometry parameters and the resulting pressure forces, in terms of S/H versus C_{p_w} and C_{p_b}, are given in the discussion of pressure measurement results for models of various aspect ratios. The flow measurement results and the correlations between group geometry and the flow parameters are given in the last two sections. The correlation between all the three parameters, the group geometry, the resulting pressure forces and the flow properties are discussed below.

9.8.2 In the case of investigations of flow over cubes in chapter 8 a logarithmic relationship was found to exist between the element spacing and the velocity at cube height U_H. A similar plot of U_H/U_1 against log S_c/H for the present results is shown in Figure 9.40 (S_c is the clear spacing between the elements), where a straight line is found to represent the experimental points. Extrapolation of this line indicates that $U_H \rightarrow 0$ as $S_c/H \rightarrow 0$. Comparison of this graph with a similar graph for the cube in Figure 8.36 shows that in the present investigation, the velocities at model height are generally lower for similar clear spacing in the case of cubes. This relationship will be later used to convert the experimental values of the drag coefficient, C_{D_1}, into C_{D_H} for their application to ventilation calculations.

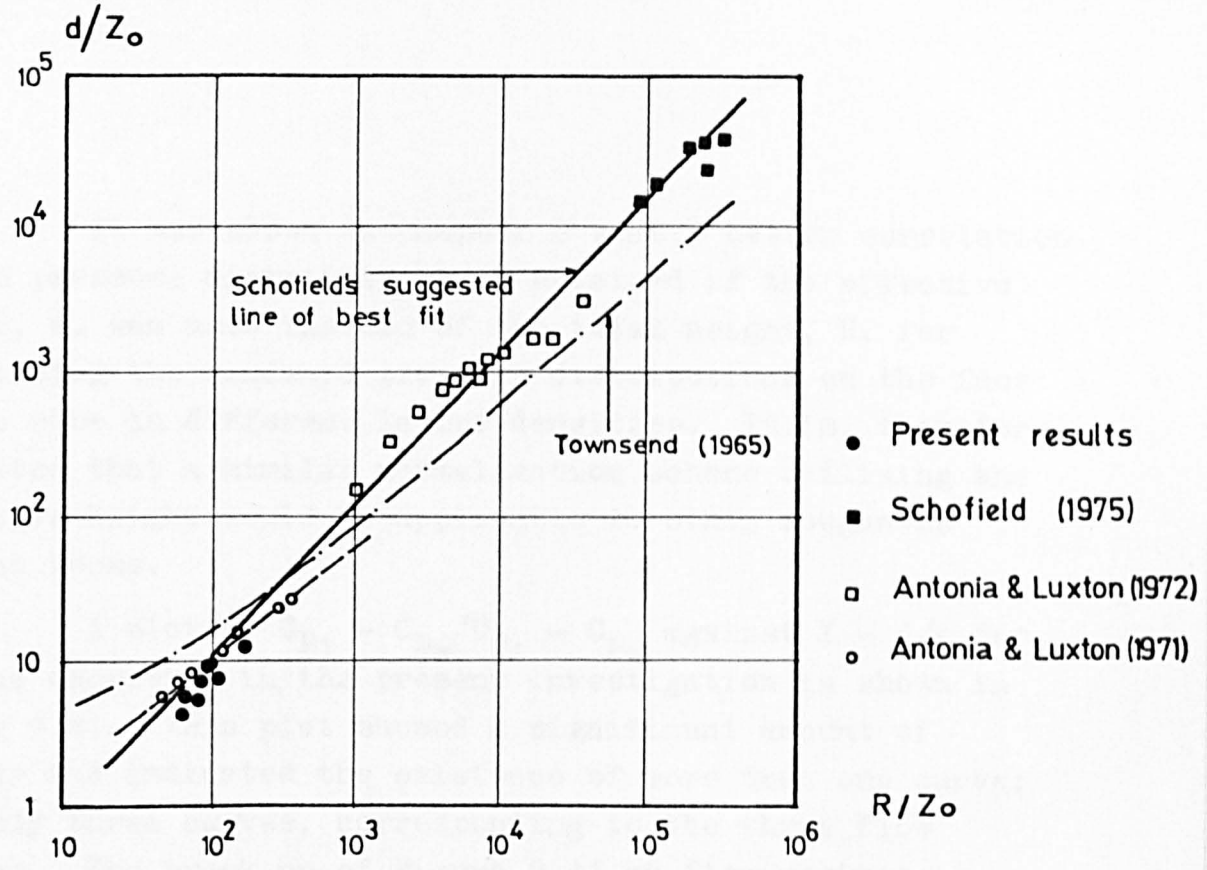

FIGURE 9.39 COMPARISON OF EXPERIMENTAL GROWTH OF INTERNAL LAYER WITH THEORY AND PRESENT RESULTS

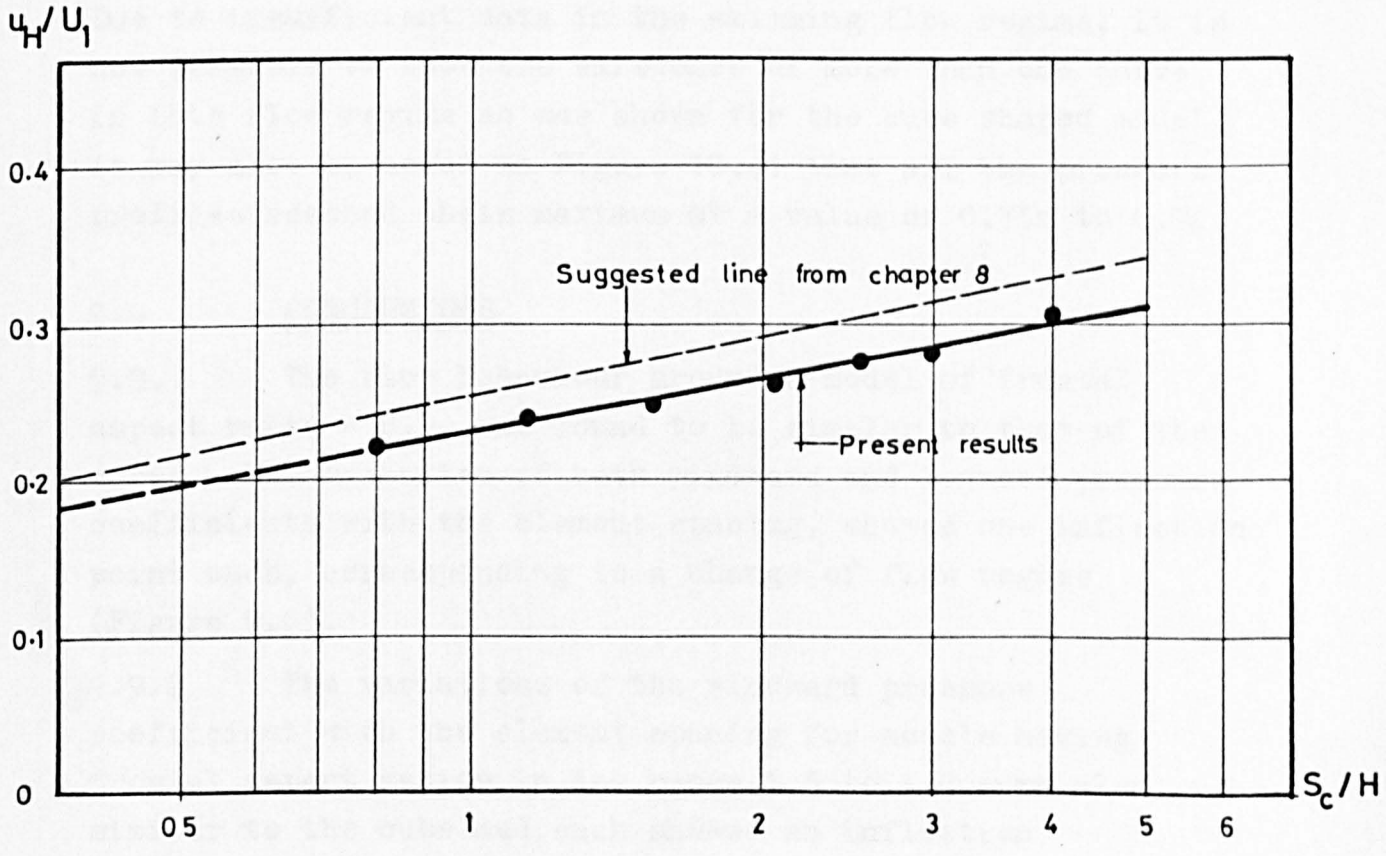

FIGURE 9.40 VARIATION OF U_H/U_1 WITH S_c/H

9.8.3 It was shown in chapter 8 that a better correlation of the pressure distributions is obtained if the effective height, ε, was used instead of the total height, H, for normalising the windward pressure distributions on the face of the cube in different layout densities. It is, therefore, suggested that a similar normalisation scheme utilising the effective height would be applicable to other roughness element forms.

A plot of $C_{p_1} - C_{p_w}/C_{p_1} - C_{p_o}$ against $Y - d/\varepsilon$ for various densities in the present investigation is shown in Figure 9.41. This plot showed a significant amount of scatter and indicated the existence of more than one curve; possibly three curves, corresponding to the three flow regimes. The break up of Figure 9.41 by flow regimes is shown in the subsequent Figures 10.42 to 10.44. It is clear from these figures that this correlation is better represented by separate curves for the three flow regimes. Due to insufficient data in the skimming flow regime, it is not possible to show the existence of more than one curve in this flow regime as was shown for the cube shaped model. It may also be noted in Figure 10.41 that all the pressure profiles reached their maximum at a value of 0.75ε to 0.9ε.

9.9 CONCLUSIONS

9.9.1 The flow behaviour around a model of frontal aspect ratio = 0.5, was found to be similar to that of the cubes. The variation of both windward and leeward pressure coefficients with the element spacing, showed one inflection point each, corresponding to a change of flow regime (Figure 9.6).

9.9.2 The variations of the windward pressure coefficient with the element spacing for models having frontal aspect ratios in the range 1.5 to 4.0 were also similar to the cube and each showed an inflection corresponding to the change from isolated roughness flow regime to the wake interference flow regime. The variation

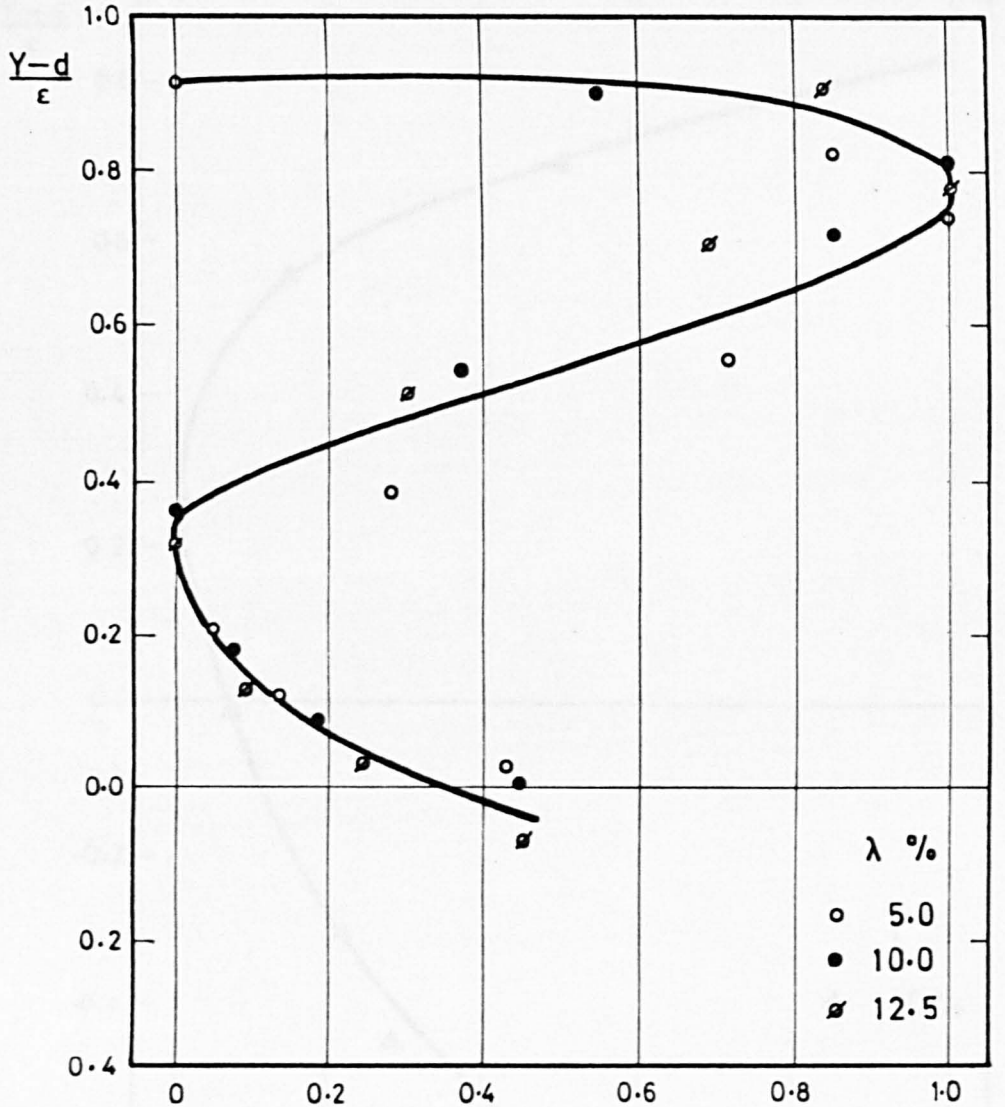

FIGURE 9.42 NORMALISED PRESSURE PROFILES FOR ISOLATED ROUGHNESS FLOW REGIME

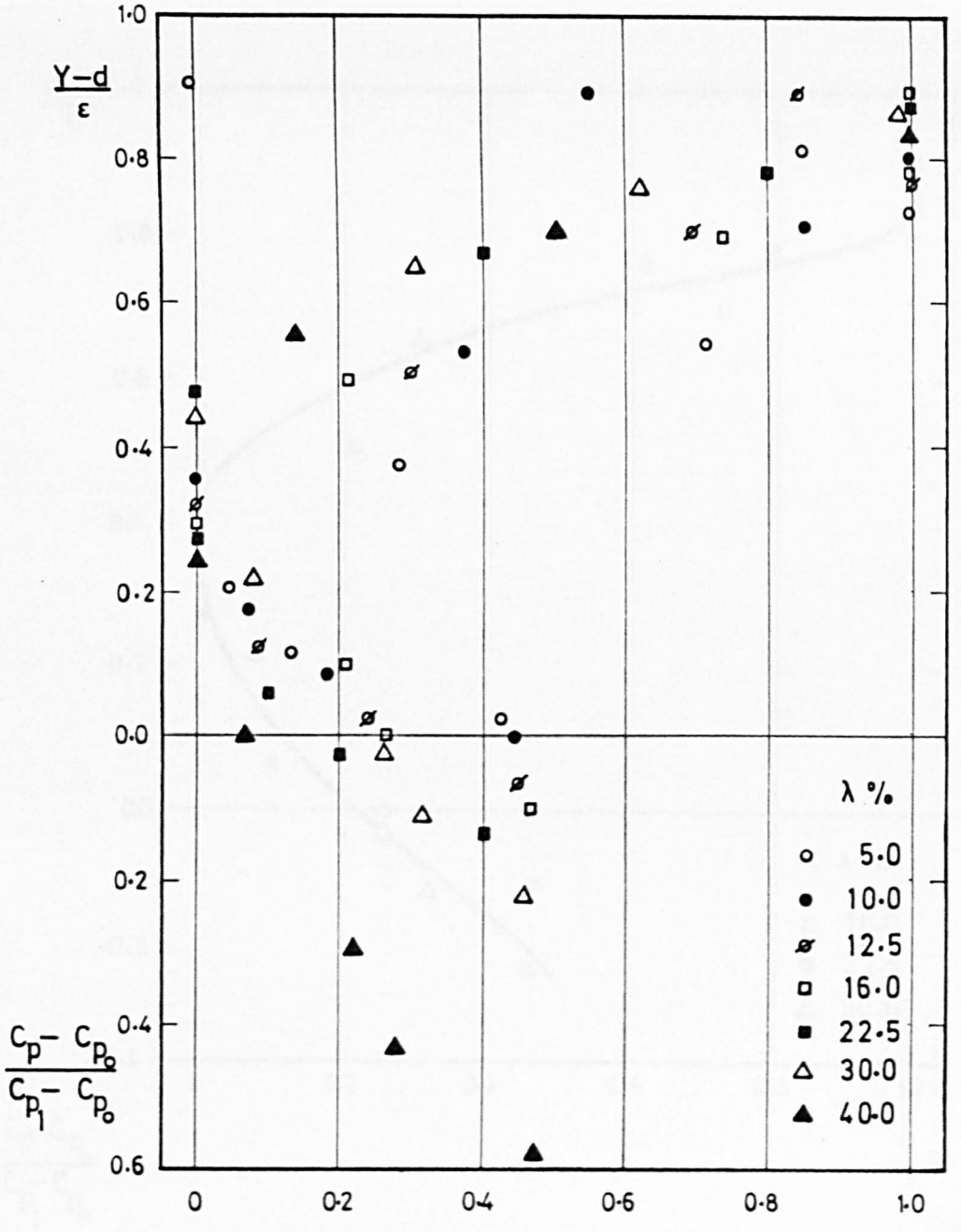

FIGURE 9.41 NORMALISED PRESSURE PROFILES FOR THE MODEL WITH A_f = 2.0 (THREE FLOW REGIMES)

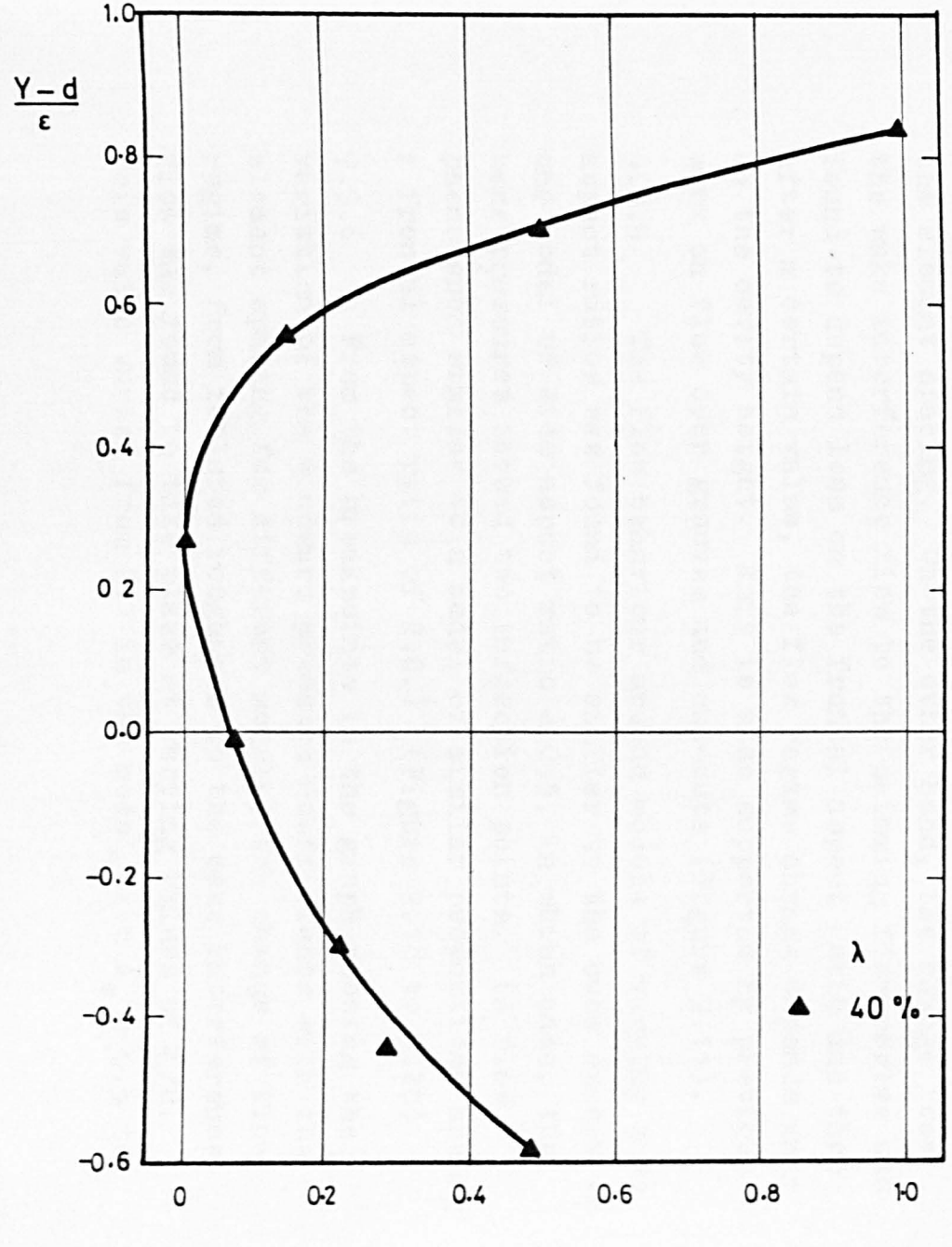

FIGURE 9.44 NORMALISED PRESSURE PROFILES FOR SKIMMING FLOW REGIME

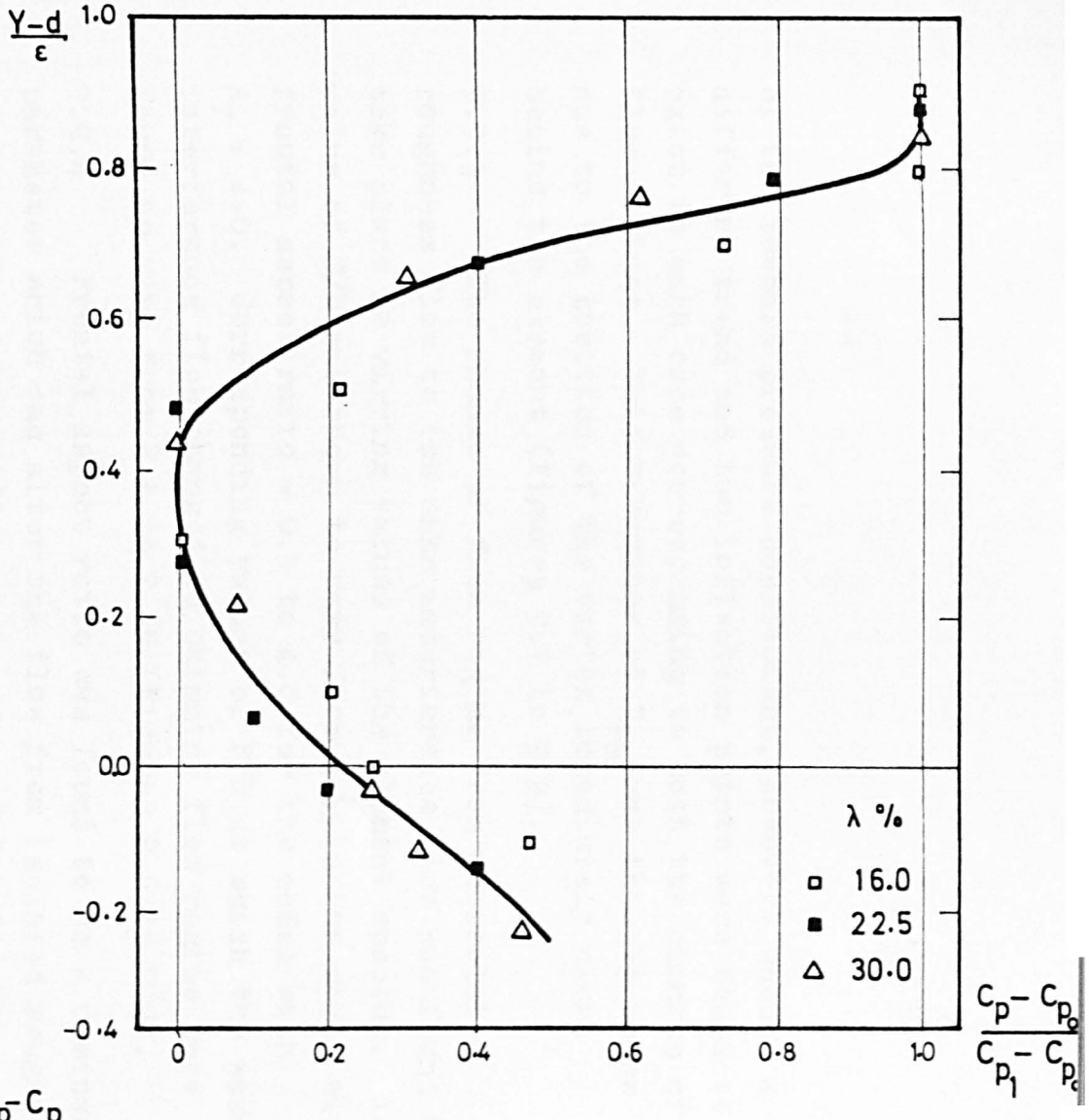

FIGURE 9.43 NORMALISED PRESSURE PROFILES FOR WAKE INTERFERENCE FLOW REGIME

of the leeward pressure coefficient, however, showed a different trend and two inflection points were found to exist in each case corresponding to both the changes of flow regimes. This behaviour of C_{p_b} was thought to be due to the position of the vortex immediately close behind the element (Figures 9.7 to 9.9).

9.9.3 The change of flow regime from an isolated roughness flow to the wake interference flow was found to take place at varying values of the element spacing. This value of S/H was shown to vary from 3.25 in the model with frontal aspect ratio = 0.5 to 4.0 for the model with A_f = 4.0. Corresponding values of S/H at which the wake interference flow changed to skimming flow regime were found to vary from 2.3 to 2.55 (Figures 9.6 to 9.9).

9.9.4 Frontal aspect ratio was found to be a dominant parameter which can alter the flow from isolated roughness to wake interference flow regime for particular values of the element spacing. On the other hand, the change from the wake interference flow to the skimming flow regime was found to depend less on the frontal aspect ratio and then after a certain value, the flow regime change depends only on the cavity height. This is also supported by previous work on flow over grooves and cut-outs (Figure 9.11).

9.9.5 The flow behaviour around models of varying side aspect ratios was found to be similar to the cube except in one model of side aspect ratio = 0.5, in which case, the base pressures showed two inflection points. (A flow phenomenon similar to a model of similar proportions having a frontal aspect ratio of 2.0.) (Figure 9.18 to 9.20)

9.9.6 From the breakpoints in the graph showing the variation of the windward pressure coefficients with the element spacing for different models, the change of flow regime, from isolated roughness to the wake interference flow was found to take place at varying values of S_c/H. This value varied from 2.1 in the model with A_s = 0.5 to

2.6 for model with a side aspect ratio of 2.0. Conversely the value of S_c/H at which the wake interference flow regime changed to the skimming flow regime remained constant at 1.4 (Figures 9.18 to 9.20).

9.9.7 Side aspect ratio is found to alter the flow from isolated roughness flow regime to the wake interference flow regime only up to a certain extent. When the side aspect ratio is large enough for the flow to reattach on the roof and sides of the model then the reattachment distance behind the element is not affected and thus the change of flow regime takes place at a fairly constant value of element spacing. Conversely, the change from the wake interference flow regime to the skimming flow regime is not affected by the side aspect ratio but is directly related to the element height as explained in 9.2.8 and 9.4.8 (Figure 9.22).

9.9.8 The roof pressure coefficients were found to be negative for all the models with the maximum suction occurring near the windward edge of the roof in most densities considered. At higher densities, however, these distributions were of a more uniform nature (Figures 9.12, 9.13, 9.23 and 9.24).

9.9.9 The variation of roof lift coefficient with the element spacing showed one break point for each model. The value of spacing at which the break point occurred was found to compare well with the values of spacing at which the wake interference flow changes to skimming flow regime. This was found to be true for all models in both the frontal and side aspect ratio ranges (Figures 9.14 and 9.25).

9.9.10 The simulated atmospheric boundary layer flow underwent only one surface change when it reached the model group layout. An internal layer was found to be growing over the group layout (Figure 9.26).

9.9.11 The logarithmic region of the inner layer of the model centre line profiles did not extend above the model height in any case (Figures 9.27 to 9.33).

9.9.12 A broken straight line relationship between the zero plane displacement and the group layout density found over the cubes was shown also to exist for the frontal aspect ratio model having $A_f = 2.0$. The break points substantiated the existence of three flow regimes found earlier (Figure 9.35).

9.9.13 The variation of the roughness length with increasing group layout density was shown to relate well with other results (Figure 9.36).

9.9.14 The variation of equivalent sand grain roughness with increasing density showed a reasonably good agreement between the present results and the results of Koloseus and Davidian (1966)(Figures 9.37 and 9.38).

9.9.15 The depth of the internal layer obtained indicated a reasonable agreement with previous experimental results as well as with the theoretical prediction by Townsend (Figure 9.39).

9.9.16 A relationship was found to exist between the velocity at model height and the clear spacing between models (Figure 9.40).

9.9.17 A normalisation scheme for the windward pressure distribution profiles which takes into account the effect of the zero plane displacement and uses the effective height has been effectively used to substantiate the flow regime hypothesis (Figures 9.41 to 9.44).

CHAPTER 10

EXPERIMENTAL RESULTS AND DISCUSSION: EFFECT OF MODEL HEIGHT VARIATIONS RELATIVE TO THE SURROUNDING ROUGHNESS

10. EXPERIMENTAL RESULTS AND DISCUSSION: EFFECT OF MODEL HEIGHT VARIATIONS RELATIVE TO THE SURROUNDING ROUGHNESS

10.1 Introduction

10.1.1 The frontal and the side aspect ratios of models have been shown to be important parameters in determining the flow around them, chapter 9. Furthermore, a study of the flow around isolated models of various heights was carried out in chapter 6, where the height was shown to be one of the important parameters in determining the wind forces on the models. In this phase of the study, a systematic investigation is made of the wind pressure variations when the test model of variable height is surrounded by uniform roughness arrays of various densities. This chapter describes the effect of the surrounding roughness in shielding the bluff model when the model height is less than the average roughness height and of the degree of exposure experienced by a model taller than the surrounding roughness. This study will also be used to substantiate the trend of the variation of C_{D_H} with the height which was established in chapter 6 for isolated models.

10.1.2 A study of the drag of a bluff body immersed in a rough wall boundary layer formed by the flow over two dimensional roughness elements, made by Joubert, Perry and Stevens (1971), showed that when the height of the individual element rises slightly above the average height of the array, the drag coefficient increases very rapidly and that the reverse was true for bodies slightly lower than the array height. They showed the variation in the drag coefficient of the order of approximately 70% with only 1% change in the height of the elements above or below the average height of the array and found this to be true only for the arrangement with stable vortices between the elements i.e. the skimming flow regime. For the "k" type

arrays, however, where the ratio of the spacing between the elements and their height is more than one so that the vortices between become unstable i.e. the isolated roughness and the wake interference flow regimes, the drag coefficient was shown to be insensitive to small misalignment of the element crest. For a 20% change in the height, they found the changes in the drag were undetectable.

Joubert et al also presented some preliminary measurements for three dimensional elements in a rough wall boundary layer growing over 3" cubes arranged in a staggered layout pattern, extending 3' beyond the model position at approximately 8% density. The height ratio of the pressure tapped model 3" wide and $1\frac{1}{4}$" deep, which was positioned in place of a cube on the centre line of the wind tunnel, was varied from 0.1 to 3.44, while the height of the array was taken as 1.0. They showed a linear variation of the drag coefficient with the height. These results have been reproduced in Figure 10.1.

10.1.3 The results of Joubert et al related to specific cases only and their experimental set up, particularly for three dimensional elements, was not rigorous as the authors themselves pointed out that more experiments were required to clarify the interaction. An effort has, therefore, been made in the present study to extend these findings generally to three dimensional elements, where the cube has been taken as having a height ratio of 1.0 and all other model heights are related to it. The length and the breadth of the model have been kept constant while the relative height was varied from 0.5 to 4.0.

10.1.4 On the basis of conclusions regarding fetch length drawn in chapter 7, and their application to subsequent investigations, the array size, R/H, of the model was kept between 10 to 25 to allow for the model wall pressures to stabilise, depending on the plan area density. The model group, however, took the form of free standing cubes on the

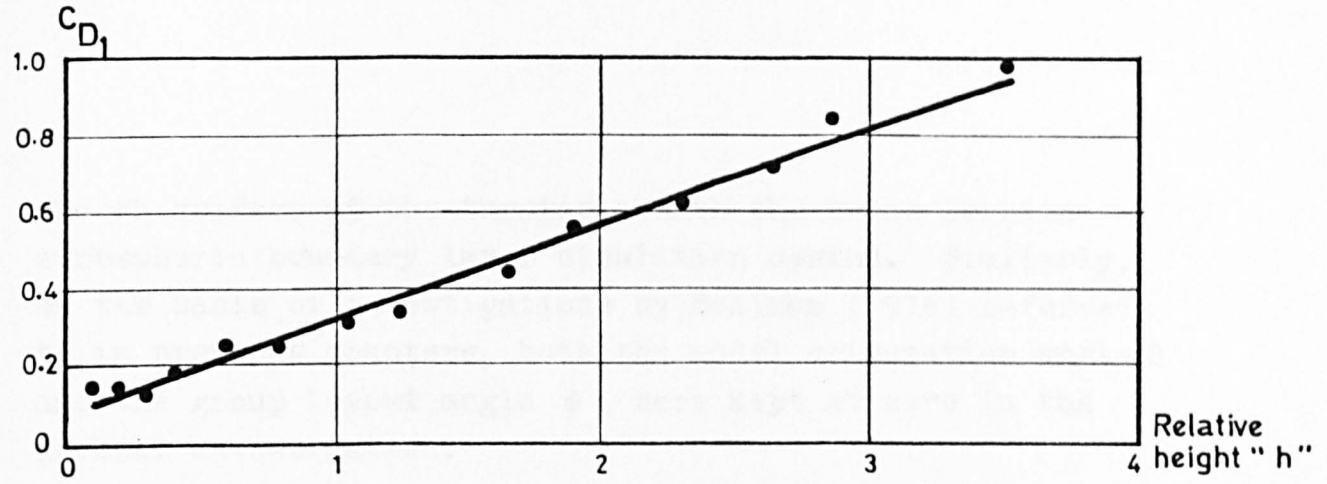

FIGURE 10.1 VARIATION OF C_{D_1} WITH RELATIVE HEIGHT (JOUBERT ET AL 1971)

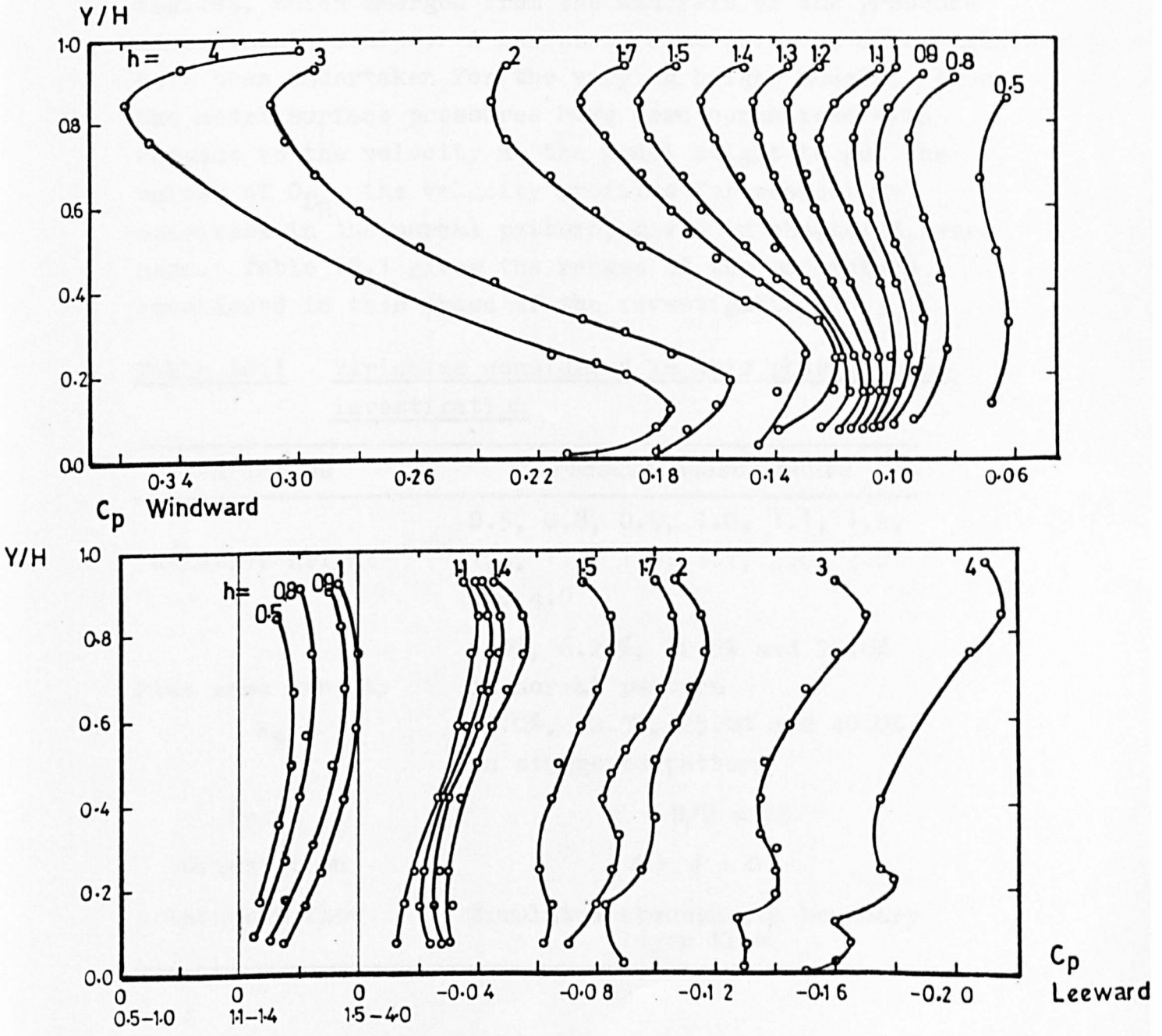

FIGURE 10.2 WALL PRESSURE COEFFICIENT DISTRIBUTIONS ON CENTRE LINE OF MODELS OF VARYING HEIGHT RATIOS - 5% NORMAL PATTERN

smooth surface of the turntable with the urban terrain atmospheric boundary layer simulation upwind. Similarly, on the basis of investigations by Soliman (1976) referred to in previous chapters, both the model orientation angle θ and the group layout angle ϕ, were kept at zero in the present investigation.

10.1.5 On the basis of observations made in chapter 8, four values of the plan area density, λ_p, in each of the layout patterns, were chosen to cover the three flow regimes, which emerged from the analysis of the pressure measurement results. A series of mean pressure measurements have been undertaken for the varying height models. Where the model surface pressures have been normalised with respect to the velocity at the model height to get the values of C_{D_H}, the velocity profiles for respective densities in the normal pattern, given in chapter 8, were used. Table 10.1 gives the ranges of the parameters considered in this phase of the investigation.

Table 10.1 Variables considered in this phase of the investigation

Variables	Pressure measurements
Relative height	0.5, 0.8, 0.9, 1.0, 1.1, 1.2, 1.3, 1.4, 1.5, 1.7, 2.0, 3.0 and 4.0
Plan area density λ_p	5.0%, 6.25%, 12.5% and 25.0% in normal pattern 10.0%, 12.5%, 25.0% and 40.0% in staggered pattern
Fetch	$10 < R/H < 25$
Orientation	$\theta = \phi = 0$
Incident flow	Simulated atmospheric boundary layer flow

10.2 Pressure measurements on the windward and leeward faces of models having varying height ratios

10.2.1 The vertical distribution of pressure coefficients normalised with respect to the free stream velocity, measured on the centre line of the windward and leeward faces of all the models in various layout densities for both the normal and the staggered patterns, are shown in Figures 10.2 to 10.9. These pressure distributions were integrated to give the mean windward and leeward pressure coefficients $C_{p_{wc}}$ and $C_{p_{bc}}$ and subsequently, the drag coefficient, C_{D_C}, in each case.

10.2.2 The shape of the windward pressure coefficient profiles were found to be similar to those for the cubes, chapter 8. In the isolated roughness flow regime cases, considered here, the shape of all the profiles was similar to an "S" shape. On the other hand, in the wake interference and the skimming flow regimes, the profiles were of a "reversed C" shape but their shape changed to an "S" type as the height of the model increased approximately 1.35 to 1.6 above the average height of the array. This is thought to be due to the limited extent of the internal layer growing over the roughness elements. It is suggested that when the height of the model was increased beyond the thickness of the internal layer (depending on the size, R/H, of the array in a particular layout density) the shape of the profile changed from a "reversed C" to an "S" shape.

On the other hand, the leeward pressure profiles for the cases where the height was larger than the average height of the array showed a kink at the average height of the array. This kink was shown to be distinct in the case of models with height ratio more than 2.

10.2.3 In an earlier investigation of flow over two and three dimensional roughness elements, Joubert et al (1971), showed different trends of the variation of drag coefficient when their relative height was varied. In the case of a

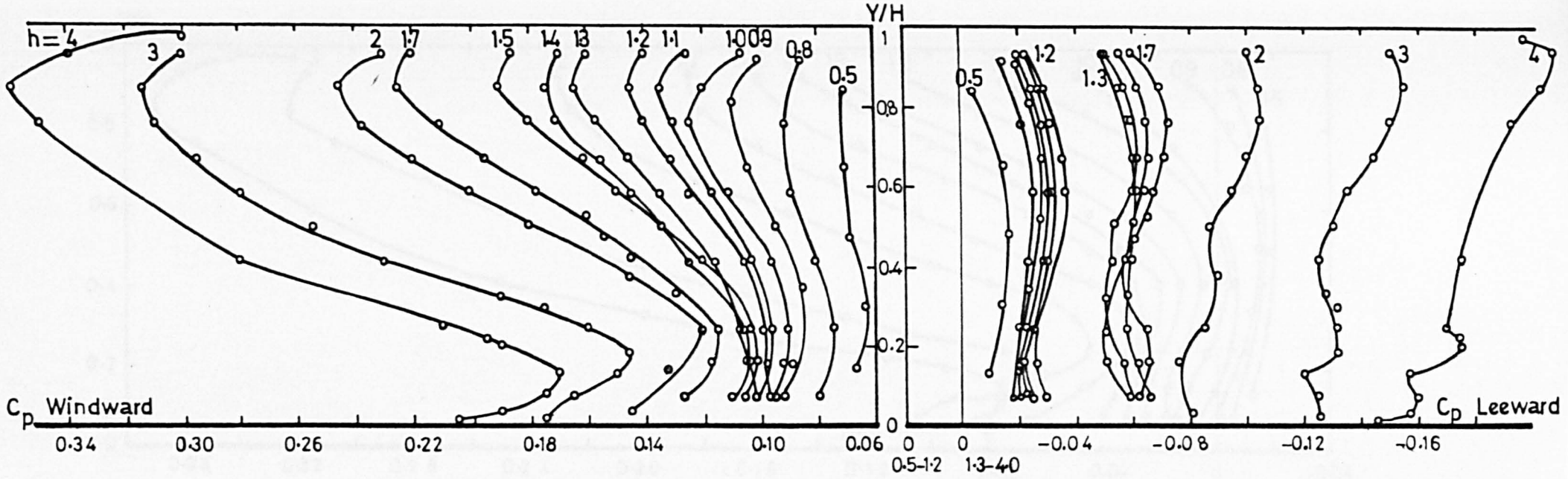

FIGURE 10.3 WALL PRESSURE COEFFICIENT DISTRIBUTIONS ON CENTRE LINE OF MODELS OF VARYING HEIGHT RATIOS - 6.25% NORMAL PATTERN

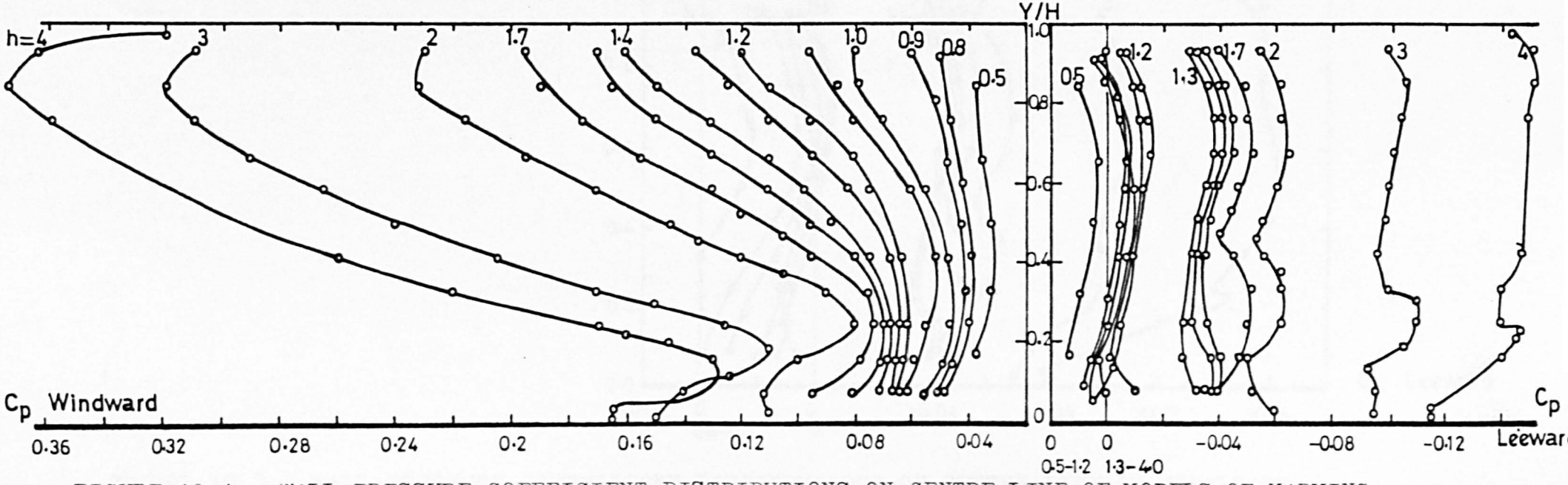

FIGURE 10.4 WALL PRESSURE COEFFICIENT DISTRIBUTIONS ON CENTRE LINE OF MODELS OF VARYING HEIGHT RATIOS - 12.5% NORMAL PATTERN

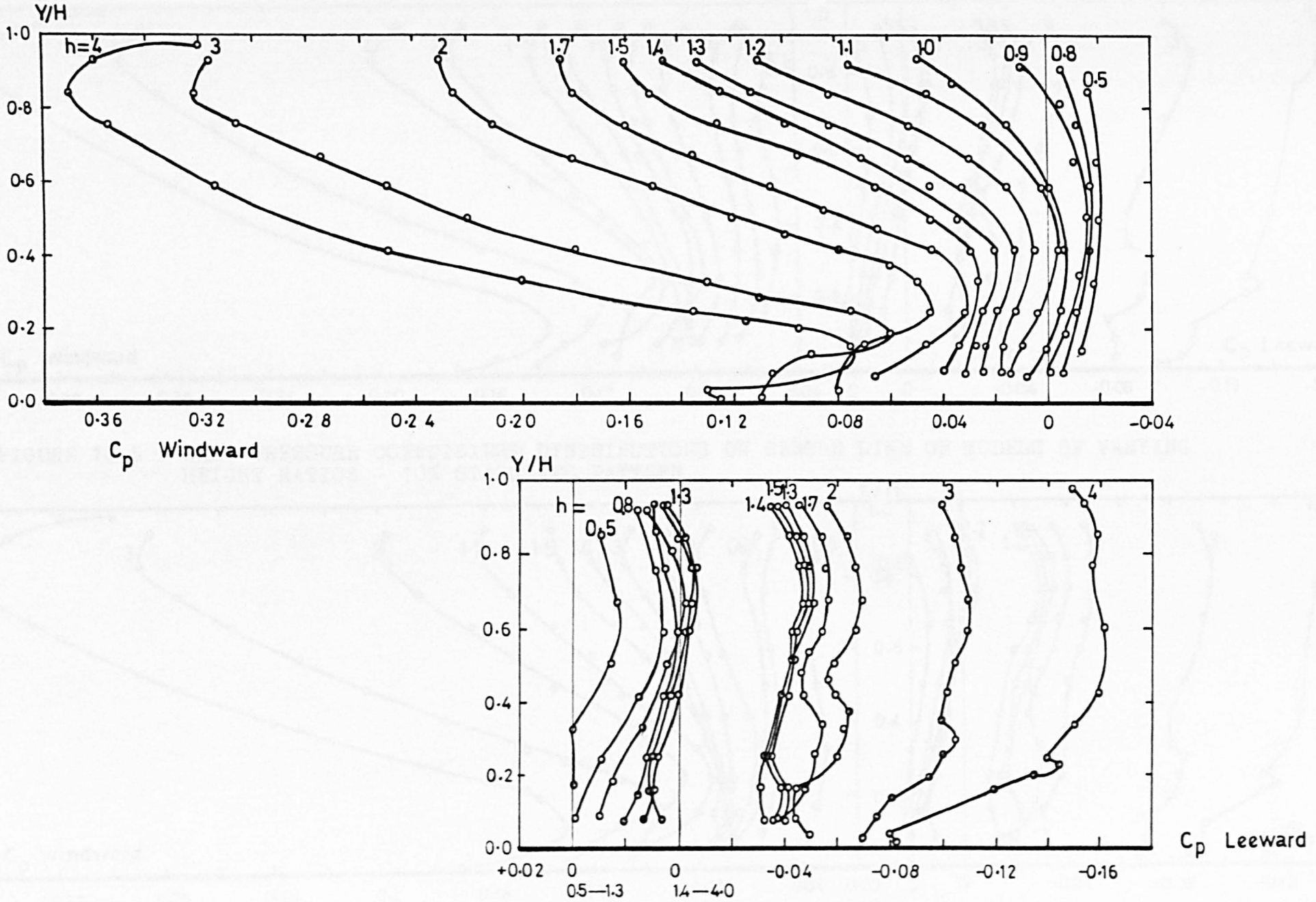

FIGURE 10.5 WALL PRESSURE COEFFICIENT DISTRIBUTIONS ON CENTRE LINE OF MODELS OF VARYING HEIGHT RATIOS - 25% NORMAL PATTERN

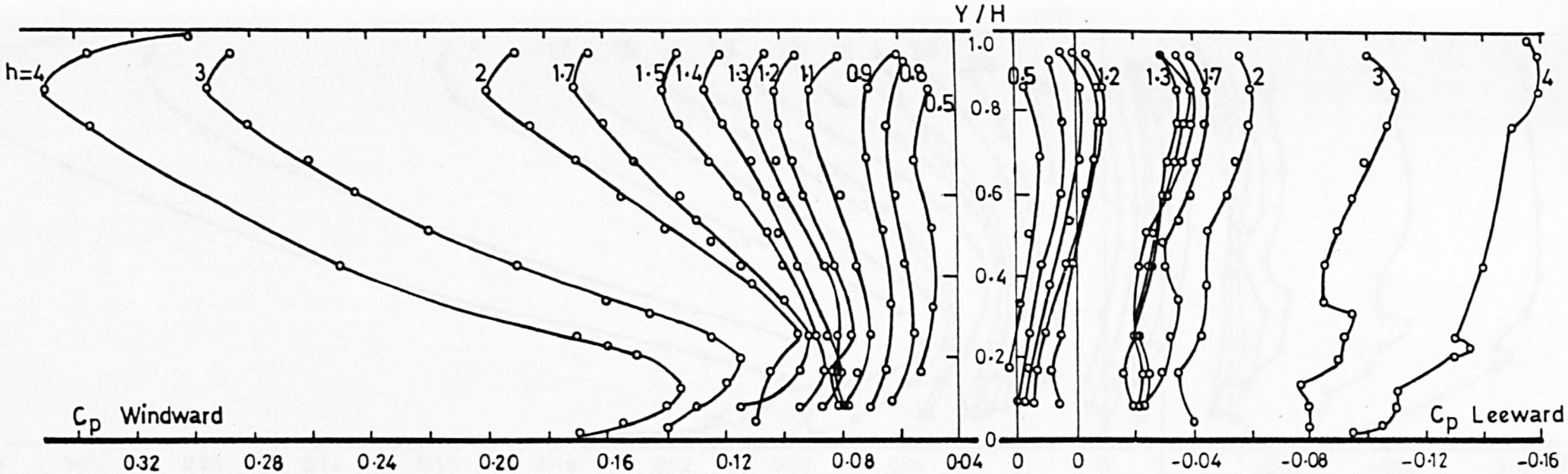

FIGURE 10.6 WALL PRESSURE COEFFICIENT DISTRIBUTIONS ON CENTRE LINE OF MODELS OF VARYING HEIGHT RATIOS - 10% STAGGERED PATTERN

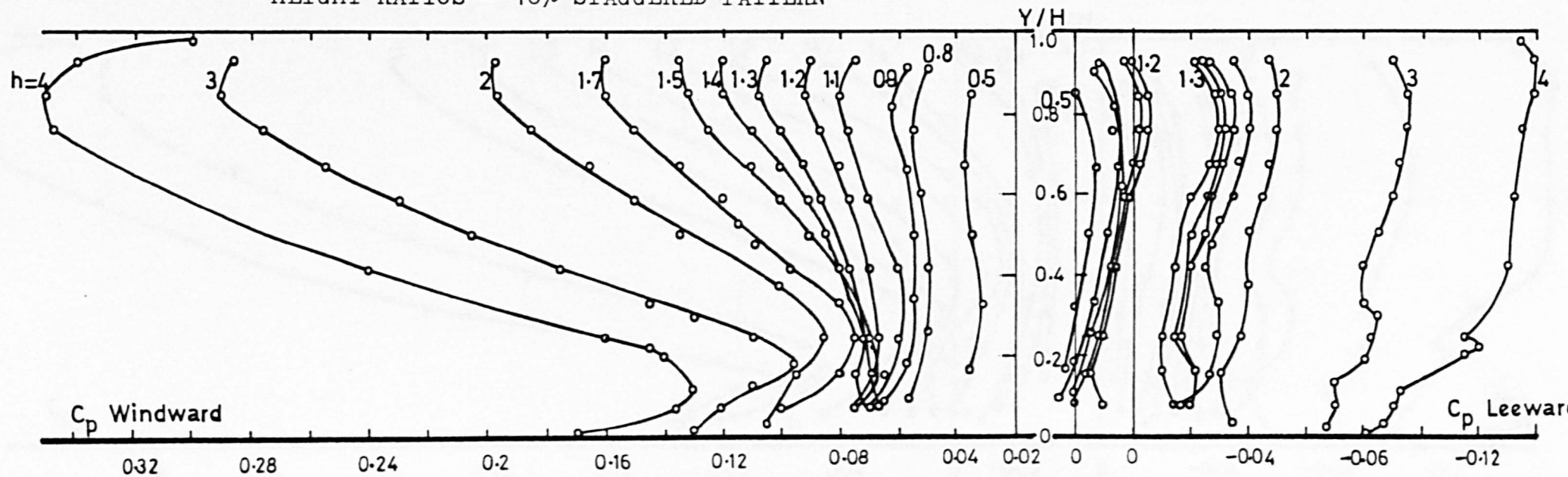

FIGURE 10.7 WALL PRESSURE COEFFICIENT DISTRIBUTIONS ON CENTRE LINE OF MODELS OF VARYING HEIGHT RATIOS, 12.5% STAGGERED PATTERN

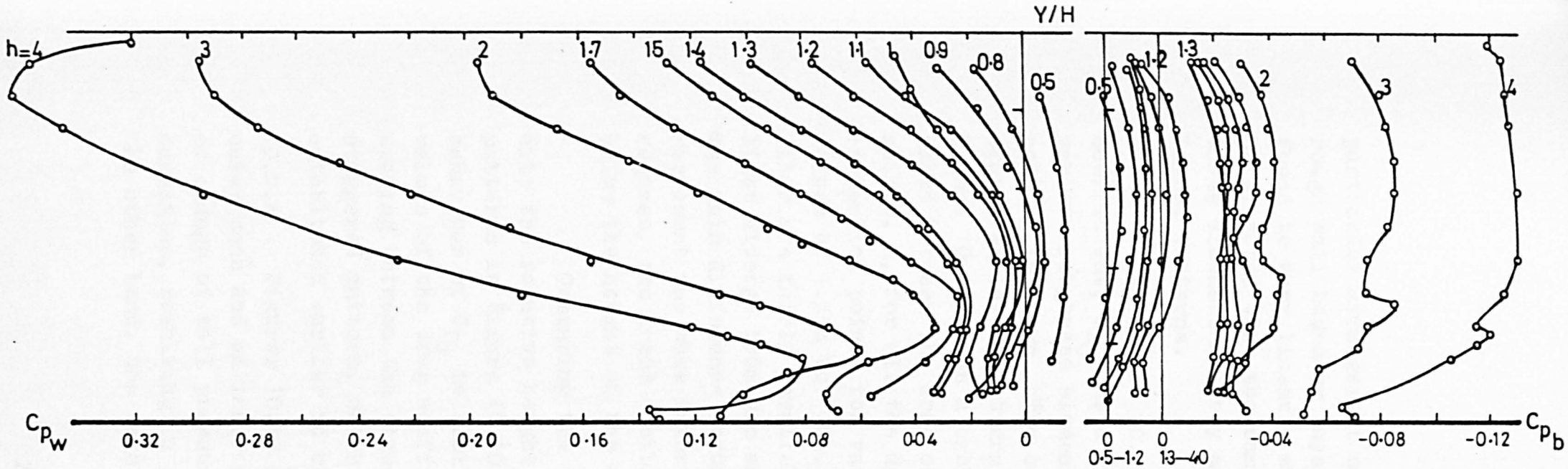

FIGURE 10.8 WALL PRESSURE COEFFICIENT DISTRIBUTIONS ON CENTRE LINE OF MODELS OF VARYING HEIGHT RATIOS, 25% STAGGERED PATTERN

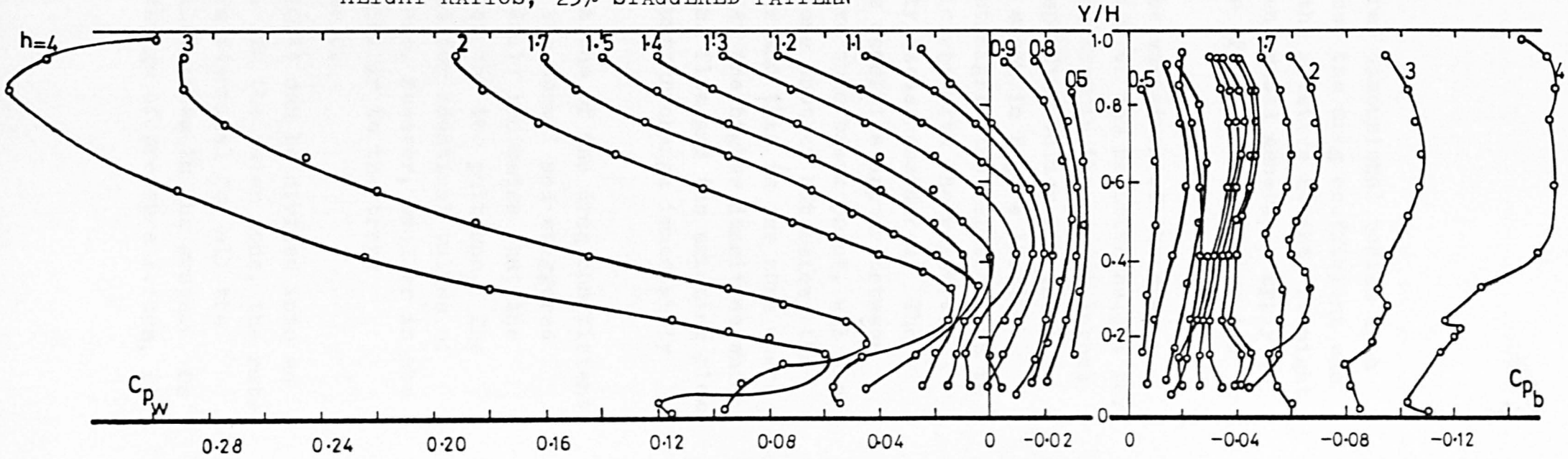

FIGURE 10.9 WALL PRESSURE COEFFICIENT DISTRIBUTIONS ON CENTRE LINE OF MODELS OF VARYING HEIGHT RATIOS, 40% STAGGERED PATTERN

particular arrangement of three dimensional bodies in a rough wall boundary layer flow, the drag coefficient was found to vary linearly with the relative height, it might be expected that the same trend would generally apply to three dimensional body arrays of various densities and layout patterns.

In Figure 10.10, the variation of the drag coefficient, C_{D_C}, as a function of the relative height for various roughness element densities in the normal layout pattern is shown. The corresponding values for the staggered layout pattern are shown in Figure 10.11. Figure 10.10 shows a broken straight line relationship to exist between the drag coefficient with the relative height, h, for all the density cases considered. The inflection points for various densities appear between values of 1.35h to 1.6h. Above this break point, all the lines are fairly parallel to one another but below, the lines diverge from one another and this is the zone where the main difference occurs. At the higher densities which represent the wake interference flow and the skimming flow regimes, the trend exhibits further change immediately below the height of the cube.

Comparing the variations of the drag coefficient with the relative height for the normal and staggered patterns in Figure 10.10 and 10.11 indicates that the behaviour of C_{D_C} is similar for the two patterns. The values of the drag coefficient for identical values of spacing between the elements are, however, smaller in the staggered pattern, which is similar to the trend established earlier in chapter 8.

10.2.4 Figures 10.10 and 10.11 can be divided into an outer zone and an inner zone. In the outer zone, the rate of change of wall pressures is identical for all the densities, resulting in parallel lines in the graph. On the other hand, the rate of change of pressure forces, in

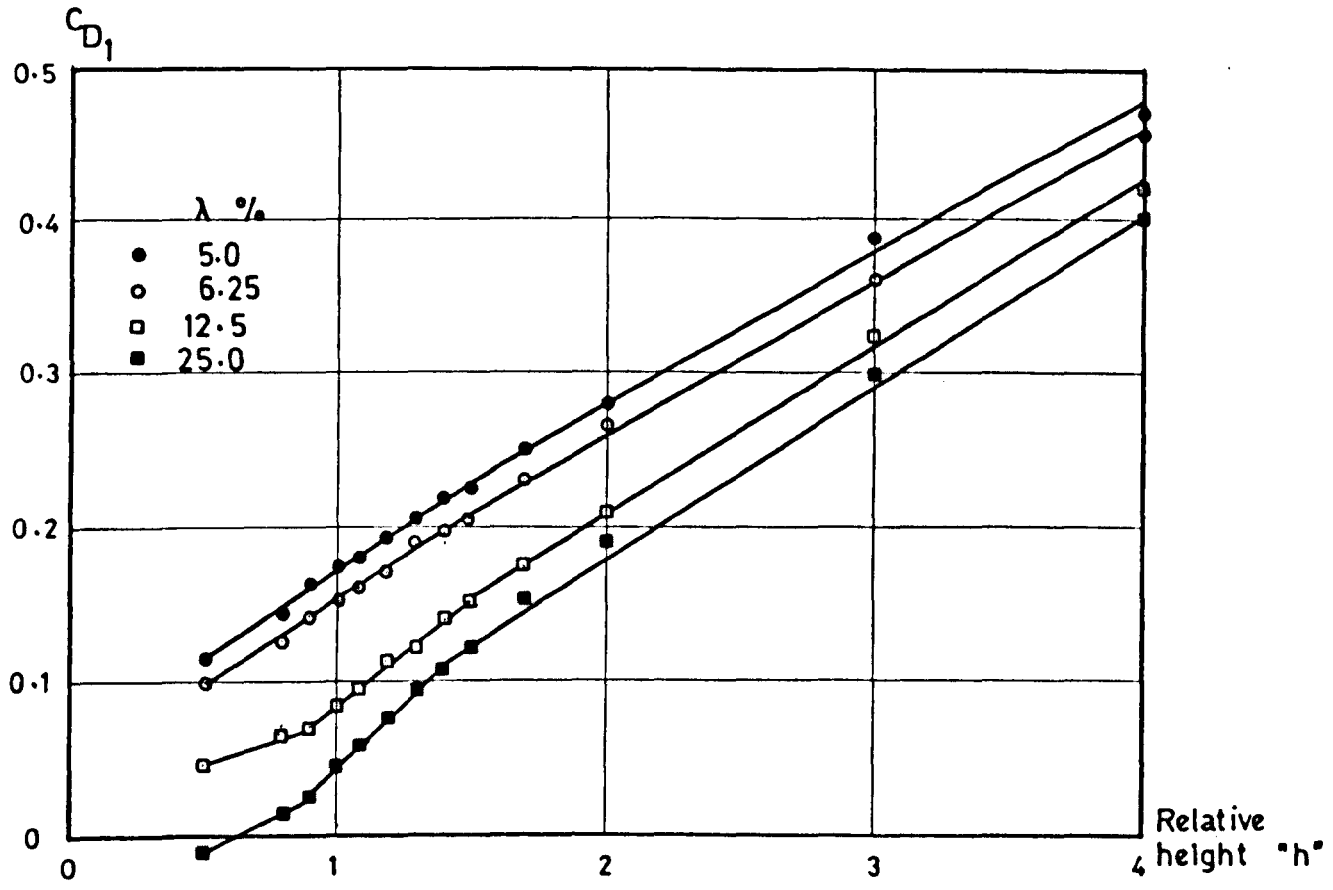

FIGURE 10.10 VARIATION OF C_{D_1} WITH THE RELATIVE HEIGHT - NORMAL PATTERN

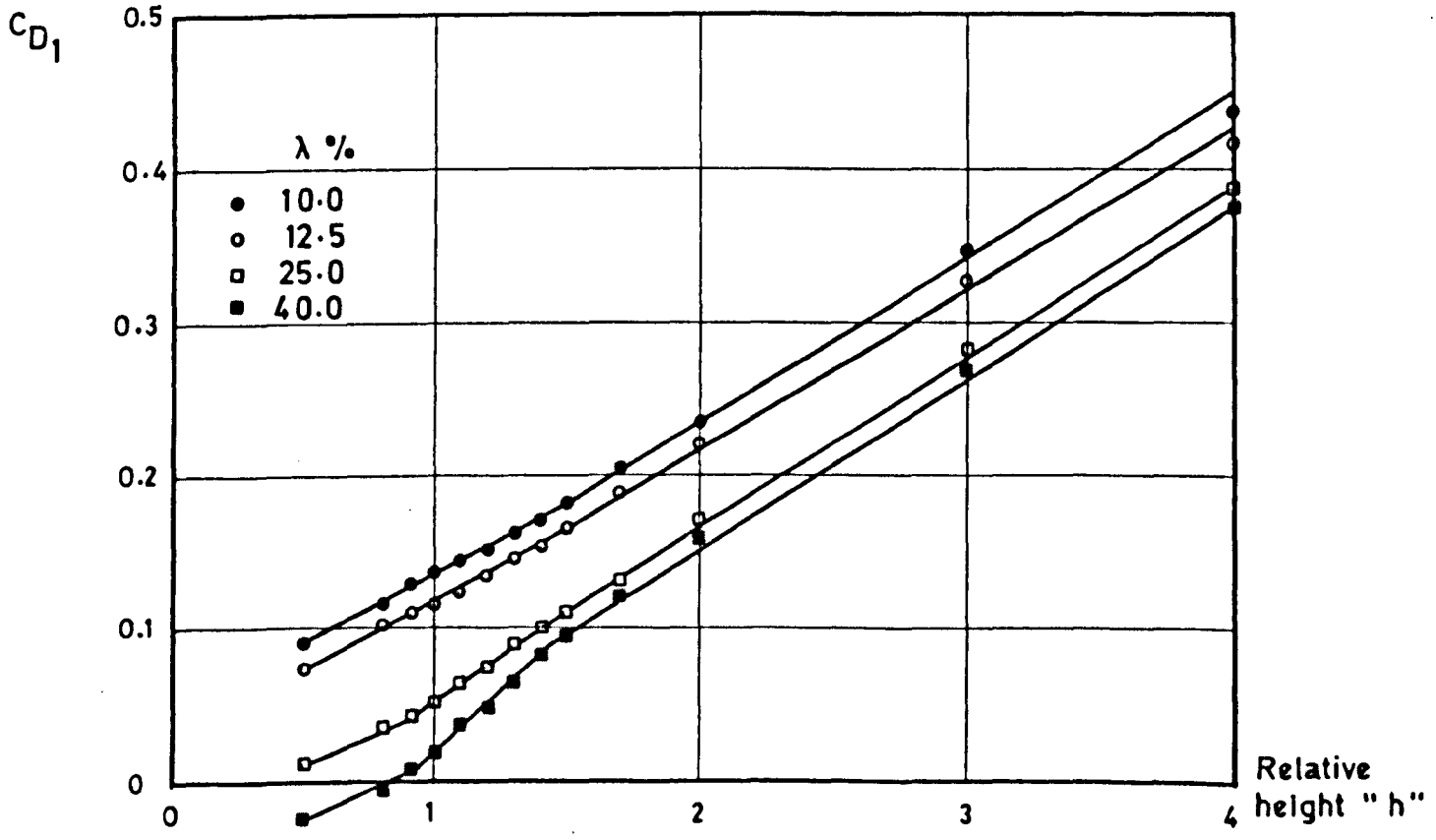

FIGURE 10.11 VARIATION OF C_{D_1} WITH THE RELATIVE HEIGHT - STAGGERED PATTERN

the inner zone, depends on the plan area density of the group layout. In this zone, the lines for various densities are no longer parallel except when they are in the same flow regime. It is suggested that in the outer zone the rate of change of pressure forces depends on the flow in the outer layer of the velocity profile which corresponds to the urban terrain atmospheric boundary layer simulated flow. This results in the lines being parallel in this zone. Conversely, the rate of change of wall pressures in the inner zone is governed by the inner layer profile which grows over the element arrays and results in different inner layer velocity profiles in each density. It is also found that the height at which the inflection points in various density cases appear correspond to the physical thickness of the inner layer growing over the model layout. The depth of the inner layer calculated in chapter 8 varies from 48mm to 56mm depending on the size of the model group in a particular density.

10.2.5 The linear variation of the drag coefficient with the relative height within the inner boundary layer substantiates the hypothesis that as the height of the individual body increases, the pressure coefficients as well as the drag coefficient on the body increase and vice versa. The trend shown by the present results also agrees with the hypothesis put forward by Joubert et al for three dimensional elements. This is, however, contrary to their results on two dimensional bodies, where they showed a rapid variation in drag coefficient of up to 70% with only 1% change in height. The rate of change of variation of the drag coefficient, governed by the inner layer profile, was shown to be different for all the densities considered in the present investigation. This again is not in line with the findings of Joubert et al that the drag coefficient is insensitive to small changes in height for two dimensional bodies with unstable vortices between them.

Figure 10.12 shows the present results for 10% density case in a staggered layout pattern and their comparison with the corresponding results for cubes in approximately 8.0% density in the identical layout pattern presented by Joubert et al. Both sets of results show a broadly similar trend though the magnitude and the rate of change of drag coefficient is different. This difference is thought to be due to the differing nature of the incident flows and the different ratios of boundary layer height to the element height in both the experiments.

10.2.6 It was shown in chapter 6 that for isolated models the drag coefficient normalised with respect to the velocity at model height, C_{D_H}, decreases sharply as the height increases before becoming constant at a value of $h \simeq 1.6$. The same general trend is shown to be true when the variable height model is surrounded by roughness arrays. Figure 10.13 shows the graph of C_{D_H} against the relative height, h, for the densities in the normal pattern. The figure shows a sudden decrease in the value of the drag coefficient, C_{D_H}, as the height increases, in all densities considered. The minimum value of C_{D_H} in various densities appears to occur at different height ratios which correspond to the physical thickness of the internal boundary layer in each case. Further increase in height, after the minimum value of C_{D_H} has been achieved, results in the graphs tending to become asymptotic at a value of C_{D_H} between 1.0 and 1.2 which is comparable to a value of 1.1 found in the case of isolated models.

10.3 Pressure measurements on the roof of models having varying height ratios

10.3.1 The pressure distributions on the roof of various models with varying heights were also studied. The pressure coefficient distributions on the centre line of the model roofs for various densities in both the normal and staggered patterns are shown in Figures 10.14 to 10.21. The

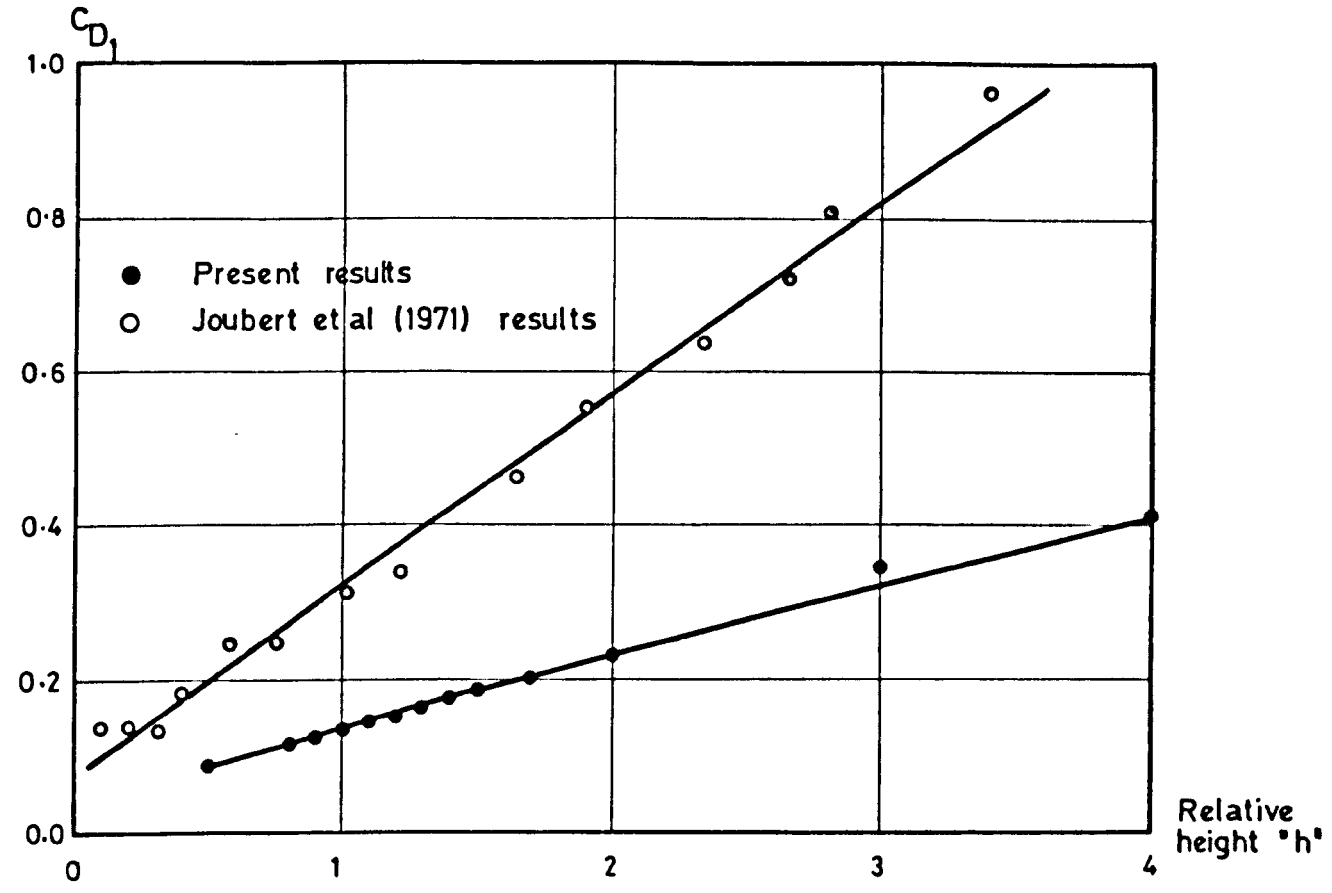

FIGURE 10.12 VARIATION OF C_{D_1} WITH RELATIVE HEIGHT AND ITS COMPARISON

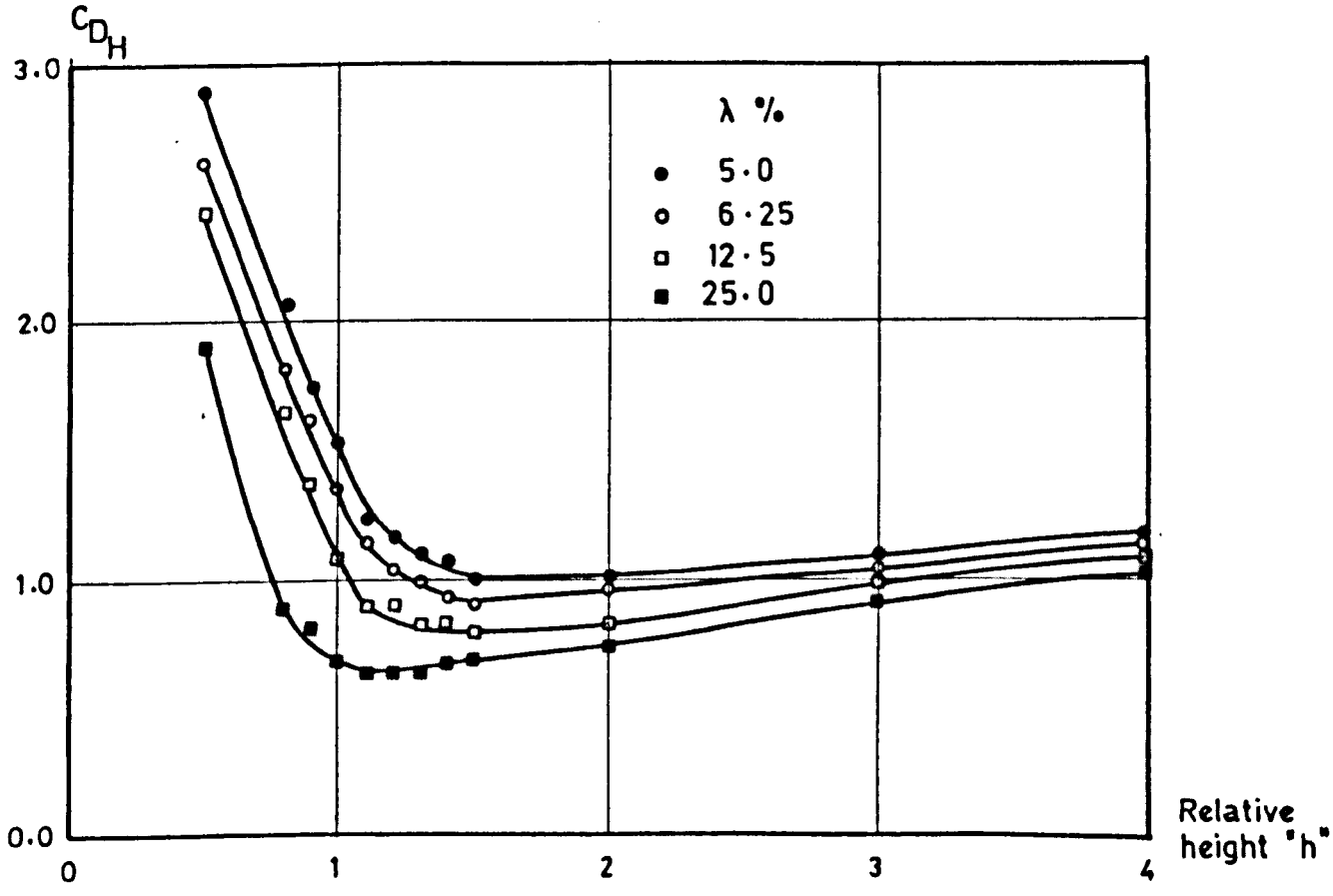

FIGURE 10.13 VARIATION OF C_{D_H} WITH RELATIVE HEIGHT

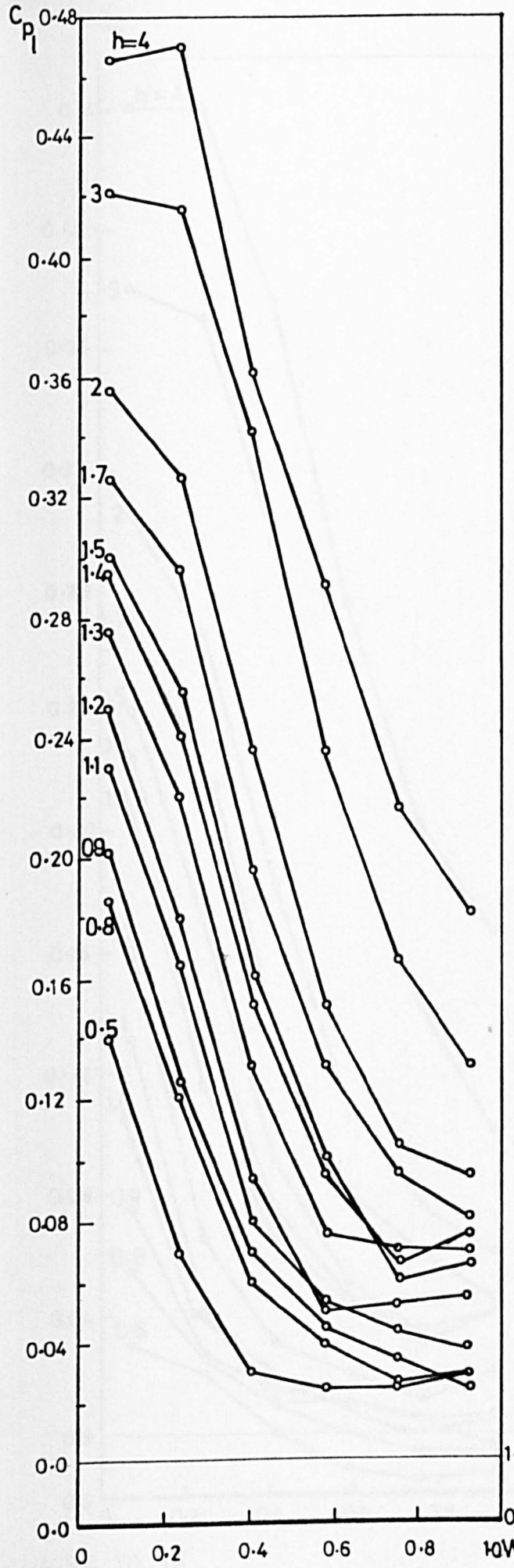

FIGURE 10.14

ROOF PRESSURE COEFFICIENT DISTRIBUTIONS FOR VARYING HEIGHT RATIO MODELS - 5% NORMAL PATTERN

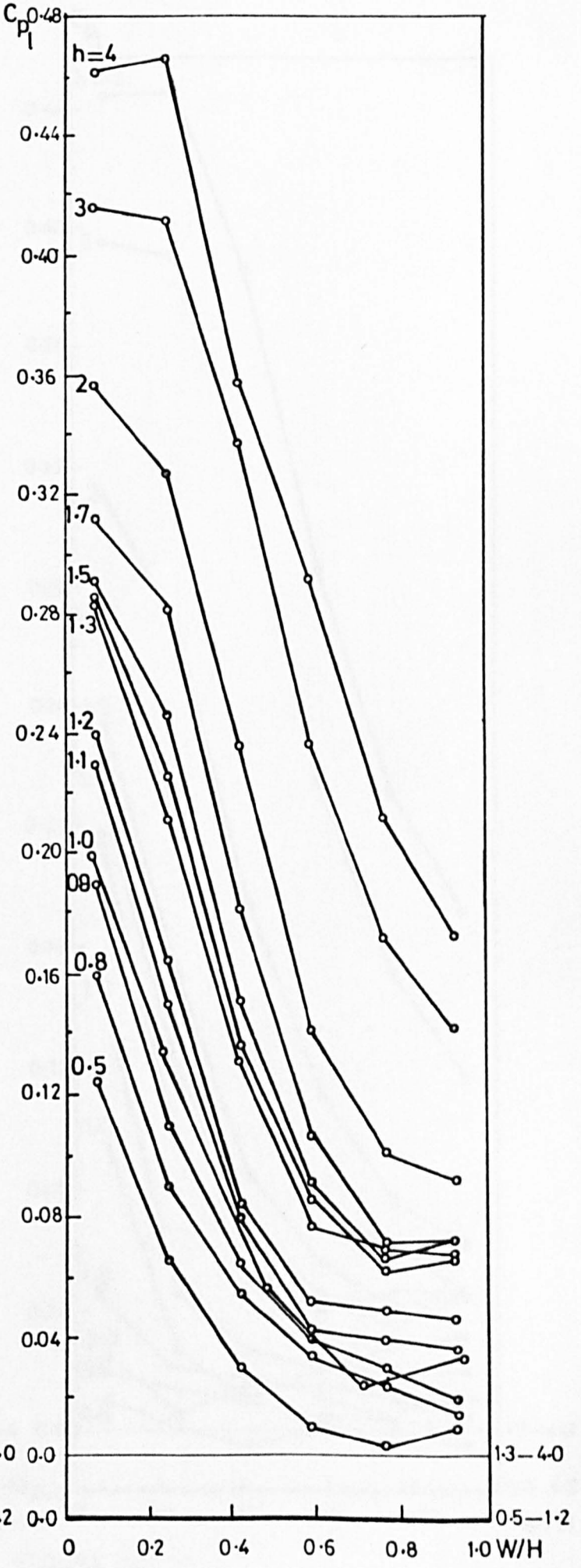

FIGURE 10.15

ROOF PRESSURE COEFFICIENT DISTRIBUTIONS FOR VARYING HEIGHT RATIO MODELS - 6.25% NORMAL PATTERN

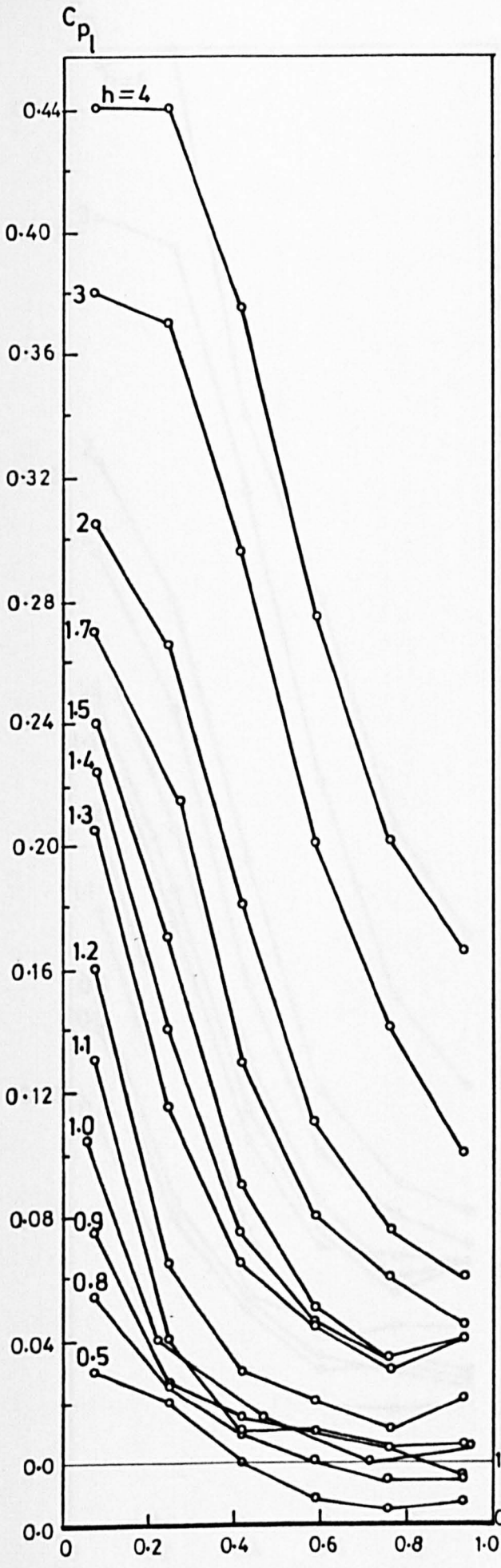

FIGURE 10.16

ROOF PRESSURE COEFFICIENT DISTRIBUTIONS FOR VARYING HEIGHT RATIO MODELS - 12.5% NORMAL PATTERN

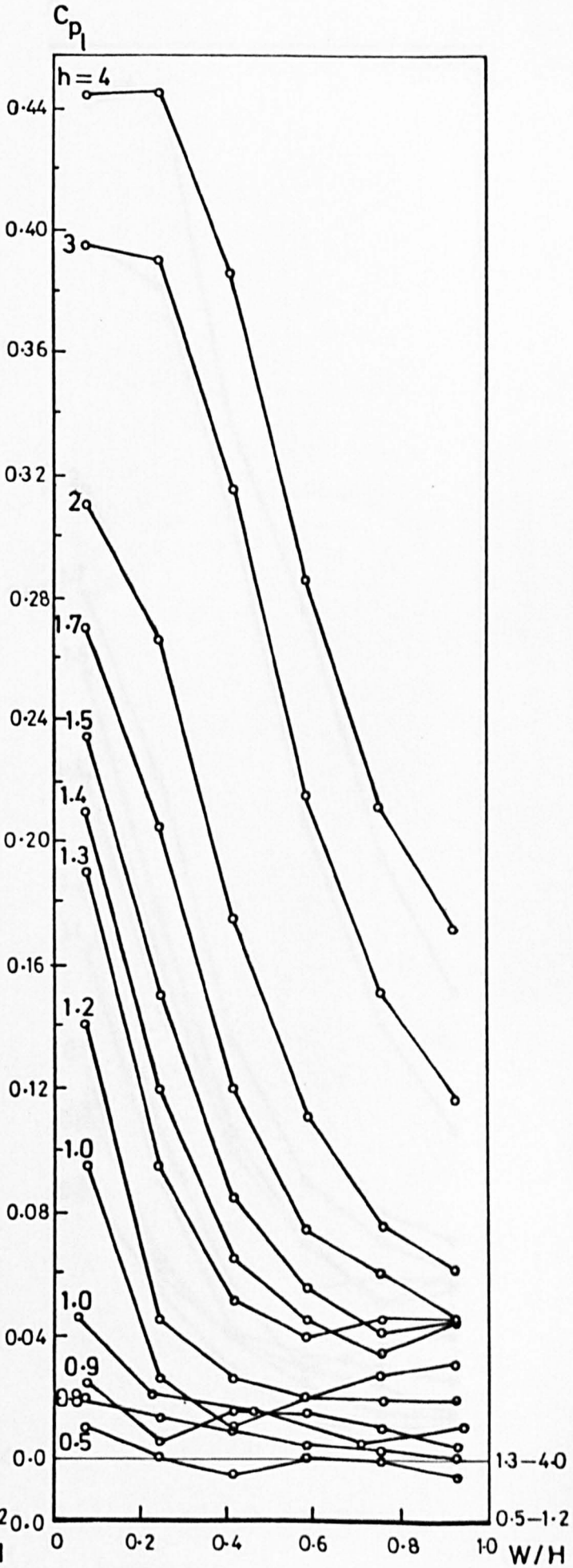

FIGURE 10.17

ROOF PRESSURE COEFFICIENT DISTRIBUTIONS FOR VARYING HEIGHT RATIO MODELS - 25% NORMAL PATTERN

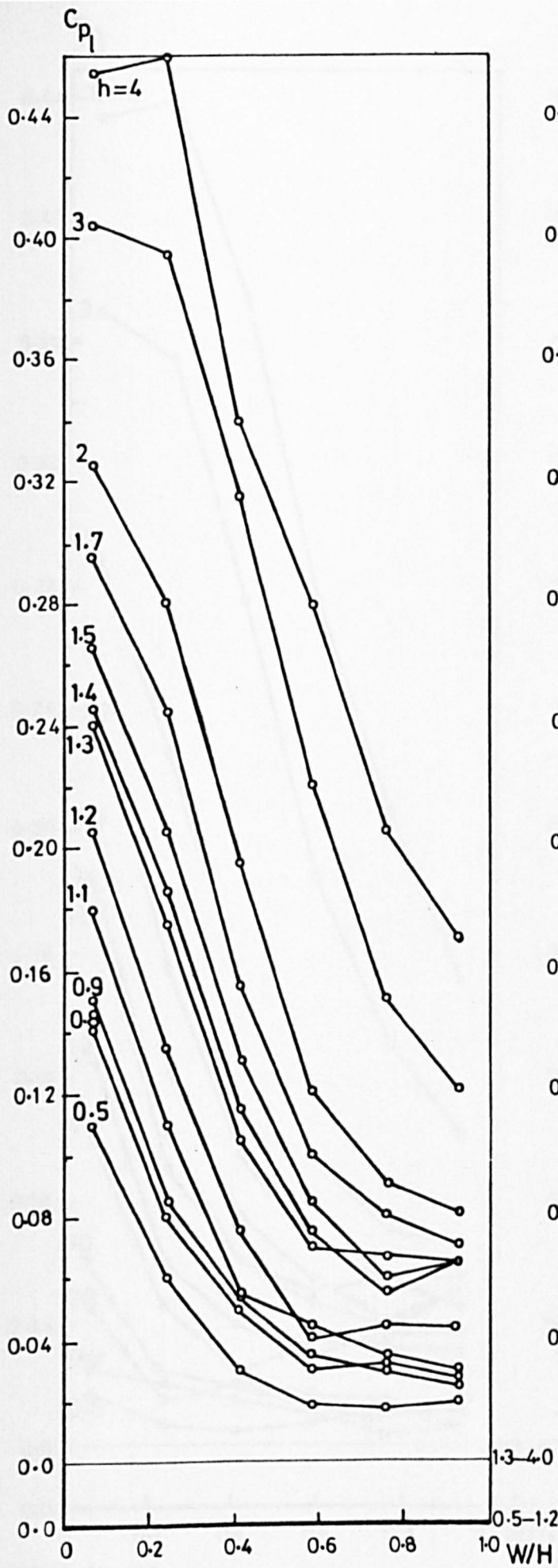

FIGURE 10.18

ROOF PRESSURE COEFFICIENT DISTRIBUTIONS FOR VARYING HEIGHT RATIO MODELS - 10% STAGGERED PATTERN

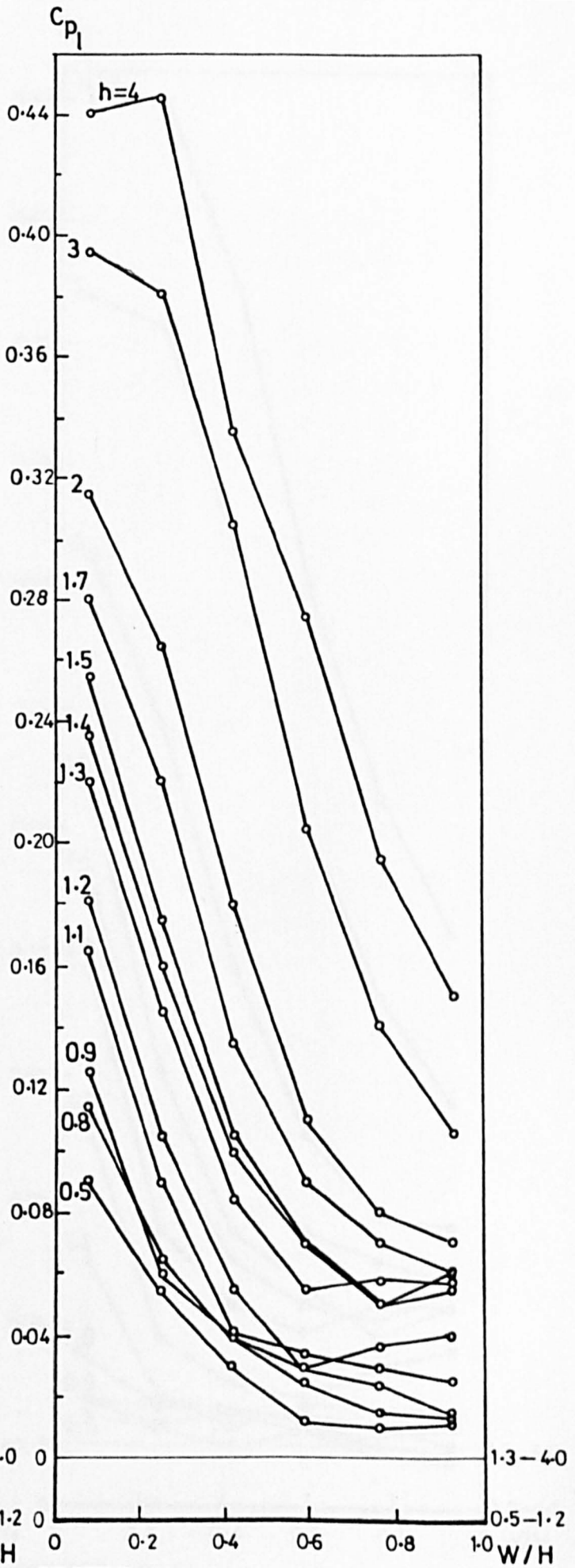

FIGURE 10.19

ROOF PRESSURE COEFFICIENT DISTRIBUTIONS FOR VARYING HEIGHT RATIO MODELS - 12.5% STAGGERED PATTERN

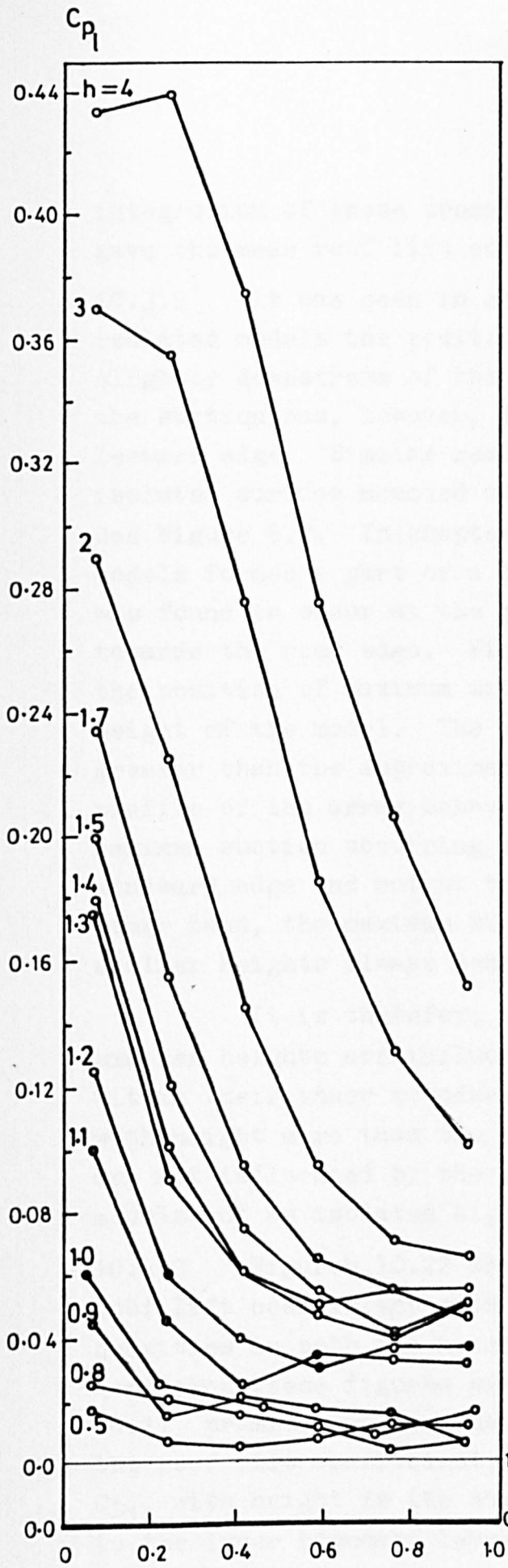

FIGURE 10.20

ROOF PRESSURE COEFFICIENT DISTRIBUTIONS FOR VARYING HEIGHT RATIO MODELS – 25% STAGGERED PATTERN

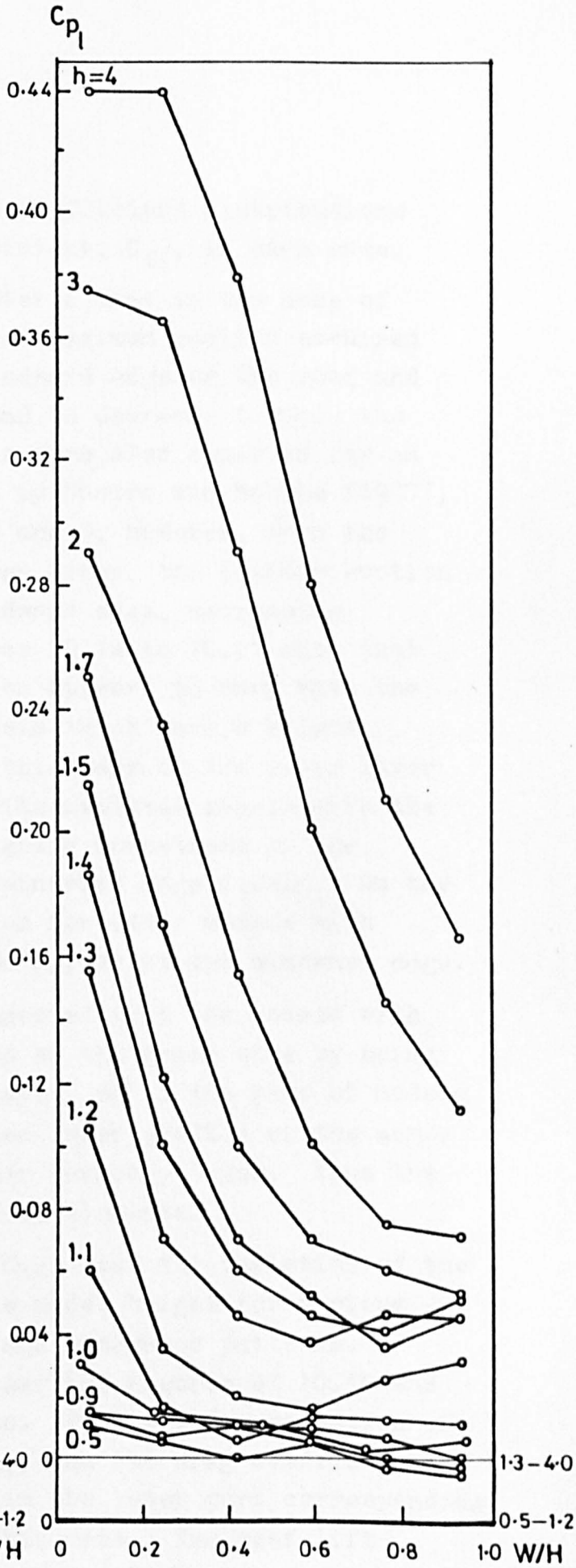

FIGURE 10.21

ROOF PRESSURE COEFFICIENT DISTRIBUTIONS FOR VARYING HEIGHT RATIO MODELS – 40% STAGGERED PATTERN

integration of these pressure coefficient distributions gave the mean roof lift coefficient, C_{L_1}, in each case.

10.3.2 It was seen in chapter 6 that in the case of isolated models the position of maximum suction occurred slightly downstream of the windward edge of the roof and the suction was, however, found to decrease towards the leeward edge. Similar results were also observed for an isolated surface mounted cube by Castro and Robins (1977), see Figure 6.2. In chapter 8 and 9, however, when the models formed a part of a large array, the maximum suction was found to occur at the windward edge, decreasing towards the rear edge. Figures 10.14 to 10.21 show that the position of maximum suction appears to vary with the height of the model. The models which have a height greater than the approximate thickness of the inner layer profile of the array behave like isolated models with the maximum suction occurring slightly downstream of the windward edge and not at the windward edge itself. On the other hand, the maximum suction for other models with smaller heights always seem to appear at the windward edge.

It is therefore suggested that the models with smaller heights are influenced by the array size by being within their inner boundary layer, while the roof of models with height more than the inner layer profile of the array are not influenced by the inner boundary layer. Thus the models act as isolated high rise elements.

10.3.3 Figures 10.22 and 10.23 show the variation of the roof lift coefficient with the model height for various densities in both the normal and staggered patterns. Comparing these figures with earlier figures of 10.10 and 10.11 prompts two conclusions. Firstly, the variation of the roof lift coefficient, C_{L_1}, and the drag coefficient, C_{D_1}, with height is the same in the lower part corresponding to the inner boundary layer thickness. The roof lift coefficient varies linearly with height in this region.

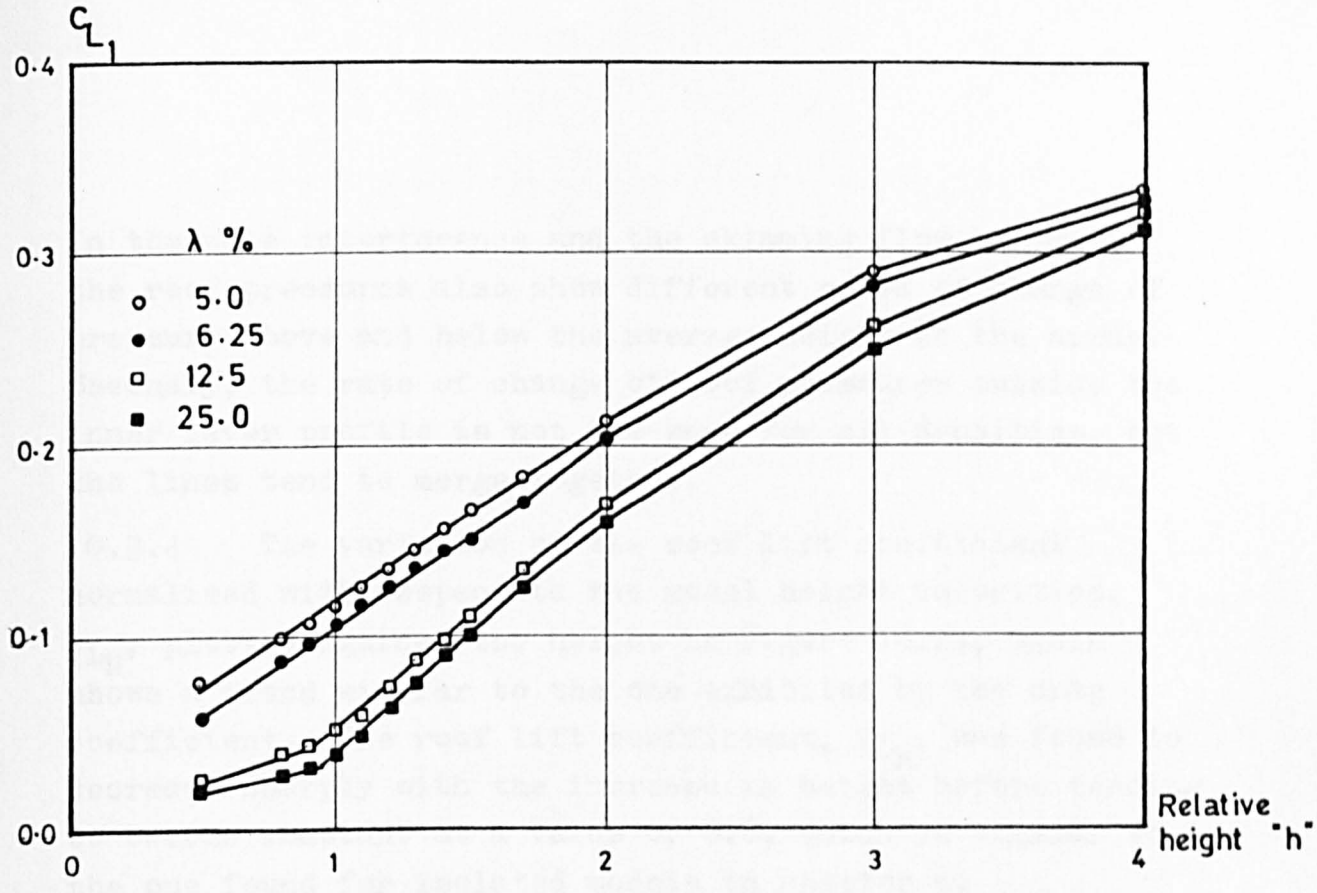

FIGURE 10.22 VARIATION OF C_{L_1} WITH RELATIVE HEIGHT - NORMAL PATTERN

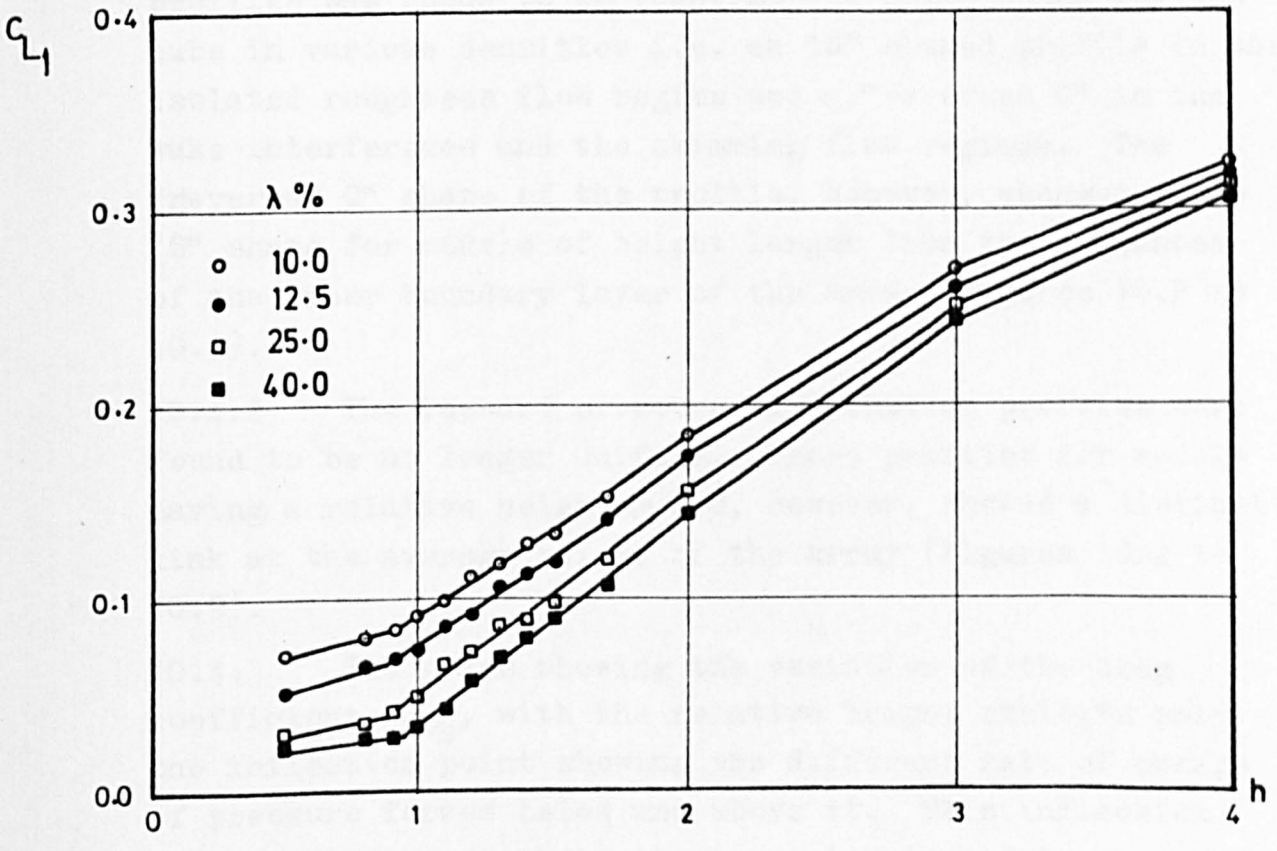

FIGURE 10.23 VARIATION OF C_{L_1} WITH RELATIVE HEIGHT - STAGGERED PATTERN

In the wake interference and the skimming flow regimes, the roof pressures also show different rates of change of pressure above and below the average height of the array. Secondly, the rate of change of roof pressures outside the inner layer profile is not the same for all densities, but the lines tend to merge together.

10.3.4 The variation of the roof lift coefficient normalised with respect to the model height velocities, C_{L_H}, plotted against the height in Figure 10.24, again shows a trend similar to the one exhibited by the drag coefficient. The roof lift coefficient, C_{L_H}, was found to decrease sharply with the increase in height before tending to become constant at a value of 0.8, which is similar to the one found for isolated models in chapter 6.

10.4 Conclusions

10.4.1 The shape of the windward pressure distribution profiles was found to be identical to those found for the cube in various densities i.e. an "S" shaped profile in the isolated roughness flow regime and a "reversed C" in the wake interference and the skimming flow regimes. The "reversed C" shape of the profile, however, changed to an "S" shape for models of height larger than the thickness of the inner boundary layer of the array (Figures 10.2 to 10.9).

10.4.2 The leeward pressure distribution profiles were found to be no longer uniform. These profiles for models having a relative height $\geqslant 2.0$, however, showed a distinct kink at the average height of the array (Figures 10.2 to 10.9).

10.4.3 The graph showing the variation of the drag coefficient, C_{D_c}, with the relative height exhibits only one inflection point showing the different rate of change of pressure forces below and above it. This inflection appears at a point where the inner layer profile merges

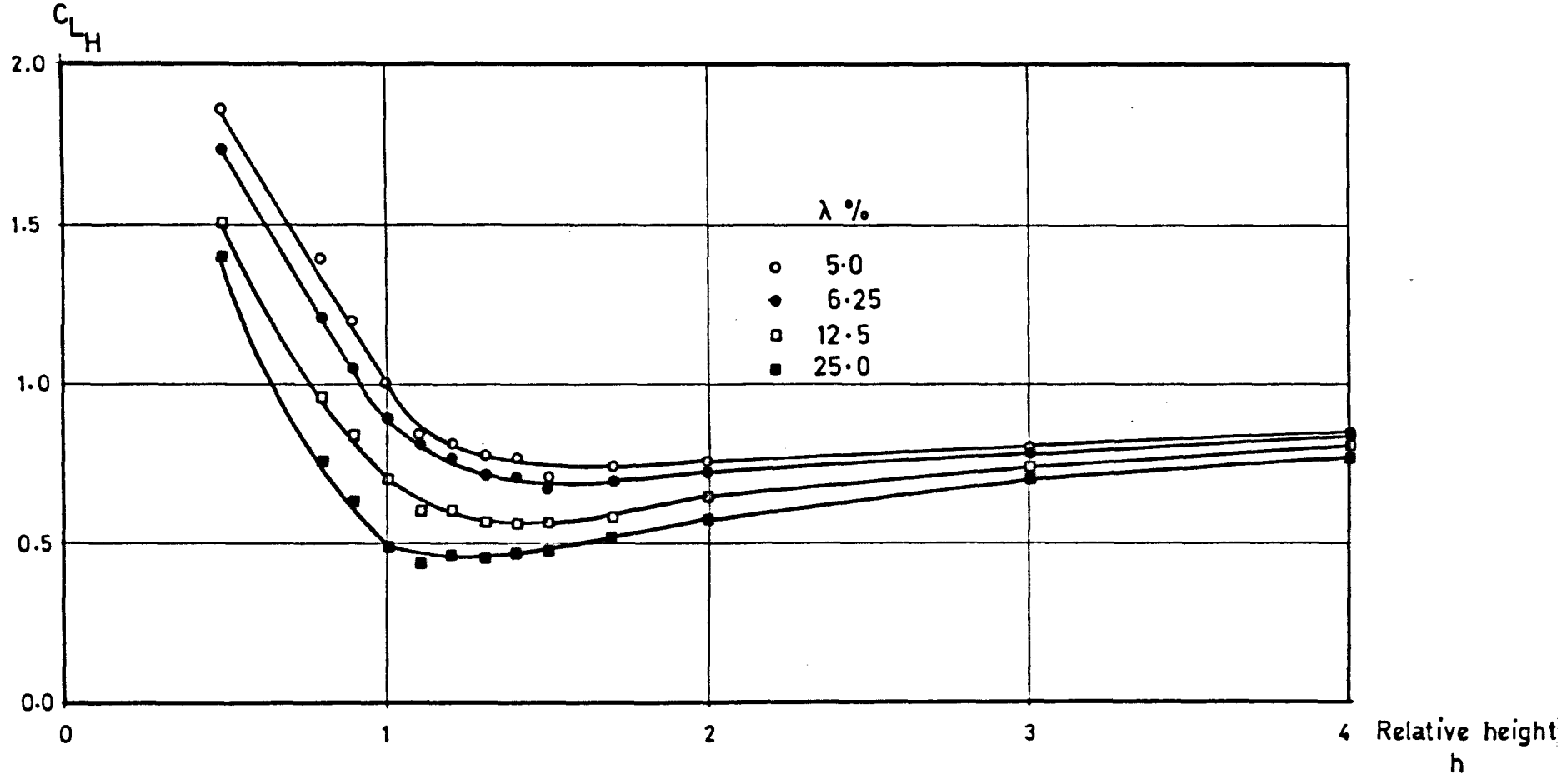

FIGURE 10.24 VARIATION OF C_{L_H} WITH RELATIVE HEIGHT

into the outer layer profile. The relative height at which this change appears varies from 1.35 to 1.6 depending upon the model fetch length in various densities (Figures 10.10 and 10.11).

10.4.4 The linear variation of C_{D_c} below this inflection point shows that the drag coefficient increases as the height increases and vice versa. Above this break point, the rate of change of pressure forces is governed by the outer layer of the profile which corresponds to the urban terrain atmospheric boundary layer simulated flow and hence is identical for various densities (Figures 10.10 and 10.11).

10.4.5 The value of the drag coefficient normalised with respect to the velocity at model heights, C_{D_H}, in all cases considered, was found to be large for buildings of smaller heights. Its value decreased as the height increased in the inner layer profile. In the outer layer profile, the value of C_{D_H} tended to become constant at a value of 1.1 found for isolated high rise buildings in chapter 6 (Figure 10.13).

10.4.6 The roof pressure coefficients were found to be negative for all models. The maximum suction for models lying within the inner layer profile appeared at the windward edge, while the maximum suction for models with height larger than the inner layer profile was found to lie downstream of the windward edge (Figures 10.14 to 10.21).

10.4.7 The roof lift coefficient varies linearly with the height in the lower part which corresponds to the inner boundary layer thickness. In higher densities, however, the rate of change of roof pressures is different below the average height of the array. Outside the inner layer profile, the rate of change of roof pressures is also different for different densities and the lines tend to merge together (Figures 10.22 and 10.23).

10.4.8 The value of the roof lift coefficient, C_{L_H}, was also found to decrease sharply with the increase in height in all densities before becoming constant at a value of 0.8. This value is identical to the corresponding value found for isolated high rise buildings in chapter 6 (Figure 10.24).

CHAPTER 11

GENERAL APPLICATION TO THE INFILTRATION CALCULATIONS OF LOW RISE BUILDING ARRAYS

11. GENERAL APPLICATION TO THE INFILTRATION CALCULATIONS OF LOW RISE BUILDING ARRAYS

11.1 Introduction

11.1.1 The crack method of natural ventilation calculations as described in the IHVE guide (1970) has been outlined in chapter 1, where it was shown how an infiltration chart is utilised to determine the infiltration rate. The infiltration chart given in Figure 11.1 is based on Jackman's (1969) study of natural ventilation for an isolated tall office building and provides a simple infiltration calculation technique from the knowledge of wind speed, the height and location of the buildings as well as the quality of windows. It does not, however, take into account some of the other relevant factors affecting the pressure difference, ΔC_{p_o}, across buildings. Furthermore, the infiltration rates calculated from this chart can be only applied to isolated high rise buildings.

11.1.2 In order to be applicable to low rise buildings, the building form and their group geometry alongwith the flow properties should be considered. These parameters have been considered in the previous chapters where a wide range of building forms were investigated in a simulated atmospheric boundary layer flow. With the detailed experimental data from the previous chapters, an attempt is made in this chapter to present an additional method of determining ΔC_p for low rise buildings which will eventually replace the left hand portion of the IHVE chart. From the pressure measurements made on the roof of various buildings, a separate procedure for determining ΔC_L has also been suggested.

11.1.3 A similar study was made by Soliman (1976) in which he investigated a wide range of building forms in a rough wall turbulent boundary layer flow and proposed a set of graphs replacing the left hand side of the IHVE chart for infiltration. The validity of his findings is, however,

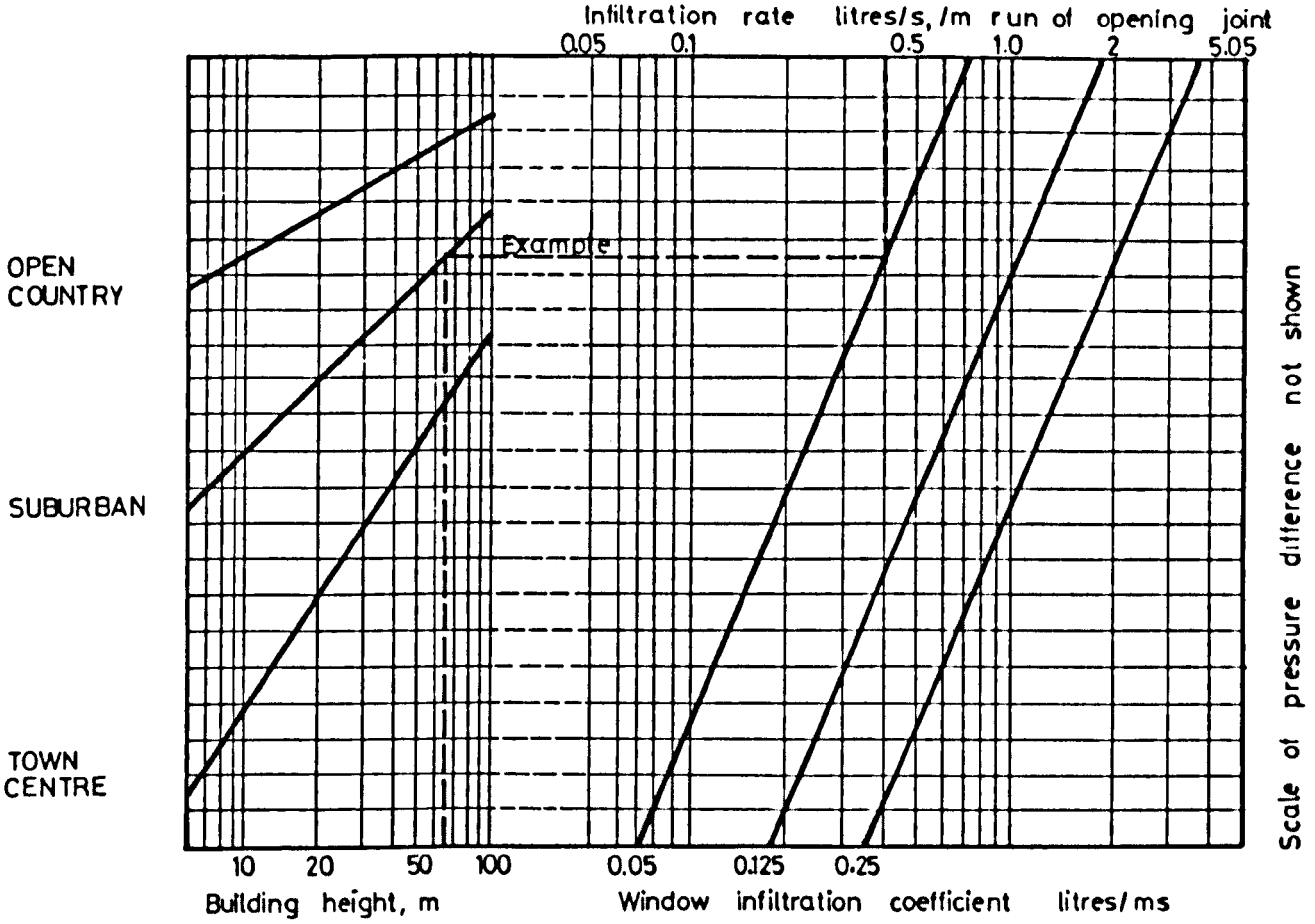

FIGURE 11.1 THE IHVE GUIDE : INFILTRATION CHART

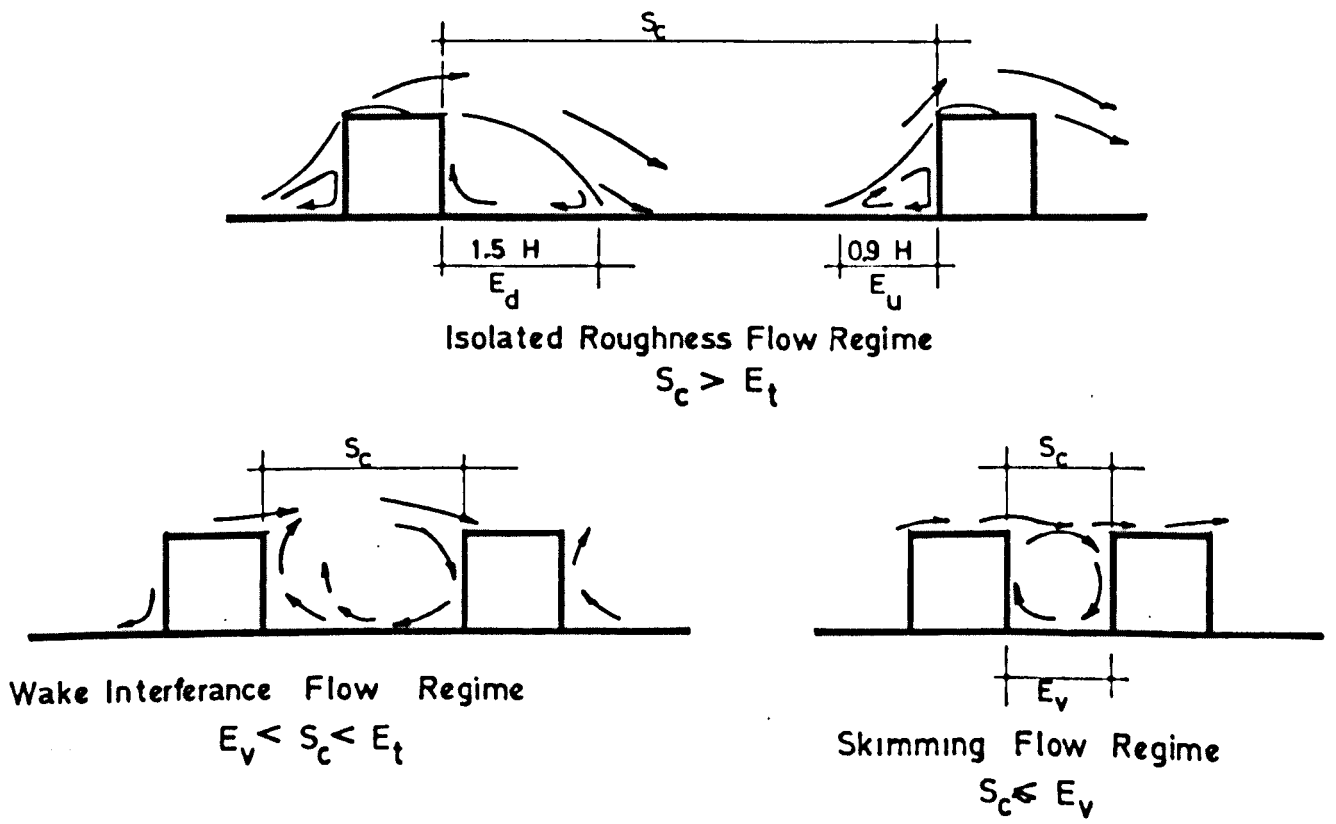

FIGURE 11.2 THE GOVERNING CONDITIONS FOR THE THREE FLOW REGIMES

questionable for two reasons: firstly the investigation was not carried out in an accurate simulation of the natural wind properties and secondly, his work for most building shapes was restricted to surface flow visualisation tests and therefore quantitative estimates of ΔC_p were not possible except in the case of cube shaped buildings. In addition to that, his results were confined to the pressure measurements on the vertical faces of the buildings and no mention of infiltration through the roof was made.

11.2 The flow regimes for various building shapes

11.2.1 The variation of the pressure forces and the velocity profile parameters with building density are shown in chapters 7 to 10. The rate of change of surface pressure forces and the limits of flow regimes for various building densities were found to be different for different individual building shapes in the previous chapters. It is, therefore, essential that the flow regimes of any building group must be defined first if any estimates of the pressure forces on them are to be made.

11.2.2 In chapter 8, it has been clearly demonstrated that the first change of regime from the isolated roughness flow to the wake interference flow regime depends on the distance of upstream separation and downstream reattachment around the cubes. The second change from the wake interference flow regime to the skimming flow regime coincides with the initiation of a stable vortex in the space between the cubes. These conditions for the flow regime limits may then be expressed as follows for the isolated roughness flow regime:

$$S_c/H > E_t/H \qquad (11.1)$$

where E_t is the sum of the upstream separation and the downstream reattachment distances E_u and E_d around the cube respectively and S_c is the clear spacing between buildings

and H is the height of buildings. For the wake interference flow regime

$$E_v/H < S_c/H < E_t/H \qquad (11.2)$$

where E_v is the stable vortex dimension in the flow direction and for the skimming flow regime

$$S_c/H < E_v/H \qquad (11.3)$$

These are shown schematically in Figure 11.2.

11.2.3 The three flow regimes for different building shapes were defined in chapter 9 where the effect of varying both the frontal as well as the side aspect ratio was investigated. It was found that the element spacing S_c/H at which the isolated roughness flow regime changes to wake interference flow regime, increases with the increase of frontal aspect ratio within the range considered, Figures 9.6 to 9.9 and 9.11. These figures also show that the change from wake interference flow regime to the skimming flow regime is relatively less sensitive to the element spacing when compared to the first change.

On the other hand, as the side aspect ratio increases, the element spacing at which the flow regime changes from isolated roughness flow to the wake interference flow regime is a function of the side aspect ratio more so for short afterbody models than for longer ones. Once the side length is sufficient for the flow to have reattached on the roof and the sides, the element spacing at which this change appears becomes insensitive, Figures 9.18 to 9.20 and 9.22. Conversely the change from wake interference flow regime to the skimming flow regime is unaffected by the side aspect ratio.

11.2.4 The dependence of the downstream reattachment distance E_d on the frontal aspect ratio L/H has been reported by Evan (1957) and Soliman (1976) for different building shapes and side aspect ratios. Conversely the upstream separation distance E_u seems to be of the same order as the building height, H, for a wide range of values of L/H studied by them. As the change from isolated roughness flow regime to the wake interference flow regime is directly related to the downstream reattachment distance, the present results substantiate the findings of Evan and Soliman. On the other hand, the relative insensitivity of the element spacing for a change from the wake interference flow to the skimming flow regime seems to agree with the findings of previous studies reported on the flow over rectangular cutouts and grooves, Rushko (1955), Tani et al (1961) and Maull et al (1963).

11.2.5 The results of Evan and Soliman showed that the effect of changing the side aspect ratio is not of prime importance. This is found to be true in the case of change from wake interference flow regime to the skimming flow regime, while the change from the isolated roughness flow to wake interference flow regime does appear at varying values of element spacing for short afterbody models. For long afterbody models, however, the element spacing at which this change appears remains constant.

11.2.6 When the work reported by Evan was plotted for the variation of E_d/H with the frontal aspect ratio L/H for different values of W/H, it was found that the downstream reattachment distance increases with L/H, Figure 11.3. It may also be noted from the figure that E_d/H tends to a constant value after a certain size of $L/H \simeq 10$. It can thus be assumed that for buildings with frontal aspect ratios $\geqslant 10$, the flow regime changes will occur at similar values of element spacing. Similar results were also reported by Soliman (1976). As the frontal aspect ratio in the present investigation could not be varied up to these limits, their

results will be used as such in the subsequent analysis.

11.3 Variation of drag coefficient C_{D_H} with frontal aspect ratio of buildings

11.3.1 The probable value of ΔC_{p_o} across the opposite faces of a building within a group of similar form and height can be estimated if the information about the individual form, the group form, the building fetch and its orientation with respect to the oncoming wind is known. These parameters have been discussed fully in the previous chapters. Their application to infiltration calculations is discussed below in a systematic manner.

11.3.2 For ventilation purposes, the building surface pressures are usually normalised with respect to the velocity pressure at the building roof height giving C_{D_H}. The roof height velocities obtained from the velocity profile measurement results given in Figure 8.36 and 9.40 for cube shaped elements and the element with a frontal aspect ratio of 2.0 were used respectively to convert the experimental values of C_{D_1} into C_{D_H} using the following relationship

$$C_{D_H} = C_{D_1}(U_1/U_H)^2 \qquad 11.4$$

When these results of C_{D_H} obtained were plotted against S_c/H, broken line relationships were obtained for both the models, Figure 11.4. It may also be noted from this figure that the inflections in the graphs correspond to the changes of flow regimes found for both models in chapter 8 and 9 where S/H was plotted against C_{D_1}. Furthermore, both the lines corresponding to the skimming flow regime can be represented by a single line within the limits of experimental scatter, and give a value of C_{D_H} as zero at $S_c/H = 0$.

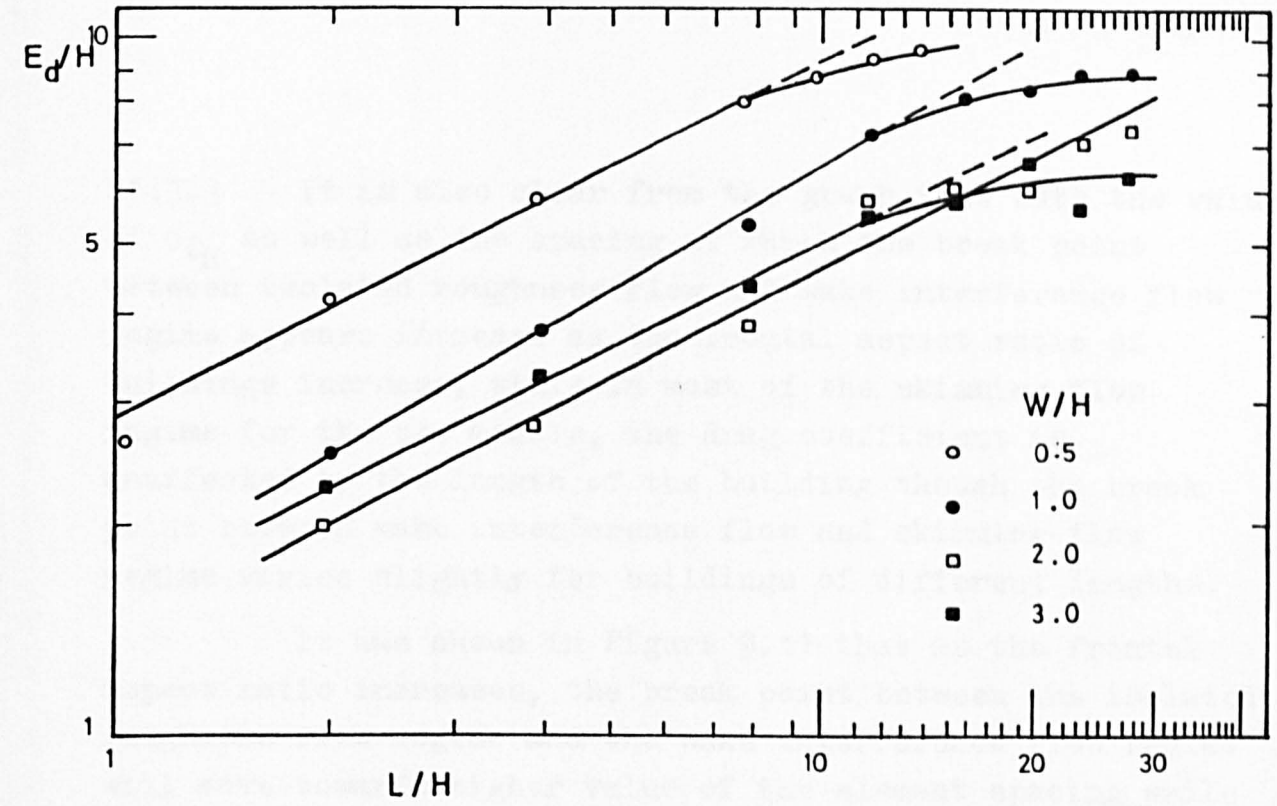

FIGURE 11.3 VARIATION OF E_d/H WITH L/H AFTER EVANS' (1957) RESULTS.

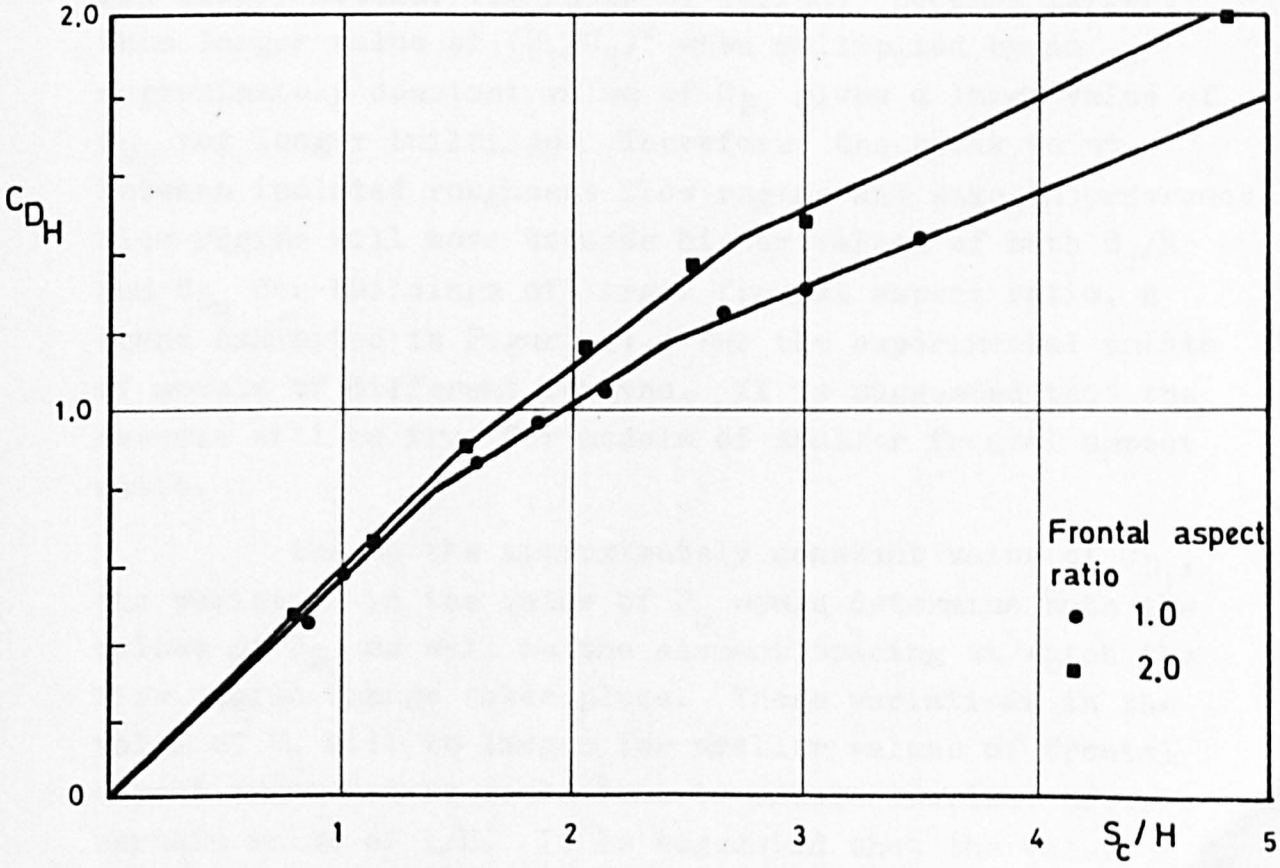

FIGURE 11.4 VARIATION OF C_{D_H} WITH S_c/H - EXPERIMENTAL RESULTS

11.3.3 It is also clear from the graph that both the value of C_{D_H} as well as the spacing at which the break point between isolated roughness flow and wake interference flow regime appears increase as the frontal aspect ratio of buildings increase, while in most of the skimming flow regime for the two models, the drag coefficient is unaffected by the length of the building though the break point between wake interference flow and skimming flow regime varies slightly for buildings of different lengths.

It was shown in Figure 9.11 that as the frontal aspect ratio increases, the break point between the isolated roughness flow regime and the wake interference flow regime will move towards higher value of the element spacing while the value of C_{D_1} remains approximately constant. It has also been shown in earlier figures of 8.36 and 9.40 that the velocity at the model height U_H decreases as the frontal aspect ratio increases. As a result of smaller values of U_H for longer models, the ratio of $(U_1/U_H)^2$ becomes larger. This larger value of $(U_1/U_H)^2$ when multiplied by an approximately constant value of C_{D_1} gives a large value of C_{D_H} for longer buildings. Therefore, the break point between isolated roughness flow regime and wake interference flow regime will move towards higher values of both S_c/H and C_{D_H} for buildings of larger frontal aspect ratio, a trend exhibited in Figure 11.4 for the experimental points of models of different lengths. It is suggested that the reverse will be true for models of smaller frontal aspect ratio.

Due to the approximately constant value of C_{D_1}, the variation in the value of U_H would determine both the values of C_{D_H} as well as the element spacing at which the flow regime change takes place. These variations in the value of U_H will be larger for smaller values of frontal aspect ratio and it would tend to become constant after a certain value of l/H. It is suggested that the value of U_H will become constant for models long enough to give constant

values of downward reattachment distance. The flow regime change will also be affected in a similar manner and it will tend to become constant for longer models.

As the change from wake interference flow regime to skimming flow regime is relatively less sensitive to the frontal aspect ratio of models (Figure 9.11) the element spacing at which this change appears for various models will vary only slightly, a trend also reflected in Figure 11.4 for two models. It is, therefore, concluded that the break point between wake interference flow and skimming flow regime will also move towards higher value of S_c/H for larger values of frontal aspect ratio, though the change will be small, compared to the first change of flow regime.

11.3.4 The experimental data given in Figure 11.4 for two buildings with frontal aspect ratios of 1 and 2 was based on the velocity profile measurements for these building models. As the velocity profile measurements for other models were not available, the relationship between U_H/U_1 and S_c/H given in Figures 8.36 and 9.40 for the two models was used to extrapolate the velocities at model heights for the remaining three models with the frontal aspect ratio as 0.5, 1.5 and 4.0 for which the pressure measurements were available.

It has been found earlier that U_H decreases with the increase of frontal aspect ratio. It has also been suggested in the previous section that the variation in the value of U_H will be larger for smaller values of L/H and it would tend to become constant for models long enough to give constant values of downward reattachment distance. From this we can conclude that the variation in the roof height velocities with the frontal aspect ratio will not be linear.

Figure 11.5 shows the graph of the frontal aspect ratio against U_H/U_1 for equal spacing increments for the two models alongwith the extrapolated values for other models. The extrapolation has been made on the assumption that the magnitude of the decrease of U_H between models of frontal

aspect ratio of 1.0 and 2.0 will be equal to the corresponding decrease between models of frontal aspect ratio = 0.5 and 1.0 as well as between models of A_f = 2.0 and 4.0.

The values of U_H/U_1 for models of frontal aspect ratio = 0.5, 1.5 and 4.0 obtained from Figure 11.5 were then used to convert the experimental values of C_{D_1} into C_{D_H} for respective models and are shown plotted in Figure 11.6. The data extrapolated for models having values of $A_f > 4$, based on the results of Evan for the reattachment distance downwind the larger models is also shown in Figure 11.6.

11.3.5 The drag coefficient C_{D_H} is found to increase with the increase of frontal aspect ratio of buildings up to a certain value of A_f before becoming constant for any particular spacing for buildings with $A_f \geq 10$, Figure 11.6. This trend is in line with the values given in ESDU 71016 for isolated buildings of various lengths which gives a value of C_{D_H} = 0.99 for buildings having a frontal aspect ratio of 0.5 and it progressively increases to 1.2 for buildings having a value of A_f = 2.0.

11.4 Variation of the drag coefficient C_{D_H} with side aspect ratio of buildings

11.4.1 Since the side aspect ratio of buildings is also found to affect the break point between isolated roughness flow regime and the wake interference flow regime, it is necessary to extend the investigation to buildings of varying side aspect ratio.

11.4.2 As the cube is the only building form in this range for which the velocity profile measurements were available, the data for other models of varying side aspect ratios was extrapolated by considering the information given in Figure 9.22, where it was found that the element spacing at which the flow regime changes from isolated roughness flow to the wake interference flow regime is a function of the side aspect ratio only for short afterbody models.

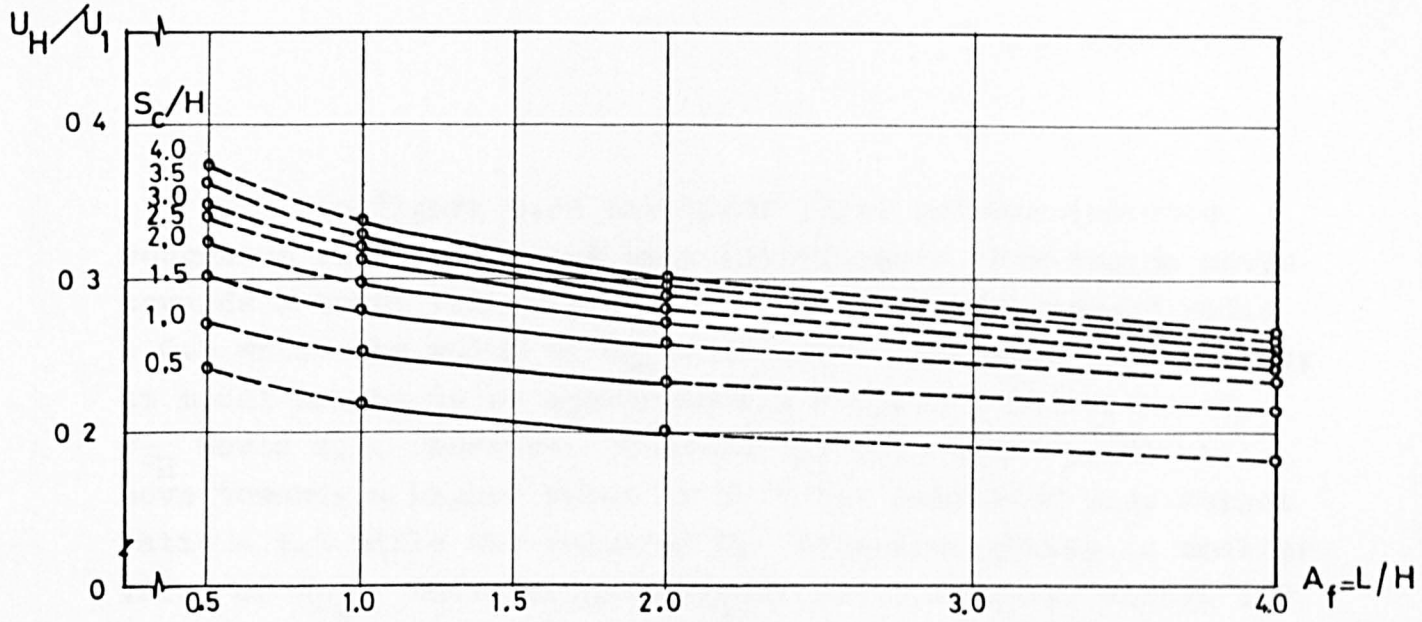

FIGURE 11.5 VARIATION OF U_H/U_1 WITH FRONTAL ASPECT RATIO FOR EQUAL SPACING INCREMENTS

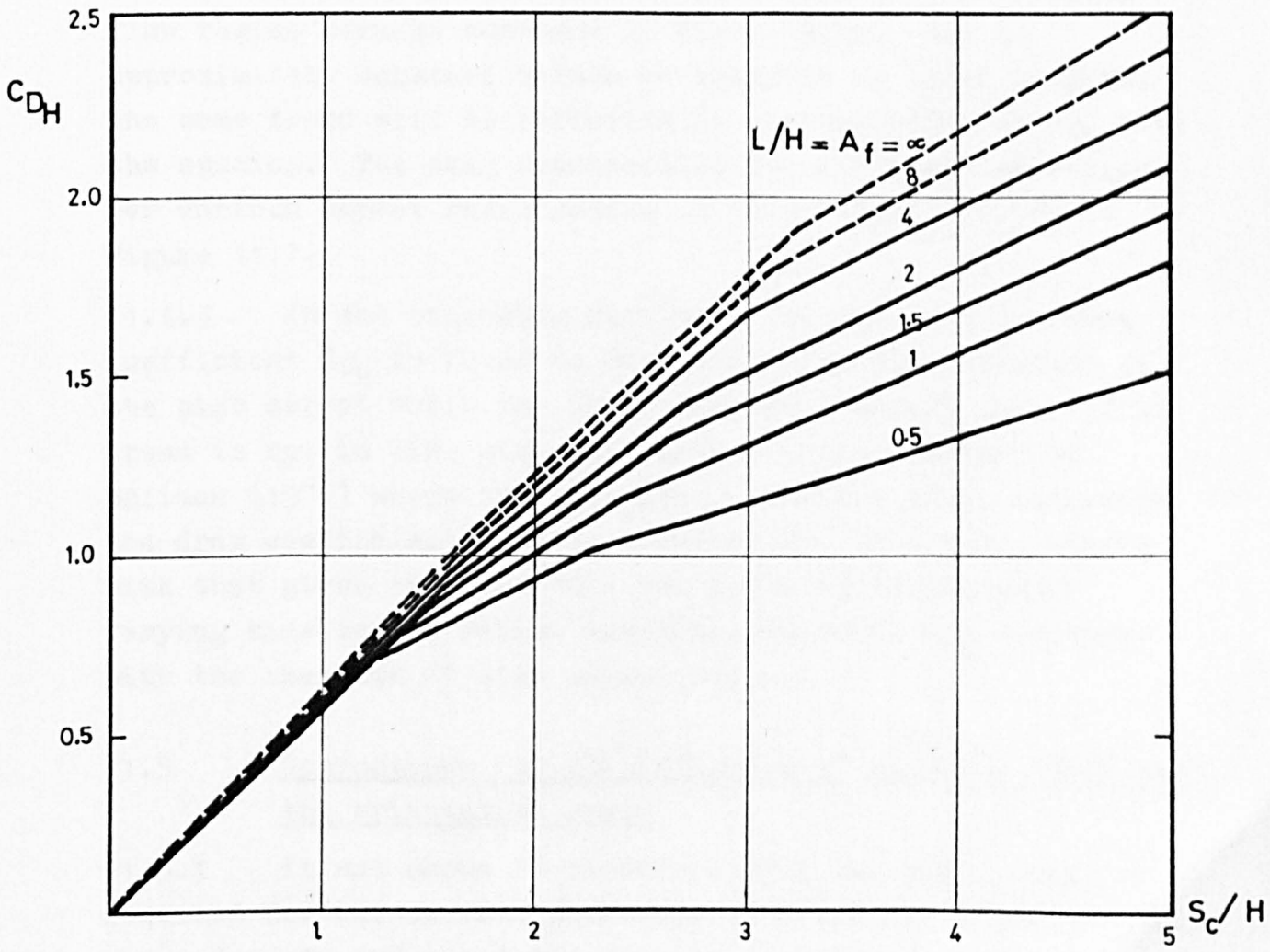

FIGURE 11.6 SUGGESTED VARIATION OF C_{D_H} WITH S_c/H FOR VARYING FRONTAL ASPECT RATIO BUILDINGS

In Figure 9.22 the break point between isolated roughness flow regime and wake interference flow regime moves towards a lower value of S_c/H for model of side aspect ratio = 0.5 while the value of C_{D_1} increases. Assuming the velocity at model height to be approximately constant, the value of C_{D_H} would also increase. Conversely, this break point will move towards a higher value of S_c/H for models of side aspect ratio = 1.5 while the value of C_{D_1} decreases giving a smaller value of C_{D_H}. Once the side aspect ratio is large enough for the flow to have reattached on the side and the roof, there will be little change as both the velocity U_H and C_{D_1} remain constant. This is shown schematically in Figure 11.7.

Conversely the value of drag coefficient C_{D_1} as well as the break point denoting the start of the skimming flow regime remains constant in Figure 9.22. Due to approximately constant values of velocity at model heights, the same trend will be reflected in the variation of C_{D_H} with the spacing. The data extrapolated for all the flow regimes for various aspect ratio models in this range is shown in Figure 11.7.

11.4.3 In the preceding sections, the value of the drag coefficient C_{D_H} is found to be affected by the variation of the side aspect ratio for short afterbody models only. This trend is not in line with the suggestion put forward by Soliman (1976) where the side aspect ratio did not influence the drag coefficient at all. Conversely, this trend agrees with that given by ESDU 71016 for isolated buildings of varying side aspect ratios where the value of C_{D_H} decreases with the increase of side aspect ratio.

11.5 Corrections for the influence of upstream fetch and the orientation angle

11.5.1 It was shown in chapter 7 that the model group size required for the surface pressures to stabilise depends on the group density and was found to vary from 10H to 25H. The

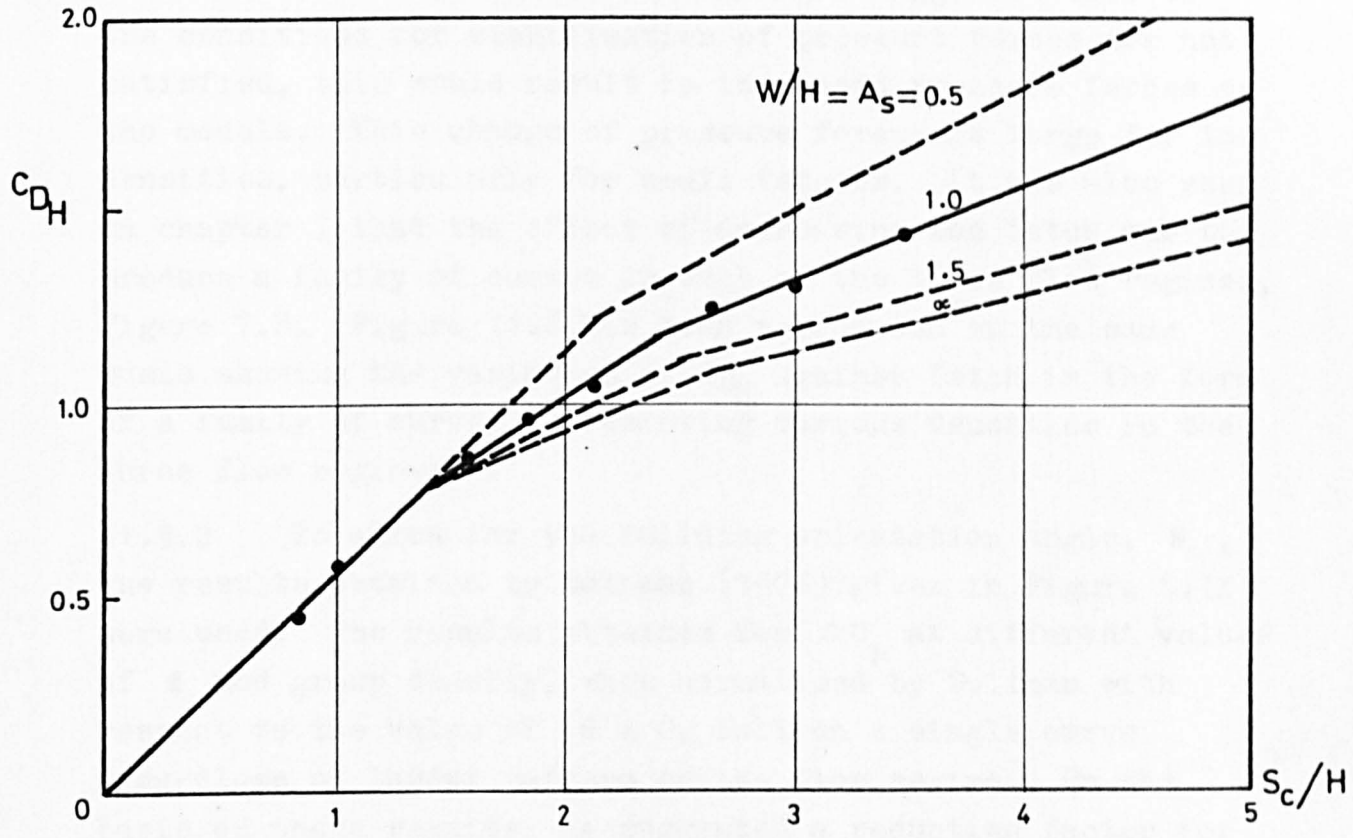

FIGURE 11.7 SUGGESTED VARIATION OF C_{D_H} WITH S_c/H FOR VARYING SIDE ASPECT RATIO BUILDINGS

stabilised values underwent a further drop with the introduction of the atmospheric boundary layer simulated flow upwind of the array size required for stabilisation of the surface pressures. It is therefore suggested that if the conditions for stabilisation of pressure forces are not satisfied, this would result in increased pressure forces on the models. This change of pressure forces is large for low densities, particularly for small fetches. It was also seen in chapter 7 that the effect of decreasing the fetch was to produce a family of curves in each of the three flow regimes, Figure 7.8. Figure 11.8 has been reproduced on the same basis showing the variation of C_{D_H} against fetch in the form of a family of curves representing various densities in the three flow regimes.

11.5.2 To allow for the building orientation angle, θ, the results obtained by Soliman (1976) given in Figure 8.14 were used. The results obtained for ΔC_p at different values of θ and group density, when normalised by Soliman with respect to the value of $\theta = 0$, fall on a single curve regardless of layout pattern or the flow regime. On the basis of these results, he suggested a reduction factor for C_{D_H} at each value of θ which is given in Figure 11.9.

11.6 The proposed method of determining the natural ventilation potential ΔC_{p_H} from the vertical faces of low rise buildings

11.6.1 The important parameters which influence the value of C_{D_H} have been discussed in the preceding sections in a systematic manner. Having seen the effect of these variables, a prediction procedure for low rise buildings is now possible. Assuming the buildings of similar height in the group, a chart can be constructed as shown in Figure 11.10, simply by placing Figures 11.6, 11.7, 11.8 and 11.9 side by side.

The value of C_{D_H} for buildings of varying frontal aspect ratio can be determined from the first part of the chart, given the group clear spacing in the flow direction

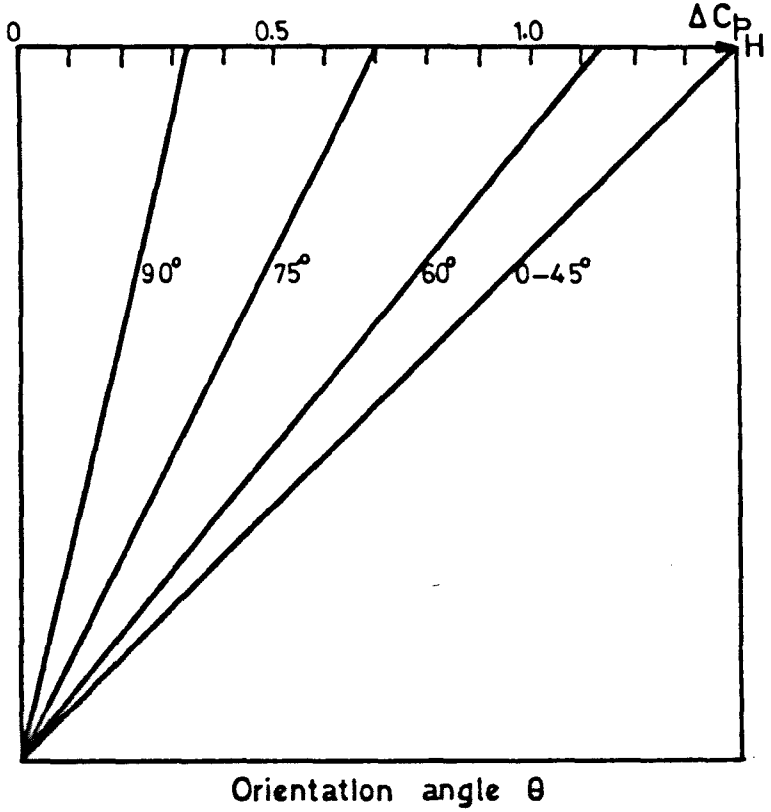

FIGURE 11.9 VARIATION OF THE NORMALISED PRESSURE DIFFERENCE WITH THE BUILDING ORIENTATION ANGLE (AFTER SOLIMAN 1976)

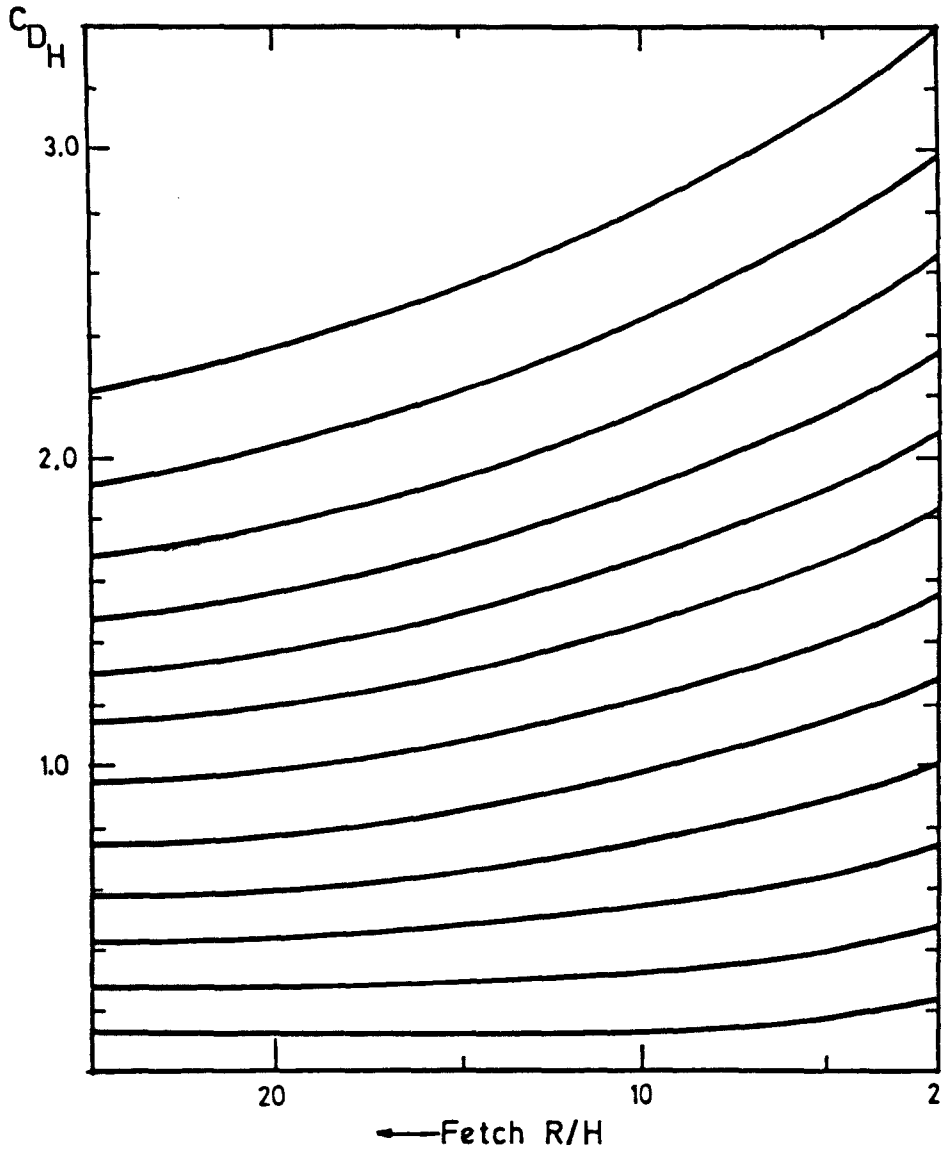

FIGURE 11.8 SUGGESTED VARIATION OF C_{D_H} WITH FETCH IN THE THREE FLOW REGIMES

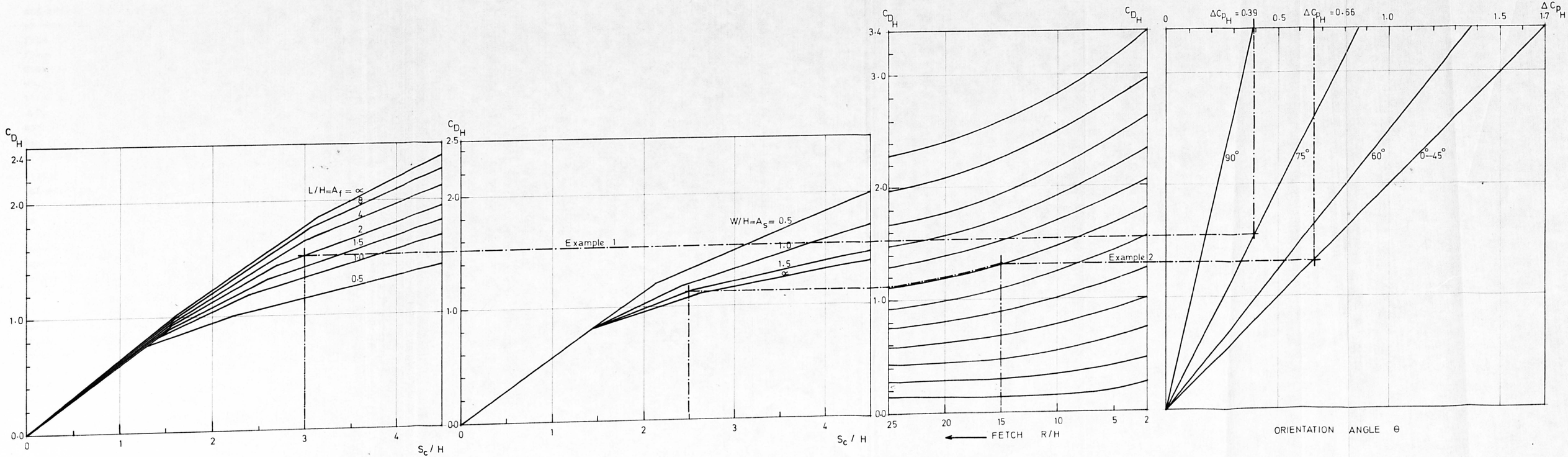

FIGURE 11.10 SUGGESTED CHART FOR THE PREDICTION OF PRESSURE DIFFERENCE ACROSS VERTICAL FACES OF VARIOUS BUILDING SHAPES.

and omitting the second part. On the other hand for buildings of varying side aspect ratios, the value of C_{D_H} can be found from the second part of the chart without considering the first. A correction to the value of C_{D_H} can then be applied from the third section of the chart if the fetch length is smaller than 25H. If the fetch length is more than 25H, the third section will also be omitted and the required value of ΔC_{p_H} across the building may be obtained from the last section of the chart where the line indicating the value of C_{D_H} intercepts any one of the lines representing the building orientation angle.

11.6.2 The chart described in Figure 11.10 can be used to calculate the infiltration rates for buildings of varying frontal aspect ratio with fixed values of width and height as 1. These proportions of structures may include buildings varying from single detached houses, semi detached houses to houses in rows of various lengths. The chart can also be used for buildings of varying side aspect ratios with fixed values of length and height taken as 1. This would also cover a wide range of building forms.

11.6.3 Two examples showing the sequence of these steps for various aspect ratio buildings is also shown in Figure 11.10. Firstly for buildings of frontal aspect ratio = 2.0, arranged in a group with a clear spacing of 3H and the wind orientation angle $\theta = 75^{o}$, the pressure difference across any opening in the building $\Delta C_{p_H} = 0.39$ when the fetch length is more than 25H. Secondly, for buildings with a side aspect ratio = 2.0, spaced at 2.5 clear spacing and an upstream fetch length of 15H, the value of ΔC_{p_H} is 0.66, for the wind blowing normal to the face.

11.6.4 Although further charts would be required to take into account the effect of both the frontal as well as the side aspect ratio simultaneously, the buildings of such dimensions are not frequently found in practice. It is, therefore, suggested that this chart would be suitable for most practical purposes and cover the majority of building

forms that are likely to be met in practical life.

11.7 Suggested method of determining the natural ventilation potential ΔC_{L_H} from the roof of low rise buildings

11.7.1 This section deals with the procedure to be adopted for the estimation of values of roof lift coefficient ΔC_{L_H} acting on the roof of a low rise building within a group of similar form and height. The procedure adopted for this method is similar to the one described in sections 11.3 to 11.6.

11.7.2 The roof height velocities obtained from the velocity profile measurement results given in Figures 8.36 and 9.40 for building models with frontal aspect ratios of 1 and 2 were used to convert the experimental values of C_{L_1} into C_{L_H} using the following relationship:

$$C_{L_H} = C_{L_1}(U_1/U_H)^2 \qquad 11.5$$

These results are shown plotted in Figure 11.11 and agree well with the trends established in earlier chapters about the variation of pressure forces in the three flow regimes. The value of C_{L_H} for a particular building model decreases in the isolated roughness flow and wake interference flow regimes while it starts to increase again in the skimming flow regime. This is suggested to be due to approximately constant value of C_{L_1} in the skimming flow regime but continually decreasing value of U_H giving larger value of U_1/U_H and thus larger roof lift coefficient C_{L_H}.

11.7.3 The data for other building models was extrapolated in a manner similar to that described in section 11.3. The values of U_H/U_1 for other models obtained from Figure 11.5 were used to convert the experimental values of C_{L_1} into C_{L_H} for respective models. This data alongwith the data extrapolated for models having larger frontal aspect ratios

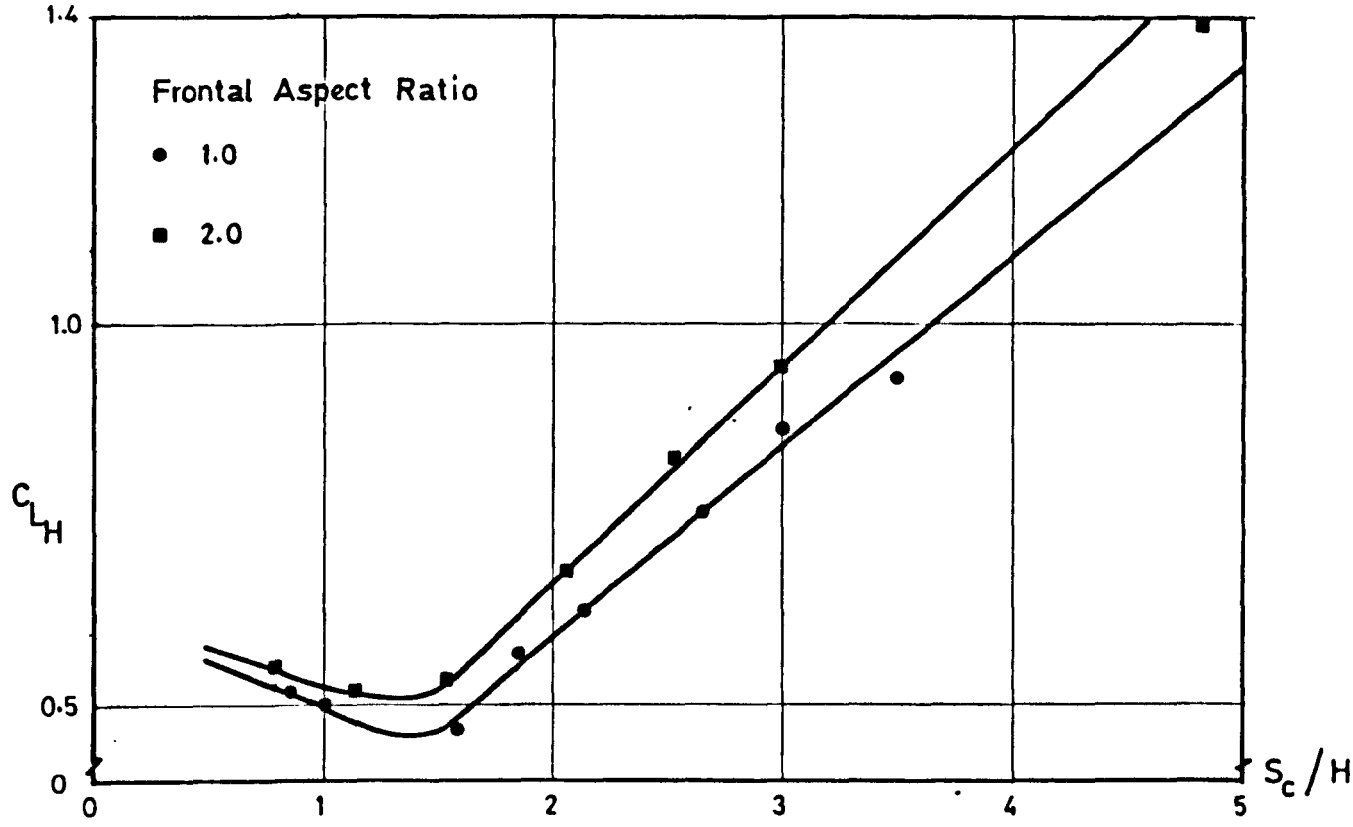

FIGURE 11.11 VARIATION OF C_{L_H} WITH S_c/H - EXPERIMENTAL RESULTS

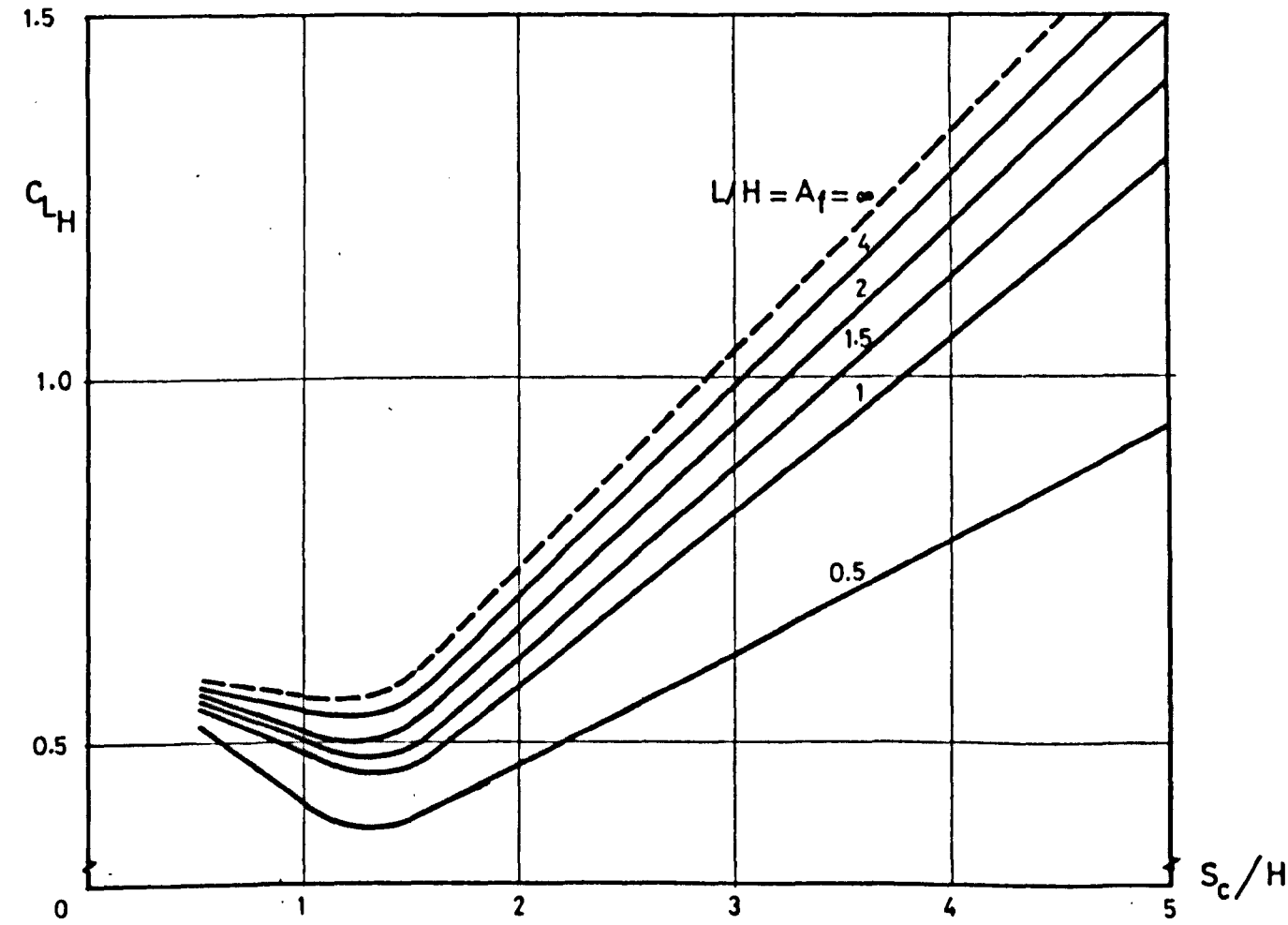

FIGURE 11.12 SUGGESTED VARIATION OF C_{L_H} WITH S_c/H FOR VARYING FRONTAL ASPECT RATIO BUILDINGS

and based on the results of Evan (1957) is shown in Figure 11.12.

11.7.4 In an attempt to extend this investigation to other building shapes of varying side aspect ratios, the data was extrapolated in the same manner as that adopted in section 11.3. In this extrapolation, the experimental values of roof lift coefficient, C_{L_1}, from chapter 9 were used. The computed values for cube shaped buildings alongwith the data extrapolated for other models of varying side aspect ratio is given in Figure 11.13.

11.7.5 The variation of the roof lift coefficient with the upstream fetch was found to be similar to the corresponding variation of the drag coefficient and was found to stabilise at similar values of fetch lengths as found in chapter 7. The effect of the introduction of atmospheric boundary layer flow upwind of the array size required for stabilisation was also similar to the one found earlier. It is, therefore, suggested that the effect of decreasing the fetch would also be similar and would be to produce a family of curves in each of the three flow regimes, Figure 11.14.

11.7.6 To allow for the building orientation angle, θ, the approximate roof pressure distributions on a surface mounted cube in datum conditions, given by ESDU 71016 were used. When this data was analysed, it was found that the roof lift coefficient averaged along the centre line of the cube did not vary much with the wind approach angle. The values of lift coefficient for orientation angles 0°, 15°, 30° and 45° were found to be 0.59, 0.51, 0.58 and 0.41 respectively.

It can also be seen from these pressure distributions that with the change of wind angle, the roof suction increased drastically at the windward corners, especially for an angle of 45° where the roof lift coefficient at the corner was approximately six times the value at the windward edge for the wind normal to the face. In the case of wind approaching

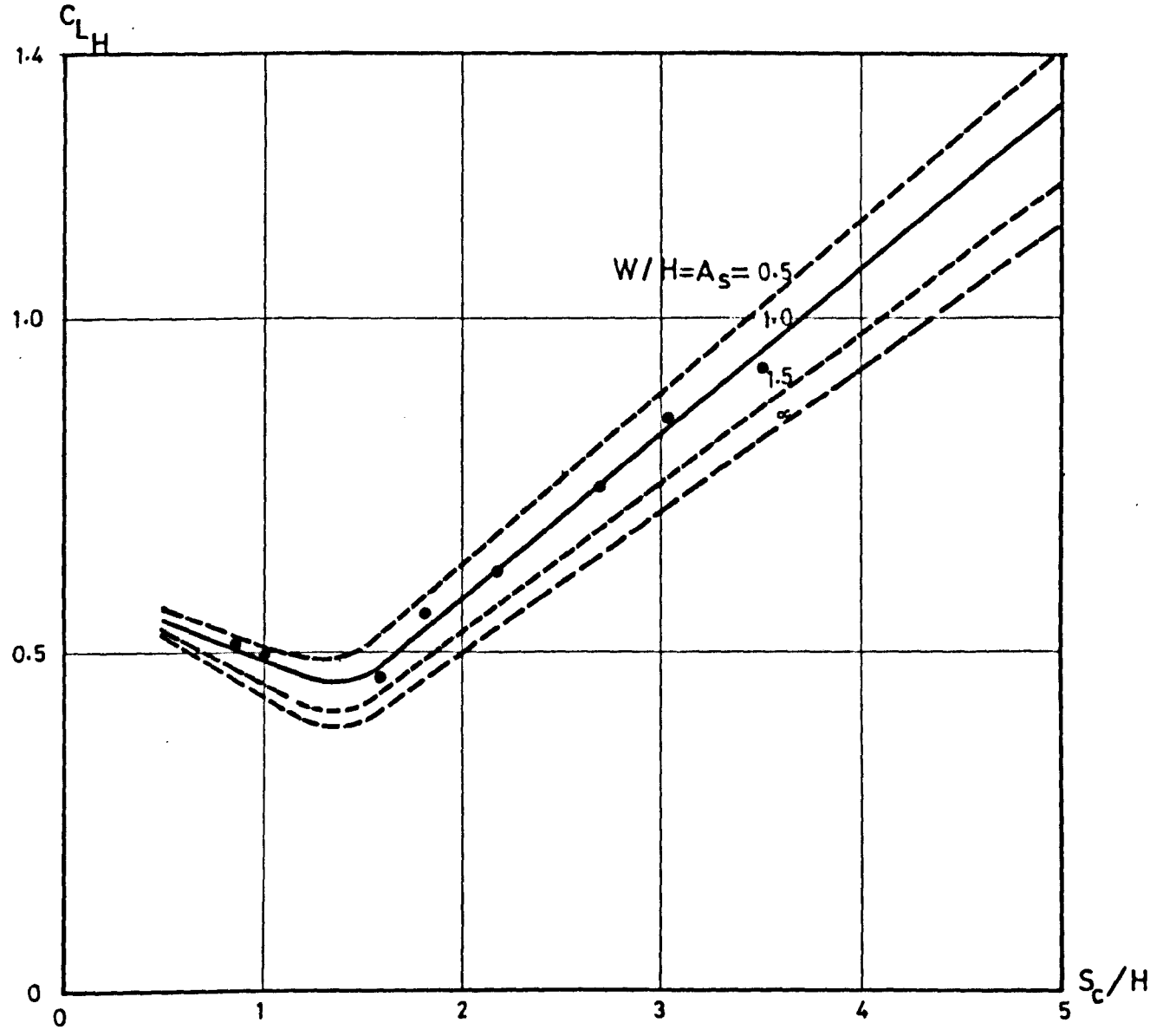

FIGURE 11.13 SUGGESTED VARIATION OF C_{L_H} WITH S_c/H FOR VARYING SIDE ASPECT RATIO BUILDINGS

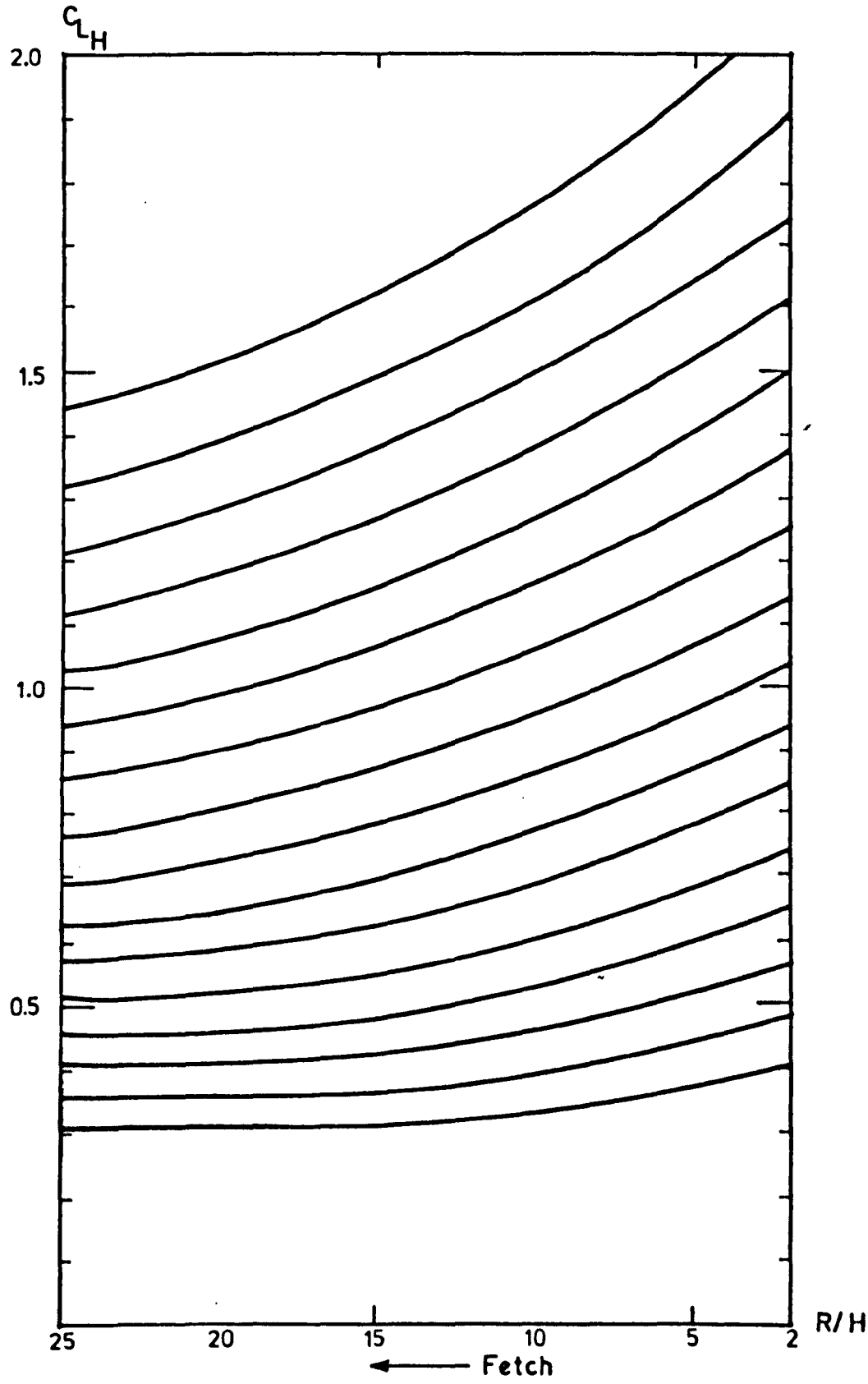

FIGURE 11.14 SUGGESTED VARIATION OF C_{L_H} WITH FETCH IN THE THREE FLOW REGIMES

at an angle of 45°, the value of pressure coefficients, however, decreased sharply and dropped to its lowest value at the trailing edge. When the total lift coefficient along the diagonal line was calculated for various angles, its value was found to be more uniform at 0.59, 0.63, 0.58, 0.56 for angles of 0°, 15°, 30° and 45° respectively.

Similar observations were also reported by Tieleman and Reinhold (1976) for their wind tunnel model investigations for 32 dwelling geometries in the simulated natural wind. They made pressure measurements on model roofs of varying geometries for wind approach angles between zero and 360 degrees for two different length to width ratios (L/W = 1.2 and 2.0). Their results for flat roof buildings show that although the mean pressures vary a great deal on different locations on the roof; their sum total is fairly uniform for wind approach angles between zero and 45 degrees.

On the basis of these observations, it is suggested that the effect of orientation angle will be negligible over the total roof suction and a reduction factor suggested earlier for the drag coefficient will not be required. If, however, the openings are not distributed over the entire roof and are only located in one particular section of the roof then the appropriate wind tunnel data will have to be referred to. In such cases, the correction to the roof lift coefficient, C_{L_H}, will be applied depending on the location of openings on the roof. The openings located near the windward edge will experience an increased roof suction and vice versa.

11.7.7 Having now arrived at a means of determining the value of C_{L_H} for systematic variation in the important parameters which influence its value, it is now possible to predict the ventilation from the roof of buildings. If the height of buildings in a group is constant, a chart can now be constructed in a manner similar to that described in the last section by placing Figure 11.12, 11.13 and 11.14 side

by side as shown in Figure 11.15. The value of C_{L_H} for a particular shape of a building can be determined from either of the first two sections of the chart to which a correction can be applied for a fetch smaller than 25H which will give the value of ΔC_{L_H} acting across the openings in the roof.

11.7.8 Two examples showing the sequence of these steps for two different buildings identical to those for whom the pressure difference across the vertical faces was calculated in section 11.6.3 is shown in Figure 11.15. For the first building of frontal aspect ratio = 2.0, arranged in a group with a clear spacing of 3H, the value of ΔC_{L_H} is 0.92 when the fetch length is more than 25H. For the second building of side aspect ratio = 2.0, spaced at 2.5H clear spacing and an upstream fetch length of 15H, the value of ΔC_{L_H} is found to be 0.725.

11.7.9 Having now calculated the pressure difference acting across the vertical faces of the building as well as acting on the roof, the sum total of the two for respective building shapes can be used to determine the infiltration from the walls as well as from the roof of buildings.

11.8 Effect of the variation of height

11.8.1 The wind loading on buildings with heights smaller or larger than the average height of surrounding buildings have been discussed in detail in chapter 6 and 10 where both the drag coefficient C_{D_H} and the roof lift coefficient C_{L_H} of buildings of height smaller than the array was found to be large. Both these values, however, decreased with the increase of height before becoming constant at values applicable to high rise buildings. It is expected that the ventilation potential will also be affected dramatically if the building height is varied relative to the surroundings. The trend, however, may or may not agree with the one found in chapter 10.

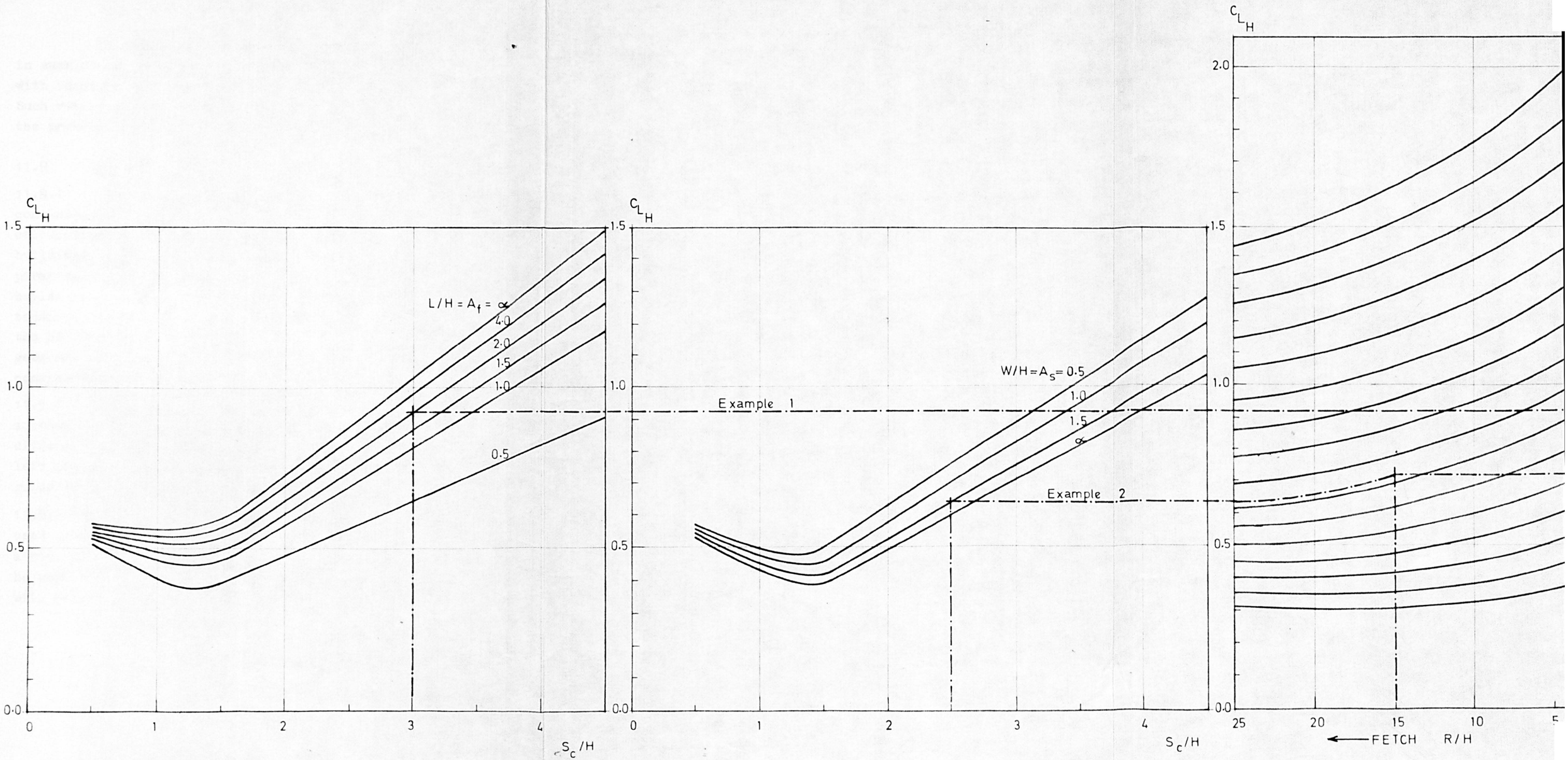

FIGURE 11.15 SUGGESTED CHART FOR THE PREDICTION OF PRESSURE DIFFERENCE ACROSS THE ROOF OF VARIOUS BUILDING SHAPES

In order to find the infiltration rates of buildings in such cases, detailed information regarding their behaviour with increased fetch and varying orientation is required. Such requirements are considered to be outside the scope of the present study and must be dealt with separately.

11.9 Conclusions

11.9.1 From the discussion made in this chapter it is concluded that the existing method of infiltration calculation given in the IHVE guide, applicable to high rise buildings, does not take into account all the relevant parameters affecting the pressure difference across low rise buildings in groups. In order to suggest an alternative technique of infiltration measurements for low rise buildings, the important parameters, i.e. the building form, their group geometry and the flow properties should be given due consideration.

11.9.2 The suggested chart, Figure 11.10, takes into account the above parameters to yield the required pressure difference across buildings. This chart can now replace the left hand side of the infiltration chart given in the IHVE guide to be used for low rise buildings.

11.9.3 Another chart suggested in Figure 11.15 can also be used profitably to give the required roof lift coefficient across any openings in the roof of buildings which can then be used to calculate the infiltration from the roof. This will form an essential addition to the IHVE guide.

CHAPTER 12

CONCLUSIONS

12. CONCLUSIONS

12.1 Available natural ventilation data

12.1.1 From the review of some previous studies of natural ventilation in buildings, wind flow round buildings and the flow over rough surfaces the following guidelines were obtained for the study.

12.1.2 The IHVE guide method (1970) for the calculation of ventilation rates through the fabric of structures is only applicable to isolated high rise buildings. It is, therefore, inappropriate to apply the same procedure of ventilation calculations to arrays of low rise buildings. The pressure difference across a particular structure in a low rise building array, estimated from this chart would result in a considerable error since important factors affecting the pressure forces, i.e. the building form, their geometry and the pattern of grouping alongwith the properties of natural wind are either oversimplified or ignored.

12.1.3 The level of accuracy of natural ventilation calculations using the crack method depends on the accuracy of determining the pressure difference across buildings. In order, therefore, to be applicable to low rise buildings in an urban built form, all the relevant factors affecting the pressure difference should be taken into consideration.

12.1.4 From the review made on the effect of flow parameters on the mean pressure forces on buildings, it was found that the turbulence and the velocity profile parameters which define the wind's structure should be modelled correctly and the wind direction taken into consideration if any accurate estimates of mean pressure forces comparable to full scale results are to be obtained.

12.1.5 From the previous studies on the simulation methods for urban terrain atmospheric boundary layer flow, it was found that a combination of a castellated fence and

triangular spires followed by floor roughness would generate the flow representing an adequate simulation.

12.1.6 From the review made of the relevant literature on natural ventilation, wind loading and external wind flows, no general relationship was found to be available which related the group geometry of built form to the resulting flow and the pressure forces on the elements of the group. However, it was evident that the flow and the pressure forces on groups of buildings are dependent on individual building form, the building group form and its fetch length.

12.1.7 Since buildings may be considered as roughness elements on the earth's surface, an investigation was also made of the flow over rough surfaces. Most of the work reported has been for two dimensional roughness elements and very little was available on three dimensional roughness elements. The main effect of changing the roughness geometry and the pattern of distribution is to produce different flow regimes. The velocity profile parameters and the pressure forces are also dependent on the flow regimes and hence the roughness geometry.

12.2 Isolated model buildings

12.2.1 From the experimental work done on surface pressure measurements on various building shapes on an empty turntable with the atmospheric simulated flow mechanism extending up to the turntable, the following conclusions are drawn.

12.2.2 In the case of the isolated models, the frontal aspect ratio affected the windward and leeward pressure coefficients in such a manner that the overall drag coefficient remained unaffected. The drag coefficient was also unaffected by the side aspect ratio of isolated models except for short afterbody models. Conversely, the effect of changing the incident flow type i.e. the parameter δ/H resulted in large variations in the pressure forces on an isolated cube. It is, therefore, suggested that a large

discrepancy in the value of δ/H would result in an inaccurate estimate of wind forces on low rise buildings, (Figures 6.1, 6.11 and 6.12).

12.2.3 The mean roof lift coefficient, on the other hand, behaves differently than the drag coefficient. The roof lift coefficient increases as the frontal aspect ratio increases and it decreases as the side aspect ratio increases for isolated models, (Figure 6.13).

12.2.4 The rate of change of surface pressure forces with the model height is different below and above a height of 1.6 times the height of the cube. The lower region may be considered to encompass low rise buildings whilst the upper region includes high rise buildings, (Figures 6.6 to 6.8).

12.2.5 The computed value of the drag coefficient, C_{D_H}, based on the velocity at roof height of an isolated cube was found to be larger than the comparable value suggested by British Standard Code of Practice for wind loading. This value increased as the height decreased. On the other hand, the value of C_{D_H} decreased as the height increased to reach a constant value at 1.6 times the height of the cube, applicable to high rise buildings, (Figure 6.8). This result suggests that the values given by the British Standard Code of Practice should be reviewed.

12.3 Groups of model buildings

12.3.1 From the experimental work done on surface pressure measurements alongwith detailed velocity profile measurements on various building shapes in groups, the following conclusions are drawn.

12.3.2 The analysis made of the flow velocity and pressure measurements on building models of various aspect ratios within groups of similar form showed that it is possible to apply the boundary layer theory for flow over rough surfaces to building model groups. The concept of the three flow regimes of flow over roughness elements has been substantiated

by the experimental measurements of pressure forces and velocity profiles for various model shapes and their grouping.

12.3.3 The effect of increasing the fetch length around the test model was to reduce the pressure forces. For small values of upstream fetch, the building model experienced a high drag coefficient and high roof lift coefficient and as the fetch was increased, these values decreased. This variation was gradual in lower density cases which became nominal when the fetch length was increased beyond 25H. On the other hand, the variation was abrupt initially for higher density cases after which the change was nominal. At a point where the change in the variation of surface pressure forces was nominal, these were taken to have stabilised. The model group size required for the surface pressure forces to stabilise depends on the group density and is found to vary from 10H to 25H, (Figures 7.8 and 7.21).

12.3.4 The nominal reduction in the surface pressure forces at increased fetch lengths when their values were taken to have stabilised, were taken into account by the introduction of the atmospheric boundary layer flow upwind of the array size, (Figures 7.9 to 7.14).

12.3.5 The surface pressure forces on the models stabilised long before the boundary layer reached equilibrium. The growth of the boundary layer over three dimensional cubical elements was found to be in reasonable agreement with the previous results and the theoretical prediction of Gartshore (Figures 7.23 and 7.24).

12.3.6 The isolated cube experienced a high drag which was found to reduce drastically even for small values of layout density. As the density in the group was progressively increased, the model drag decreased before going to zero at 100% density, (Figures 8.4 to 8.6).

12.3.7 From the detailed pressure measurements on the cube shaped elements in various layout densities, different flow regimes were shown to be characterised by a change of behaviour in the mean windward and leeward wall pressures as well as the roof lift coefficient, as the spacing between the buildings in the flow direction is varied, (Figures 8.4 to 8.6).

12.3.8 The governing conditions of these changes of behaviour in the pressure forces supported both by previous works and the present investigation may be given as follows:

a) In the isolated roughness flow regime, the clear spacing between blocks is greater than the sum of the distances of separation and reattachment round the block obtained in the isolated element case.

b) In the skimming flow regime the space between the blocks contains a stable vortex. The onset of the formation of vortex appears to be entirely dependent on the ratio between the clear spacing and the block height. This ratio was found to be 1.4 for the present study of flow over cubes, a value which is in good agreement with corresponding figures given previously for flow over two dimensional grooves.

c) The wake interference flow regime occurs if the clear spacing between the blocks takes any value between the previous two cases.

12.3.9 In the case of flow over groups of elements, different than the cube shape, the frontal aspect ratio was found to be a dominant parameter which can alter the flow from isolated roughness to wake interference flow regime for particular values of the element spacing. On the other hand, the change from the wake interference flow to the skimming flow regime was found to depend less on the frontal aspect ratio and then after a certain value, this flow regime change depends only on the cavity height. This is also supported by

previous work on flow over grooves and cut-outs, (Figure 9.11).

12.3.10 The side aspect ratio of elements is also found to alter the flow from isolated roughness to the wake interference flow regime only up to a certain extent. When the side aspect ratio is large enough for the flow to reattach on the roof and the sides of the model then the reattachment distance behind the element is not affected and the change of flow regime takes place at a fairly constant value of element spacing. Conversely, the change from the wake interference flow regime to the skimming flow regime is not affected by the side aspect ratio but is directly related to the element height, (Figure 9.22).

12.3.11 On the basis of the flow phenomenon round various shaped models and their behaviour in the variation of leeward pressure coefficients, these can be divided into two broad categories of short afterbody models and long afterbody models. The short afterbody models show two inflection points in the variation of their base pressures with spacing corresponding to both the changes of flow regimes, (Figure 9.7 to 9.9 and 9.18). The long afterbody models on the other hand show only one inflection point corresponding to the change from wake interference to skimming flow regime, (Figures 8.4 to 8.6, 9.6, 9.19 and 9.20). Conversely, all the models show only one inflection point in their variation of windward pressure coefficients which represents the change from isolated roughness flow to the wake interference flow regime.

12.3.12 The roof pressure coefficients were always found to be negative with the maximum suction occurring near the windward edge of the roof and decreasing towards the rear edge. At higher densities, however, these distributions were of a more uniform nature, (Figures 8.12, 9.12, 9.13, 9.23 and 9.24).

12.3.13 The variation of roof lift coefficient with the element spacing showed only one break point for all the models. The value of spacing at which this break point appeared was found to compare well with the values of spacing at which the wake interference flow changes to skimming flow regime. This was found to be true for all models in both the frontal as well as the side aspect ratio ranges, (Figures 8.13, 9.14 and 9.25).

12.3.14 Any slight misalignment in the element layout could be shown to change the flow within the cubes, for the same overall density, resulting in changes of C_{p_w} and C_{p_b}. This phenomenon was more pronounced in the transition range between the adjacent flow regimes.

12.3.15 A collapse of the windward pressure distribution profiles for the cube was obtained when the profiles were classified by flow regimes. These profiles, in the isolated roughness flow, took the form of an "S" and those in the skimming flow regime took the form of a reversed "C" while the profiles in the wake interference flow regime collapsed only in the lower 85% of their height. In the remaining 15% of the element height, the collapse was poor owing to the transition from an "S" to a reversed "C" shape. The leeward pressure profiles in the isolated roughness and wake interference flow regimes were of a more uniform distribution and collapsed as one family, whilst they were no longer uniform in the skimming flow regime, (Figure 8.9). The shape of the pressure distributions for other models show that the same would be true for them also.

12.3.16 The variation of the effective skin friction coefficient with density reflected a behaviour similar to the reported behaviour of the equivalent sand grain roughness with density, (Figure 8.11).

12.3.17 From the velocity profile measurements for the two models, the logarithmic region of the internal layer did not extend above the model height in any case, (Figures 8.19 to 8.26 and 9.27 to 9.33).

12.3.18 A broken line relationship is shown to exist between the zero plane displacement and the group layout density for both the models for which the velocity profile measurements were available. The break points correspond to the three flow regimes already suggested (Figures 8.30 and 9.35). It is suggested that the same trend may be true for other models.

12.3.19 The variation obtained for both the roughness length and the equivalent sand grain roughness with density showed good agreement with previous work for both the models, (Figures 8.31 to 8.34 and 9.36 to 9.38). Similarly, good agreement with the theoretical prediction of the internal layer depth was also demonstrated, (Figures 8.35 and 9.39).

12.3.20 A relationship is found to exist between the velocities at model height and the clear spacing between models, (Figures 8.36 and 9.40).

12.3.21 A normalisation scheme for the windward pressure distribution profiles, which takes into account the effect of the zero plane displacement and uses the effective height, has been suggested for both the models. In this scheme, all the pressure distribution profiles collapsed on three different curves in each model representing the three flow regimes, (Figures 8.38 to 8.41 and 9.41 to 9.44).

12.4 Central model height variations

12.4.1 From the experimental work done on surface pressure measurements on the central model of variable height, surrounded by uniform roughness arrays of various densities, the following trends are established.

12.4.2 When the height of the test model is varied with respect to the average height of the model group, the variation of the drag coefficient, C_{D_1}, with relative height shows different rate of change of pressure forces within and outside the inner layer profile growing over the model group. The relative height at which this change appears depends on

the model fetch length. Below this inflection point, the rate of change of pressure forces is governed by the inner layer profile and above it, the outer layer profile governs this rate, (Figures 10.10 and 10.11).

12.4.3 The value of the drag coefficient, C_{D_H}, is shown to be large for buildings of height smaller than those surrounding it. As the height increases, the value of C_{D_H} decreases. When the height of the building is increased beyond the inner layer profile i.e. the buildings considered as high rise, the value of C_{D_H} becomes constant, (Figure 10.13).

12.4.4 The roof lift coefficient, C_{L_1} behaved in a similar manner as the drag coefficient, C_{D_1}, in the inner layer profile. Outside the inner layer, the rate of change of roof suction is different for different densities and the lines tend to merge into one another (Figures 10.22 and 10.23). The roof lift coefficient based on the roof height velocities C_{L_H}, on the other hand, behaves in a manner identical to the drag coefficient, C_{D_H}, (Figure 10.24).

12.4.5 The trend of the variation of the drag coefficient as well as the roof lift coefficient based on the model height velocities, C_{D_H} and C_{L_H}, respectively with the height is not in line with the British Standard Code of Practice.

12.5 Natural ventilation design methods

12.5.1 On the basis of conclusions drawn in sections 12.2 to 12.4 from the work of models of various shapes, their application to natural ventilation design methods and wind forces on low rise buildings was studied and the following recommendations are made.

12.5.2 For the purposes of general application to infiltration rate calculations of low rise building arrays, the relevant important parameters i.e. building form, the group geometry and the resulting flow properties have been considered in this study. On the basis of the conclusions drawn from this study, a chart has been produced to yield

the required pressure difference across buildings. This chart can replace the left hand side of the infiltration chart given in the IHVE guide to be applicable to low rise building groups, (Figure 11.10).

12.5.3 Another chart has also been suggested which can be used profitably to give the required pressure difference across the roof of buildings to calculate the infiltration from any openings in the roof. This will form an essential addition to the IHVE guide, (Figure 11.15).

12.5.4 In addition to this, it is also suggested that the current British Standard Code of Practice for wind loading should be reviewed to incorporate the trends discussed earlier in this investigation.

REFERENCES

REFERENCES

Antonia, R.A. and Luxton, R.E. 1971 — "The response of a turbulent boundary layer to a step change in surface roughness: Part I, Smooth to Rough". Jr. Fluid Mechanics, 48, Part 4.

Antonia, R.A. and Luxton, R.E. 1972 — "The response of a turbulent boundary layer to a step change in surface roughness: Part II, Rough to Smooth". Jr. Fluid Mechanics, 53, Part 4.

Armitt, J. 1966 — "The simulation of the atmospheric boundary layer in a wind tunnel". Central Electricity Research Laboratory, Note RD/L/N, 83/66.

Armitt, J. and Counihan, J. 1968 — "The simulation of the atmospheric boundary layer in a wind tunnel". Jr. Atmospheric Environment, Vol. 2.

Armitt, J. 1974 — "Wind loading on a rectangular block". Central Electricity Research Laboratory, Report No. RD/L/N, 59/74.

A.S.H.R.A.E. 1972 — "Handbook of Fundamentals". American Society of Heating, Refrigerating and Air Conditioning Engineers, New York.

Bailey, A. and Vincent, N.D.G. 1943 — "Wind pressure on buildings including effect of adjacent buildings". Jr. Institute of Civil Engrs, 20(8), Paper No. 5367.

Bedingfield, P.S. and Lapraik, R.D. 1970 — "Boundary layers in an urban environment". B.Sc. Dissertation 136, Dept. of Aeronautical Engineering, University of Bristol.

Bettermann, D. 1965 — "Contribution a l'Etude de la Couche Limite Turbulente le Long de Plaques Rugueuses". Rapport 65-6, Centre National de la Recherche Scientifique, Paris.

Bilsborrow, R.E.
1973
"Natural ventilation of buildings". Ph.D. Thesis, Dept. of Building Science, University of Sheffield.

Bilsborrow, R.E. and Fricke, F.R.
1975
"Model verification of analogue infiltration prediction". Jr. Building Science, Vol. 10.

Blom, J. and Warner, L.
1969
"The influence of change in surface roughness on the development of the turbulent boundary layer in the lower layers of the atmosphere". Jr. Atmos. Sciences, Vol. 26.

Bradley, E.F.
1968
"A micrometeorological study of velocity profiles and surface drag in the region modified by a change in surface roughness". Q. Jr. Royal Met. Society.

B.R.E. Digest
1970
"The assessment of wind loads". Building Research Station Digest 119.

B.S.I.
1972
"Basic data for the design of buildings". British Standard Code of Practice for Wind Loading, CP3, Chapter V, Part II, 1972.

Castro, I.P., Jackson, N.A. and Robins, A.G.
1975
"The structure and development of a 2m deep simulated suburban boundary layer". Central Electricity Generating Board, Research Report, R/M/N-800.

Castro, I.P. and Robins, A.G.
1977
"The flow around a surface mounted cube in uniform and turbulent streams". Jr. Fluid Mechanics, Vol. 79, Part 2.

Caton, P.G.F.
1975
"Standardised maps for hourly mean wind speed over UK and some implications regarding wind speed profiles". Fourth International Conference on "Wind Effects on Buildings and Structures", Heathrow, London.

Cermak, J.E., Sadeh, W.Z. and Hsi, G.
1969
"Fluctuating moments on tall buildings produced by wind loading". Tech. meeting of National Bureau of Standards. Building Science series 30, US Dept. of Commerce.

Clauser, F.H.
1954
"Turbulent boundary layers in adverse pressure gradients".
Jr. Aero. Society, 21.

Clauser, F.H.
1956
"The turbulent boundary layer".
Advances in Applied Mechanics 4.

Cockrell, D.J. and Lee, B.E.
1969
"Methods and consequences of atmospheric boundary layer simulation".
Paper presented at the Fluid Dynamics Panel specialists meeting, AGARD Conference Proceeding No. 48.

Cook, N.J.
1971
"Effects of scale of turbulence on the flow around buildings".
Ph.D. Thesis, Dept. of Aeronautical Engineering, University of Bristol.

Cook, N.J.
1972
"Wind tunnel simulation of the atmospheric boundary layers".
Symposium on external flows, University of Bristol.

Cook, N.J.
1974
"On applying a general atmospheric simulation method to a particular urban site for ad hoc wind loading or wind environment studies (Technical Note)".
Jr. Atmospheric Environment, Vol. 8.

Cook, N.J.
1976
Private communication.

Cook, N.J.
1976 (a)
"Data for the wind tunnel simulation of the adiabatic atmospheric boundary layer - Part C".
B.R.E. Note, N-135/76.

Counihan, J.
1969
"An improved method of simulating an atmospheric boundary layer in a wind tunnel".
Jr. Atmospheric Environment, Vol. 3.

Counihan, J.
1971
"Wind tunnel determination of the roughness length as a function of the fetch and roughness densities of three dimensional roughness elements".
Jr. Atmospheric Environment, Vol. 5.

Counihan, J.
1973
"Simulation of an adiabatic urban boundary layer in a wind tunnel".
Jr. Atmospheric Environment, Vol. 7.

Counihan, J.
1975
"Adiabatic atmospheric boundary layers. A review and analysis of data from the period 1880-1972. (Review paper)".
Jr. Atmospheric Environment, Vol. 9.

Dalgliesh, W.A.
1969
"Experience with wind pressure measurements on a full scale building".
Paper presented at Tech. meeting of National Bureau of Standards. Building Science Series 30, U.S. Dept. of Commerce.

Davenport, A.G.
1963
"The relationship of wind structures to wind loading".
Paper presented at symposium no. 16 at N.P.L., UK.

Davenport, A.G.
1967
"The dependence of wind loads on meteorological parameters".
Paper presented at a symposium on Wind Effects on Buildings and Structures, Ottawa, Canada.

Davenport, A.G.
1971
"The response of six building shapes to turbulent wind".
Phil. Trans. Royal Society, London, A-269.

Dean, R.B.
1974
"An investigation of shear layer interaction in ducts and diffusers".
Ph.D. Thesis, Dept. of Aeronautics, Imperial College, London.

Dick, J.B.
1949
"Experimental studies in the natural ventilation of houses".
Jr. I.H.V.E. Vol. 17.

Dick, J.B.
1951
"Ventilation research in occupied houses".
Jr. I.H.V.E. Vol. 19.

Dvorak, F.A.
1969
"Calculation of turbulent boundary layers on rough surfaces in pressure gradients".
Jr. A.I.A.A. Vol. 7, No. 9.

Euromech 50
Hunt, J.C.R. and Fernholz, H.
1974
"Wind tunnel simulation of the atmospheric boundary layer".
(A report on Euromech 50), Jr. Fluid Mech. Vol. 70, Part 3.

Eaton, K.J.
Mayne, J.R. and
Cook, N.J.
1976
"Wind loads on low rise buildings, effect of roof geometry".
Building Res. Stn. C.P. 1/76.

Elliot, W.P.
1950
"The growth of the atmospheric internal boundary layer".
Trans. Amer. Geophys. Union Vol. 39.

ESDU 71016
1971
"Fluid forces, pressures and moments on rectangular blocks".
Engg. Science Data Unit, item 71016.

ESDU 72026
1972
"Characteristics of wind speed in the lower layers of the atmosphere near the ground: strong winds (neutral atmosphere)".
Engg. Science Data Unit, item 72026.

Evans, B.H.
1957
"Natural air flow around buildings".
Texas Engg. Experimental Stn. Res. Report 59.

Gartshore, I.S.
1973
"A relationship between roughness geometry and velocity profile shape for turbulent boundary layers (low speed aerodynamics)".
National Research Council, Canada, Internal Report No.LTR-LA-140

Gartshore, I.S.
1977
Discussion of the paper on "An investigation of the forces on three dimensional bluff bodies in rough wall turbulent boundary layers" by B.E. Lee and B.F. Soliman. Trans. of the ASME Jr. of Fluids Engg.

Gartshore, I.S. and
De Croos, K.A.
1977
"Roughness element geometry required for wind tunnel simulation of the atmospheric wind".
Trans. of the ASME Jr. of Fluid Engg.

Givoni, B.
1968
"Ventilation problems in hot countries".
Technion - Israel Institute of Tech.
B.R.S. Dept. of Building Climatology.

Good, M.C. and
Joubert, P.N.
1968
"The form drag of two dimensional bluff plates immersed in turbulent boundary layers".
Jr. Fluid Mech. Vol. 31, Part 3.

Harris, R.I. 1968 — "Measurements of wind structure at heights up to 598 ft. above ground level". Symposium on wind effects on buildings and structures. Loughborough University.

Harris, R.I. 1970 — "The nature of the wind". Symposium on the modern design of wind sensitive structures, C.I.R.I.A. London. Institute of Civil Engg. Seminar Proceedings.

Harris, R.I. 1972 — "Measurements of wind structure". Symposium on external flows, University of Bristol.

Harris, R.I. 1977 — "The atmospheric boundary layer". Paper presented in a seminar on the statistical assessment of wind loads, B.R.E. Dept. of Environment.

Hillier, R. 1973 — "An investigation of the cladding wind loads on a model of Hartlepool switch house". C.E.G.B. Laboratory Note RD/L/N, 227/73.

Hillier, R. 1978 — "Effects of free stream turbulence on separated flows". Lecture at the Dept. of Aeronautics, Imperial College, London. February.

Hinze, J.O. 1975 — "Turbulence". 2nd Edition, McGraw Hill, New York.

Houghton, E.L. and Carruthers, N.B. 1976 — "Wind forces on buildings and structures - An introduction". Edward Arnold Ltd., London.

I.H.V.E. guide 1970 — "Air infiltration, section A4". Institution of Heating and Ventilating Engineers, Book A; Design Data, London, 1971.

Jackman, P.J. 1969 — "A study of the natural ventilation of tall office buildings". H.V.R.A. Laboratory Report No. 53.

Jensen, M. and Franck, N. 1965 — "Model scale tests in turbulent wind". Danish Tech. Press, Copehagen.

Johnson, J.W.
1944
"Rectangular artificial roughness in open channels".
Am. Geophys. Union Trans. Part 6.

Jones, P.M., Delarrinage, M.A.B. and Wilson, C.B.
1971
"The urban wind velocity profile".
Jr. Atmos. Env. Vol. 5.

Joubert, P.N., Stevens, L.K. and Perry, A.E.
1962
"The effect of aspect ratio on wind forces on building models".
Civil Engg. Trans. Institute of Engg. Australia, C.E.4.

Joubert, P.N., Perry, A.E. and Stevens, L.K.
1971
"Drag of a bluff body immersed in a rough wall boundary layer".
Proceedings of Third Int. Conference on Wind Effects on Buildings and Structures, Tokyo, 1971.

Kamei, I.
1955
"Studies on natural wind pressure on buildings and other structures".
Rep. No. 1, Building Research Inst., Min. of Construction, Japan.

Kelnhofer, Wm. J.
1971
"Influence of a neighbouring building on flat roof wind loading".
Proc. of Third Int. Conf. on Wind Effects on Buildings and Structures, Tokyo, 1971.

Koenigsberger, O.H., Ingersoll, T.G., Mayhew, A. and Scokolay, S.V.
1973
"Manual of tropical housing and building climatic design".
Part I. Longman Group Ltd.,

Koloseus, H.J. and Davidian, J.
1966
"Free surface instability correlation and roughness concentration effect on flow over hydrodynamically rough surfaces".
Geol. Surv. Water Supply paper 1592-C.D., US Govt. Printing Office.

Lee, B.E.
1975(a)
"The effect of turbulence on the surface pressure field of a square prism".
Jr. Fluid Mech. Vol. 69, Part 2.

Lee, B.E.
1975(b)
"The wind climate of Sheffield".
Dept. of Building Science, Int. Report BS 27, Fac. of Arch. Studies, Sheffield University.

Lee, B.E.
1976
"Some effects of turbulence scale on the mean forces on a bluff body". Jr. Ind. Aerodynamics I.

Lee, B.E.
1977
"The simulation of atmospheric boundary layers in the Sheffield University 1.2 x 1.2m boundary layer wind tunnel".
Dept. of Building Science, Int. Report BS 38, Faculty of Arch. Studies, Sheffield University.

Lee, B.E. and Soliman, B.F.
1977
"An investigation of the forces on three dimensional bluff bodies in rough wall turbulent boundary layers".
Trans. of the ASME Jr. of Fluids Engg.

Liu, C.K., Kline, S.J. and Johnston, J.P.
1966
"An experimental study of turbulent boundary layer on rough walls".
Report MD 15, Dept. of Mech. Engg. Stanford University, California.

Marshall, J.K.
1971
"Drag measurements in roughness arrays of varying density and distributions".
Jr. Agricultural Meteorology, Vol. 8.

Maull, D.J. and East, L.F.
1963
"Three dimensional flow in cavities". Jr. Fluid Mech. Vol. 16.

Melbourne, W.H. and Joubert, P.N.
1971
"Problems of wind flow at the base of tall buildings".
Proceedings of Third Int. Conference on Wind Effects on Buildings and Structures, Tokyo, 1971.

Miyoshi, S., Ida, M. and Miura, T.
1971
"Wind pressure coefficients on exterior wall elements of tall buildings".
Proceedings of Third Int. Conference on Wind Effects on Buildings and Structures, Tokyo, 1971.

Morris, Jr. H.M.
1955
"Flow in rough conduits".
Trans. ASCE Vol. 120, Paper No. 2745.

Munn, R.E.
1966
"Descriptive micrometeorology".
Academic press, New York and London.

Nelson, L. (Lokmanhekim, Ed.) 1971 — "An algorithm for infiltration rate calculations". ASHRAE Task Group on Energy Requirements for Heating and Cooling.

Newberry, P.S. and Obee, R.W. 1971 — "Flow in building complexes". B.Sc. Thesis 146. Dept. of Aero. Engg. University of Bristol.

Newberry, C.W., Eaton, K.J. and Mayne, J.R. 1973. — "Wind loading on tall buildings - further results from Royex house". B.R.S. Current Paper 29/73.

Nikuradse, J. 1933 — "Stomungsgesetze in Rouhen Rohren". Forschungsheft 361.

Norton, D.J. and Oldham, G.A. 1975 — "Modelling roughness element size structures". Second US National Conference on Wind Engg. Research, Colorado State University.

Olgyay, V. and Olgyay, A. 1963 — "Design with climate". Princeton University Press, Princeton.

Panofsky, H.A. and Townsend, A.A. 1964 — "Change of terrain roughness and the wind profile". Q. Jr. Royal Met. Society, Vol. 90.

Panofsky, H.A. and Peterson, E.L. 1972 — "Wind profiles and change of terrain roughness at Riso". Q. Jr. Royal Met. Society 98.

Pasquill, F. 1970 — "Wind structure in the atmospheric boundary layer". Phil. Trans. Roy. Soc. London, A, Vol. 269.

Pasquill, F. 1972 — "Some aspects of boundary layer description". Q. Jr. Royal Met. Society, Vol. 98.

Perry, A.E. and Joubert, P.N. 1963 — "Rough wall boundary layers in adverse pressure gradients". Jr. Fluid Mech. 17.

Perry, A.E., Schofield, W.H. and Joubert, P.N. 1969. — "Rough wall turbulent boundary layers". Jr. Fluid Mech. Vol. 37, Part 2.

Peterka, J.A. and Cermak, J.E. 1974 — "Simulation of atmospheric flows in short wind tunnel test sections". Centre for Building Tech. I.A.T. National Bureau of Standards, USA.

Plate, E.J. 1964 — "The drag on a smooth flat plate with a fence immersed in its turbulent boundary layer". ASME Paper No. 64-FE-17.

Powell, R.W. 1944 — "Discussion of rectangular artifical roughness in open channels by J.W. Johnson". Am. Geophys. Union Trans. Pt. 6.

Prandtl, L. 1952 — "The essentials of fluid dynamics". Blackie and Sons Ltd., London.

Rand, W. 1952 — "Investigation of open channel flow over artificially roughened bottom". Iowa Institute of Hydraulic Research, Unpublished Thesis.

Robertson, L.E. and Chen, P.W. 1969 — "The treatment of wind in the design of very tall buildings". Building Science Series 30. Proceedings of Tech. meeting. US National Bureau of Standards.

Rushko, A. 1955 — "On the wake and drag of bluff bodies". Jr. Aero. Soc. 22.

Schlictling, H. 1968 — "Boundary layer theory". 7th Edition, McGraw Hill, New York.

Schofield, W.H., Perry, A.E. and Joubert, P.N. 1974 — "Pressure distributions in slot type rough walls under turbulent boundary layers". Australian Dept. of Supply Report, ARL/M.E.-TN 345.

Schofield, W.H. 1975 — "Measurements in adverse pressure gradient turbulent boundary layer with step change in surface roughness". Jr. Fluid Mech. Vol. 70.

Simpson, R.L. 1973 — "A generalised correlation of roughness density effects on the turbulent boundary layer". Jr. A.I.A.A. Vol. 11, No. 2.

Shellard, H.C. 1963 — "The estimation of design wind speeds". N.P.L. Symposium No. 16 on Wind Effects on Buildings and Structures.

Shiotani, M.
1962
"The relation between wind profiles and the stability of the air layer in the outskirts of the city". Jr. Met. Society, Japan, Vol. 11, 40(6).

Soliman, B.F.
1976
"A study of the wind pressure forces acting on groups of buildings". Ph.D. Thesis, Dept. of Building Science, University of Sheffield.

Stathopoulos, T.
1975
"Wind pressure loads on flat roofs". M.Sc. Thesis, Faculty of Engg. Science, University of Western Ontario, Canada.

Sutton, O.G.
1953
"Micrometeorology. A study of physical processes in the lowest layers of the earth's atmosphere". McGraw Hill Publishing Co.

Tani, I., Iuchi, M. and Komoda, H.
1961
"Experimental investigation of flow associated with a step or a groove". Report No. 364, Vol. 27, No. 4, Aeronautical Res. Institute, University of Tokyo.

Tieleman, H.W. and Gold, R.R.
1976
"Wind tunnel investigation of CARE, inc. single family dwelling". Rep. No. VPI-E-76-22, Dept. of Engg. Science and Mech. Virginia Polytech. Institute and State University, Blacksburg.

Tieleman, H.W. and Reinhold, T.A.
1976
"Wind tunnel model investigation for basic dwelling geometries". Rep. No. VPI-E-76-8. Dept. of Engg. Science and Mech., Virginia Polytech. Institute and State University, Blacksburg.

Townsend, A.A.
1951
"The structure of the turbulent boundary layer". Proc. Cambridge Phil. Soc. Trans. Vol. 47.

Townsend, A.A.
1965
"The response of a turbulent boundary layer to abrupt changes in surface conditions". Jr. Fluid Mech. Vol. 22, Part 4.

Tripp, W.
1936
"Friction losses in an artificially roughened rectangular channel". Jr. Aeronaut. Science, Vol. 4.

Van der Hoven, I.
1957
"Power spectrum of horizontal wind speed".
Jr. Meteorology, Vol. 14.

Weston, E.T.
1956
"Air movement in industrial buildings: Effect of nearby buildings".
Special Rep. No. 19, Commonwealth Experimental Building Station, Sydney.

Wise, A.F.E., Sexton, D.E. and Lillywhite, M.S.
1965
"Air flow round buildings".
Urban Planning Research Symposium, Min. Technology, B.R.S.

Wise, A.F.E.
1970
"Wind effects due to groups of buildings".
B.R.E. Current Paper 23/70

Wood, D.H. and Antonia, R.A.
1975
"Measurements in a turbulent boundary layer over a d-type surface roughness".
Trans. ASME Jr. of Applied Mech.

Wooding, R.A., Bradley, E.F. and Marshall, J.K.
1973
"Drag due to regular arrays of roughness elements of varying geometry".
Boundary Layer Meteorology 5.

Yu, C.C.T.
1975
"Flow round a square block measurement of mean and fluctuating pressure. Effect of incident turbulence".
M.Sc. Thesis, Dept. of Aeronautics, Imperial College of Science and Tech., Univ. of London.